The Detection of Ancient Mines by NASA Space Shuttle Imaging RADAR: Scotland, the Sinai and Spain

Gary McKay, 2003

Ph.D. Geography
The University of Edinburgh
2003

I hereby declare that this work has been composed by myself and has not been previously submitted for any other degree, professional qualification, or publication. Copyright protection exists under the Federal Code of the United States of America.

Submitted this day 8 May 2003 by

The Detection of Ancient Mines by NASA Space Shuttle Imaging RADAR: Scotland, the Sinai and Spain

Gary McKay, 2003

Abstract

The pre-history of mining for metals is poorly understood. A number of reasons may be postulated such as the re-working of mine sites with the consequent loss of early mining evidence, urbanization, particularly within coastal regions of the world, and changes in vegetation coverage. This study examines the ability of space-borne remote sensing technologies to detect potential ancient mineral extraction and processing sites with a view to understanding the regional impact of mineral extraction over areas too large to be amenable to conventional archaeological survey techniques.

A determinative and comparative analytical methodology of how ancient mines may be detected, surveyed, and analyzed using space-borne remote sensing technology, chiefly multipolarimetric Space Shuttle Imaging RADAR, was employed. This methodology used three elements, polarimetric RADAR analysis of mine sites, examination of performance characteristics within three distinctly different climatic environments, as well as modeling and visualization of mines within their geoarchaeological landscapes. The sites studied were South Ardachy, Scotland, Serabit El Khadim in the Sinai, and Conil, Spain. The selection of mining regions was based on a number of factors, including commentaries of classical writers, mine types, climatic conditions, the availability of Space Shuttle Imaging RADAR data, CORONA satellite data, and Advanced Very High Resolution Radiometer (AVHRR) data.

The results of the comparative investigation between the C and L RADAR bands using phase difference analysis at the South Ardachy and Conil ancient mine sites were unable to determine a specific reflecting surface type due to low sensor resolution and the unique shapes of the mines; the Serabit El Khadim mine site did not possess dual polarimetric data and could not be analysed. Decibel responses for both C and L RADAR bands performed within known standards in their various polarimetric modes and were shown to be unaffected by the various climates. All three sites were modeled and visualized three-dimensionally to demonstrate the capability of Imaging RADAR to map geoarchaeological landscapes and to display the extent of landscape change due to mining extraction and processing.

This study demonstrated the potential of space-borne remote sensing for archaeological prospection and discovery on regional and continental scales.

Acknowledgements

A research work of this scale could not be achieved without the support of numerous individuals. There is no first amongst the many listed here, merely a succession of fellow academic adventurers encountered on a journey to gather knowledge.

Former teachers and mentors, Dr. Dan Good, Dr. Nancy Shumaker, Dr. Ben Richason III, Dr. Jim Rankin, and Dr. Donnie Richards, all of whom could be relied upon for support; at NASA and JPL, Dr. Thomas Sever, Dr. Thomas Farr, Dr. Ellen O'Leary, Dr. Ronald Blom and Dr. Jakob Van Zyl. At the Thomas Edison House in London, where invaluable support was rendered when it was most needed, John Dowling. At the Naval Research Laboratory where ideas and innovation were paramount and where the golden rule was "there are no rules, we're trying to get something done around here"!

Far afield, Dr. Mario Olmo and the Geography Department of the University of Granada, who with Dr. Antonio Aragon of the Casa Cultural in Barbate, Spain, and his colleague Mariano Nunez, explained where Tartessos was in an evening.

In Egypt, Ali Ben Hassan and his gracious family, who thought it was all marvelous madness.

In Scotland, Dr. David Caldwell at the National Museum of Scotland and his modern Islemen, Mr. Nigel Ruckley (BGS-ret.) and Mr. Roger McWee, all gentlemen who merrily chattered away as we walked many a mile over the heather and hill of Islay.

At the University of Edinburgh's Department of Geography, Mr. Chris Place, Mr. Gavin Park and Mr. Steve Dowers, who helped in the early days with the struggle to control the massive amounts of remote sensing data.

The Department of Archaeology at the University of Edinburgh rendered essential assistance throughout this work. Dr. Dennis Harding, Dr. Eddie Peltenberg, Dr. Trevor Watkins and Dr. Gordon Thomas, who all took time to point the way when direction was needed. Finally, Mr. Ian Morrison, a computer expert without parallel, who calmed many a fear and saved many a piece of data from disappearing into oblivion; there are not enough words of thanks!

At the Oriental Institute, Mr. John Sanders and Mr. Chuck Jones, who responded with all due speed when vital questions were posed from very distant places around the world.

Finally, my supervisors, Dr. Tim Malthus, Dr. Geraint Coles and Dr. McGuire Gibson; they survived an ocean of data and a tidal wave of ideas. It was truly global in scale.

Dedication

The last years of the Cold War were momentous times for those of us directly involved in historic events. Yet, merely a decade later academics, journalists and students frequently underestimate the Herculean achievements of the Cold War era in the collection of scientific data. Formerly classified environmental data is now being released at such a rate that it has inundated the world's scientific community and it has also overwhelmed their ability to analyze the secrets this information may hold about the world.

These prizes of information, just as any discovered during the Age of Discovery, were not gathered without cost. Those of us who survived the Cold War carry with us the dreams denied to fellow crewmates and friends, knowing that that our own dreams might be deferred in order to fulfill theirs. This work is a debt fulfilled to past crewmates and friends, whom dreamed of looking down upon the earth merely to discover.

In memory of the NASA Space Shuttle Challenger and her crew, friends whom perished on January 28, 1986. They carried the first civilian multipolarimetric Imaging RADAR system into space.

In memory of U.S. Navy aircraft "Ranger 11" and her crew, fellow crewmates at Fleet Air Reconnaissance Squadron Number Two, VQ-2, who perished on Jan. 25, 1987. Classified.

Their mission is complete.

Foreword

The title of this work suggests to the reader that it is merely a remote sensing technology application directed at various archaeological sites around the world. This can be forgiven in the context of today's obsession with technology within the Science of Geography. Since the early 1980s and throughout the 1990s, Geographical Information Systems (GIS) and Remote Sensing (RS) technologies benefited from dramatic advances in computational power and speed. These technologies, coupled with the creation and development of the Global Positioning System (GPS) at the same time, equipped geographers with spatial analysis tools that scarcely could have been imagined a mere half-century before. Unfortunately, this has given rise to the misconception that these tools are sciences themselves, which they are not, and to a certain languishing in pure geographic and topographic work.

Geography is defined as "a science that deals with the description, distribution, and interaction of the diverse physical, biological, and cultural features of the earth's surface". It is also frequently called the "first science". The development of the discipline itself is from the Greeks, their body of work being translated and synthesised into Western Civilisation by the Moorish culture of Spain between the 8th and 15th centuries. No pure geographic work would have been considered suitable without meeting the previously described definition of the science, the *Al-Muqqadima* of Ibn-Khaldun being the supreme example, as stated by Toynbee.

Yet, there is another science that predates Geography, that being Topography.

Topography was derived from the Greek word *topographein*, which is comprised of *topos,* or place, and *graphein*, to write. Its modern definition is "the description of the configuration of a surface including its relief and the position of its natural and man-made features". The subject of this study, ancient mines, are man-made features whose constructions have changed the configuration of the earth's surface and whose positions are poorly understood, thus a topographic approach seems more than apt. Further, the remote sensing technology employed within this study was designed to be a topographic mapping instrument; its latest iteration was used in the Year 2000 to perform a global mapping campaign entitled the "Shuttle RADAR Topographic Mapping" (SRTM) mission.

Finally, different cultures were involved in constructing these mining features. This demands a pure geographic approach as well for only by understanding the aspirations and outlooks of these cultures can we understand why vast efforts were expended upon the location of mineral ores and their extraction.

This study, therefore, is a work of topographic science. It utilises terrain analysis via digital terrain models, surface configuration detection by a remote sensing instrument and toponymic analysis by linguistic methodology to derive certain ideas about the shape of particular areas of the world. It then employs geographic science in the form of comparative historical, geological, climatological and locational information to correlate the findings of the topographic analysis.

G.L. McKay, Topographer of the United States Army.

Table of Contents

List of Figures vii

List of Tables xi

Chapter 1 - Introduction 1
1.1 Approach and Aims 4
1.2 Thesis Structure 6

Chapter 2 – Ancient Mines: A Review of their History and Remote Sensing Detection Methods 8
2.1 Introduction 8
2.2 A Review of Ancient Mining in the Study Regions 9
2.2.1 Scotland 9
2.2.1.1 Characteristics of Pre-Industrial Age Mines in Scotland 11
2.2.2 Egypt and the Sinai 12
2.2.1 Characteristics of the ancient mines of the Sinai 14
2.2.3 Ancient Mining in Andalucian Spain 16
2.2.3.1 Characteristics of the ancient mines of Andalusian Spain 18
2.3 Detection of ancient mines and remote sensing technology 20
2.3.1 Traditional methods of ancient mine detection 20
2.3.2 Remote sensing of ancient mine sites: techniques and research .. 21
2.3.2.1 Remote sensing archaeology techniques 23
2.3.2.2 Remote sensing archaeology research 24
2.3.2.3 Imaging RADAR: applications relevant to archaeology 26
2.4 Conclusions 28

Chapter 3 - Principles of Imaging RADAR and Archaeological Use 30
3.1 Introduction 30
3.2 Electricity 30
3.3 The Electromagnetic Theory 31
3.4 RADAR 32
3.5 Basic Concepts of RADAR 33
3.6 SAR 34
3.7 Polarimetric SAR 37
3.8 Target and microwave interaction 41
3.9 SAR Configuration and control 46
3.10 Understanding SAR imagery 54
3.11 NASA SIR-C/X-SAR multipolarimetric Imaging RADAR 56

Chapter 4 - Methods 61
4.1 Introduction 61
4.1.1 Ancient mines: a general model 62
4.2 Physical Geography and Geology 65
4.2.1.1 Regional Selection 68
4.2.1.2 Britain and the Hebridean Islands 68
4.2.1.3 Egypt and the Sinai 68
4.2.1.4 Spain 69
4.2.2 The Geology 69
4.2.3 The Minerals and Mines 69
4.3 Historical Geography 69
4.3.1 Historical Geography: research methods 69

4.4	Location of the Mine Complexes	70
4.4.1	Site Topography and Analysis	70
4.4.1.1	Topographic Analysis	70
4.4.1.2	Slope	71
4.4.1.3	Aspect	71
4.4.1.4	Shaded Relief	71
4.4.1.5	Profile Convexity	71
4.4.1.6	Plan Convexity	71
4.4.1.7	Longitudinal Convexity	72
4.4.1.8	Cross-sectional Curvature	72
4.4.1.9	Minimum Curvature	72
4.4.1.10	Maximum Curvature	72
4.4.2	Geology of the Sites	72
4.4.3	Geomorphology	73
4.4.4	Vegetation	73
4.5	Site History and Archaeology	73
4.5.1	Historical Background	73
4.5.2	Site Archaeology and Survey	73
4.5.3	Ground Features	73
4.5.4	Archaeological Assessment	74
4.5.5	Ground control campaign	74
4.6	CORONA Satellite Imagery	75
4.6.1	CORONA Imagery	75
4.6.1.1	CORONA Satellite Imagery Processing and Subsets	75
4.7	AVHRR Satellite Imagery	76
4.8	Meteorological Data	77
4.8.1	Meteorological Office Data	77
4.9	NASA SIR-C/X-SAR Imaging RADAR, Data and Analysis Techniques	77
4.9.1	The Imaging RADAR	77
4.9.2	Data Processing	77
4.9.3	Imaging RADAR Data Analysis	78
4.9.3.1	Analysis Form and Test Site	78
4.9.3.2	C Band Imaging RADAR Analysis	78
4.9.3.3	L Band Imaging RADAR Analysis	78
4.9.3.3.1	Comparative Transects	78
4.9.3.4	Comparative Analysis	79
4.9.4	Imaging RADAR Topographic Modeling and Visualization	79
4.9.4.1	Data Fusion and Representation	79
4.9.4.2	Filter Processes	80
4.10	Summary of Results	81
4.10.1	Imaging RADAR and the Topography	81
Chapter 5	**South Ardachy, Isle of Islay**	82
5.1	Introduction	82
5.2	Physical Geography and Geology	82
5.2.1	The Physical Geography of Islay	82
5.2.2	The Geology of Islay	84
5.2.3	The Minerals and Mines of Islay	85
5.2.3.1	Minerals	85
5.2.3.2	Mining	85
5.3	Historical Geography	87
5.3.1	The Historical Geography of Islay until the Industrial Revolution	87

5.4 Location of the South Ardachy Mine Complex 88
5.4.1 Site Topography and Analysis 89
5.4.1.1 Topographic Analysis 91
5.4.1.2 Slope 92
5.4.1.3 Aspect 93
5.4.1.4 Shaded Relief 94
5.4.1.5 Profile Convexity 95
5.4.1.6 Plan Convexity 96
5.4.1.7 Longitudinal Convexity 97
5.4.1.8 Cross sectional curvature 98
5.4.1.9 Minimum curvature 99
5.4.10 Maximum curvature 100
5.4.2 Geology of the site 101
5.4.3 Geomorphology 101
5.4.4 Vegetation 101
5.5 Site History and Archaeology 102
5.5.1 Historical Background 102
5.5.2 Site Archaeology and Survey 102
5.5.3 Ground features 103
5.5.4 Archaeological assessment 104
5.6 CORONA Satellite Imagery 104
5.6.1 CORONA Satellite Imagery details 104
5.6.1.1 CORONA Satellite Imagery subset 105
5.7 AVHRR Satellite Imagery 105
5.8 Meteorological Data 106
5.8.1 United Kingdom Meteorological Office Data 106
5.9 NASA SIR-C/X-SAR Imaging RADAR Data and Analysis 107
5.9.1 The Imaging RADAR data 107
5.9.2 Data processing 107
5.9.3 Imaging RADAR data analysis 108
5.9.3.1 Analysis form and test site 109
5.9.3.2 C band Imaging RADAR phase difference analysis 110
5.9.3.3 L band Imaging RADAR phase difference analysis 115
5.9.3.3.1 Comparative Transect 120
5.9.3.4 Comparative Analysis of the South Ardachy Mine RADAR Data 125
5.9.4 Imaging RADAR Topographic Modeling and Visualization 132
5.9.4.1 Data Fusion and Representation 132
5.9.4.2 Filter Processes 133
5.9.4.3 Visualization: West 134
5.9.4.4 Visualization: North 135
5.9.4.5 Visualization: East 136
5.9.4.6 Visualization: South 137
5.10 Summary of Results 138
5.10.1 Imaging RADAR and the Topography 138

Chapter 6 - Serabit El Khadim, the Sinai 139
6.1 Introduction 139
6.2 Physical Geography and Geology 139
6.2.1 The Physical Geography of the Middle Sinai 139
6.2.2 The Geology of the Sinai 141
6.2.3 The Minerals and Mines of the Western Sinai 143
6.2.3.1 Minerals 143

6.2.3.2 Mining 143
6.3 Historical Geography 143
6.3.1 The Historical Geography of the Sinai until the Fourth Dynasty 143
6. 4 Location of the Serabit El Khadim Mine Complex and Topographic Analysis 146
6.4.1 Site Location 146
6.4.1.1 Topographic Analysis 147
6.4.1.2 Slope 148
6.4.1.3 Aspect 149
6.4.1.4 Shaded Relief 150
6.4.1.5 Profile Convexity 151
6.4.1.6 Plan Convexity 152
6.4.1.7 Longitudinal Convexity 153
6.4.1.8 Cross-sectional Convexity 154
6.4.1.9 Minimum Curvature 155
6.4.1.10 Maximum Curvature 156
6.4.2 Geology of the Site 157
6.4.3 Geomorphology 158
6.4.4 Vegetation 159
6.5 Site History and Archaeology 161
6.5.1 Historical Background 161
6.5.2 Site Archaeology and Survey 161
6.5.3 Ground Features 163
6.5.4 Archaeological Assessment 164
6.6 CORONA Satellite Imagery 164
6.6.1 CORONA Satellite Image Details 164
6.6.1.1 CORONA Satellite Imagery Subset 164
6.7 AVHRR Satellite Imagery 166
6.8 Meteorological Data 167
6.8.1 Egyptian Meteorological Office Data 167
6.9 NASA SIR-C/X-SAR Imaging RADAR Data and Analysis 167
6.9.1 The Imaging RADAR Data 167
6.9.2 Data Processing 168
6.9.3 Imaging RADAR Data Analysis 170
6.9.3.1 Analysis Form and Test Site 170
6.9.3.2 C band Imaging RADAR phase difference Analysis: “B” Mine, Serabit El Khadim 171
6.9.3.3 L band Polarimetric Imaging RADAR Analysis: “B” Mine, Serabit El Khadim 174
6.9.3.3.1 Comparative Transect 177
6.9.3.4 Comparative Analysis of the C band and L band RADAR Data 180
6.9.4 Imaging RADAR Topographic Modeling and Visualization 182
6.9.4.1 Data Fusion and Representation 185
6.9.4.2 Filter Processes 185
6.9.4.3 Visualization: West 187
6.9.4.4 Visualization: North 188
6.9.4.5 Visualization: East 189
6.9.4.6 Visualization: South 190
6.10 Summary of Results: Serabit El Khadim 191
6.10.1 Imaging RADAR and the Topography 191

Chapter 7: Conil, Spain 192
7.1 Introduction 192
7.2 Physical Geography and Geology 192
7.2.1 The Physical Geography of Cadiz and The Gaditano Maritime 192
7.2.2 The Geology of Conil and the Cadiz Province 195
7.2.3 The Minerals and Mines of the Cadiz Province 196
7.2.3.1 Minerals 196
7.2.3.2 Mines 196
7.3 Historical Geography 197
7.3.1 The Historical Geography of the Conil Mines until the Roman Era 197
7.4 Location of the Conil Mines and Topographic Analysis 200
7.4.1 Site Location 200
7.4.1.1 Topographic Analysis 201
7.4.1.2 Slope 202
7.4.1.3 Aspect 203
7.4.1.4 Shaded Relief 204
7.4.1.5 Profile Convexity 205
7.4.1.6 Plan Convexity 206
7.4.1.7 Longitudinal Convexity 207
7.4.1.8 Cross-sectional Convexity 208
7.4.1.9 Minimum Curvature 209
7.4.1.10 Maximum Curvature 210
7.4.2 Geology of the Site 211
7.4.3 Geomorphology 212
7.4.4 Vegetation 213
7.5 Site History and Archaeology 214
7.5.1 Historical Background 214
7.5.2 Site Archaeology and Survey 214
7.5.3 Ground Features 216
7.5.4 Archaeological Assessment 217
7.6 CORONA Satellite Imagery 217
7.6.1 CORONA Satellite Image Details 217
7.6.1.1 CORONA Satellite Imagery Subset 218
7.7 AVHRR Satellite Imagery 219
7.8 Meteorological Data 220
7.8.1 U.S. Navy Meteorological Office Data 220
7.9 NASA SIR-C/X-SAR Imaging RADAR Data and Analysis 221
7.9.1 The Imaging RADAR Data 221
7.9.2 Data Processing 221
7.9.3 Imaging RADAR Data Analysis 222
7.9.3.1 Analysis Form and Test Site 223
7.9.3.2 C band Imaging RADAR phase difference analysis: "C" Mine, Conil 224
7.9.3.3 L band Imaging RADAR phase difference analysis: "C" Mine, Conil 229
7.9.3.3.1 Comparative transect 234
7.9.3.4 Comparative Analysis of the C band and L band RADAR Data 240
7.9.4 Imaging RADAR Topographic Modeling and Visualization 248
7.9.4.1 Data Fusion and Representation 248
7.9.4.2 Filter Processes 249
7.9.4.3 Visualization: West 250
7.9.4.4 Visualization: North 251

7.9.4.5 Visualization: East 252
7.9.4.6 Visualization: South 253
7.10 Summary of Results: Conil 254
7.10.1 Imaging RADAR and the Topography 254

Chapter 8 - Site Result Comparison 255
8.1 Introduction 255
8.2 Physical Geography and Geology 255
8.2.1 Comparing the Physical Geography 255
8.2.2 The Geology 256
8.2.3 The Minerals and Mines 257
8.2.3.1 Minerals 257
8.2.3.2 Mines 257
8.3 Historical Geography 258
8.3.1 The Historical Geography 258
8.4 Location of the Mine Works and Topographic Analysis 259
8.4.1 Site Location 259
8.4.1.1 Topographic Analysis 260
8.4.1.2 Slope 260
8.4.1.3 Aspect 261
8.4.1.4 Shaded Relief 261
8.4.1.5 Profile Convexity 262
8.4.1.6 Plan convexity 263
8.4.1.7 Longitudinal convexity 263
8.4.1.8 Cross-sectional Convexity 264
8.4.1.9 Minimum Curvature 265
8.4.1.10 Maximum Curvature 265
8.4.2 Geology of the Site 266
8.4.3 Geomorphology 266
8.4.4 Vegetation 267
8.5 Site History and Archaeology 268
8.5.1 Historical Background 268
8.5.2 Site Archaeology and Survey 269
8.5.3 Ground Features 270
8.5.4 Archaeological Assessment 270
8.6 CORONA Satellite Imagery 271
8.6.1 CORONA Satellite Image Details 271
8.6.1.1 CORONA Satellite Imagery Subset 271
8.7 AVHRR Satellite Imagery 272
8.8 Meteorological Data 273
8.8.1 Isle of Islay, Mid-Sinai and Straits of Gibraltar Meteorological Data 273
8.9 Comparative Analysis of the NASA SIR-C/X-SAR Imaging RADAR Data 273
8.9.1 The Imaging RADAR Data 273
8.9.2 Data Processing 274
8.9.3 Imaging RADAR Data Analysis 274
8.9.3.1 Analysis Form and Test Site 274
8.9.3.2 Imaging RADAR Analysis 275
8.9.3.2.1 C band 277
8.9.3.2.2 L band 278
8.9.3.3 Comparative Surfaces and Transects 279
8.9.4 Imaging RADAR Data fusion, modeling and visualisation 280

Chapter 9: Conclusions 285
9.1 Principal conclusions 285
9.2 Discussion and future prospects 287

Bibliography 293

Appendix I 305

Appendix II 313

Appendix III 322

Appendix IV 358

Appendix V 363

Appendix VI 369

Appendix VII 425

List of Figures

Fig. 2-1 The world and the three ancient mining areas investigated by Imaging RADAR 9
Fig. 2-2 Britain and Ireland; created from NOAA data, 1:2m 10
Fig. 2-3 The Isle of Islay, Scotland, UK 12
Fig. 2-4 Ancient Egypt Based on Oriental Institute, Univ. of Chicago map 13
Fig. 2-5 Egypt and the Sinai; created from NOAA data, 1:2m 14
Fig. 2-6 The Middle Sinai including Serabit El Khadim mines 15
Fig. 2-7 Andalusian Spain; created from NOAA data,1:2m 17
Fig. 2-8 Southwest Andalucia including the Conil mine site 18
Fig. 3-1 A circulating magnetic field. Its direction is dependent on the current's direction of flow and on the polarity of the voltage being applied. (After U.S. Navy, Vol. 1, "Matter and Physics".) 31
Fig. 3-2 Electromagnetic portion of the spectrum 32
Fig. 3-3 Band designations for various RADAR frequencies 33
Fig. 3-4 SAR target illumination principles 35
Fig. 3-5 Foreshortening, layover and shadow, left to right. (CCRS 2001) 36
Fig. 3-6 Phase and its representation in degrees 39
Fig. 3-7 Degree/radians circle 40
Fig. 3-8 Left to right, top-hat reflector, dihedral reflector and trihedral reflector 43
Fig. 3-9 General representations of typical RADAR targets 56
Fig. 3-10 Main antenna array of the NASA SIR-C/X-SAR 57
Fig. 3-11 The SRTM instrument showing the main radar antenna, the mast, and the outboard radar antenna 59
Fig. 5-1 The Isle of Islay, Scotland (Based on NIMA, OSGB data) 83
Fig. 5-2 Northeast Islay mining areas and relevant geology; based on Cressey (1995) and OSGB 1:50k geology data (2001) 86
Fig. 5-3 Location of South Ardachy mines (based on Cressey, 1995) 89
Fig. 5-4 South Ardachy mine complex (based on Cressey, 1995) 90
Fig. 5-5 Rate of change for slope, eastern Islay 92
Fig. 5-6 Aspect characteristics of eastern Islay 93
Fig. 5-7 Shaded relief of eastern Islay; illumination from southeast 94
Fig. 5-8 Profile convexity for eastern Islay 95
Fig. 5-9 Plan convexity of the eastern Islay area 96
Fig. 5-10 Longitudinal curvature of the eastern Islay area 97
Fig. 5-11 Cross sectional curvature of the eastern Islay area 98
Fig. 5-12 Minimum curvature of the east Islay region 99
Fig. 5-13 Areas of maximum curvature in eastern Islay 100
Fig. 5-14 South Ardachy mine complex geology 101
Fig. 5-15 AVHRR GAC image subset, Isle of Islay, Scotland,UK 105
Fig. 5-16 The Isle of Islay: Ground Control Points and South Ardachy area outlined 108
Fig. 5-17 The South Ardachy mines complex – Chh band 109
Fig. 5-18 Target scene mine shaft and adit at South Ardachy (Adapted from Cressey 1995 and OSGB 1:25k map) 110
Fig. 5-19 Chh raw RADAR data, South Ardachy,Islay 111
Fig. 5-20 C band, total power RADAR data image map 112
Fig. 5-21 Decibel image and phase difference absolute value image for C band, pixels 1208 by 1637 to 1646, South Ardachy, Islay 113
Fig. 5-22 Lvv raw RADAR data, South Ardachy, Islay 116
Fig. 5-23 L band, total power RADAR data image map 117

Fig. 5-24 Decibel image and phase difference absolute value image of L band, pixels 1208 by 1637 to 1646, South Ardachy, Islay..... 118
Fig. 5-25 Comparative transect (left) and mine site transect (right) in red, top; image of transect area terrain, bottom..... 121
Fig. 5-26 Decibel image and phase difference absolute value image, pixels 1203 by 1645 to 1654 (C band, comparative transect), South Ardachy, Islay..... 122
Fig. 5-27 Decibel image and phase difference absolute value image, pixels 1203 by 1645 to 1649 (L band, comparative transect), South Ardachy, Islay..... 124
Fig. 5-28 Mine shaft of pixel 1208 x 1640, Site "A", South Ardachy; view to south..... 126
Fig. 5-29 A general map of the mine shaft at pixel 1208 x 1640, Site "A", South Ardachy..... 127
Fig. 5-30 Mine tailings area southwest of Site "A", South Ardachy; view to south..... 128
Fig. 5-31 Shuttle RADAR illumination of a dihedral reflector 129
Fig. 32a South Ardachy polarimetric phase difference records for all transects.....131
Fig. 32b South Ardachy decibel responses for all transects..... 131
Fig. 5-33 The South Ardachy mines viewed from the west..... 134
Fig. 5-34 The South Ardachy mines as viewed from the north..... 135
Fig. 5-35 The South Ardachy mines complex viewed from the east..... 136
Fig. 5-36 The South Ardachy mines as viewed from the south..... 137
Fig. 6-1 The Sinai and Serabit El Khadem. NIMA and DCW data..... 140
Fig. 6-2 A general map of the Sinai's geology; adapted from USGS, 1:500,000 map..... 142
Fig. 6-3 The Middle Sinai from Abu Rudeis to the Gulf of Aqaba; created from U.S. Army Topographic Corps, 1:250,000 map (1958).....146
Fig. 6-4 Serabit El-Khadim mine complex slope analysis..... 148
Fig. 6-5 Serabit El Khadim mine complex aspect analysis..... 149
Fig. 6-6 Serabit El Khadim mines shaded relief analysis..... 150
Fig. 6-7 Serabit El Khadim mines complex profile convexity analysis..... 151
Fig. 6-8 Plan convexity for the Serabit El Khadim mines region..... 152
Fig. 6-9 Longitudinal curvature for the Serabit El Khadim area.....153
Fig. 6-10 Serabit El Khadim mines cross sectional convexity analysis..... 154
Fig. 6-11 Serabit El Khadim mines complex minimum curvature analysis.....155
Fig. 6-12 Serabit El Khadim mines complex maximum curvature analysis..... 156
Fig. 6-13a and 6-13b Examples of the geology of the jebel near Serabit El Khadem..... 158
Fig. 6-14 The geomorphology regions of the Sinai, based on USGS 1:500,000 map..... 159
Fig. 6-15 Typical vegetation in wadis, Phoenician juniper (centre), palm and birr.....160
Fig. 6-16 A view of Site "B" mine and wadi; view to north-northwest..... 161
Fig. 6-16a Generalised area survey map of Serabit El Khadim..... 162
Fig. 6-17 An image subset of the Serabit El Khadim mines area at 2.5 m. resolution..... 165
Fig. 6-18 An AVHRR image subset over the Sinai proper on 11 April 1994..... 166
Fig. 6-19 The Middle Sinai: Ground Control Points.....169
Fig. 6-20 The Serabit El Khadim mines complex – Chh band..... 170
Fig. 6-21 Mines near Serabit El Khadim..... 171
Fig. 6-22 Chh raw RADAR data image map: Serabit El Khadim "B" target mine area.... 172
Fig. 6-23 C band total power RADAR data image map: Serabit El Khadim.....173
Fig. 6-24 Lhh raw RADAR data image map: Serabit, "B" target mine site..... 175
Fig. 6-25 L band total power RADAR data image map: Serabit, "B" target mine site..... 176
Fig. 6-26a Comparative transect near Serabit El Khadim, top..... 178
Fig. 6-26b Image of the transect area, bottom..... 178
Fig. 6-27 Mine pit and miner's huts; pixel 4274 x 1664-65, Site "B", Serabit..... 180
Fig. 6-28 A general map of the mine site at pixel 4274 x 1664-65, Site "B", Serabit..... 181
Fig. 6-29 Comparison of decibel responses for all Serabit El Khadim transects..... 182

Fig. 6-30 Left to right, top-hat reflector, dihedral reflector and trihedral reflector..... 184
Fig. 6-31 The Serabit El Khadim mines viewed from the west..... 187
Fig. 6-32 The Serabit El Khadim mines as viewed from the north..... 188
Fig. 6-33 The Serabit El Khadim mines complex viewed from the east..... 189
Fig. 6-34 The Serabit El Khadim mines as viewed from the south..... 190
Fig. 7-1 Conil, Spain and region; created from NOAA data, 1:2m..... 193
Fig. 7-2 Example of mining, Ojen slag heap, Cadiz, Spain..... 197
Fig. 7-3 Conil mine site location, geomorphologic zones, and mining related toponyms underlined. Created from DCW and Junta de Andalucia data..... 200
Fig. 7-4 Conil site topography; southwest view..... 201
Fig. 7-5 Slope analysis, Conil..... 202
Fig. 7-6 Aspect analysis, Conil..... 203
Fig. 7-7 Shaded relief analysis, Conil..... 204
Fig. 7-8 Profile convexity analysis, Conil..... 205
Fig. 7-9 Plan convexity analysis, Conil..... 206
Fig. 7-10 Longitudinal convexity analysis, Conil..... 207
Fig. 7-11 Cross-sectional curvature analysis, Conil..... 208
Fig. 7-12 Minimum curvature analysis, Conil..... 209
Fig. 7-13 Maximum curvature analysis, Conil..... 210
Fig. 7-14 Conil mine rakes and surrounding geology..... 211
Fig. 7-15 Conil mine slag heap with sparse vegetation..... 213
Fig. 7-16 Generalised survey map of Conil de Frontera mining complex..... 215
Fig. 7-16a Collapsed side gallery, Site "C" mine rake, approx. 1 metre in height..... 216
Fig. 7-17 CORONA image subset of Conil, Spain mine rakes, ~3m resolution..... 218
Fig. 7-18 AVHRR LAC image subset, Conil, Spain..... 219
Fig. 7-19 The Conil mines region: Ground control point (GCP) sites..... 222
Fig. 7-20 The Conil mine site – Chh (R), Lhh (G) and Lvv (B) bands..... 223
Fig. 7-21 Chh raw RADAR data image map: Conil "C" target mine rake..... 225
Fig. 7-22 C band, total power RADAR data image map: Conil "C" target mine area..... 226
Fig. 7-23 Decibel image and phase difference absolute value image of C band, pixels 125 x 366 to 125 x 370, Conil, Spain..... 227
Fig. 7-24 Lhh raw RADAR data image map: Conil "C" target mine shaft..... 230
Fig. 7-25 L band, total power RADAR data image map: Conil "C" target mine area..... 231
Fig. 7-26 Decibel and phase difference absolute value image of L band, pixels 125 by 366 to 370, Conil, Spain..... 232
Fig. 7-27 Comparative transect, near Conil mine complex, top, image of transect area terrain, bottom..... 235
Fig. 7-28 Decibel image and phase difference absolute value image (C band, comparative transect) pixels 225 x 266 to 270..... 236
Fig. 7-29 Decibel image and phase difference absolute value image (L band,, comparative transect) pixels 225 x 271 to 275..... 238
Fig. 7-30 Mine rake of pixel 125 x 372 , Site "C", Conil mine rakes..... 240
Fig. 7-31 A general map of the Site "C" target mine; pixel 125 x 372, Site "C", Conil.... 241
Fig. 7-32 Pixel 89 x 308; Comparative open pit mine image and map..... 242
Fig. 7-33 Comparative transect area, view from southwest to northeast with hill of Cerro Cantabria in distance..... 243
Fig. 7-34 Shuttle Imaging RADAR illumination of a theoretical dihedral reflector similar in shape to the Site "C" mine rake, Conil, Spain..... 246
Fig. 7-35a Decibel responses for Conil de la Frontera mine and comparative transects.. 247
Fig. 7-35b Polarimetric phase difference statistics for Conil de la Frontera mine and comparative transects..... 247

Fig. 7-36 The Conil mines viewed from the west..... 250
Fig. 7-37 The Conil as viewed from the north..... 251
Fig. 7-38 The Conil mines complex viewed from the east..... 252
Fig. 7-39 The Conil mines as viewed from the south..... 253
Fig. 8-1 Rate of change for slope, eastern Islay, Serabit El Khadim and Conil..... 260
Fig. 8-2 Aspect characteristics for eastern Islay, Serabit El Khadim and Conil..... 261
Fig. 8-3 Shaded relief of eastern Islay, Serabit El Khadim and Conil..... 261
Fig. 8-4 Profile convexity for eastern Islay, Serabit El Khadim and Conil..... 262
Fig. 8-5 Plan convexity of the eastern Islay area, Serabit el Khadim and Conil..... 263
Fig. 8-6 Longitudinal curvature of the east Islay area, Serabit El Khadim and Conil..... 263
Fig. 8-7 Cross-sectional curvature of the east Islay area, Serabit El Khadim and Conil... 264
Fig. 8-8 Minimum curvature of the east Islay region, Serabit El Khadim and Conil..... 265
Fig. 8-9 Areas of maximum curvature in eastern Islay, Serabit, and Conil..... 265
Fig. 8-10 AVHRR GAC subsets, Isle of Islay, Sinai and LAC subset for south Spain.... 272
Fig. 8-11 Left to right, South Ardachy (Site "A"), Serabit (Site "B"), and Conil, (Site "C")..... 276
Fig. 8-12 Target mine maps for South Ardachy (Site "A"), Serabit El Khadim (Site "B"), and Conil (Site "C"), left to right..... 277
Fig. 8-13 Comparative transect areas for South Ardachy (left), Serabit El Khadim (middle) and Conil (right)..... 279
Fig. 8-14 The Isle of Islay (top)..... 281
Fig. 8-15 The Sinai from the Red Sea (top), foreground to the El Tigh Plateau..... 282
Fig. 8-16 A view of the Bay of Algeciras, Gibraltar (top), and southern Spain..... 283

List of Tables

Table 4-1 The model for archaeological mine detection. 64
Table 4-2 Potential remote sensing signatures for ancient mining features 66
Table 5-1 Calibrated brightness temperatures 106
Table 5-2 24 hour averaged weather data, Met Station, Machrihanish, Scotland 106
Table 5-3 Mine site transect, South Ardachy, Islay, C band decibel and phase difference statistics. 114
Table 5-4 Mine site transect, South Ardachy, Islay, L band decibel and phase difference statistics. 119
Table 5-5 Comparative transect, South Ardachy, Islay, C band decibel and phase difference statistics. 123
Table 5-6 Comparative transect, South Ardachy, Islay, L band decibel and phase difference statistics. 125
Table 5-7 Pixel 1208 x 1640 decibel response and phase difference report 126
Table 5-8 Pixel 1215 x 1660 decibel response and phase difference report 128
Table 6-1 Calibrated brightness temperatures in degrees Kelvin, NOAA-11, 1994. 167
Table 6-2 Mine site transect, Serabit El Khadim, C band decibel statistics. 174
Table 6-3 Mine site transect, Serabit El Khadim, L band decibel statistics. 177
Table 6-4 Comparative transect, C band decibel returns, Serabit el Khadim. 179
Table 6-5 Comparative transect, L band decibel returns, Serabit el Khadim. 179
Table 6-6 C and L band decibel responses, mine pit and miner's hut, Serabit El Khadim 182
Table 6-7 C and L band decibel responses for comparative transect, centre pixel, Serabit El Khadim 182
Table 7-1 Calibrated brightness temperatures, degrees Kelvin, NOAA-11, 1994. 220
Table 7-2 24 hour averaged weather data, Met Station, Rota, Spain. 220
Table 7-3 Mine site transect, Conil, Spain, C band decibel and phase difference statistics. 228
Table 7-4 Mine site transect, Conil, Spain, L band decibel and phase difference statistics. 233
Table 7-5 Comparative transect, Conil, Spain, C band decibel and phase difference statistics. 237
Table 7-6 Comparative transect, Conil, Spain, L band decibel and phase difference statistics. 239
Table 7-7 Pixel 125 x 372: Conil mine rake. 242
Table 7-8 Pixel 89 x 308, C band phase difference and decibel responses on top, L band beneath; small open pit mine. 242
Table 7-9 Pixel 225 x 270, Comparative transect, C and L band phase difference with decibel responses. 243
Table 8-1 Physical Geography and characterisation 255
Table 8-2 Geology and characterisation 256
Table 8-3 Minerals and characterisation 257
Table 8-4 Mining and characterisation 257
Table 8-5 Historical geography and characterisation 258
Table 8-6 Site location and characteristics 259
Table 8-7 Site geology and characterisation 266
Table 8-8 Geomorphology and characteristics 266
Table 8-9 Vegetation and characteristics 267
Table 8-10 Historical background and characteristics 268
Table 8-11 Site archaeological survey characteristics 269
Table 8-12 Ground features and characteristics 270
Table 8-13 CORONA satellite imagery subset characteristics 271

Table 8-14 24 hour averaged regional weather data for Site "A", "B" and "C". 273
Table 8-15 C band decibel returns and phase difference for Site "A", "B" and "C" 276
Table 8-16 L band decibel returns and phase difference for Site "A", "B" and "C" 276
Table 8-17 C band decibel returns and phase difference for Site "A", "B" and "C", comparative transects 279
Table 8-18 L band decibel returns and phase difference for Site "A", "B" and "C", comparative transects 279

"Now I have come in as you see, with my ship and companions sailing over the wine-blue water to men of alien language, to Temese, after bronze, and my cargo is gleaming iron". Athene, the goddess, appearing as Mentes the Taphian before Telemachos in the "The Odyssey of Homer"(Homer, translated by Richard Lattimore, 1967:32, verse 180).

The rise of civilisation goes hand in hand with an ability to extract and employ an increasingly complex range of metals. The development of mineral extraction technology is relatively poorly understood by the archaeologists (Craddock, 1998). A number of reasons may be postulated such as the re-working of mine sites with the consequent loss of early mining evidence, urbanisation, especially within the coastal fringes of the world, and changes in vegetation coverage over the landscape (Alessandro, 1994, Bartlett, 1993, Budge and Morain, 1978 and Tylecote, 1976).

The archaeological rationale for this research study is simple. The archaeological community, attempting to ascertain the scope of ancient metallurgical practices, has largely focused on mineral refining, metal products and metals trade (Tylecote, 1976). Works by individuals such as Rothenburg (1979) and Meyer (1997), though some two decades apart, have intensively studied particular ancient mining sites and complexes, while remarking upon their level of industrialisation and possible mineral refining capabilities. However, neither of these research efforts attempted to create a model or methodology for the detection of ancient mines or considered new survey technologies.

Metal products have offered archaeology a means for determining the region of the world from which a particular artefact may have originated by using isotope analysis, for instance (Cressey, 1995, Rothenberg, 1981, Craddock, 1998). However, this method is unable to precisely match a particular metal component with a specific geographic location. Understanding the geographic and topographic locale is of utmost importance in comprehending the extent of metalliferous mining landscapes around the world.

Archaeologically speaking, it has been difficult to ascertain the correct temporal depth within mining landscapes since there has been little work on determining key temporal markers; this is has been a problem in mines which date from the early medieval to early industrial era (Craddock, 1998). Using Great Britain as an example, organisational changes in how mining was carried out in Devon mines during the late medieval period led to substantial changes in the mining landscape. The English Crown, taking direct control of these mines implemented a capital intensive program which required larger numbers of labourers whom were required to be housed nearby; these new communities obscured previous mine workings (Roe and Davies, 2000, Tylecote, 1976).

Metals trade, also thoroughly researched, has largely revolved around the issue of tracing trade routes. Trade with sub-Saharan Africa, as an example, has played a key role in the history and development of Mediterranean cultures from the appearance of the Phoenicians in the west (sometime in the eighth or seventh centuries BC) to the rise of Greek and Roman Civilisation and ultimately to the present. West Saharan Africa was central to these developments; forming a crucial corridor and link between different cultures, north and south, for several millennia. The prosperity of interior settlements such as the near legendary Timbuktu waxed and waned as the fortunes of remote civilisations rose and fell; all this depended upon a trade of extracted West African gold with salt from Mediterranean cultures. Yet, the locations of these mines, which largely funded the rise of Mediterranean cultures, is unknown (Barnard and Tamotsu, 1975, Bovill, 1995, Collis, 1984, Craddock, 1998, Ehrenreich, 1975 and Healy, 1978).

Consequently, the basic archaeological question is unanswered: *how are ancient mines detected?* What is the methodology for the detection of ancient mines? What technology may be employed to rapidly and efficiently detect ancient mines? Finally, how may ancient mines be observed within their particular topography? In essence, the simple question is this: where are the *sources* of metals for a particular civilisation located?

This study sets out to examine new technologies for the detection of potential ancient mineral extraction and processing sites with a view to understanding the regional impact of mineral extraction over areas too large to be amenable to conventional survey techniques.

The importance of developing new techniques and methodologies for archaeology in the employment of remote sensing technologies cannot be overestimated. While this archaeological research problem endeavours to approach the questions of ancient mining detection and mapping, the basic *modus operandi* may be employed for any archaeological area of interest. Therefore the importance of this work to the science of archaeology is to demonstrate a methodology which rapidly and efficiently detects, surveys, analyses and models landscapes at the scale which would otherwise be unfeasible, both from a financial or labour point of view.

To this end this study attempts to construct a determinative and comparative analytical methodology of how ancient mines may be detected, surveyed, and analysed using space-borne remote sensing technology, namely multipolarimetric Imaging RADAR. This methodology had three key elements:

- The employment of multipolarimetric Imaging RADAR (Chap. 3 and 4) to perform geoarchaeological and topographic analyses of the landscapes surrounding each target mine site.

- To model the mine sites characteristically for indications of similarity in geographical and geological locations by a process of visualisation.
- To examine the performance characteristics of Imaging RADAR under different climatic and ground conditions using decibel response and polarimetric phase difference analysis.

The rationale for the choice of Imaging RADAR data for archaeological reconnaissance of ancient mining areas over conventional space-borne spectral systems, such as LANDSAT, is based on the unique characteristics of the microwave sensor (Daily, Farr, Elachi and Schaber, 1979). Imaging RADAR is an all-weather active remote sensing system able to penetrate all but the most extraordinary weather conditions, thus making it better equipped to deal with this particular remote sensing archaeology problem, the detection of ancient mines in under different climatic conditions (Ulaby and Dobson, 1989). To pause, active remote sensing systems, by definition, are those which transmit a signal at a particular wavelength of the electromagnetic spectrum towards a target and then record the reflected signal for analysis. Passive remote sensing systems, such as LANDSAT, rely on reflected signals from the Earth's surface which are generated by the sun and then recorded in various bands or wavelengths of the electromagnetic spectrum for analysis. (Chap. 3). As will be explained in Chapters 2 and 3, while optical, thermal and multi-spectral remote sensing systems have been used for archaeological research, they have been limited because of weather and their inherently passive remote sensing design. Since these systems are unable to transmit their own signals, they are at the mercy of climatic events which may obscure a particular archaeological target area. Their employment in archaeological work is discussed in Chapter 2 and Chapter 3 as well.

Returning to the Imaging RADAR system, it is a topographic mapping instrument, designed specifically for the charting of large-scale geologic landscapes (Chapter 3). This again is a key difference between the active and passive remote sensing systems. The active remote sensing characteristics of Imaging RADAR make it possible for the system to characterise features, determine the interaction of the transmitted signal with these ground features, and in this study ascertain whether certain ground depressions are ancient mines and what microwave interactions are occurring (Chap. 3). It would not be far off the mark to say that Imaging RADAR systems are able to assess the texture and consistency of a given target, as a generalisation.

The all-weather advantage of Imaging RADAR is demonstrated by the use of CORONA (Chapter 4) optical data for comparative purposes over all the target sites within this research project for the visual detection of mines, geology, geomorphology and vegetation. As will be discussed in Chapter 5 on the Isle of Islay, Scotland, the target mine site at South Ardachy was obscured in every available CORONA image scene from the years 1961 through 1972 (USGS, 2001).

AVHRR (Chapter 4) data is employed as an aid to visualisation of target scene area ground based meteorological observation by displaying cloud cover and water vapour amounts. This, in effect, is a double confirmation of local meteorological conditions which may have affected Imaging RADAR performance and are discussed in each of the relevant chapters and the final comparative results chapter (Chapters 5, 6, 7 and 8).

Finally, Digital Terrain Elevation Data Level 0 (known as DTED; see Chapter 4) was chosen as the base digital elevation data from which to construct more detailed local Digital Elevation Models (known as DEM). DTED Level 0 is the highest resolution, publicly available DEM data that has global coverage and high-accuracy surveyed corner points for each cell area (NIMA, 2001).

In consequence of the requirement for three distinctive climatic areas, the study area is hemispheric in scope, encompassing contrasting environments ranging from temperate mid-latitudes to arid desert regions.

In setting out to employ this space-borne technology to archaeological prospection and reconnaissance a number of technical challenges had to be overcome. Since there was no prior research or body of literature regarding the detection of ancient mine sites by any type of space-borne remote sensing system, much of this study has *per force* to focus on the creation of initial base line data.

1.1 Approach and aims

The purpose of this study was to comparatively analyse the capability of space-borne multipolarimetric imaging RADAR to detect, survey, and analyse, ancient mining sites in three distinctly unique climatic and geomorphologic settings. The regions were selected based on references by classical writers. The sites chosen within these regions are the 17th century mine workings of Ardachy on the Hebridean Island of Islay, Scotland, UK, the copper and turquoise mines of Serabit El-Khadim, the Sinai, Egypt, and a mine of mixed provenance, displaying 1st century AD Roman and earlier artefacts, in Conil, Spain. In order to accomplish this purpose, the following questions were posed:

- First, can references by classical writers be used to locate ancient mining regions? Does historical geography provide sufficient historical references and geographic descriptions to select specific ancient mining sites for remote sensing analysis by Imaging RADAR?
- Second, can a correlation between metallurgical toponyms and the historical geography and geology of the mining regions be used as a means of establishing a methodology for the application of remote sensing? Do toponyms and corresponding geology indicate a maximum likelihood of ancient mining within an area?
- Third, can the geology and geomorphology of each mine site area be analysed by Imaging RADAR?
- Fourth, does the local climate of each mining area affect the performance of the multipolarimetric Imaging RADAR?
- Finally, can a comparative performance matrix showing the decibels returns and polarimetric phase difference analyses between all sites reveal unique signatures for the target mine sites?

Consequently, the specific aims of this work will be:

- To research the available biological, cartographic, geographic, geological, historical and topographic records to gain a historical geographic understanding of each mine site within its ancient landscape.
- To develop a geo-linguistic model for the location of ancient mine sites which may be used to target remote sensing technologies in support of archaeological reconnaissance (Appendix IV). It should be noted that only the region surrounding the Conil, Spain site (Chap. 7) was analysed during this research work. Toponym information for the South Ardachy, Scotland site was found to be invalid due to inaccurate Gaelic transliteration over time by the Ordnance Survey of Great Britain (Chap. 5). The lack of proper mapping in the Sinai by the Egyptian government precluded toponym analysis in that region because place names had not been accurately recorded (Chap. 6).
- To investigate the ability of multipolarimetric Imaging RADAR map to determine the extent of mining activity.
- To compare each mine site's multipolarimetric Imaging RADAR returns with the earliest high-resolution optical space-borne remote sensing system.
- To investigate the performance of Imaging RADAR by comparing Advanced Very High Radiation Radiometer (AVHRR) satellite imagery with the Imaging RADAR scenes.

- To examine the performance of the C and L band multipolarimetric Imaging RADAR wavelengths in HH, HV, and VV modes, within three distinct climatic conditions, temperate, (Scotland), arid (Sinai), and semi-arid (Spain), by producing a comparative performance matrix of RADAR responses to the targeted ancient mine sites.
- To create new methods of landscape visualisation for archaeological analysis of ancient mine areas.

1.2 Thesis Structure

The focus of Chapter 2 will be a review of the history of ancient metal mining, the types of mining, and the remote sensing techniques which may aid in the detection and discovery of mines. The first portion of the chapter will be a discussion of ancient mining areas, techniques employed, and the anecdotal, cartographic, geographic and historical sources used to ascertain the locations of ancient mine sites.

The second portion of the chapter deals with an overview of remote sensing research and applications which may have an archaeological use, as well as directed remote sensing efforts in support of archaeology, i.e. remote sensing archaeology. The emphasis will be on qualitative applications and spatial analysis.

Chapter 3 begins with a basic discussion of the operational principles of RADAR. After laying this foundation, Synthetic Aperture RADAR (SAR) systems are introduced in order to familiarise the reader with and understanding of Imaging RADAR. Following this section of the chapter, the technique of multipolarimetric Imaging RADAR is discussed. The effect of antenna pattern correction, incident angles, pedestal height, and other variables that may affect Imaging RADAR returns over a given terrain are discussed, as well as microwave interaction with the earth's surface.

Chapter 4 will deal with the research design of this work and the methodologies chosen to examine the hypotheses. The process of site selection using references from classical writers is presented first, followed by a discussion of the desk-based studies regarding physical geography, geology, historical geography and geomorphology.

The second portion of Chapter 4 deals with the methods and techniques employed in topographic analysis, site geomorphology, vegetation survey, mine site history, mine site archaeology, ground feature identification, and archaeological assessment.

The final portion of Chapter 4 discusses the data processing techniques and analysis of CORONA, AVHRR and NASA SIR-C/X-SAR remote sensing data. The methods of data fusion and visualisation for virtual landscape creation are also covered.

Chapter 5 discusses the results of the examination of the South Ardachy mine site on the Isle of Islay, Scotland. Chapter 6 presents the data resulting from the study of the Serabit El-Khadim mine site, in the Sinai of Egypt. Finally, Chapter 7 covers the results obtained from the Conil, Spain site. Chapter 8 will compare the results of each sector of analysis concerning the mine sites; a comparative matrix of the multipolarimetric Imaging RADAR decibel responses and phase difference for all target mine sites will be presented as well. Chapter 9 will conclude the work with a concise review of the results as well as a discussion of possible future research areas.

Chapter 2

Ancient Mines: A Review of their History and Remote Sensing Detection Methods

"I shall now discuss metals and the natural resources we use to pay for goods. We search for these deep within the earth, diligently and in a number of ways". Pliny (translated by John Healy, 1991:286).

2.1 Introduction

Research concerning ancient mines, smelting processes, equipment of smiths and the artefacts produced by them, has shown that knowledge of metals was discovered independently in several parts of the world (Cotterell, 1980). Copper appears to have been the first metal used for creating tools and weapons, appearing some 9000 years ago (Tylecote, 1976). Excluding the continent of Australia, where metals were unknown before European discovery, metallurgical technology was established around the world by 1000 AD (Cotterell, 1980).

It is apparent then that ancient mining has left its mark in some fashion or another around the world with possibly only agriculture having an equal effect upon global landscapes. Equally, the scale of ancient mining operations has created a dramatic influence upon the environment, ranging from local to global levels. Mining for the base metals by past civilisations with less modern refining capabilities has created a plethora of environmental problems (Bell, 1998). Highly contaminated soils and sediments in hydrological systems are some of the problems faced by modern communities when previously unknown mine systems are taken in by urbanisation.

This chapter is divided into four sections. In Section 2.2, the rise of mining within the geographic regions of Scotland, the Sinai, and southern Spain, is defined within the context of their cultural and technological circumstances. Section 2.3 discusses remote sensing research relevant to the detection of ancient mine sites. It must be stated that there is *no* existing *body* of research literature concerning the detection of ancient mine sites by any form of space-borne remote sensing. Section 2.4 concludes the review.

2.2 A Review of Ancient Mining in the Study Regions

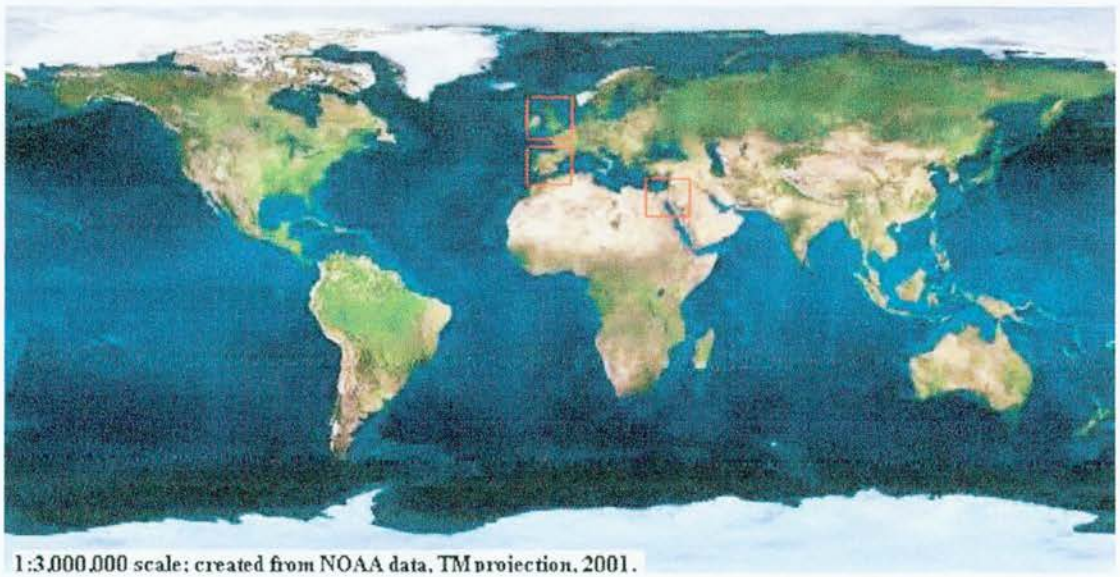

Fig. 2-1 The world and the three ancient mining areas investigated by Imaging RADAR in this study.

2.2.1 Scotland

The early history and diffusion of metal work in Western Europe has been well explained by Forbes (1950) and Tylecote (1976). Around 5000 BC the first cold-copper and gold working had occurred in the Balkans with smelting technology appearing at the end of the same millennium (Champion *et al.*, 1984). By the end of the 4th millennium casting and molding of metals had spread to central Europe (Renfrew, 1969). The end of the 3rd millennium saw the appearance of fine articles made from gold and copper throughout Europe, even to the remote British Isles (Clark, 1952 and Fig. 2-1).

The European Bronze Age began around 2300 BC with its first indications in the British Isles being seen at a site near Parys Mountain and also the Llandudno Mines, both in Wales (Muhly, 1985). Iron working reached the British Isles around 800 BC during what is known as the Celtic Iron Age c. 7th century BC. (Ehrenreich, 1975). However, archaeological evidence for the earliest pre-historic mining in the British Isles is limited with sites such as West Water Reservoir, Peebleshire, Scotland and Calduthel Mains, Scotland, being among the more prominent (Scarre, 1995).

Tin was found in large quantities in Cornwall and was the subject of trade by the Greeks and Phoenicians sailing from the Iberian Peninsula by 1000 BC (Boardman, 1999). However, other than implied accounts noted by later historians and geographers such as Pliny or Strabo, nothing is known about the earliest mining in what today is Scotland (Pliny, 1991). The Roman writer Tacitus would finally bring the subject of metals into historical view with his commentaries on the invasion campaign of Claudius in Britain c. 44 AD (Gibbon, 2000). Even so, northern Scotland and its Celtic culture remained outside the stream of history, as the Roman Empire did not conquer them. The Isle of Islay, located on Scotland's south-western coast belonged to this unconquered area (Fig. 2-2).

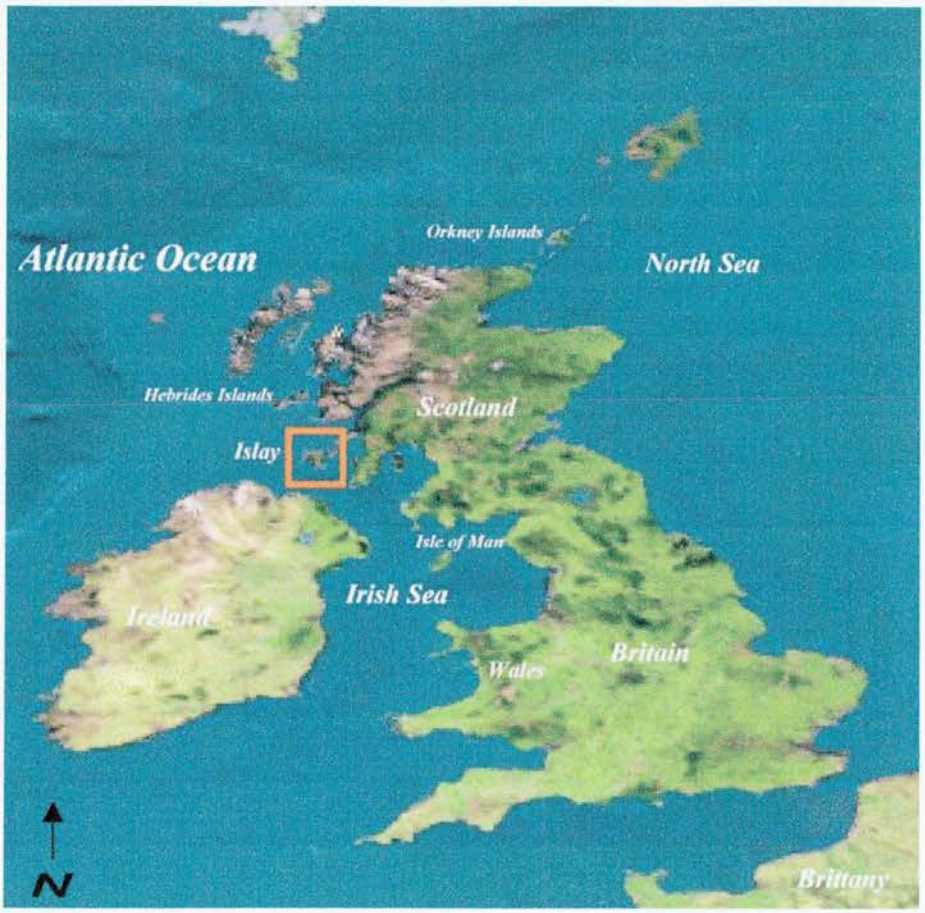

Fig. 2-2 Britain and Ireland showing Islay's location; created from NOAA data, 1:2m.

While Roman historians could make anecdotal reference to mining in conquered Britain, the area now known as England and the Scottish Borders, the archaeological record for the rest of Scotland has scant evidence regarding organised mining during pre-history. Not until the 13th century do references concerning mining appear, with these being monastic sponsored gold and lead mining efforts (BGS, 1995).

By the end of the medieval period and certainly by the beginning of the 17th century, advances in technology had pushed mining to new levels of production and refinement in Britain (Kakela, 1978). However, as the focus of this work is on the earliest mines, that is pre-Industrial, it is necessary to provide a description of the type of mines, mining landscapes and processing techniques which would be seen in Scotland.

2.2.1.1 Characteristics of Pre-Industrial Age Mines in Scotland

Generally speaking, pre-historic man in Scotland extracted flint, chert, copper, gold, lead, mercury and tin, in surface deposits where available (Shepherd, 1980). Methods of ore detection were primitive at best and, considering the minimal evidence for any organised mining in pre-historic Scotland, the vague later historical commentaries on gold, for instance, must have been based on the discovery of large placer or alluvial deposits. Remarkably enough, an area of the far north Highlands near Ben Loyal has been the scene of a 'gold-rush' in modern times with occasional small nuggets still found, thus lending possible credence to ancient accounts (BGS, 1995).

In modern mining parlance ancient man worked what are now known as bedded deposits, irregular intrusions and veins (Weisberger and Pernicka, 1995). Quarrying, which would be a major form of mining for the Egyptian civilisation and to a much lesser degree for the Iberian cultures, was evident in Britain from c.3200 BC to c.1500 BC (Shepherd, 1980). For most of Scotland's earliest miners though, place, or alluvial deposits, would have been the main source for metals like gold and tin (BGS, 1995). Alluvial deposits are formed from water sources eroding ore bearing materials from hills and mountains, then depositing them downstream as currents slow in riverbanks, sandbars and riverbeds (Shepherd, 1980). Base metals, such as the lead on the Isle of Islay, would have been mined from exposed veins in outcrops (See Fig. 2-3 and Pliny, trans. 1991). After exhausting the surface deposits, mine rakes would be created which are literally broad ditches dug along the path of the mineral vein. Finally, trial mine pits and shafts would have been dug, following the metal vein to it's end, or to the limit of the mining technology (Pliny, trans. 1991).

It can be seen that in Scotland, the mining landscape would be one where pits, rakes and shafts could be expected, along with small spoil tips and slag heaps. Vegetation would likely be minimal due to the leaching effect of metals into the soils and the paucity of soil quality and quantity in these mining areas.

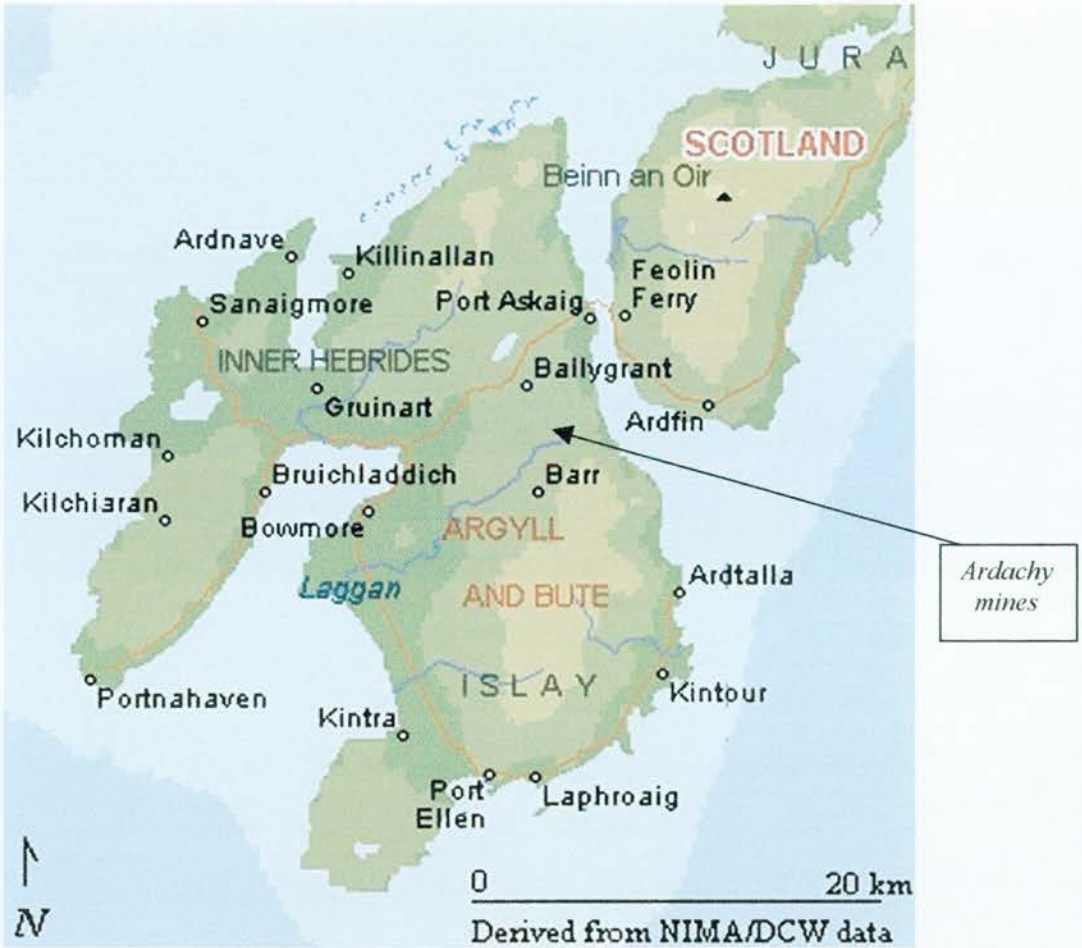

Fig. 2-3 The Isle of Islay, Scotland, UK.

2.2.2 Egypt and the Sinai

The history of ancient mining within the geographic region defined as the Kingdom of Egypt is both long and complex. Moreover, the cultural and political dimensions of ancient Egypt can be considered amorphous, having constantly fluctuated with the various fortunes of its rulers, its climate, and threats of invasion (Fig. 2-4 and Shaw, 2000).

The development of metalworking is similarly complex with the progressive development of copper, gold and silver working from c. 3500 BC onward (Alfred, 1998 and Moorey, 1985). The expansion of Egyptian civilisation created a considerable demand for metals leading to the progressive development of both trade networks and extensive mining activities. Examples of the latter include the mines at Timna and Bir Um Fawakir (Rothenberg, 1979 and Meyer, 1994). The discussion here focuses on what little is known of Egyptian mining activity in the Sinai Peninsula.

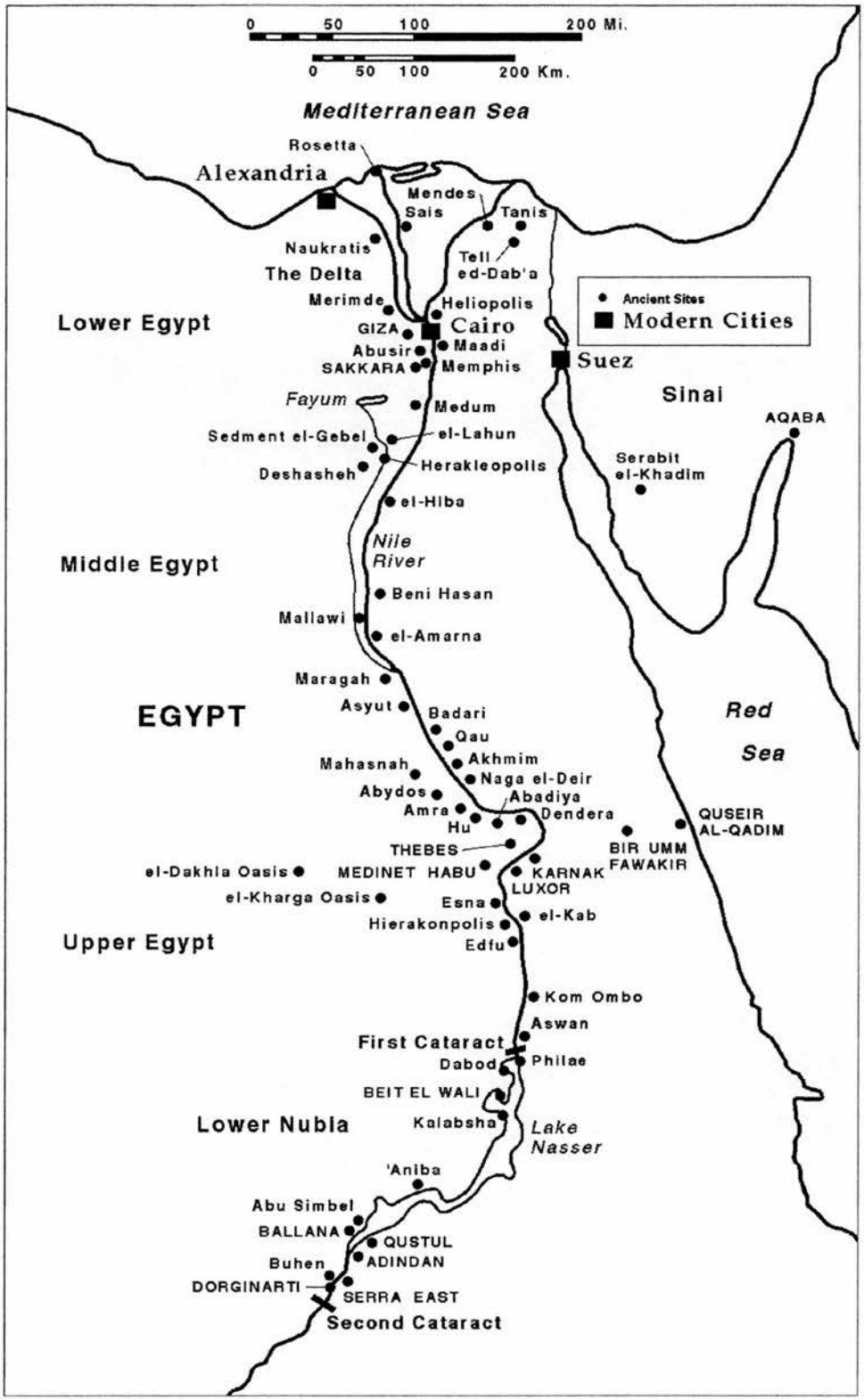

Fig. 2-4 Ancient Egypt with important sites from the Pre-Dynastic period (3500 BC) through the Twelfth Dynasty (1800 BC. Based on Oriental Institute, Univ. of Chicago map).

2.2.2.1 Characteristics of the ancient mines of the Sinai

While the rock used in the construction of buildings and monuments during the Third and Fourth Dynasties was generally quarried nearby, the Egyptians performed copper mining in the Sinai Peninsula due to the richness of the raw ores (Cotterell, 1980). The scale of copper mining in the Sinai would reach such a size in later Dynasties that it would become the first real industry of the ancient world (Aldred, 1998). The Egyptians mined deposits of the green copper mineral malachite, a copper carbonate, because it was the easiest copper mineral to reduce and refine into copper metal; the blue-copper carbonate mineral azurite also was discovered (Rothenburg *et al.*, 1979). Near these two copper ore minerals, the early prospectors often found another copper mineral derivative, blue-green turquoise, highly prized by the Pharaohs and traded by caravan throughout the Middle East (Malek, 2000). Fig. 2-5 displays the Sinai Peninsula in relationship to greater Egypt.

Fig. 2-5 Egypt and the Sinai; created from NOAA data, 1:2m.

Located on the edge of the El-Tigh escarpment in the western portion of the Sinai, and accessible from the coast of the Gulf of Suez by Wadi Bugma, Serabit El-Khadim and the associated Wadi Maghara complex were convenient for shipment of copper products to mainland Egypt (Fig. 2-6). The copper mines in the Sinai desert at Serabit El-Khadim and Wadi Maghara were the aim of the first major Egyptian forays abroad during the reign of Djoser in the Third Dynasty (Malek, 2000). Initially, only limited armed expeditions were sent into the Sinai in order to mine copper and turquoise. However by the Twelfth Dynasty (1849-1801 BC) Amenemhet III began to build fixed armed encampments along with large mining complexes in the copper-rich mineral areas (Shepherd, 1993). Ruins of the old mines, the miners' huts, and inscriptions to the Goddess Hathor, can be found at Wadi Maghara as well as at Serabit El-Khadim, attesting to the level of long-term organization (Petrie, 1906). Copper mining in the Sinai Peninsula continued until the reign of Ramses III, in 1150 BC, over 2,000 years later (Van Dijk, 2000).

Fig. 2-6 The Middle Sinai including Serabit El Khadim mines.

The mines of the Serabit El Khadim and Wadi Maghara region tend to be of the quarry type, but there are numerous examples of galleries carved into cliff-sides, mineshafts and short tunnels. Large slagheaps may be found as well; one of which was estimated to contain 100,000 tons of dross, which would have resulted in some 5,500 tons of copper (Petrie, 1906). Details of the Serabit El Khadim target mine site will be discussed in Chapter 6.

The mining landscape of Serabit El Khadim can be said to be one in which quarries, galleries, mineshafts, tunnels and large spoil tips may be found. Due to the extreme aridity of the environment, virtually no vegetation is found in these areas; this is addressed in more detail in Chapter 6.

2.2.3 Ancient Mining in Andalusian Spain

The history on mining in Andalusian Spain, that is to say the south central and south-western most portion of the Iberian Peninsula, is among the oldest documented in Europe (Pliny, 1991). Due to the extensive nature of ore-bearing deposits, as well as the numerous rivers draining the centre of Andalucia, early civilisations found it easy to engage in metal extraction activities (Savory, 1968). Though it is an ancient region culturally, its name is derived from the 8th century Arabic toponym, Al-Andalus, or the "Garden of Allah" (Baird, 1986). Fig. 2-7 displays an image map of the region.

Mining in Andalusian Spain can be dated to the Neolithic period with the discovery of crude fire pits containing minute fragments of slag (Galan, 2000). The first notices of Iberian Spain entering into written history contain references to its mineral wealth with the semi-legendary kingdom of Tartessos, or Tarshish, being the best known entity (Herodotus, 1972). By the arrival of the Greek and Phoenician maritime traders c. 1000 BC, the quantity of metal being extracted and processed was such that they only needed to transport the product, thus obviating the necessity of engaging in mining themselves (Aubet, 1994). The major attraction for Phoenician traders in Andalusian Spain, or Tartessus, appears to have been lead and silver. The Greeks endeavoured to penetrate the rivers leading north out of the Mediterranean Sea into the interior of Spain and France searching both for routes to Brittany and for tin (Boardman, 1999).

By c. 550 BC the main area of mining in Andalusian Spain was located north of the Guadalquivir River in the foothills of the Sierra Morena mountains, with copper being the primary metal extracted (Fig. 2-7). This area is now known as the "Rio Tinto Zone", due to long association of the name of the river with mining in the region, and it's history of being tinted red from copper mine wastes (Baird, 1988). Around 535 BC, Andalucia fell under the rising power of the Carthaginian Empire which would continue for 3 centuries before the first wars with the growing Roman Empire (Herodotus, 1972).

Fig. 2-7 Andalusian Spain; created from NOAA data, 1:2 million scale.

Initially Rome negotiated treaties with Carthage for trade with its Iberian entrepots; this occurred as early as c. 508 BC (Ogilvie, 1980). Relations were never cordial and by 264 BC the First Punic War had broken out and lasted until 241 BC (Pliny, 1991). In 220 BC the Second Punic War broke out, which is known for the military campaigns of Hannibal against Rome (Warmington, 1980). By 205 BC the Carthaginians had been driven from Iberia with the Andalusian region coming under the sway of Rome by 193 BC (Ogilvie, 1980). Insofar as mining in the southern region of Spain was concerned it meant not only a change of control, but also the entrance of more advanced mining techniques (Pliny, 1991). It should be stated that the focus of the Second Punic War was the control of the vast, rich mines of Iberia (Warmington, 1980).

2.2.3.1 Characteristics of the ancient mines of Andalusian Spain

The best known area of ancient mining in Andalusian Spain has been the Rio Tinto zone, located north of the Guadalquivir River (See Fig. 2-7). Various parts of this area have been worked for some 6,000 years, which has lead to the destruction of some of the earliest mine sites by modern industrial mining concerns (Shepherd, 1993). However, it also has to be said that the Roman period destroyed many early mines by using intensive methods of mineral survey and mining (Pliny, 1991). Virtually every form of mine may be seen in the region, ranging from trenches, also known as rakes, mineshafts, tunnels and pits. (Rothenburg and Blanco-Freijeiro, 1981). It should be reiterated that in commentaries by the classical writers, mine rakes are sometimes referred to as trenches, or channels, which are essentially ditches that have been excavated to follow the trend of an exposed mineral vein (Shepherd, 1993).

In the south of Andalusia, along the Mediterranean coastline from Estepona to Cartagena (See Fig. 2-8), metals were mined from placer deposits in rivers flowing down from the Sierra Nevada mountains as well as from shafts and tunnels (Semmler, 1986). During the Greek and Phoenician period, c. 8th century BC, these were processed and traded at numerous entrepots such as Abdera, Alumencar and Malaga, with other known sites being Cerro del Prado and the mouth of the Guadalhorce River (Collins, 1998).

Fig. 2-8 Southwest Andalucia including the Conil mine site.

The general mining landscape of the south-west Andalucian region can be seen to be one in which, like Islay in Scotland, mine rakes, shafts, pits, slag heaps and spoil tips may be found. The climate and soil typology being more amenable, vegetation is not as sparse as Islay or Serabit El Khadim (Chapter 7).

The area chosen for this study lies in the extreme south-western quadrant of the Andalusian region, near the greatest Phoenician trade port, Gadir, known today as the city of Cadiz (See Fig. 2-8 and Aubet, 1994). More will be detailed concerning Gadir in Chapters 3 and 7, but a striking feature is that although the sea port was established to trade silver from the Tartessan empire, virtually no examples of ancient or pre-industrial mining exist in the nearby hinterland of the city (ITG, 1994: *Cadiz)*.

Before discussing issues associated with mine detection using remote sensing, the types of features that may be encountered within a mining landscape are summarised here. First, the antiquity of a particular mining landscape must be taken into account. Mining that is primarily based on placer deposits, that is ore deposits found in stream beds or on surface outcroppings, may leave little external cultural evidence of extraction efforts. These landscapes may be as varied as a *wadi* in the Sinai (Chap. 6 and Appendix 4) or a Scottish stream. Vegetation, as given in the previous example of the Sinai, may be nought, whereas in Scotland trees and lush vegetation masses might well populate the areas.

Ancient mining landscapes that are the results of more organised extraction efforts will of course exhibit more noticeable features (Shepherd, 1980). As discussed in the previous three sections, these features may be mine rakes, essentially large ditches dug to follow near surface ore deposits, mine pits, which may be merely test efforts or large, continuously worked diggings (Craddock, 1998). Even more extensive extraction efforts may result in galleries, limited shafts and tunnels, though again this dependent upon the particular area's geology (Rothenberg, 1981). In the Sinai numerous galleries and short tunnels are found, as well as more typical pit extraction efforts (Rothenberg, 1979). The mines studied in this work in Scotland and Spain (Chap. 5 and 7), on the other hand, revealed only trial pits and rakes (Cressey, 1995).

Other features related to ancient mining landscapes include slag heaps, spoil tips, puddling ponds and leats. Slag heaps are essentially the by-products of mine ore processing, be it by fire or water, while spoil tips include the by-products of crushing as well (Shepherd, 1980). Puddling ponds, created to separate particular minerals from their base ores during processing may also be present in a mining landscape, although these were not seen during the course of this research (Shepherd, 1980 and Craddock, 1998). Slag heaps and spoil tips, seen during the course of this research may be rather small such as those seen in Scotland and Spain (Chapter 5 and 7), or immense, such as viewed in the Sinai (Chapter 6). The features yield innumerable artefacts and evidences of the particular type of mining activity carried on within a landscape as well as the quality of mineral ore available for extraction.

Leats, seen only in the Scotland portion of this research, are a method of draining a mining area of water, be it from a working or processing area (Shepherd, 1980 and Chap. 5). They appear as narrow ditches in the landscape.

These mining landscape features, and how RADAR and other remote sensing technologies may observe them, will be discussed in Chapter 3 and 4.

2.3 Detection of ancient mines and remote sensing technology.

2.3.1 Traditional methods of ancient mine detection

Ancient mines have been sought largely by later cultures to assess the further extraction of valuable mineral ores, and not with any interest in archaeology (Tylecote, 1976). It should be pointed out as an aside that the science of archaeology only began to be formed and recognised as a discipline in the late 19th century, so consciousness of ancient mining sites at any earlier period would have been extraordinarily prescient (Shepherd, 1980).

The specific landscape features that were clues to the previous existence of an ancient mine would of course have been the mine rakes, pits, disused shafts, slag heaps and spoil tips discussed in the previous section. Shepherd notes that the geographic method, based on observation and reference by historic and classical writers, is, and has remained, the most common method of ancient mine detection, though this is a methodology which has not changed over several millennia (Shepherd, 1993). An expansion of this time-tested methodology is to observe an entire cultural landscape for evidence of locally produced metallurgical products by noting the types of settlements, transport networks and ports contained within its area; these might be considered general landscape features as well (Rothenberg, 1979). This expansion of the basic geographic and historical methodology of ancient mine detection presents its own problem in an exponential fashion. The archaeologist is now contending with an enormous landscape, which must be surveyed on foot or by vehicle, to observe possible mining relating features. This of course means that valuable time and resources have been expended, which reduce the available investigation time should a potential ancient mine site be detected. This is also an obvious rationale for the employment of *any* remote sensing technology as a reconnaissance tool, since sites of potential interest may be targeted first for ground investigation (Lyons, 1980). Ironically, the geographic method would be considered an essential portion of a remote sensing archaeology campaign, though now identified as the *ground truthing* portion of a campaign (Chap. 4).

Finally, other than the sole commentary on methods of ancient mine detection by Shepherd, there is no body of literature regarding the subject of ancient mine detection (Sehpherd, 1980). This is made doubly frustrating by the fact that although Craddock's recent work regarding ancient mines takes Shepherd to task over many issues, his work leaves the subject of mining detection virtually untouched (Craddock, 1998). There is clearly a failure to comprehend a basic scientific principle here, in that the better the capability of the archaeological community to detect new mining complexes, the greater the ability to comprehend the scope, scale and technological level of a particular culture.

The discussion will now move onto potential remote sensing Imaging RADAR research, techniques and technologies, which have already been utilised in ways that could be easily modified to assist in the detection, survey and analysis, of ancient mine sites.

2.3.2 Remote sensing of ancient mine sites: techniques and research

Other than one work concerning optical detection of ancient mine sites by Cech and Walach (1998) and a work entitled *Phyto-archaeology* only a very limited quantity of literature exists concerning *the methodology for detection of ancient mining sites* using Imaging RADAR systems or other spectral sensors (Brookes and Johannes, 1990). The work mentioned above, *Phyto-archaeology*, is of some interest as it was somewhat ahead of its time in concept. The authors discuss the spectral responses of vegetation throughout the electromagnetic spectrum in a manner that today, in the year 2002, would be termed *full-spectral analysis*. Although the work was written only a few years after the work of Sever and Sheets in Central America, where multiple types of remote sensing technologies were employed, this book did a good job in laying out the conceptual process of full-spectral analysis (Sever and Sheets, 1988). The discussion of vegetation patterns in and near various cultural sites is specifically worth noting for the occasional remarks regarding ancient mine workings.

It again should be pointed out that while there have been other remote sensing campaigns in support of archaeological research, there have been no papers, journals or books written strictly on the *methodology* for *ancient mine detection* by *remote sensing* (Sever, 2001 and El Baz, 2001). This review does not dismiss previous *general* work performed in remote sensing archaeology, but rather notes the lack of ancient mining related work in this area. This author has bi-annually produced a digital publication entitled the "Annotated Bibliography of Remote Sensing Archaeology" which reviews and critiques every available text on the subject ranging from SONAR to RADAR applications and which has been regarded as the most extensive available (McKay, 2001, Sever, 2001, El Baz, 2001).

The size of the "Annotated Bibliography of Remote Sensing Archaeology", which in its latest iteration is now some 20,000 words, gives an idea of the general work in the field and an adapted version of this review served as the literature resource pool for this study. An analogue version of this review is provided in Appendix VI and should be considered as a supplementary in-depth review to this chapter's discussion on remote sensing archaeology and ancient mining.

Proceeding onward, although there is a dearth of texts regarding ancient mines or their detection, foundation research has been performed using Imaging RADAR and other spectral systems in the fields of general archaeology, geo-archaeology, geology, geomorphology and remote sensing archaeology. Those seminal pieces that have the most relevance to this work were reviewed and critiqued; again referral to the more general *Annotated Bibliography of Remote Sensing Archaeology* in Appendix VI is useful for further information.

The employment of remote sensing technology is commonplace in the reconnaissance of *modern* mining by mapping potential ore-bearing geology. Again, it must be re-iterated that this work endeavours to develop and demonstrate a methodology for the detection of *ancient* mining. Other archaeological campaigns where mines have been discovered in the course of a survey by remote sensing technologies are not dismissed, such as Goettler *et al* (1991), but once more it must be said that a simple criteria was employed in the review of previous works regarding this subject. *Was there a remote sensing archaeological methodology for the detection of ancient mining? Was the methodology then employed in a remote sensing archaeology campaign strictly for the detection of ancient mining?* No existing academic literature was able to answer "yes" to either question. Finally, the underlying point of this entire research study is to answer a basic science question that has not been answered or posed by the archaeological community, a question which this author has posed time and again to archaeologist and geologists: *how are ancient mines detected? What is the method?*

The science of remote sensing is defined as the collection of data about an object, or phenomena, without the data sensors being in direct contact with the object. Thus, sensors are said to be operating in a remote sensing mode that begets our terminology (Jensen, 1986). While numerous sensors are commonly used to monitor geophysical processes of the earth, such as seismic events, these sensors are defined as transducers since they are in direct contact with phenomena and merely translate an analogue occurrence into a digital form for scientific analysis. Remote sensing archaeology, mentioned in the previous paragraph, is a subset of the overall discipline of remote sensing.

Remote sensing archaeology may be defined as the methodologies and techniques pertaining to the identification, quantification, spectral and spatial analysis, of those areas of the world suspected of being impacted by humankind's cultural actions in both historic and pre-historic time periods. Furthermore, the ability of both basic and complex geophysical remote sensing systems to capture scientific data which may explain humankind's position within its overall environment is coupled with its capability to spatially map humankind's structural development over the landscape (McKay, 1996). The next section will address those works concerning techniques of remote sensing archaeology.

2.3.2.1 Remote sensing archaeology techniques

The basic techniques for remote sensing archaeology were first laid out in the U.S. Department of the Interior series, "Remote Sensing: Aerial And Terrestrial Photography for Archaeologists" (Avery and Lyons, 1978). This first supplement addressed the basic techniques employed for obtaining high quality aerial and terrestrial photogrammetric products for archaeological survey. Development of aerial interpretation skills, and the use of optical imagery for ground truthing in support of more robust systems such as RADAR and Multi-Spectral Sensors (MSS), is endorsed for cultural site assessment.

The fifth pamphlet in the series described the techniques involved in the collection and analysis of multispectral data taken over Chaco Canyon, New Mexico. Five pueblos of the Anazasi were the focus of these efforts: Pueblo Alto, Kin Bineola, Pueblo Bonito, Chetro Ketl, and Wijiji. Airborne missions were conducted to provide field support by gathering soil moisture and vegetation structure data at Pueblo Alto, Kin Bineola, and Wijiji. Extensive treatment is given to the entire image-processing regimen within this work (Lyons, 1981).

After this initial burst of activity concerning the development of remote sensing archaeology, there is sparse literature until the 1990s. After the entry of viable personal computer (PC) systems and the establishment of functional geographical information system (GIS) technologies, commentaries regarding the integration of remote sensing technology into GIS systems to perform advanced archaeological analysis begin to appear (Stine and Decker, 1991 and Farley *et al.*, 1990).

Among the most significant are Cutting *et al.* (1994) and Gaffney *et al.* (1996). In Cutting's work, the usefulness of medium resolution MSS sensor data in detecting large scale area transport routes is noted, as well as techniques for integrating and fusing the analysis results via a GIS (Ehlers, 1989).

A successful series of maps was generated which defined caravan and migration routes across the Altay region of Central Asia (Cutting *et al.*, 1994). Gaffney's team in 1996, explored the more theoretical aspects of remotes sensing imagery and GIS technology by testing the viability of landscape visualisations created from image analysis and digital terrain models, or DTMs as they are commonly termed (Gaffney *et al.*, 1996).

This concludes a basic overview of remote sensing archaeology techniques. While there are many GIS works regarding archaeological analysis, the body of literature regarding the development of specific archaeological techniques is limited at best (Davis and Simonett, 1991). The next section will describe the most significant remote sensing archaeology campaigns.

2.3.2.2 Remote sensing archaeology research

In the late 1980s, Dahlin and Pope mounted an effort attempting to ascertain the viability of the hypothesis that ancient Mayan canal systems were located throughout the Yucatan Peninsula. The authors reported that, on the contrary, they were found only in northern Belize, southern Quintana Roo, Mexico, and the Candelaria River tributaries of Campeche, Mexico. Dahlin and Pope noted that the existing SAR platforms were unable to detect small canals due to speckle noise (extraneous image artefacts, see Chap. 4) and spatial resolution capabilities of the technology. SAR imagery and LANDSAT TM data were proven useful, however, in detecting large canals that served as feeders to small lattice canal systems. Their study showed that the canals were located near perennially moist soils and wetlands with predominately high water tables or artesian springs (Dahlin and Pope, 1989).

At approximately the same time, Sever and Sheets (1988) detailed their research on Indian trails of Costa Rica with LIDAR (Laser Indicating Detector And Ranging), TIMS, or Thermal Infrared Multispectral sensors, SAR, and optical systems. Centred on north-western Costa Rica, the investigation attempted to discover the relationship between various ancient villages, cemeteries, and other ruins, which appeared to be rather widely dispersed.

The investigators first utilised LIDAR sensing technology after noting several apparent trails that appeared under infrared analysis. LIDAR is a LASER device that makes profiles of the earth's surface, in this case emitting pulses to the ground 400 times per second, striking the surface every ~ 8-9 cm., which bounces back to a receiver. Sever and Sheets (1988) followed up this analysis with a Synthetic Aperture RADAR run. Noting the application of varying wavelengths to discover subsurface features, the authors were able to find several suspected prehistoric features.

Finally, Sever and Sheets (1988) used a TIMS (Thermal Infrared Multispectral Scanner) platform to investigate intermittent vegetation growth patterns. The TIMS system used six channels to measure the thermal radiation given off by the ground, with accuracy to 0.1 degree centigrade. After completing this extensive remote sensing effort of the target areas, the authors then employed an aircraft to fly over the site and obtain high altitude photographs, including colour infrared photography (Sever and Sheets, 1988).

The results of this effort by Sever and Sheets (1988) were that the complimentary uses of remote sensing technologies that covered distinct portions of the electromagnetic spectrum enabled them to locate anomalies that would not have been detected if only one sensor type had been employed. As an example, the SAR data implied that the vegetation canopy in one particular area appeared to be substantially lower and of a non-natural spatial pattern. A follow-on survey by a LIDAR system substantiated this observation, thus leading to ground investigation and survey. On the other hand, problems with filtering of the SAR data, due to the inhomogenous vegetation canopy and the type of backscatter generated, led to considerable computer processing problems in reference to imagery products (Chap. 3). This campaign should still be considered a landmark effort in the development of remote sensing archaeology techniques and in particular for its attempt to perform full-spectral analysis of a target area.

Finally, in 1991 came the well-known remote sensing archaeology campaign for the lost trade city of Ubar, located in Oman. An expedition lead by archaeologist Juris Zarins and remote sensing scientist Ron Blom of NASA's Jet Propulsion Laboratory (JPL), employed NASA-SIR-C/X-SAR Imaging RADAR, SPOT imagery, and LANDSAT imagery, to reconnoitre the presumed site of the caravan city. Imaging RADAR was able to detect unknown caravan trails due to the embedded sand particulates in the limestone of the surrounding area. A combination of spectral and microwave imagery was used to generate a target site list, which was used by Zarins to prioritise his investigations, which led to the discovery of a previously unknown ruin dating to the period of the lost city (Fiennes, 1992).

This concludes the review of dedicated remote sensing archaeology research. Again, as with the technique section, there is a limited body of literature. While there may be occasional use of remote sensing imagery as a supplement to ongoing archaeological work, rarely has it been used to drive the archaeological investigation, even with the availability of nominal cost data (Fowler, 1996). Again, it should be noted that the *Annotated Bibliography of Remote Sensing Archaeology* reviews all known archaeological applications and it should be consulted for additional context. The next section discusses relevant Imaging RADAR applications.

2.3.2.3 Imaging RADAR: applications relevant to archaeology

The possible use of space-borne Imaging RADAR to assist in archaeological reconnaissance and analysis can be dated to 1981 when McCauley described the detection of geo-archaeological features beneath the hyper-arid sands of the Eastern Sahara by the NASA Shuttle Imaging RADAR System A (NASA SIR-A) during its 1981 mission (McCauley, 1982). The initial version of the NASA SIR series carried an L band wavelength Imaging RADAR system that operated in an HH polarisation mode, which is described in detail in Chapter 3. The discovery that hyper-arid desert regions could be penetrated by as much 10-15 metres by the microwave system provoked a significant effort concerning detection of geo-archaeological features.

Among the subsequent research is Allan and Richards (1983) who advocated the use of SAR in Libya for archaeological survey. Blom *et al.* (1981) examined returns in the Mojave Desert of California by SEASAT. Elachi *et al.* (1982) followed with a comprehensive report of the entire mission and similar results from around the planet. El Shazly reported on the implications for the re-shaping of baselines for human cultural development in Egypt by his interpretation of mega-hydrological features detected by the Shuttle Imaging RADAR system A (El Shazly, 1981).

The flight of the NASA SIR-B system in 1984, followed a decade later by the NASA SIR-C/X-SAR system, both described in Chapter 3, led to another advance in geo-archaeological process research. McCauley *et al.* (1986) released work concerning the development of the mega-geomorphology of the Eastern Sahara in 1986, which described a system of east-west trending watercourses, now covered by sand. McHugh *et al.* (1988) released findings regarding Acheulian sites in the south-eastern region of the Sahara, which further supported the hypotheses of McCauley regarding drainage systems, that being that dramatic climatic change had occurred which had obscured previously functioning systems which flowed west to east in present day north Africa. A joint paper in 1989 which married their ideas on the paleo-drainage systems of Egypt and the Sudan, which speculated that massive climate change had caused dramatic changes in the hydrological systems, although the cause was unknown (McHugh and McCauley, 1989).

The capability of the NASA-SIR-C/X-SAR to detect land degradation, which is a key issue for archaeology in discovering the amount of landscape change within a particular region was highlighted by Ray *et al.* (1992). More importantly for this investigation, it discussed the use of polarimetry in surface detection and change.

Since 1986, Schaber *et al.* (1986, 1996, 1997) have released a series of papers concerning subsurface scattering in deserts, signal penetration and the use of multipolarimetric Imaging RADAR for geological interpretation (Schaber *et al*, 1986, 1996 and 1997). These works by Schaber *et al.* (1986, 1996, 1997) are seminal works in the surface scattering mechanisms of the multipolarimetric Imaging RADAR systems when interrogating desert environments, particularly when confronted by extremely inhomogeneous surfaces, which will be discussed further in Chapter 3.

Finally, Zebker *et al.* (1996) produced a work which surveyed the penetrative capabilities of NASA-SIR-C/X-SAR data in its various modes and wavelengths. They noted that in certain environments the penetrative characteristics of the shorter C band wavelength (~3.5 cm) and the longer L band wavelength (~23.8 cm) were similar when using the horizontal send and receive conditions, or HH mode. This will be discussed further in Chapter 3.

A primary use of the NASA multipolarimetric Space Shuttle Imaging RADAR system, in all its variants, has been to perform landscape change analysis on a global scale. Unique penetrative capabilities discovered during the 1980 overpasses of hyper-arid regions in Africa revealed unknown paleo-drainages, which focused the archaeological community on the system's capability to detect sub-surface features. However, the archaeological community has overlooked the capability of such systems to precisely map the geology and geomorphology of a given area.

The ability of Imaging RADAR to render quality, large area geological mapping renders it highly suitable for detecting and mapping the dykes and strike lines that can indicate areas of mineralisation (Abdelsalam *et al.* 1995, Bell, 1998, Berlin *et al.*, 1986, Blom *et al.* 1981, CCRS, 2001, Elachi *et al.* 1982, Evans, *et al.*, 1986, Farr and Gillespie, 1984, Fung *et al.* 1981). As will be pointed out in Chapter 5, while some of the world is well mapped, geologically speaking, much more of the world it is not, and Imaging RADAR can detect new features even in well-mapped areas. This is an important feature for archaeologists operating in areas that have little or no geological cartography in existence.

Finally, as mentioned in the introductory chapter of this work, Imaging RADAR was chosen for its all-weather remote sensing capability. While optical and spectral remote sensing systems offer their own particular benefits, such as spectral analysis of mineral bearing geological structures, they are not all-weather capable.

It should also be noted that with the exception of certain recent high-resolution multi-spectral satellite systems, such as IKONOS (1-4 metres in resolution), the resolution of NASA Shuttle Imaging RADAR (12-m resolution) is typically better than more common sensors such as LANDSAT 7 (30 m resolution) or its predecessors (USGS, 2001).

NASA Shuttle Imaging RADAR data also tends to be much less costly, though it should be pointed out that at present there is only coverage for some 10 percent of the world (JPL, 2001 and USGS, 2001). The Shuttle RADAR Topographic Mapping Mission during early 2001 which employed only the C and X bandwidths will supplement this data collection, however, it is the L band which is most useful for archaeological reconnaissance and survey (JPL, 2001 and USGS 2001, Chapter 3 and 4). NASA Shuttle Imaging RADAR was chosen for this research over other remote sensing systems because of its advantages in cost, resolution, all-weather data collection and topographic mapping capabilities, thus allowing geological mapping in all climatic regions of the world. This author should point out that, in his perspective, *no* one type of remote sensing technology is considered better than another type of remote sensing technology and believes that the various sensors are complimentary in the information which they provide. Further, it is this author's opinion that the responsibility for choosing the best *primary* remote sensing technology to investigate an archaeological site lies with the investigator. In the case of ancient mines, they are cultural disturbances of naturally homogenous geological structures. Since these cultural disturbances leave telltale indications of their occurrence, it would appear logical to employ a remote sensing system designed to map geological structures, hence the use of Imaging RADAR in this research project.

2.4 Conclusions

A concise review of what is known about ancient mining within the three study regions selected for this study has been outlined. The characteristics of mining within each of these regions has been explored with reference to their development and the types of mine structures which may be found within them. A discussion of the established method of ancient mine detection was presented, which noted that the methodology for the discovery of these sites still fundamentally relies on classical and historical geographic commentary.

The second portion of the review noted that there was virtually no body of literature which discussed the detection of ancient mine sites by remote sensing methods, either by Imaging RADAR systems or any other type sensor. A short discussion regarding remote sensing archaeology and its techniques was followed by an overview of the few remote sensing archaeology campaigns. Imaging RADAR research was examined for those investigations that had research that may lend assistance to ancient mine detection. It was seen that while much work has been done on geo-archaeological investigation in the last twenty years, no work had been done in exploring the detection of ancient mine sites within the context of potentially suitable geological structures.

Finally, the literature search revealed no evidence of polarimetric investigations in regards to mine detection, ancient or modern. This study is therefore moving into a new basic research area by defining what the microwave characteristics of various ancient mine sites are, and further, by observing what unique polarimetric responses were recorded by the instrument. In Chapter 3, a discussion of basic RADAR theory and the operation of Imaging RADAR will be explained.

Chapter 3

Principles of Imaging RADAR and Archaeological Use

"In 1961 the U.S. Navy bounced a RADAR wave carrying telemetry off the moon and back to the earth from a ship in the Pacific Ocean". James Bamford, "Body of Secrets", 2001: 94.

3.1 Introduction

When an active microwave remote sensing instrument aboard a spacecraft sends an electromagnetic pulse of energy to the Earth's surface, the energy travels in the form of a wave to the Earth's surface, where after striking the surface it scatters back towards the sensor's receiving antenna. This pulse propagation, which is a simplified description of a RADAR remote sensing system, can be described in physical terms using the electromagnetic equations of Maxwell. Knowledge of the interplay between the Earth's surface and the reflected electromagnetic microwave is vital to the comprehension of the detected signal and the remote sensing data recorded. This is of particular importance in correctly analysing and interpreting the Imaging RADAR data used in this research project to detect ancient mining sites. This chapter will outline, in sequence, the basic principles for comprehension of multipolarimetric synthetic aperture RADAR function and the imagery that it produces. The explanation will conclude with a basic description of surface interaction with the NASA Space Shuttle SIR-C/X-SAR multipolarimetric system, the most advanced and complex RADAR system yet constructed. This chapter is provided as background material for the reader ignorant on the subject of remote sensing and in particular, RADAR.

3.2 Electricity

Electricity is the fundamental physical occurrence related to negative or positive electrical charges. Electrical charges are a basic aspect of matter and are carried by elementary particles. These particles are known as electrons and defined by scientific convention as being negative. Consequently, the activities of electricity are the end product of masses of electrons or their motions (Encyclopaedia Britannica, 2000).

The Greeks were the first to study electrical phenomena, primarily stationary charges, or static electricity (Snodgrass, 1980). Significant study of electricity began at the end of the 16th century, with William Gilbert studying static electricity and magnetism (U.S. Navy, 1996). Benjamin Franklin showed the electrical nature of lightning in 1752 in his kite experiment, and established the standard nomenclature of negative and positive to distinguish charge types (Doren, 1991). Joseph Priestley established in 1767 that electric charges attract with a force inversely proportional to distance, just as gravity was shown to do by Sir Isaac Newton (U.S. Navy, 1996). Building upon this, Davy in 1806, and later Faraday during the 1820's, explored electrochemistry, creating the foundations for electromagnetism (Fig. 3-1, Davy, 1823 and Faraday, 1993).

3.3 The Electromagnetic Theory

James Clerk Maxwell converted Faraday's physical observations into mathematical formulae in his "Treatise on Electricity and Magnetism" in 1873, thus establishing the theory of electromagnetism (U.S. Navy, 1996). Maxwell's theory, in greatly simplified terms, postulated that the energy of the electromagnetic field is in the space around the conductor as well as in the conductors themselves; thus, an elegant description of Faraday's magnet and copper wire dynamo. This theory of electromagnetism made possible the inter-related inventions of radiotelegraphy by Marconi (Masini, Stella and Segre, 1999) and Tesla (Childress, 1993), television by Logie-Baird (McArthur, 1985), and RADAR by Baird (U.S. National Archives, 2001: pers. comm), Taylor of the U.S. Naval Research Laboratory (U.S. Navy, 1996, Vol. 18) and Watson-Watt (Latham and Stobbs, 1999).

This work will not go into any further detail on these basic theories, but the best descriptions may be found in the U.S. Navy's publicly available works (U.S. Navy, 1996).

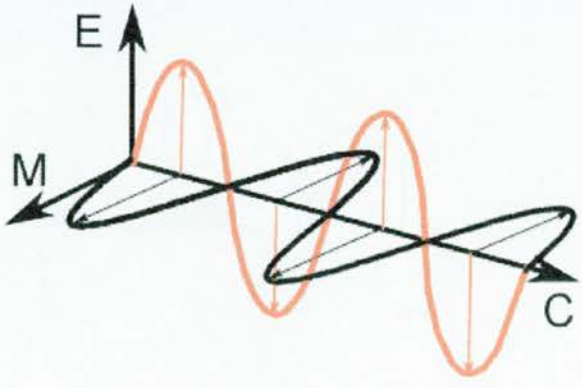

3-1 An electromagnetic wave (CCRS, 2001)

As mentioned in the introduction to this chapter, when a spacecraft emits a microwave towards the earth, this energy travels in the shape of a wave. Electromagnetic waves have magnetic and electrical oscillating fields that are perpendicular to each other in orientation. These in turn lie perpendicular to the propagation direction. As mentioned before, each field is oscillating and has the form of a sine wave (Fig. 3-1). The distance between the peak of each of these waves is known as a wavelength. The number of times that one of these peaks passes a specific point in a second is known as frequency (U.S. Navy, 1996). Therefore, if the spacecraft emits a microwave in which the wave peaks are closer together, the frequency is said to be higher and if the electrical field within the microwave is changed to another orientation, its polarity is changed. This is the basis for RADAR polarimetry, which will be discussed further on within this chapter (Kong, 1975).

3.4 RADAR

It was previously stated in Section 3.3 that the invention of RADAR may be attributed to Baird, Taylor and Watt. It is also worth mentioning that in 1886 Heinrich Hertz noted an anomaly within his early radio experiments that indicated a capability of target detection by electromagnetic waves (Ulaby, Moore and Fung, 1981).

The term RADAR is an acronym made up of the words RAdio Detection And Ranging and dates from World War II (Rowe, 1948). RADAR operates at the micro and radio portion of the spectrum with a wavelength ranging from approximately 1cm to 1m, though the precise boundaries are debated (Fig. 3-2, CCRS, 2001, JPL, 2001).

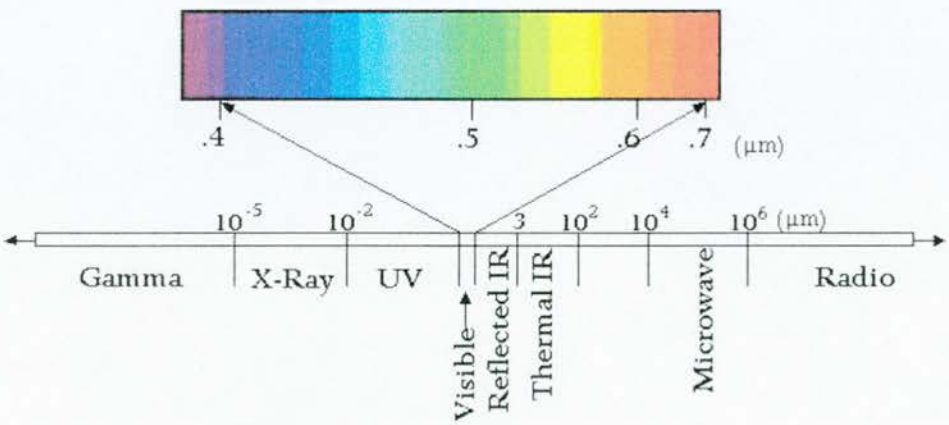

Fig. 3-2 The electromagnetic spectrum (GSFC 2001)

RADAR is defined as electronic equipment, or apparatus, that detect the presence, and distance of objects by using reflected electromagnetic energy (US Navy, 1996). Electromagnetic energy of the frequency used for RADAR is unaffected by darkness and also penetrates clouds, fog, smoke, haze, rain and other precipitants. RADAR systems may be terrestrial or space-based. On earth they are used to determine ship positions, plane locations and characteristics of landmasses; they may be also used to monitor bodies of water for pollution and ice conditions that are invisible to the naked eye because of distance, darkness, or weather. In space RADAR is used for navigation and analysis of extraterrestrial bodies such as the other planets within the solar system or the Earth itself (Barrett and Lilley, 1963 and JPL, 1994 and 2000).

3.5 Basic Concepts of RADAR

RADAR operates in a way similar to the principle of sound-wave reflection. If a shout is made in the direction of a sound-reflecting object (like a rocky canyon or cave), an echo will be heard. If one knows the speed of sound in air, then the distance and general direction of the object can be estimated. The time required for a return echo can be converted to distance if the speed of sound is known. RADAR uses electromagnetic energy pulses in much the same way. The radio frequency (*rf*) energy is transmitted to and reflects from the reflecting object. A small portion of the energy is reflected and returns to the RADAR set. This returned energy is called an echo, just as it is in sound terminology (Kerr and Goldstein, 1951). Conventional RADAR systems use the echo to determine the direction and distance of a reflecting object. Further discussion on conventional RADAR systems may be found in the three-volume work of Ulaby, Fung and Moore (1981-86). It should be noted that RADAR frequencies have been named in a somewhat standardised fashion since World War II; the NASA Space Shuttle Imaging RADAR employs the X, C and L bands (Fig. 3-3).

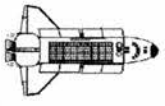

P = 0.225 - 0.390 GHz	K = 10.90 - 36.0 GHz
L = 0.390 - 1.550 GHz	Q = 36.0 - 46.0 GHz
S = 1.550 - 4.20 GHz	V = 46.0 - 56.0 GHz
C = 4.20 - 5.75 GHz	W= 56.0 - 100 GHz
X = 5.75 - 10.90 GHz	

Fig. 3-3 RADAR frequencies and their band designations

In RADAR science the amount of surface reflected energy, or *backscatter*, from a target, is expressed in *decibels*. When normalised to target area, the *normalised RADAR cross-section* is calculated (JPL, 2001). *Radar cross section* has several definitions, but the most generally accepted one states that it the measure of a target's ability to reflect radar signals in the direction of the radar receiver (US Navy, 1996). This is to say that it is a measure of the ratio of backscatter power per steradian (unit solid angle) in the direction of the radar (from the target) to the power density that is intercepted by the target (JPL, 2000, CCRS, 2001).

3.6 SAR

The NASA Space Shuttle Imaging RADAR data used in this study is the product of a multipolarimetric Synthetic Aperture RADAR (SAR) system (See Section 3-9). A SAR uses an advanced technical process to create an artificially longer antenna than would be physically impossible to carry aboard a platform, hence the term "synthetic". Details of these systems are found in Ulaby, Fung and Moore (1981-87). Before addressing the complexities of polarimetry and the data it produces, the operational characteristics of SAR and how it records the image data must be explained.

Just as with the previously described RADAR system, a SAR measures distance by calculating the delay in time between transmission and reception of an electromagnetic pulse, thus enabling it to plot where various targets are in relation to each other in the *range* direction. *Range* is defined as the direction in which the signal or RADAR wave is transmitted (CCRS, 2001 and JPL, 2001). *Range* is also one of several terms used to define a SAR system's *viewing geometry* (CCRS, 2001 and JPL, 2001). Other key terms related to SAR geometry are listed below and quoted from the Canadian Centre for Remote Sensing's Internet tutorial on RADAR systems (CCRS, 2001). Fig. 3-4 portrays these principles.

- *"**altitude:** the vertical distance from the SAR sensor platform to a point on the Earth's surface directly below (CCRS, 2001)".*
- *"**nadir**: the point directly below a SAR sensor platform on the Earth's surface (CCRS, 2001)".*
- *"**azimuth:** the direction on the ground parallel to the motion of the SAR sensor platform (CCRS 2001)".*
- *"**range vectors:** the vector representing the direction and distance from the SAR sensor platform to the Earth's surface being image during a single transmitted pulse of the signal; also, the vectors representing the directions and distances to each imaged element of the target surface (CCRS, 2001)".*
- *"**Earth normal vector:** the perpendicular to the Earth's surface (per the reference model of the Earth) (CCRS, 2001)".*
- *"**slant range:** the distance from the sensor to a target located in the range direction; also known as the SAR perceived distance (CCRS, 2001)".*
- *"**ground range:** the slant range projected onto the Earth's surface; also known as the actual or geographic distance (CCRS, 2001)".*
- *"**near range:** the ground range closest to nadir and also the shortest slant range in the image (CCRS, 2001)".*

- ***"far range:*** *the ground range farthest from nadir and also the longest slant range in the image (CCRS, 2001)".*
- ***"swath width:*** *the slant or ground range distance images by the SAR in the range direction* ***(CCRS, 2001)".***
- ***"illumination angle:*** *the angle between the Earth normal vector (at nadir) and the range vector measured at the SAR position. This angle determines the distribution of RADAR illumination across the SAR swath (see above). As the altitude of the SAR sensor platform increases, the illumination angle range that corresponds to the SAR swath, from near to far range, decreases (CCRS, 2001)".*
- ***"incidence angle:*** *the angle between the RADAR range vectors and the local vertical direction (CCRS, 2001)".*
- ***"local incidence angle:*** *the angle between the range vector and the surface normal to each terrain element imaged by the SAR. It is common practice to replace the exact definition (used only in RADAR scattering theory) with an angle between the range vector and a mean terrain surface normal defined over the minimum area resolvable by the SAR (also referred to as a resolution cell) (CCRS, 2001)".*
- *"radar cross-section: RCS is expressed in terms of the physical size of an hypothetical uniformly scattering sphere that would give rise to the same level of reflection as that observed from the sample target (CCRS, 2001").*

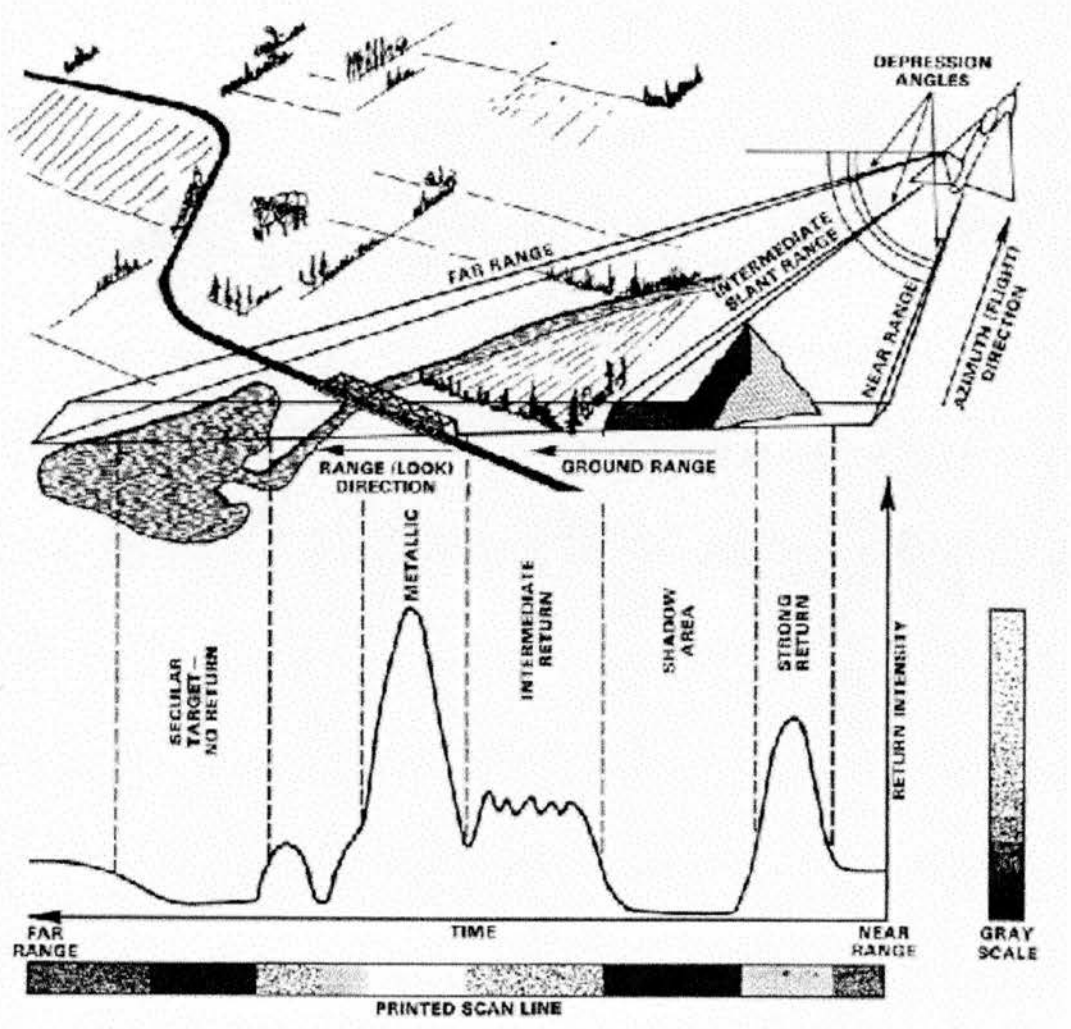

Fig. 3-4 SAR target illumination principles (from NASA GSFC 1986-2001)

Since a RADAR system operates on the principle of measuring where features are in relation to the transmitter by calculating time delay and the sensor is *side-looking*, certain features may be portrayed incorrectly in the recorded data in comparison to their actual appearance. An example of this would be when a space-borne SAR is illuminating a mountain range on the earth. Because the peak of the mountain is closer to the SAR than the base of the mountain, a transmitted RADAR wave could arrive at the peak of the mountain before the base is illuminated (CCRS, 2001 and JPL, 2001). The recorded image data will then show the peak of the mountain as if it is skewed, or leaning, towards the space-borne SAR system's position. If the terrain has extreme topographic relief, then large distortions may occur in the recorded image data (Sabins, 1987).

The distorting effects of extreme topography on SAR recorded data are known as *foreshortening*, *layover* and *shadow*. The degree of effect is based on *local incident angle*, which is determined by the illumination angle of the SAR and the slope angle in the local area of the topography. In this work, the best image examples of these effects may be found in Chapter 7, Fig. 7-19, while Fig. 3-4 and Fig. 3-5 portray these effects over a hypothetical terrain and how they will appear on recorded image data, (CCRS, 2001 and JPL, 2001 and Sabins, 1987). Finally, Appendix VII gives a more detailed definition of these effects.

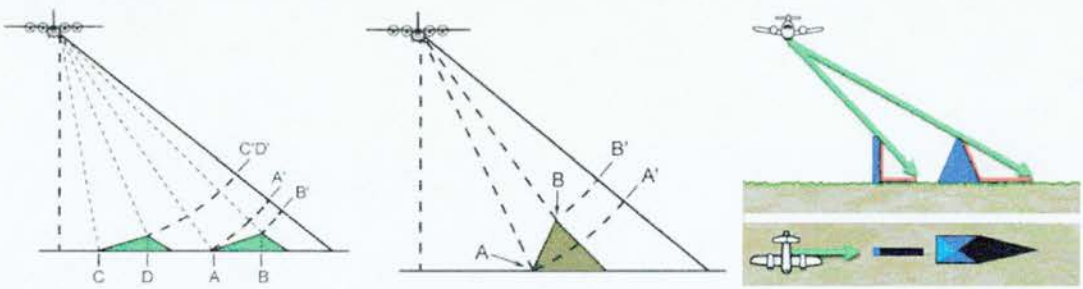

Fig. 3-5 Foreshortening (l), layover (m) and shadow (r). The red surfaces of the far right image are completely in shadow. Black areas in image are shadowed and contain no information (Appendix VII and CCRS 2001).

It should be noted that *all* forms of remote sensing systems are unable to correctly image physical features in a topography that has relief (CCRS, 2001 and JPL, 2001, Berlin *et al* 1982 and Daily *et al*, 1969). The comparison of optical imagery with SAR imagery displays a very different representation of topography, though both systems are subject to the same effects of observation geometry and terrain surface geometry (CCRS, 2001). It is how these two systems go about measuring a target terrain surface that makes them create different images in regards to the positions of physical features and their relief.

A SAR remote sensing system measures the distance to a targeted physical feature on the terrain's surface by calculating the time delay in the broadcast microwave's return to the antenna. These distances are then represented in an image. The distances to physical features on the terrain surface are related to the measured *slant range distance* (Fig. 3-4 and Curlander 1992, CCRS, 2001 and JPL, 2001). In an optical system, the distances to physical features on the terrain are computed from the geometry of the terrain surface, the observation geometry of the sensor and measured angles (CCRS, 2001 and JPL 2001). It should be noted that the effects of atmospheric distortion could also play a role in optical sensor accuracy (USGS, 2001).

It is now that the difference between the two systems and how they view terrain surfaces can be clearly seen. In a SAR system, a high mountain peak is closer to the sensor and concurrently the distance in the image decreases; the illuminated mountain peak is displaced closer to the SAR system. This is an example of *foreshortening* (Appendix, VII, Fig. 3-4 and CCRS 2001, JPL 2001). In the optical sensor's case, the exact opposite is true if in an oblique view. The high mountain peak is seen as a greatly increased angle and consequently greater image distance. The viewed mountain peak is therefore placed further away from the optical system. This is of course an example of *layover* (Appendix VII, Fig. 3-4 and CCRS, 2001 and JPL, 2001). It can be said that a complementary data set is useful when viewing any terrain surface with any type of remote sensing system to confirm the characteristics and position of a physical feature in the targeted area. This was the rationale for the employment of CORONA imagery in this research project (Jensen, 1986 and Sabins, 1987).

3.7 POLARIMETRIC SAR

The basic concepts underlying RADAR and SAR systems have been defined so that the reader might better understand the NASA SIR-C / X-SAR Imaging RADAR (or Shuttle Imaging RADAR) which produced the data for this research project. Shuttle Imaging RADAR belongs to the previously described family of SAR; it also belongs to the group of RADAR systems known as polarimetric SAR (JPL, 2001, Kingsley and Quegan, 1992).

In Section 3.3 the basic theory of how an electromagnetic wave may be transmitted through space was discussed as well as the particulars of the orientation of the electrical field which surrounds it. It was noted that a change in the orientation of that electrical field in relation to the magnetic field denoted a change in *polarity*. Thus, if a SAR system has the capability to transmit and receive a RADAR wavelength in at least one other *mode* of polarity, it may be said to be *polarimetric*.

If a SAR system is capable of transmitting and receiving a RADAR wave in every possible orientation and combination thereof, it is commonly referred to as *fully polarimetric*. This is of course a greatly simplified definition and full technical descriptions are best found in Ulaby, Fung and Moore's works (1981-87).

As was noted, polarimetric SAR systems operate in different *modes* of *polarisation*. Polarisation is defined in RADAR science as the orientation of an electrical field about a transmitted microwave signal (CCRS, 2001 and JPL, 2001 and Ulaby, Fung and Moore, 1981-87). Mode applies to the orientation of the electrical field using a *reference surface* (or *plane*). The reference surface is based on the earth normal vector and SAR *range* direction, or *vector* of the transmitted signal (CCRS, 2001 and JPL, 2001).

Therefore, a RADAR wave can be said to be transmitted in a *vertical mode* if the antenna of the SAR system is positioned to put the electrical field of the signal into the plane of the reference surface (CCRS, 2001 and JPL, 2001 and Ulaby, Fung and Moore, 1981-87). Conversely, the RADAR wave is said to transmitted in a *horizontal mode* if the electrical field has been positioned in a plane which is perpendicular to the earth normal vector and the SAR reference surface (CCRS and JPL, 2001, Ulaby, Fung and Moore, 1981-87). RADAR waves transmitted in a horizontal mode have a spatial orientation that is unrelated to illumination angle (Fig. 3-4 and CCRS, 2001).

When a space-borne SAR system transmits signals in a specific polarisation mode towards a feature, or *target,* on the surface of the earth, the interaction with the earth's terrain may cause the polarisation of the signal to change. A signal transmitted in the vertical polarisation mode may interact with a physical feature that has surfaces that cause multiple polarised orientations to be reflected back to the receiving antenna. This principle is caused *depolarisation* (Ulaby, Fung and Moore 1981-87). Thus, the SAR systems receiving antenna may record horizontally polarised signal reflections from the earth's surface along with reflections from the original vertically polarised signal. The degree of depolarisation that may occur is related to the electrical and physical properties of the particular surface (CCRS, 2001 and JPL, 2001, Ulaby, Fung and Moore 1981-87).

The majority of the airborne SAR systems presently deployed are capable of transmission and reception in both horizontally and vertically polarised modes; most spaceborne are single polarimetric capable (Lillesand and Kiefer, 2000). There is a standardised nomenclature used by the RADAR community to describe these modes of operation as well. RADAR waves transmitted on a horizontal plane are known as H, while those received in the same plane are designated in the like manner.

Following this mode of nomenclature, a C band RADAR wave transmitted in the horizontal mode and received in the horizontal mode would be designated as C hh. The same holds true for the RADAR waves transmitted in the vertical plane, or mode; if transmitted in a vertical plane and received on the vertical plane it will be designated C vv. Further, in the RADAR community, when RADAR wave is transmitted and received in the same plane, or mode, it is generally referred to as *like polarised*. It is possible to receive a RADAR response in an opposite plane to what was emitted, i.e. transmitted in a vertical plane and received in the horizontal plane. When this occurs, it is referred to as being *cross-polarised*. Cross-polarisation is caused by the scattering of the transmitted RADAR wave by the particular target in multiple directions, thus creating a weaker recorded response at the antenna than if it were like polarised.

At this point, key concepts relating to polarisation must be discussed, as it is the foundation for the analysis of the NASA SIR-C/X-SAR data utilised in this research work. These concepts are *phase* and *phase difference* (JPL, 2000 and CCRS, 2001).

Phase is a characteristic of an intermittent phenomenon, which in this case is an electromagnetic wave, and refers to its source and its progress in relation to an arbitrary source (CCRS, 2001 and JPL, 2000, US Navy, 1996). In RADAR science, the idea of phase refers to how electromagnetic waves oscillate. When seen as a cyclical occurrence, similar to the action of a wave or even the crankshaft motion of an engine, phase may be represented in *degrees* (Fig. 3-6 and CCRS, 2001 and JPL 2000). Therefore, if one-fourth of a cycle equals a 90 degree *phase rotation*, then one complete cycle equals a 360 degree phase rotation (CCRS, 2001 and JPL, 2000). Those waves that have a source where the phase 0 degrees are in perfect alignment are considered *in-phase*, while those waves that have phase 180 degrees in alignment are considered to be *out-of-phase* (CCRS, 2001 and JPL, 2000).

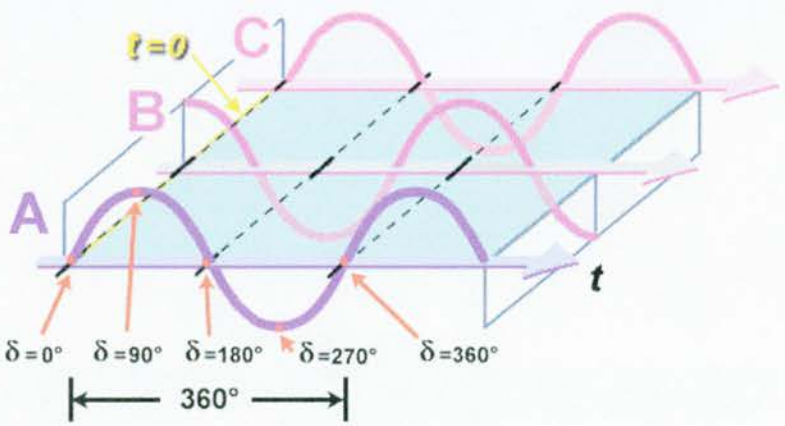

Fig. 3-6 Phase and its representation in degrees (from CCRS 2001)

Many SAR systems can calculate the phase of an incoming RADAR pulse and then calculate the *phase difference* (in degrees) in the return of the hh and vv signals. The time-delay, or *difference*, in the response of transmitted signals, for example between hh and vv polarised RADAR waves, is many times caused by scatterers with unique spatial and structural characteristics (CCRS, 2001 and JPL, 2000). SAR systems of this same type are also able to calculate correlation coefficients for the hh and vv responses, which can be thought of as a measurement of likeness/unlikeness between the hh and vv scatterers (CCRS, 2001 and JPL, 2000). Phase difference was the method chosen to detect ancient mining sites because of its ability to define and discriminate particular types of reflecting surfaces known as *corner reflectors* (pg. 43 and Fig. 3-8).

Finally, one point related to phase difference and the measurement system used to represent this concept should be mentioned. Phase difference may be expressed as either *degrees* or *radians*.

Radian size is based is on the mandate that there are 2 π radians in a circle, or 360 degrees; therefore, 360 degrees is the same as 2 π radians (Fig. 3-7). Of course this means that 1 radian is equal to $180/\pi$ degrees, and 1 degree is equal to 1 π /180 radians. The rationale for the popularity of this system lies in the fact that scientific formulae are easier to express and comprehend when radians are used to measure angles (Rice, 2001). However, since this study is directed towards a wider audience phase difference results will be presented as the magnitude of change in degrees along with decibel responses.

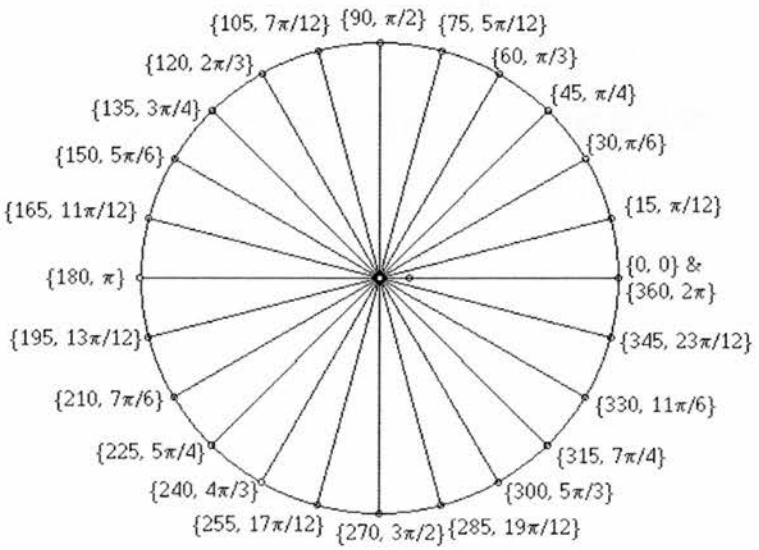

Fig. 3-7 Degree/radians circle (from Rice University 2001)

A *phase difference absolute value image* was generated for each mine site as a product of the calculations used to measure the phase difference between the horizontal and vertical polarisations of the NASA SIR-C/X-SAR data. Phase difference is calculated in *degrees* with ranges from 0 degrees to 180 degrees; results are presented in graphical images that use a piece-wise linear stretch to map these values. (ENVI, 2000 and CCRS, 2001).

Knowledge of a target area's scattering properties as a function of polarisation can yield important information about the roughness of surfaces and orientations of the structural components of vegetation (Wang *et al*, 1995). The next section will discuss how microwaves interact with earth's surface, how they are recorded as images and how they are interpreted.

3.8 Target and Microwave Energy Interaction

Using grey values that represent the variation in microwave response from a particular target, a SAR image may be produced which can aid in both digital and visual interpretation of a landscape. How the topography of the earth's landscape interacts with transmitted microwaves, how they are recorded by the RADAR system and how they are represented in SAR imagery is the focus of this section.

Generally speaking, RADAR targets that reflect a considerable amount of the microwave energy transmitted towards them will be represented as light grey or white colour tones in SAR imagery. Conversely, targets that reflect a small amount of microwave energy, or none at all, will appear as very dark grey to black areas in SAR imagery. Finally, RADAR targets that have surface properties which fall between maximum and minimum reflectance capabilities may be regarded as intermediate reflectors and are represented in SAR imagery by medium grey colour tones (JPL, 2000).

The quantity of backscatter received by a RADAR sensor is a function of the qualities of the target and the performance characteristics of the RADAR system. Some of the target qualities that affect the quantity of microwave backscatter are dielectric constant, geometric shape, local incidence angle, and surface roughness. RADAR system characteristics that will affect microwave backscatter are incidence angle, look direction, polarisation and wavelength or frequency. These components decide the total quality and quantity of microwave backscatter against a target and therefore the intensity or brightness of colour that is displayed on a given piece of SAR imagery. Any change in the characteristics of these components affects the amount of backscatter received by the RADAR and the resultant imagery; these components are described in the following paragraphs.

Dielectric Constant is a measurement system where the electrical properties of a material are calculated for the amount of absorption, reflection and transmission of microwave energy after being subjected to an incident signal (JPL, 2001). Examples of materials with high dielectric constants that produce strong backscatter responses are living vegetation, metals, salt and water. Materials that have weaker interactions with transmitted microwave energy and thus produce lower backscatter responses are dry soils, dry sands, dead vegetation, lake ice and rocks. As may be imagined, the introduction of any material with a high dielectric constant within an overall low dielectric constant target medium, will result in an increased backscatter response recorded by the RADAR system. An example in an archaeological situation would be the filling of an ancient hollow way located on a flat plain with water after a heavy rain shower. Because the hollow way has a concave shape created over thousands of years of use which tends to hold water, it will be detected by the RADAR sensor as a high dielectric constant target, in comparison to its less interactive surroundings i.e. the flat rapidly draining soils of the plain.

Target geometry or geometric shape is the actual physical shape of a target illuminated by a RADAR system. It would appear obvious that an object that is larger in size would typically generate a larger backscatter response than a smaller object. A forest may be considered a general target, yet within the forest various trees, flowers, and other plants, grow which all have different leaf concentrations, leaf sizes, branch sizes, trunk lengths, heights and orientations thereof. All of these characteristics affect the quality and quantity of measurable backscatter. A target such as the forest is sometimes referred to as a *localised distributed target* (CCRS, 2001).

A special form of geometric shapes, known as *coherent point targets*, produce backscatter responses which are far out of proportion to their actual physical size. These targets are able to reflect a large amount of the transmitted microwave signal back to the SAR system in comparison to a *localised distributed target* such as a forest. While localised distributed targets have a fading effect when subjected to SAR transmission, coherent point targets do not. In fact coherent point targets generally occur only in areas that have been created by humankind, and are not as common in nature. The SAR backscatter responses from these types of targets tend to be smooth in relation to the transmitted wavelength and have a normal orientation in respect to the RADAR range vector. If the geometry of the particular target surface is right, multiple coherent scattering processes can produce very strong RADAR responses (CCRS, 2001).

Coherent point targets are also known as *corner reflectors* and usually fall into three categories (pg. 40). They are *top-hat* (180° phase difference), a conductive smooth cylinder which stands upon a smooth plane, *dihedral* (also 180° phase difference), which has two flat conducting surfaces at right angles to each other, and *trihedral* (0° phase difference), which has three flat conducting surfaces that are all perpendicular to each other (Fig. 3-8, CCRS, 2001). A top-hat reflector exhibits a RADAR response which is independent of the SAR viewing angle, but which is also much weaker than the responses which may be recorded from a dihedral or trihedral corner reflector. A dihedral reflector, on the other hand, produces a strong response only if its reflecting surfaces are perpendicular to the direction of illumination by the SAR system. Trihedral reflectors produce the strongest responses of the three corner reflectors. This is because when microwave energy is transmitted incident onto any surface of a properly oriented corner reflector, the transmitted energy will return directly to the source of emission, i.e. the SAR antenna. Human-made corner reflectors are features such as multi-storey buildings, highway bridges and radio towers. An ancient mine rake, with a u-shaped profile, might be expected to exhibit characteristics of a dihedral reflector. Thus, hh-vv phase difference might be a useful tool in the detection of such sites.

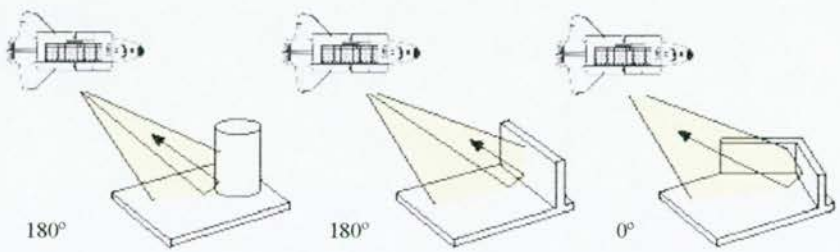

Fig. 3-8 Left to right, top-hat reflector, dihedral reflector and trihedral reflector with the expected HH-VV polarimetric phase difference values that allow them to be identified by phase difference analysis (from CCRS 2001, JPL, 2001, Raney, 1992)

Local incidence angle affects the quantity of backscatter received back from a target because of the angle that transmitted microwave energy is incident on the target's surface. As an example, a hill with maple trees directly facing the SAR transmitter's illumination will appear brighter on SAR imagery because it has a smaller local incidence angle. Conversely, if the hill was oriented indirectly or away from the SAR transmitter's illumination it would appear darker and have a large local incidence angle. Local incidence angle must be taken into account particularly in areas with hilly to mountainous terrain (Lillesand and Kiefer, 2000 and CCRS, 2001).

Surface roughness has been generally described in the RADAR science community as surface irregularities, such as height and width of terrain features, which are described by statistical mathematics. Common statistical representations include root-mean-square (RMS), which is derived by averaging horizontal and vertical scale lengths, and by creating two-dimensional distribution models that describe the variation in the surface topography over a given area. In the SAR science community, roughness scale lengths will be computed and normalised to the characteristics of the particular RADAR wavelength used in a given target area. As a general rule of thumb, RADAR remote sensing scientists consider a surface area smooth if the vertical variation is beneath one-tenth of a wavelength across a horizontal area of three or more wavelengths (CCRS, 2001 and Lillesand and Kiefer, 2000).

Surface roughness is one of the most important factors affecting microwave backscatter responses. Smooth surfaces that are horizontal to the SAR will cause almost all of the incident microwave energy to reflect away from the receiving antenna, thus causing these areas to appear dark grey, or black, on SAR imagery. These are referred to as specular surfaces. Examples of these type reflectors are large, calm bodies of water such as lakes and highways that have been paved with very smooth macadam. If a lake should have a small breeze occur while being imaged, and its surface become slightly choppy, or rough, then it becomes a *diffuse reflector.*

Diffuse reflectance occurs when a smooth horizontal target area, such as a desert plain, begins to grow low shrubs intermittently over time. This slight "roughening" of a previously "smooth" target area causes microwave energy to be reflected in multiple directions with a little more backscatter being recorded by the SAR receiving antenna. On SAR imagery these diffuse reflectance areas will generally appear as brighter grey values than areas of specular reflectance will. If an area being imaged by a SAR contains a river that has large, exposed areas of coarse gravel that are approximately the same size as the transmitted wavelength, then strong diffuse reflectance will occur. This is also seen in bodies of water where high winds have created short, cyclic wave actions. When these types of features are imaged by SAR systems, the imagery records very bright grey tones (CCRS, 2001 and JPL, 2001).

Volume scattering is defined as the multiple scattering of a transmitted RADAR wavelength within a particular medium. This medium may be the canopy of a forest, an ice field where years of snowfall have created different layers of ice density, or the sands of a desert where complex sub-surface structures may exist (CCRS, 2001 and JPL, 2001 and McHugh *et al* 1988, Sever and Sheets 1988, Aslam *et al*, 1988).

In volume scattering the medium reflects some of the microwave energy transmitted from the SAR system back to the antenna, while other microwaves penetrate the interior volume of the medium to reflect from some particular structural component back to the sensor's antenna. The characteristics of the medium, and the quantity of moisture present as well as the configuration of the SAR system, are the determining factors in the amount of volume scattering that occurs and what the receiving antenna records (JPL, 2000 and CCRS, 2001 and Lillesand and Kiefer, 2000).

A moderate amount of volume scattering occurs in most agricultural fields or in other intermittently occurring plants (Guo, *et al* 1996). Vegetation height is important as low-growing plants or grasses may cause the same volume scattering effect. In any of these type target areas, or mediums, three scattering mechanisms can usually be observed taking place. They are diffuse scattering from the terrain, direct or single bounce scattering from the components of the vegetation and *double-bounce* vegetation to ground reflection (CCRS, 2001 and JPL, 2000). While the first two types of scattering have been discussed previously, double-bounce has not. The double-bounce effect occurs when a transmitted microwave strikes a component such as tree limb, reflects downwards towards the ground where it is reflected upwards and back to the SAR sensor's receiving antenna (Guo, *et al* 1996, Lillesand and Kiefer, 2000).

Forests present a difficult problem for the study of RADAR backscatter. The density of the canopy, the various reflecting surfaces due to the presence of different species and height differences make forests subject to numerous scattering effects. While it is not possible within this work to detail them all, the most important scattering effects are:

- diffuse scattering from the terrain
- shadowing, by an overhanging canopy, of the terrain or even other portions of the surrounding forest
- direct backscatter from the peaks of the trees or the total canopy of the forest
- multiple scattering from the internal components of the forest's canopy
- double-bounce scattering effects off tree trunks and terrain (CCRS, 2001)

The interaction between transmitted microwave energy and the earth's surface has been examined, but the role of a SAR system's configuration, and how it affects the transmission of RADAR wavelengths still remains to be discussed. The following sections will do so, by detailing SAR system configuration and its ramifications for microwave transmission.

3.9 SAR Configuration and control

The *frequency* of a RADAR wavelength is one of the most important factors in regards to calculating the quantity of backscatter, the level of surface penetration and volume scattering of targets (CCRS, 2001). The reason for the importance of frequency lies in two factors. Firstly, the dielectric constant of a bulk material relies upon the RADAR frequency in a few materials and second, the scattering ability of a scattering element in a material relies upon the scale of the element and the dielectric constant of the scattering element material (CCRS, 2001).

For example, sands found along a beach are generally fine, smooth and moist. If targeted by a SAR, any anomalies in dielectric constant in the sand structure of the beach will be so small that they may be ignored and the observer may conclude that the microwave interactions worthy of investigation will have happened at the sand's surface. How microwave energy is scattered at the *surface* and how it penetrates a soil is governed by the difference between the air and soil beneath it and is related to RADAR frequency (CCRS, 2001 and Fung *et al*, 1981). The small amount of microwave energy that permeates a soil will get propagated via a refracted pathway and will be attenuated by the soil at a ratio which is reliant upon the chosen RADAR frequency and the soil's electrical conductivity. The total penetration depth of a RADAR frequency is therefore based upon the distance of propagation where the microwave energy has become attenuated to approximately 37% of its strength as measured at the surface (CCRS, 2001 and Lillesand and Kiefer, 2000 and Sabins, 1987). Thus, soils that have a medium level of conductivity will usually have a penetration depth of 1-5 wavelengths, while extremely dry soils that have an electrical conductivity approaching zero may be penetrated up to 100 wavelengths (CCRS, 2001 and Guo, 1996).

If a material has dielectric constant discontinuities within it that have a major scattering force, every time a microwave meets a scatterer some of the microwave energy will be scattered in multiple directions away from the original propagation source (CCRS, 2001). Consequently, many scatterers will be able to reflect scattered signals upwards through the surface of a material, as described in the section on volume scattering, and thereby dramatically lessen the penetration depth of a RADAR wave. For example, when a C-band (5.3 GHz) wavelength is transmitted against sea ice that has compacted over several years, the penetration depth will be around six wavelengths. This is because the sea ice is considered to be a low-loss material filled with bubbles of air. If an L-band (1.5 GHz) wavelength were used, the size of the bubbles of air within the sea ice would be considerably smaller than the RADAR wavelength and the volume scattering effect would be negligible. Penetration depths would be on the order of 10 wavelengths in this case (CCRS, 2001).

When the material imaged by a SAR system is composed of intermittent high dielectric constants, the level of wavelength penetration will be governed by the size of the scatterer in relation to wavelength ratio as well as the quantity of scatterers per unit volume at each wavelength-normalised size (CCRS, 2001). Referring back to volume scattering mechanisms, the constituent parts of a forest canopy, i.e. branches, leaves, limbs etc., would be an example of this particular function. The transmitted RADAR wavelength loses energy because it is influenced by an extinction coefficient; the amount or effect of this coefficient is based on the frequency employed (CCRS, 2001 and Evans, 1986). While this is a great simplification of the overall body of research regarding canopy penetration, it is generally true that the longer the wavelength, the greater the depth of microwave penetration. Thus, P band has the ability to provide information about the terrain beneath a forest, while C band would have considerable difficulty in penetrating the forest canopy, depending on the type of tree species of course (CCRS, 2001 and JPL, 2001).

Finally, the frequency of the RADAR wavelength affects whether or not a surface will appear darker (smooth) or lighter (rough) in SAR imagery. Anomalies in the surface that are less than one tenth of the overall wavelength's amplitude, as mentioned in the section on surface roughness, will be ignored because they are not large enough to be resolved by the signal. Thus, the area within a piece of imagery that has this characteristic will be represented by dark grey tones because of the smoothness of the surface. As a typical example, if an L band frequency is used to image a portion of the ocean where the wave cycle and height are low, then the imagery will record a dark (smooth) area. On the other hand, if C or X band frequencies were used, then the wave cycle and height would approximate their wavelengths causing the same area to appear bright, or rough, in the imagery (Fung *et al*, 1981, Ulaby and Dobson, 1989).

In a previous section, *incidence angle* was described as the resulting angle created between the local vertical direction and the RADAR range vector (CCRS, 2001). Since SAR systems usually record over long distances in the range direction, the incidence angle will of course change from the point beneath the sensor to the farthest edge of the imaging swath. One of the most important effects of incidence angle is in the way that surfaces appear, insofar as smoothness and roughness are concerned. An object that may appear dark, or smooth, in the near range might appear brighter (rougher) in the far range should the incidence angle have changed markedly over the total distance. Consequently, the categorisation of backscatter responses, or signals, with particular target materials has to take into consideration incidence angle as an influencing factor.

Targets observed at various incidence angles have many unique scattering responses because of the interplay between the view geometry and the physical structure of the target material. However, these unique characteristics aid in categorisation. It should be noted that changes in target illumination due to incidence angle are more common in aerial SAR systems than in space borne platforms. This is because the high altitude of the space borne system creates a smaller range in the incidence angle of an image scene area (CCRS, 2001).

Thus, how a RADAR wave is affected after striking a particular target is based on the transmitted signal's composition, the target's size, structure, and physical composition, as well as the geometric relationship between the target and the signal (CCRS, 2001 and JPL, 2000). During this complicated process a RADAR wave may experience numerous responses or reflections from the target that can change the original transmitted signal's polarisation. A transmitted RADAR signal which experiences a single-bounce reflection will not experience a polarisation change, in other words a signal transmitted in a vertical mode will be received in the same vertical mode (CCRS, 2001 and Fung *et al.*, 1981). However, more complex scattering responses can cause a transmitted signal to become *depolarised*, that is to say a signal transmitted in a vertical mode will be received in the horizontal mode (CCRS, 2001 and Fung *et al*, 1981, 1986). The amount of depolarisation experienced by the transmitted signal and the polarisation set-up of the SAR sensor will affect how a target appears on SAR imagery. Thus, it is extremely important to ground-truth any research area of interest to determine those targets that may potentially cause depolarisation.

Look direction is the term used by RADAR scientists to portray how a SAR sensor's transmitted RADAR signal is directed in relation to the orientation of the features beneath it (CCRS, 2001 and JPL, 2000). The look direction of sensor can have a major effect on how areas appear on SAR imagery, in particular if the imaged areas include fields of organised agriculture, such as cornrows, or extremely lineated geological features such as dykes or faults (Blom and Daily 1982, Daily *et al.*, 1979, Evans, *et al.* 1986 and Guo, 1996). Therefore, in geological applications, if the SAR sensor is able to direct its transmission signal perpendicular to dykes, faults or other lineaments, it will create enhanced tonal differences in the resultant SAR imagery. Because these features will have greatly enhanced contrasts, tones and shadows, the geological features and topography should be easier to discern. This is of key interest to this research work is concerned since the location and analysis of geological structures is essential to understanding the locations of ancient mines.

If the SAR sensor has a transmission direction which is perpendicular to the rows in agricultural fields, the resulting backscatter will be consistent with the particular crop; i.e. corn or sunflowers, which are normally represented as intermediate grey tones (CCRS, 2001, Ulaby and Dobson, 1989). On the other hand, if the SAR sensor's transmission direction is parallel to the linear crop rows, the microwave energy will be able to reach the soil beneath. Because the soil is a smoother reflecting surface in comparison to the surrounding crop vegetation the SAR imagery will represent the field as an area of darker grey colour tones (CCRS, 2001 and Aslam *et al.*, 1978). However, the soil might become obscured as the vegetation grows, thus changing the backscatter response over the course of a growing season.

Spatial resolution is described as a SAR sensor's capability to detect, identify and discern two targets that are located near each other as separate points within a target area (CCRS, 2001 and Fung *et al*, 1981). While higher resolution imagery is generally desired, all levels of resolution have their uses. High resolution (1-10m res.) SAR imagery is useful for the mapping of individual cultural and natural features, but a medium (10m-50m res.) or even low resolution (above 50m. res.) SAR product is more useful when mapping large areas such as oceans, forests or ice fields (CCRS, 2001 and JPL, 2000 and Zebker *et al*, 1996).

A SAR system has its spatial resolution determined separately in the range direction and azimuth direction, and is dependent on the configuration of the sensor and its RADAR apparatus (CCRS, 2001 and JPL 2000). The resolution within the azimuth direction is generally assumed to be half of the length of the SAR system's antenna. The azimuth resolution is then made independent of range by processing the signal (CCRS, 2001 and JPL, 2000). The range resolution is determined by the transmitted pulse's frequency bandwidth, which is a product of the range-focused pulse's width, or time duration (CCRS, 2001, Cutrona, 1970 and Fung *et al*, 1986). Thus, bandwidths which are larger will create pulse widths that are small and focused (CCRS, 2001 and JPL, 2000).

Since signal pulse length determines the range resolution of Imaging SAR platforms, the distance resolved, in reality, is the distance from the beginning and ending of the pulse's edges (CCRS, 2001 and Fung *et al.*, 1986). Therefore these pulses may be portrayed as signal wave fronts propagated from a SAR system's antenna to illustrate their relationship with the earth's surface (Fung *et al.*, 1981). If the arcs of the propagated wave fronts are portrayed as intersecting a planar, or flat, portion of the earth's topography, then the resolution distance in the ground range will be greater than that of the resolution in the slant range; the smaller the incidence angle, the larger the ground range resolution (CCRS, 2001 and Fung *et al*, 1986).

It has been explained in this chapter that a space borne SAR system transmits a signal that is composed of a continuous series of short pulses from the microwave portion of the electromagnetic spectrum (JPL, 2000 and Lillesand and Kiefer, 2000). Only a small portion of the transmitted energy is reflected back to the SAR system receiving antenna as backscatter, which is recorded and archived by onboard computers as time delays (CCRS, 2001 and JPL, 2000). Before useful SAR imagery can be created from the archived groups of time delays, it must undergo a digital processing and calibration protocol before downlinking to ground stations (CCRS, 2000 and JPL, 2000). Sub-routines to this overall-processing regimen include *geometric correction*, *multilooking*, *radiometric correction* and *signal processing*; only the procedures essential to this work will be discussed here for simplicity (CCRS 2001, JPL 2000, and USGS, 2000). Further processing routines that may be utilised to enhance the SAR imagery's usefulness include *radiometric scaling*, *spatial enhancement*, and *data fusion*; these are routines that are normally accomplished by end-users utilising remote sensing software (ENVI, 2001 and USGS, 2000). However, before proceeding, the basic steps for the creation of SAR imagery will be outlined, with *signal processing* being first.

As mentioned, a SAR signal history contains data on the amount of time delay between the transmission and reception of a particular RADAR wave as well as the strength of the responses from the imaged terrain and the targets within it (CCRS, 2001 and JPL, 2000). The signal history data is in an unusable form at this stage insofar as visual interpretation is concerned, and so must be processed first. This is called *compression* and involves a process where the signal history data is manipulated so that the range and azimuth directions are now seen as a gridded product that is two-dimensional (CCRS, 2001 and JPL, 2000, Elachi *et al.*, 1981 and Jensen, 1986). The two-dimensional grid product is subdivided on the basis of the size of the slant range resolution cell (CCRS, 2001 and Jensen, 1986). The slant range resolution cell is defined as the smallest terrain area that a value for reflection intensity may be computed for in the compression procedure (CCRS, 2001 and Jensen, 1986). These procedures are necessary in order to construct a digital product capable of being understood by an interpreter. (Jensen, 1986).

After creating the basic digital SAR image product, further procedures may be needed or required by the end-user to facilitate the interpretation and usefulness of the data. As previously mentioned, these procedures are *radiometric correction, geometric correction,* and *multilooking*. They and their sub-routines will now be discussed.

Radiometric calibration may be used on digital SAR data in two forms. *Absolute calibration* is used to create a correlation that is time-free between the brightness on a SAR image and the recorded backscatter of a ground target (CCRS, 2001 and Jensen, 1986). Absolute calibration ensures that firm targets have the same level of image intensity at each overpass of the SAR system and makes it possible to perform precision measurements of both terrain and topography (JPL, 2000 and CCRS, 2000).

Relative radiometric calibration is used to create a continuous correlation between the image's intensity and the recorded backscatter of a ground target (CCRS, 2001 and Jensen, 1986). Relative calibration produces an effect where a target has the same level of image intensity independent of its location within the SAR image (CCRS, 2001 and NASA GSFC, 2000). This form of calibration is used when quantitative SAR research is being performed and is generally done at data downlink and processing centres but absolute calibration is not possible (CCRS, 2001 and NASA GSFC, 2000).

Geometric correction is a procedure used on SAR imagery to rid it of geometric distortions created by the SAR system's geometry as it passes over a target area. This procedure creates, in essence, an image map that presents a true geographic visualisation of the target area (CCRS, 2001 and JPL, 2000). As with the radiometric calibration process, there are two forms of correction.

The *slant range* to *ground range correction* is used on SAR imagery because the data is collected in the slant range direction, as defined previously it is not unusual for the relative distances on the earth's surface to be inaccurate (CCRS, 2001 and JPL 2000, Elachi *et al*, 1981). If accurate ground distances are required, then the data gathered in the slant range require conversion into a ground range format (CCRS, 2001 and JPL, 2000, Elachi *et al* 1981, 1986). If an uncorrected SAR imagery is visualised in ground range, it will be viewed by the interpreter as if compression had occurred in the near range, since this is the area that the highest level of distortion will happen (CCRS, 2001 and JPL, 2000). In order to establish a high level of precision, the ground range conversion should be done by the interpreter since it demands an intimate knowledge of the topography of the target area and the configuration of the imaging geometry used (CCRS, 2001 and JPL, 2000, Elachi *et al,* 1981). Digital elevation models (DEM), are useful in this process (CCRS, 2001 and Kober, 1991).

Geometric rectification is used to properly associate objects portrayed on remote sensing imagery to their actual forms (shapes) and alignments (CCRS, 2001 and JPL, 2000). The process can reduce or eliminate the geometric distortions that are introduced into the data by the SAR system's occasional uncontrolled motions in space i.g. pitch, roll or yaw, or altitude changes due to orbital deviation caused by gravity, platform correction, or even subtle atmospheric drag from earth (CCRS, 2001 and NASA GSFC, 2001).

Geometric rectification is also used to change an image's orientation so that is conforms to cartographic norms, i.e. ensuring that image scene "north" is the same as real world conventions (CCRS, 2001, Jensen ,1986 and Lillesand and Kiefer, 2000). The primary reasons for employing geometric correction processes are that as the SAR images the earth's surface, the rotation of the globe causes each collected line of image data to appear skewed. Further, in general the SAR systems currently in orbit do not collect data from a true north-to-south flight direction (CCRS, 2001 and NASA GSFC, 2001). Most of the SAR systems in space image from a near polar orbit perspective. It should be noted that aerial SAR systems are unlimited in their direction of flight and are constrained only by flying altitude (NASA GSFC, 2001).

One of the SAR image data processing sub-routines that is commonly performed is *radiometric scaling* (Elachi *et al*, 1981 and Jensen, 1986). As SAR imagery is composed of grey colour tones that represent the intensity of the backscatter recorded by the SAR system, two things influence the colour range, the first being the total dynamic range of the RADAR responses within the image scene and the second being the computer encoding process utilised to output an image (CCRS, 2001 and Jensen, 1986).

The first of the two items, the total dynamic RADAR range of a SAR image scene, is determined by these parameters: the imaging geometry of the SAR, the RADAR frequency employed by the SAR and the resolution of the SAR (CCRS, 2001 and Sabins, 1987). An example of this would be an image scene that is composed of, featureless plains, which are interrupted by large rock escarpments. A SAR system using the C band frequency to image the scene at 45° of incidence angle will have to encompass a dynamic range of some nine orders of magnitude (CCRS, 2001 and JPL, 2000 and Elachi *et al*, 1986). Such an example may be seen in Chapter 6 in the images concerning Serabit El Khadim

The second influence on dynamic tonal range is the digital encoding process. Normally, the encoding will reduce the value of returns recorded from strongly reflecting targets (i.e. bright) and represent them at a standardised saturated level; this sometimes referred to a "signal clipping" (CCRS, 2001, Elachi *et al*, 1981 and 1986, Jensen, 1986 and US Navy, 1996). Signal clipping may also set the returns recorded from a weakly reflecting target to zero in order for the majority of the mid-level grey colour tones to be portrayed in either a digital or hard copy product (CCRS, 2001 and JPL, 2000 and Elachi *et al*, 1981 and 1986). Care should be taken to observe the rescaling constants of a SAR data set and to save them. This is because the digital encoding process removes the image calibration (JPL, 2000).

The range of grey in a SAR image scene that has been properly calibrated can be greater than the value range that a computer monitor can display (Jensen, 1986). The computer monitor will frequently distort, compress and otherwise scale the actual colour range representations of the SAR image, making the subtle tonal variations impossible to see (CCRS, 2001, Lillesand and Kiefer, 2001, and JPL, 2000, Jensen, 1986). Radiometric enhancement overcomes this problem by calculating the total possible range of grey colour tones that a display can handle and creating an output that matches the display's capability (CCRS, 2001 and Jensen, 1986). Gathering the grey colour values of the SAR data before their manipulation and then calculating their values over a wider range performs this process and this is typically done up to the maximum range of the computer display (CCRS, 2001, Lillesand and Kiefer, 2000 and Jensen, 1986). This process is also known by remote sensing analysts as contrast "stretching" (ENVI, 2000). The stretching process allows a greater level of contrast to be shown between targets, enabling the subtle tonal variations to be observed by the interpreter (Jensen, 1986).

The *spatial filtering* routine is used to change the level of *signal noise*, or *speckle*, in the grey tones of a SAR image scene that has a generally average tonal composition (Jensen, 1986 and Lee, 1981). *Speckle* appears as a "salt and pepper" or grainy texture in an image (CCRS, 2001). The effect is caused by random constructive and destructive interference from the multiple scattering returns that will occur within each resolution cell (JPL, 2001, and CCRS, 2001). For example, a homogeneous target, such as a grassy field, without the effects of speckle would generally produce light-toned grey colour pixel values within an image (Jensen, 1986). However, if the field had some individual blades of grass that were uniquely oriented, then there would be reflections within each resolution cell resulting in some image pixels being brighter and some being darker than the average tone such that the field appears speckled (CCRS, 2001).

Spatial filters are a way of limiting *speckle* or signal noise and enhancing the contrast within an image scene. However, care must be taken when using spatial filters as they may remove critical information from the SAR data (Holcomb, 1992 and Sabins, 1978). There are several distinct families of filters commonly used, among them *low pass* filters, which average the grey colour tone values within a specified number of surrounding pixels to lower the range of the overall grey scale value and hence smooth an image, and high *pass* filters to indicate areas where significant levels of change in tone are observed, such as edges (CCRS, 2001 and ENVI, 2000).

Adaptive filters are essentially high pass filters that are utilised to reduce speckle. What makes them subtly different from conventional high pass filters is their ability to change the statistics of image scene based on its own overall characteristics (CCRS, 2000 and ENVI, 2000). Adaptive filters are the riskiest routines to employ as their results can result in products that are impossible to reproduce (CCRS, 2001, ENVI, 2000 and Jensen, 1986).

All of the key processes and terminology related to the production of SAR imagery have now been described and a basic overview of the appearance of SAR imagery given. Key visual pointers that will assist an end-user in properly interpreting SAR imagery will now be defined.

3.10 Understanding SAR imagery

Although SAR remote sensing data has been available in limited quantity for many years, there has been little development in its use until recent years (Elachi *et al*, 1981 and Sabins, 1987). This coincided with the arrival of widely available commercial SAR imagery from Russia's ALMAZ, Japan's JERS-1, Europe's ERS-1,2 and Canada's RADARSAT; only ERS-2 and RADARSAT are still operating in a functional program (Lillesand and Kiefer, 2000).

Consequently, the transferral of technological understanding and education about SAR systems and their imagery has lagged behind that of the better-known conventional spectral systems such as LANDSAT (CCRS, 2001 and Lillesand and Kiefer, 2000). Still, many of the basic image interpretation skills required by image analysts to study spectral imagery are valid in analysing SAR imagery. The *visual interpretation* pointers outlined in the following paragraphs are for basic understanding of the *hard copy* image product displayed in this research work. Texts on *digital image analysis* are given in the accompanying bibliography for this work, which provide further guidance.

Condensing the previous sections of this chapter, it can be seen that four key items must be known to understand any RADAR image. These key items are RADAR system configuration, how microwave energy works with a RADAR remote sensing system, how transmitted microwave energy reacts with the Earth's surface in regards to objects or targets, and how recorded microwave responses, or backscatter, are represented in an image product (CCRS, 2001 and JPL, 2000 and Elachi *et al*, 1981).

Upon understanding the essential characteristics behind a given piece of SAR imagery, an interpretation template may used which is similar to that used in the analysis of conventional optical or spectral imagery (CCRS, 2001). However, the interpretation of SAR imagery must also take into consideration the sensor system's unique characteristics, i.e. that it is an active illuminating sensor, unlike optical and spectral sensors which are passive (USGS, 2000). The essential components of an interpretation template for SAR imagery should include such characteristics as association, colour tone, pattern, shape, size, and texture (Fig. 3-9, CCRS, 2001, Lillesand and Kiefer, 2000). These are defined as follows:

- *Association* - The process of identifying features within an image scene based on the context of their local or regional position (CCRS, 2001 and JPL, 2000). An example being the observance of a small well-vegetated area with a carefully cultivated landscape in the middle of a desert. This is usually understood to be an oasis.
- *Colour tone* - The tonal colour within a SAR image is based on the intensity and quality of the recorded backscatter for a particular RADAR frequency (CCRS, 2001 and JPL, 2000).
- *Pattern* - This is the spatial distribution or regular occurrence of objects or features. How they are spaced, their orientation, density or even uniformity is characteristic of pattern in a remote sensing context (CCRS, 2001 and JPL, 2000).
- *Shape* - This is the spatial form of an object or area (CCRS, 2001 and JPL, 2000). For example, RADAR shadow can be used to determine terrain characteristics, or to calculate feature height (CCRS, 2001).
- *Size* - Feature size is determined by comparison with the surrounding area and is useful to discern and isolate individual features in relation to each other (CCRS, 2001 and Lillesand and Kiefer, 2000).

- *Texture* - This characteristic is commonly described as the distribution pattern of tonal variation in a given image scene area (CCRS, 2001 and JPL, 2000). Common terminology for the various forms of texture are fine, flecked, grainy, linear or speckled, although others may been seen on occasion, such as chequered (CCRS, 2001 and Sabins, 1987). Texture is an important consideration in the analysis of geological features and is a key feature of this research study (Blom and Daily, 1982, El Shazly, 1983, Fig. 3-9).

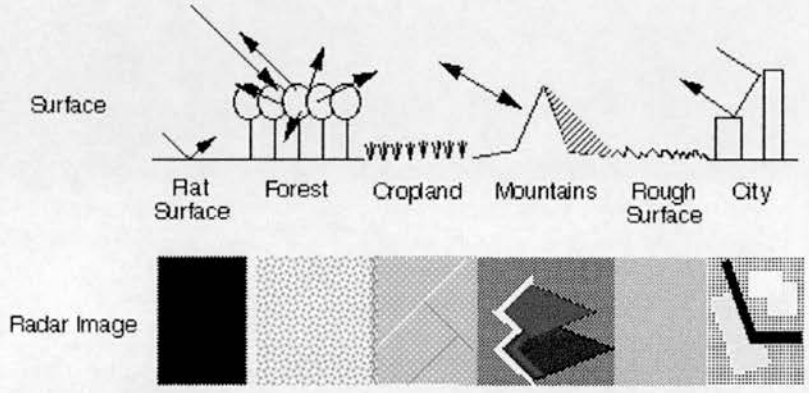

Fig. 3-9 General representations of typical RADAR targets (JPL 2000)

SAR systems are able to determine the texture of the earth's surface and by polarimetric means also determine the orientation of scattering surfaces within an area (Lopes *et al.*, 1993). Since ancient mine structures are found in homogenous geological formations and have a distinct shape or structure, they may produce a characterisable decibel value and a measurable phase difference in response to a polarised RADAR wave striking them (Ulaby and Dobson, 1989). Therefore, a *multipolarimetric* Imaging RADAR, the NASA SIR-C/X-SAR system was chosen for this study; it characteristics are explained in the following section.

3.11 NASA SIR-C/X-SAR multipolarimetric Imaging RADAR

SIR-C/X-SAR, built by the Jet Propulsion Laboratory and the Ball Communications Systems Division for NASA, is a three-frequency RADAR including L-band (23-cm wavelength), C-band (6-cm wavelength) and X-band (1.5-cm wavelength) (Stuhr *et al.*, 1994). It is the third major evolution in the NASA Imaging RADAR program which was begun in 1982 with SIR-A and followed by SIR-B in 1984 (Jordan *et al*, 1995). SIR-C is the first space-borne RADAR with the ability to transmit and receive horizontally and vertically polarised waves at both frequencies (Schmullius and Evans, 1997).

Since the SIR-C/X-SAR Imaging RADAR system has the ability to transmit and receive multiple wavelengths and polarisations, it is termed *multipolarimetric*. The sensor system also includes an X-band RADAR operating in a single-polarisation (VV) mode designed by the Italian Space Agency (ASI) and the German Space Agency (DARA). The X-band RADAR antenna is mechanically tilted (U.S. Navy, 1996), unlike the main C and L band antennas which are electronically tuneable allowing for electronic steering without physically moving the entire large antenna. This feature, combined with the roll and yaw manoeuvres of the Space Shuttle, allows for target scene image capture from 15 to 55° angles of incidence. Technical upgrades to the original system allow the SIR-C/X-SAR to capture simultaneous image scenes with both C and L band frequencies in all polarisation configurations-hh, vv, hv, and vh (Fig. 3-10 and JPL, 1994).

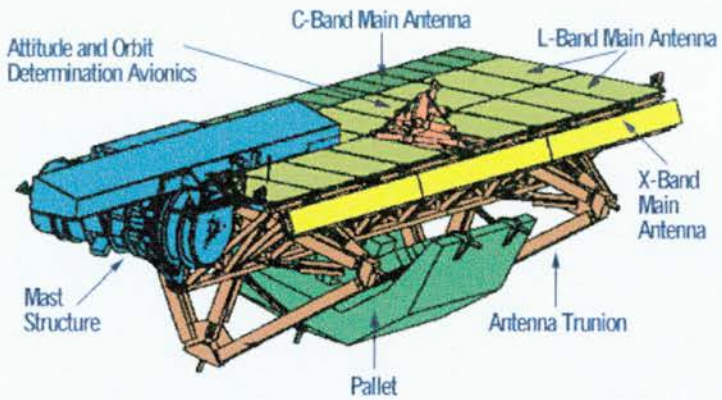

Fig. 3–10 Main antenna array of the NASA SIR-C/X-SAR. (Adapted from JPL.)

Both the SIR-C and X-SAR systems may be operated simultaneously or in conjunction with each other. The width of the ground swath, or the area on the target surface covered by the particular wavelength, varies from 15 to 90 kilometres, depending on the orientation of the antenna beams. The resolution of the various RADAR sensors can be varied from 10 to 200 metres as well as in a variable power mode.

SIR-C/X-SAR moves across the Earth much like a conventional airborne SAR; as it passes over an area a pulse is transmitted at each position; the return echoes pass through a receiver and are then recorded in an echo store (JPL, 2000). Then, because the RADAR is moving relative to the ground, the returned echoes are Doppler-shifted for motion compensation (negatively as the RADAR approaches a target; positively as it moves away). Comparing the Doppler-shifted frequencies to a reference frequency allows the many returned signals to be focused on a single point, effectively increasing the length of the antenna that is imaging that particular point, i.e. the SAR principle.

The unique characteristics and its performance parameters of the NASA SIR-C/X-SAR system can be seen in Tables 3-1 and 3-2.

Platform	Orbital altitude	Resolution	Look angle range	Bandwidth	Pulse Repetition Rate	Instrument Mass
NASA SIR-C/X-SAR	~225 km.	~30m (mode dependent)	17° to 63° from nadir	10, 20, 40 Mhz	1395 to 1795 pulses per second	11,000 kg.

Table 3-1 NASA SIR-C/X-SAR system characteristics (JPL 2001)

NASA SIR-C/X-SAR	C-Band	L-Band	X-Band
Wavelength	5.8 cm.	23.5 cm.	3 cm.
Swath width	15-90 km.	15-90 km.	15-40 km.
Pulse length	33.8, 16.9. 8.5 us	33.8, 16.9, 8.5 us	40 us
Data rate	90 Mbits/s	90 Mbits/s	45 Mbits/s
Data format	8, 4 bits BFPQ	8, 4 bits BFPQ	8, 4 BFPQ

Table 3-2 NASA SIR-C/X-SAR system parameters (JPL 2001)

The SIR-C/X-SAR's main value to Earth observation and monitoring has been its ability to measure the earth's surface using the RADAR signature from three different wavelengths, and to make measurements for different polarisations at two of those wavelengths, C and L (Table 3-2, JPL, 2001). This ability to perform polarimetric analysis of geological structures at two different wavelengths made it a primary choice for ascertaining the potential of remote sensing technology to detect ancient mining sites and other related archaeological sites. Scientific investigations using the SIR-C/X-SAR RADAR image data have been performed in the following discipline areas (JPL, 2001):

- Biology, to determine vegetation classification, extent and deforestation
- Geomorphology, to study soil moisture content and structure
- Oceanography to study ocean dynamics, wave and surface wind speeds and directions
- Geology, to study volcanism and tectonic activity
- Hydrology, to soil erosion and desertification

Unfortunately, total ground coverage for all SIR (SIR-A, B and C) missions yielded only 11 percent coverage of the earth's surface, though it was intended to be a precursor for the Earth Observation system (EOS) (NASA, 2001 and JPL, 2001).

However, in February 2000, a specially modified Shuttle Imaging RADAR mission was launched that may herald a new technical step forward towards a full-time, multipolarimetric and interferometric Imaging RADAR satellite (NASA, 2001). Dubbed the Shuttle RADAR Topographic Mapping Mission, or SRTM, this flight utilised a modified SIR-C RADAR instrument to map 80 percent of the world's surface by means of RADAR interferometry (Fig. 3-11, NASA, 2001 and JPL, 2001).

In RADAR interferometry, two radar images must be taken from slightly different locations (JPL, 2001). The differences between these two images are then calculated to allow for the surface elevation, or change. In order to get two radar images taken from different locations, and to preserve the necessary orbital accuracy, the original SIR-C/X-SAR system was highly modified, first by removing the L-band RADAR antenna system. This was done in order to reduce the lift-off weight and to make way for a new RADAR system and antenna. This new RADAR system had its antenna attached to the end of a mast that could be extended 60 meters out from the shuttle, thus enabling the Shuttle to send and receive the second necessary RADAR signal to create an interferometric data set (JPL, 2001). This is known as *single-pass interferometry* since two RADAR antennae located at two different locations on the platform are imaging the same target to ensure the previously mentioned orbital accuracy (JPL, 2001).

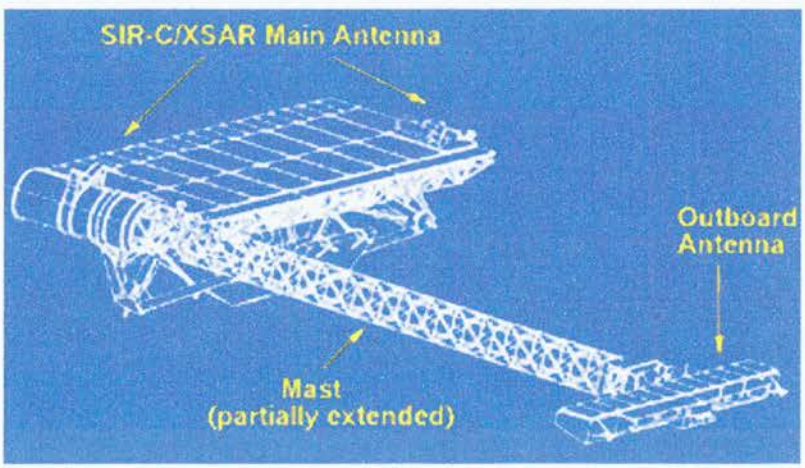

Fig. 3-11 The SRTM instrument showing the main radar antenna, the mast, and the outboard radar antenna (JPL, 2001).

The SRTM launched into an orbit with an inclination of 57 degrees, allowing the Earth's surface between 60° N and 56° S latitude to be imaged by the SRTM RADAR systems. This equates to approximately 80 percent of the world's surface (JPL, 2001).

The major technical innovation of the SRTM was in proving that single pass interferometry could accurately and efficiently collect elevation data (JPL, 2001). However, insofar as SRTM data use goes for archaeological purposes, its usefulness will be primarily limited to creating more precise landscape models because the interferometric nature of the mission precluded the gathering of L-band data. This was due to the Shuttle being unable to fit the L-band RADAR system into its cargo bay after the installation of the mast RADAR system and because the Shuttle Transport System (STS) would have been unable to lift the combined RADAR systems due to their weight (JPL, 2001). Thus, the RADAR system that has demonstrated the most potential for archaeological reconnaissance was idled (Dahlin and Pope, 1989, McCauley *et al.* 1982 and 1986, McHugh *et al.*, 1988, Schaber *et al.* 1997). Consequently, until some form of full-time long-wavelength Imaging RADAR system is deployed, the archaeological community will continue to be hampered by the lack of useful data. The Shuttle Imaging RADAR data archive for the 1994 missions is still among the most valuable for archaeological use due to its use of the L band RADAR system in various polarimetric modes.

This chapter has defined the theory, operation, and function of RADAR. It has further detailed the theory of SAR systems including SAR configuration and control, target and microwave interaction, as well as polarimetry. An overview of the interpretation of RADAR imagery was given. It has also described the operational capability and characteristics of the active microwave sensor used for this research piece, the NASA Space Shuttle Imaging RADAR SIR-C/X-SAR multipolarimetric system. Finally, it has introduced a derivative Imaging RADAR system carried by the Shuttle Transport System (STS), known as the Shuttle RADAR Topographic Mapping (SRTM) instrument, which performs interferometric remote sensing of the earth's surface.

The next chapter will introduce the methodology employed during this study.

Chapter 4
Methods

"I have measured the coastline of Alba (Britain) and believe it to be 4,875 miles in circumference". Pytheas of Massalia, from "On the Oceans" c. 250 BC. (Healy: 1991: 53).

4.1 Introduction

This chapter describes the methods, materials and technology used within this work. The focus of this investigation was to explore the ability of NASA Space Shuttle multipolarimetric Imaging RADAR (SIR-C/X-SAR) to detect, survey, and analyse, ancient mine sites for their polarimetric RADAR phase difference responses. These sites would also be geographically and topographically analysed to determine their potential to provide archaeological evidence of ancient base-metal mining. Next, the performance capabilities of the Imaging RADAR within temperate, hyper-arid, and semi-arid regions of the world would be examined. As such, supplementary remote sensing data was used to support the microwave investigation in the form of declassified CORONA optical imagery for ground verification and Advanced Very High Resolution Radiometer (AVHRR) imagery for climatic analysis of the Space Shuttle overpass period for each site. The satellite weather imagery was supplemented by local ground-based meteorological data.

Section 4.1.1 presents a general model of remote sensing and mines while potential remote sensing signatures over the mine complexes are discussed in Section 4.1.2. Section 4.2 and 4.3 discuss the geographical and historical desk-based study undertaken to obtain information regarding the site and location of known ancient mines within the study areas. The geographical study covered the physical and historical aspects of ancient mining and was used to create a list of potential target mine sites.

Topographical studies were subsequently performed to obtain information regarding the locations of the selected mines within the area landscape. Digital terrain elevation models, or DEMs, were created from available sources and fused with ground information to perform topographic analysis of each target mine site. This is described in Section 4.4.

The methodology for collecting ground information regarding the target mine sites, area geology, geomorphology and vegetation are then covered in Section 4.5. Mine site history and archaeology based on field survey within the study areas is also covered in this section.

CORONA and AVHRR satellite data processing are described in Section 4.6 and 4.7. Ground based meteorological information is detailed in Section 4.8. Finally, Section 4.9 covers the NASA SIR-C/X-SAR Imaging RADAR data processing and analysis methodology, including filter processes, data fusion and visualisation.

4.1.1 Ancient mines: a general model

Chapter Two of this work discussed the mines found within the study regions of this work; western Scotland, the Sinai and southern Spain. The mines in the study areas shared certain similar characteristics, for example both the South Ardachy, Scotland (Chap. 5) and Conil, Spain (Chap. 6) complexes had rakes, but also numerous differences. Consequently, it is not possible to establish a general model of the spatial layout and industrial features of an ancient mining area. However, it is possible to establish a *general* model of expected remote sensing responses from the features commonly found in a typical mining complex. The following flow-chart illustrates the model process, while Appendix V presents examples of remote sensing signatures from an ancient mining complex that contains a wide variety of industrial and geological features.

The flow-chart should serve as a reference as the remainder of this chapter is read as it is designed to visualise the decision making process utilised in this particular research work.

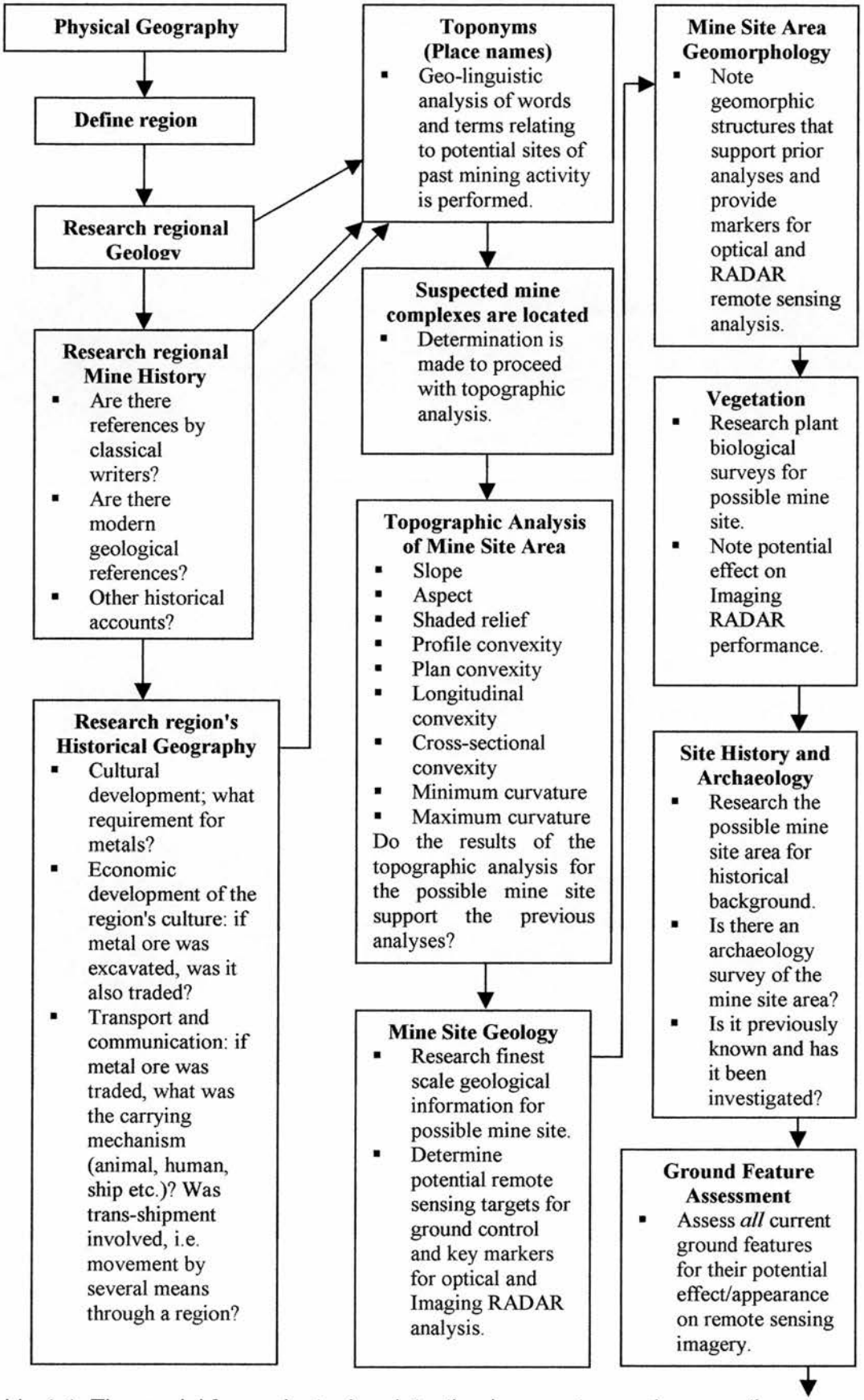

Table 4-1 The model for ancient mine detection by remote sensing - *continues*

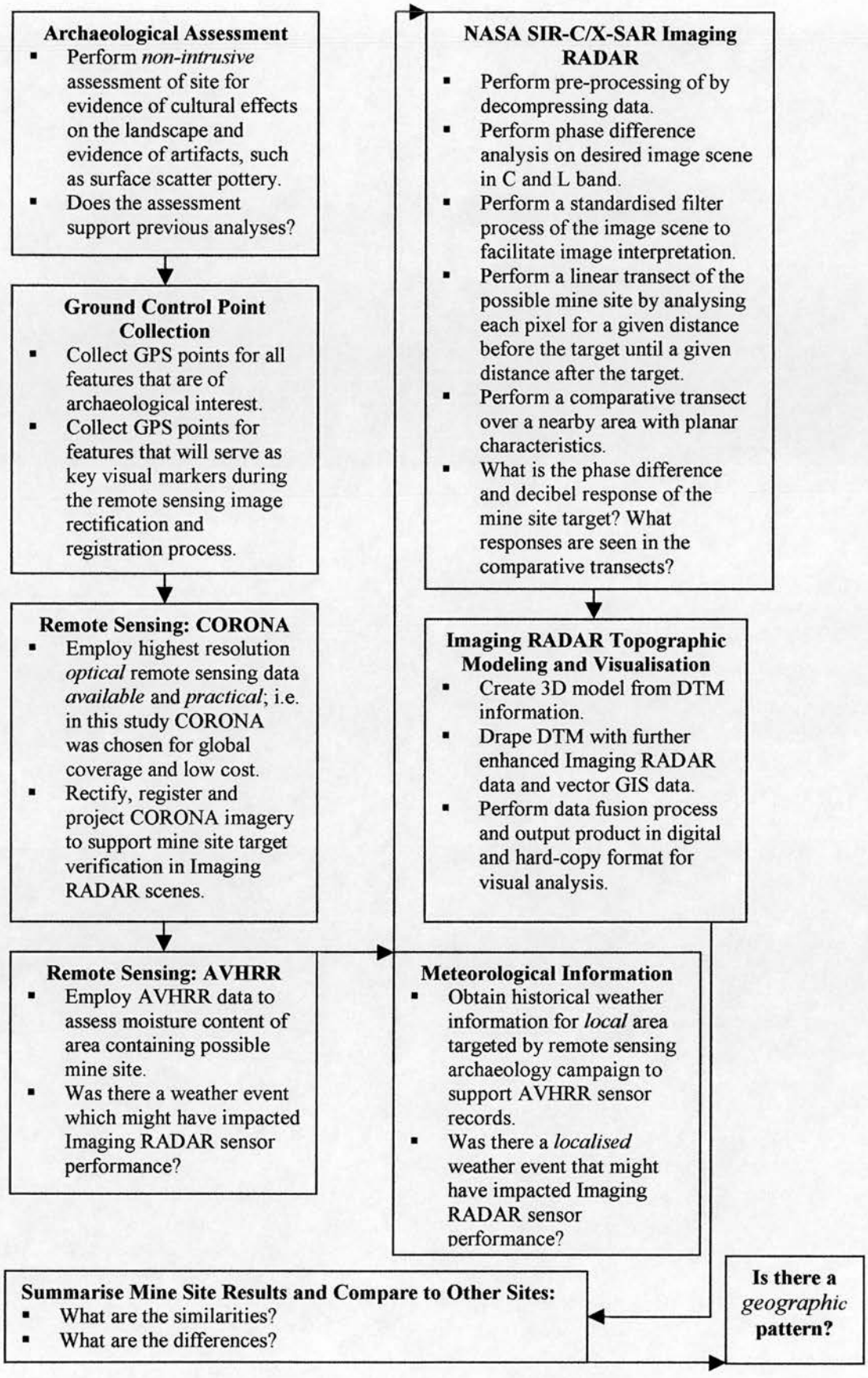

Table 4-1 The model for ancient mine detection by remote sensing

4.1.2 Potential remote sensing responses

As stated, the object of the research was to compare Imaging RADAR responses over ancient mine features in three different environmental regions of the world. However, it was recognised that each mining complex would have unique extraction and processing features. Consequently, it was not possible to compare the same cultural feature at all three sites; for example mine rakes occur only at South Ardachy and Conil. Thus, it was recognised that a specific signature for particular mining features would not be able to be determined based on this limited research, but that probable responses of various sensors could be postulated based on their known performance characteristics.

Table 4-2 displays possible remote sensing responses for a hypothetical mining complex that contains all the cultural features observed at the three research sites. The characteristic column of the table describes the particular mine related feature while the potential effects and responses column describes the responses that may be recorded by optical, RADAR and multispectral systems. This column also notes which band or wavelength of a remote sensing system may be useful in detecting a specific mining related feature.

The three remote sensing systems represented in the table should be understood to be CORONA or SPOT as the optical sensor, NASA SIR-C/X-SAR Imaging RADAR as the RADAR system, and finally, LANDSAT 7 ETM+ as the multispectral system, though it also has optical capabilities as well. While the first two systems (CORONA and SIR-C/X-SAR) are utilised in this research work, LANDSAT 7 ETM+ was not used due to its resolution capabilities and the fact that it was not placed into orbit and calibrated until well after research had begun (Lillesand and Kiefer, 2000 and USGS, 2000). However, it was felt that due to the enhanced capability of LANDSAT 7 ETM+, and its widespread use as a remote sensing data source, that it should be included here. The point is to demonstrate widely available, low-cost remote sensing data providers and how they may assist in remote sensing archaeological work.

It should be stressed here that it would be impossible to predict exact signatures for each and every cultural feature contained within an ancient mining complex due to a multitude of factors such as sensor orientation, mode, set-up, look-angle, range and many more. It is important that Chapter 3 and Appendix V be used as supplementary background to this table. Finally, where the cultural features shown in the hypothetical mining complex of Table 4-2 actually occurred in this research work is represented in the characteristic column. They are represented as follows, South Ardachy = *A*, Serabit El Khadim = *B* and Conil de la Frontera = *C*.

Characteristic feature	Potential effects and possible remote sensing responses for ancient mining features for optical, multi-spectral and RADAR sensors
Topography (*A, B, C*)	Complex or convoluted topography may affect both optical and RADAR systems ability to detect target, especially if a hill or mountain obscures sensor line of sight. Multiple reflecting surfaces may create more noise or *speckle* in RADAR imagery. Medium resolution (10 -30m) optical imagery is good for large area mapping; band 8 (0.52-0.90 at 15m res.) in LANDSAT 7 ETM+ (Appendix V).
Geology (*A, B, C*)	Optical and RADAR responses - Optical systems can provide colour discrimination of geology type; RADAR can assess structure, texture, and surface orientation. LANDSAT 7, band 7 (2.09-2.35) good for determining rock and mineral type (Chap. 3 and Appendix V).
Vegetation (*A, C*)	Optical systems can discriminate colour of geology; RADAR in C-band can possibly determine leaf orientation, density. L-band in hh polarimetric mode can possibly penetrate vegetation cover to assess soil moisture and structure; RADAR dependent on sensor orientation and settings. LANDSAT 7, band 4 (0.75-0.900) for determining vegetation type and biomass, band 5 (1.55-1.75) for vegetation moisture content, band 6 (10.40-12.50) for vegetation stress analysis potentially caused by metal contaminants (Chap. 3 and Appendix V). LANDSAT band *combinations* are critical in this process.
Quarry (*B*)	Detection by optical system dependent on available light, sensor orientation and weather; RADAR detection dependent on size, geology and surrounding complexity of the topography; RADAR dependent on sensor orientation and settings to the target. LANDSAT 7, band 7 may prove useful for geologic analysis if feature is sufficient size, band 8 may be able to map feature (Chap. 3, Appendix V).
Trial workings (*A, B, C*)	Optical systems offer no descriptive value; depends on sun angle. RADAR should register change in phase difference but decibel response depends on shape and orientation of the feature to the antenna as well as mode, wavelength, sensor orientation and settings (Chap. 3). Medium resolution optical systems (10-30m) have insufficient resolution to identify individual workings.

Table 4-2 Potential remote sensing signatures for ancient mining features *continues*

Tailing dump, spoil and slag heaps (*A, B, C*)	Optical system detection dependent on sunlight, sensor orientation, spatial resolution and weather; appearance will vary with sunlight amount. RADAR in C band may show brighter responses on cracked rock that is close in size to wavelength. L-band in vv polarimetric mode may detect moisture content while hh polarimetric mode determines assists in determining orientation; RADAR dependent on sensor orientation, settings and resolution. LANDSAT 7, band 6 (10.40-12.50) may determine vegetation stress due to pollution if plants present on feature are of sufficient size or biomass; other bands in the visible region will also assist in this process. Band 7 (2.09-2.35) could determine rock type if close to resolution capability of sensor (Chap. 3 and Appendix V). As before, *combinations* of bands are important in detection of appropriate geological features.
Rakes and adits (*A, C*)	Optical system detection dependent on sunlight, sensor orientation, resolution and weather; appearance will vary with sun elevation. RADAR in C band may show brighter responses on cracked rock that is close in size to wavelength. L-band in vv polarimetric mode may detect moisture content or orientation in hh polarimetric mode; RADAR dependent on sensor orientation, settings and resolution. LANDSAT 7 or other medium resolution optical sensors may detect features using panchromatic data in band 8 (0.52-0.90)(Appendix V).
Buildings (*B*)	Optical sensors dependent on solar elevation, sensor orientation, resolution and weather. RADAR may record double-bounce effect in either wavelength; RADAR dependent on sensor orientation, settings and resolution. LANDSAT 7, band 8 (0.52-0.90) may detect individual structures for mapping purposes (Chap. 3 and Appendix V).

Table 4-2 Potential remote sensing signatures for ancient mining features

4.2 Physical Geography and Geology

4.2.1 The Physical Geographies

The mine study areas were chosen on the basis of commentaries from three classical writers, Herodotus of Halicarnassus, Pliny the Elder, and Strabo. The first two were historians, the latter a geographer. Regional selection of mining is described below.

4.2.1.1 Regional Selection

4.2.1.2 Britain and the Hebridean Islands

Strabo remarked upon the voyage of Pytheas of Massalia, possibly the first sailor to circumnavigate the British Isles c. 250 BC (Cunliffe, 2001). Strabo records that Pytheas visited the tin mines of Cornwall and from other sources noted that, "of the metals, they have tin and lead" throughout "at least ten islands" (Strabo, trans. Jones, 1906). Unfortunately, a book written by Pytheas entitled *On the Ocean* has been lost to modern historical geographers, but Strabo may have worked from a copy (Cunliffe, 2001). Pytheas may have been alluding to the Hebridean Islands and Ireland. The island most well known for lead mining in the Irish Sea is the Isle of Islay. Furthermore, it was known that silver was sometimes processed from the large quantities of silver ore (Smith, 1895). The location, historical commentary, extensive archaeological surveys, complex geology, and previous geo-chemical analysis of mine sites, coupled with a temperate climate, made Islay a logical choice as a target mine site.

4.2.1.3 Egypt and the Sinai

Pliny the Elder describes "copper from Egypt" and "emeralds so hard that they are not able to be marked" (Pliny, trans. by Rackham, 1991). The ancient Egyptian mining area most well known for having both copper ore and gemstones within the same context is Serabit El Khadim, in the Sinai Peninsula. This was also a site with an arid climate, moderate historical commentary, and rudimentary archaeological survey (Petrie, 1906). Some modern archaeological work based on examining the metallurgical processes used at Serabit El Khadim was performed in the late 1970s and early 1980s, but extensive examination is still lacking at the mine workings (Bartov, 1985, Greenwood, 1997, and Rothenburg, 1979).

4.2.1.4 Spain

Herodotus records that Colaios, a seaman from Greece, was forced through the Straits of Gibraltar on a voyage to Africa because of a storm. After the storm ended, Colaios entered the mouth of a large river north of the Straits, thought to be today's Guadalquivir River in Spain. After sailing upstream, he discovered a region wealthy with silver and managed to trade for 60 talents of silver, which was equivalent to some 1000 to 2000 kg of ore (Herodotus, 1972). This silver rich region came to be known as Tartessos, or Tarshish, today's Andalucian region in Spain. The discovery of silver caused the Phoenician Trade Empire to expand westward and led to the construction of the port of Gadir, today's Cadiz (Aubet, 1987). Based on this historical commentary, demonstrated archaeological evidence of ancient mining north of the Rio Guadalquivir, and the presence of a semi-arid climate, the Andalucian region was chosen as a study area for mine site detection. The model used to detect the previously unknown ancient mine site at Conil is described in Appendix IV.

4.2.2 The Geology

The geology for each region surrounding a target mine site was scrutinised by a desk-based study of available publications and was extensive in scope. The British Geological Survey provided information regarding Islay, the Egyptian Geological Survey for Serabit El Khadim, and the Instituto de Geominera de Espana for the discovery at Conil in Andalucian Spain.

4.2.3 The Minerals and Mines

Since the classical writers knew each mine site for a particular metal ore, information was sought concerning the known presence of other minerals and mining works. Sources for the economic mineral history of each target mine site region were evaluated during the desk-based study. Sources included modern geological surveys, historical accounts, archaeological reports and other published sources.

4.3 Historical Geography

4.3.1 Historical Geography: research methods

An extensive desk-based historical geographic study was undertaken for each site after a thorough understanding of the physical geography of each site had been reached. It was decided that the historical geography for each site would be reviewed up until the period of time when each mine site was alleged to have been in existence.

The rationale for this approach was that understanding the particular characteristics of the culture and economy in existence at the time of the mine's operation would yield information concerning its size, location, and transport access. Other issues, such as post-abandonment use of the landscapes e.g. agriculture at Islay and Conil, and any remedial land recovery efforts were also noted.

4.4 Location of the mine complexes

The desk-based study of the physical and historical geography of each mining region revealed the location of each mine complex, with the exception of Conil, which was discovered during the field survey campaign.

4.4.1 Site topography and analysis

After determining the location of the target mine sites, a topographic analysis of the region surrounding each mine complex was performed using a Digital Terrain Elevation Data subset equivalent to a level 1 parameter, i.e. one verifiable elevation point every 90 metres on average (NIMA, 2001). This was deemed necessary in order to model each mine site within its surrounding landscape.

The Islay and Serabit El Khadim data sets were Level 0 products (1 elevation point per kilometre), improved by converting the data product to a point GIS coverage, plotting in elevation points from topographic maps of the area immediately surrounding each mine site, then re-converting the data into a grid in ENVI 3.4 software (ENVI, 2000). The Conil data set was a Level 1 product provided by the Oficina de Cartografia de Junta de Andalucia. The data subset boundary for each mine site was set to the same limits as the NASA SIR-/X-SAR Imaging RADAR data subset for three-dimensional modelling purposes and to speed processing time.

4.4.1.1 Topographic analysis

The topographic analysis was composed of the following examinations: slope, aspect, shaded relief, profile convexity, plan convexity, longitudinal convexity, cross sectional convexity, minimum curvature, and maximum curvature (Wood, 2001). Each analysis process is defined in the following sections.

4.4.1.2 Slope

Slope was measured in degrees with the convention of 0 degrees for a horizontal plane. The slope and curvature of the surface determined the morphometric feature. For example, a sloping surface that is concave in the cross-sectional direction is a channel. A sloping surface that is convex in the cross-sectional direction is a ridge. Peaks have a convex cross-section and convex longitudinal curvature while pits have concave curvatures. Passes have one convex curvature orientation and one concave curvature orientation (Wood, 2001).

4.4.1.3 Aspect

Aspect, in topographic terms, describes the orientation of primary terrain faces toward a given point. The aspect angle of the terrain surrounding each mine complex was measured with the convention of 0 degrees to the north (up) and angles increasing clockwise (Wood, 2001).

4.4.1.4 Shaded Relief

A shaded relief for each mine complex was computed using a sun elevation angle in conjunction with a sun azimuth angle. This gives an invaluable representation of how the target scene on the earth's surface would normally be illuminated in cloud free conditions by visible sunlight in comparison with the Imaging RADAR data (Wood, 2001 and NIMA, 2001).

4.4.1.5 Profile convexity

Profile convexity analysis measures the rate of change of the slope along the profile of each ridgeline. Intersecting the plane of the Z-axis and the direction of the aspect does this. Profile convexity works in conjunction with the following plan convexity analysis, so they should be considered in conjunction. The plan convexity (intersecting with the XY plane) measures the rate of change of the aspect along the plan. These two surface curvature measures are in orthogonal directions with profile convexity in the direction of maximum gravity effects and plan convexity in the direction of minimum gravity effects (Wood, 2001).

4.4.1.6 Plan Convexity

As mentioned in Section 4.4.1.5, the plan convexity (intersecting with the XY plane) measures the rate of change of the aspect along the plan. This analysis was performed in conjunction with the profile convexity analysis (Wood, 2001).

4.4.1.7 Longitudinal Convexity

Longitudinal curvature (intersecting with the plane of the slope normal and aspect direction) and cross-sectional curvature (intersecting with the plane of the slope normal and perpendicular aspect direction) are measures of the surface curvature orthogonally in the down slope and across slope directions, respectively (Wood, 2001).

4.4.1.8 Cross sectional curvature

As mentioned in Section 4.4.1.7, cross-sectional convexity, or curvature (intersecting with the plane of the slope normal and perpendicular aspect direction) is a measure of the surface curvature orthogonally across slope directions (Wood, 2001).

4.4.1.9 Minimum curvature

An analytical technique where the surface area with the least amount of curvature is detected (ENVI, 2001).

4.4.1.10 Maximum curvature

This analysis performs the opposite analysis of the minimum curvature process by computing the areas of maximum curvature within a given area, thus defining feature areas that demonstrate increased water flow velocity or more aspect, as examples (ENVI, 2001 and Wood, 2001).

After topographic modelling of each mine complex was performed, field surveys were undertaken to determine an appropriate mine working, or feature, which would become the actual test Imaging RADAR site. The Isle of Islay was visited during April in 1999 and November 2000, the Sinai was visited from December 1999 to January 2000, while Spain was visited from February until May of 2000. During the field surveys, geology, geomorphology, vegetation, site history, archaeology, ground feature inventory and image ground control were performed. These processes are described in the following sections.

4.4.2 Geology of the sites

Significant geological features for each site were noted against the applicable geological surveys and maps acquired during the desk-based study, as well as those obtained during fieldwork. Features, which would be prominent from RADAR interrogation, were noted.

4.4.3 Geomorphology

The geomorphology of each mine site area was noted and compared against the U.S. Soil Conservation Service's guide on soil taxonomy as well as the applicable surveys reviewed during the desk-based survey of the physical geography of each region (U.S. Conservation Service, 1985). The structure of the geomorphology was noted for its possible effect on microwave response.

4.4.4 Vegetation

The vegetation of each mine site was noted and compared against the reference materials uncovered during the desk-based study of each region's physical geography. Where possible, local names for vegetation were recorded. Particular attention was paid to vegetation that may have had an effect on microwave backscatter processes. For example, leaf size was measured and vegetation density was noted.

4.5 Site History and Archaeology

4.5.1 Historical Background

The historical background for each mine complex, where available, was examined against the actual existing site features and any local knowledge, if available. In the case of South Ardachy, extensive historical material was available, for Serabit El Khadim there was moderate commentary, and for Conil there was no historical documentation.

4.5.2 Site archaeology and survey

Site archaeology and survey for South Ardachy and Serabit El Khadim were based on previously archaeological research campaigns to discover the extent of site change. The South Ardachy survey was based on the 1994-95 campaign of Cressey (1995), while the Serabit El Khadim survey was a re-examination of Petrie's 1904-5 Sinai campaign (Petrie, 1906). Conil was a new discovery in an ore-bearing region.

4.5.3 Ground Features

Current ground features such as earthworks and local high points, were noted and described in order to determine their existence at the time of the NASA SIR-C/X-SAR Imaging RADAR campaign in 1994 and to determine their effect, if any, on microwave responses. Site changes from the original archaeological surveys were also noted for South Ardachy and Serabit El Khadim.

4.5.4 Archaeological assessment

A walkover survey was carried out at each site to identify any new features such as surface scatter of pottery or any other significant artifacts. Assessment was limited to surface artefacts and features, as the purpose of this study was to be a non-intrusive remote sensing survey of each target mine site.

4.5.5 Ground control campaign

During the field surveys, ground control points were collected using a Magellan 2000 Global Positioning System (GPS) receiver with 12-channel acquisition capability. Since the Selective Availability (SA) function had been removed by the U.S. Air Force, it was deemed unnecessary to use a survey-quality GPS system. This is because the resolution of the GPS signal ensured a resolution of within 10 metres of actual ground point; the Imaging RADAR data had a resolution of ~9.5 to ~12.5 metres (Wysocki, 1991 and USCGNC, 2001).

Averaging of the GPS positions was performed, as it is a well-known technique for improving the accuracy of the reading (Wysocki, 1991). Each position is the result of taking 5 position readings at eight-minute intervals, then deriving the average. In particular, this was important in Spain due to image layover, which caused displacement of mountain peaks in some areas of the image scene (Sabins, 1987). This caused no local displacement for the Conil site area, however, due to its coastal location.

The registration and projection process used ENVI 3.4 in which a cubic convolution re-sampling procedure was applied to each image (ENVI, 2001). The cubic convolution procedure uses 16 pixels to approximate the *sinc* function while using cubic polynomials to re-sample the image scene, giving a greater level of accuracy in the projected image scene and generally better visual clarity (Jensen, 1986, ENVI, 2001).

On Islay, sixteen ground control points (GCP) sites were utilised in conjunction with co-ordinates obtained from an Ordnance Survey topographic map to obtain a root-mean-square (RMS) error of 0.92 pixels for the RADAR scene (Appendix I). In the Sinai at Serabit El Khadim, twenty-three external GCP sites were used, with 122 GCP internal sites within a 2-kilometre range of the target mine site (Appendix II). This was done to ensure high, local area ground accuracy to image scene position, ensuring that the target mine site was properly identified and analysed (Druss, 1992). RMS for both the Imaging RADAR scene and CORONA imagery was 0.8 pixels for the target mine site area. In Spain, over 250 GPS positions were taken and averaged at 90 GCP stations (Appendix III). The RMS for the Imaging RADAR scene and CORONA imagery was 0.0297 pixels.

4.6.1 CORONA Imagery: Implications and Uses

CORONA was the first fully operational space reconnaissance project for the United States government. The CORONA program was originally endorsed and begun under the administration of President Eisenhower in February 1958. Its first successful mission was on August 18, 1960, and it operated for twelve years during the Cold War. It was developed as a joint project of the CIA and the USAF, a relationship that evolved into the National Reconnaissance Office (NRO). On the 24th of February 1995 this data was declassified by presidential order (Day *et al.*, 1998).

The declassified imagery provides an extensive and inexpensive optical coverage of the Earth. It contains imagery collected during the period 1960-1972 from throughout the world with significant emphasis on Eastern Europe and Asia. Due to the large image archive and its near-global coverage it was chosen as the sensor system for target scene verification (USGS, 2001).

4.6.1.1 CORONA satellite imagery processing and subsets

The spatial and temporal characteristics of the declassified historical satellite imagery were 2 metres on the KH-4 and KH-6 platforms, which were the systems that supplied the data for this study (USGS, 2000). The data for this investigation were taken from the following temporal collection dates: Ardachie, Islay on 20 August 1960, Serabit El-Khadim, the Sinai on July 12, 1972 and Conil, Spain on April 14, 1972. The Islay data were taken in single, panoramic mode, while the Serabit El-Khadim and Conil data were taken in stereographic mode.

Figured resolution for the Islay data was approximately 3 metres due to orbital wobble as the early CORONA platforms suffered from primitive navigational guidance systems (Day *et al.*, 1998). The Serabit El-Khadim and Conil data, on the other hand, were examples of the later CORONA stereographic systems operating at optimum conditions with a figured resolution of *less* than 2 metres. The performance of this system exceeded all but the most expensive commercially available panchromatic imagery at the time of this study (Fowler, 1996).

The CORONA data for this study were received from the United States Geological Survey's Earth Data Archive Centre in South Dakota in the form of high-resolution KODAK images reproduced from an original camera negative. The paper-backed image product was approximately one-half metre in length by some 75mm in width (USGS, 2001).

The image products were scanned into a digital product at 2,400 dpi for induction into the ENVI 3.4 remote sensing software. The Targa Interchange File Format (TIFF) was used for ease of conversion to a Geo-TIFF product, which upon image registration, rectification and projection stores the world co-ordinates within the first lines of the file itself. Geo-TIFF is the accepted international image files standard for cross-platform use between remote sensing and GIS softwares (ENVI, 2001).

The digital CORONA images were then projected, registered and rectified using ground control position obtained during field surveys. The Universal Transverse Mercator (UTM) co-ordinate system and WGS-84 datum were used for standardisation to the global positioning system (GPS) system (NIMA, 2001). Geocorrection accuracy, or RMS, for the Sinai data set was 0.8 pixels and 0.0297 pixels for the Conil, Spain data set.

4.7 AVHRR Satellite Imagery

The Advanced Very High Resolution Radiometer (AVHRR) is a broad-band, four or five channel (depending on the model) scanner, sensing in the visible, near-infrared, and thermal infrared portions of the electromagnetic spectrum. It was chosen for use in this study to supply imagery indicating weather conditions at the time of RADAR coverage as it had an on-line data archive maintained by the U.S. National Oceanographic and Atmospheric Administration (NOAA) which contained 1994 climate data (NOAA, 2001).

AVHRR data are acquired in three formats: High Resolution Picture Transmission (HRPT), Local Area Coverage (LAC), and Global Area Coverage (GAC). Only LAC and GAC imagery were used in this study. LAC imagery has a nominal resolution of 1.1 km while the GAC imagery has a 4.4-km nominal resolution.

The AVHRR data used for this study were obtained from the U.S. Government's NOAA Internet Satellite Active Archive (SAA) archive site (NOAA, 2001). Data takes were downloaded for the 48 hour period preceding the NASA Space Shuttle Imaging RADAR system mission overpass at each target scene mine site.

The data were processed using ENVI 3.4 by first performing a calibration routine, then geo-referencing the data into the UTM co-ordinate system, using a WGS 84 datum, where applicable. GAC imagery was processed over the Isle of Islay and Sinai Peninsula region, while only LAC imagery was available over the southern Spain area. It should be noted that the calibration routine for this data was developed for NOAA-12 to 16 series satellites. The data used in this study was from NOAA-11, and the level of data degradation is unknown (ENVI, 1999).

4.8 Meteorological Data

4.8.1 Meteorological Office Data

Ground-based meteorological information was provided by the United Kingdom Meteorological Office, the Egyptian Meteorological Service, and the United States Navy Meteorological and Oceanographic Command, Naval Station Rota, Spain. Data, where available, were averaged for the 24 hour period immediately preceding the NASA SIR-C/X-SAR orbital overpass in 1994. Information collected included temperature, rainfall, wind direction, relative humidity, and wind speed.

4.9 NASA SIR-C/X-SAR Imaging RADAR, data and analysis techniques

4.9.1 The Imaging RADAR

The NASA SIR-C/X-SAR is a multipolarimetric Imaging RADAR system flown aboard the space shuttle with two flights from April 9-20, 1994 and September 30 to October 11, 1994. A modified version of the original unit was re-configured for interferometry and designated as the Shuttle RADAR Topographic Mapping system in 1999. This system flew in 2000, however data from this system was unavailable during the course of this investigation (NASA, 2001). A detailed description of the operational principles of Imaging RADAR and this system are given in Chapter 3 of this work.

4.9.2 Data Processing

Data was selected from the interactive USGS satellite data archive and ordered (USGS, 2001). The data were received from the USGS Earth Data Centre in a Stokes Matrix compressed data format stored on 8mm hi-quality digital tape cassettes (Curlander *et al.*, 1992). The data were decompressed from their stored format using ENVI 3.4 remote sensing software and stored on a computer hard drive.

4.9.3 Imaging RADAR data analysis

4.9.3.1 Analysis form and test site

A standard process was used to evaluate the capability of NASA SIR-C/X-SAR Imaging RADAR to detect, survey and analyse ancient mine sites. A portion of each mine site was selected and transected in a linear fashion by analysing each pixel for x pixels, beginning at a point which was deemed to give a normal decibel return and phase difference.

The transect for each mine site was oriented north to south, beginning at pixel x by y and ending at pixel $_x$ by $_y$, again spanning the mine from normal signal return surface to normal signal return surface for reference purposes. Both C and L bands were analysed for decibel strength and polarimetric phase difference.

4.9.3.2 C band Imaging RADAR analysis

An image subset was created from each overall image scene to facilitate processing time. South Ardachy, dubbed Site "A" utilised a 200 x 200 pixel subset, with each pixel encompassing 12.5 metres of earth terrain. An 11 pixel transect was used. A comparative transect was taken on nearby flat terrain.

The Serabit El Khadim site, known as Site "B", used the same dimensions. This site used an 11 pixel transect. A comparative transect was taken within a nearby wadi, or desert ravine, which was flat and composed of alluvial and aeolian depositional materials.

Conil, designated Site "C", used a 374 x 350 pixel subset. This is because the mine complex was previously unknown and extended in length outside a 200 x 200 pixel subset area. A 10 pixel transect was used at this site. The comparative transect was taken on nearby fallow agricultural field.

4.9.3.3 L band Imaging RADAR analysis

L band Imaging RADAR data were analysed in the same manner as the C band, described in Section 4.9.3.2.

4.9.3.3.1 Comparative transects

A portion of the South Ardachy mine complex was chosen to demonstrate the capability of the multipolarimetric Imaging RADAR system in sensing topographic change. A similar number of pixels were used as the primary transects. These data were analysed in the same manner as data described in Section 4.9.3.2.

Comparative transects were taken at Serabit El Khadim and Conil in the same manner as South Ardachy. However, at the Conil mine site a nearby operational open pit mine was also used for comparison. In this case a sample pixel was extracted from an area within the mine which was similar in shape and examined for decibel and polarimetric phase difference.

4.9.3.4 Comparative analysis

At each target mine site, the polarimetric phase difference was examined and compared against the opposing wavelength. A photograph and map of the feature accompanied this comparison. After this analysis, the entire image scene was subjected to filter and image enhancement processes before three-dimensional modelling and visualisation, which is described in Section 4.9.4. This was done to provide maximum enhancement of the analysis results and demonstrate the potential for result visualisation within a virtual landscape.

4.9.4 Imaging RADAR topographic modelling and visualisation

4.9.4.1 Data fusion and representation

It has been an accepted practice for RADAR remote sensing analysts to utilise Digital Terrain Models (DTM) whenever available with imagery to verify ground range correction (overlay problems) and for techniques such as SAR shape-shading (Kober, 1991). It also assists archaeologists in site and settlement pattern analyses, for precise analysis of micro-topographies can reveal subtleties not apparent to the human eye (Barasino and Helly, 1985).

DTED (Digital Terrain Elevation Data) Level 0, a product of the National Imagery and Mapping Agency (NIMA) of the U.S. government was used to produce a grid of the same area as the MLC data set. This grid was then converted to a point file. Elevation points from each mine area were then extracted from available topographic maps and added as additional points to the master points file. This file was then re-converted into a grid file and ingested by ENVI 3.4 to create a Digital Terrain Model (DTM). The preference for NIMA terrain products are that they are data sets that are available for global coverage with verifiable corner point accuracy.

The most important factor in RADAR terrain analysis is high accuracy in target location. The master DTM, originally in a geographic co-ordinate system and WGS-84 datum was then rectified, registered and projected into the Universal Transverse Mercator projection, using WGS-84 where applicable.

Before the projected RADAR images were overlaid onto the DTM, it was decided to further enhance the visualisation of the topography by creating a pseudo-colour image (Kruse and Dietz, 1991). The premise behind this technique was to enable of comparison of the different detection capabilities of the particular RADAR wavelengths and polarisations, and if desired, other spectral remote sensing data (Daily *et al.*, 1992). But first, a filtering process was employed to give maximum enhancement to image scene features.

4.9.4.2 Filter processes

An adaptive filter regimen was used against all data sets. Adaptive filters are utilised to diminish the speckle noise in a RADAR image while preserving textural information. The Lee and Frost filter processes were chosen for these data sets due to their usefulness in preserving textural information (Lee, *et al.*, 1994).

The Lee filter is a standard deviation based (sigma) filter used to reduce data with considerable noise whose relative intensity is related to the overall image scene, but which has an additive and/or multiplicative component. It filters the data based on statistics acquired from the calculations performed within individual filter windows (Lee, 1981). This type of filter processing also preserves maximum image detail. After reviewing the results of the Lee filter process, it was decided to employ a Frost filter due to its capacity to preserve edges in RADAR imagery (ENVI, 1997). As the focus of the overall endeavour was to locate the edges and extents of the target mines and surrounding topography, it was felt that this step would be fruitful.

While the Frost filter is an adaptive filter, its function is different than the Lee. It derives its results by operating as an exponentially damped circularly symmetric filter utilising the local area statistics (Lee *et al.*, 1994). The pixel that is subjected to filtering is replaced by a value calculated upon the distance from the filter centre, the damping factor, and the local variance. Thus, it may be seen that this form of filtering is localised to the specific variances of the image data, thus preserving and subtly enhancing topographic features.

The Frost filter was used only once on each data set as favourable results were achieved and because further processing would cause data degradation (Holcomb, 1992).

A pseudo-color Imaging RADAR scene may be generated from 3 different polarisations and by then assigning them as a Red, Green, and Blue band to form a false colour image (Kruse, 1996).

Finally, the composite image was created and overlaid upon the Digital Elevation Model (DEM). Three-dimensional image scenes of the fused RADAR and DTM data were created from a north, south, east and west vantage-point for each image scene subsets. Results were interpreted for the viewer.

4.10 Summary of results

4.10.1 Imaging RADAR and the topography

A summary of results was created for each target mine site area, then compared against each other, for overall conclusions, which are presented in Chapter 8 and 9.

The methodology employed in this research study has been outlined. The next chapter, Five, will discuss the results of the Imaging RADAR investigation of the South Ardachy mines located on the Isle of Islay, Scotland.

Chapter 5
South Ardachy, Isle of Islay

5.1 Introduction

This chapter presents the results of the Imaging RADAR (NASA SIR-C/X-SAR) archaeological survey of the South Ardachy mines located on the Isle of Islay, Scotland. Section 5.2 is a description of the physical geography of the island, which is followed by a historical geography in Section 5.3. Site topography and analysis are outlined in Section 5.4. Section 5.5 presents site history and archaeology, while Section 5.6 displays the CORONA satellite imagery. Section 5.7 presents AVHRR data immediately preceding the overpass of the Space Shuttle and its Imaging RADAR system. Section 5.8 covers the local meteorological data immediately preceding the overpass of the Shuttle Transport System (STS). Detailed Imaging RADAR analysis data is outlined in Section 5.9. Section 5.10 concludes the chapter with a summation of the data presented.

5.2 Physical Geography and Geology

5.2.1 The Physical Geography of Islay

The Isle of Islay (55° 50′ N, 6° 15′ W) is the southernmost island in the chain of islands known as the Inner Hebrides, which lie alongside mainland Scotland to the west (BOS, 1987). Islay lies 30 miles from the north coast of Ireland and virtually the same distance away from the Scottish mainland at Kintyre (Fig. 5-1).

The dominant physical geographic components of Islay are Loch Indaal, Loch Gruinart and Beinn Bheigier. Loch Indaal and Loch Gruinart are sea lochs that almost divide Islay in two with only low flat land lying between the eastern and western halves of the island. Beinn Bheigier is the dominant high ground on the island and is located on the south-eastern portion of its mass with an elevation of 494 m.a.s.l. Other significant topographies on the island are the Rhinns of Islay, a rugged set of low rock hills running in a north-easterly direction up Islay's Atlantic flank, and The Oa, a high rugged terrain on its south-eastern side bisected by steep valleys running inland from the sea (Jupp, 1994).

Due to its seaward location and the proximity of Ireland, and its physical isolation from mainland Scotland due to the latter's mountainous western spine, the development of Islay has been based on maritime transport and communication (Williams, 1997).

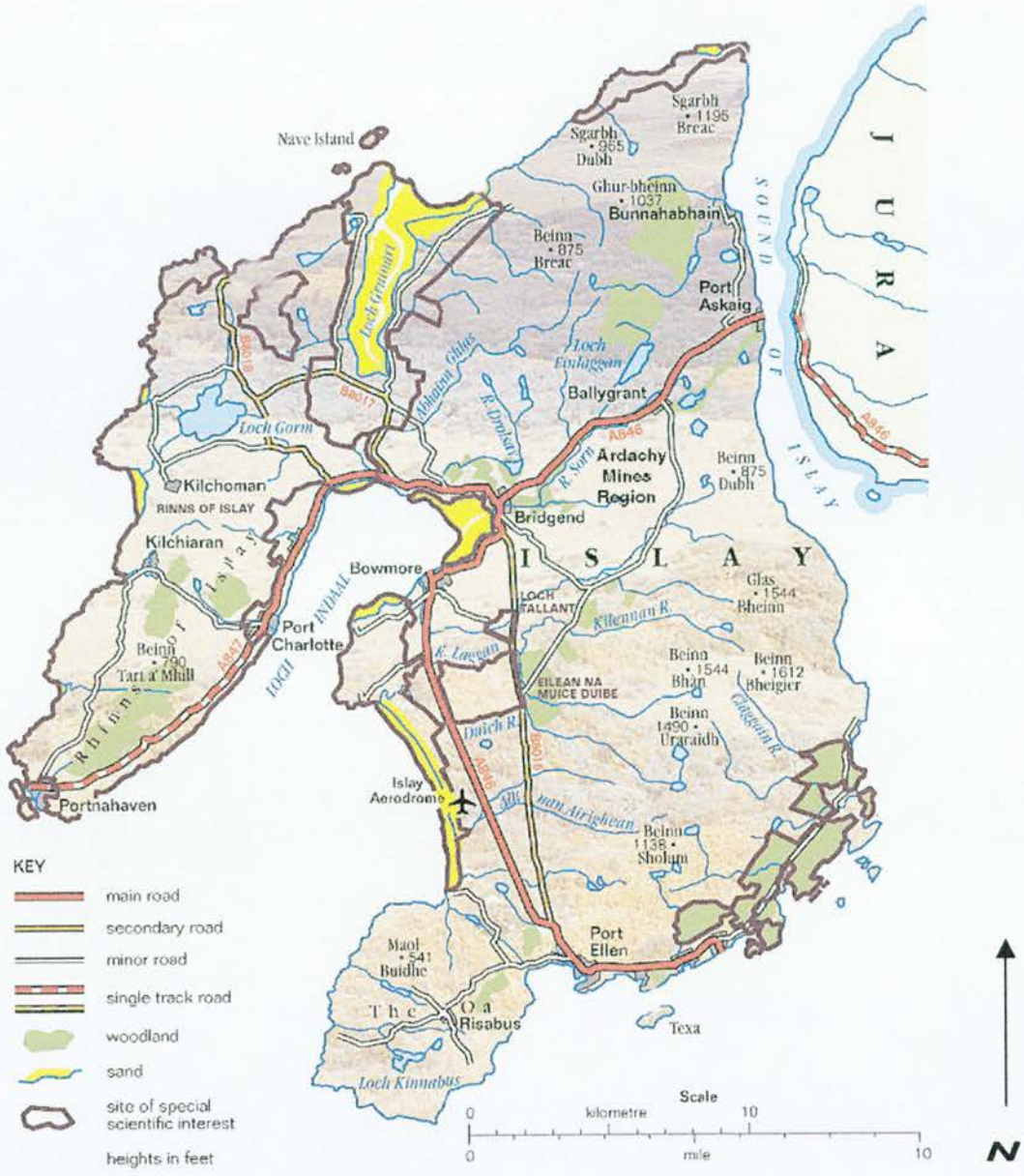

Fig. 5-1 The Isle of Islay, Scotland (Based on NIMA, OSGB data).

5.2.2 The Geology of Islay

Islay displays both unique and shared geological characteristics within a very small geographic area; this is due to its proximity to the northernmost coast of Ireland and the Argyll Peninsula of western Scotland. The island's unusual geological construction has been of interest to geologists due to its complex and convoluted lithologies, but it may be understood to contain three basic components.

The eastern portion of the island is comprised primarily of Dalradian metamorphic rocks such as quartzites, limestones and phyllites, which immediately represent all of the island's three basic components (Fig. 5-2). The blue-gray limestones are generally to be observed within the Lossit Limestone (formerly dubbed Islay limestone) and Ballygrant Formations that lie within the Blair Atholl sub-group of the Dalradian sequence. The major slates and phyllite sequences of Islay form part of the Bharradil Member of the Ballygrant Formation.

The underlying geological structure of the western area of the island is known as the "Rhinns Geological Complex". There are two principal lithologies forming the structure in this region, one of which is composed of Lewisian gneiss with the intrusive epidiorite and hornblende schists (Muir et al. 1994). The soils are young in geological terms having been formed only over the previous 10,000 years, providing fertile arable and improved pasture on the limestone with rough grazing in acidic regions. Peat can be found on Islay in large tracts that account for some 25 % of the island's surface area (Cressey, 1995).

The second major structural influence on Islay's geology is the glacial erosion experienced throughout the Scottish Highlands and Inner Hebrides during the Quaternary Period. Due to the location of the Inner Hebrides immediately west of the Highlands they were mostly glaciated by the Highlands ice-sheet (Late Devensian ice-sheet). The islands of Mull and Skye are the exception to this action; having been covered only by locally nourished ice sheets during the last glacial period (Sissons, 1974, 1977, 1983).

Sissons also suggested that the Loch Lomond Readvance terminated within the Inner Hebridean Islands (Sissons, 1981). Synge and Stevens, however, have refuted this, claiming that the western area of the ice-limit in western Islay lies in the form of an end moraine complex that transects the middle of the Rhinns region below Loch Gorm (Synge and Stephens, 1966). Dawson (1982) further refutes this claim with the evidence of an ice-limit near the head of Loch Indaal where an end moraine extends for some 8 km. It is here that a series of deposits occur as an assemblage of ridges and depressions that include many linear features of fluvial-glacial origin. Islay also hosts series of Late Glacial raised beaches along with impressive Post Glacial shorelines. These can be seen at the head of Loch Indaal and were extensively surveyed by Dawson (1982).

5.2.3 The Minerals and Mines of Islay

5.2.3.1 Minerals

Copper, iron, lead and manganese are found on Islay. Silver was also produced during the late 19th century at the Mulreesh mine complex where some 2500 troy ounces were produced from lead gangue (Cressey, 1995).

5.2.3.2 Mining

While historical evidence and Gaelic oral stories suggest that the mining of minerals on Islay began in the 12th century, no firm evidence has been found to support this claim. However, the culture of the Hebrides during the period of the "Lord of the Isles" was that of a maritime power based on good communications by sea with easily transportable and marketable commodities (McDonald, 1997). The economic significance of exploiting mineral deposits would have been important in the development of the Islesmen's cultural, military and political power.

Lead was mined from some 12 narrow veins that trend along a 035-135° axis over an area of some 40 km² (Gallagher 1991). The lead mineralisation is associated with the Dalradian Limestone, dolorites and phyllites, known collectively as the Lossit Limestone which outcrop around Ballygrant village. The dominant sulphide mineral in the area is galena, with lesser chalcopyrite and sphalerite also in abundance. The principal gangue minerals in association with the galena are breccias of calcite and dolomite with subordinate quartz (Fig. 5-2). It should be stated here that the definitive work concerning mining on Islay is Cressey's environmental archaeological study, which was the foundation for the ground truthing campaign of this work (Cressey, 1995).

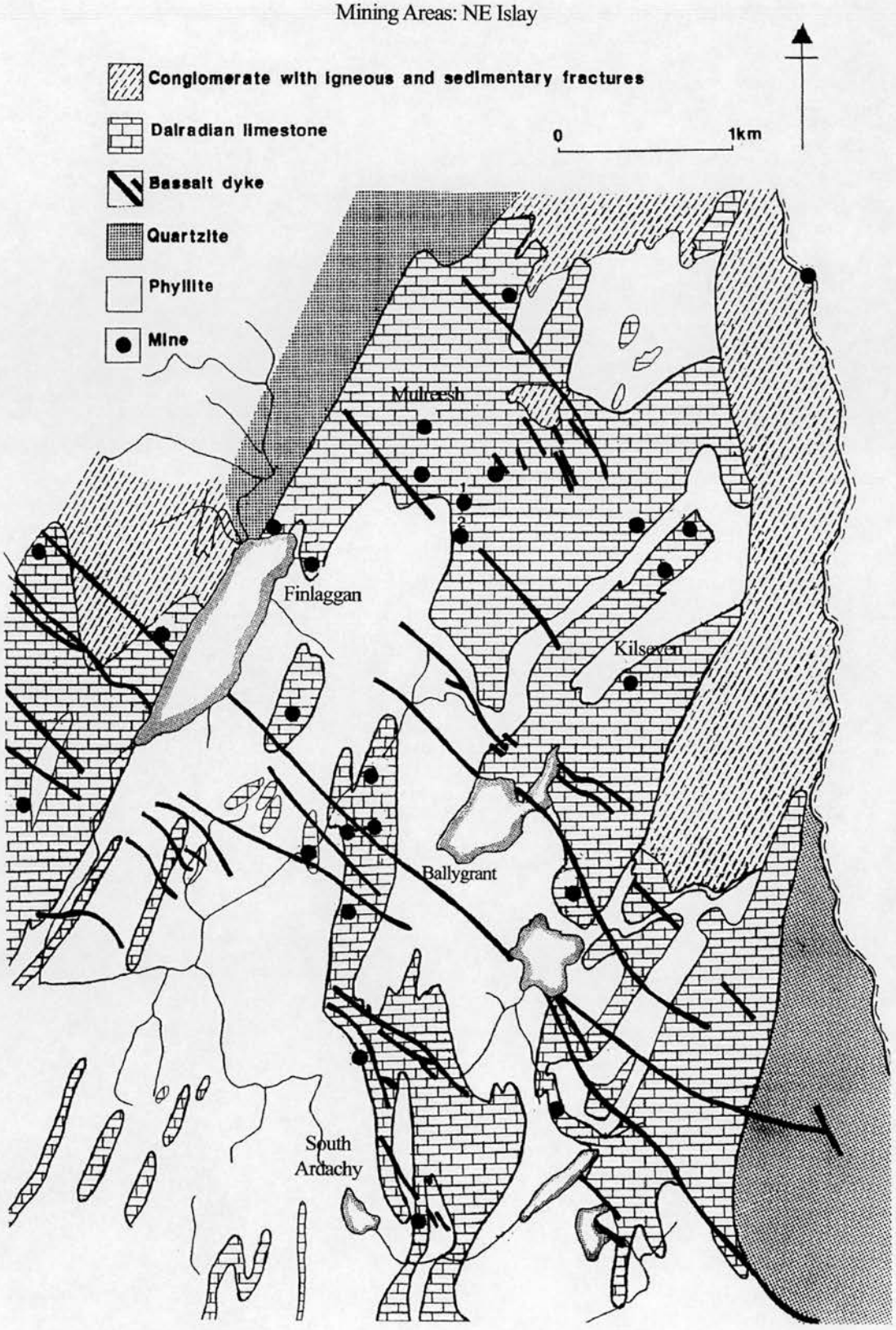

Fig. 5-2 Northeast Islay mining areas and relevant geology; taken from Cressey (1995) and OSGB 1:50k geology data (2001).

Copper was mined at Kilseven, located some 1.5 km northeast of Loch a' Chuirn and 1 km northeast of Loch Ballygrant. Wilson and Flett (1921) state that a vein with a northeast trend was seen to be some 0.5-1 m in width with a total distance of some 400 m. This mine was discovered in 1760 and it is unknown if previous activity occurred at the site, although later lead mining did occur there.

Manganese was mined in the 19th century on a small scale on the Dun Athad peninsula on the Mull of Oa, the most southerly of Islay's two protruding landmasses. Here former workings have been identified but their date is uncertain. The ore appeared as pyrolussite forming metal veins that were seen in association with replacement bodies of quartzite (Wilson and Flett, 1921).

Thomas Pennant mentions in 1772 during his travels through Islay and the Hebrides a "species of iron called bog ore" located in a stratified deposit not far from the lead mines of Ballygrant (Pennant, 1774). The feasibility of extracting iron ore from bogs was considered but later analysis show these deposits to have been sporadic and not economically viable for exploitation. However, during the late Viking era and the early Middle Ages, these small deposits may have had a much higher value.

Finally, limestone is the most predominant rock that may have some intrinsic economic value, though quite likely not so much during the early Middle Ages. Mined presently at Ballygrant and used for agricultural improvement and road surfacing, it is mostly a modern product.

It may be seen that the Isle of Islay has supplied wealth by two distinct means to its inhabitants over time, one being its mineral wealth and the second being the richness of its limestone laden soil. The historical geography of the island will now be examined.

5.3 Historical Geography

5.3.1 The Historical Geography of Islay until the Industrial Revolution

The first evidence of human habitation on Islay appears during the Mesolithic period (c. 7000 – c. 3500 BC) at Rubha Bolsa. From this earliest inhabitation, Islay has flourished through each of the various archaeological ages with Neolithic (c. 3000 – c. 2500 BC) sites at Nerabus, Bronze Age (c. 2500 – 600 BC) sites at Cultoon in the Rhinns of Islay and Iron Age (c. 600 BC – AD 400) sites at Ardnave (Jupp, 1994). However, the principal time periods for which we are concerned within this work are the Dark Ages until the pre-Industrial Revolution (750 AD – 1700 AD).

In the year 787 AD, the first of what would later come to be known by historians as the Viking Raids began in an attack on the coast of present day England by Norwegians. By 795 AD Iona had been sacked and burned while the Isle of Man and the mainland of Ireland had been pillaged by 800 AD (Williams, 1997). Sometime in this period just after 800 AD, the Isle of Islay fell to the Norsemen and began its journey into history as a centre of maritime power and commerce (Graham-Campbell and Batey, 1998).

Islay's first years in its new use as a logistical base for Viking depredations in the Irish Sea are tumultuous and chaotic for historians to discern. It is clear, however, that with the death of Godfrey (853 AD), who was the Toiseach or Thane of the Isles, all Celtic influence ended in the Hebridean chain, as after this date until the ascendancy of Somerled in 1158 all king lists contain exclusively Norse names (Williams, 1997). Therefore, the foundation and development of the maritime economy and its related components throughout the Irish Sea can be seen to have a distinctly Norse influence. From the construction and design of sailing ships to the types of cargoes and products traded, the supporting infrastructure of this system such as ports, roads, and manufacturing centres, were developed in such a way as to enhance the projection of maritime power (Smyth, 1998). In no other place in the Irish Sea was this brought to such a high level of refinement as on the Isle of Islay and is relevant to the story of mining on the island. Metalworking, whether skills, technology, or products, were introduced and exchanged by maritime means, and the success of such an industry would have been wholly dependent upon on a robust naval capability.

In the year 1158 AD the leader Somerled managed to gain control over the majority of the Hebridean chain of islands after several land and sea battles, a fortuitous marriage, and extraordinary diplomatic skills (Cowan and McDonald, 2000). Thus, while it would be one of Somerled's ancestors whom titled himself "Rex Insularum" or "Lord of the Isles", the ascendancy of the western isles of Scotland into its own autonomous military and political power had begun. It would not be completely extinguished for four centuries.

5.4 Location of the South Ardachy Mine Complex

As previously stated, the site chosen on Islay for the mine detection, survey and analysis regimen using Imaging RADAR was the South Ardachy mine complex. This site was chosen because of documented environmental evidence of mining activity dating to the middle 14th century (Cressey, 1995). Fig. 5-3 gives a more detailed topographic and geological view of the site.

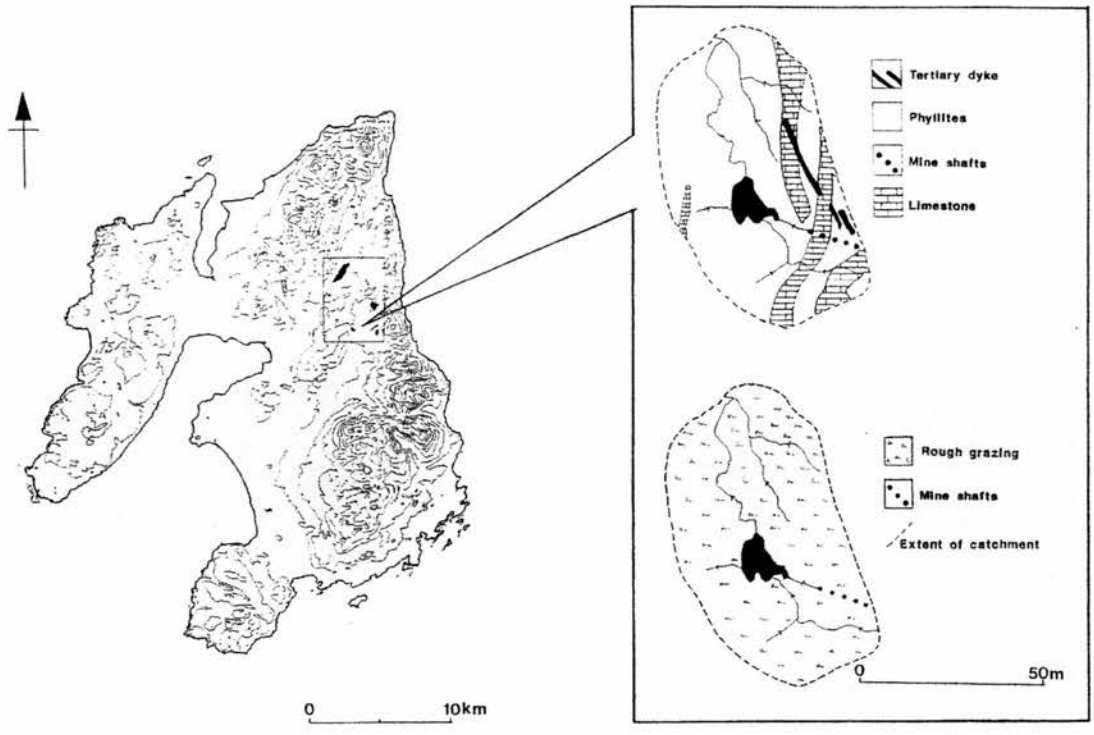

Fig. 5-3 Location of South Ardachy mines (based on Cressey, 1995).

5.4.1 Site topography and analysis

The centre co-ordinate of the South Ardachy mine complex is 302097 E by 6187660 N, UTM. Loch Bharradil, which is triangular in shape with a small island, possibly, a crannog, near its northern end, borders the western edge of the mine complex. The northern boundary of the mine complex is regarded as the Gleann Maraiche track for the purposes of this study. The southern boundary of the complex is the foot of the hill Airigh Ghuaidhre, at 139555 E by 663653 N, UTM. The Ballygrant to Cluanach road marks the eastern boundary of the mines (Fig. 5-4).

The site map also includes an overlay of the approximate pixel locations discussed in the Imaging RADAR section, with the southernmost pixel of the analysed transect being on the right and the northernmost on the left. Due to cartographic representation and the nature of the sensor, an active continuous microwave emitter, the pixels are a systematic portrayal of the data by the computer software for purposes of analysis in a Cartesian form i.e. x and y.

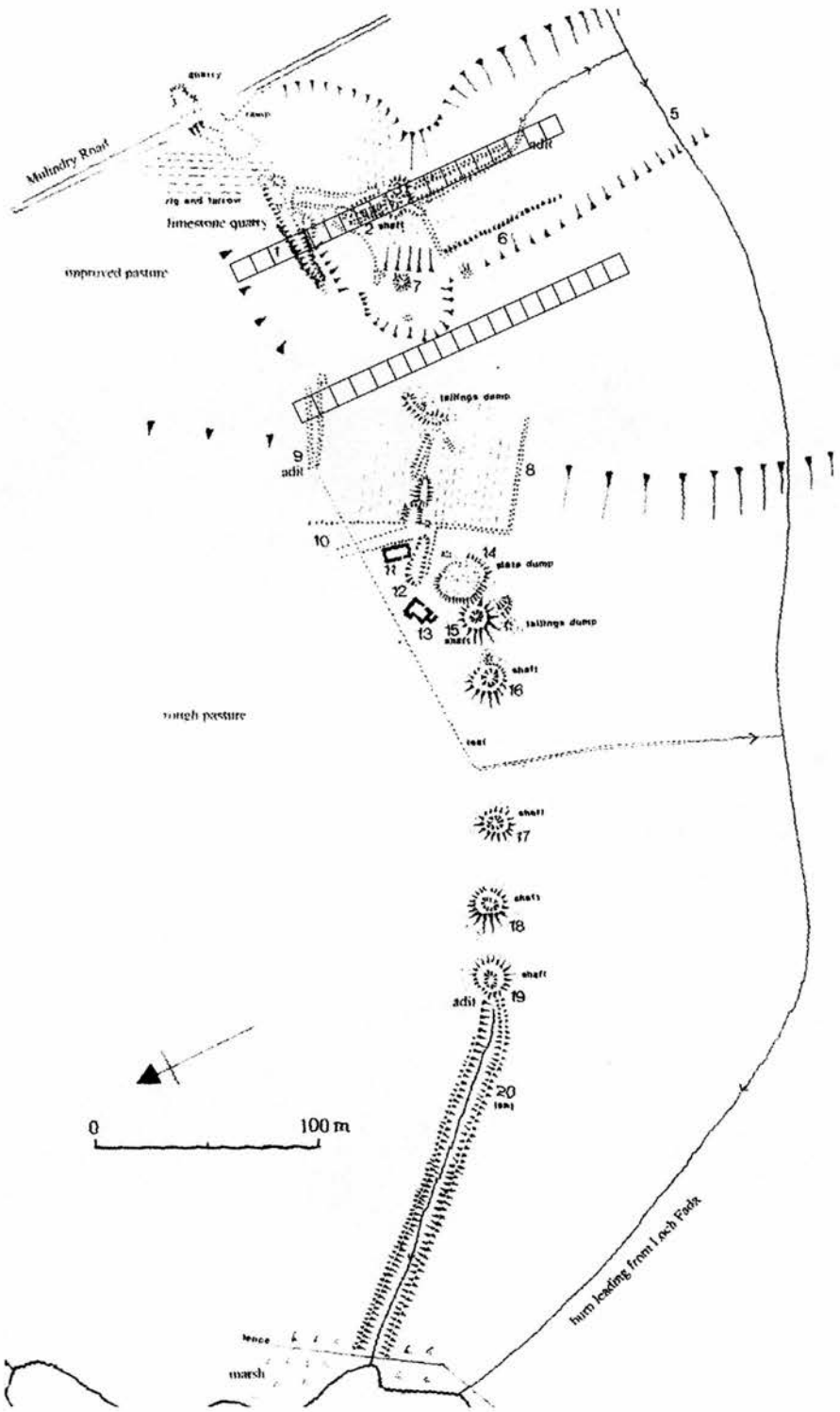

Fig. 5-4 South Ardachy mine complex (based on Cressey, 1995). The transect method used throughout the study is shown here by the two series of contiguous boxes representing the pixels, the top transect bisecting the target mine, the bottom transect covering a more planar surface for comparison.

5.4.1.1 Topographic analysis

A complete topographic analysis of the region surrounding the South Ardachy mine complex was performed using a Digital Terrain Elevation Data subset equivalent to a level 1 parameter i.e. one verifiable elevation point every 90 meters on average (NIMA, 2001). The data subset used here was verified to an elevation point every 70 meters. The data subset boundary was set to the exact limits of the NASA SIR-/X-SAR Imaging RADAR data subset for three-dimensional modelling purposes and to speed processing time. The data set geographic co-ordinates are as follows: upper left corner pixel 55° 49′ 10.53″ latitude by -6° 11′ 16.16″ longitude; the lower right corner pixel 55° 46′ 36.51″ latitude by – 6° 6′ 10.69 ″ longitude, or some 2.5 km x 2.5 km.

Topographic analysis is necessary to understand the manner in which microwave emissions interact with the earth's surface and to support valid analyses and assumptions. It must again be re-iterated that the analytical processes employed here are those which will applicable with the forthcoming Shuttle RADAR Topographic Mission (SRTM) data release and so were included in this study to demonstrate archaeological applications for landscape analysis (NIMA, 2001 and JPL, 2001). Topographic analysis followed the methodology outlined in Chapter 4, which comprise examinations of the following characteristics: slope, aspect, shaded relief, profile convexity, plan convexity, longitudinal convexity, cross sectional convexity, minimum curvature, maximum curvature and topographic feature classification (i.e. hill, peak, depression etc.).

5.4.1.2 Slope

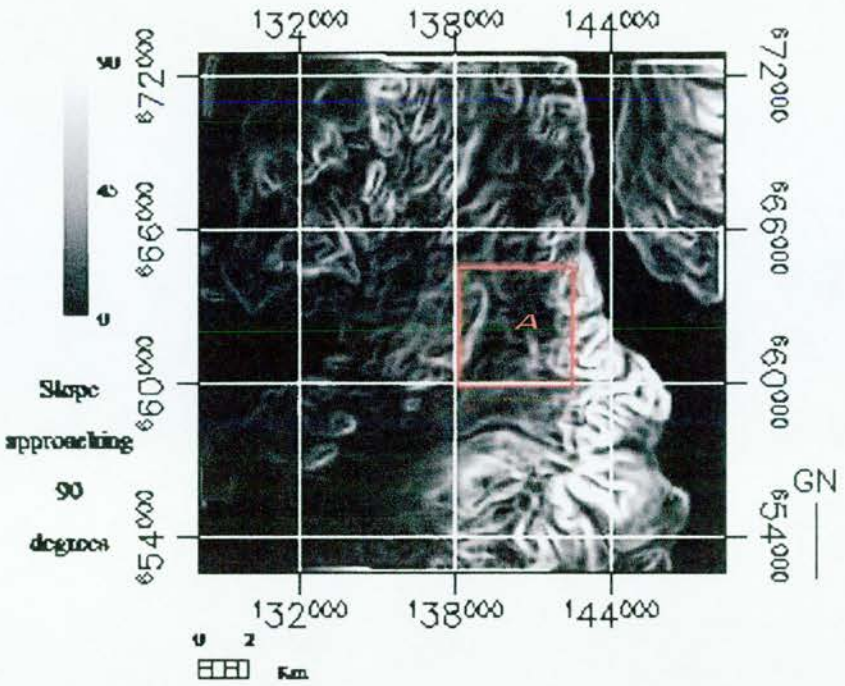

Fig. 5-5 Rate of change for slope, eastern Islay.

The predominate area of measurable slope change lies along the axis traversed by the longitude line at UTM 138000 W. This region lies to the east of the South Ardachy mining area, defined by the red box and the letter "A", and is bordered on the east by the Sound of Jura. The numerous beinns, or sharp hill peaks, are the dominate features responsible for the strong changes in slope; drainage is primarily to the west.

A small area of significant slope change may be seen to the upper right of UTM co-ordinate 660000 N by 138000 W. This is the ridge-hill of Beinn Bharradail, which obscures drainage to the immediate west of both Loch Bharradil and the South Ardachy mine sites. It can be seen from the lesser rate of slope change between these two regions that two circumstances may arise from mining in such an area. First, heavy metal pollution from the South Ardachy site would tend to migrate in the hydrological system to the south and southwest, and second, with a low rate of slope change the concentration of heavy metal pollution should be localised due to slow water velocities.

5.4.1.3 Aspect

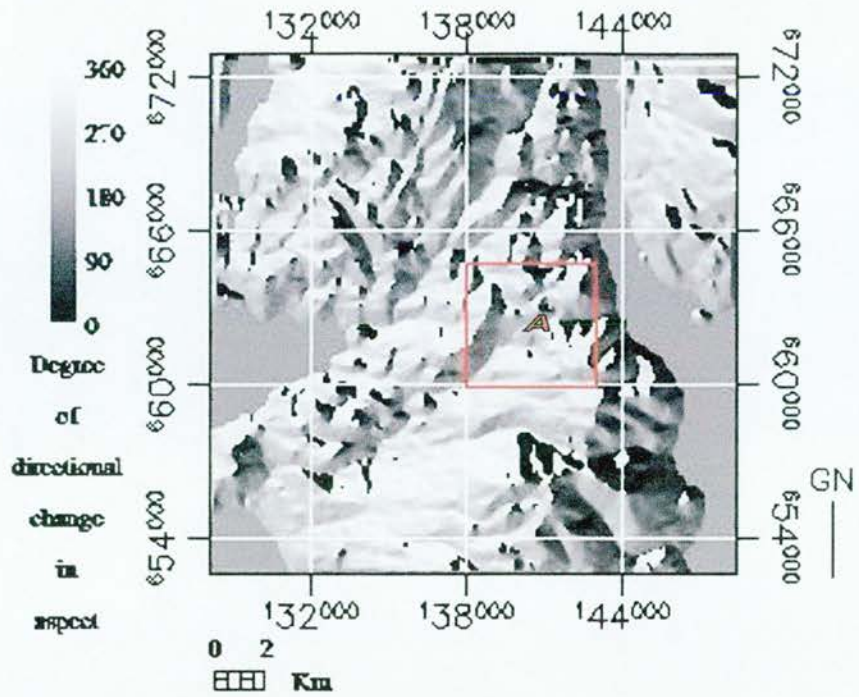

Fig. 5-6 Aspect characteristics of eastern Islay.

Chapter 3 described aspect as the orientation of primary terrain faces toward a given point. In the above image scene due north is given as 0° for purposes of aspect orientation. With that in mind it can be seen that a large proportion of eastern Islay is oriented between 270° and 360° of aspect. Considering that the dominant wind direction throughout much of the year on Islay is from 280°, these slopes in the past would not have been primary points of human habitation due to exposure. Based on that premise, potential habitation sites of the earliest miners who worked the South Ardachy mines would have been ideally situated beneath the sheltering ridge of Beinn Bharradil, located to the upper right of UTM co-ordinate 660000 N by 1380000 W.

Shuttle Imaging RADAR performance over Islay was optimal due to this dominant aspect orientation. This was because of the ascending orbit using a right-looking antenna mode.

5.4.1.4 Shaded Relief

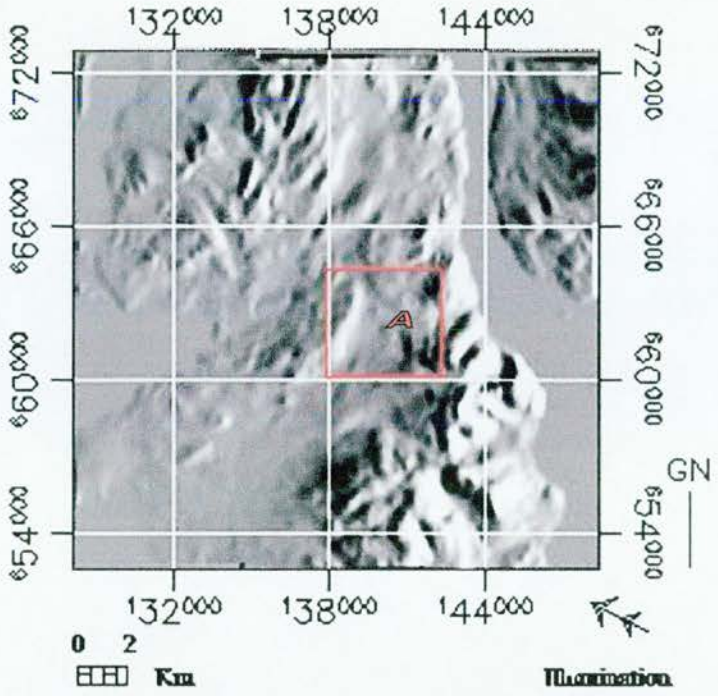

Fig. 5-7 Shaded relief of eastern Islay; illumination from southeast.

A shaded relief of the South Ardachy mine complex was computed using the following figures: a sun elevation angle of 18.25 in conjunction with a sun azimuth angle of 97.50. These are the values for 0731 GMT on April 18,1994, the moment at which the STS Endeavour and the NASA SIR-C/X-SAR Imaging RADAR system passed overhead. This gives an invaluable representation of the how the target scene on the earth's surface would normally be illuminated in cloud free conditions by visible sunlight in comparison with the Imaging RADAR data further along in this chapter.

It is archaeologically important to note that the surfaces in the image displaying illumination are generally in agreement with the previous aspect analysis. The sun illuminated surfaces offer maximum solar heating and secondly, protection from the predominant winds.

5.4.1.5 Profile convexity

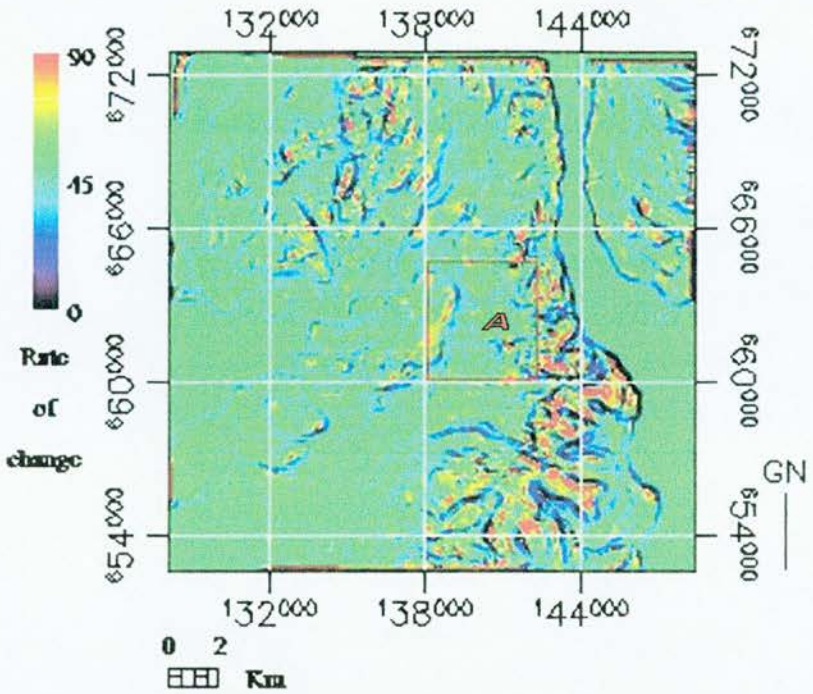

Fig. 5-8 Profile convexity for eastern Islay.

Profile convexity analysis measures the rate of change of the slope along the profile. It can be seen that the quadrant surrounding the South Ardachy mines shows medium levels of convexity along the Beinn Bharradil ridgeline. However, immediately opposite the edge of the lead-bearing limestone outcrop may be detected trending from north to south with only minimal change in slope profile. This feature is significant also for the fact that it indicates an eastern boundary for the hydrological system that fills Loch Bharradil.

There is minimal influence on imaging RADAR performance over the target area based on this particular topographic analysis.

5.4.1.6 Plan Convexity

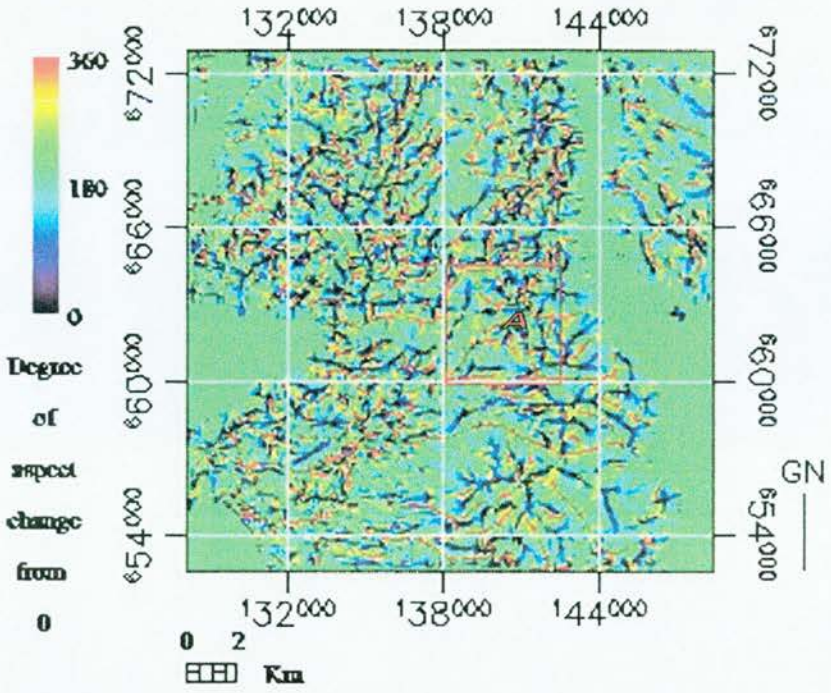

Fig. 5-9 Plan convexity of the eastern Islay area.

As discussed in Chapter 4, plan convexity (intersecting with the XY plane) measures the rate of change of the aspect along the plan. As may be seen, there are areas of aspect change along the plan of the terrain surfaces within the area containing the South Ardachy mines, indicating an undulating series of hills and hillocks. This provides possible insight into transport routes leading from the mines to ports of shipment. Assuming that both raw and finished ore products would have been transported in some form of wagon, or wheeled cart, routes would have been established based on the capabilities of these vehicles to transit the terrain. Further, as draft animals perform best under hauling conditions when traversing low angle slopes in roughly parabolic arcs, then the area displaying the least profile and plan convexity change lies to the south of the South Ardachy mines (U.S. Army, 1876).

Plan convexity for the target region is not of a significant amount to impede imaging RADAR emissions, however, the various degrees of aspect change present an opportunity for further study of naturally occurring multifaceted reflecting surfaces and their influence on returns.

5.4.1.7 Longitudinal Convexity

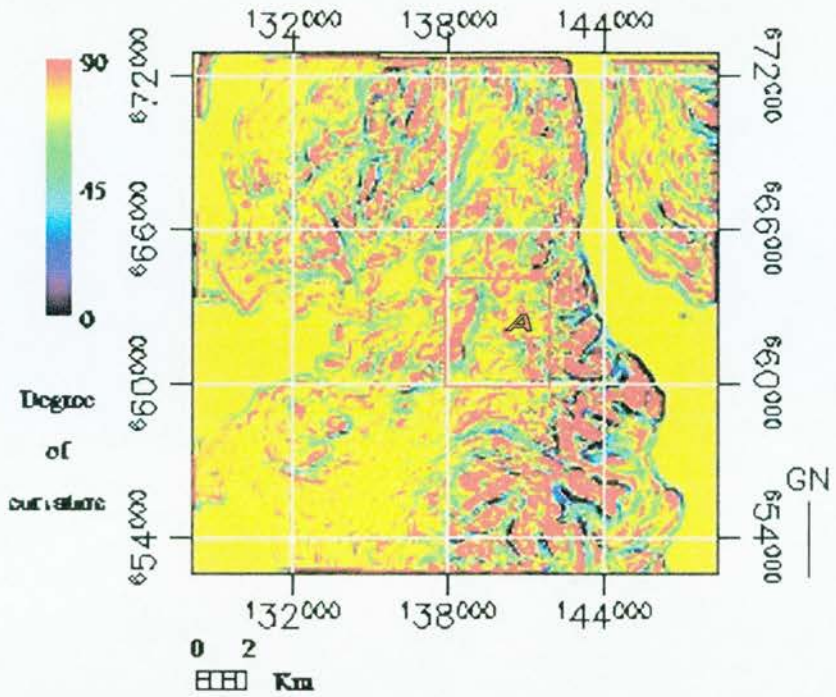

Fig. 5-10 Longitudinal curvature of the eastern Islay area.

As explained in Chapter 3, longitudinal curvature and cross-sectional curvature are measures of the surface curvature orthogonally in the down slope and across slope directions, respectfully. The previous profile and plan analyses showed limited topographic change in those vectors and the same can be said for longitudinal curvature.

The foremost area of longitudinal curvature which is of any importance to the South Ardachy mine complex is the limestone outcrop, which may be seen in the image map as a subtle yellow-green trending north to south between UTM longitude 138000 W and 144000 W.

There are no impediments to imaging RADAR performance that may be observed from this analysis.

5.4.1.8 Cross sectional curvature

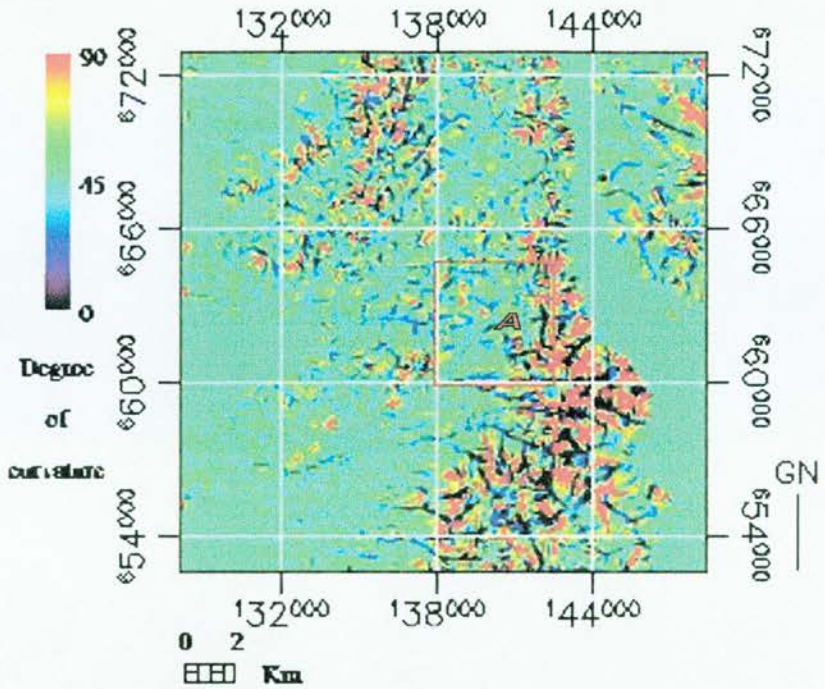

Fig. 5-11 Cross sectional curvature of the eastern Islay area.

As mentioned in Chapter 3, cross-sectional convexity, or curvature (intersecting with the plane of the slope normal and perpendicular aspect direction) is a measure of the surface curvature orthogonally across slope directions. In the above image map, it can be seen that Islay's eastern portion is characterised by cross sectional curvature which is resultant from the underlying geological structure, that of contact areas which have created the necessary heat and pressure for mineralisation. This may be seen in rather more detail in the discussion area concerning Islay's geology.

The effect of such topography is significant on the hydrology of Islay as limited drainage networks exist which empty a large area. This is yet another significant implication for the influence of ancient mines on the environment as concentrations of heavy metals are unlikely to be highly mobile.

There is no noticeable affect within the target area on imaging RADAR performance due to the nominal resolution of the sensor.

5.4.1.9 Minimum curvature

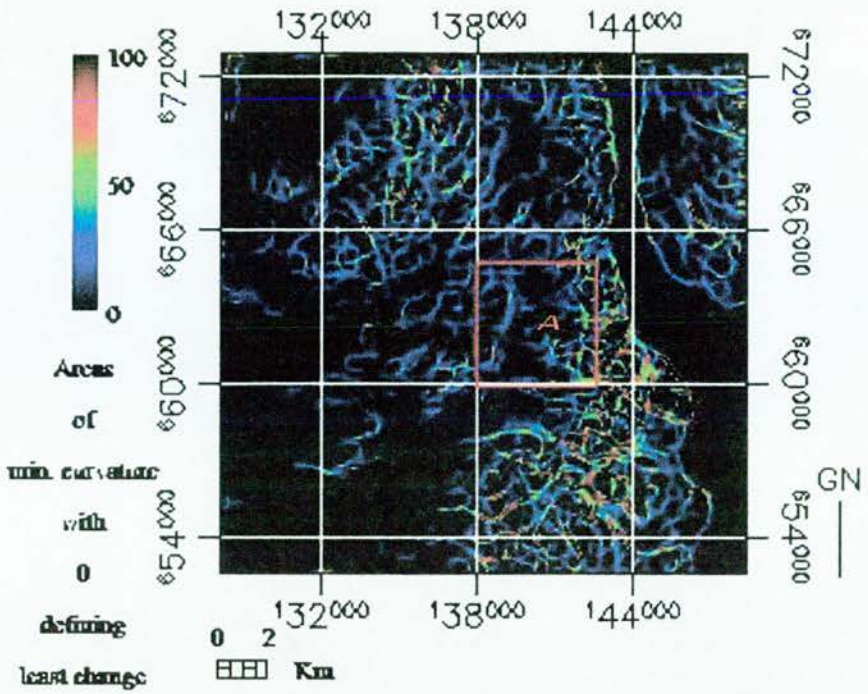

Fig. 5-12 Minimum curvature of the east Islay region.

The most self-explanatory topographic analysis form, minimum curvature is a profound picture of the area surrounding the Ardachy mines. This is a vivid portrayal of the lack of influential topographic structures, which when present, create watercourses that would empty an area through a developed hydrological network. In this case, the numerous small lochs near the South Ardachy mines have provided water for mineral production over the years, but have also tended to keep by-products of heavy metal refinement localised.

5.4.1.10 Maximum curvature

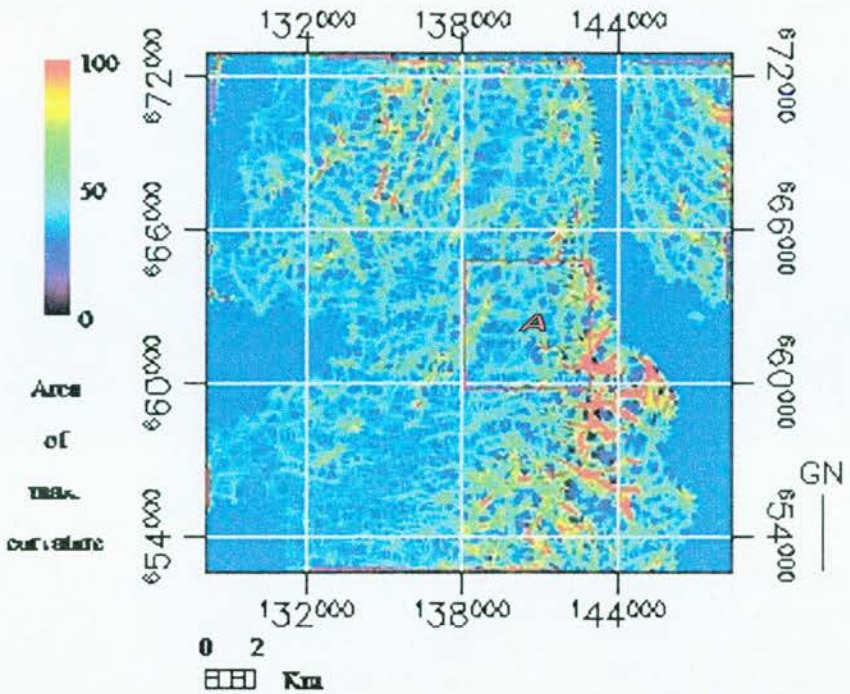

Fig. 5-13 Areas of maximum curvature in eastern Islay.

A computation of the inverse of the previous analysis, maximum curvature shows again that there are virtually no macro dominant topographic features in the South Ardachy mines area. While there are localised factors that affect the micro-topography, which are discussed in the section on the site survey, as the resolution scale of the available data presented here, this is not a calculable factor. The lack of curvature is significant in terms of the lack of hydrological drainage and the localisation of heavy metals deposition by generations of mining activity.

The topographic analysis of the mining area having now been discussed, the following section will present an overview of the underlying geology that creates this topography.

5.4.2 Geology of the site

The South Ardachy mine complex is comprised of acidic slates and phyllites bisected by a Dalradian limestone feature which trends from the south-east of the area to the north-northwest (Fig. 5-14). This limestone feature is paralleled roughly by a Tertiary dyke. Extensive mineralisation has occurred in this area and Pb (lead) was extracted in large quantities here as well as at the North Ardachy mine complex (Smith, 1895).

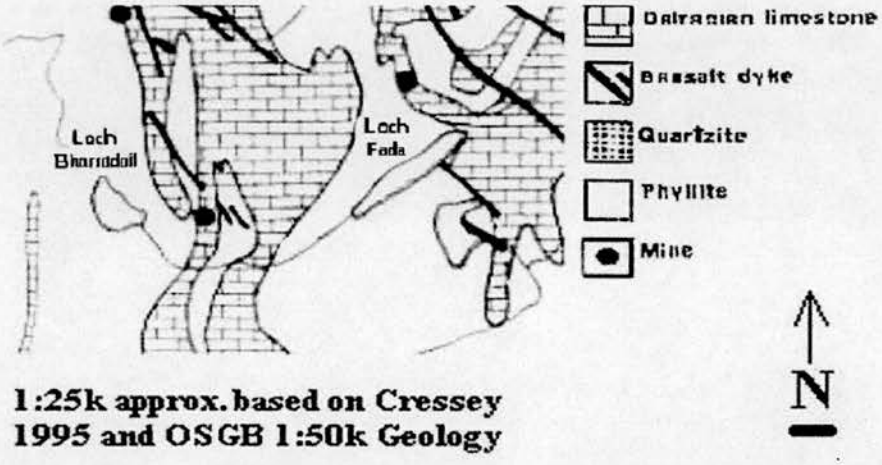

Fig. 5-14 South Ardachy mine complex geology.

5.4.3 Geomorphology

The soil types within the mine area are of the Foundland Series of drift deposits. These deposits are comprised of slates and phyllites. The limestone outcrops that contain the heavy mineralisation are covered by a shallow Deecastle Association of brown rankers intermixed with light loams.

Some grazing by cattle is supported on the lower slopes of the hills where phyllites and shale have heavily deposited. Around the shores of Loch Bharradil, west of the centre of the mine complex, are peaty glays and podsols (Cressey, 1995).

5.4.4 Vegetation

The bogs, which are intermittent throughout the lower-lying regions of the mine complex, are populated by *Festuca* (grasses) and *Calluna vulgaris*. *Campanula rotundifolia* and *Orchis mascula* represent species that thrive best in the alkaline conditions of the area. Vegetation around Loch Bharradil is dense with the species of *Phragmites australis* mixed with *Cladium*. Mine spoil heaps and piles are sparse of vegetation due to high levels of heavy metals. The only vegetation noted on these heaps are *Plantago lanceolata L* and *Rumex obtusifolius* as observed by Cressey in 1994 (Cressey, 1995).

5.5 Site History and Archaeology

5.5.1 Historical Background

The most detailed source for mining activity on Islay is the Book of Islay (Smith, 1895). However, this book does not contain any drawings or maps which detail the South Ardachy mines prior to the Industrial Revolution. Several descriptions from the period of the middle 18th century allude to the size of the mines and their operations as well as area mineralisation.

Alexander Shiriff stated that South Ardachy was the most important mine on Islay in his 1770 report, State of the Mines in Islay. Shiriff noted that: "An east-west vein is presently being worked for a length of 30 fathoms (approx. 55 metres); the vein is crossed by two whindykes (today's Tertiary dykes) and ore is up to 2 ½ feet wide along one of their sides".

Other visitors to the workings such as Freeburn in the late 1760s also noted the rich metal veins among the Tertiary dykes; this would be an astute observation of the metamorphic interface zone between Dalradian limestone and Olivine Basalt (Smith, 1895).

5.5.2 Site archaeology and survey

This archaeological survey is a reassessment of Cressey's 1994-5 site inspection. Significant changes will be noted as they may affect the remote sensing analysis. This site was visited on several occasions, the first being 16 April 1999 and the most recent 15-20 November 2000.

The limitations of traditional archaeological survey methods in examining ancient mine sites are evident from the outset of such an undertaking. Difficulties in positioning features detailed in historical works, usually without maps, and changed surface features due to new land uses are but a few of the problems. Islay's historical records only note numbers of workers and the qualities of the ores that they extracted. Information regarding mine layout, supporting infrastructure and transport mechanisms is largely non-existent. The majority of the South Ardachy mine complex is comprised of open cast workings with the odd surface working and mine shafts. Spoil heaps, or tips, range from local rock to fine secondary tailings. These secondary tailings are found along the edges of the mineshafts as well as around the valley slopes south and west of the centre of the complex. There are also small limestone heaps that were dumped around the mouths of the mineshafts that contain associated slates as well.

5.5.3 Ground Features

The Mulindry Road acts as a northern-eastern border for the target scene area; the road itself crosses a former quarry that is oriented along an east-west axis. It is estimated that the quarry covers an area some 50 metres in length by 7 metres in width. Other workings are located along the same axis nearby. Mine spoils are to be seen in a terraced fashion leading to an adit which has been back-filled with refuse. A shaft crosses the trial mine associated with this feature. This shaft has an adit situated alongside it. This feature has been well preserved due to the effects of a small stream issuing from Loch Fada and draining away into Loch Bharradil. Ascending from the adit is a steep slope leading up to a large square embankment that surrounds a rig and furrow. A test pit cut into the limestone outcrop at the peak of the hill may also be seen. Looking southwards reveals an area of sizeable tailings that stretch away down a hill sloping towards the southern portion of the mine complex.

The southern area of the South Ardachy mine complex is dominated by trial pits oriented on an east-west axis and is surrounded by an embankment. The northeastern trial is the most significant with a minimum depth of 5 metres. Unfortunately, the majority of the features have been back-filled over the passage of time by local farmers with refuse and spoil. However, it is interesting to note that the refuse and spoil are lightly packed in relation to the surrounding geomorphology.

A building of squared construction may be seen backing onto a bank alongside the track; its relation to mine activity is unknown. Another construction is located west of this building and again, its use in mining operations is unknown. Finally, due Southwest is a building which has a large opencast feature. This building has numerous mine tailing deposits associated with it, which are oriented on an east-west axis.

Southwest of the area of mine tailings is a large, oval shaped tailings dump. The tailings are comprised of phyllites interspersed with iron pyrite as well as slate. Immediately west of the tailing dump are five mine shafts that are filled with refuse. The average internal diameters of the shafts are 8.1 metres. The mineshaft furthest from the centre of the site is located near a leat, which is some 3.5 metres in depth. This leat has significant banks and crosses some 185 metres of open pasturage. The embankments alongside the shoulders of the leat are evidently interspersed with significant quantities on mine tailings due to the lush vegetation dominated by *Campanula rotundifolia*.

It should be noted here that a key change has occurred since the 1994-1995 site survey by Cressey in that the northeastern trial mine shaft has been partially filled with rubbish and other refuse. Additionally, the region immediately east of Loch Bharradil up to the leat has been under the plow for crop planting.

5.5.4 Archaeological assessment

The open-cast features most closely coincide with the historical commentary concerning South Ardachy. These trial shafts were noted by in the 18th century writings as pre-dating the current workings i.e. those of the 17th and 18th century when South Ardachy was in full production.

The remaining features of the South Ardachy mine complex probably belong to the period of time ranging up to the 19th century. However, as the focus of this study is the detection, survey and analysis of ancient mining features i.e. pre-Industrial and early Industrial Revolution, it is those pre-17th and early 18th century features that will be focused upon.

5.6 CORONA Satellite Imagery

5.6.1 CORONA Satellite Image Details

Satellite imagery from the CORONA program was obtained from the USGS GLIS Archive. There was only one image from the entire CORONA satellite program that had overpasses of the Isle of Islay region, an image that reached from Leuchars, Scotland to Northern Ireland. The imagery was obtained on 30 August 1961 (Appendix 1). However, due to orbital skew caused by the lack of inertial systems in the early platforms, blurred imagery was produced in all of this early series making it unusable for its original analytical purposes (Day *et al*, 1998). Additionally, no cloud free image area was available over Islay within the selected imagery. Still, much of the early CORONA data is very useful for remote sensing archaeology as it covers areas of the world prior to the massive industrialisation of the late 1960s and 70s. The chapters covering the results in Egypt and Spain will demonstrate the remarkable quality of this imagery for archaeological use.

5.6.1.1 CORONA Satellite Imagery Subset

No CORONA imagery was available for this study area due to cloud cover.

5.7 AVHRR Satellite Imagery

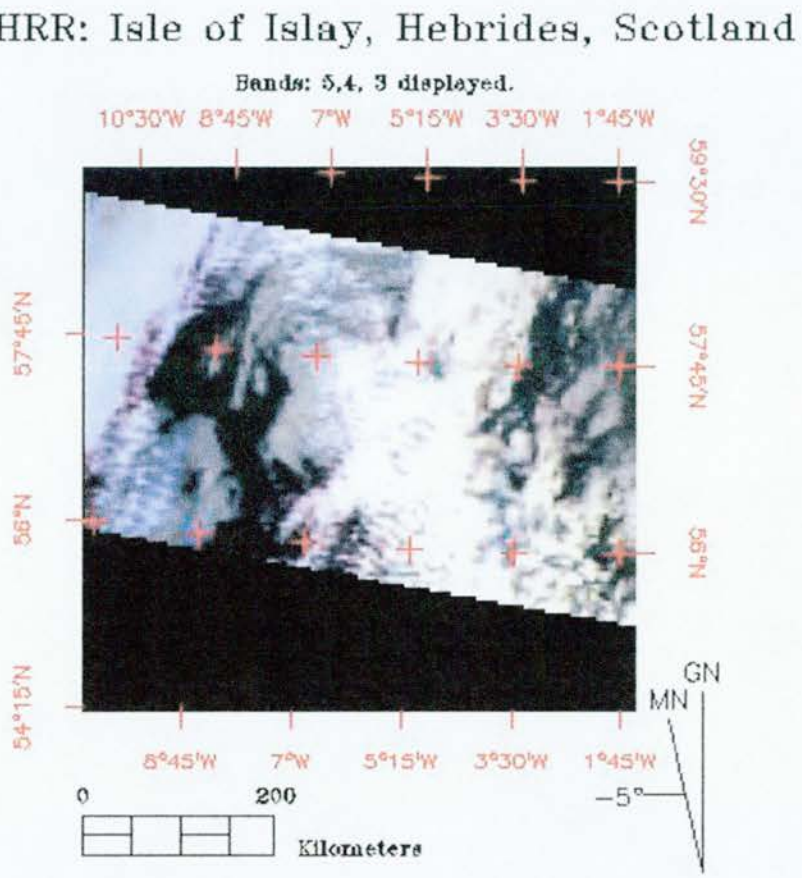

Fig. 5-15 AVHRR GAC image subset, Isle of Islay, Scotland, UK.

AVHRR Global Area Coverage (GAC) data for the orbital pass immediately preceding the overflight of the SIR-C/X-SAR Imaging RADAR system on 18 April 1994 was obtained from the NOAA Satellite Active Archive for analysis. Resolution of the data is 4 kilometres in GAC mode. It can be seen that the area above Islay, 57° 45′ N by 8° 45′ W to 57° 45′ by 7° W, is cloud free with no impediments to maximum RADAR performance.

Calibration of the AVHRR data for brightness temperature was computed for bands 3, 4 and 5 using algorithms developed for the NOAA-12 platform, and presented in degrees Kelvin which represent the brightness temperatures (ENVI, 2001and Table 5-1). The data displayed here is from the NOAA-11 platform, therefore it is unknown as to the performance differences per the calibration algorithm; Chapter 4 details this data set (NOAA, 2001).

NOAA 11 – Band 3	3.74 K
NOAA 11 – Band 4	10.82 K
NOAA 11 – Band 5	12.00 K

Table 5-1 Calibrated brightness temperatures, degrees Kelvin, NOAA-11, 1994.

5.8 Meteorological Data

5.8.1 United Kingdom Meteorological Office Data

Averaged weather data for the Isle of Islay region immediately prior to the STS Endeavour overpass was provided by the Meteorological Office of the United Kingdom from data collected at the Machrihanish Station for the 24 hours immediately preceding the Shuttle overpass on 18 April 1994. The station is located at UK national grid reference, NR 663226, at a height of 10 m.a.s.l., some 50 kilometres from Islay. The 24 hour averaged data is presented in Table 5-2.

Temperature (degrees, Celsius)	6.13°
Rainfall (mm)	.005
Wind direction (degrees, compass)	295°
Relative humidity (percent)	92.5
Wind speed (km)	3.91

Table 5-2 24 hour averaged weather data, Meteorological Station, Machrihanish, Scotland.

As can be seen in Fig. 5-15, and from the ground data gathered at Meteorological Station Machrihanish, Scotland, there were no significant quantities of rainfall within the period of time prior to the overpass of the Shuttle Imaging RADAR system which would have affected RADAR signals. Consequently, it was assumed that decibel responses recorded over the target mine site would correlate with previously known RADAR performance data observed by Ulaby and Dobson (1989).

5.9 NASA SIR-C/X-SAR Imaging RADAR Data and Analysis

5.9.1 The Imaging RADAR Data

The Imaging RADAR data for Islay were obtained on the 16th and 18th of April 1994 during NASA STS (Shuttle Transport System) Mission SRL-1. C and L wavelengths were transmitted in the horizontal send and receive polarisation (hh) as well as the vertical send and receive polarisation (vv) modes to create the Multi-Look Complex (MLC) product.

The Cvv polarisation was operating at a 5.298 Ghz frequency while the Lvv polarisation was functioning at a 1.249 Ghz frequency. The orbital direction of the Space Shuttle was ascending while the look direction of the Imaging RADAR was right looking.

The track angle at the image centre was 83.2° East of North with an incidence angle of 28.0° for the MLC mode data. The centre latitude and longitude of the entire image scene are 55° 46.4′ N by 6° 5.7′ W with a time plot of 106:07:38:31.2 (GMT) over the same point. The nominal resolutions are 12.5 metres in range and azimuth for the MLC product. Actual pixel size and spacing of the digital product is 12.5 metres. The image scene was Ground Range corrected in initial data compilation and has a Doppler Centroid of -54 Hertz. The pulse bandwidth was functioning at 20 Mghz.

5.9.2 Data Processing

Initially, MLD (Multi-Look Detected) data tapes were decompressed using ENVI 3.4 (SP1) software in their separate Cvv and Lvv bandwidths as raw CEOS images. However, after discovering data inconsistencies with the MLD product and checking the data validity with Dr. Ellen O'Leary of JPL, an MLC data set was found in the USGS Global Land Information System archives which covered the Isle of Islay and South Ardachy mines complex area.

Upon receiving the MLC data set and decompressing the data sets, the data were then synthesised via the ENVI 3.4 image processing software. First, for cartographic purposes, each data set was projected into the Universal Transverse Mercator co-ordinate system using the British Ordnance Survey Airy Datum of 1936 for presentation purposes. Ground control points (GCPs) were taken at 16 locations (Fig. 5-16) (Appendix 1 for GCP information). Next, all phase difference analysis, filtering and test enhancements were performed on a raw data subset comprising a standard size area of 200 x 200 pixels. This was done to ease processing and analysis time due to the large sizes of the data sets. The South Ardachy mines complex study area may be seen roughly outlined in the small-scale image map of Fig. 5-16.

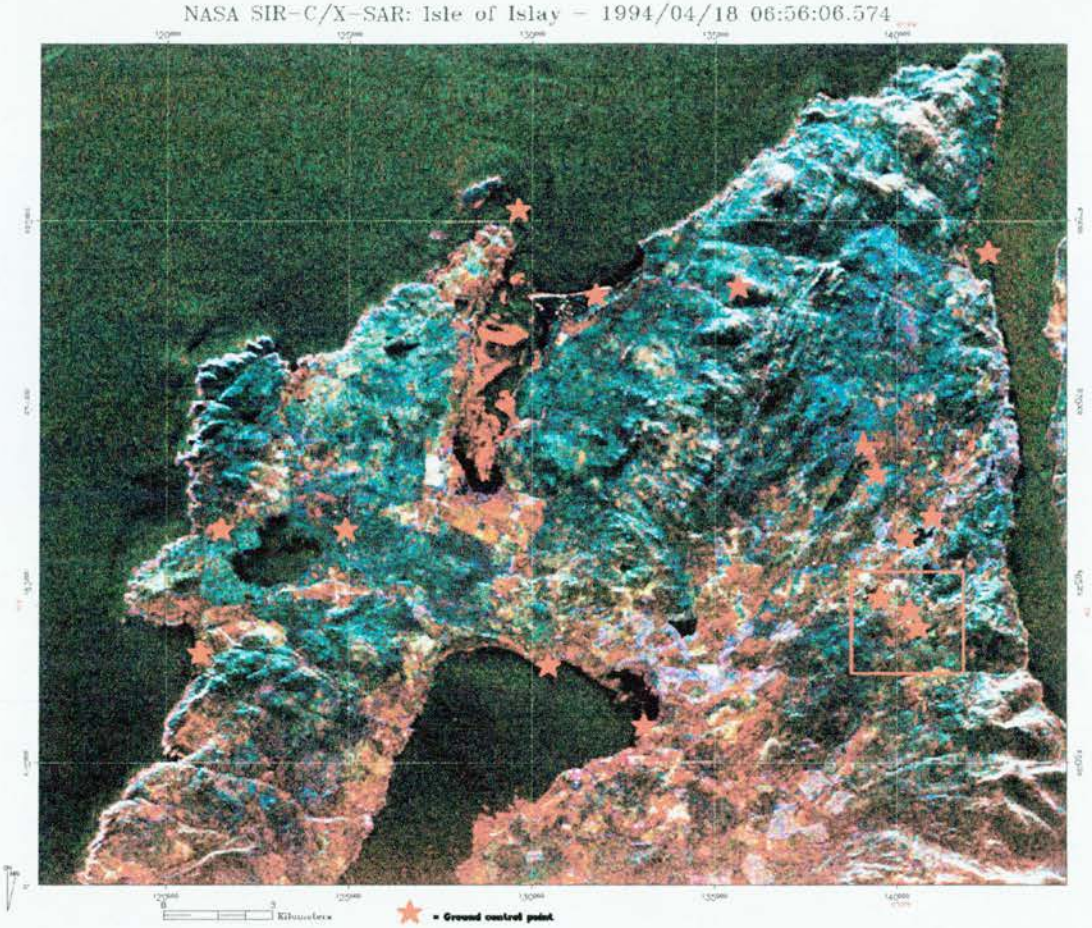

Fig. 5-16 The Isle of Islay: Ground Control Points (GCP) with South Ardachy area outlined.

5.9.3 Imaging RADAR data analysis

A reference Imaging RADAR map of the South Ardachy mines complex is presented in Fig. 5-17 to facilitate interpretation of the following RADAR data sets which have not been registered and projected to a co-ordinate system. Registration and projection processes artificially skew visual image results and frequently lead to misinterpretation, thus the data sets were analysed in base form; this image may be referred to for general placement of the target area within the overall image scene.

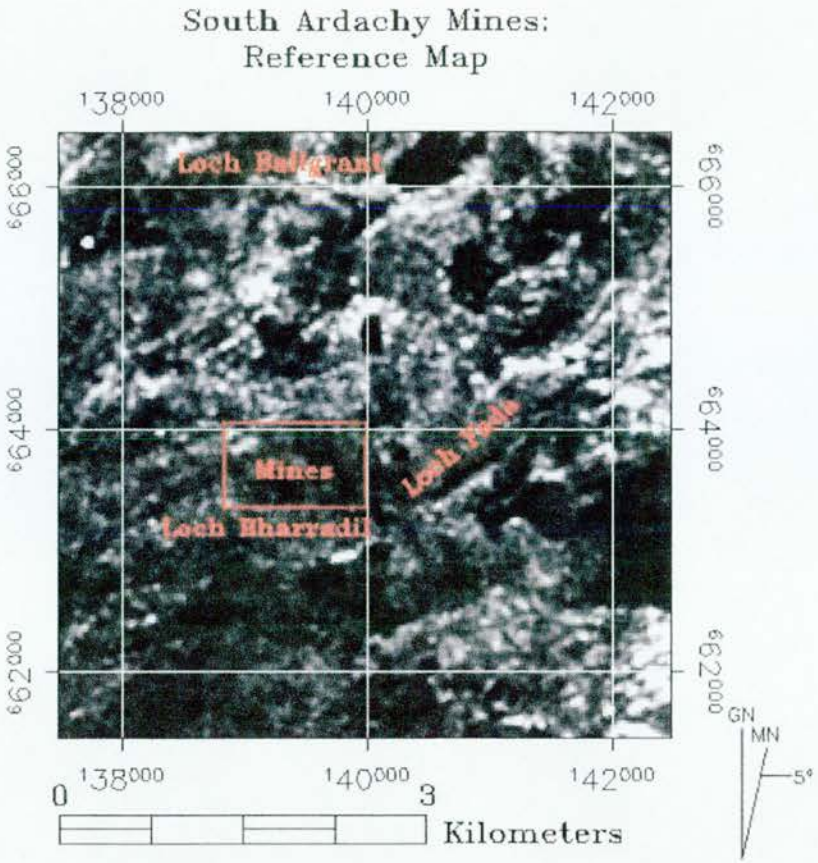

Fig. 5-17 The South Ardachy mines complex – Chh band.

5.9.3.1 Analysis form and test site

Evaluation of the capability of NASA SIR-C/X-SAR Imaging RADAR to detect, survey and analyse the South Ardachy mines was a straightforward process. It was decided to pick a portion of the mine site and transect it in a linear fashion by analysing each pixel's decibel response and phase difference for 10 pixels, or approximately 130 metres. The transect was oriented north to south, beginning at pixel 1208 x 1637 and ending at pixel 1208 x 1646. This distance was chosen to span the mine from normal signal return surface to normal signal return surface for reference purposes. Both C and L bands were analysed for decibel strength and phase difference response.

The test area chosen was mine shaft "A" as seen in below in Fig. 5-18. The UTM co-ordinate (OSGB datum) of the centre area of the mine shaft is approximately 663678 N by 139730 E and corresponds to pixel 1208 by 1641 in the data sets.

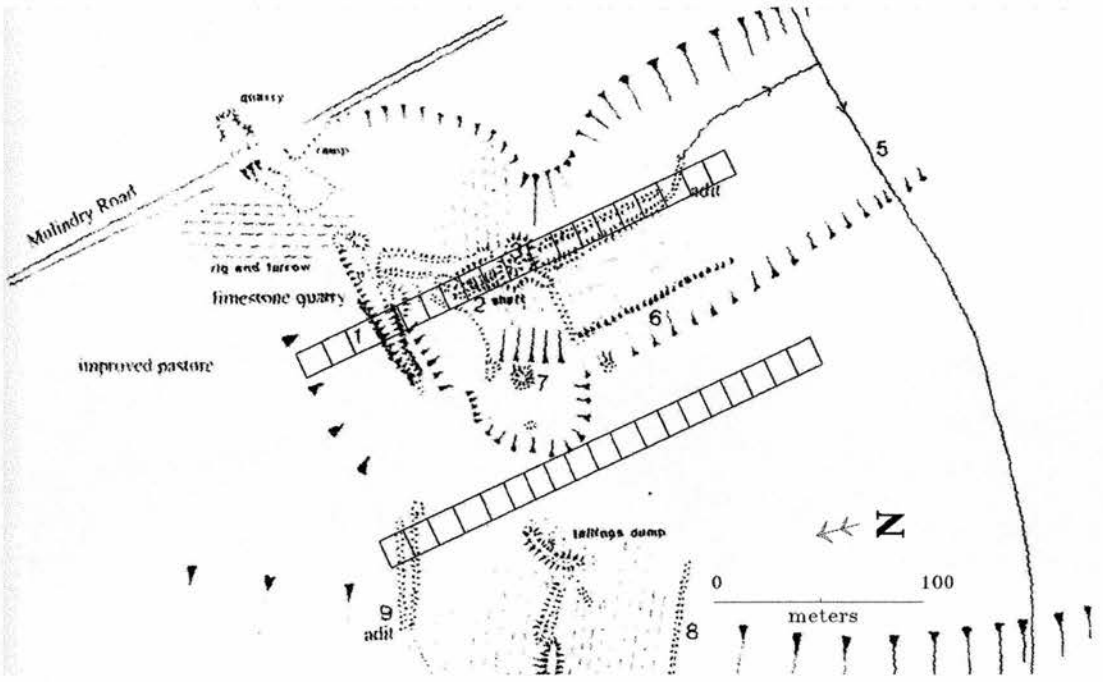

Fig. 5-18 Target scene mine shaft and adit at South Ardachy (Adapted from Cressey 1995 and OSGB 1:25k map).

5.9.3.2 C band Imaging RADAR phase difference analysis: "A" mine, South Ardachy

The image data set for the "A" mine target site at South Ardachy measures 200 x 200 pixels, with each pixel encompassing 12.5 metres of earth terrain. The transect of decibel and phase difference analysis concerning the mine begins at pixel 1208 by 1637 and ends at 1208 by 1646. An overview image map of the *raw* Chh RADAR data is provided in Fig. 5-19, with an explanation regarding the target illumination image map seen in Fig. 5-20 on the following page. The direction of analysis is from the northernmost pixel to the southernmost pixel with 1208 by 1637 being the *northernmost* pixel; pixel 1208 by 1646 is the *southernmost.* Immediately following this map are the analysed pixels and their statistics in Figures 5-21 and Table 5-3 to. It should be noted that Figure 5-21 contains a *polarimetric phase difference absolute value* image produced as a result of the software's analytical routine (ENVI, 2001). It should not be confused with the overview and raw RADAR images seen in the text, which are representations of the recorded *decibel responses* of the system (Chap. 3).

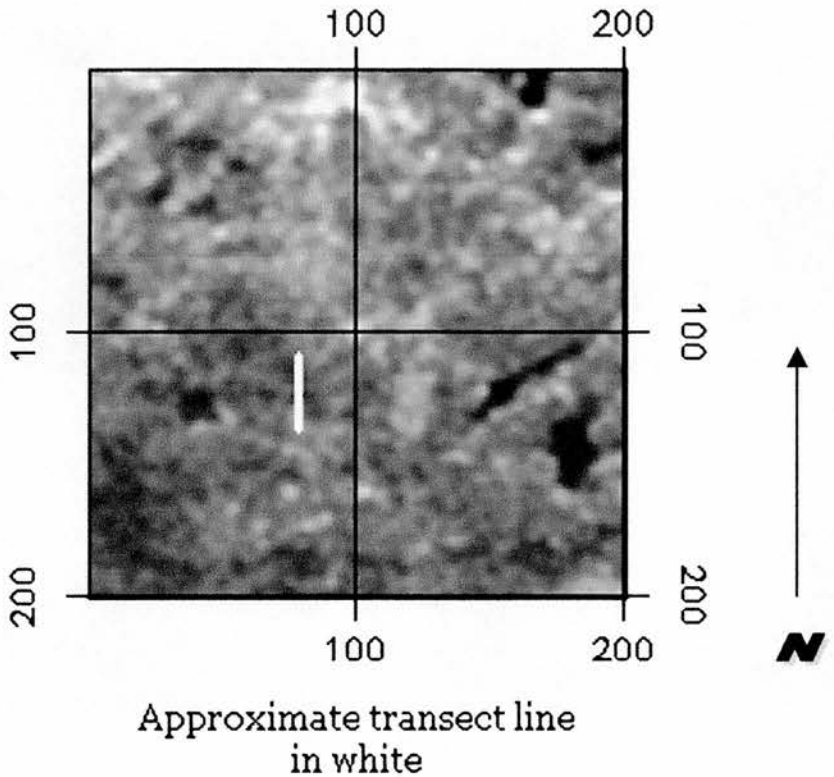

5-19 Chh raw RADAR data, South Ardachy, Islay.

The following image, Figure 5-20, is a scene area illumination map, and as explained in Chapter 4, a *mandatory* requirement for proper interpretation of the Imaging RADAR data in regards to flight direction of the sensor, antenna look direction and incidence angle information (Farr, Blom and O'Leary, 2001, pers. comms). These will be seen for each of the RADAR wavelengths analysed in this chapter as well as the other study regions.

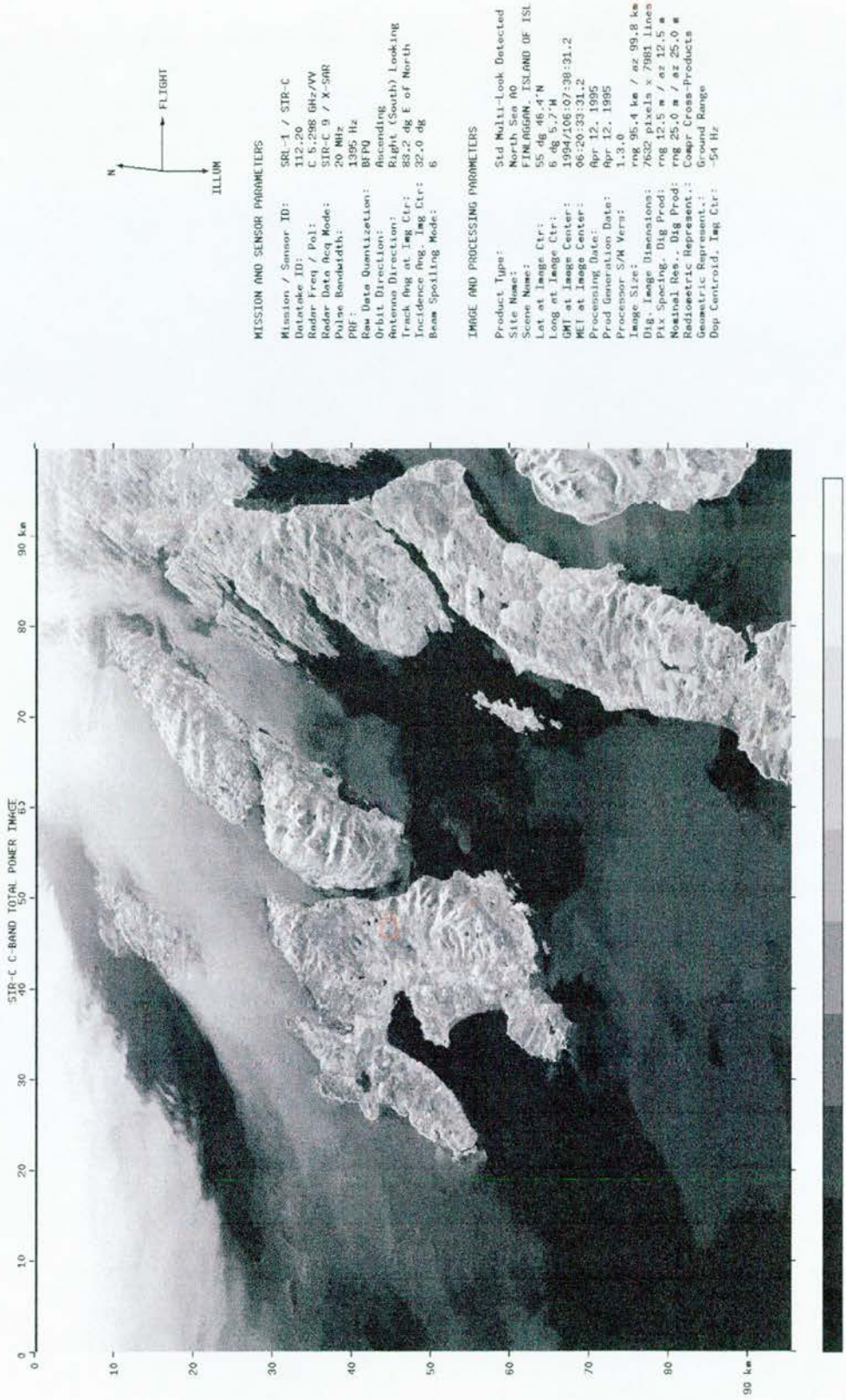

Fig. 5-20 C band, total power RADAR data image map: South Ardachy "A" target mine area in red. Image and information created from CEOS software and header file, NASA/JPL.

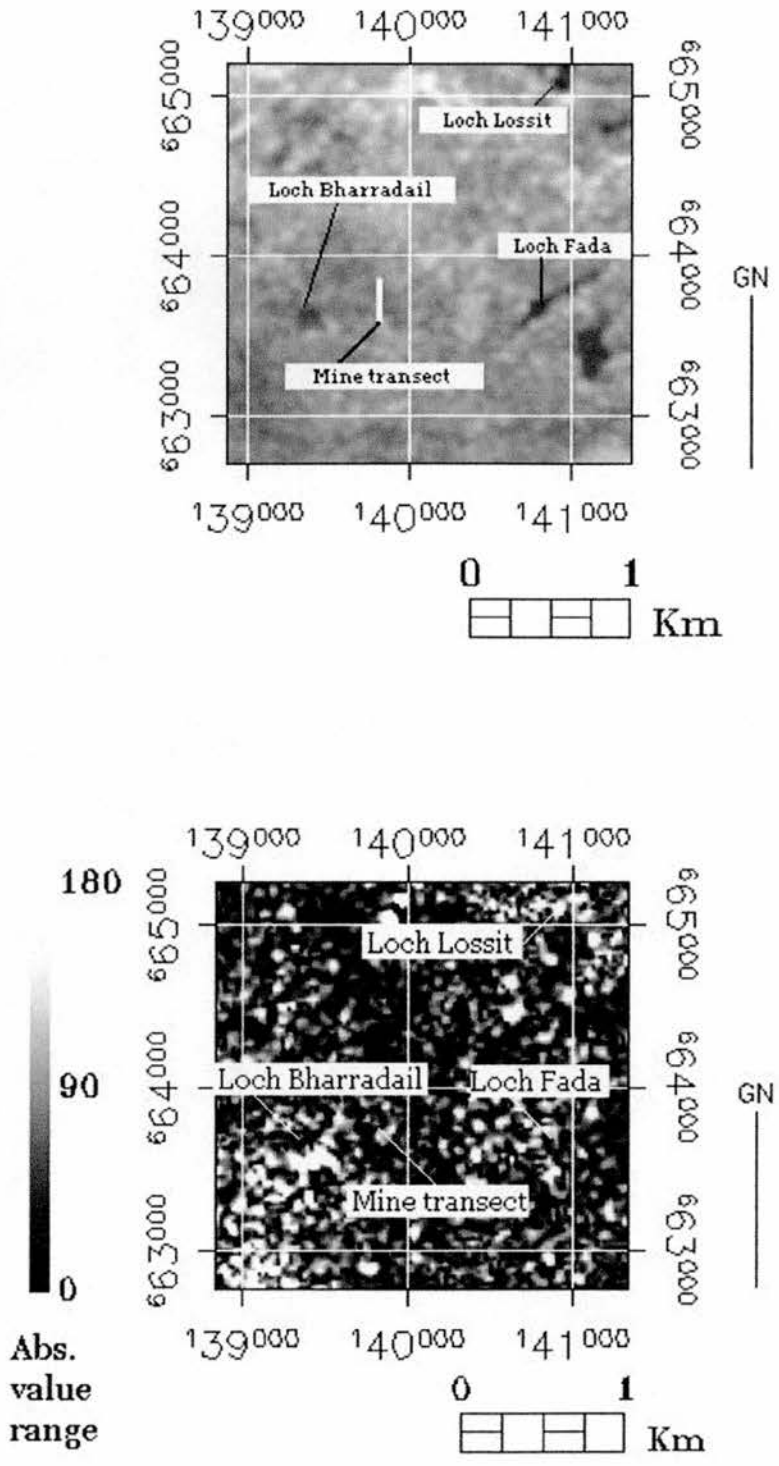

Fig. 5-21 Decibel image (Chh, above) and phase difference absolute value image (below) for C band 1208 by 1637 to 1646, South Ardachy, Islay

Pixel Co-ordinate	Chh (db)	Cvv (db)	Phase Difference
1208x1637	-7.03	-8.93	-4.44°
1208x1638	-6.46	-8.22	-5.71°
1208x1639	-5.65	-7.42	-10.98°
1208x1640	-6.26	-7.74	-6.99°
1208x1641	-8.11	-9.45	-3.81°
1208x1642	-9.20	-10.33	-9.36°
1208x1643	-8.91	-10.60	-3.07°
1208x1644	-8.23	-10.27	5.24°
1208x1645	-7.68	-9.09	1.08°
1208x1646	-7.15	-8.56	-4.80°

Table 5-3 Mine site transect, South Ardachy, Islay, C band decibel and phase difference statistics.

The first observation is that C band responds to the earth's topography at the target mine by registering a -6.99° change in phase difference. The phase difference absolute value image shown in Figure 5-21 (red arrow) indicates a change in magnitude in the area *near* the mine transect ranging between 90° and 180°, which is inconsistent with this result. This may be caused by the reflecting surfaces influencing the backscatter recorded over the mine transect, but again ground position error must be taken into account. Strong Cvv decibel responses in the target site transect are reported until the pixel corresponding with the mine, where the Chh decibel response is nearly equal to that of the Cvv. Perhaps this indicates a concentrating effect for the Cvv polarisation, due to the depth of the trial mine inhibiting backscatter to the sensor's antenna or more likely, equally responsive reflective surfaces which are larger than the bandwidth. It should be noted that the mine may lie on the border of pixel 1208 x 1639, which shows a large change in magnitude, since the registration of the image set will have an inherent inaccuracy versus the actual ground range of the RADAR data (Chap. 3). It should also be noted that the absolute phase difference image highlights other areas of large phase differences within the image window, but which are not associated with mine features.

5.9.3.3 L band Imaging RADAR phase difference analysis: "A" mine, South Ardachy

The image data set for the "A" mine target site at South Ardachy was the same as for the C-band data set. The transect of decibel and phase difference analysis over the mine begins at pixel 1208 by 1637 and ends at 1208 by 1646. An overview image map of the raw Lhh RADAR data is provided in Fig. 5-22 and a target illumination map in Fig. 5-23. The direction of analysis is from the northernmost pixel to the southernmost pixel. Again, pixel 1208 by 1637 is the northernmost pixel within the transect with 1208 by 1646 being the southernmost. Immediately following this map are the pixels analysed for their decibel response qualities and their phase difference statistics in Figure 5-24 and Table 5-4.

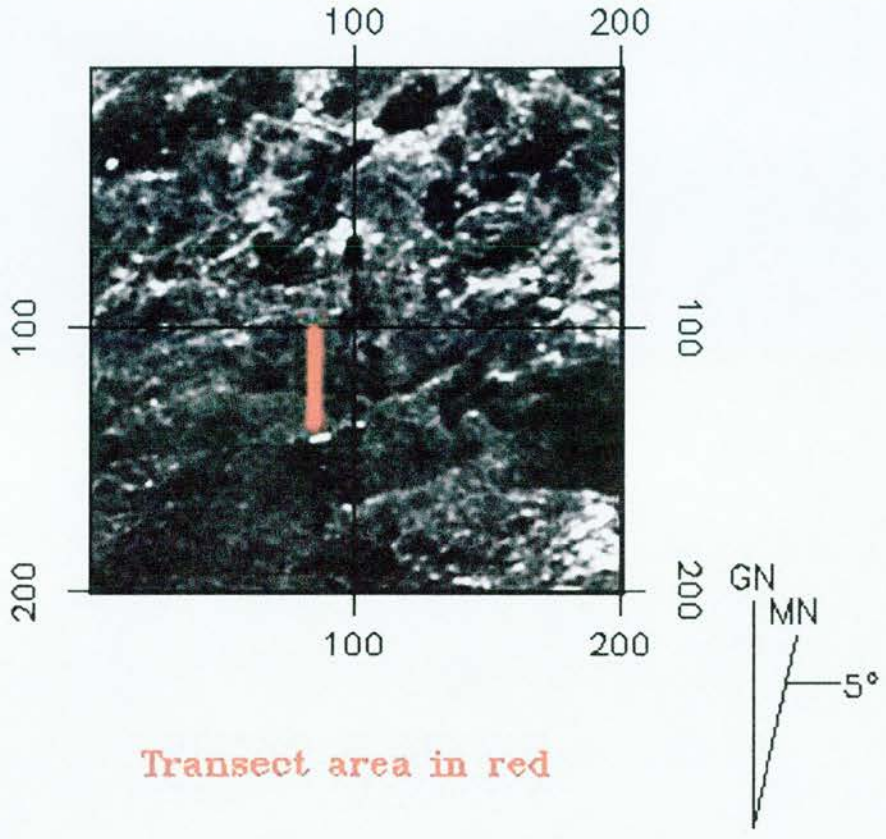

Fig. 5-22 Lvv raw RADAR data, South Ardachy, Islay.

Fig. 5-23 L band, total power RADAR data image map: South Ardachy "A" target mine area in red. Image and information created from CEOS software and header file.

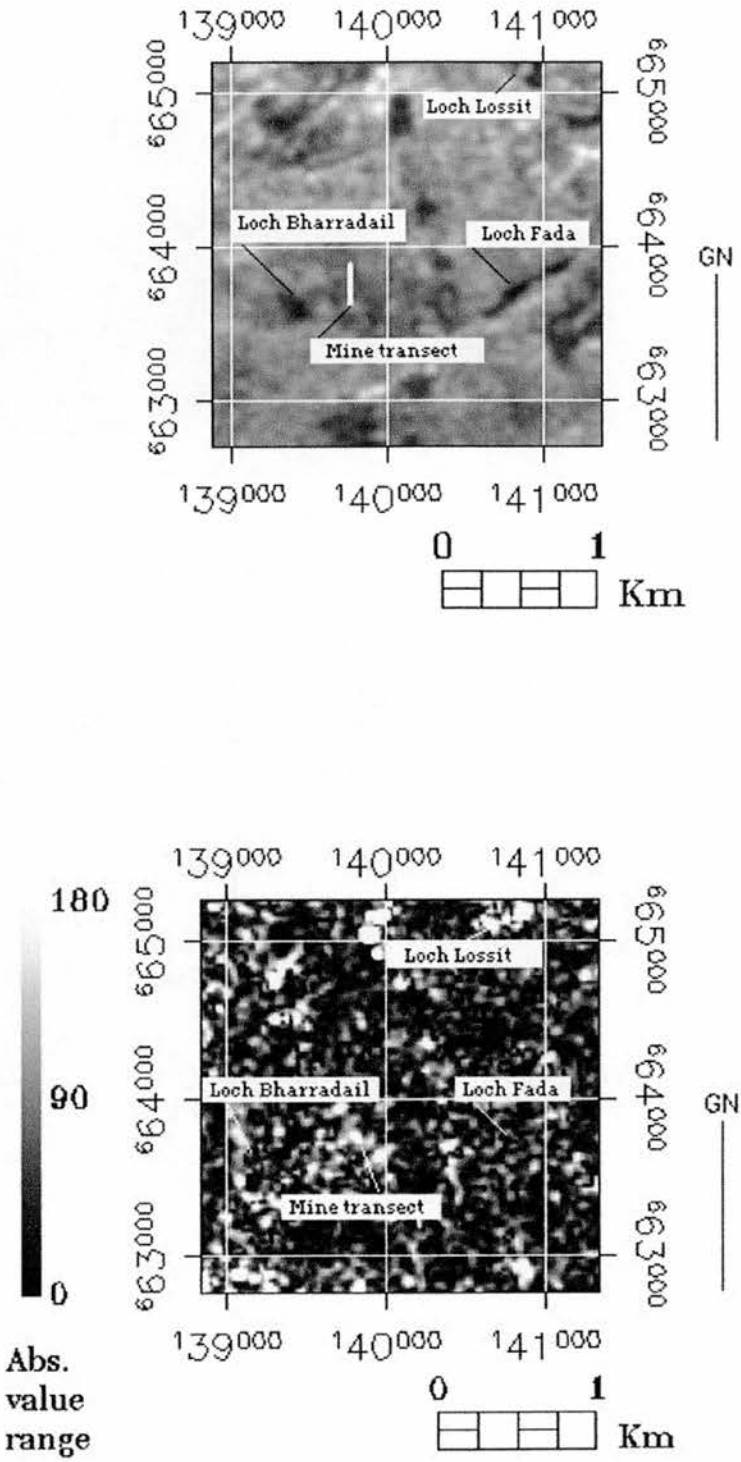

Fig. 5-24 Decibel image (Lhh, above) and phase difference absolute value image (below) of L band, pixels 1208 by 1637 to 1646, South Ardachy, Islay.

Pixel Coordinate	Lhh (db)	Lvv (db)	Phase Difference
1208x1637	-11.05	-10.61	12.63°
1208x1638	-12.79	-12.55	12.22°
1208x1639	-15.55	-14.42	9.28°
1208x1640	-15.26	-13.99	6.11°
1208x1641	-14.08	-13.36	5.85°
1208x1642	-14.86	-14.34	3.54°
1208x1643	-16.17	-14.76	7.05°
1208x1644	-16.62	-14.79	14.57°
1208x1645	-15.28	-13.66	2.20°
1208x1646	-13.69	-12.28	-4.15°

Table 5-4 Mine site transect, South Ardachy, Islay, L band decibel and phase difference statistics.

While the C band responds to the earth's topography at the target mine by registering a -6.99° change in phase difference, the L band reported a 6.11° change in magnitude. Further, when compared to the C band phase difference absolute value image of Fig. 5-21, the L band absolute value image of Fig. 5-24 (red arrow) shows a greater area of magnitude change along the entire transect represented by the values ranging between 90° and 180° (ENVI, 2000). The L band transect of the trial mine area indicates a rough surface in the Lhh decibel responses until the moment it crosses the trial mine, where the difference between the Lhh and vv responses becomes reduced; there is also a change in polarimetric phase difference (Ulaby and Dobson, 1989). As noted before, the mine may lie on the border of pixel 1208 x 1639, which shows a large change in magnitude, thus the registration of the image set may have an inherent inaccuracy versus the actual ground range of the RADAR data (Chap. 3). As with the C-band data analysis, it should also be noted that the absolute phase difference image highlights other areas of large phase differences within the image window, but which are not associated with mine features.

5.9.3.3.1 Comparative transect

A nearby portion of the South Ardachy mine complex was chosen to demonstrate the capability of the multipolarimetric Imaging RADAR system. Referring back to Fig. 5-18, of the mine site, a transect was chosen which bisected the area east of the tailings dump and west of the isolated shafts leading towards Loch Bharradil. The same transect parameters were used, with each pixel encompassing 12.5 metres of earth terrain, for approximately 125 metres total. The comparative transect of decibel and phase difference analysis begins at pixel 1215 by 1656 and ends at 1215 by 1665. An overview image map of both the comparative transect and the mine site transect is provided in Fig. 5-25. The direction of analysis is from the northernmost pixel to the southernmost pixel. Again, pixel 1215 by 1656 is the northernmost pixel within the transect with 1215 by 1665 being the southernmost. Immediately following this map are the pixels analysed for their decibel response qualities and phase difference statistics with the C band data presented first, followed by the L band data.

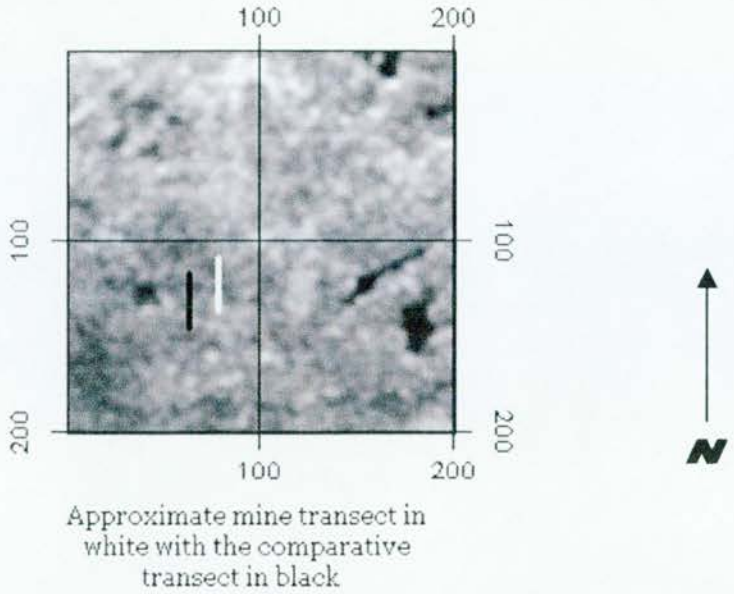

Fig. 5-25 Comparative transect (left) and mine site transect (right) in red, top; image of transect area terrain, bottom. View is from the north to the south with the hills of Beinn Bhreac, Sgorr nam Faoileann and Maol a Bharra in the distance, left to right. Comparative transect is the field in the top centre of image.

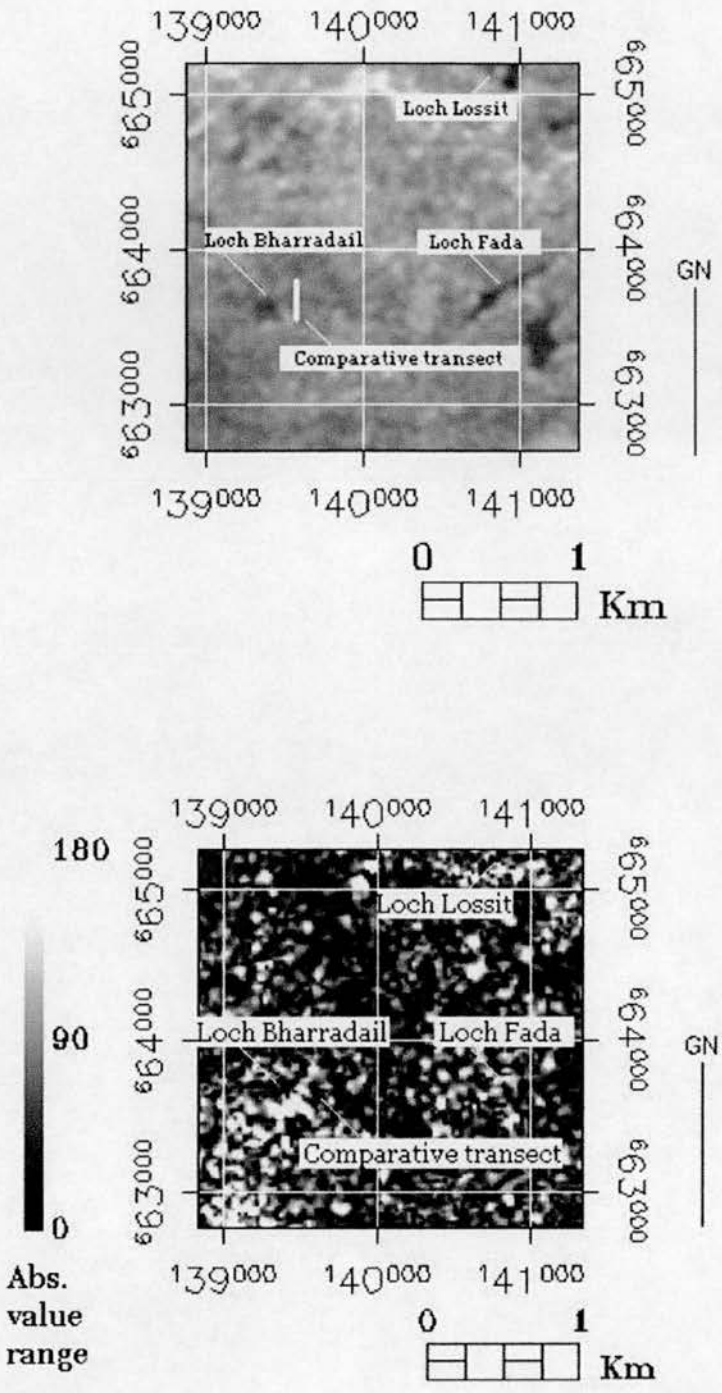

Fig. 5-26 Decibel image (Chh, above) and phase difference absolute value image (below), pixels 1215 by 1656 to 1665 (C band, comparative transect), South Ardachy, Islay.

Pixel Co-ordinate	Chh (db)	Cvv (db)	Phase Difference
1215x1656	-10.08	-8.41	0.00°
1215x1657	-8.58	-7.38	-1.03°
1215x1658	-9.84	-8.99	-0.54°
1215x1659	-11.49	-11.25	-0.62°
1215x1660	-11.53	-11.36	2.07°
1215x1661	-11.10	-12.09	4.93°
1215x1662	-11.96	-12.33	0.73°
1215x1663	-11.91	-9.31	2.26°
1215x1664	-11.36	-9.79	4.39°
1215x1665	-11.21	-9.66	6.63°

Table 5-5 Comparative transect, South Ardachy, Islay, C band phase difference image with decibel statistics.

The phase difference reports from the middle pixel of the comparative transect, as well as those along the entire transect are different than those along the target mine rake transect, which are well represented by the phase different absolute value image in Fig. 5-26 (red arrow). The topography is flatter with a slight downward slope to the south-east, thus the C band reports no phase difference change similar to the Site "A" mine rake.

The C band decibel responses and phase difference statistics are consistent with those reported by Ulaby and Dobson (1989) when imaging a field with short, pasture grass. The L band information, presented next, will also indicate nearly the same situation.

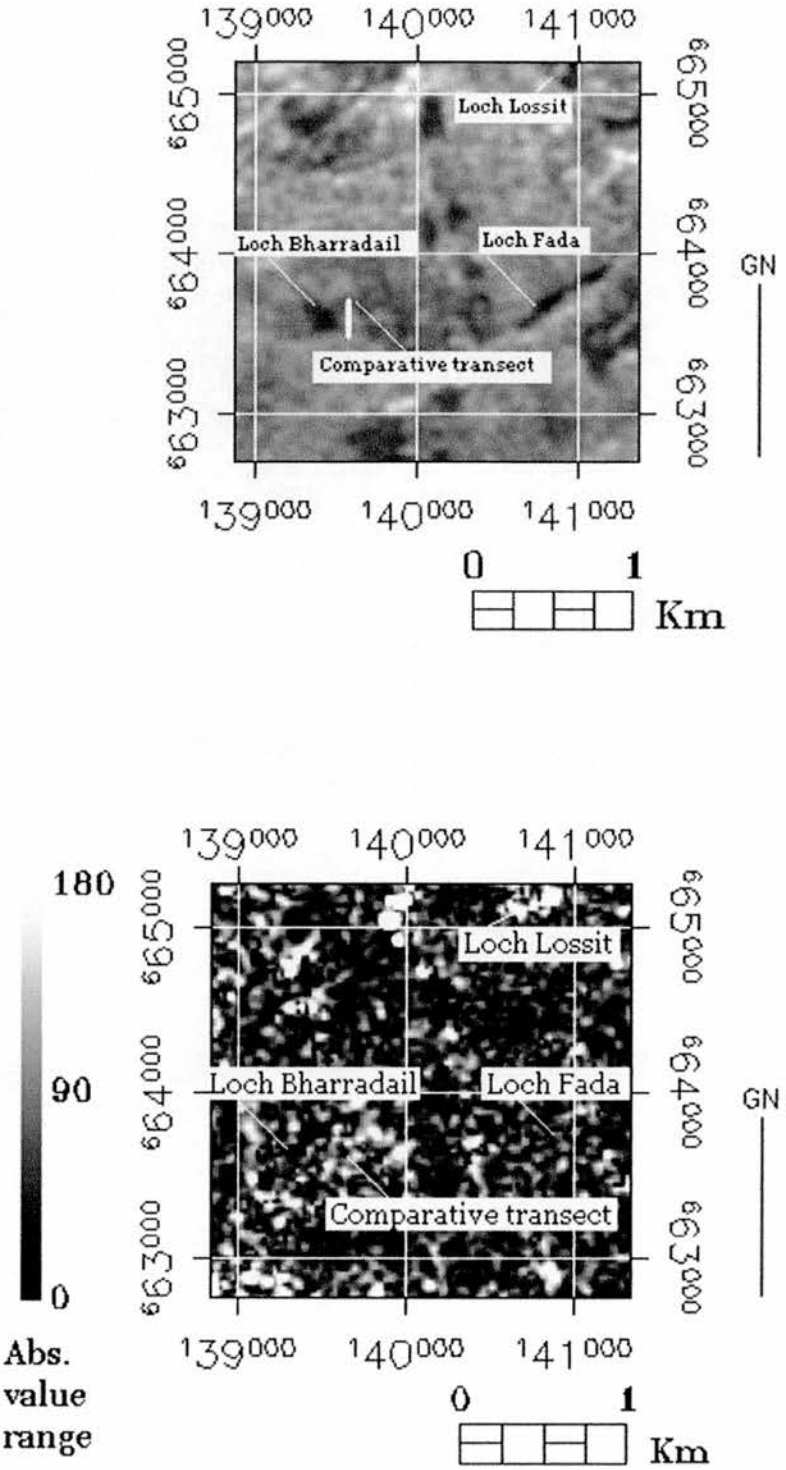

Fig. 5-27 Decibel (Lhh, above) and phase difference absolute value image (below), pixels 1215 by 1656 to 1665 (L band, comparative transect), South Ardachy, Islay.

Pixel Co-ordinate	Lhh] (db)	Lvv (db)	Phase Difference
1215x1656	-14.58	-14.38	0.51°
1215x1657	-10.70	-11.28	2.96°
1215x1658	-10.48	-10.99	3.91°
1215x1659	-13.83	-13.18	0.00°
1215x1660	-16.31	-14.12	-1.57°
1215x1661	-17.89	-15.33	2.67°
1215x1662	-19.11	-16.63	2.98°
1215x1663	-16.40	-15.06	0.00°
1215x1664	-13.37	-13.20	0.00°
1215x1665	-13.35	-13.52	-0.55°

Table 5-6 Comparative transect, South Ardachy, Islay, L band decibel response and phased difference statistics.

Again, the phase difference reports observed from the middle pixel of the comparative transect are different than for those covering the target mine rake. The phase difference absolute value image in Fig. 5-27 (red arrow) indicates this as well as there is minimal change in magnitude according to the 0 to 180 grey scale mapping of the data (ENVI, 2001). Since the topography is relatively flat with a slight downward slope to the south-east, thus the L band reports no phase difference change similar to the Site "A" mine rake pixel. Thus, the L band can be said to demonstrate decibel responses and phase difference statistics consistent with the type surface being recorded, a field with short, pasture grass (Ulaby and Dobson, 1989).

5.9.3.4 Comparative analysis of the South Ardachy mine site RADAR data

Pixel 1208 x 1640 is the pixel which coincides with the location of the upper trial mine shaft at Site "A" in the South Ardachy mines complex (See Fig. 5-28). There is a particular difference between the C and L band decibel responses and phase difference analysis reports. They are displayed in Table 5-7 for comparison.

Fig. 5-28 Mine shaft of pixel 1208 x 1640, Site "A", South Ardachy; view to south.

Pixel Co-ordinate	C/HH (db)	C/VV (db)	Phase Difference
1208x1640	-6.26	-7.74	-6.99°

Pixel Co-ordinate	L/HH (db)	L/VV (db)	Phase Difference
1208x1640	-15.26	-13.99	6.11°

Table 5-7 Pixel 1208 x 1640 decibel response and phase difference report

The distance across the trial mine shaft in Fig. 5-28 is 9.1 metres in the east-west axis and 11.2 metres in the north-south axis. It is approximately 4 metres deep at the north end and rises to 1.5 metres at its shallowest depth in the southern end (See Fig. 5-29). The map in Fig. 29 is generalised, as the resolution of the RADAR sensor does not see smaller surface facets.

The first observation is that C band responds to the earth's topography at the target mine by registering a -6.99° change in phase difference, while the L band reports a 6.11° change in magnitude, which are both displayed in Fig. 5-21 and Fig. 5-24 as phase difference absolute value images. Strong Cvv decibel responses in the target site transect are reported until the pixel corresponding with the mine, where the Chh decibel response is nearly equal to that of the Cvv. Perhaps this indicates a concentrating effect for the Cvv polarisation, due to the depth of the trial mine inhibiting backscatter to the sensor's antenna or more likely, equally responsive reflective surfaces which are larger than the bandwidth. The L band transect of the trial mine area indicates a rough surface in the Lhh decibel responses until it reaches the trial mine, where the difference between the Lhh and vv responses becomes reduced; there is also a slight reduction in polarimetric phase difference (Ulaby and Dobson, 1989). It should be noted that the mine may lie on the border of pixel 1208 x 1639, since the registration of the image set will have an inherent inaccuracy versus the actual ground range of the RADAR data (Chap. 3).

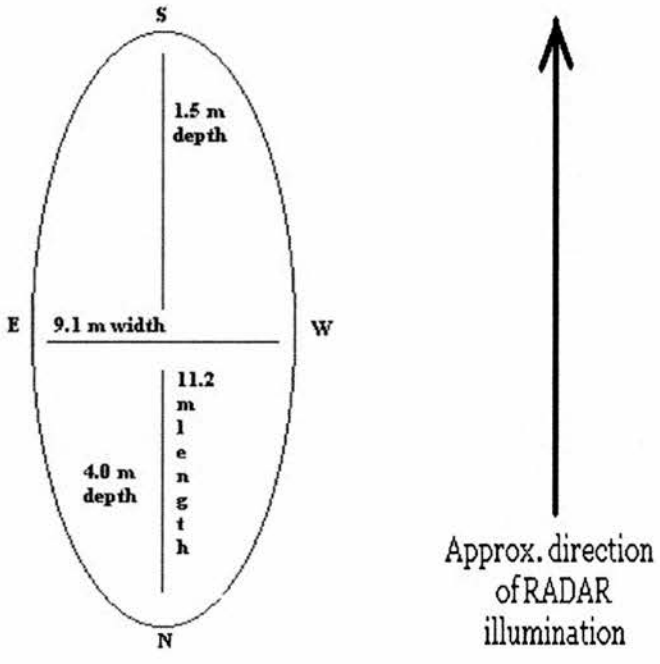

Fig. 5-29 A general RADAR target map of the mine shaft at pixel 1208 x 1640, Site "A", South Ardachy

A comparative pixel from the tailings region transect, south-west of Site "A", coincides with pixel number 1215 x 1650, seen below in Fig. 5-30. The C band and L band decibel responses and phase difference report may be seen in Table 5-8.

Fig. 5-30 Mine tailings area Southwest of Site "A", South Ardachy; view to south.

Pixel Co-ordinate	Chh (db)	Cvv (db)	Phase Difference
1215x1660	-11.53	-11.36	2.07°

Pixel Co-ordinate	Lhh (db)	Lvv (db)	Phase Difference
1215x1660	-16.31	-14.12	-1.57°

Table 5-8 Pixel 1215 x 1660 decibel response and phase difference report

The phase difference reports observed from the middle pixel of the comparative transect are characteristically different than for those over the target mine rake and are graphically presented in Fig. 5-26 and Fig. 5-27 as phase difference absolute value images. Here, the topography is relatively planar with only a slight downward slope to the south-east, thus the C band reports no phase difference change similar to the Site "A" mine rake. Both C and L band demonstrate decibel responses and phase difference statistics commensurate with the type surface being recorded, a field with short, pasture grass (Ulaby and Dobson, 1989).

In referring to the Lvv raw data image scene subset (See Fig. 5-22) and the Lvv overview image (See Fig. 5-23), the darker grey colour tones in the image scene correspond with pixels which exhibit the decibel return levels in pixels such as 1208 x 1640, as an example (Chap. 3). These image scenes, as an example, should be compared with the graphical representation of the phase differences reported for the same image scene subset where the piece-wise linear stretch is used to map the degree of difference between the hh and vv polarisations (ENVI, 2001). It can be seen that two distinct characteristics of the Imaging RADAR system are being visualised in these images, decibel response and phase difference. The first reports the *quantity* of RADAR backscatter, polarised or otherwise, from a target while the second reports the *quality* of a polarised RADAR band after striking a target. If an attempt were made to *qualify* a trial mine solely on its RADAR decibel return, this would provide only some information as it is obvious from the just mentioned overview images that there are numerous dark pixels within most RADAR image scenes that represent weak returns that may be caused by surfaces which are specular (Chap. 3).

Polarimetry, as discussed in Chapter 3, permits us to *qualify* and *quantify* the particulars of the target mine site due to the position of each of the unique reflecting surfaces in relation to the horizontal or vertical mode of the emitted microwave *and* the strength of their backscatter returns; i.e. in this case, essentially a roughly elliptical excavation in the earth's surface. Again, referring back to the discussion on corner reflectors and phase difference in Chapter 3, it was assumed that the South Ardachy trial mine (pixel 1208 x 1640) would function as a dihedral in response when viewing the L results since it is known to be more responsive to lineal features (Fig. 5-31 and Abdelsalam *et al*, 1995). The C band results were expected to be somewhat significant due to fact that there was only a small vegetation canopy that would inhibit backscatter response. Decibel and phase difference reports for both bands show that the Imaging RADAR can detect the subtle deviations in topography created by an ancient mine working. However, it cannot categorise the mine as a specific reflector due to its irregular shape and the low sensor resolution.

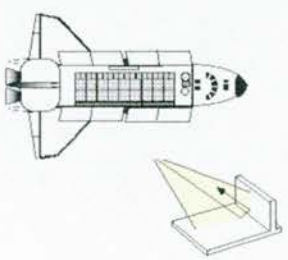

Fig. 5-31 Shuttle RADAR illumination of a dihedral reflector (Adapted from CCRS and JPL 2001).

The decibel response and polarimetric phase difference information for the comparative transect sample pixel, 1203 x 1645, is indicative of a field covered with very short grass (Fig. 30 and Table 5-8). The planar nature of the topography is notable by the lack of large phase difference responses until the last pixels, 1215 x 1663 through 1215 x 1665. The C band comparative transect shows increasing changes in magnitude in Tables 5-5, which may be due to small scatterers of mine spoil that are still present at the margins of the field bordering the spoil heaps; these are seen in the foreground of Fig. 5-30, stretching towards the field. The phase difference absolute value image of Fig. 5-26 demonstrates the magnitude of change along the C band transect by grey scale colour mapping the statistical change to a 0 and 180 schema, which shows minimal veering to the 180 end of the scale (ENVI, 2001). It should be noted that the limitations of analogue representation of these data make it difficult to perceive these subtle variations outwith the viewing of the data in a digital format.

The use of decibel response and polarimetric phase difference via absolute value images to perform analysis at South Ardachy revealed two problems in its limitations, sensor resolution and the unique shape of the target mine. Addressing the resolution issue first, the nominal resolution of the Shuttle Imaging RADAR was 12.5 metres for this data set and it was expected that the size of the target mine, which approximated the sensor's resolution, and the area's surface roughness, speaking in RADAR terms, would make a target such as the trial mine site evident (See Chapter 3). However, when viewing an image subset of the target scene area in its native digital format the mine complex features are not exceptionally distinct though they do seem to appear as anomalies in what would be an otherwise homogeneous rock structure (i.e. the Dalradian limestone) when viewed in a pseudo-colour composite image (Section 5.9.4).

The second issue, that of the shape of the target mine site, was more difficult to assess. It is likely that the unique shape and depth of the mine creates a trapping effect in the vertical orientations of the transmitted RADAR waves, thus affecting backscatter response. The ideal mechanism to have tested this hypothesis would have been the construction of a physical model utilising the same materials, environmental conditions, and the Shuttle Imaging RADAR instrument; this was of course impossible. Modelling by computer methods was also not possible, as there was no polarimetric modelling and analysis software available during the course of the study, nor fully polarimetric data in a proper format (Chap. 9, Chapman, Farr and O'Leary, 2001, pers. comms.).

Still, transects of decibel and absolute phase difference analysis indicated that differences between a mine site and the surrounding area may be detectable through an analysis of absolute phase differences. However, the large phase difference was not a unique signature to the mine as the distribution of large phase differences across the images showed.

Finally, as an additional aid in visualising how the microwaves are interacting with the terrain at South Ardachy, line charts which display the polarimetric phase difference and decibel responses recorded by the sensor are presented in figures 5-32a and 5-32b. Pixel 1 represents the southernmost pixel in each transect and Pixel 10 represents the northernmost pixel in each transect.

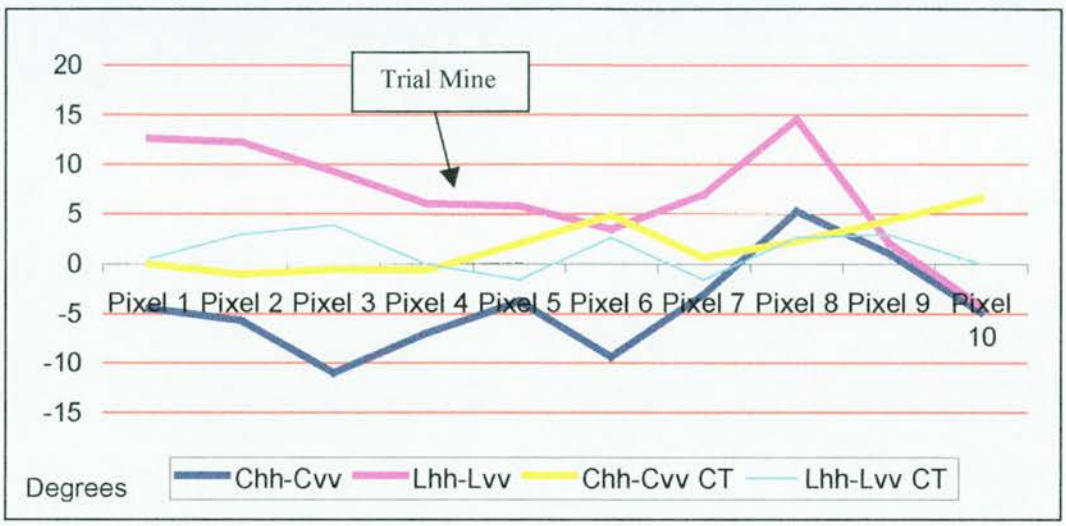

Fig. 5-32a South Ardachy polarimetric phase difference records for all transects

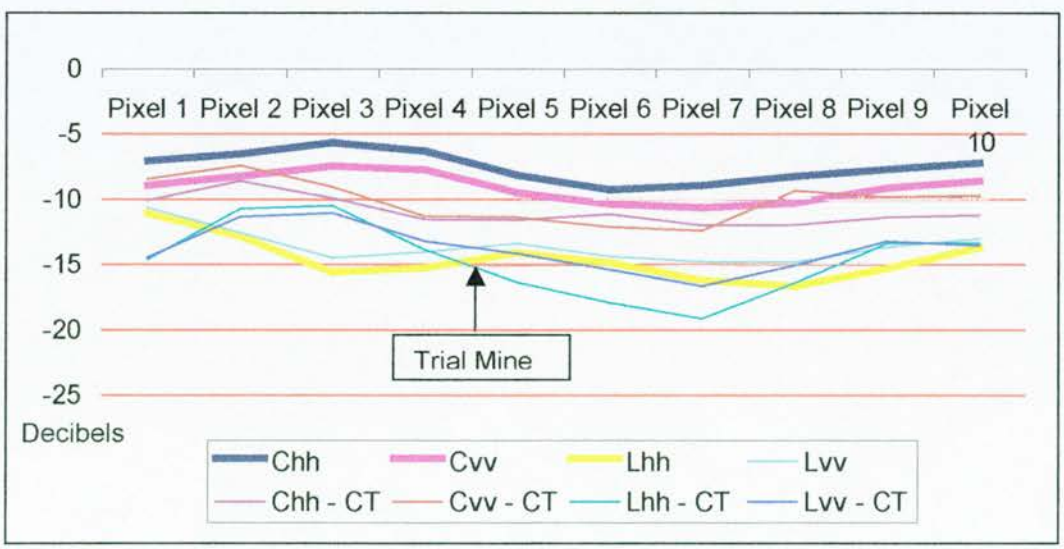

Fig. 5-32b South Ardachy decibel responses for all transects

In Chapter 3 it was noted that stray backscatter will occur as RADAR wavelengths strike the earth's surface and rebound in odd manner of axis, thus creating extraneous signal noise or speckle in recorded images (See Fig. 5-23). De-speckling, or noise reduction, in Imaging RADAR data is important and as in all RADAR processing, the balance between speckle reduction and loss of data is a very fine line. Since the particular emphasis in using Imaging RADAR for this archaeological study was the detection of ancient mines, it was decided to use a filtering process that would retain maximum detail while ridding extraneous noise. The results of this portion of the RADAR data analysis are described in the following section concerning visualisation.

5.9.4 Imaging RADAR topographic modelling and visualisation

5.9.4.1 Data fusion and representation

Chapter 4 described the general process by which Imaging RADAR data was processed and manipulated to enhance analysis. Only specific alterations to the general processes will be discussed here, as reference back to Section 4.9.4 will provide in-depth descriptions.

The master DTM, originally in a geographic co-ordinate system and WGS-84 datum, was rectified, registered and projected into the Transverse Mercator projection, using the standardised U.K. spheroid known as the Airy, with the 1936 OSGB datum as its reference (BOS, 1987: Sheet 60 – Islay).

The Cvv, Lhh and Lvv MLC polarisation images, having been fully processed and analysed, were then rectified, registered, and projected to the same U.K. co-ordinate system. Sixteen Ground Control Points (GCPs) were utilised with a RMS of 0.9 pixels accuracy.

The projected images were overlaid, or fused with the DTM after creating a pseudo-colour image as mentioned in Chapter 4 and below in Section 5.9.4.2 (Kruse and Dietz, 1991). The premise behind this additional technique was to enable comparison between the Cvv detection of surface rock structures with the lineal detection of Lvv and the capability of Lhh to survey geomorphology (Blom and Daily, 1982). In some instances sub-surface detection of geological structures has occurred beneath jungle canopy and deserts depending on the soil aridity and near term climatology (Blom *et al*, 1981).

5.9.4.2 Filter processes

An adaptive filter regimen was used against the Islay MLC data set as described in Chapter 4, Section 4.9.4.2. After suitable processing a pseudo-colour image was created. This image was then sub-sampled to create an image which had a pixel resolution of 3 metres. This was done in order to create a finer detail in the three-dimensional imagery of the fused DTM and RADAR landscape models. It was observed during the creation of the visualisation landscapes that fine resolution images appeared less fragmented upon data fusion than they did as image data at their native resolution.

It was decided to utilise the Cvv wavelength as the Red colour band, the Lvv wavelength as the Green colour, and the Lhh wavelength as the Blue colour band to produce a false composite image. The reasoning behind these colour choices are as follows: Cvv has a wavelength of 3.8 cm ~ which since the area of South Ardachy is largely treeless, means that exposed rock outcroppings would give strong returns. Lvv at 23.5 cm~ is known to enjoy very subtle moisture detection capabilities, thus it was chosen as the Green colour band. Mine shafts, adits, disused puddling ponds and other remnants of mining activities, tend to be moisture collectors. Finally, Lhh, well known in geo-archaeological work for its lineal detection capability, was chosen as the Blue colour band (Abdelsalam *et al*, 1995)

Finally, the composite image was created and overlaid upon the Digital Elevation Model (DEM). Three-dimensional image scenes of the fused RADAR and DTM data are presented in Figures 5-33 through 5-36 with views from the primary compass points of west, north, east and south, surrounding the South Ardachy mines complex. Numerous geological features may be seen by this composite as well as cultural features both recent and of unknown origin.

5.9.4.3 Visualisation: west

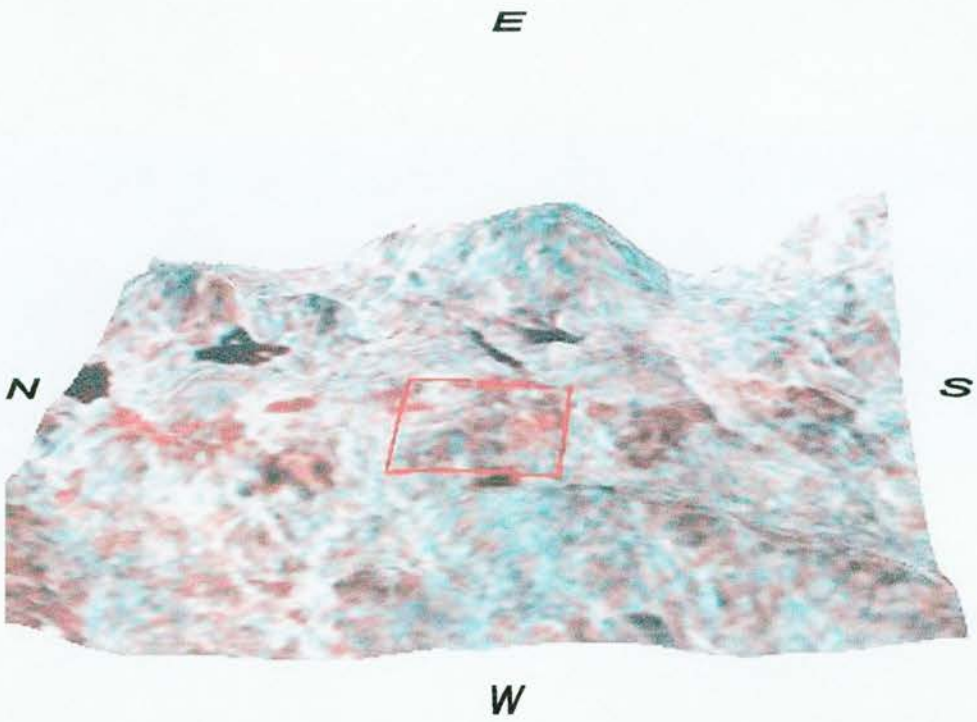

Fig. 5-33 The South Ardachy mines viewed from the west (1:22,784).

In Figure 5-33 the Cvv band (Red) is providing strong returns over the Dalradian limestone outcrops running from the southwest (lower right) to northeast (upper left) and south (middle right edge of image) to north (middle left) near Loch Ballygrant. The Cvv band is giving graphic evidence of a metamorphic interface as the two areas of red-coloured trends collide near the loch. Loch Fada is located above the red box delineating the mine complex, for orientation. The strong blue tones in the right foreground of the image are coincident with a region of heavy concentrations of phyllites and are responding to the Lhh band. The light green tones beneath the left corner of the mining area box are the Lvv returns responding to the Glenn Maraiche area. For comparison of this imagery with area geology see Fig. 5-3, the map of Northeast Islay geology and mines.

5.9.4.4 Visualisation: north

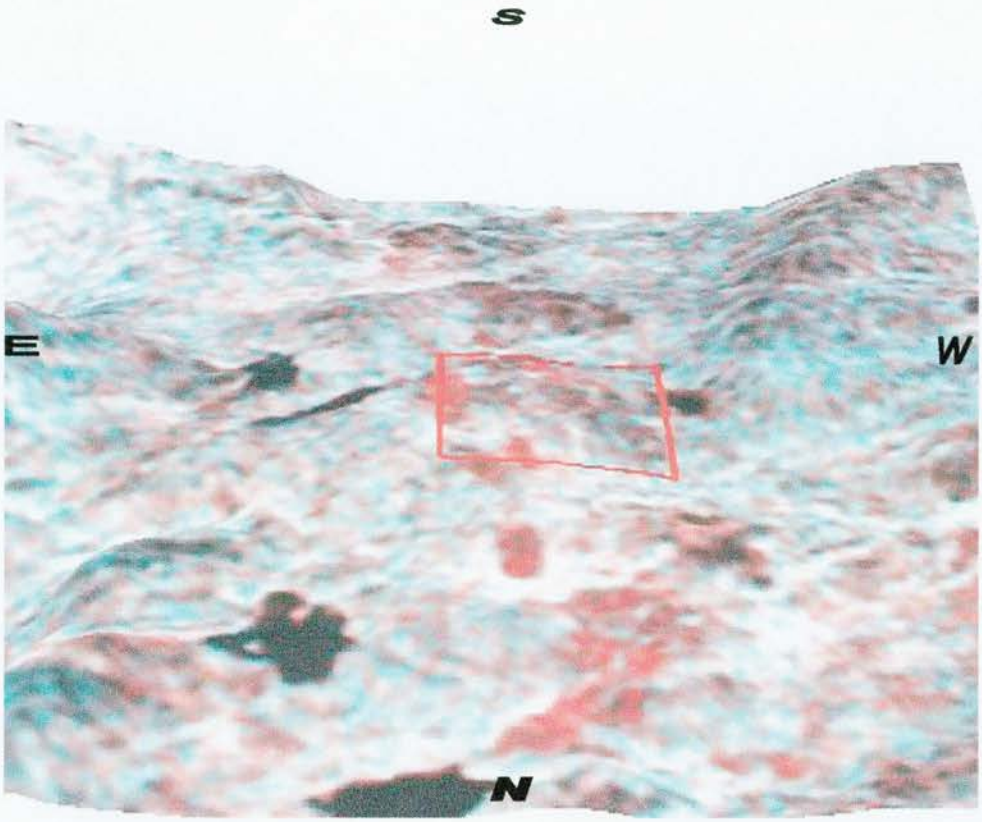

Fig. 5-34 The South Ardachy mines as viewed from the north (1:22,784).

In Fig. 5-34, the Dalradian limestone outcrop which is the primary ore-bearing structure for lead on Islay can be seen trending south (up in this image) and in the foreground to the west (right in this image) as detected by the Cvv band (Red). Loch Lossit displays a dyke bisecting it from the upper left (southeast) to the lower right (northwest) detected by the Lhh band (Blue). The northwest portion of this dyke was unknown cartographically and geologically according to British Geological Survey maps. Lvv band (Green) provides interesting return information over the Baleachdrach region in the northwest (lower left in the image) which is comprised of mixed forest and pasture. Finally, the dominant hill ridge which channels rainfall into Loch Bharradil, Beinn Bharradil, may be seen on the upper right corner of the image, leading down to its terminus at the western edge of the loch.

5.9.4.5 Visualisation: east

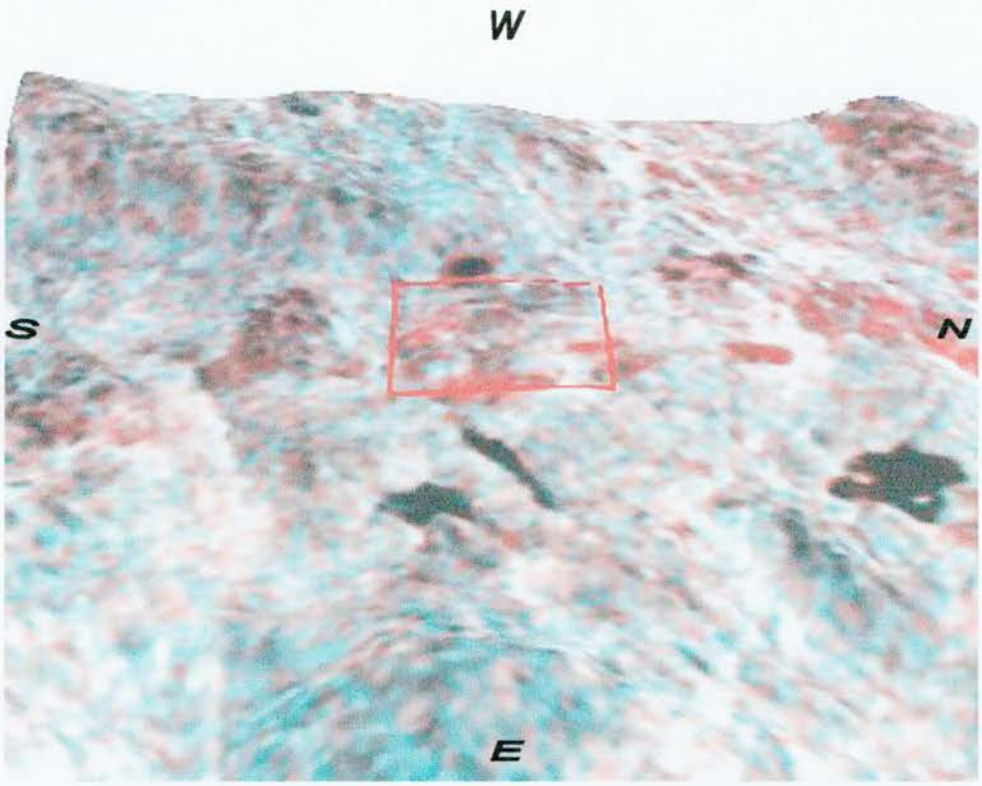

Fig. 5-35 The South Ardachy mines complex viewed from the east (1:22,784).

Fig. 5-35 gives the most demonstrative example of Islay's convoluted topography and geology. The Dalradian limestone that fed the South Ardachy mines complex is obvious as it trends south (left) to north (right) detected by Cvv (Red). However, in this image the present day region of quarrying and mining may be seen to the west (upper right in image) of Loch Lossit near the white tones. The white tones are corner reflectance from the buildings and roof tops of the village of Kilmeny and the nearby industrial workings of the present-day mine. The phyllite rich slopes of Cnoc nan Uan, Beinn Bharra-dail, and Beannan Tir Mhacaimh to the west of the South Ardachy complex are evident in their blue tones from the Lhh band returns. Note the slight green tones at the foot of these hills indicating higher moisture content from the Lvv band. Finally, the crannogs of Loch Ballygrant, located on the lower right of the image scene, are quite prominent and well delineated by both the Cvv band and Lhh band; the geological dyke is well visible from this view angle as well.

5.9.4.6 Visualisation: south

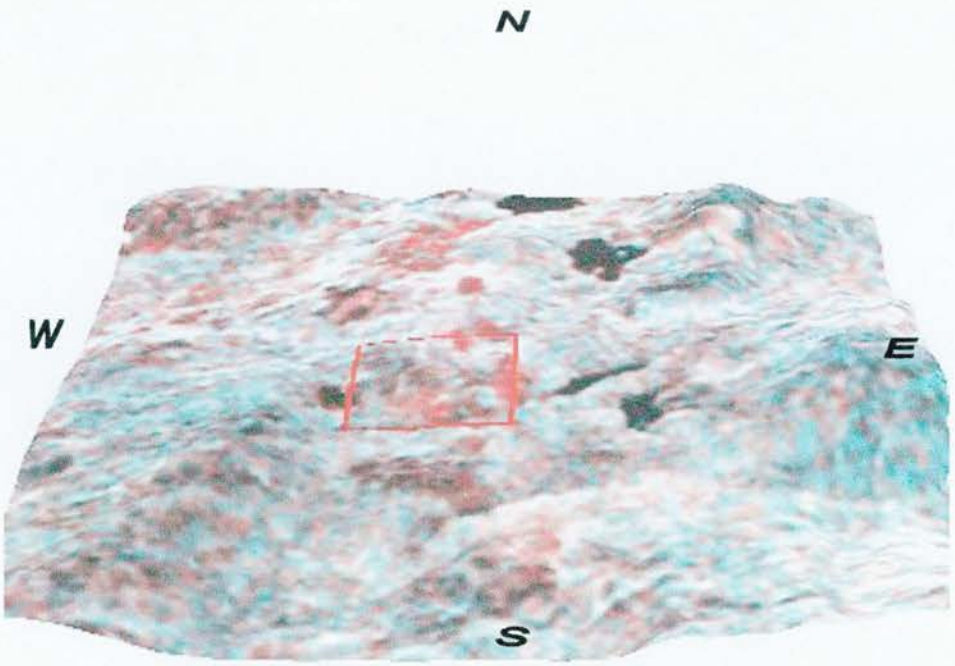

Fig. 5-36 The South Ardachy mines as viewed from the south (1:22,784).

Fig. 5-36 provides an excellent view of the Dalradian limestone outcrops oriented north to south and the intersecting south-west trend. The red box defining South Ardachy has been situated further southward in this view to draw attention to the dark returns within the limestone outcrops. The centre, lower dark return is the major area of ore extraction surrounding pixels 1208 x 1640 and 1208 x 1641.

These images demonstrate an additional objective of this study. While South Ardachy is a previously known area of mining, and the objective was to determine if it were possible to observe a peculiar multipolarimetric RADAR waveform related to mine shafts, it was also important to demonstrate Imaging RADAR's capability to map an area's geology as this would best determine a region's ability to support ancient mining. While that may be done in area such as the United Kingdom, which has been fairly well mapped geologically, in other remote areas of the world where ancient mining is known to have occurred, these cartographic resources are non-existent. It should also be added that several unknown larger scale geological features were discovered on the entire Islay RADAR data set, such as the geological dykes near Loch Ballygrant (Ruckley, 2000, pers. comm).

5.10 Summary of results: South Ardachy, Isle of Islay

5.10.1 Imaging RADAR and the topography

After a description of the historical and physical geographic setting behind ancient mining on the Isle of Islay, a detailed topographic analysis was performed on an area surrounding the chosen test site, the South Ardachy mining complex. Topographic analysis revealed a terrain surface of undulating hills, marked by a geological interface.

A Space Shuttle Imaging RADAR data set covering the South Ardachy mine complex on the Isle of Islay was then analysed using the polarimetric phase difference method to determine if the RADAR system was capable of detecting a trial mine shaft by its unique shape within the topography. It was not possible to ascertain, however, whether or not the multi-polarimetric Imaging RADAR system viewed the shape of the target mine site, which is essentially an elliptical depression in the ground, as a dihedral or some other type of corner reflector using polarimetric phase difference analysis. A sample pixel from the mid-section of a comparative transect traversing a portion of the terrain south of the trial mines was also examined; it revealed no significant reflectors in the C band or L band either; this was expected due to the planar nature of the area's topography. Fully polarimetric data and analysis results and the construction of a computer model would likely reveal the complex microwave interaction with the mine's unique shape and position.

Finally, a false colour composite of the South Ardachy mines region was created from the Cvv, Lvv, and Lhh bands of the MLC data subset. This false colour composite was then draped over a DTM for three-dimensional visualisation of the archaeological landscape surrounding the mines. The false-colour composite highlighted the Imaging RADAR capability to map the geo-archaeology of the South Ardachy region, revealing further possible areas of ancient mining activity.

The next chapter will present the results of the investigation of the mines of Serabit El-Khadim, located in the Sinai Peninsula of Egypt. Following that chapter, the investigation results for the mines of Conil in Spain will be presented.

Chapter 6

Serabit El Khadim

"Pharaoh Neco, after calling off construction of the canal between the Nile and the Red Sea, sent out a fleet manned by a Phoenician crew with orders to sail round and return to Egypt and the Mediterranean by way of the Pillars of Hercules...after two full years, and during the course of the third, they returned, reporting what they saw". "The Histories" by Herodotus (Herodotus, translated by de Selincourt, 1996: 128).

6.1 Introduction

This chapter presents the results of the Imaging RADAR (NASA SIR-C/X-SAR) archaeological survey of the Serabit El-Khadim mines located in the Sinai Peninsula, Egypt. Section 6.2 is a description of the physical geography of the peninsula, which is followed by a historical geography in Section 6.3. Site topography and analysis is outlined in Section 6.4. Section 6.5 presents site history and archaeology, while Section 6.6 displays the CORONA satellite imagery. Section 6.7 presents AVHRR data immediately preceding the overpass of the Space Shuttle and its Imaging RADAR system. Section 6.8 covers the local meteorological data immediately preceding the overpass of the Shuttle Transport System (STS). Detailed Imaging RADAR analysis data are outlined in Section 6.9. Section 6.10 concludes the chapter with a summation of the data presented.

6.2 Physical Geography and Geology

6.2.1 The Physical Geography of the Middle Sinai

Physical geographers commonly divide the Sinai of Egypt into eight main regions. Listed from the Mediterranean Sea to the southern tip of the Sinai they are: 1) the Dune sheet of the Littoral reach of the Mediterranean, 2) the Insular Massifs of the jebels or mountains, 3) the sand deserts of the Suez foreshore area, 4) the gravel and rock terrain of the El Tigh escarpment, 5) the Dividing Valleys lying between the El Tigh and Sinai Massif, 6) the Sinai Massif, 7) the plains of Qa and finally, 8) the Aqaba foreshore (Greenwood, 1997). This study is concerned only with the Insular Massifs or jebels of the Maghara and the nearby Dividing Valleys that skirt the ancient mining site of Serabit El Khadim. The approximate centre of the site i.e. geographic co-ordinate, is 29°02' N by 33°28' E. Fig. 6-1 displays the region to be discussed.

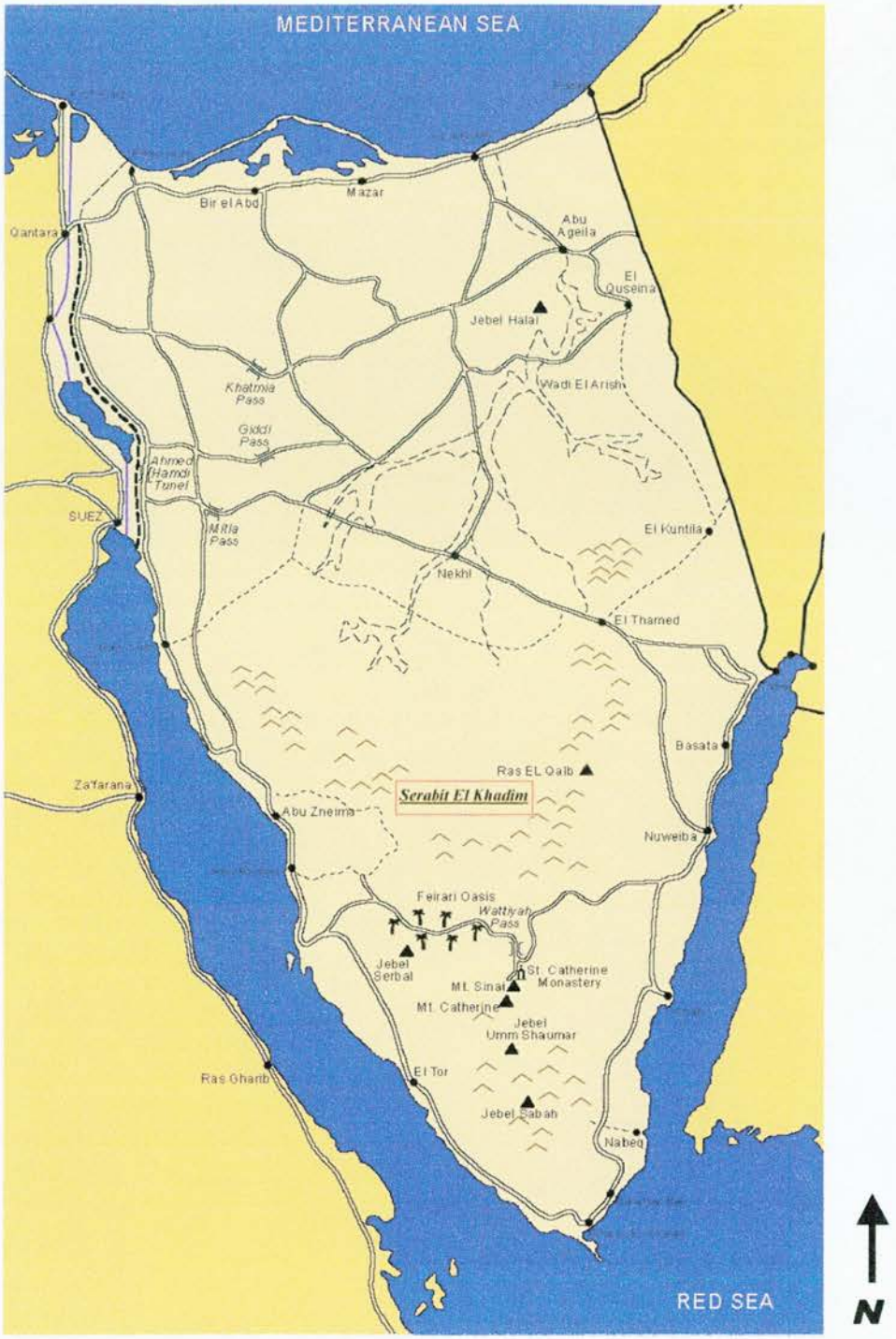

Fig. 6-1 The Sinai and Serabit El Khadim; from NIMA data at 1:350,000 map.

Although the study area is focused some 40 kilometres in a direct line from the Gulf of Suez, like much of the rest of the Sinai Peninsula the area enjoys no mitigating effects from the surrounding seas. Hyperarid conditions dominate as the Atlantic Subtropical High Pressure System exerts its influence over the entire peninsula (Thomas, 1965).

The land of the Middle Sinai along the Gulf of Suez consists of wide featureless alluvial plains. Proceeding towards Serabit El Khadim through any of the principle wadis, or valleys, the land rises dramatically into barren, gravel and rock strewn mountains. The edge of the Middle Sinai bordering on the Sinai Massif to the south looks upon exposed, crystalline mountains that are significant indicators of the underlying geological stresses that created the region (Bartov, 1985).

6.2.2 The Geology of the Sinai

The geological structure of the Sinai falls within two groups, a Precambrian base which is largely exposed in the south and a triangular area of sedimentary layers in the north that becomes thicker and more pronounced near the Mediterranean coast. The boundary between the two lies on an east-west plane from Gebel Hamman Faraun on the Gulf of Suez to Nuweiba on the Gulf of Aqaba; this coincides with the El Tigh and Egma escarpments in the high centre of the peninsula. Based on age, the surface geology can be broken into seven groups. From oldest to youngest they are: Precambrian intrusives and metamorphics, Jurassic sedimentary strata, Cenomanian-Turonian limestones and dolomites, Senonian chalk, Eocene chalk and limestones, Oligocene and Miocene sediments and Miocene dikes, and Quartenary alluvium (Eyal, 1985).

The Sinai massif that borders the southern area of the Dividing Valleys is composed largely of ancient Precambrian rocks dominating the south of the peninsula. Approximately 75% of the area are crystallised rock indicating a substantial geological interface during formation (Greenwood, 1997). See Fig. 6-2 for a geology map of the entire Sinai Peninsula.

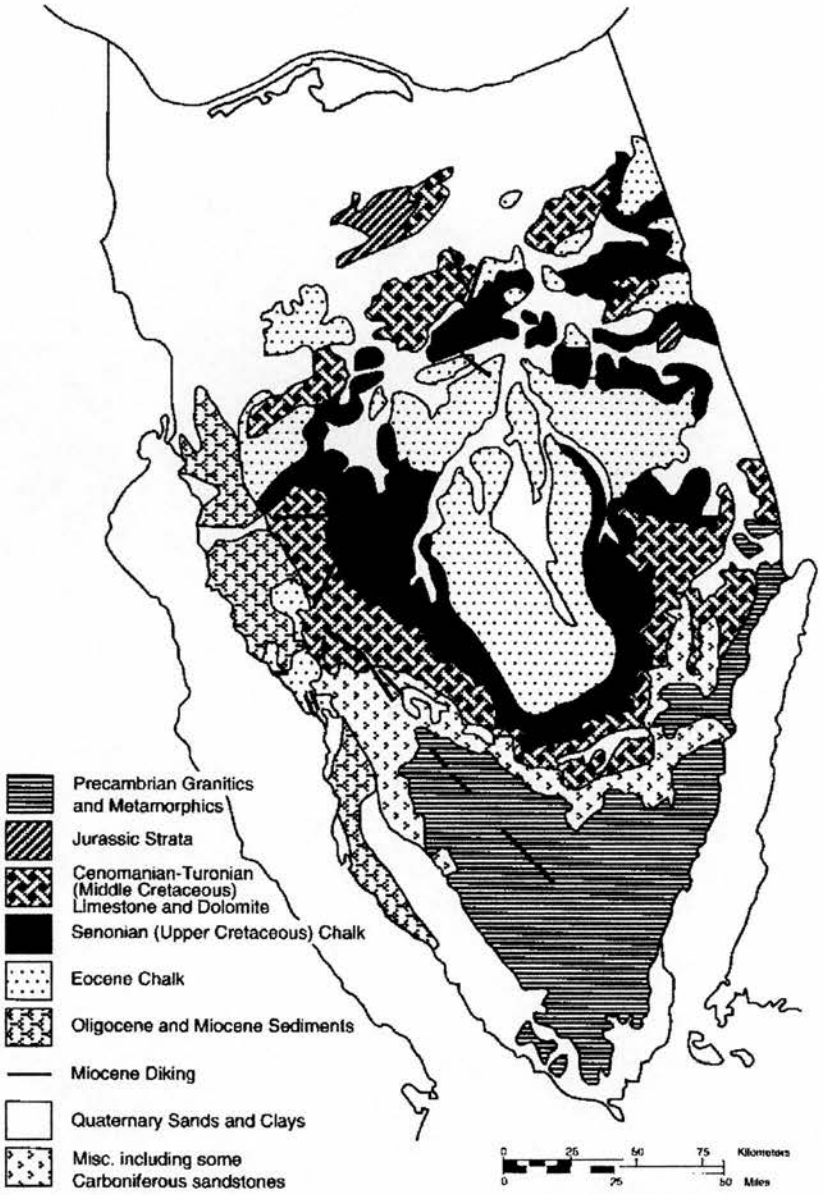

Fig. 6-2 A general map of the Sinai's geology; adapted from USGS, 1:500,000 map and Greenwood (1997).

6.2.3 The Minerals and Mines of the Western Sinai

6.2.3.1 Minerals

In the ancient world copper and turquoise were extracted both at Serabit El Khadim and around the region of Umm Bugma in large quantities, as is well known (Butts, 1954). These areas ceased production as the technology of the ancient period failed to meet the difficulty of ever-deeper extraction. Deposits of iron, manganese, copper, gold, lead, tin and zinc were known in the Umm Bugma area by the Egyptians, Greeks and Romans, but difficulties in extraction, refinement and transport, negated their economic extraction until modern times (Dame and Moores *et al.*, 1982).

6.2.3.2 Mining

In the Sinai ancient mining revolved principally around three sites, Serabit El Khadim, the oldest and longest producing, Timna in the northeast near the present-day border with Israel and Palestine, and Umm Bugma on the Wadi Maghara. Timna was extensively mined with over 7,000 mineshafts and galleries with potentially more buried under aeolian deposition over time (Rothenberg, 1979). Production in all these regions in an organised manner ceased by the close of the Roman Empire, although there were attempts during the Byzantine era (Meyer, 1997).

Production in all these areas has ceased with the exception of the Umm Bugma region; in the 1980s it was reopened for exploration and extraction, with titanium added to the list of minerals discovered there now (USGS, 2001). The ancient deposits of iron, manganese, copper, gold, lead, tin and zinc are presently being extracted while a developing industry in gypsum is beginning in the Wadi Halal region (Greenwood, 1997).

6.3 Historical Geography

6.3.1 The Historical Geography of the Sinai until the Fourth Dynasty of Egypt

The historical geography of the Sinai, unlike Egypt, is very problematic, as limited in-depth work has been performed. As previously discussed in Chapter 2, the Neolithic sites at Merimda on the western periphery of the Nile Delta were among many sites strung along the littoral of the Mediterranean Sea eastwards to Palestine (Aldred, 1998).

The Chalcolithic cultures of the Badari may have had contact with their contemporaries in Sinai based on as yet limited evidence of possible turquoise trade (Hendrickx and Veermersch, 2000).

Copper made its entrance at Mostagedda and Matmar in Upper Egypt, and near Badari c. 3500 BC (Aldred, 1998). However, the quality of that copper, as well as the rough constructions of the tools, suggest that local copper ores were used and that no trade had yet sprung up with the primitive beginnings of copper mining near Serabit El Khadim (Midant-Reynes, 2000). Inhabitants of the Sinai at the time were not unlike the last of the Bedawi, or Bedouin today, pastoral in nature and seeking to preserve precious water resources (Hobb, 1989). Still, as the Sinai's historical geography is inextricably linked with that of Egypt, this era of time is commonly referred to as the Predynastic period.

The First Dynasty of Egypt began some 200 years after the conclusion of the Predynastic period under King Menes (Walters, 1980). Egypt may be seen at this time, around 3200 BC, as reaching from the sixth cataract of the Nile River, south of ancient Meroe, north to the Mediterranean Sea and the Nile Delta. On the west, Egypt only extended into the furthest reaches of arable land and adequate water, which is to say the Nile Valley and intermittent oases. On the east, Egypt extended its reach along the Mediterranean Sea towards present-day Israel and Palestine, then south through the Sinai Peninsula to the Red Sea (Malek, 2000).

While mining in the Sinai may have preceded the creation of the cultural and political entity of Egypt, as discussed in Chapter 2, its organised extraction only began in the Third Dynasty under Djoser (Walters, 1980). Until that time the Sinai had essentially functioned as a vast tract to be crossed for purposes of trade (Malek, 2000). Still, the copper mines in the Sinai desert were the aim of the first major Egyptian forays abroad and an important reason for imperial expansion into southern Palestine later to protect them (Sandars, 1980).

During the Third Dynasty, Djoser began the great era of stone tomb and monument construction. Utilising copper implements that were likely fabricated from copper extracted from the Sinai, Zoser's engineers built the first great pyramid, the Pyramid of Saqqara, about 2900 BC (Aldred, 1998). The copper extracted from Serabit El Khadim was transported across the Red Sea to eastern Egypt from an imperial port constructed expressly for mine ore shipping near the present day town of Abu Rudeis (Rothenburg, 1979: 18-36). The Great Pyramid of Giza, built by King Khufu, followed the Saqqara pyramid by only some 100 years later (Malik, 2000).

Thereafter, an unprecedented scale of development occurred during the Fourth Dynasty (Aldred, 1998). The pyramids and other great buildings of the Egyptian civilisation were built of stones that had been quarried and shaped using copper tools (Walters, 1980). Egypt would later develop its other metal resources with gold, iron, and silver being produced in various documented quantities into the Byzantine period (Meyer, 1997)

As discussed in Chapter Two, the scale of copper mining in the Sinai would reach such a size in later Dynasties that it would become the first real industry of the ancient world. Evidence of the level of sophistication achieved by the Egyptians lies near Abu Zenima on the Red Sea, where a sea port was constructed strictly for the shipment of metal ores (Rothenburg, 1979).

The Egyptians generally mined deposits of the green copper mineral malachite since it was the easiest copper mineral to reduce and refine into copper metal; they also discovered the closely related blue-copper carbonate mineral azurite. Near these copper ore minerals, the early miners often found turquoise (Malek, 2000).

Turquoise was prized not only in Egypt, but also around the ancient world as a gemstone, and as such it has been found widely dispersed throughout the ancient Near Eastern world due to vast trade routes stretching as far as the Caspian Sea (Shaw, 2000). The status of turquoise in Egyptian religion may be seen by its inclusion with the funerary jewellery of the boy-king, Tutenkhamen, discovered by Howard Carter in 1922 (Desroches, 1969).

It is apparent that the Egyptians viewed the Sinai as a vast mineralogical treasure house. Petrie estimated in 1904-5 that one slag heap contained an estimated to 100,000 tons of dross, which would have resulted in 5,500 t of copper (Petrie, 1906). This estimate by captures the scale of the old workings during the early 1900s. It is probably impossible to calculate the industrial output of the mines. However, it can be envisioned that the impact upon the environment must have been severe with wide-scale pollution, a legacy that is still apparent in the landscape today.

6.4 Location of the Serabit El Khadim mine complex and topographic analysis

6.4.1 Site location

The approximate geographic Coordinate for Serabit El Khadim is 29°02' N by 33°28' E. The mine complex is reached by travelling some 40 kilometres due east of Abu Rudeis on the Red Sea via a track along the Wadi Baba and Wadi Garf. The final approaches to the Temple of Hathor are impassable by vehicle, and it is necessary to enter via foot along an eight-kilometre footpath. The surrounding wadis are accessible by all-terrain vehicles.

It should be noted here that it is a dangerous area to traverse without proper maps and experienced guides. Varying from the designated tracks may lead to wadis and sabkhas that contain unexploded ordnance and mines from the 1967 Arab-Israeli war. Extreme care is necessary for research in the outlying area. The middle Sinai may be seen in Fig. 6-3.

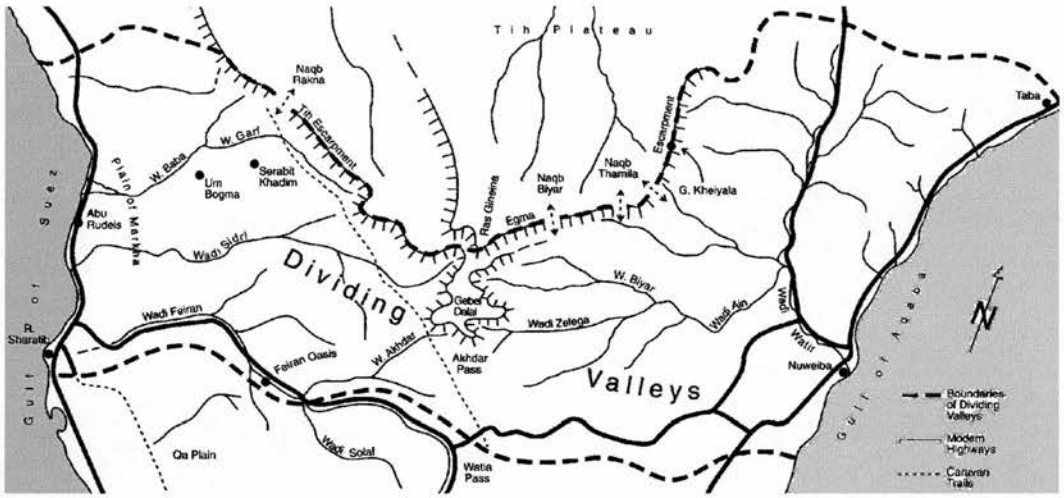

Fig. 6-3 The Middle Sinai from Abu Rudeis to the Gulf of Aqaba; created from U.S. Army Topographic Corps data (1958), USGS (2000) and Greenwood (1997). 1:250,000 map.

Sir William Flinders Petrie was the first archaeologist to draw a plan of Serabit El Khadim and the positions of the mines in relation to the temple during his campaign in 1904-5 (Drower, 1995). Petrie's survey is the most detailed of the entire mine workings to date, although there have been recent German and Israeli visits during the 1960s and 1970s (Fig. 6-21 and Rothenberg, 1979). The most important group of mines at Serabit El Khadim lies on a ridge between the heads of valleys that are offshoots of the Wadi Serabit.

6.4.1.1 Topographic analysis

A complete topographic analysis of the region surrounding the Serabit El-Khadim mine complex was performed using a Digital Terrain Elevation Data subset equivalent to a level 1 parameter i.e. one verifiable elevation point every 90 metres on average. The data subset used here was verified to an elevation point every 70 metres and meets USGS cartographic and NIMA standards (NIMA and USGS, 2001). The data subset boundary was set to the exact limits of the NASA SIR-/X-SAR Imaging RADAR data subset three-dimensional modelling purposes and to speed processing time. Thus, topographic analytical processes demonstrated here will be applicable to the forthcoming SRTM data (JPL, 2001).

The topographic analysis comprised the following examinations as discussed in Chapter 4: slope, aspect, shaded relief, profile convexity, plan convexity, longitudinal convexity, cross sectional convexity, minimum curvature, maximum curvature and topographic feature classification (i.e. hill, peak, depression etc.). An exhaustive topographic analysis is necessary to understand the manner in which microwave emissions interact with the earth's surface and to understand the situation of the mines in relation to its potential archaeological landscape.

Finally, a quick perusal of the shaded relief analysis in Section 6.4.1.4 and its accompanying image map, Fig. 6-6, serves as an excellent comparative visual reference to the other topographic analyses.

6.4.1.2 Slope

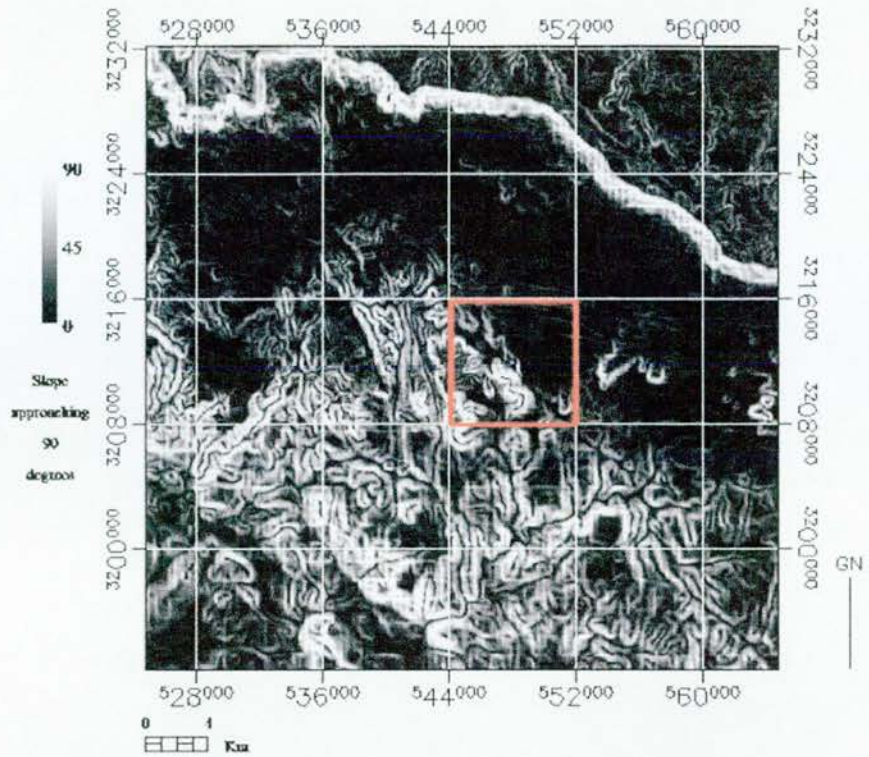

Fig. 6-4 Serabit El-Khadim mine complex slope analysis.

Slope, as discussed in Chapter 4, is measured in degrees with the convention of 0 degrees for a horizontal plane. Subtle striations and other imperfections in the image are due to imperfect DEM data processing by NIMA (2000) and the lack of enough field collected elevation points to allow creation of a smooth and continuous grid or TIN surface (ESRI 2000).

In Fig. 6-4, the area immediately surrounding Serabit El Khadim and the target scene mine has been highlighted in red. It can be seen that there is a heavy predominance of high slope angles indicating that any rainfall will rapidly scour away existing soils and cause erosion due to high water velocity. The areas closer to 0 indicate areas where water collection would have been most likely; a necessary resource for any mining effort as well as supporting the existence of any settlements for mine workers.

The convoluted terrain indicated here is also a considerable challenge for an imaging RADAR system. Due to the numerous valleys and wadis, some areas will be shadowed from microwave interrogation while over-illumination will result from some slopes functioning as perfect corner reflectors (Berlin *et al*, 1982).

6.4.1.3 Aspect

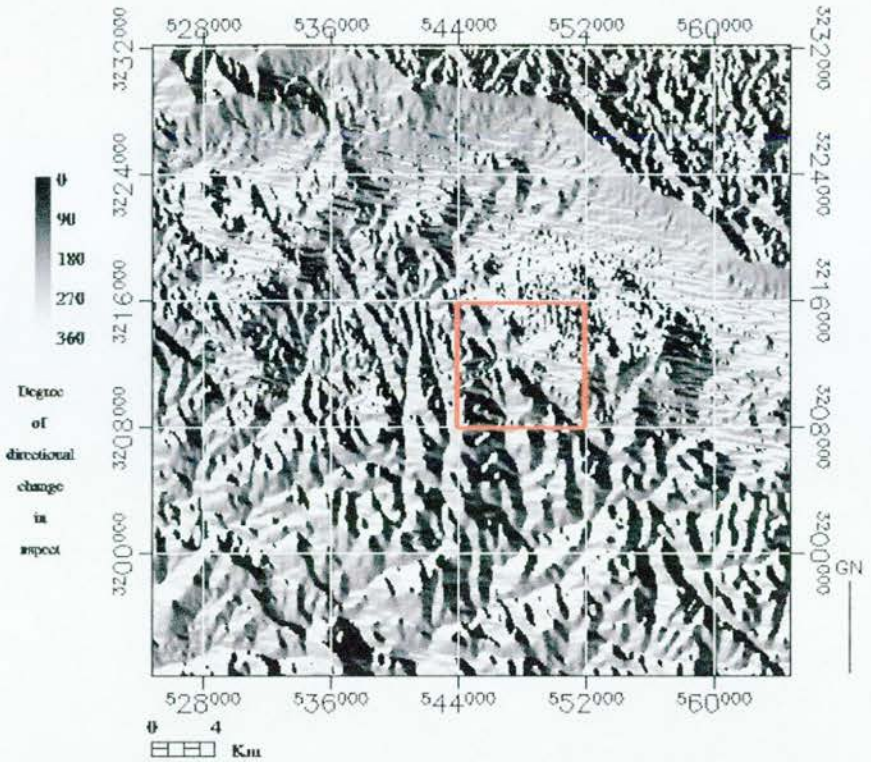

Fig. 6-5 Serabit El Khadim mine complex aspect analysis.

Aspect, in topographic terms, describes the orientation of primary terrain faces toward a given point. The aspect angle of the terrain surrounding the Serabit El-Khadim mine complex was measured with the convention of 0 degrees to the north (up) and angles increasing clockwise (Chap. 4).

The prominent feature in Fig. 6-5 is the delineation of the massive wall of the Maghara trending diagonally from the lower right to the upper left of the highlighted area. The Wadi Garf to the east of the highlighted box is the primary route in modern times to access the Serabit El Khadim site.

The predominance of slope faces in the target area oriented towards the direction of the illumination of the Shuttle Imaging RADAR on its overpass indicate that only areas within wadis should fail to provide viable backscatter returns.

6.4.1.4 Shaded Relief

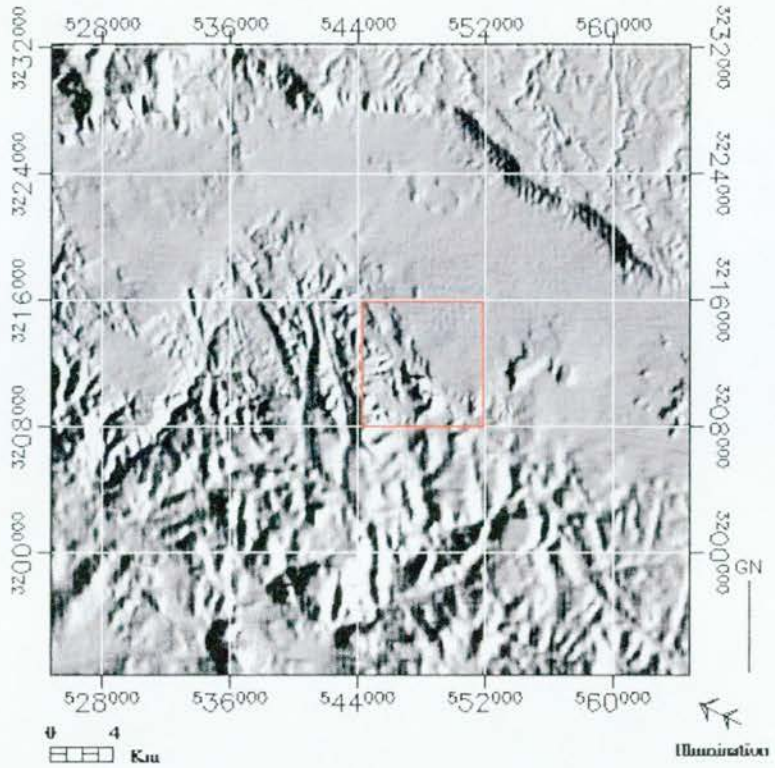

Fig. 6-6 Serabit El Khadim mines shaded relief analysis.

A shaded relief of the Serabit El-Khadim mine complex (Fig. 6-6) was computed using the following figures: a sun elevation angle of 45.25° in conjunction with a sun azimuth angle of 109.87°. These are the values for 1000 GMT on April 10,1994, the day at which the NASA SIR-C/X-SAR Imaging RADAR system passed overhead. This gives an invaluable representation of the how the target scene on the earth's surface would normally be illuminated at mid-morning in cloud free conditions by visible sunlight in comparison with the Imaging RADAR data further along in this chapter.

6.4.1.5 Profile Convexity

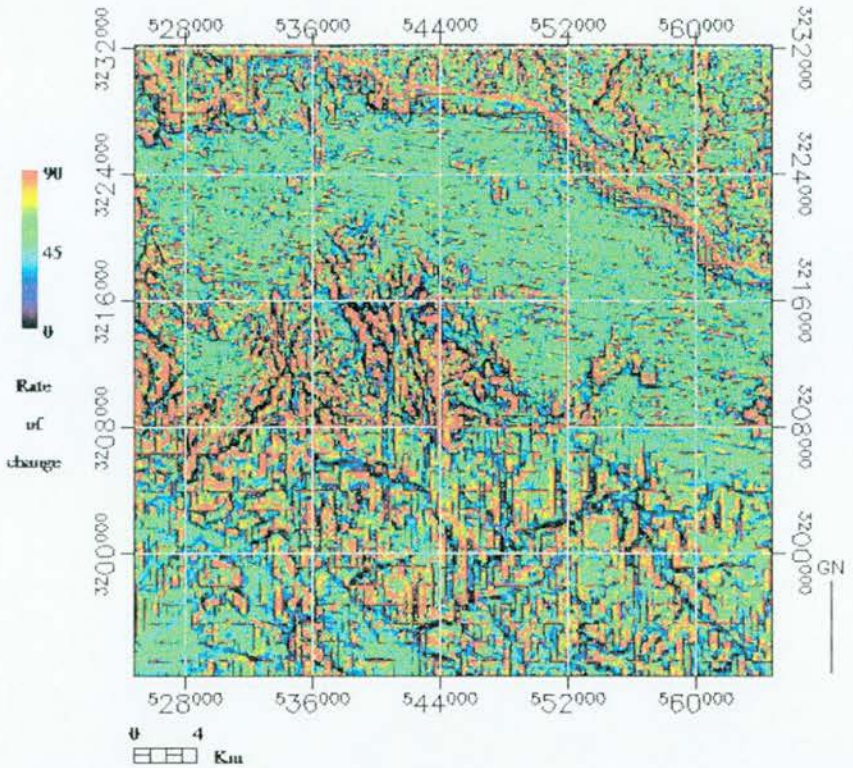

Fig. 6-7 Serabit El Khadim mines complex profile convexity analysis.

Chapter 4 explained that profile convexity analysis measures the rate of change of the slope along the profile by intersecting the plane of the Z-axis and the direction of the aspect. The area highlighted in Fig. 6-7, as well as the region surrounding it, profoundly demonstrate a region on contorted and convoluted topography indicating a conflict point in the underlying geology. Numerous changes in slope profile may be observed to the south-west and north-east of the primary mine sites. Due to this topographic structure, transport of resources to and from the mines must have been considerably difficult; as indicated here, access routes would have been easiest from the giant Wadi Garf, the region to the right of the target scene highlight box.

6.4.1.6 Plan Convexity

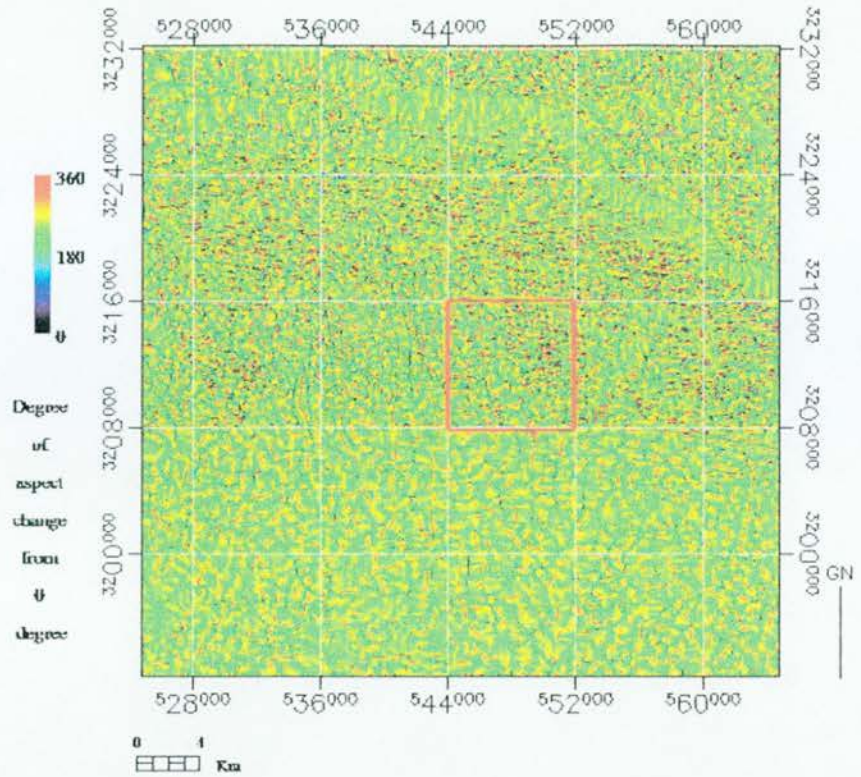

Fig. 6-8 Plan convexity for the Serabit El Khadim mines region.

Chapter 4 noted that plan convexity (intersecting with the XY plane) measures the rate of change of the aspect along the plan. As may be seen in Fig. 6-8, there are numerous areas of aspect change along the plan of the terrain surfaces, within the target scene area.

In cultural terms, this has the same influence upon movement by humans as the previously noted analyses. In scientific terms as related to the performance of an imaging RADAR system over the terrain it further demonstrates the highly convoluted nature of the reflecting surfaces. Coupled with the previous profile analysis, and based on known performance parameters, L band RADAR operating in an horizontal send and vertical receive polarimetric mode would seem to offer the best results in ground interrogation (Ulaby and Dobson, 1989, 119-123)

6.4.1.7 Longitudinal Convexity

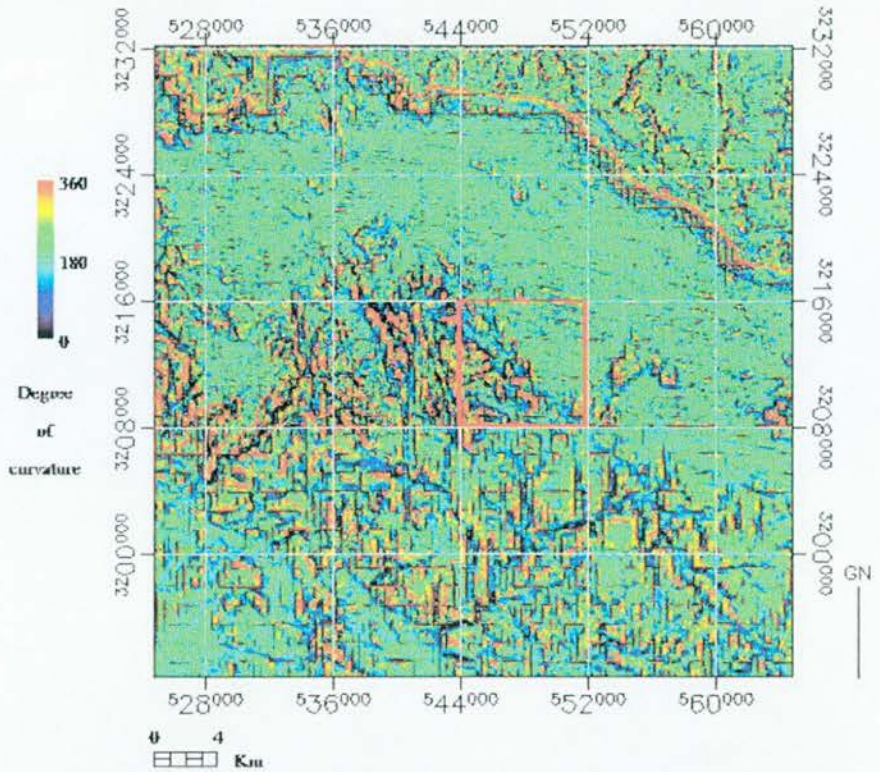

Fig. 6-9 Longitudinal curvature for the Serabit El Khadim area.

Longitudinal curvature (intersecting with the plane of the slope normal and aspect direction) and cross-sectional curvature (intersecting with the plane of the slope normal and perpendicular aspect direction) are measures of the surface curvature orthogonally in the down slope and across slope directions, respectfully. Therefore, the longitudinal convexity analysis in this instance indicates the hills that have the most similarity to a large, upside down bowl and having gentler water runoff slopes.

The region within the target scene box in Fig. 6-9 indicates numerous areas conducive to containing water flow, which in an area populated by deep, narrow wadis is to be expected. Rates of evaporation should be lower within these recesses, thus raising the chances of infiltration into the local geology and creating small springs or pools.

6.4.1.8 Cross Sectional Convexity

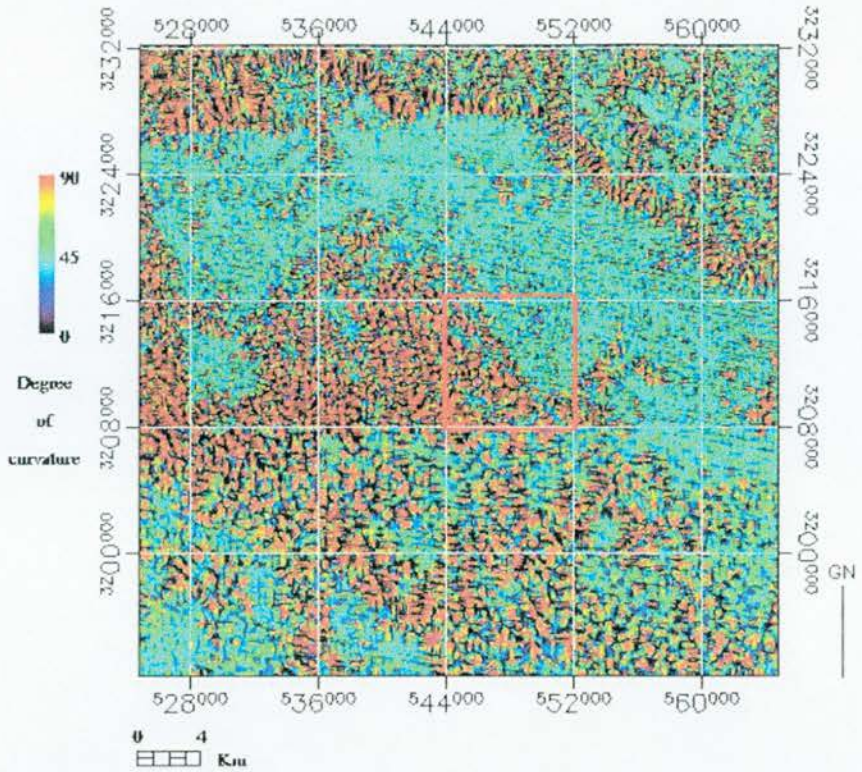

Fig. 6-10 Serabit El Khadim mines cross sectional convexity analysis.

In Chapter 4, cross-sectional convexity, or curvature (intersecting with the plane of the slope normal and perpendicular aspect direction) is defined as a measure of the surface curvature orthogonally across slope directions. The effects of data processing by NIMA to create the underlying raw DEM data used here and the residual no-data areas produced by the topographic calculations are not understood at present and should be borne in mind.

Again, the defining feature within the area of interest seen in Fig. 6-10 is a thoroughly convoluted topography with multiple facets influencing both natural and cultural activities upon its surface. The extraordinary level of cross-sectional curvature within this region, and its aridity, obviously preclude any agriculture and all but the hardiest of vegetation, as has been previously mentioned. Heavy rainfall events as well as constant winds over such a surface topography will lead to massive alluvial and arenal erosion over centuries, further exacerbating any attempt at land resource use; limited research suggests that the climate during the early Egyptian dynasties was significantly wetter (Scarre, 1995).

6.4.1.9 Minimum Curvature

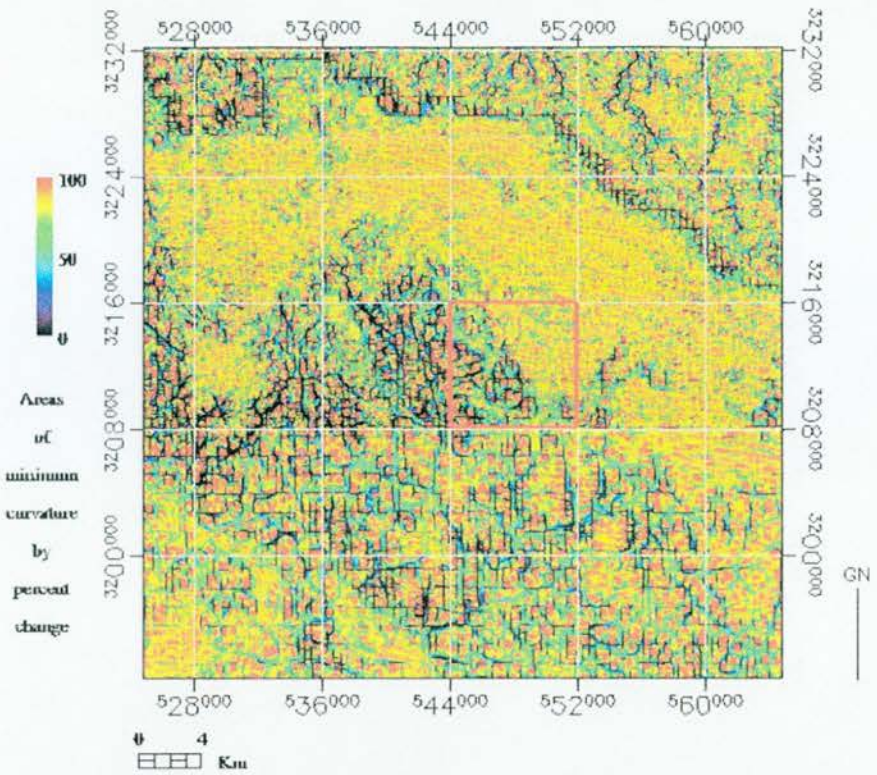

Fig. 6-11 Serabit El Khadim mines complex minimum curvature analysis.

Chapter 4 described minimum curvature as an analytical technique where the surface areas with the least amount of curvature are detected and colour mapped. As seen in Fig. 6-11, the areas with minimum curvature are those with values closest to 0. It can be seen once again that the areas which contain minimum levels of curvature lie within the floors of the narrow wadis, indicating areas scoured by heavy rainfall events filled with alluvial mud over time by deposition from slowing water velocities. It is particularly difficult for imaging RADAR systems to penetrate and receive useful backscatter information from these areas due to their being surrounded by high angle slopes and rock overhangs (Berlin, 1982).

6.4.1.10 Maximum Curvature

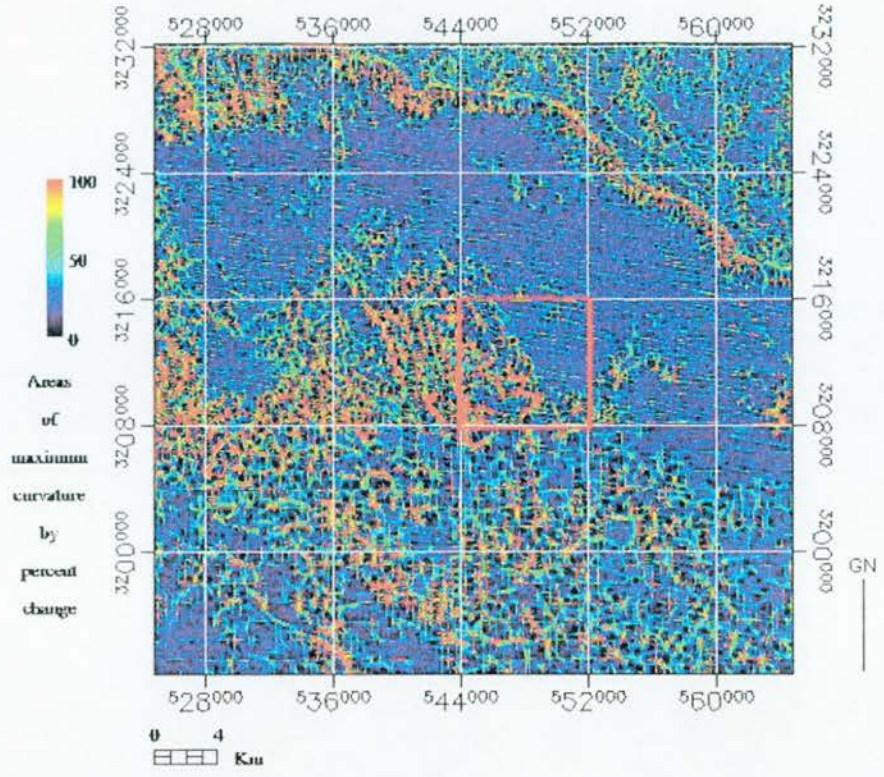

Fig. 6-12 Serabit El Khadim mines complex maximum curvature analysis.

This analysis performs the inverse of the minimum curvature process by computing and colour mapping the areas of maximum curvature within the Serabit El Khadim mines area. It can be seen in Fig. 6-12 that the entire centre area of the region of interest exhibits high curvature, again demonstrating an underlying geological structure of considerable size exerting influence on the surface structure. This is a very strong indicator of the type of geological characteristics required for the creation of metal ores, those being heat and pressure created from colliding and uplifting structures.

The overall impression that may be gained from the topographic analyses is that the importance of metal extraction and processing at Serabit El Khadim superseded all terrain and climate problems which the Sinai presented to the Egyptians. The technical and logistical audacity to overcome the problems of water and food supplies as well as transport are to be admired as a reflection of the sophistication of the Egyptian culture.

The topographic analysis of the mining area having been discussed, the following section will present an overview of the underlying geology that creates the topography surrounding Serabit El Khadim.

6.4.2 Geology of the site

The area specific to the Site "B" mines of Serabit El-Khadim consists of schists, gneisses, and migmatites (granite intrusives). There are also occasional marble and limestone outcroppings throughout the surrounding hills and wadis. This is to be understood as numerous limestone outcroppings in the Serabit primary further support its long history as a site of copper and turquoise mining.

The barren ravines around the temple of Serabit had never been mapped until Petrie's expedition in 1904-5; nor had the positions of the mines been mapped, or even described in relation to the temple. A generalised map of the Sinai geology is shown in Fig. 6-2. No detailed local geology map of the Serabit El Khadim mine site was available.

First, as a general rule, the most important mines tend to be located at the heads of the numerous wadis surrounding Serabit El Khadim. There is also evidence of a great up-thrust of the central table of granite, as much as 500 metres above the area norm. This has probably taken place since the Carboniferous sandstone was deposited; and indeed, probably since it flowed in the Tertiary age (Bartov, 1985).

The Carboniferous sandstone was evidently carved out into the valleys by rapid water inundation. Observing the very smooth outline along its harder and better-preserved parts it is possible to see this, which is quite different from the enormous hollows of aeolian erosion. Here, wind carried particles have scoured the softer strata down to the next stratum, which is composed of ferrites. This layer ranges from dark reddish-brown sandstone at Wadi Maghara to a striated band occasionally appearing at Wadi Serabit El Khadim along its walls (See Fig. 6-13a and 6-13b).

The sand depths at the bottoms of the wadis vary from 10 metres to well over 35 metres beneath the great cliffs of Serabit El Khadim, due east of the Temple of Hathor. At Al Aghara on the Garf lower sandstone deposits are some 50 metres in depth over the floor of the valley. The thin ferrite-bearing stratum appears to be deposited at one level, which are approximately 10 metres at Wadi Maghara and some 200 metres at Wadi Serabit. Beneath these ferrite strata are where turquoise was, and still is, found (See Fig. 6-13b). The iron-bearing layer at Wadi Maghara is a stratum of 15 metres within the sandstone that is of a pink or light-red colour (See Fig. 6-13a and 6-13b).

Fig. 6-13a and 6-13b Examples of the geology of the jebel near Serabit El Khadim.

6.4.3 Geomorphology

The geomorphic regions of the Sinai are dominated primarily by the erosional wear of water. Greenwood (1997) describes the peninsula as having nine geomorphic regions: Dune Sheet in the north and northwest, Insular Massifs, Suez Foreshore, The El Tigh Escarpment or Plateau, Dead Sea Drainage, Dividing Valleys, Plain of Qa, Sinai Massif and Aqaba Foreshore. Serabit El-Khadim belongs to the Dividing Valleys geomorphic region in the lower middle south of the peninsula (Fig. 6-14).

There are varied soils within the region of the Dividing Valleys. Entisols, composed of alluvial soils of recent deposition are found in wadi bottoms. Typic torripsamments, sandy entisols which lack contact within 50 cm of a lithic surface are widely distributed, as well as lithic torripsaments, having contact within 50 cm of a lithic surface and virtually never moist (Dan, 1982 and Soil Conservation Service, 1975).

The larger region around Serabit El-Khadim, stretching from Wadi Garf to Wadi Baba is heavily eroded by cuts into the underlying sandstone. At the point where Wadi Garf enters Wadi Baba the sandstone gives way to marine deposits in the Carboniferous age. Here, as mentioned in the previous section, are found the ancient workings of turquoise with the outlying areas for copper extraction (Bartov, *et a*l, 1985).

South of this area lies the modern manganese mine workings at Umm Bugma which are reached via the track leading east up the Wadi Sidra or north, then south from the Wadi Baba track to the main workings (See Fig. 6-3).

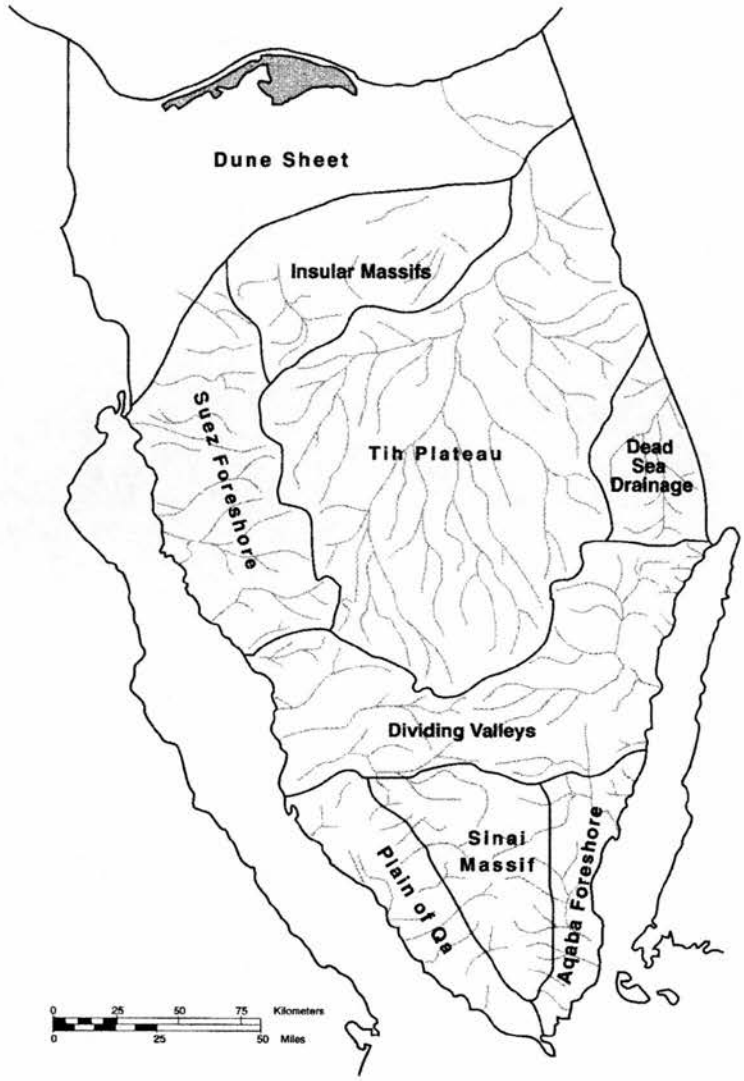

Fig. 6-14 The geomorphological regions of the Sinai, based on USGS 1:500,000 map and Greenwood (1997).

6.4.4 Vegetation

The area surrounding Serabit El Khadim has a plant ecology that consists of basically only two classifications, shrub formations and semi-shrubs. The shrub formations are comprised of the following species: *Juniperus phoenicea* (Phoenician juniper), *Noaea mucronata* (referred to by Bedouins as "sirr" and also known as "saltwort"), and are noted primarily existing towards the western fringe of the El Tigh escarpment. The *Noaea mucronata*, or *sirr*, is found more upon hard-rock outcroppings, while the Phoenician juniper is found in dispersed groups along the fluvial bottoms of the wadis. Interestingly, the Phoenician juniper also tends to be found on smooth limestone areas in profundity if the outcrop has experienced sufficient erosion (Danin, 1979).

The dominant semi-shrubs, which are found at the bottom of the wadis containing the mine workings at Serabit El Khadim, are *Salsola tetrandra*, *Halgeton alopecuroides*, *Artesmisia herba-alba* and *Hammada salicornica*. They are generally in a dispersed pattern of compact growths along the wadi channels. *A. setifera*, known by the Bedouin as "gilu", is to be found to the south and east of the mines and is a colony species that apparently now has extended throughout two-thirds of the Sinai (Hobbs, 1989).

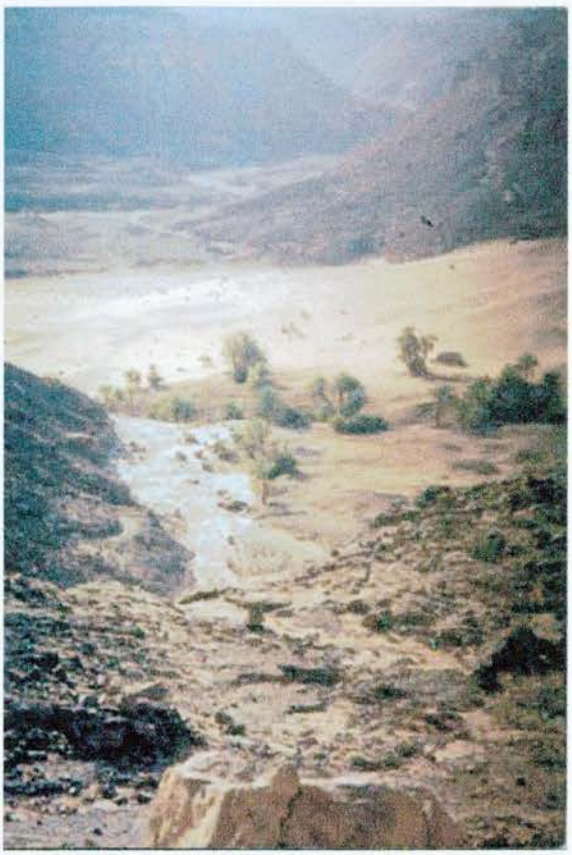

Fig. 6-15 Typical vegetation in wadis, Phoenician juniper (centre), palm and birr.

As with the mines of South Ardachy on the Isle of Islay, Scotland, there is, however, no sufficient vegetation canopy, nor mass, to significantly impede or disturb Imaging RADAR returns. In fact, the desert environment of Serabit El Khadim is a near perfect operating environment for Imaging RADAR. Only the contorted, narrow and twisting topography of the wadis presents problems for adequate RADAR signal return (Berlin, 1985).

6.5 Site History and Archaeology

6.5.1 Historical Background

The history of archaeological investigation at Serabit El Khadim essentially begins with Sir William Flinders Petrie's expedition during 1904-5 (Petrie, 1906). Petrie noted considerable destruction by speculating mining companies and engineering consultants throughout the site. In his estimation the oldest mine was that which began beneath the inscription of Sa-nekht, of the Third Dynasty (Petrie, 1906).

Fig. 6-16 A view of Site "B" mine and wadi per McKay designation; view to north-northwest.

6.5.2 Site archaeology and survey

This survey was a reassessment of the Flinders Petrie visit discussed in *Researches in the Sinai* (Petrie, 1906) and was carried out in a field visit between 28 November 1999 and 14 December 1999. The mine cited by Petrie under the inscription of Sa-nekht is substantial and well formed. This mine is a very wide, irregular cut, 3 metres high and 7 metres across. The sides were apparently cut by chisel, as the marks are apparent on the walls.

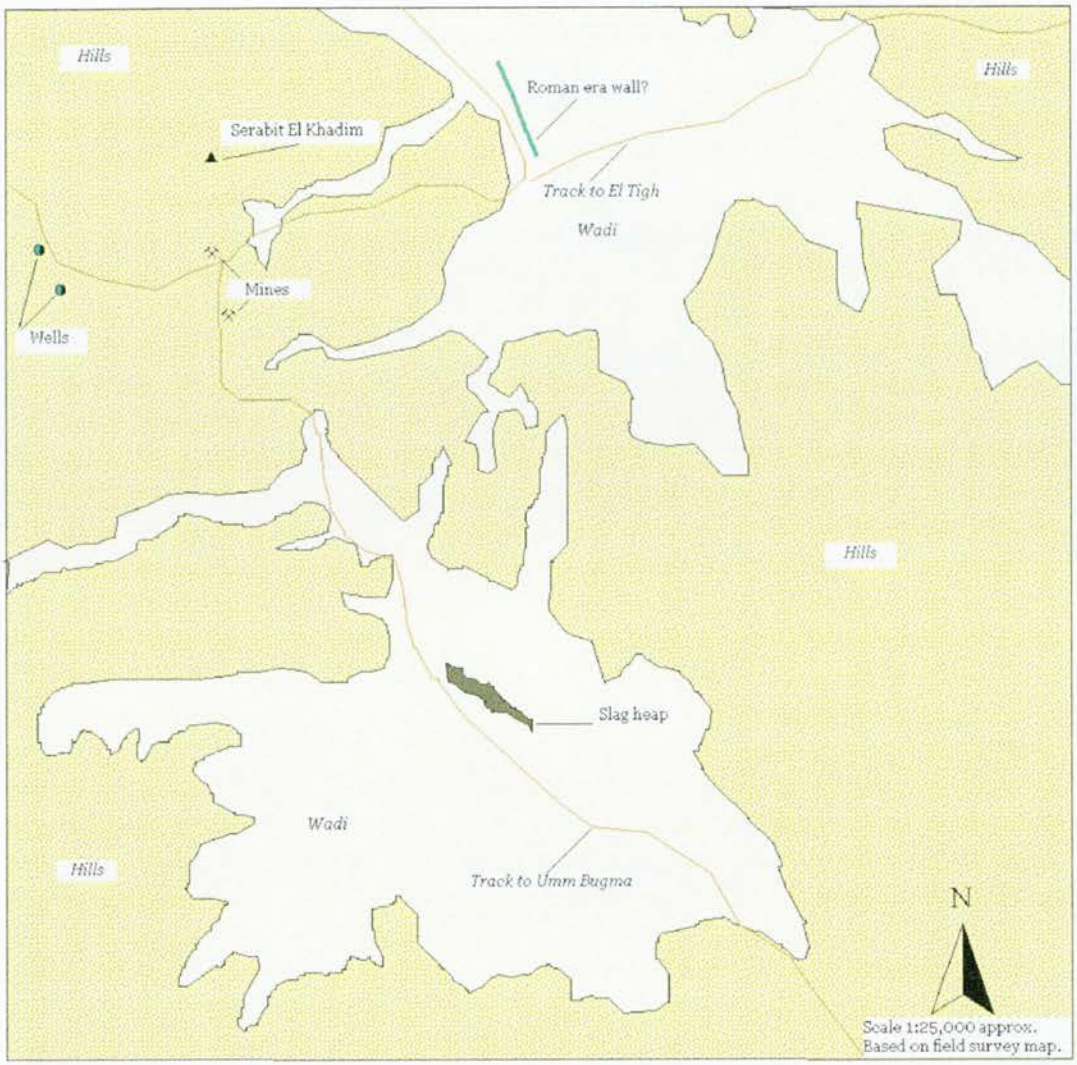

Fig. 6-16a Generalised area survey map of Serabit El Khadim.

There are two very large mine waste heaps on the valley floor near Site "B". Casual surface survey shows that numerous flints are interspersed with the waste rock. Quite likely thorough examination would produce thousands of such items, however the sheer size of the mine heaps would deter this process (Fig. 6-16, 6-16a, 6-21).

The most important group of mines are clearly those west of the Site "B" target scene. These mines lie upon a ridge between the heads of two valleys. Mine workings extend down the sides of the ridge to the floor of Wadi Serabit. On the face of the ridge at the head of valley are two inscriptions dedicated to Amenemhat II (Malek, 2000). It is here that the most unusual aspect of mining at Serabit is revealed (Fig. 6-16a).

Beneath the inscriptions to Amenemhat II an enormous amount of chiselling and cutting is in evidence while near by is a tunnel in the rock following a turquoise vein. This tunnel extends throughout various mine galleries within the hill, and opens out on the opposite side of the ridge, cutting through some 8 metres of rock. The complexity of these galleries appeared to require an opening for air as a small tunnel was dug downward from the hill to the main mine on the hilltop. This is a distance of some 4 metres through solid rock.

West of Site "B" is an inscription credited to Sebek-her-heb, military leader of the expedition in the forty-fourth year of Amenemhet III (Shaw, 2000). These mines may have already been opened by then, as there is an inscription of the thirty fifth year of Amenemhet There are also inscriptions to Amenemhet III and Tutmes IV (Shaw, 2000).

6.5.3 Ground Features

The evident feature at Site "B" is the remains of miner's huts situated nearby and the deeply cut mine working itself. The huts appear to have been constructed of blocks of sandstone some half a metre in length and 20 centimetres in thickness.

The mine working is rectangular in shape and has a depth of some 3 metres on average, with one area reaching 8 metres at its maximum. Its length is approximately 20 metres. Its rectangular shape has a width of some 11 metres on average.

6.5.4 Archaeological assessment

The features that most closely coincide with the historical commentary concerning Serabit El Khadim are the nearby tribute inscriptions to the Pharaoh Sanakht of the Third Dynasty, which is the period when the site area was industrialised. Other information that may point to whom these miners may have been is subject to conjecture without further intensive archaeological investigation (Rothenberg, 1979 and Malek, 2000).

6.6 CORONA Satellite Imagery

6.6.1 CORONA Satellite Image Details

The satellite imagery shown in Fig. 6-17 was obtained from the USGS GLIS Archive. This image is the imagery freest of clouds from the entire CORONA satellite program that had overpasses of the Sinai region. Unlike the Isle of Islay in Chapter 5, there was cloud free imagery over the Serabit El Khadim site as can be seen in the image subset under Section 6.6.2. This imagery was obtained on CORONA utilising a 70mm optical camera; estimated resolution was to have been 1.8 metres (Appendix I).

The entire coverage area of the image set spans from eastern Egypt to the Gulf of Aqaba. Due to the image's large coverage area ground registration and projection were accomplished only in the western portion of the image set. Thus, the displayed image was registered in UTM Zone 36 using the WGS 84 datum as described in Chapter 4. This is an important consideration in using CORONA as due to its large image coverage area an image may bisect two UTM zones, thus necessitating splitting the image for ground control registration and projection accuracy.

6.6.1.1 CORONA Satellite Imagery Subset

An image subset was extracted from the overall image set to match the coverage area of the Site "B" NASA SIR-C/X-SAR Imaging RADAR data set. This data set may be seen in Fig. 6-17.

While the limitations of analogue reproduction inhibit the resolution of the CORONA optical set, it is safe to specify here that in digital form the miner's huts of Serabit El Khadim as well as the Temple of Hathor, are quite visible. Furthermore, it is highly likely that significant change has occurred due to aeolian erosion in the area surrounding the mines, particularly in the Wadi Serabit (Fig. 6-17).

Viewing the area immediately left of UTM Coordinate 546000 E by 3213000 N, one may see the remains of a wall traversing the wadi Southeast to northwest. Petrie does not note this wall on his 1904-05 expedition survey map. On the other hand, a boundary wall mentioned by Petrie, northwest of UTM co-ordinate 546000 E by 321000 N is barely visible. A rough field survey map that depicts the area may be referred back to in Fig. 6-16a.

Based on Petrie's observations and the observations recorded by the CORONA overpass in 1972, there has been significant sand deposition over the boundary wall in the lower wadi, while the wall noted in the upper wadi appears to have been uncovered by scouring winds.

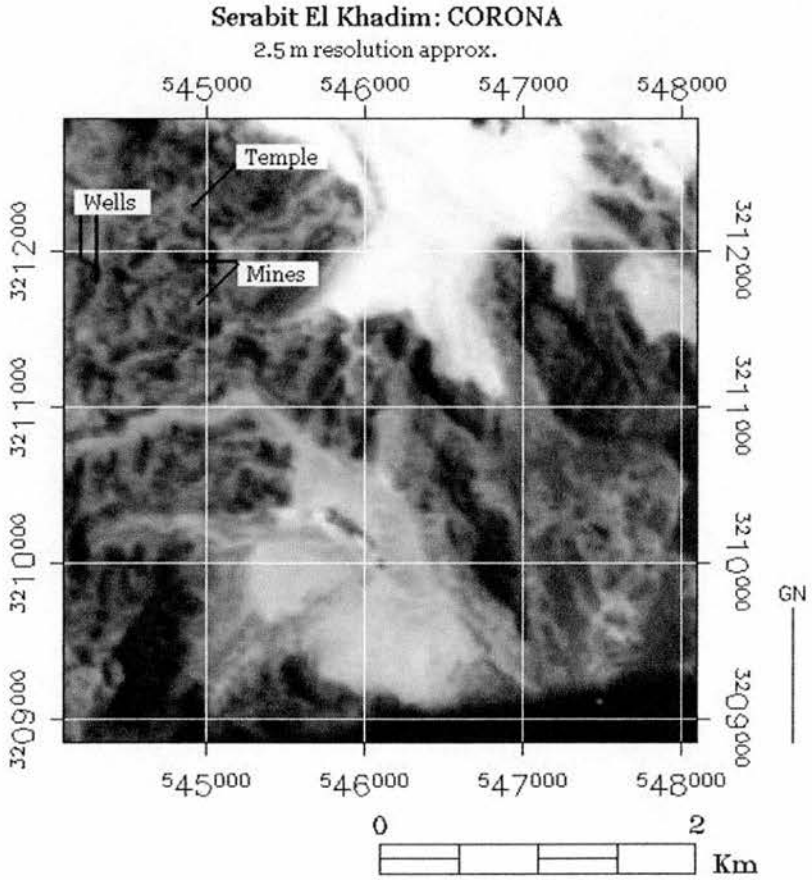

Fig. 6-17 An image subset of the Serabit El Khadim mines area at 2.5 m. resolution.

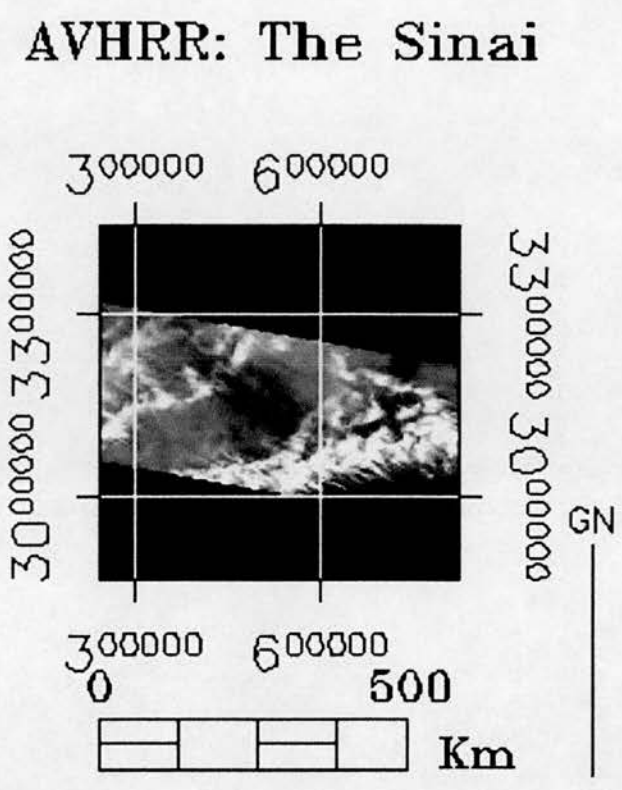

Fig. 6-18 An AVHRR image subset over the Sinai proper on 11 April 1994.

AVHRR Global Area Coverage (GAC) data for the orbital pass immediately preceding the overpass of the STS Endeavour SIR-C/X-SAR Imaging RADAR system on 11 April 1994 was obtained from the NOAA Satellite Active Archive for analysis (Fig. 6-18). Resolution of this data is approximately 4 kilometres in GAC mode. Bands 5 (Red), 4 (Green) and 3 (Blue) are displayed as a false colour image for ease of visual interpretation. The colour designators refer to display bands. It may be seen from this image that cloud cover was intermittent throughout the region and that the moisture content, as registered by the infrared bands, is minimal (NOAA, 2000 and ENVI, 2000).

Calibration of the AVHRR data for brightness temperature was computed for bands 3, 4 and 5 using algorithms developed for the NOAA-12 platform, and presented in degrees Kelvin (Table 6-1).

The analysis shows little atmospheric moisture present over the central Sinai, which corresponds to the available ground information. The thermal results show the reflectance values from cloud structures to the west and south-east of the study area to be high though.

It was originally hoped to obtain Defence Meterological Satellite Organisation (DMSO) data at 1 km resolution for the area, but this proved impossible due to data archive limits i.e. no more than five years of catalogued metereological history (NOAA, 2000).

NOAA 11 – Band 3	3.74 K
NOAA 11 – Band 4	10.82 K
NOAA 11 – Band 5	12.00 K

Table 6-1 Calibrated brightness temperatures in degrees Kelvin, NOAA-11, 1994.

6.8 Meteorological Data

6.8.1 Egyptian Meteorological Office Data

The Egyptian Meteorological Office station at Abu Rudeis, the Sinai, reported the following weather information for the region near Serabit El Khadim in April of 1994. The station is located on the Gulf of Suez at sea level 45 kilometres from Serabit El Khadim.

The mean annual monthly temperature for the Abu Rudeis region is 22 C; in April of 1994 the total precipitation was 2 mm with an average temperature for the month of 21 C. On 11 April 1994 the temperature was 23 C with no measurable precipitation recorded for the previous 19 days. No further data was available. The region is classified as arid.

As such, the conditions for data acquisition by the SIR-C/X-SAR Imaging RADAR system was optimal with virtually no measurable atmospheric or ground moisture to affect microwave interaction. Wind speed information was unavailable.

6.9 NASA SIR-C/X-SAR Imaging RADAR Data and Analysis

6.9.1 The Imaging RADAR Data

The Imaging RADAR data for Serabit El Khadim were obtained on 11 April 1994 during NASA STS (Shuttle Transport System) Mission SRL-1. Both C and L wavelengths used the horizontal send and receive polarisation (hh) mode as well as the horizontal send and vertical receive polarisation (hv) mode in the Multi-Look Complex (MLC) product. The C band polarisations were operating at a 5.304 Ghz frequency while the L band polarisations were functioning at 1.254 Ghz.

The orbital direction of the Space Shuttle was ascending with the Imaging RADAR operating in a right-looking look direction. The sensor platform heading at the image centre was of 36.268° with an incidence angle of 46.922° for the MLC mode data. The centre latitude and longitude of the entire image scene was 28.5290184° N by 32.8416634° E at the same point. The nominal resolutions are 12.5 metres for the MLC product, with actual pixel size and spacing being the same (Appendix II).

6.9.2 Data Processing

Upon receiving the MLC data and following decompression, the information was then synthesised via the ENVI 3.4 image processing software (ENVI 2001). First, for cartographic purposes, the data set was projected into the Universal Transverse Mercator co-ordinate system using the WGS-84 datum. Ground control points (GCPs) were taken at locations as seen in Fig. 6-19 represented by red stars (See Appendix 1 for GCP information). Next, decibel response analysis, filtering and test enhancements were performed on a raw data subset comprising a standard size area of 200 x 200 pixels. This was done to facilitate processing and analysis time due to the enormous sizes of the data sets. The Serabit El-Khadim mines complex study area can be seen in the small-scale image map of Fig. 6-20.

It should be pointed out that the original focus of this research was to compare polarimetric responses between all three sites in this work. However, due to data format problems (full polarimetric versus fully polarimetric), software input problems (inability to synthesise RADAR data correctly due to a missing byte in the header file structure), and finally, the lack of comparable data sets (i.e. hh/vv polarisations), analysis was restricted to phase difference examination (ENVI, 1997 and JPL, 2000-01). The key failure was the inability of the software to recognise the incorrect header file structure and to then render it impossible to generate three-dimensional polarimetric response figures. Failing to recognise this subtle byte and file structure difference caused a total re-working of all RADAR analyses within this research work. At any rate, phase difference analysis was impossible at Serabit El Khadim due to the lack of a hh/vv data take during the 1994 Shuttle mission; as such, decibel responses will be commented upon in this chapter where applicable and useful. Chapter 9 will discuss data problems during this research work.

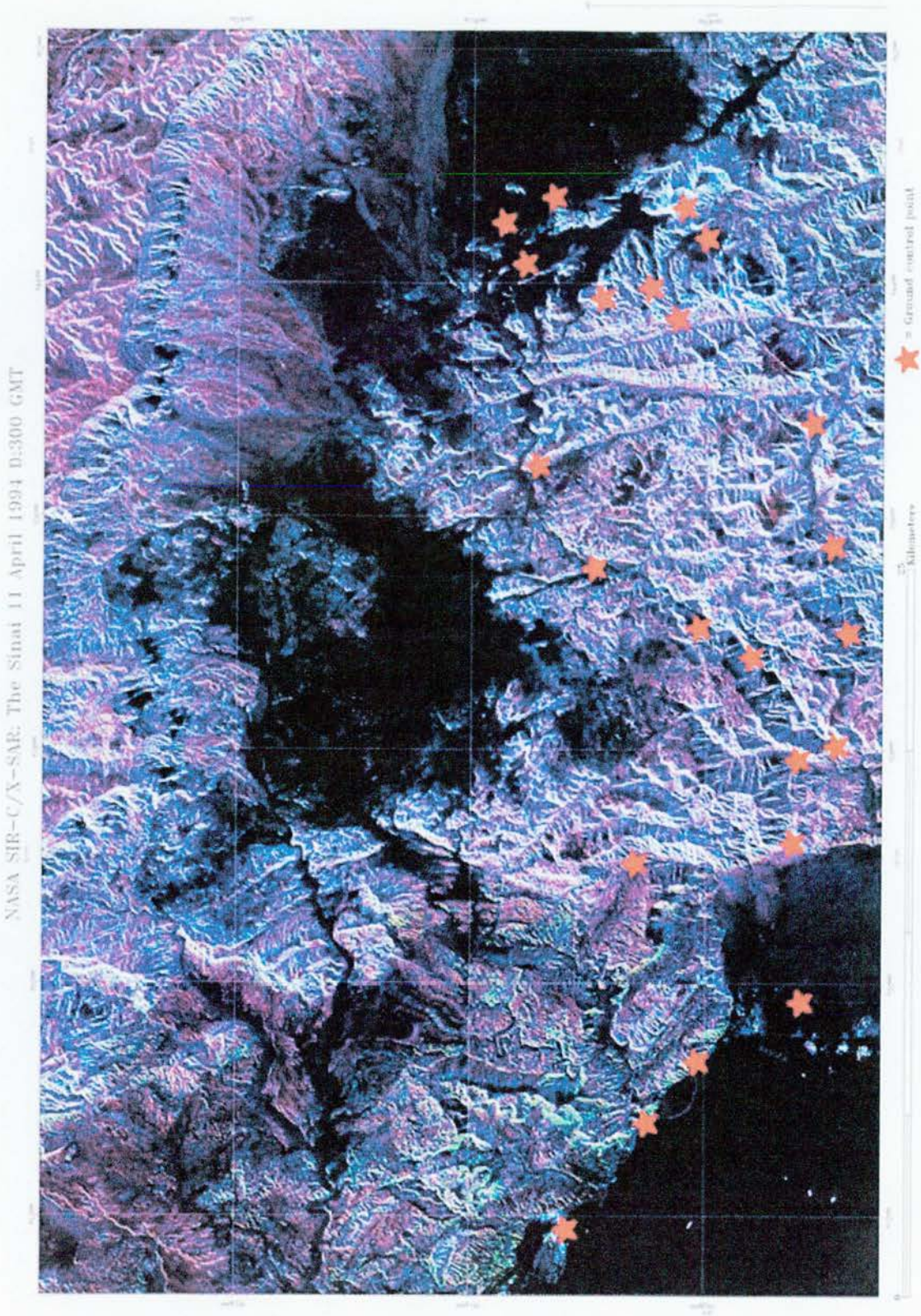

Fig. 6-19 The Middle Sinai: ground control points.

6.9.3 Imaging RADAR data analysis

A reference Imaging RADAR map of the Serabit El Khadim mines complex is presented in Fig. 6-20 to facilitate interpretation of the following RADAR data sets which have not been registered and projected to a co-ordinate system. Registration and projection processes artificially skew visual image results, thus the data sets were analysed in base form.

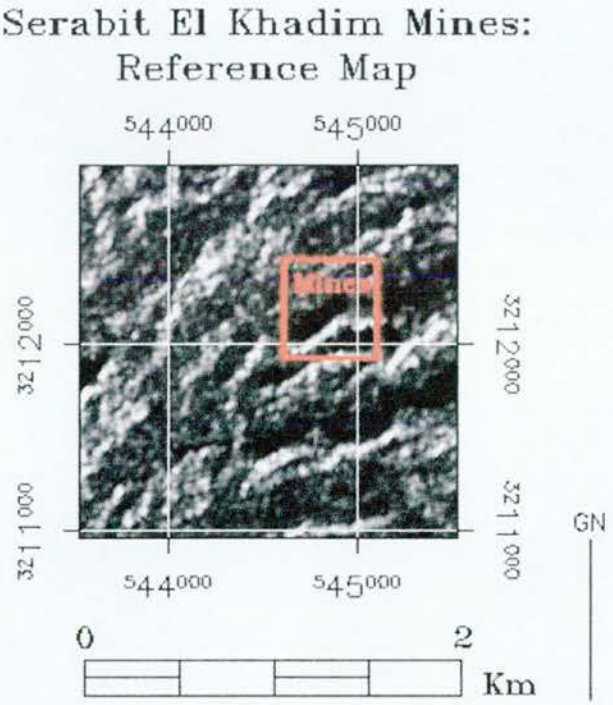

Fig. 6-20 The Serabit El Khadim mines complex – Chh band.

6.9.3.1 Analysis form and test site

Evaluation of the capability of NASA SIR-C/X-SAR Imaging RADAR to detect, survey and analyse the Serabit El Khadim mines was conducted in the same manner as the South Ardachy mines described in Chapter 5. It was decided to select a portion of the mine site and transect it in a linear fashion analysing each pixel within the selected transect, which was 12 pixels or approximately 150 metres. The transect was oriented north to south, beginning at pixel 4274 x 1668 and ending at pixel 4274 x 1657. This distance was chosen to span the mine from normal signal return surface to normal signal return surface for reference purposes. Both C and L bands were analysed only for decibel strength as it was not possible to perform phase difference analysis due to the lack of *vv* polarisation information for both C and L bands.

The test area chosen was mineshaft "B" as seen in below in Fig. 6-21. The UTM Coordinate (WGS-84 datum datum) at the centre area of the mine quarry is 321223 N by 544748 E UTM and corresponds to pixel 4274 by 1664 in the data sets. The red line beneath the nomenclature "Target mine Site "B" corresponds to the transect of the mine quarry.

Fig. 6-21 Mines near Serabit El Khadim; Petrie's 1:25,000 scale 1904 survey map with additional text by McKay.

6.9.3.2 C band Imaging RADAR phase difference analysis: "B" mine, Serabit El Khadim

The image data set for the "B" mine target site at Serabit El Khadim measures 200 x 200 pixels, with each pixel covering 12.5 metres of terrain. The transect of decibel analysis concerning the mine begins at pixel 4274 by 1668 and ends at 4274 by 1657. The mine quarry is located at pixel 4274 by 1668. An overview image map of the raw Chh RADAR data is provided in Fig. 6-22 with a target illumination image map in Fig. 6-23. The direction of analysis is from the southernmost pixel to the northernmost pixel. Following this map, the pixels are analysed for their decibel statistics in Table 6-2.

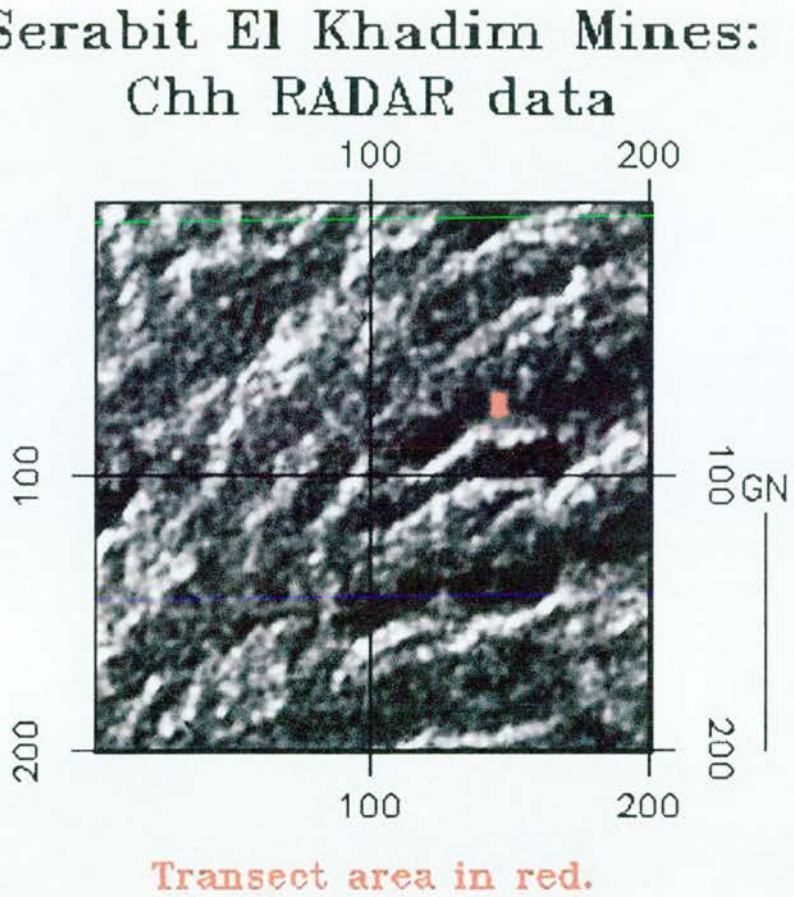

Fig. 6-22 Chh raw RADAR data image map: Serabit El Khadim "B" target mine area.

The following page displays the C band illumination image map (See Fig. 6-23) for the entire scene area with the target scene area outlined (Elachi *et al,* 1984).

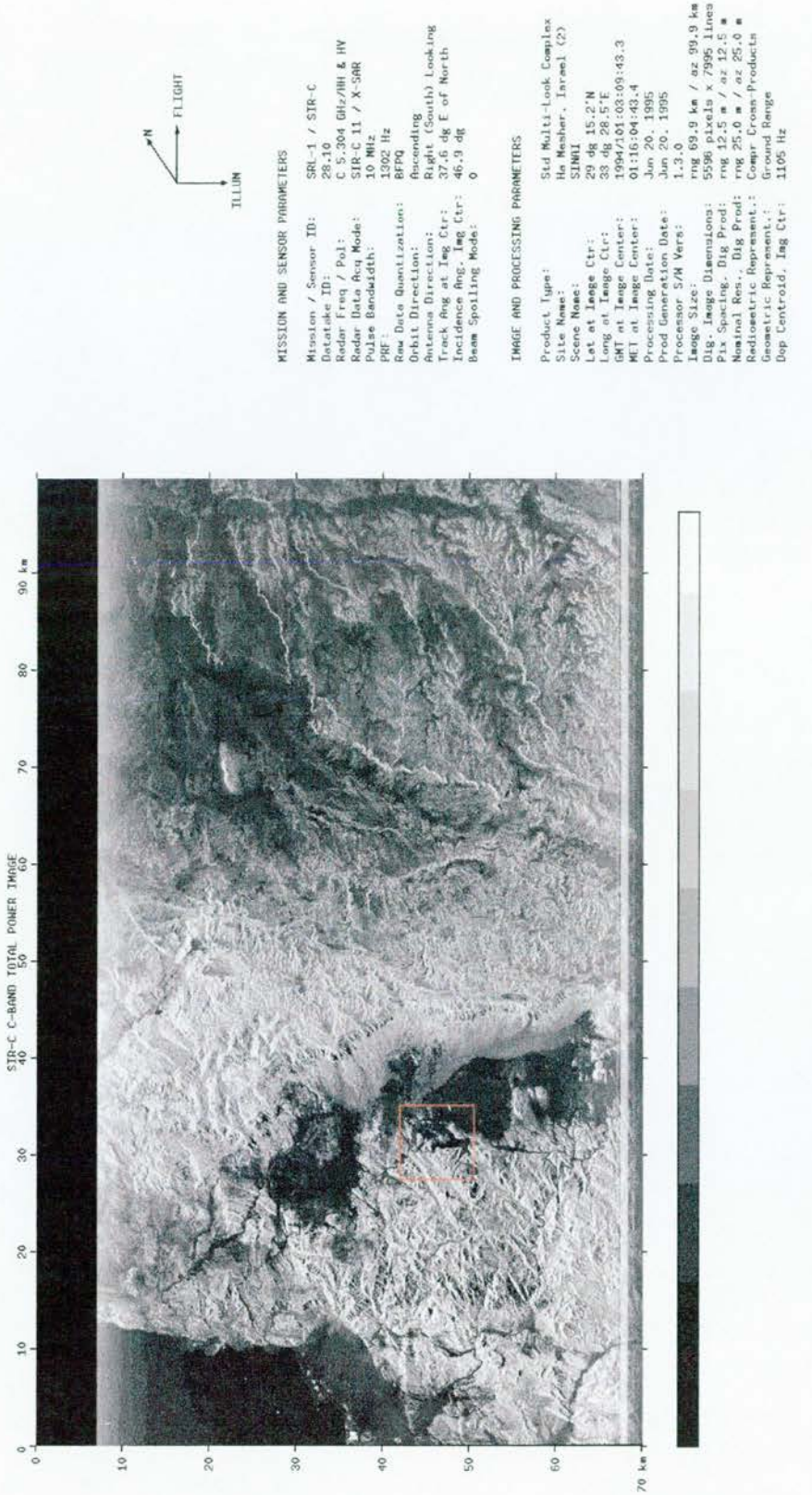

Fig. 6-23 C band total power RADAR data image map: Serabit El Khadim "B" target mine area within red box. Image and information derived from CEOS software and header file.

Pixel Co-ordinate	C/hh	C/hv
4274x1668	-10.18	-18.76
4274x1667	-12.08	-25.19
4274x1666	-10.48	-24.46
4274x1665	-12.40	-23.15
4274x1664	-14.69	-23.49
4274x1663	-14.72	-23.99
4274x1662	-14.10	-24.59
4274x1661	-12.59	-22.70
4274x1660	-10.03	-22.66
4274x1659	-9.07	-24.40
4274x1658	-10.43	-24.05
4274x1657	-11.07	-20.69

Table 6-2 Mine site transect, Serabit El Khadim, C band decibel statistics.

As can be seen by viewing the RADAR sensor settings in Appendix II, the incidence angle for Serabit El Khadim was greater than when the sensor was above South Ardachy on Islay. Even so, the decibel responses are comparable to the figures reported by Ulaby and Dobson (1989) for terrain and geology of this type at this incidence angle and wavelength. It is interesting to note that a work by Berlin *et al.* (1982) concerning the extreme topography of the Grand Canyon in America, discusses various incidence angle settings for such areas.

6.9.3.3 L band Imaging RADAR phase difference analysis: "B" mine, Serabit El Khadim

The image data set for the "B" mine target site at Serabit El Khadim measures 200 x 200 pixels, with each pixel encompassing 12.5 metres of earth terrain. The transect of decibel analysis concerning the mine begins at pixel 4274 by 1668 and ends at 4274 by 1657. An overview image map of the raw Lhh RADAR data is provided in Fig. 6-24 with a target illumination map in Fig. 6-25. The direction of analysis is from the southernmost pixel to the northernmost pixel. Immediately following this map are the pixels analysed for their decibel statistics in Table 6-3.

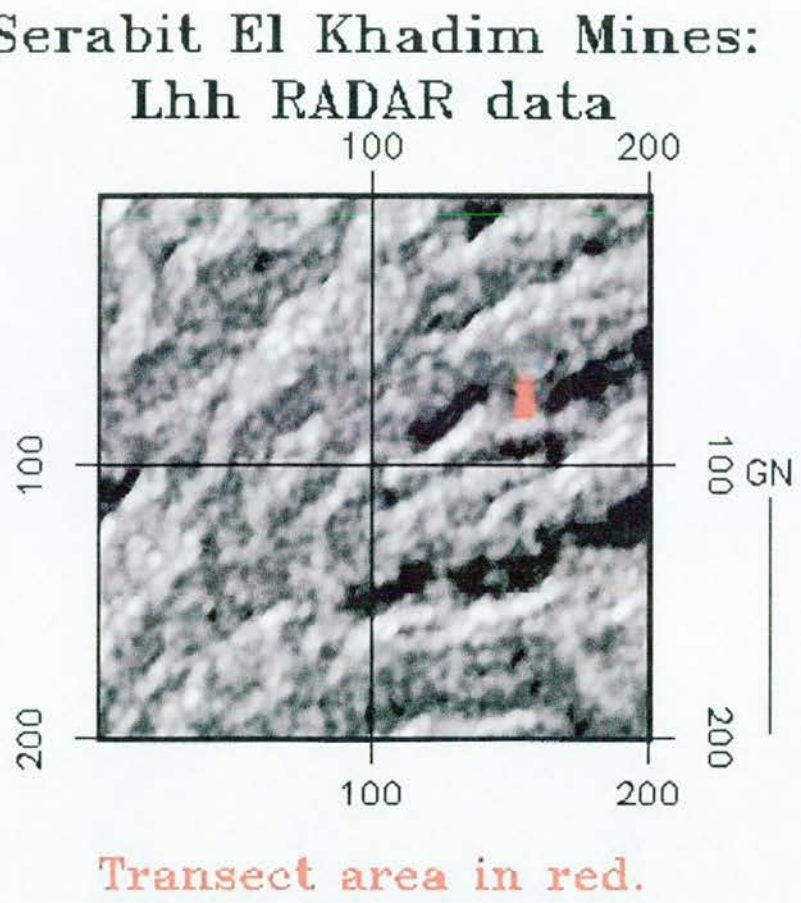

Fig. 6-24 Lhh raw RADAR data image map: Serabit, "B" target mine site.

Fig. 6-25 L band total power RADAR data image map: Serabit, "B" target mine site area outlined in red box. Image and information created from CEOS software and header file, NASA/JPL.

Pixel Co-ordinate	L/hh	L/vv
4274x1668	-20.11	-29.73
4274x1667	-19.80	-30.04
4274x1666	-21.22	-30.96
4274x1665	-21.48	-27.70
4274x1664	-21.74	-27.10
4274x1663	-20.11	-29.73
4274x1662	-29.58	-30.68
4274x1661	-12.78	-25.57
4274x1660	-13.54	-23.04
4274x1659	-14.19	-24.06
4274x1658	-13.40	-24.29
4274x1657	-15.42	-23.45

Table 6-3 Mine site transect, Serabit, L band decibel statistics.

What may be said of the C band decibel responses may be said of the L band responses (Table 6-3). They are consistent with the known responses for a RADAR operating around 45° incidence angle (Ulaby and Dobson, 1989). It was expected that a stronger response would have been seen over pixel 4274 x 1664 (miner's pit), but this was not so.

6.9.3.3.1 Comparative Transect

A nearby area of the Serabit El Khadim mine complex was chosen to compare the capability of the multipolarimetric Imaging RADAR system. Referring back to Fig. 6-20, of the mine site, a transect was chosen which bisected the area east of the mine in the wadi area in a north-south fashion. The same transect parameters are used, with each pixel encompassing 12.5 metres of earth terrain, for approximately 125 metres total. The comparative transect of decibel analysis begins at pixel 4286 by 1668 and ends at 4286 by 1659. An overview image map of both the comparative transect and the mine site transect is provided in Fig. 6-26a, while a photograph of the area terrain may be seen in Fig. 26b. The direction of analysis is from the northernmost pixel to the southernmost pixel. Again, pixel 4286 by 1659 is the northernmost pixel within the transect with 4286 by 1668 being the southernmost. Immediately following this map are the pixels analysed for their decibel statistics with the C band data presented first, followed by the L band data.

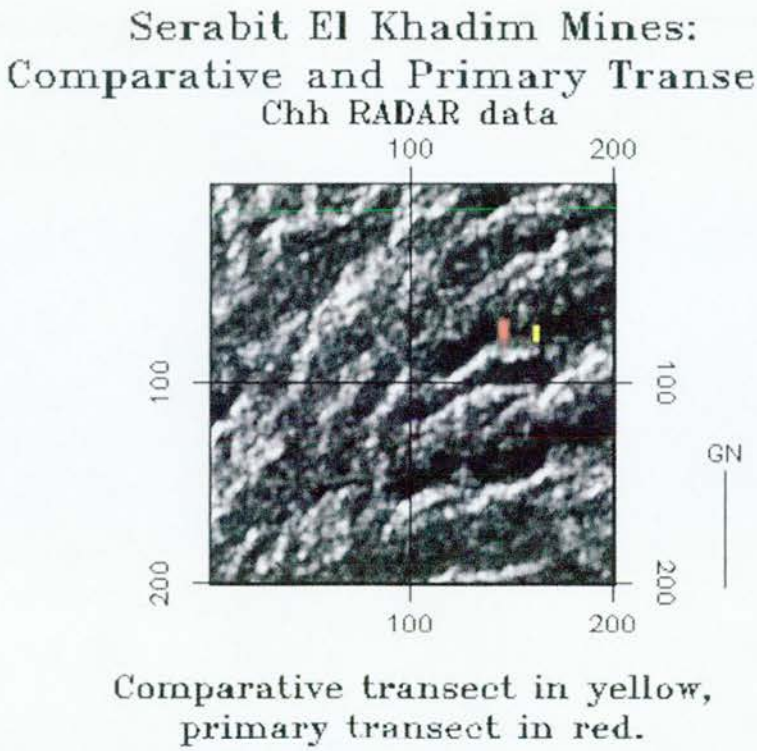

Fig. 6-26a

Fig. 6-26b

Fig. 6-26a Comparative transect near Serabit El Khadim, top, and Fig 6-26b with an image of the transect area, bottom. View from the east towards the west with the El Tigh escarpment in the distance.

Pixel Co-ordinate	Chh	Chv
4286x1668	-16.56	-21.11
4286x1667	-16.07	-93.31
4286x1666	-13.95	-167.04
4286x1665	-13.54	-169.73
4286x1664	-15.96	-24.54
4286x1663	-17.63	-25.88
4286x1662	-18.12	N/a
4286x1661	-20.71	-99.33
4286x1660	-18.74	-173.16
4286x1659	-18.74	N/a

Table 6-4 Comparative transect, C band decibel returns, Serabit El Khadim.

Pixel Co-ordinate	Lhh	Lhv
4286x1668	-17.18	-179.31
4286x1667	-17.25	-176.25
4286x1666	-20.51	-99.33
4286x1665	-22.87	-179.37
4286x1664	-25.25	-184.97
4286x1663	-27.76	-187.07
4286x1662	-26.89	-185.80
4286x1661	-23.91	-182.82
4286x1660	-22.16	-181.88
4286x1659	-23.10	-183.72

Table 6-5 Comparative transect, L band decibel returns, Serabit El Khadim.

As expected the C-band decibel responses recorded over the essentially flat terrain of the comparative transect are weaker than those seen occurring along the mine transect. This was to be expected as the heavy, alluvial deposition of the wadi bottom offered minimal geological reflectors with only the occasional Phoenician juniper tree as a potential vegetation reflector.

Lhh band responses were weaker than the mine transect, which was expected over such a heavy depositional mud plain with few horizontal reflectors such as low cliff lines or ridges. The Lhv responses are unexplained, though conversations with personnel at JPL (2000) referred to calibration problems with this data set.

6.9.3.4 Comparative Analysis of the C band and L band RADAR data

Pixels 4274 x 1664 and 4274 x 1665 are the two pixels which coincide with Site "B" in the Serabit El Khadim mines complex (See Fig. 6-27). Pixel 4274 x 1664 corresponds with the mine pit, while 4274 x 1665 covers a nearby mine hut.

Fig. 6-27 Mine pit (background) and miner's huts (foreground); pixel 4274 x 1664-65, Site "B", Serabit.

As previously mentioned in the section on ground features, the mine working is rectangular in shape and has a depth of some 3 metres at its maximum. Its length is approximately 20 metres. On average the width of the feature is 11m and is rectangular in shape (See Fig. 6-28). A landscape sketch map of the target mine area may be found in Fig. 6-16a of this work.

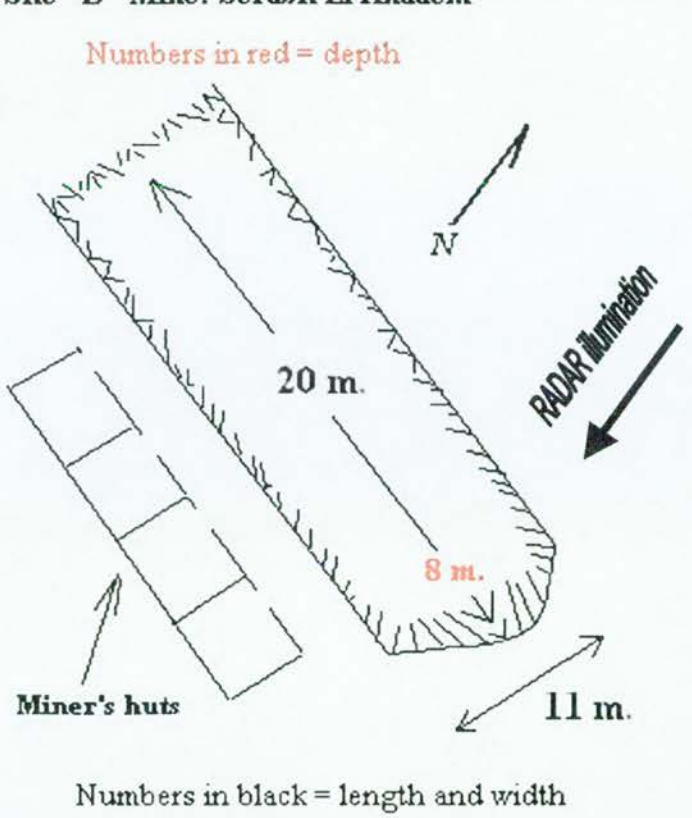

Fig. 6-28 A general map of the mine site at pixel 4274 x 1664-65, Site "B", Serabit.

The miner's huts at Serabit El Khadim are unique to all the sites in this work as they were the only structures related to an ancient mining workforce outside of possible structures related to processing at South Ardachy. It was therefore considered worthwhile to examine the decibel return of the pixel overlying the hut structure adjacent to Site "B". The pixel which coincides with this structure is pixel 4274 x 1665. The C band and L band decibel responses for this structure as well as the mine pit may be seen in Table 6-6. Immediately following, Table 6-7 displays the decibel response of a pixel from the mid-section of the comparative transect to illustrate performance differences. Figure 6-26b shows the general overview of the comparative transect area.

Pixel Co-ordinate	hh	hv
4274x1665 Miner's hut - C band	-12.40	-23.15
4274x1664 Mine pit - C band	-14.69	-23.49
4274x1665 Miner's hut - L band	-21.48	-27.70
4274x1664 Mine pit - L band	-21.48	-27.10

Table 6-6 C and L band decibel responses, mine pit and miner's hut, Serabit El Khadim

Pixel Co-ordinate	hh	hv
4286x1664 C band	-15.96	-24.54
4286x1664 L band	-25.25	-184.97

Table 6-7 C and L band decibel responses for comparative transect, centre pixel, Serabit El Khadim

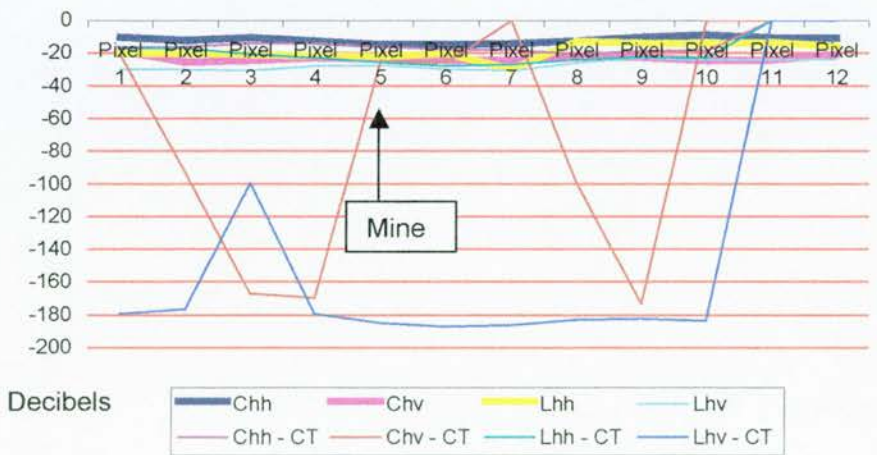

Fig. 6-29 Comparison of decibel responses for all Serabit El Khadim transects

While only the decibel responses for the mine pit and miner's hut are shown in Table 6-6, it is useful to refer back to their respective transect tables in commenting on the Imaging RADAR returns. Just as was mentioned in Chapter 5 regarding the registration precision of the image scene data versus the actual ground range placement of the recorded RADAR data, some error is inevitable. Still it is interesting to note when viewing the decibel responses for the C band over the miner's hut that the structure displays one of the stronger responses in the transect at -12.40 dB for the hh polarisation and if one considers probable error, then pixel 4274 x 1666 displays an even firmer response in the same mode. It may be that the wall of the miner's hut, which has a considerable amount of smaller rubble aligned along its length, is providing a firmer reflecting surface for there are no plants or other materials in the site which approximate the C band (See Chapter 3). Pixel 4274 x 1664, which approximates the position of the mine pit or quarry, exhibits a weaker decibel response at -14.69 dB for the hh polarisation which is logical since it essentially has little or no reflectors for the C band; the target mine area is considerably rough. C band responses for the miner's hut and quarry in the hv polarisation mode are essentially unchanged, again this must be charged to the lack of useful reflectors, sensor incidence angle and surface material (Appendix II, Chapter 3 and Ulaby and Dobson, 1989).

The L band decibel record over the miner's hut and the mine pit showed no change in response at -21.48 dB and -21.74 dB respectively for the hh polarisation; hv polarisation responses for the same two pixels were almost the same at -27.70 dB for the hut and -27.10 dB for the quarry.

Pixel 4286 x 1664 was selected from the middle section of the comparative transect to assess against the results of the target mine site (Table 6-7). The C band decibel response reveals an unremarkable and weaker response in the hh polarisation mode, although certainly less than that recorded at the miner's hut pixel, 4274 x 1665, this is probably correct as the terrain which the comparative transect crosses is a flat wadi bottom comprised of dense alluvial material with a thin aeolian deposition layer on top. The L band hh polarisation response is weak as well, which is logical based on the lack of reflectors on the featureless wadi bottom. The hv polarisation of the C band recorded at this pixel is only marginally than that recorded at the mine quarry, while the L band hv response is virtually non-existent.

Finally, Fig. 6-29 graphically represents the decibel responses for all the transects of Serabit El Khadim. Pixel 1 represents the southernmost pixel in each transect while pixel 12 represents the northernmost pixel. Visual interpretation of the combined transect responses can be difficult due to the results of the Lhv band, but it does provide additional insight into the microwave responses over the area's terrain.

It was not possible to determine if the mine at Serabit El Khadim could be classified as any particular type of corner reflector by the Imaging RADAR using phase difference analysis due to the lack of hh-vv polarisation data for this site, as has been explained previously (Appendix II, Chapter 9 and See Fig. 6-30). The results of this data set were discussed with Dr. Thomas Farr, Director of the Shuttle RADAR Topographic Mapping (SRTM) group and Bruce Chapman at NASA Jet Propulsion Laboratory (JPL) on 14 June 2001, who suggested that a later version of the data set utilised in this study may be more valid, due to a new calibration standard (Farr, 2001: pers. comm.). Still, no dual or fully polarimetric set of data for this area exists from the Shuttle Imaging RADAR program.

Consequently, unlike the South Ardachy mine site discussed in Chap. 5, information is limited insofar as determining what type of reflecting surface the SIR-C system may have been observing (Fig. 6-30).

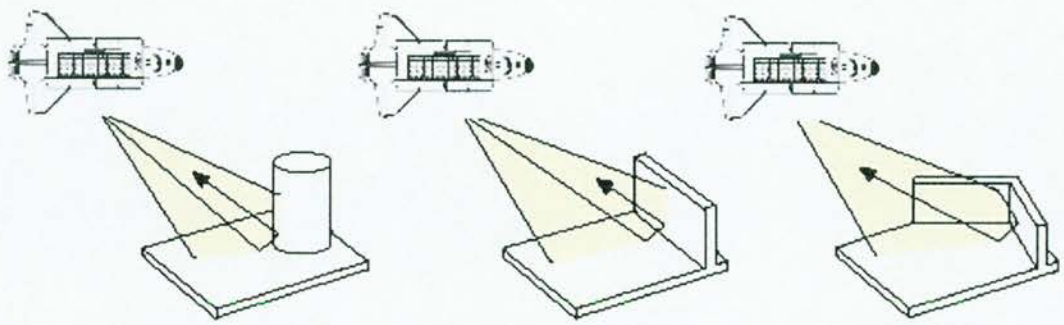

Fig. 6-30 Left to right, top-hat reflector, dihedral reflector and trihedral reflector (Adapted from CCRS 2001, JPL 2001 and Raney 1992)

In Chapter 3 it was described that the wavelengths emanating from a polarimetric RADAR system's antenna may strike the earth's surface along either the horizontal or vertical axis of the wave, and depending on the mode, they may or may not be received in a like manner. However, stray backscatter will occur as these broadcast wavelengths strike the earth's surface and rebound in odd manner of axis, thus creating extraneous signal noise or speckle in the final derived image. De-speckling and the filtering mechanism used to achieve a reduction in extraneous signal noise is important in all RADAR processing and particularly so when attempting to produce an image for visual interpretation, yet there is a delicate balance between speckle reduction and the loss of data, which was mentioned in Chapter 5. How the Serabit El Khadim data set was filtered and visualised is discussed in the following section.

6.9.4 Imaging RADAR topographic modelling and visualisation

6.9.4.1 Data fusion and representation

Chapter 4 described the general process by which Imaging RADAR data was further processed and manipulated to enhance analysis. Only specific alterations to the general processes will be discussed here, as reference back to Section 4.9.4 will provide in-depth descriptions.

DTED (Digital Terrain Elevation Data) Level 0, a product of the National Imagery and Mapping Agency (NIMA) of the U.S. government was used to produce a grid of the same area as the MLC data set. This grid was then converted to a point file. Elevation points from the Serabit El Khadim mines area were then extracted from a 1943 U.S. Army Engineering Survey map and added as additional points to the master points file. This file was then re-converted into a grid file and ingested by ENVI 3.4 to create a precision Digital Terrain Model (DTM) for the area of interest (AOI). Spatial resolution of the final grid exceeded NIMA DTED Level 1 standard, as discussed in Chapter 4 (NIMA, 2000).

The master DTM, originally in a geographic coordinate system and WGS-84 datum was then rectified, registered and projected into the Universal Transverse Mercator projection, using the standardised WGS-84 spheroid and datum.

The Chh, Lhv and Lhh MLC polarisation images, having been fully processed and analysed at this point, were then rectified, registered, and projected to the same UTM/WGS-84 Coordinate system. Ground Control Points (GCPs) were utilised with a RMS of 0.9824 percent accuracy of the original map source data.

6.9.4.2 Filter processes

As described in Chapter 4 and Chapter 5, an adaptive filter regimen was used against the Serabit El Khadim data set and after filter processing, a pseudo-colour Imaging RADAR scene was generated from 3 different polarisations and by assigning them Red, Green, and Blue, to form a false colour composite image (Kruse, 1996). It was decided to utilise the Chh wavelength as the Red colour band, the Lhv wavelength as the Green colour, and the Lhh wavelength as the Blue colour to produce this image.

The reasoning behind these colour choices are as follows: Chh has a wavelength of 3.8 cm and is useful for determining surface texture qualities of geological and geomorphological structures. Lhv at 23.5 cm is known to enjoy very subtle detection capabilities for vegetation, thus it was chosen as the Green colour band. Mine quarries, shafts, adits, disused puddling ponds and other remnants of mining activities, tend to be moisture collectors. Finally, Lhh, well known in geo-archaeological work for its lineal detection capability, was chosen as the Blue colour band (Abdelsalam *et al.*, 1995)

Finally, the composite image was created and sub-sampled as described in Chapter 5, then overlaid upon the Digital Elevation Model (DEM). Three-dimensional image scenes of the fused RADAR and DTM data are presented in Figures 6-31 through 6-34 with views from the primary compass points of north, south, east and west, surrounding the Serabit El Khadim mines complex.

6.9.4.3 Visualisation: west

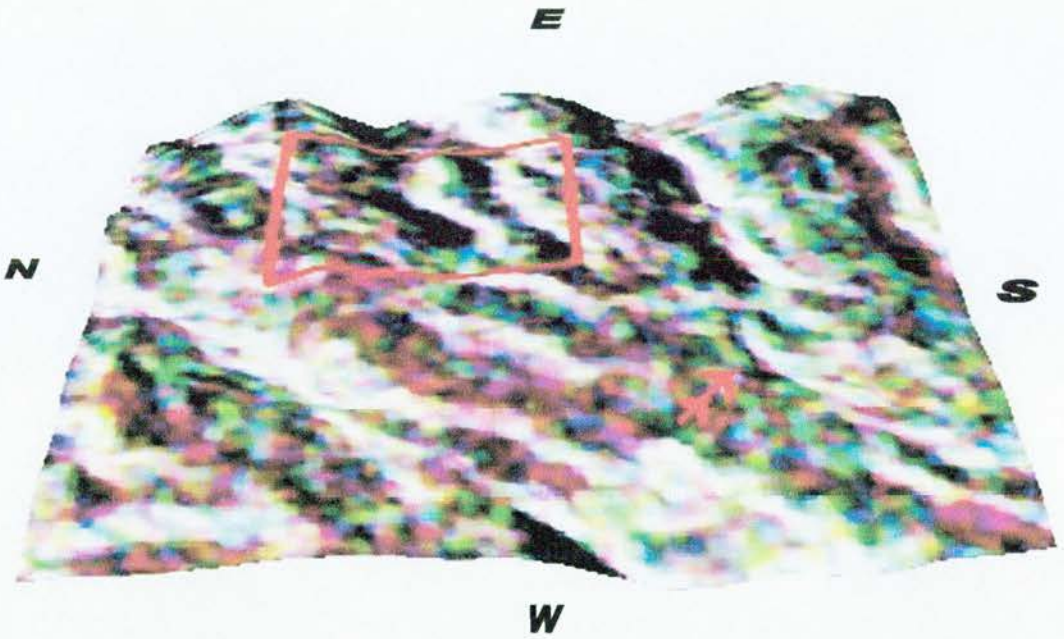

Fig. 6-31 The Serabit El Khadim mines viewed from the west (1:22,784).

In Figure 6-31 a track leading across the top left edge of Wadi Bateh's northern rim may be detected. This is located in the lower right quarter of the figure as a dark line leading towards the lower edge of the scene and indicated by a red arrow. The archaeological history of this track is unknown, but it is assumed to post-date the first mining activities at the site. This assumption is based on the dearth of archaeological evidence dating prior to the Pre-Dynastic period (Rothenberg, 1979).

The numerous intensities and hues of the selected band colours demonstrate the analyses provided in the topographic section concerning aspect and how it affects RADAR returns. Note the tendency for over-illumination on faces more oriented to the north, or left in this image, and the red hues of the Chh band returns varying in intensity as their reflecting surfaces are situated in less angular positions to the emitting antenna.

6.9.4.4 Visualisation: north

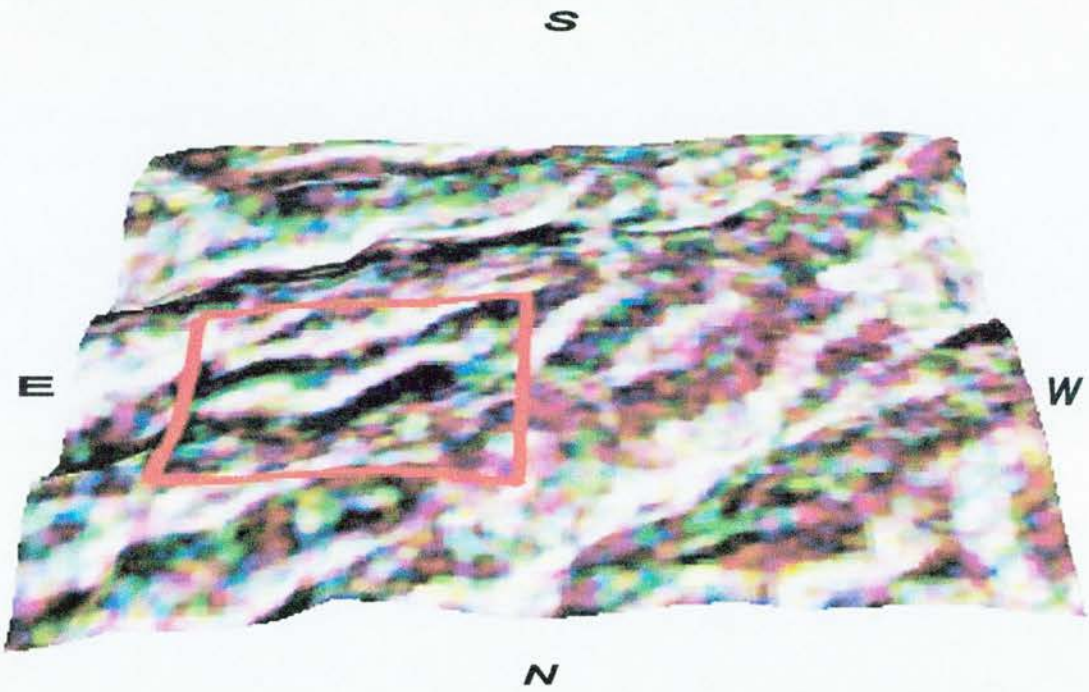

Fig. 6-32 The Serabit El Khadim mines as viewed from the north (1:22,784).

In Fig. 6-32 the depth of the northeast-southwest trending wadis is evident due to the failure of any strong returns to escape the steeply walled interiors. Note the whitish colours in the right side of the image, indicative of extremely rough surfaces with angles closely corresponding to the sensor's emitting antenna.

Archaeologically, it would be thought from the terrain model and the indications of the RADAR returns, or lack thereof, that the primary areas of potential human habitation or activity would be within the wadis. This is because, as demonstrated in the topographic analysis, these are the areas most protected from solar radiation, serve as collection points for rainfall as well as having low evaporation rates, and finally, offer easier transportation routes to the greater Sinai region. However, many settlements have been found atop the hills, confounding this idea (Rothenberg, 1979 and Malek, 2000). It could be postulated that the discovery of useful metals within the region might have occurred because of early inhabitants of the wadis discovering eroded ore structures, which were then exploited.

6.9.4.5 Visualisation: east

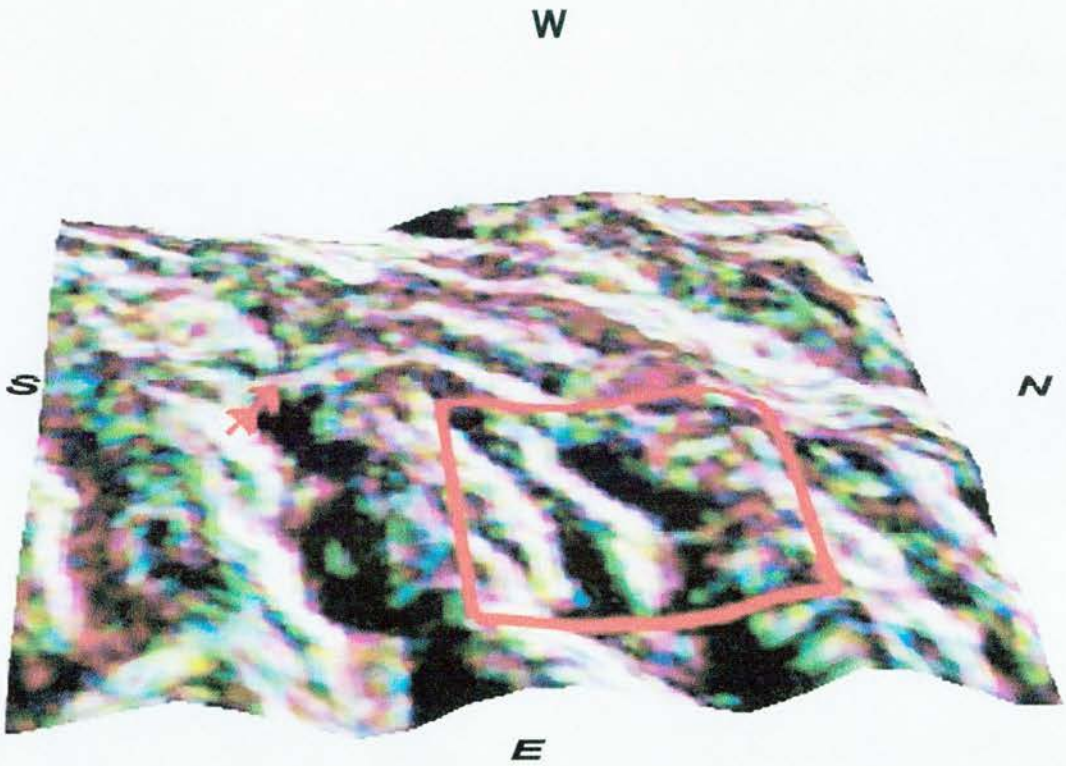

Fig. 6-33 The Serabit El Khadim mines complex viewed from the east (1:22,784).

Fig. 6-33 gives the most demonstrative example of the depth and steep slopes of the main wadis leading out of the Serabit El Khadim area. The wadi second from the left is closest to the Site "B" mine site. The ability of imaging RADAR to detect tracks in a hyper-arid environment is seen again here as several tracks may be seen intersecting above the two centre wadis, as indicated by the red arrow. These tracks lead to water sources on the Wadi Bateh, the dark area in the top centre of the image. Wadi Bateh is noted for its springs by Petrie in 1904 and has two functional springs presently (Petrie, 1906).

6.9.4.6 Visualisation: south

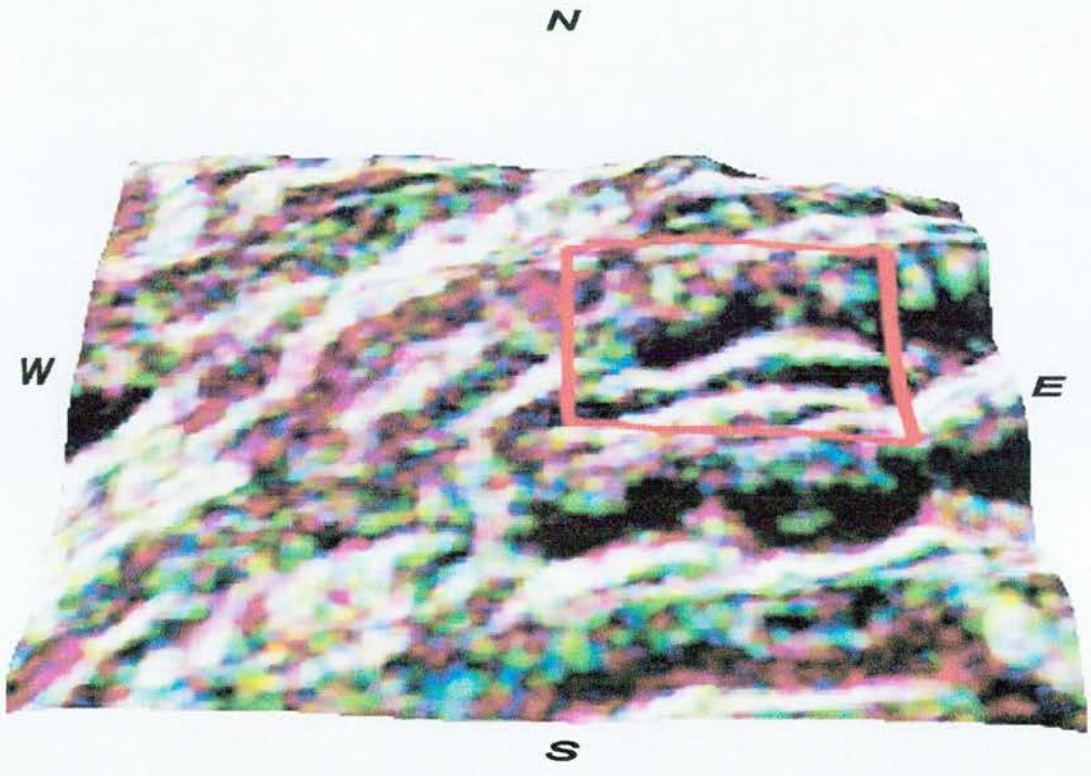

Fig. 6-34 The Serabit El Khadim mines as viewed from the south (1:22,784).

Fig. 6-34 provides an excellent view of the same effect used in the South Ardachy mines analysis. Note the red areas (Chh band) located on the ridges in between the wadis, on the sides of the wadis, and in an arcing pattern from lower left in the image to the top right wadi; these areas correspond with the local limestone outcrops as with South Ardachy on Islay. The Lhv band, assigned to green here, is apparently responding to the structure of the red sandstones exposed along the north walls of the wadis visible to the sensor. The blue colour area in the bottom centre of the image is an area of alluvial deposition running into the Wadi Garf; this area has moisture soaked mud beneath its surface of loose sands and gravels.

6.10 Summary of results: Serabit El Khadim, the Sinai

6.10.1 Imaging RADAR and the topography

After a description of the historical and physical geographic setting behind ancient mining on the Sinai, a detailed topographic analysis was performed on an area surrounding the chosen test site, the Serabit El Khadim mining complex. Topographic analysis revealed a terrain surface of extreme convolution, marked by a geological interface around the site.

The unusual nature of the data set used for this target mine site made it impossible to perform either phase difference analysis or polarimetric analysis as neither dual nor fully polarimetric Space Shuttle Imaging RADAR data was available (Chapter 9). Further, the RADAR propagation and reception mode utilised for this data set, the incidence angle and the lack of calibration for the data, make even the decibel responses somewhat circumspect, although it should be noted that the statistics observed fall in line with those of Ulaby and Dobson (1989). Since the completion of the analysis for this site a calibration program utilising a new standard has been implemented at the USGS with this data set scheduled for re-assessment. However, as of the date of this writing, it had still not been examined and again, no full or fully polarimetric data set resides in the archives at JPL or the United States Geological Survey (USGS, 2001: http://www.usgs.gov).

Finally, a false colour composite of the Serabit El Khadim mines region was created from the Cvv, Lhv, and Lhh bands of the MLC data subset. This false colour composite was then draped over a DTM for three-dimensional visualisation of the archaeological landscape surrounding the mines. The false-colour composite highlighted the Imaging RADAR capability to map the geo-archaeology of the Serabit El Khadim region, revealing further possible areas of ancient mining activity. Tracks leading from the mine site to water sources were also detected, indicating the level of organisation surrounding the complex. It is also possible that climate change over several thousand years reduced, or negated more local water sources for mine production use.

The next chapter will present the results of the investigation of previously unknown mines near Conil, Spain. Following that chapter, a summary of inter-site comparison results will be presented.

Chapter 7

Conil, Spain

"Hanno sailed from Gades to the extreme part of Arabia and published a note of his voyage, as did Himilcar, when sent at the same time to explore the coastlines of Europe". Pliny, from "Natural History, translated by John Healy, 1991: 33.

7.1 Introduction

This chapter presents the results of the Imaging RADAR (NASA SIR-C/X-SAR) archaeological survey of the Conil mines located on the Gaditano coast of Andalusia, Spain. Unlike the previous two sites, the Conil mine is a new archaeological discovery made by applying a geographical model constructed during the research for this study, as discussed in Chapter 3. Section 7.2 is a description of the physical geography of the island, which is followed by a historical geography in Section 7.3. Site topography and analysis is outlined in Section 7.4. Section 7.5 presents site history and archaeology, while Section 7.6 displays the CORONA satellite imagery. Section 7.7 presents AVHRR data immediately preceding the overpass of the Space Shuttle and its Imaging RADAR system. Section 7.8 covers the local meteorological data immediately preceding the overpass of the Shuttle Transport System (STS). Detailed Imaging RADAR analysis data is outlined in Section 7.9. Section 7.10 concludes the chapter with a summation of the data presented.

7.2 - Physical Geography and Geology

7.2.1 – The Physical Geography of Cadiz and the Gaditano maritime

The physical boundaries of the Gaditano maritime region are much different than the modern day political boundaries of Cadiz, which mark its extent. The word Gaditano is derived from the ancient Phoenician word for the city of Cadiz, that being Gadir (Escacena, 1985). Modern geographers, including many Iberian specialists, observe the standard definition of the maritime region being located entirely within the province of Cadiz, which is located on the extreme southwestern tip of Andalusian Spain (see Fig. 7-1). This is a fallacy which not only ignores historical fact, but one which ignores physical evidence. The following description provides a more correct geographical definition.

Moving clockwise around the compass rose, the region's northern borders would be defined by the foothills of the Sierra Morena Mountains with the Guadalquivir River flowing beneath them to the southwest. At the north-northeast border lies the city of Cordoba, with further inland navigation of the Guadalquivir River halted by rapids, shoals, and siltation.

Figure 7-1 Conil, Spain and region; created from NOAA data, 1:2m.

Moving south through the lower reaches of the Sierra Ronda Mountains, the southeast border finds the headwater of the Guadalhorce River, east of the ancient Roman city of Antequera, and some forty miles north of Malaga on the Mediterranean Sea. Rocky, crescent-shaped bays and shallow waters dot the coastline southwest from Malaga to the southernmost border. These rocky bays and shallow beaches are the home of many ancient seaports such as Malaga, or Malacca, as it was known to the Greeks, and Estepona, founded by the Carthaginians, and in the Bay of Gibraltar, Carteia, begun by the Phoenicians (Baramki, 1961).

Located deep within the furthest reaches of the Bay of Algeciras, Carteia was protected by the massive Rock of Gibraltar on its east, and the cliffs of the Los Pinos Blancos Mountains on the west. Today's modern city of Algeciras now serves as a massive point of transhipment for Europe and North Africa, serving the same purpose as Carteia did several millennia beforehand for the Phoenician, Punic and Roman empires (Collins, 1998).

Rounding the extreme southwestern point of Spain and Europe through the Straits of Gibraltar, the maritime region is now bounded on the west by the Atlantic Ocean. The coastline is known as the Costa de la Luz because of the lengthy white sand beaches that illuminate the shoreline under moonlight. At Cadiz itself, the enormous bay is surrounded by great salt marshes which have produced salt from evaporative methods for trade since 1000 BC (Bonald, 2000).

Some 65-kilometre north-northwest of Cadiz on the Costa de la Luz, at the western border on the region's perimeter, lies the mouth of the Guadalquivir River and the salt marsh wilderness of the Coto de Donana. The Guadalquivir River is the largest river in Andalusia with its headwater flowing from the Sierra Nevada, Sierra Morena, Serrania de Ronda, and Sierra de Segura Mountains (Hopkins, 1995).

The extreme northwest position of the Gaditano maritime region is punctuated by the shallow tidal marshes of Huelva. The Rio Tinto river derives its name from the early, well known mining district located at its headwaters, which polluted its waters with the erosion and by-products of copper mining (Moscati, 1988). It should also be mentioned that artefacts belonging to pre-historic Celto-Iberians have been found along the lower reaches of the stream, leading some archaeologists to speculate on the sea-going aspects of that culture (Arribas, 1964).

The Gaditano area consists of an enormous valley; bordered on two sides by great mountain ranges and on the other two sides by an ocean and a great sea. These conditions have enabled the region to enjoy a mild climate, with summer temperatures being abated somewhat along the Guadalquivir River and coastlines, while the rapidly rising elevations of the mountains also guarantee some thermal relief. Winters are generally noted for exceptional rainfall, this obviously being a Mediterranean climate and are occasionally dominated by either poniente or levante winds. Levantes blow across the Straits of Gibraltar from North Africa, usually from the east-southeast, thus their name, which is derived from the ancient word for the eastern Mediterranean (NOAA, 2001). Ponientes blow from the west-northwest, thus creating the dangerous autumnal gales which have destroyed many vessels, in the days of sail and most certainly influenced early Mediterranean sea-traders (Aubet, 1994).

7.2.2 The Geology of Conil and Cadiz Province

Although Conil lies outside the Straits of Gibraltar on the Atlantic Ocean, it is the geologic processes that created the Mediterranean Sea that have had, and still have, the most influence on its stratigraphy. The Mediterranean is a remnant of the vast ancient sea called Tethys, which was squeezed almost shut in the Oligocene Epoch, 30 million years ago, when the crustal plates carrying Africa and Eurasia collided. The plates are still grinding together, causing the eruption of volcanoes such as Mount Etna, Mount Vesuvius, and Stromboli, all in Italy, and triggering frequent earthquakes, which have devastated parts of Italy, Greece, Turkey, and in the past, Spain (Instituto Tecnologico Geominero, 1990).

From these geological processes two immense undersea sills have been created. The first ranges from Tunisia to Sicily and divides the Mediterranean into eastern and western basins. Another seafloor sill, from Spain to Morocco, lies at the outlet of the Mediterranean. Only 300 metres deep, it restricts circulation through the narrow Strait of Gibraltar, thereby greatly reducing the tidal range of the sea and, coupled with high rates of evaporation, making the Mediterranean much saltier than the Atlantic Ocean. Another geological feature traversing from the southwest to the northeast, the Rif-Betic Cordillera, intersects this sill (Instituto Tecnologico Geominero de Espana, 1994).

The Rif-Betic Cordillera is a structure which has its roots in the Cretaceous and Tertiary time and extends from the southwest of Morocco, rising as the Atlas Mountains, then dipping slightly under the Straits of Gibraltar to rise as the Sierra Ronda and Sierra Nevada Mountains in Spain. It is this feature which has influenced Cadiz's geology the most over time (Instituto Tecnologico Geominero de Espana, 1994).

The most notable characteristics of the geology in the Conil region are deposition of disturbed sediments throughout the lower Cretaceous-Miocene, frequent tectonic activity, and an abundance of upward structural movement (Fig. 7-3 and 7-14). The oldest sediment samples in the area date from the Triassic, but only have limited representation in the area. There is then found a succession of clays and gypsum with insertions of dolomite and sandstone, resulting in an elevated plasticity and making it easily deformed since the beginning of the Jurassic until present; the marls and limestone are representative of the upper Cretaceous-Paleocene time (Instituto Tecnologico Geominero de Espana, 1994). Thus, it can be seen that the heat, stress and motion required for mineralisation has existed in the area for millennia.

The soils of the region are typically brown and red with yellow podzolics. They are generally indicative of the higher plains in the surrounding valleys (Benson, 1989:12-13). As with the rest of the Iberian Peninsula, no point is further than sixty miles from a mountain range, and so it is with this region as well. Minerals such as iron, tin, and silver, may be readily found throughout the Serrania de Ronda, which is a component of the Sistema Penibetico mountain range (Collins, 1998). This southern range of mountains towers over the western Mediterranean Sea and contains both the Serrania Ronda and Sierra Nevada, as well as one of the highest altitudes in Europe, the Cerro de Mulhacen near Granada (Hammond, 1995). Great clay deposits are found near Cordoba, which may have been the source of the Iberian Peninsula's earliest known ceramic pottery. The clays of the region were well known to the Greeks by the year 900 BC and would later find its greatest expression in the famous Malacca pottery, the name being taken from the Greek name for the seaport Malacca, or Malaga as it is now known (Boardman, 1999).

The salient features of the Gaditano Maritime's physical geography have now been noted. A short discussion of the known mines and mining areas of Cadiz are presented in the following section, after which the historical geography of the region surrounding the Conil mines will be presented.

7.2.3 The Minerals and Mines of Cadiz Province

7.2.3.1 Minerals

The primary sources of economic geology within the Province of Cadiz today are primarily construction-related materials. These are a) clays, which are used in the pottery and tile manufacturing industry, b) sulphur, an extraction industry almost abandoned, c) gypsum, suitable for wall construction materials, d) marl, extracted primarily for construction materials and e) the attendant sands suitable for concrete (Instituto Tecnologico Geominero de Espana, *Cadiz,* 1994, Fig. 7-3 and 7-14).

7.2.3.2 Mines

At the present time there are no mines operating in the province of Cadiz extracting non-ferrous or ferrous metals. Historical records suggest a much more varied mining past, as discussed in Chapter Two. The private library of the Duquesa de Medinia-Sidonia is a source of potential historical documentation as it contains papers dating from the 9th century to present regarding land use in the province (Baird, 1988).

As an example of unknown mine works, thirty kilometres from the Conil mine rakes, near the mouth of the Valle de Ojen, are the remaining slagheaps of a lead mine of undetermined provenance (Fig. 7-2 and 7-3 for location). Also nearby are the remains of pocket mining for coal (Instituto Tecnologico Geominero de Espana, *Tahivilla,* 1990: Map 1.074, 13-47).

Fig. 7-2 Example of mining, Ojen slag heap, Cadiz, Spain.

7.3 Historical Geography

7.3.1 The Historical Geography of the Conil mines area until the Roman era

The pre-historical and historical geographic record of the Iberian Peninsula is continually being altered. The long held belief by many anthropologists has been that humankind did not make its first arrival into Europe until sometime after 500,000 BP. However, humankind's earliest ancestors were at the edge of Europe long before 500,000 BP. In Northwest Africa, just over the Straits of Gibraltar in the foothills of the Atlas Mountains, artefacts at least one million years old have been found (Hublin, 1996). Recently, discoveries at the Gran Dolina located near Atapuerca, Spain, have dramatically revised previous conclusions of humankind's earliest ventures into Europe.

Investigations led by Eudald Carbonell of Rovira y Virgli University at Atapuerca have shown a geological record which dates the human artefacts to relate to a paleomagnetic inversion around 780,000 years BP. The evolutionary record of these people points to an ancestry from the Bosphrus and eastern Mediterranean (Bahn, 1996). Thus, the pre-historic record of the Iberian Peninsula points to a time some three-quarters of a million years ago. There are numerous sites in Andalusia indicating the presence of Mesolithic and Neolithic peoples. However, the historical records begin less than 10, 000 years ago (Scarre, 1995).

The earliest organised inhabitants of the region now known as Andalusian Spain were Celto-Iberians who, based on archaeological records, seemed to have been largely clustered in sites near the present day cities of Huelva and Sevilla (Perez, 2000). If so, this may be the origin of the Kingdom of Tartessos (Casanova, 2000). This period of time coincides with the Atlantic Bronze Age (1100-800 BC) and could prove to point to the resources, which gave Tartessos its power (Aubet: 1994).

The inhabitants of Andalusia, as well as the rest of the Iberian Peninsula, had understood the need for one of their natural resources, tin, as a vital component in the manufacture of high quality bronze for both weapons and other goods. Sitting astride a natural trade route crossroad, the Celto-Iberian peoples probably developed a high economic state within a short time, serving as suppliers and middlemen for traders from the Mediterranean and Atlantic. It is well known that by the 8th century BC King Gergon of the Tartessans was in touch with the Phoenicians of the eastern Mediterranean, trading silver and lead (Arribas 1964).

The Phoenicians are one of the great maritime cultures of history. Though their fame in modern times is largely derived from their development of a standard, simplified, and flexible alphabet, they should be equally renowned for their skill as mariners. Pomponius Mela, a Hispano-Roman historian, wrote in the first century AD,

"The Phoenicians were a clever race, who prospered in war and peace. They excelled in writing and literature, and in other arts, in seamanship, in naval warfare, and in ruling an empire" (Harden, 1962).

Mela's words are significant, for without their maritime business ventures, the Celto-Iberic cultures of the Gaditano maritime might never have achieved the benefits of their naturally presented position on the tip of Southwestern Europe.

While the Phoenicians are well known for having been among the first of the Mediterranean cultures to sail through the Pillars of Hercules, or Straits of Gibraltar, into the Atlantic, it was actually the Greeks who first reached the Gaditano maritime (Harrison, 1988). Both groups utilised a route of travel that skirted the North African coast until within sight of the Andalusian coast, probably at the southern Pillar, or Ceuta, then used the northerly thrusting coastal current to cross over to the Iberian Peninsula. This path avoided the strong central currents which tended to send a ship far into the Atlantic Ocean, usually never to be seen again (Pernetta 1995).

Both groups were in intense competition with each other for several centuries, with the Greeks establishing forward seaport trading colonies on Sicily, Corsica, and the high coast of the Costa del Sol of Andalusian Spain (Angelis and Tsetskhadze, 1994). The seaport colonies of the Phoenicians were first located across the North African coast stretching from the Levantine homeland to Cyprus, Crete, and Tunis. Later expeditions extended this westward reach through the Straits of Gibraltar to Mogador, on the southwest Moroccan coast and Cadiz, or ancient Gadir, on the southwestern coast of Andalusia. Gadir became the central trade outpost of the Phoenicians in their trade efforts throughout the eastern Atlantic Ocean and western Mediterranean (Aubet: 1994). The ninth century BC saw Phoenician tradeports established at Mostaganem, in present-day Algeria, and Carteia on the Bay of Algeciras in Andalusian Spain (Moscati, 1988).

The entire region, centred on Cadiz, may also have had an unusual function as well, serving as a shortcut into the inland area of the Tartessan Empire. The Phoenicians attempted to bypass Tartessan middlemen in the tin trade by establishing two trading and mineral production centres of their own in the Sierra Gazules, a branch of the Sistema Penibetico mountains. Known to historians as Lascut and Iptuci, until recently little was known either of their location or of their success in tin production, although recently the village of Alcala de Gazules has been identified as Lascut (Sola, 1957 and Perez, 2000). Their success was undoubtedly tied to the effectiveness of Cadiz in supplying their needs as well as exporting their products. It is possible that Conil belonged to this same early network of mining entrepots.

Whatever the case, the Conil mining site appears to have been established sometime in the third century BC and was surely in operation by as early as the middle of the first century BC (Aragon, 2000). It was then either abandoned by the Carthaginians or captured by the Romans (Burn and Selincourt 1972).

7.4 Location of the Conil mines and topographic analysis

7.4.1 Site location

The Conil site was discovered in April of 2000 after three months of extensive fieldwork. The site is located at approximately 297685 E by 402120 N, UTM (See Fig. 7-3). The primary site is bounded on the southwest by the N-340 coastal highway, the Conil or Rio Salado, on the north at some 1000 metres distance, and the mountain Cerro Patria to the southeast. The Rio Salado is the closest supply of freshwater at 1 kilometre to the north. The Atlantic Ocean is 4 kilometres to the west. There is no eastern boundary to the mines as a continuous series of undulating, ore bearing hills, trends some 40 kilometres inland towards the city of Medina-Sidonia. This region has not been surveyed by archaeo-metallurgists or ancient mining experts, according to the Junta de Andalucia in Seville as of May 2000.

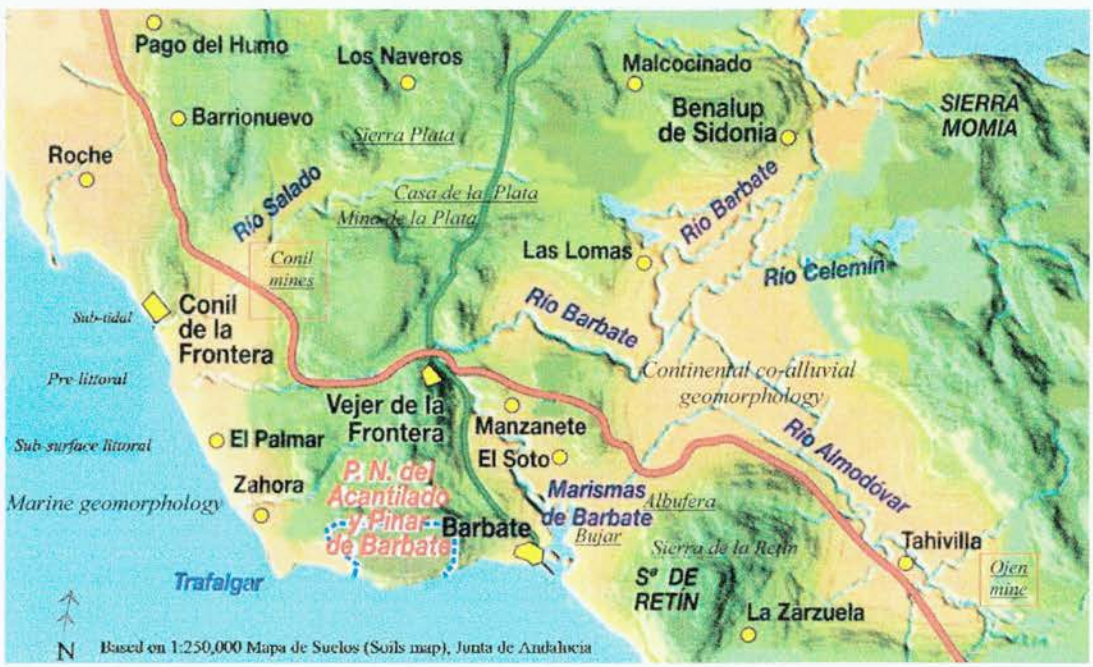

Fig. 7-3 Conil mine site location, geomorphologic zones, and mining related toponyms underlined. Created from DCW and Junta de Andalucia data.

7.4.1.1 Topographic analysis

A complete topographic analysis of the region surrounding the Conil mine site was performed using a Digital Terrain Elevation Data subset equivalent to a level 1 parameter i.e. one verifiable elevation point every 90 meters on average. The data were obtained from the Oficina de la Junta de Andalucia, Departamento de Cartografía; data drop-outs are due to processing problems (NIMA, 2001). The data subset used here was verified to an elevation point every 70 meters. The data subset boundary was set to the exact limits of the NASA SIR-/X-SAR Imaging RADAR data subset for three-dimensional modelling purposes and to speed processing time. The data set geographic co-ordinates are as follows: upper left corner pixel 36° 19′ 52.32″ latitude by -6° 1′ 26.46″ longitude. The lower right corner pixel 36° 17′ 16.26″ latitude by –5° 58′ 25.25″ longitude, with overall dimensions of some 5.0 km x 5.0 km approximately.

Just as with the two previous sites, topographic analysis is necessary to understand the manner in which microwave emissions interact with the earth's surface and to support valid analyses and assumptions. The topographic analysis followed the methodology outlined in Chapter 3, which comprise the following examinations: slope, aspect, shaded relief, profile convexity, plan convexity, longitudinal convexity, cross sectional convexity, minimum curvature, maximum curvature and topographic feature classification (i.e. hill, peak, depression etc.). A general landscape view of the site is presented in Fig. 7-4. Figure 7-5 and 7-7 may be referred to as reference maps for this data as they portray the DEM data in a standardised cartographic manner familiar to most viewers.

Figure 7-4 Conil site topography; southwest view.
Note the mine rake in the foreground, centre hill and far hill.

7.4.1.2 Slope

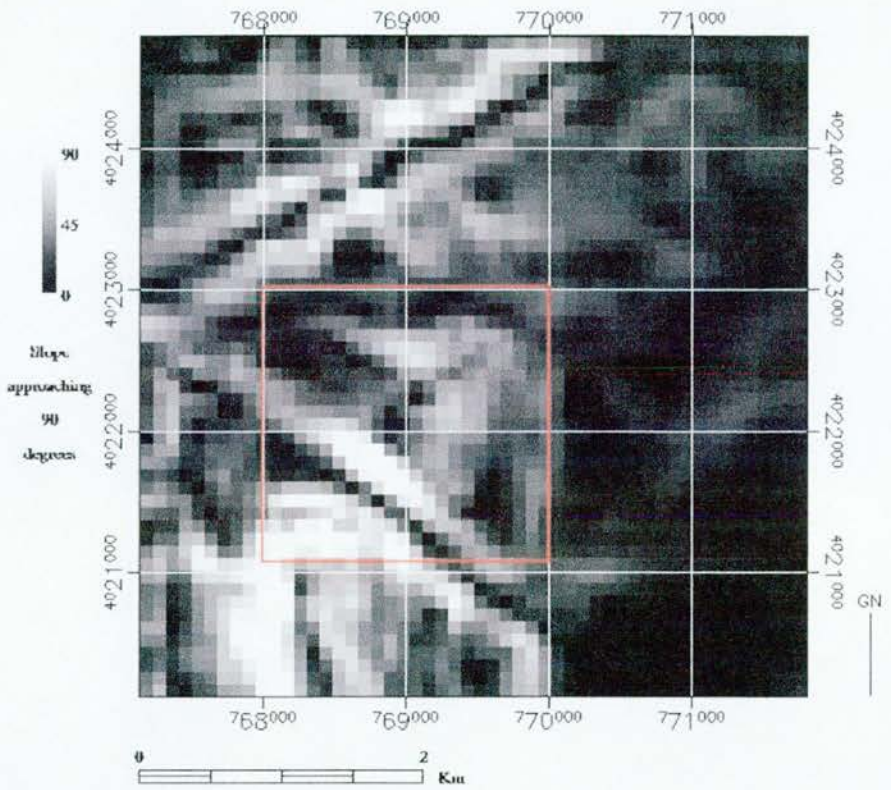

Fig. 7-5 Slope analysis, Conil.

It can be seen in Fig. 7-5 that the most significant slope change occurs in the lower left grid square of the red area of interest (AOI) box and then in the left lower grid square outside the box. The lower left grid square within the red box corresponds with the Site "C" target mine rake. The area at the upper right portion of the grid displaying slope change is a result of the embankment construction for the N-340 coastal highway (Fig. 7-3, 7-17, 7-31 and Appendix III, Fig. III-1). This construction destroyed the middle portion of the original mine rake system. Indications of the convoluted nature of the ore-bearing hillocks in the northern portion of the Conil mine rake complex can be seen in the upper two grid squares within the AOI box.

The trend of the Rio Salado from the west to the northeast can be seen at grid Coordinate 402300 N by 768000 E. It should be noted here that the location of a nearby source of fresh water is a key factor for any metals extraction and processing, and once again, the Conil site follows that well-known model.

7.4.1.3 Aspect

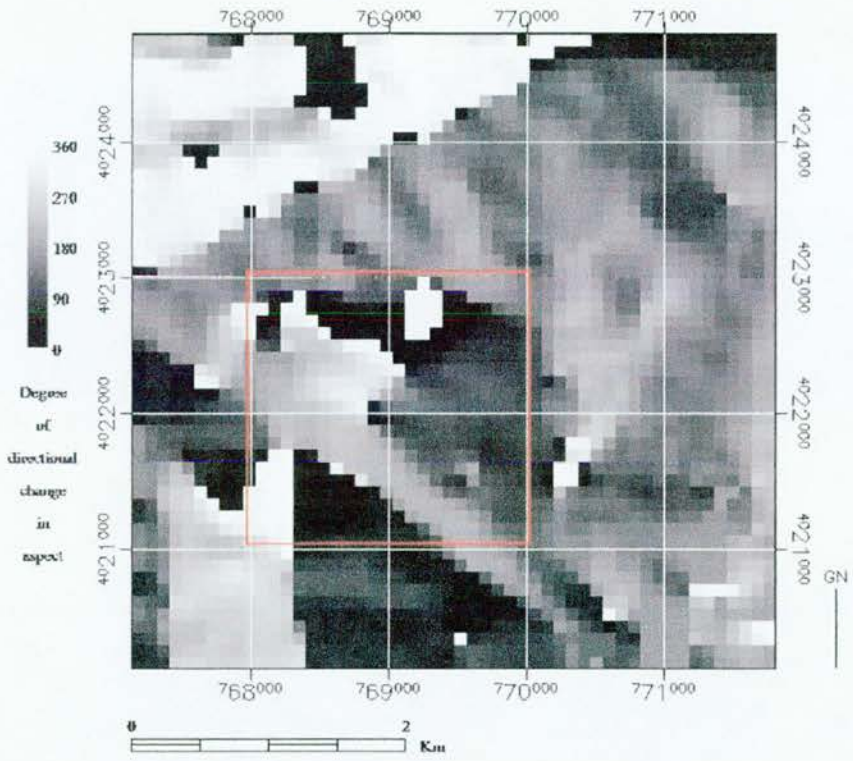

Fig. 7-6 Aspect analysis, Conil.

In Fig. 7-6, the dramatic change in aspect between the topography located north and south of the banks of the Rio Salado is remarkable. The aspect of the topography along the south bank of the Rio Salado gives a clear indication of the small ore-bearing hillocks trending towards the northeast. The area of interest box shows a topography that is clearly influenced by underlying geological stresses and indicates that the conditions necessary for mineralisation are present.

In regards to human habitation, it is unlikely that the banks of the Rio Salado would have been utilised due to its exposure angle to solar radiation, as well as the deep fluvial mud pans. Unlike on Islay, the early inhabitants of the Iberian Peninsula would have taken pains to obtain shaded, wind protected locations (Perez, 2000). The areas exposed to solar illumination will be examined in the shaded relief analysis of the following section.

7.4.1.4 Shaded Relief

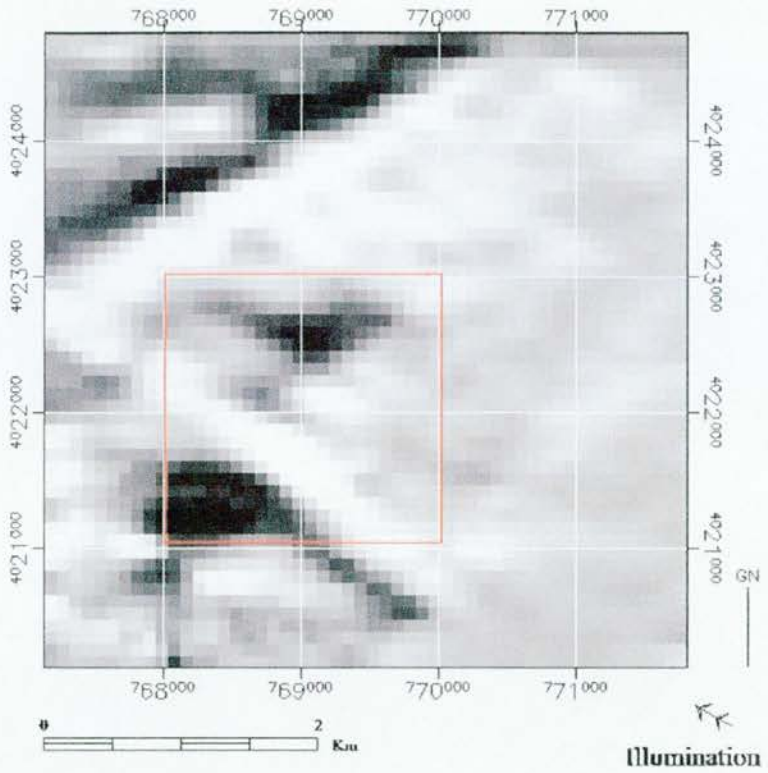

Fig. 7-7 Shaded relief analysis, Conil.

Shaded relief for the Conil mine complex was computed using the following figures: a sun elevation angle of 40.004063° in conjunction with a sun azimuth angle of 135.897994°, 1000 hours. Fig. 7-7 shows a topography that provides little respite from either solar illumination or the evaporative effects of wind. The solar illumination was calculated for the angularity of the sun in early October over the lower Iberian Peninsula. It is interesting to note that the modern open pit mine, as well as the mine rakes area, is of sufficient depth to offer some mitigation from illumination. The long hours of solar illumination would have hindered mineral processing on some points, such as in washing of ores, which requires large amounts of fresh water, which of course would have evaporated rapidly in the Mediterranean climate. Conversely, the intense solar radiation would have rapidly dried ores, readying them for processing more rapidly.

7.4.1.5 Profile Convexity

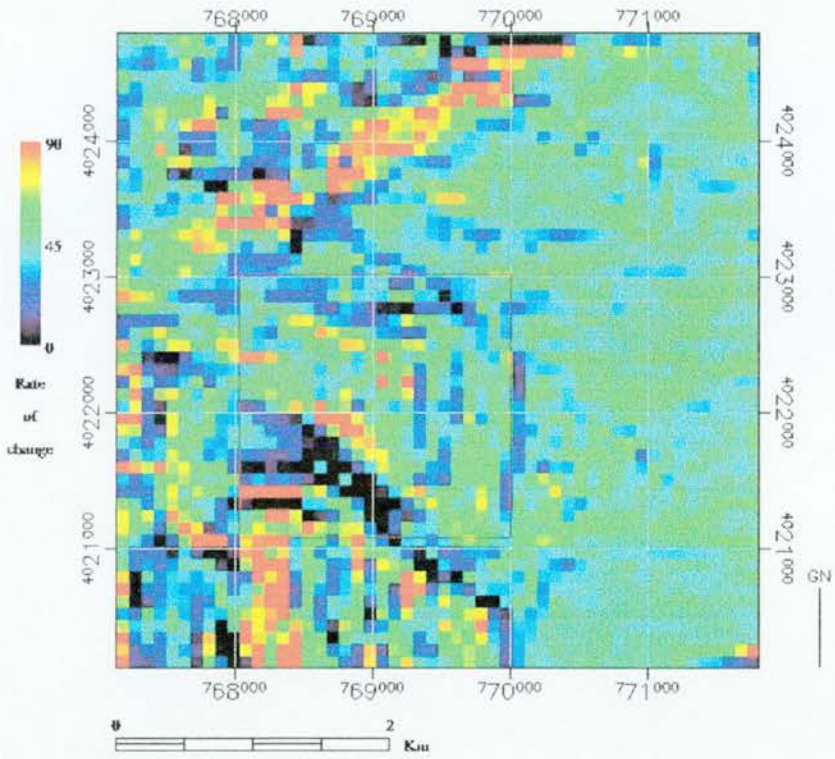

Fig. 7- 8 Profile convexity analysis, Conil.

As can be seen in Fig. 7-8 profile change, which measures the rate of change of the slope along the profile, is concentrated along the banks of the Rio Salado in the upper left grid squares and the lower left grid squares, which contain the Site "C" target mine rake. Once more, the hillocks that contain ore extrusions may be detected in the upper two grid squares of the area of interest box by their 80-90 percent change in profile.

The area observed in the right portion of the image may be seen to have moderate changes. However, note that the general pattern of profile change is trending towards the northeast. This again is indicative of an underlying geological structure that is exerting strong influence on the geomorphology.

7.4.1.6 Plan Convexity

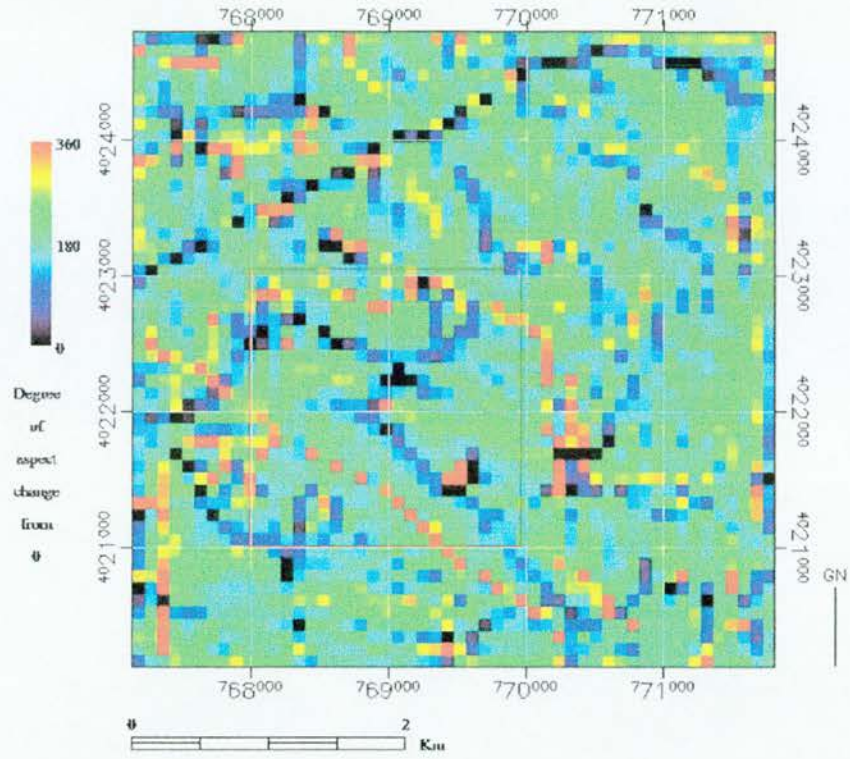

Fig. 7-9 Plan convexity analysis, Conil.

As discussed in Chapter 3, plan convexity (intersecting with the XY plane) measures the rate of change of the aspect along the plan. The analysis here reveals a numerous quantity of irregular protruding surface faces that change direction within a small surface area (Fig. 7-9). This is a precise description of the small hills, hillocks and exposed rock extrusions, which dot the landscape. Transport difficulties to and from a mine site located within this type of topography would normally be regarded as moderate, in particular when using cart or wagon transport. However, due to the proximity of the Rio Salado and the Atlantic Ocean it is likely that at some point water transport was employed. This is a point that requires future archaeological investigation of the area between the northern portion of the Conil mines area and the Rio Salado.

7.4.1.7 Longitudinal Convexity

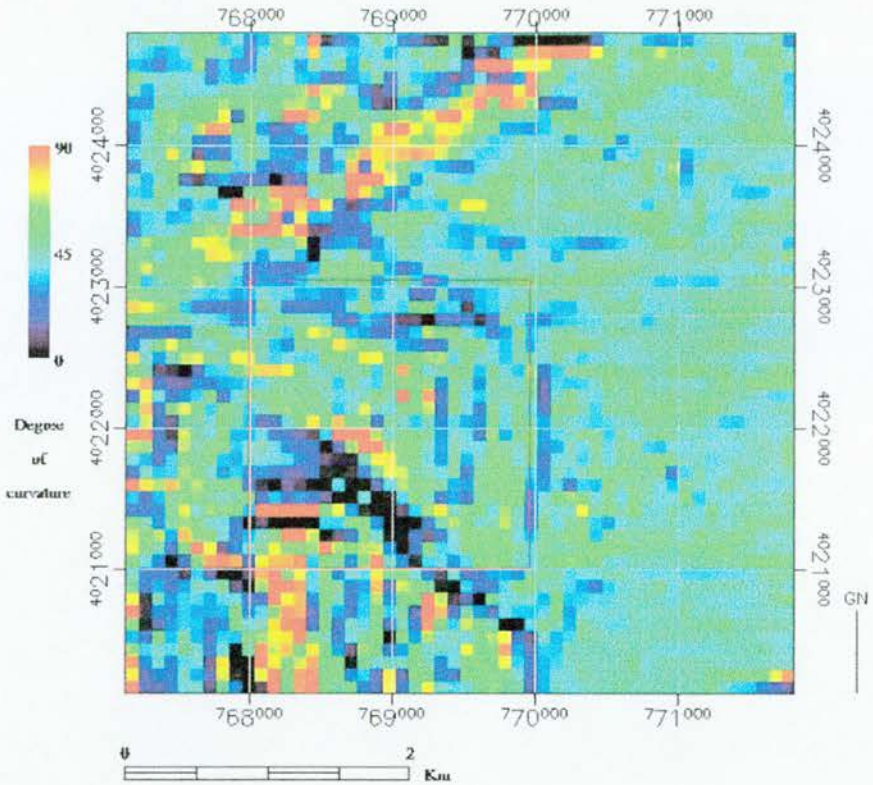

Fig. 7-10 Longitudinal convexity analysis, Conil.

As explained in Chapter 3, longitudinal curvature and cross-sectional curvature are measures of the surface curvature orthogonally in the down slope and across slope directions, respectfully. The previous profile and plan analyses have shown limited topographic change in those vectors and the same can be said for longitudinal curvature.

Again, areas of curvature may be seen along the Rio Salado, the upper left grid squares in the image above, and in the lower left grid squares, which contain the Site "C" target mine rake (Fig. 7-10). These would also be the areas which have the potential for elevated erosion from both water and air, for as heavy rainfall within the winter months is common in the Iberian Peninsula, surfaces with high longitudinal convexity would transport water more rapidly. These same areas would also be more exposed to the high average wind conditions of the area. Consequently, areas of mineral extrusion within the Conil mine rake area were likely to have been exposed over time by these factors coupled with a rising local geology.

7.4.1.8 Cross-sectional curvature

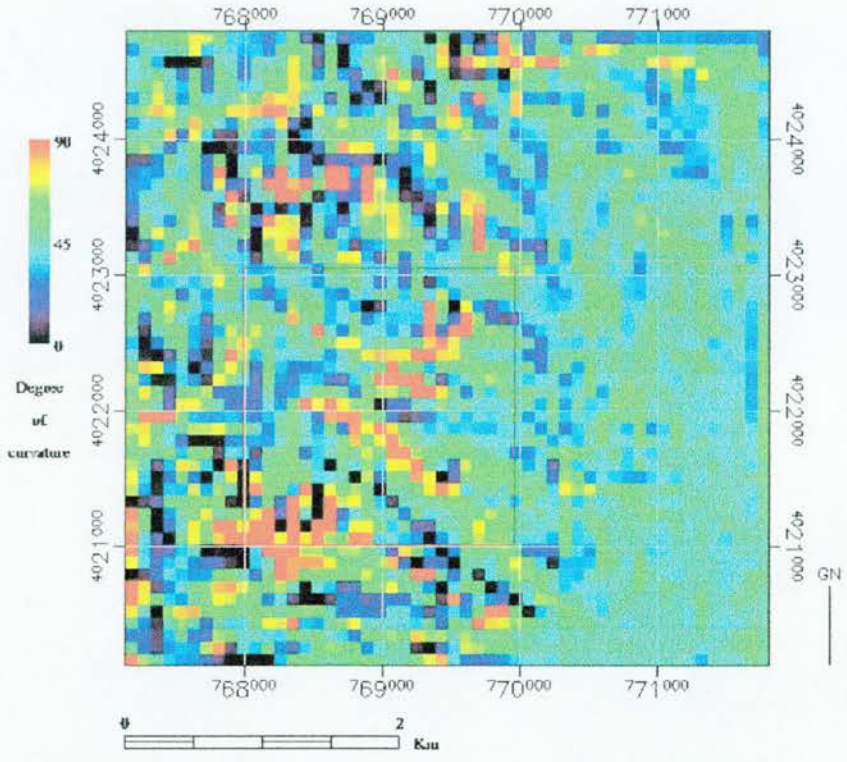

Fig. 7-11 Cross-sectional curvature analysis, Conil.

As mentioned in Chapter 3, cross-sectional convexity, or curvature (intersecting with the plane of the slope normal and perpendicular aspect direction) is a measure of the surface curvature orthogonally across slope directions. In the previous section the aspect of hydrological and aeolian erosion over a rising geology was presented as a potential hypothesis for the exposure of the mineralogy of the Conil mine rakes. Here, the cross-sectional analysis process highlights the major ore bearing hillocks within the area of interest box surrounding the rakes (Fig. 7-11).

Referring to the geology map in Fig. 7-14, it can be seen that these areas of high cross-sectional convexity correspond with the dolomite extrusions, which are surrounded by gypsum deposits. Once more, it might be inferred from this evidence that the underlying geology is affecting the surface topography.

7.4.1.9 Minimum curvature

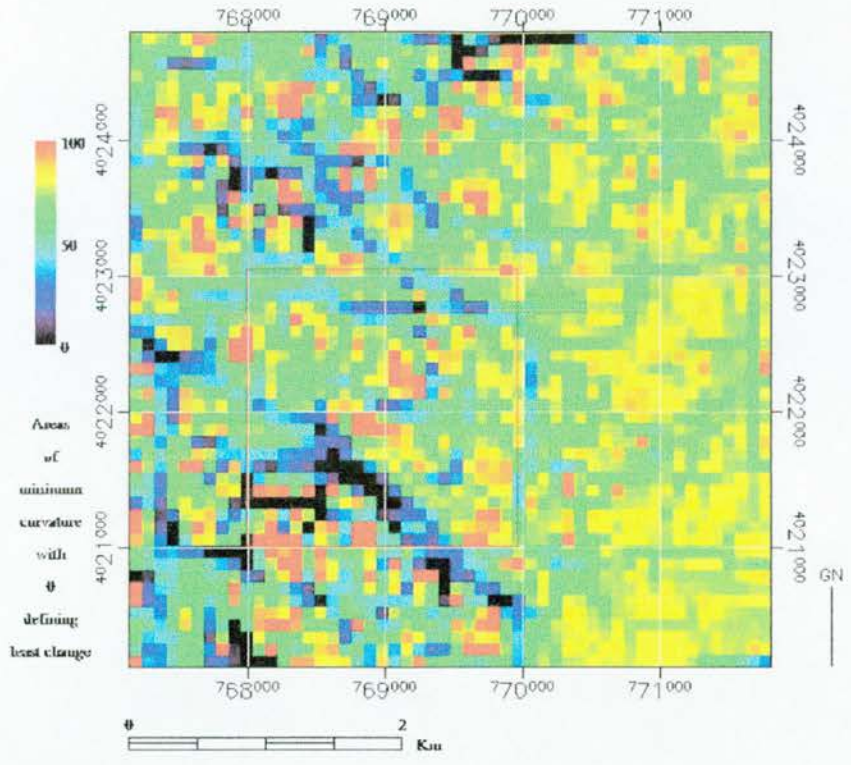

Fig. 7-12 Minimum curvature analysis, Conil.

Minimum curvature analysis of the Conil mine rakes area similarily reveals a local topography that is convoluted by change, with only the Rio Salado basin and the man-made route of the N-340 highway displaying significant areas of no change (Fig. 7-12). Note that the small open pit mine located in the lower left grid of the area of interest box is evident in this analysis just below the trend of the N-340. Once again, the region in the right portion of this image scene is dominated by moderate change in curvature.

In topography such as this, water from rainfall will find few places to collect. Coupled with a primarily sand-based soil structure, high amounts of solar radiation and high average wind speeds, then all the ingredients for a semi-arid environment are in place. This again stresses the requirement that mineral processing at the Conil mine rakes, if it occurred in any significant quantity, must have relied on the Rio Salado as a fresh water source.

7.4.1.10 Maximum curvature

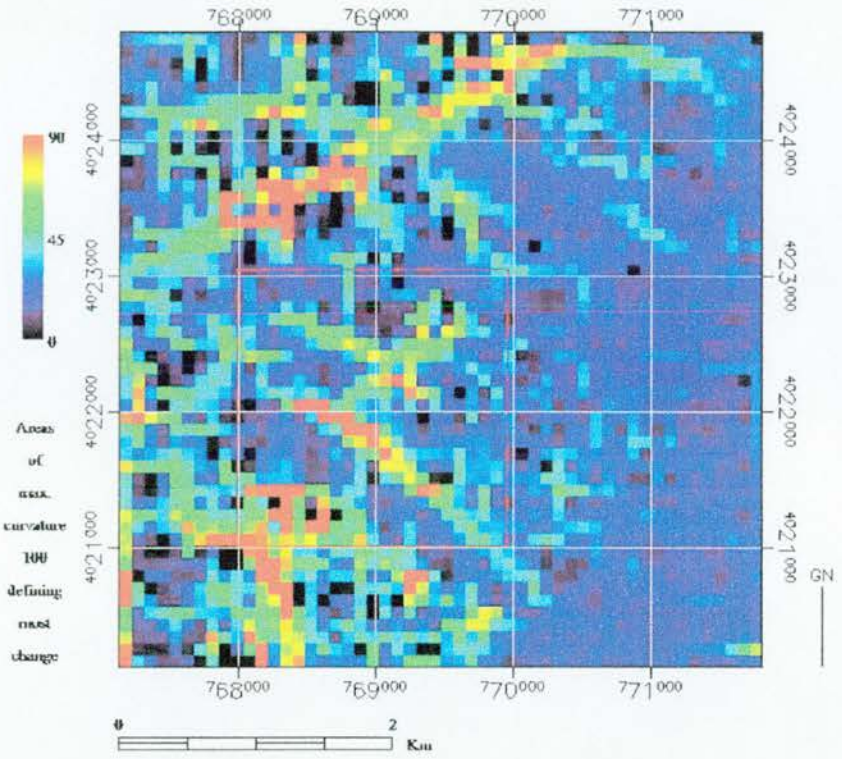

Fig. 7-13 Maximum curvature analysis, Conil.

The inverse of the previous analysis, maximum curvature detects the areas in topography that have maximum change across all planes of the given surface. The Site "C" target area can be seen in the lower left grid of the area of interest box as exhibiting these characteristics (Fig. 7-13), as well as the north face of the intruding N-340 embankment, and of course the central banks of the Rio Salado in the northern grids squares.

Subtle indications of the mine ore bearing hillocks in the northern portion of the Conil mine rakes may be seen in the upper two grid squares of the area of interest box. Again, these correspond to the dolorite extrusions surrounded by clay and gypsum deposits.

7.4.2 Geology of the site

The Conil mine site is largely comprised of red clays, gypsum, sandstone and dolomite (Fig. 7-14). Within this overall composition are to be found extrusions of black table dolomite, so named for their shape. These extrusions form a series of small hillocks that dot the landscape, trending towards the northeast. Co-located within these hillocks are pockets of lead, galena and copper (Instituto Tecnologico Geominero de Espana, 1994).

The areas lying above the site along the Rio Conil, also known as the Rio Salado, are composites of alluvial deposition and various marls. The larger mine rakes are represented on the map by red and black parallel lines denoting mixed ores.

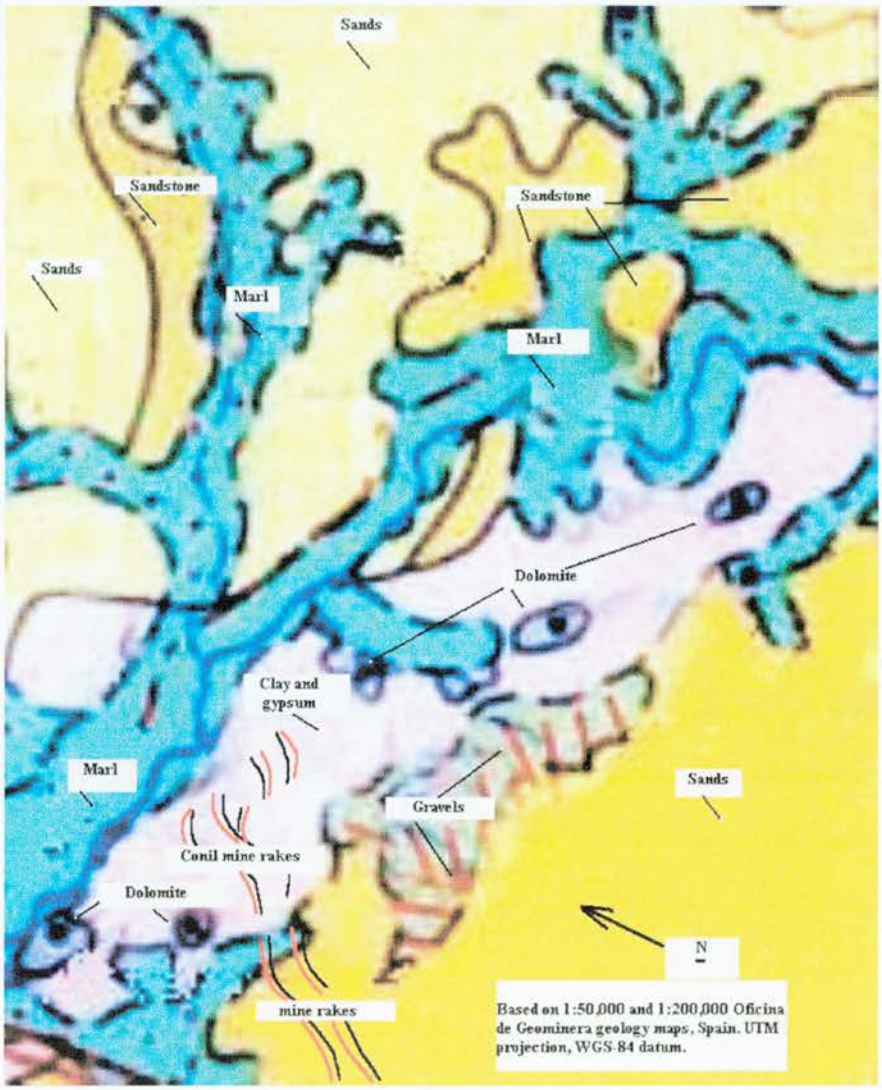

Figure 7-14 Conil mine rakes and surrounding geology.

7.4.3 Geomorphology

Conil is located approximately 3 kilometres due east of the Atlantic Ocean, and lies on the interface between two zones of geomorphology, marine and continental (See Fig. 7-4). The first, a marine geomorphology, has three categories, subsurface, pre-littoral and sub-tidal (Instituto Tecnologico Geominero de Espana 1994).

The subsurface littoral geomorphology extends from some 2 kilometres off-shore to the granite reefs of Trafalgar. The waters are constantly filled with fine silts and dissolve minerals as a result of scouring by the clashing currents.

The pre-littoral geomorphology begins about 2 kilometres offshore and extends inward to the sub-tidal zone, or areas that are exposed upon low tide. The geomorphology in the pre-littoral region is primarily an area of accumulation for sands and light gravels eroded from the outer reefs.

The sub-tidal zone is the area exposed by tidal action. This area displays the evidence of Quaternary marine terraces and ladder-like platforms of rock from tectonic activities (Instituto Tecnologico Geominero de Espana 1994)

The continental geomorphology zone, which begins at the Conil site, has two categories. The first is an aeolian geomorphology which has ancient longitudinal dunes, trending north and south, and immense ramp dunes, such as those at Los Canos de Meca with a height of 162 metres (Servicio Geografico del Ejercito, 2000).

The second type of continental geomorphology present in the area is fluvial. It can be seen in the geology map of the mine site that there is a mixture of sand deposits interspersed with alluvial deposition and marls (Fig. 7-14). This is a good example of hydrological erosion stripping away ancient aeolian deposition to reveal underlying geology as well as transported materials (Instituto Tecnologico Geominero de Espana 1994). The presence of Pleistocene and Holocene geologic materials may also be seen here as well (Junta de Andalucia, 2000).

A description of the vegetation populating the Conil mine site will now be presented before discussing the site history and archaeology.

7.4.4 Vegetation

The mine rakes at Conil have numerous small slagheaps associated with them, which are composed of loose soil and which may have polluted components. Therefore, few species of vegetation are successful in thriving within the site. However, on the southeastern periphery of the site, near the foot of the mountain named Cerro Patria, may be found an interesting sight, a large stand of *Juneripus phoenicea* or Phoenician juniper, known in Spain as Sabina, and noted in Chapter 6 at Serabit El Khadim.

Upon the slagheaps of Conil may be found a small bush, known locally as arrayan, or mirto. In English, this is a myrtle belonging to the *Myrtus communis* species. It may be found to be in dense colonies atop the slagheaps and hillocks bearing dolomite with other intrusive ores (See Fig. 7-15).

Fig. 7-15 Conil mine rakes: slag heap vegetation.

The remaining significant vegetation within the mine site is largely comprised of grasses such as *Argostis, Vulpia, Bromus and Hordeum.* Translated from the Spanish vernacular of the region in order, these are iron, fox, sheep and herd grasses (Clavero, 1997).

7.5 Site History and archaeology

7.5.1 Historical background

There is no historical provenance for this site. Archaeologists or archaeo-metallurgists had not previously investigated the site.

7.5.2 Site archaeology and survey

The site was visited for the first time on 12 May 2000 and was entered by utilising a gravel track that led from highway N-340. After 300 metres, another track leading northeast was followed for 150 metres before continuing on foot. Traversing a small cattle pasture of 100 metres in width, the first rake was found. After surmounting the highest of the slagheaps for a landscape view, it could be seen that the series of mine rakes and slagheaps trended towards the northeast horizon. Meanwhile, a view to the southwest indicated rakes that could be seen on the western side of N-340 extending a kilometre towards the sea (Fig. 7-4 and 7-16).

Immediately upon cresting a large flat hill that overlooked the entire site, large amounts of fragmented surface pottery and ceramics could be seen. Descending the hill towards the northern terminus of the Site "C" mine rake, gullies created by erosion revealed further indications of embedded pottery shards beneath the surface. At this point in time, the Casa Cultural de Barbate, located in Barbate, Spain, was consulted before retrieving any surface artefacts, as there was no license for archaeological investigation. It should be noted that the goal of remote sensing archaeology is to be non-intrusive and non-destructive.

On May 13, 2000 a collection of sample surface artefacts was retrieved from the hill overlooking Site "C", as well as from one of the gullies which had eroded into a mine rake. These artefacts were deposited with Dr. Antonio Aragon, Director of the Casa Cultural de Barbate for analysis. While collecting the artefacts from the gully, pieces of mine slag were also collected for metallurgical analysis by the Universidad de Cadiz.

The entire mine rake complex was walked on May 14, 2000 to observe its particular ground features, which are discussed in the following section.

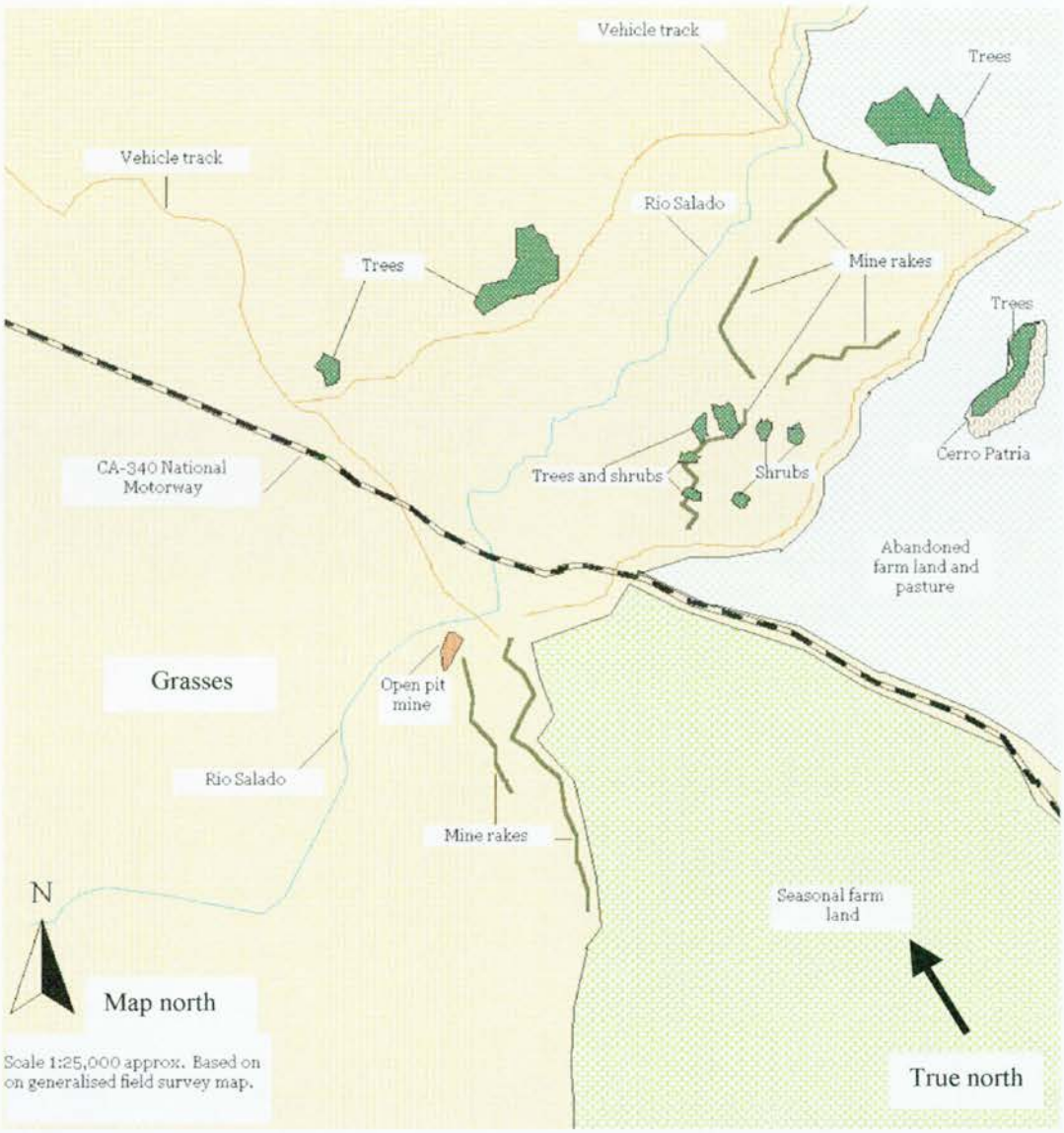

Fig. 7-16 Generalised survey map of Conil de Frontera mining complex

7.5.3 Ground features

Three features dominate the site, mine rakes of various lengths bisecting small hillocks, numerous small slagheaps and modern small pits, those currently being disused. The mine rakes tend to zigzag across the terrain. Following extrusions of mineral ores, the rakes seem to disappear after bisecting an ore bearing hillock and reaching level ground, only to reappear on another nearby hillock. This is the case for the lengthy mine rake targeted for analysis in this comparative study and dubbed Site "C".

The Site "C" mine rake begins 500 metres south of the Rio Salado, then zigzags across the landscape where its middle section is interrupted by the N-340 highway, then continues on its western shoulder (Fig. 7-4 and 7-16). The total length is 2 kilometres conservatively, excluding directional changes. The width of the rake varies from 5 metres in width to 3 metres in width, with depths ranging from 0.5 metres to 4 metres. At numerous points along the rakes, side galleries may also occur within the section analysed by the imaging RADAR data. These galleries may be as short as 1 metre in length, to as much as 3 metres, often appearing as short tunnels and appear to have been constructed to reach pockets of ore extending contrary to the primary direction of the rake. An example of a collapsed gallery may be seen in Fig. 7-16a.

Fig. 7-16a Collapsed side gallery, Site "C" mine rake.

The slag heaps range in height from 1-4 metres with one exceptional slagheap reaching 6 metres (See Fig. 7-15). The slag heap seen in Fig. 7-15 lies in the centre of the mine complex due east of the northern end of the Site "C" mine rake.

The small modern open pit mine may be the result of dolorite and galena extraction, which is used by a nearby road pavement factory. The owner was unavailable for query on this point of interest. At any rate, this small open pit mine fell within the target area image scene and was selected as a comparative site for the imaging RADAR analysis.

7.5.4 Archaeological assessment

The surface artefacts collected from the hill overlooking the northern end of the Site "C" mine rake were analysed and compared with a diagnostic collection held by Dr. Antonio Aragon of the Casa Cultural de Barbate, Spain, a branch of the Departmento de Arqueologia, Universidad de Cadiz. These artefacts were found to match Roman pottery from the 1st century BC and 1st century AD.

Pottery shards extracted from the gully at Site "C" were found to be of mixed provenance, being Punic and Tartessan. The Punic artefacts matched samples from the 4 and 5th century BC, while those of Tartessan origin appeared to fall within the 6th century BC (Aragon, 2000: communication).

The analysis of the metal slag retrieved from Site "C" and analysed by the Universidad de Cadiz metallurgical group revealed evidence of copper, lead and iron ore processing; further data from the site will be obtained during a detailed geo-chemical and geo-physical campaign during late 2001.

7.6 CORONA Satellite Imagery

7.6.1 CORONA Satellite image details

Satellite imagery from the CORONA program was obtained from the USGS GLIS Archive. The imagery was obtained on May 24, 1972 by a KH-2 series CORONA utilising a 70mm optical camera; estimated resolution was 3 metres (See Appendix 1). (Day *et al*, 1998).

7.6.1.1 CORONA Satellite imagery subset

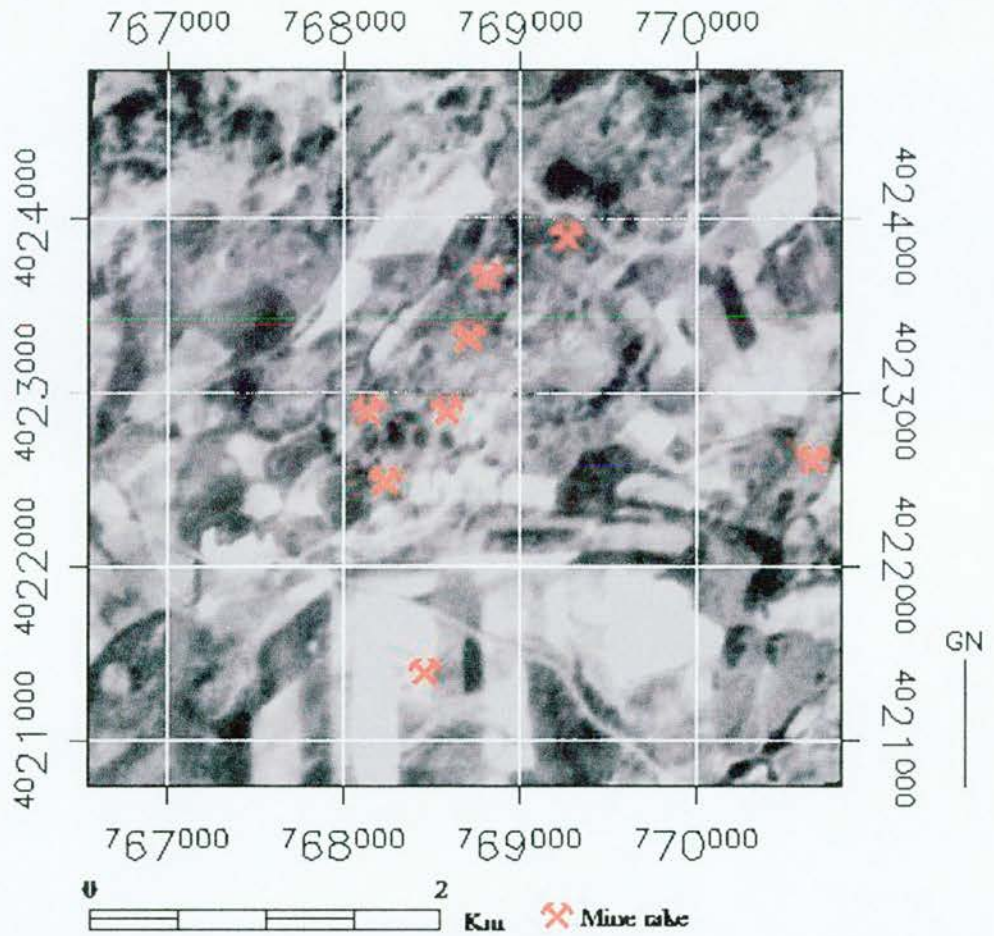

Fig. 7-17 CORONA image subset of Conil, Spain mine rakes, ~3m resolution.

There are two important features to the CORONA imagery of the Site "C" target scene area seen in Fig. 7-17. The first is that the dense colonies of myrtle atop several of the slagheaps may be detected in the centre of the image as dark areas next to the mine rake symbols. Furthermore, subtle indications of other mine rakes may be seen in the digital version of this image, although here in an analogue media it is difficult to observe.

The second feature of interest is the change in the landscape to the south, or right, of the mine rakes since 1972 when this image was collected; the present day landscape is one of dry pasture land or sunflower fields. The 1994 Shuttle imagery reveals a fairly unremarkable landscape, which can be seen in Fig. 7-19, by comparison.

7.7 AVHRR Satellite Imagery

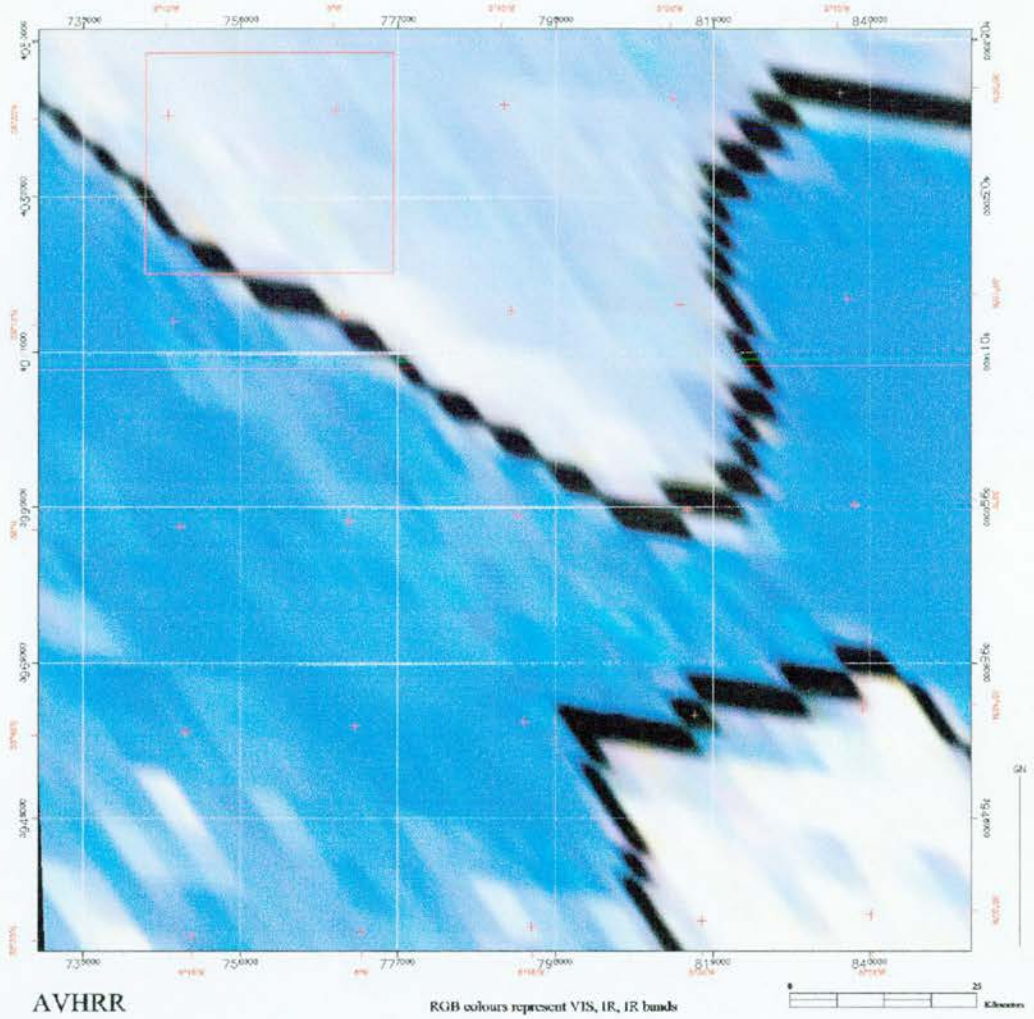

Fig. 7-18 AVHRR LAC image subset, Conil, Spain.

AVHRR Local Area Coverage (LAC) data for the orbital pass immediately preceding the overflight of the STS Endeavour SIR-C/X-SAR Imaging RADAR system on 1994 was obtained from the NOAA Satellite Active Archive for analysis. Resolution of this data is approximately for 1 kilometre in LAC mode, though the representation of this data in Fig. 7-18 is displayed in a much coarser manner. This coarseness is due to the use of digital cartographic software package to highlight the coastlines of Morocco (Africa) and Spain (Europe). A red box highlights the Conil area.

There was no cloud cover over the target scene area therefore Imaging RADAR performance would have had no degrading climatic conditions.

Calibration of the AVHRR data for brightness temperature was computed for bands 3,4 and 5 using algorithms developed for the NOAA-12 platform, and presented in degrees Kelvin (Table 7-1). It should be noted here that the data displayed here is from the NOAA-11 platform, therefore it is unknown as to the performance differences per the calibration algorithm.

NOAA 11 – Band 3	3.74 K
NOAA 11 – Band 4	10.82 K
NOAA 11 – Band 5	12.00 K

Table 7-1 Calibrated brightness temperatures, degrees Kelvin, NOAA-11, 1994.

In essence, any significant moisture within the region should be recorded and observed by the NOAA-11 sensor. However, just as with the region over Serabit El Khadim in the Sinai, very little atmospheric moisture can be observed, thus no major impedance to microwave performance can be observed.

7.8 Meteorological Data

7.8.1 U.S. Navy Meteorological Office Data

Meteorological data for the 72 hours immediately preceding the Shuttle Transport System overpass on October 3,1994, was provided by U.S. Navy Meteorological Command Detachment, Rota, Spain. Data from the Tarifa station, located some 35 kilometres due south on the Straits of Gibraltar, was the closest automated collection point. Co-ordinates for the collection station are 36.00 N by 5.36 W, with an elevation of 40 metres.

Temperature (degrees, Celsius)	22°
Rainfall (mm)	0
Wind direction (degrees, compass)	185°
Relative humidity (percent)	83
Wind speed (km)	43.2

Table 7-2 72 hour averaged weather data, Met Station, Rota, Spain.

The meteorological conditions for microwave sensor acquisition of terrain information in the Conil de la Frontera area, based on ground and satellite information, may be understood to be good.(Fung *et al.*, 1981). Both wind speed, soil moisture conditions and atmospheric moisture levels were optimal for microwave performance (Fung *et al.*, 1981).

7.9 NASA SIR-C/X-SAR Imaging RADAR Data and Analysis

7.9.1 The Imaging RADAR Data

The Imaging RADAR data for Conil, Spain were obtained on the 3rd of October 1994, during NASA STS (Shuttle Transport System) Mission SRL-2. Both C and L wavelengths used the horizontal send and receive polarisation (hh) mode as well as the vertical send and vertical receive mode polarisation (vv) mode in the Multi-Look Complex (MLC) product. The Cvv polarisation was operating at a 5.298 Ghz frequency while the Lvv polarisation was functioning at a 1.249 Ghz frequency. The orbital direction of the Space Shuttle was descending while the direction of the Imaging RADAR was right looking. The sensor platform heading at the image centre was 139.480° with an incidence angle of 24.158° for the MLC mode data. The centre latitude and longitude of the entire image scene was 36.18° N by -5.38° W at the same point. The nominal resolutions are 12.5 metres in range and azimuth for the for the MLC product. Actual pixel size and spacing of the digital product is 12.5 metres. The image scene was Ground Range corrected in initial data compilation.

7.9.2 Data Processing

Upon receiving the MLC data set and decompressing the data sets, the data were then synthesised via the ENVI 3.4 image processing software. First, for cartographic purposes, each data set was projected into the Universal Transverse Mercator coordinate system using the WGS-84 for *visual* presentation purposes. Data analysis was performed on *raw* uncorrected data (Chap. 3 and 4) Ground control points (GCPs) were obtained in the field at over 200 locations using a mean of 5 GPS positions taken over 8 minutes. This was done to ensure high precision due to the mountainous terrain of the region and the overlay problems inherent in RADAR imagery over such a region (USCNG, 2001 and Wysocki, 1991).

GCP averaged positions may be seen in Fig. 7-19 represented by red stars (See Appendix III for GCP information). Next, all phase difference analysis, filtering and test enhancements were performed on a raw data subset comprising an area surrounding the target mine site.

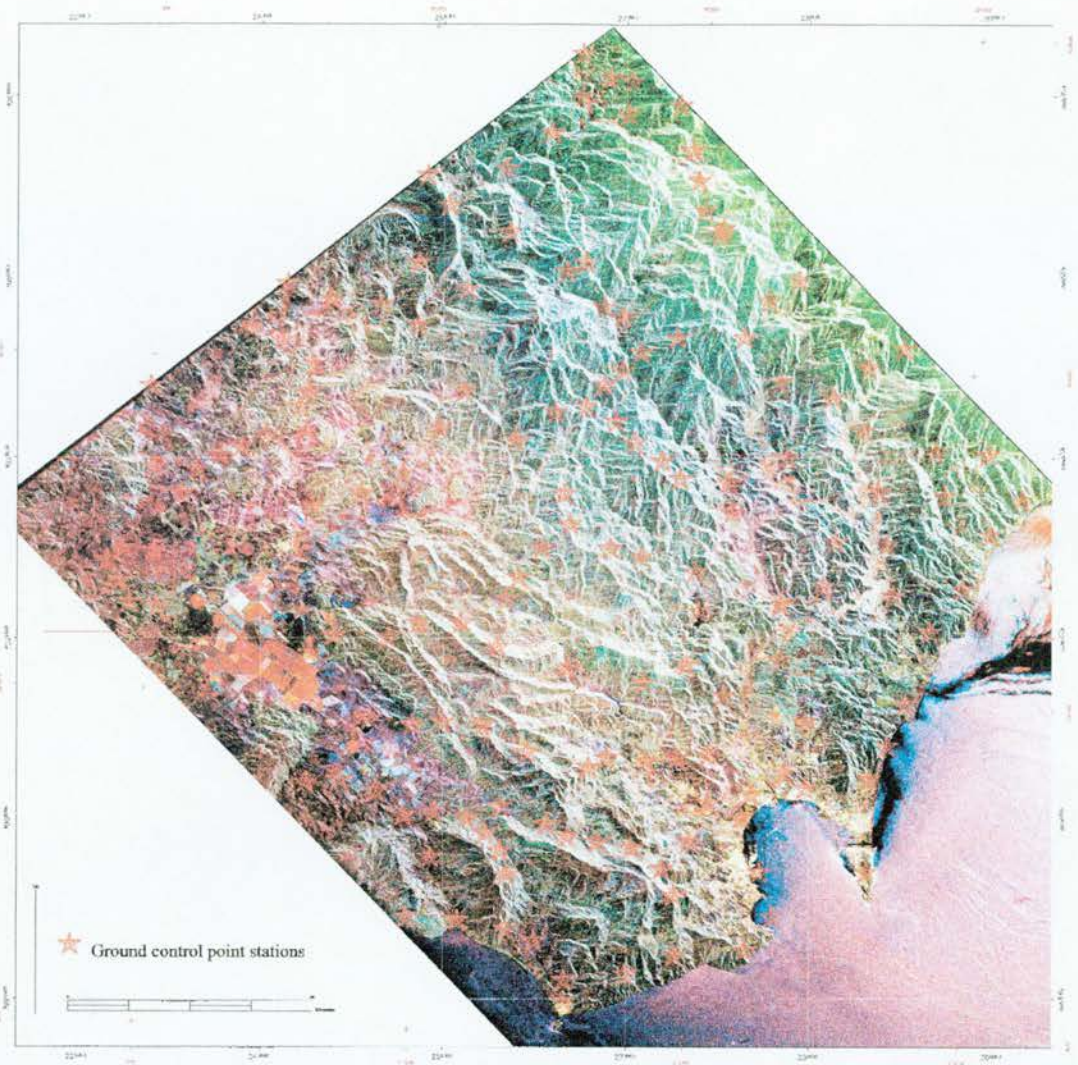

Fig. 7-19 The Conil mines region: Ground control point (GCP) sites superimposed on the NASA SIR-C/X-SAR RADAR data.

7.9.3 Imaging RADAR data analysis

A reference Imaging RADAR map of the Conil mine site is presented in Fig. 7-20 to facilitate interpretation of the following RADAR data sets.

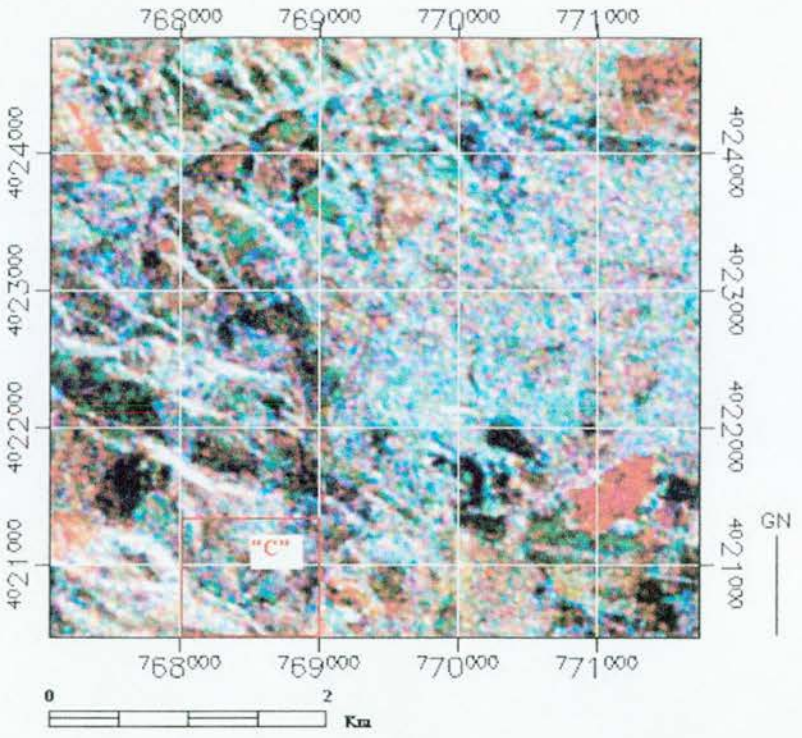

Fig. 7-20 The Conil mine site – Chh (R), Lhh (G) and Lvv (B) bands.

7.9.3.1 Analysis form and test site

Evaluation of the capability of NASA SIR-C/X-SAR Imaging RADAR to detect, survey and analyse the Conil mine site was, unlike Serabit El Khadim, a straightforward process and similar to South Ardachy. Still, as with the Site "A" and "B" targets, a portion of the mine site was transected in a linear fashion by analysing each pixel for 10 pixels, or approximately 125 metres. The transect was oriented north to south, beginning at pixel 125 x 366 and ending at pixel 125 x 375. This distance was chosen to span the mine from normal signal return surface to normal signal return surface for reference purposes. Both C and L bands were analysed for decibel response and phase difference.

The test area chosen was mine rake "C" as seen above in Fig. 7-20,outlined by a red box. The UTM Coordinate (WGS-84 datum) of the centre area of the mine rake is 402083 N by 768270 E and corresponds to pixel 125 by 371 in the data sets.

7.9.3.2 C band Imaging RADAR phase difference analysis: "C" mine, Conil

The image data set for the "C" mine target site at Conil measures 370 x 370 pixels, with each pixel encompassing 12.5 metres of earth terrain. The transect of decibel and phase difference analysis concerning the mine begins at pixel 125 by 366 and ends at 125 by 375. An overview image map of the raw Chh RADAR data is provided in Fig. 7-21 and a target illumination image map in Fig. 7-22. The direction of analysis is from the northernmost pixel to the southernmost pixel with 125 by 366 being the *northernmost* pixel; pixel 125 by 375 being the southernmost. Immediately following this map are the analysed pixels and their statistics in Tables 7-3. Finally, it should be noted that the image data subset is not centred around the target mine site as were South Ardachy and Serabit El Khadim because the western edge of the entire image scene fell within the boundaries of the 200 x 200 subset standard employed within the rest of this research work. Consequently, for purely visual and aesthetic purposes an image subset area was chosen which displayed only data; the same principle was used for the L band data.

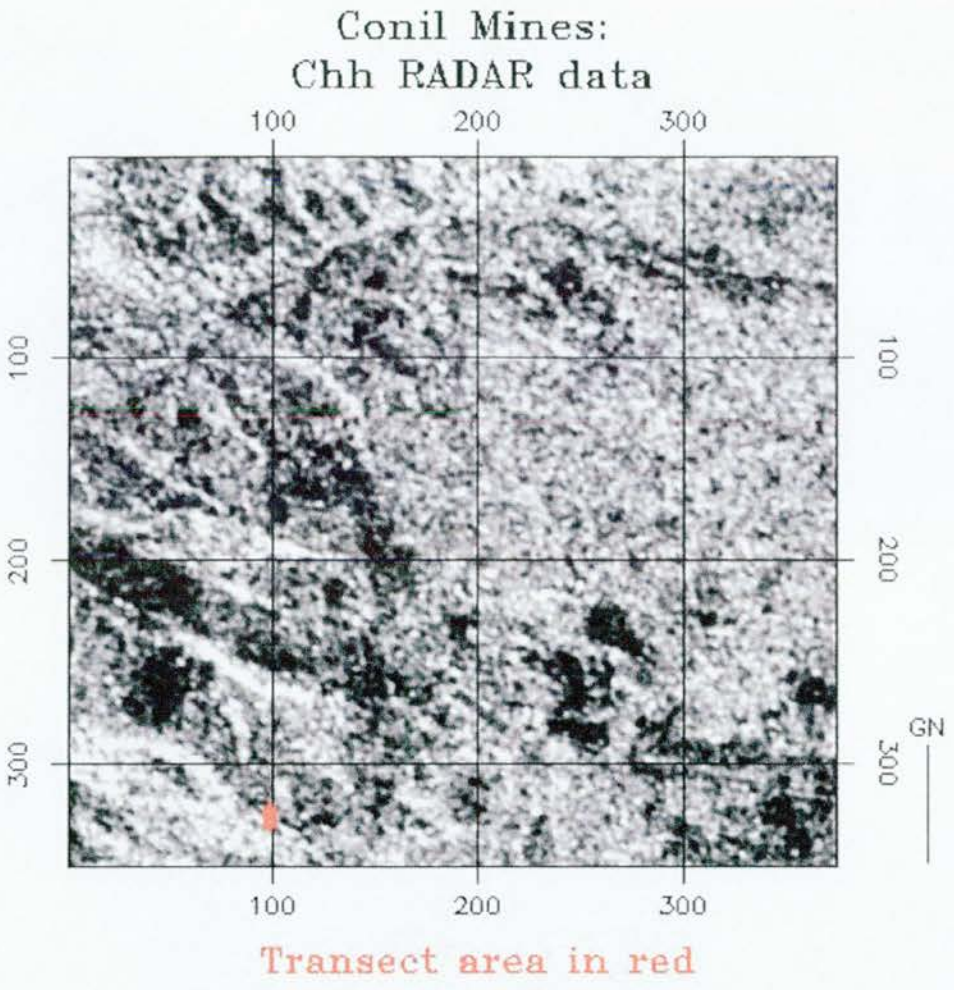

Fig. 7-21 Chh raw RADAR data image map: Conil "C" target mine rake.

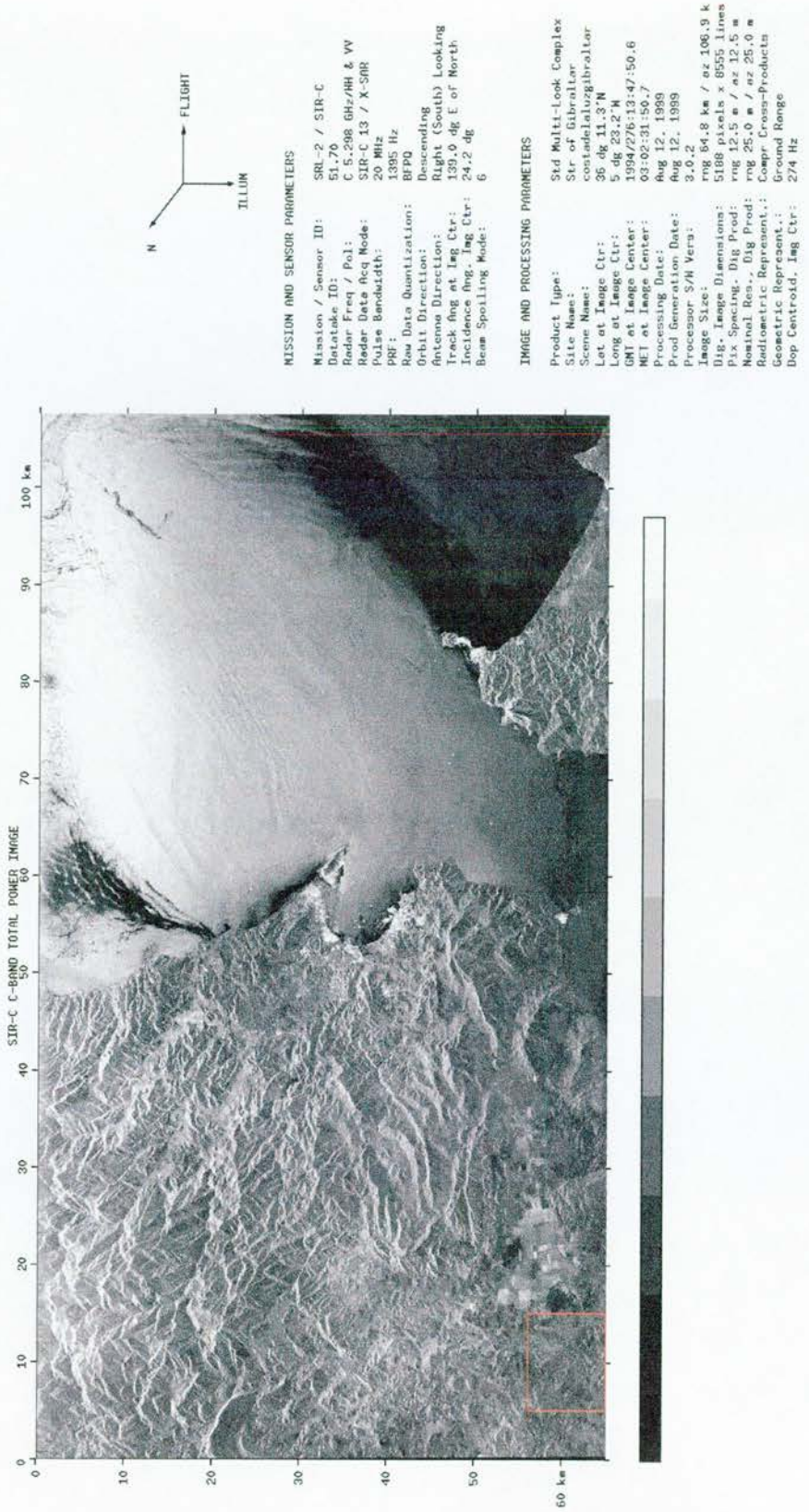

Fig. 7-22 C band, total power RADAR data image map: Conil "C" target mine area in red. Image and information created from CEOS software and header file.

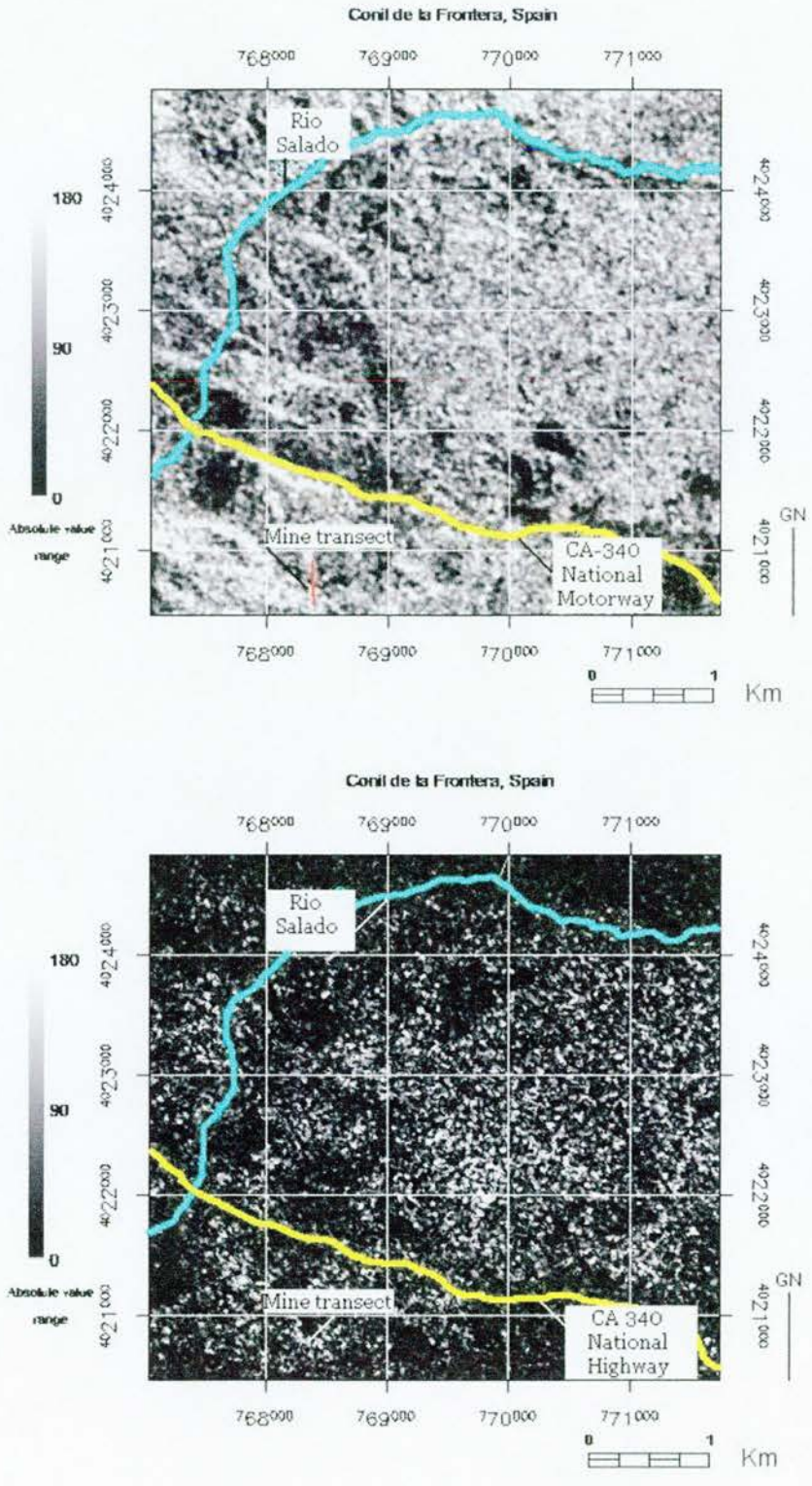

Fig. 7-23 Decibel image (above) and phase difference absolute value image (below) analysis for C band, pixels 125 x 366 to 125 x 370, Conil, Spain.

Pixel Co-ordinate	C/hh (dB)	C/vv (dB)	Phase difference
125x366	-12.25	-4.95	-86.08°
125x367	-9.72	-5.50	-64.80°
125x368	-9.24	-5.68	-53.76°
125x369	-9.47	-4.26	-61.45°
125x370	-9.65	-4.24	-71.75°
125x371	-8.83	-3.52	-40.37°
125x372	-9.71	-3.13	-7.84°
125x373	-12.25	-4.95	-19.37°
125x374	-12.70	-4.72	-14.71°
125x375	-11.60	-3.48	-26.48°

Table 7-3 Mine site transect, Conil, Spain, C band decibel and phase difference statistics.

Pixel 125 x 372 displays similar C-band phase difference statistics to those observed at the South Ardachy site on Islay. Interestingly, the phase difference absolute value image in Fig. 7-23, which maps the magnitude of change in phase difference to a grey-scale colour mapping schema ranging from 0 to 180, appears to portray a series of high magnitude values trending south-east to north-west across the transect. Due to the large number of abandoned mine rakes and their concordant vegetation, this may be a combination of both reflecting surfaces functioning together in some unique fashion. Still, the decibel responses recorded along the entire transect are different than those on Islay. This is likely due to the fact that the Ardachy transect occurred over a terrain which had no vegetation coverage except short grasses, unlike Conil, which has the waxy leafed myrtle bushes obscuring the mine rakes. These *arrayan* leaves are fairly dense and may be sufficiently oriented to be the cause of a stronger vv response decibel response.

7.9.3.3 L band Imaging RADAR analysis: "C" mine, Conil

The image data set for the "C" mine target site at Conil measures 370 x 370 pixels, with each pixel encompassing 12.5 metres of earth terrain. The transect of decibel and phase difference analysis concerning the mine begins at pixel 125 by 366 and ends at 125 by 375. An overview image map of the raw Lhh RADAR data is provided in Fig. 7-24 with a target illumination map in Fig. 7-25. The direction of analysis is from the northernmost pixel to the southernmost pixel. Again, pixel 125 by 366 is the northernmost pixel within the transect with 125 by 375 being the southernmost. Immediately following this map are the pixels analysed for their phase difference qualities and their decibel response statistics in Fig. 7-26 and Table 7-4.

Finally, it is important to note that the data subsets were analysed in their *raw*, un-projected and unregistered forms, thus noted cartographic scales are *approximate* and are referenced to the final warped image product (Chap. 3 and 4).

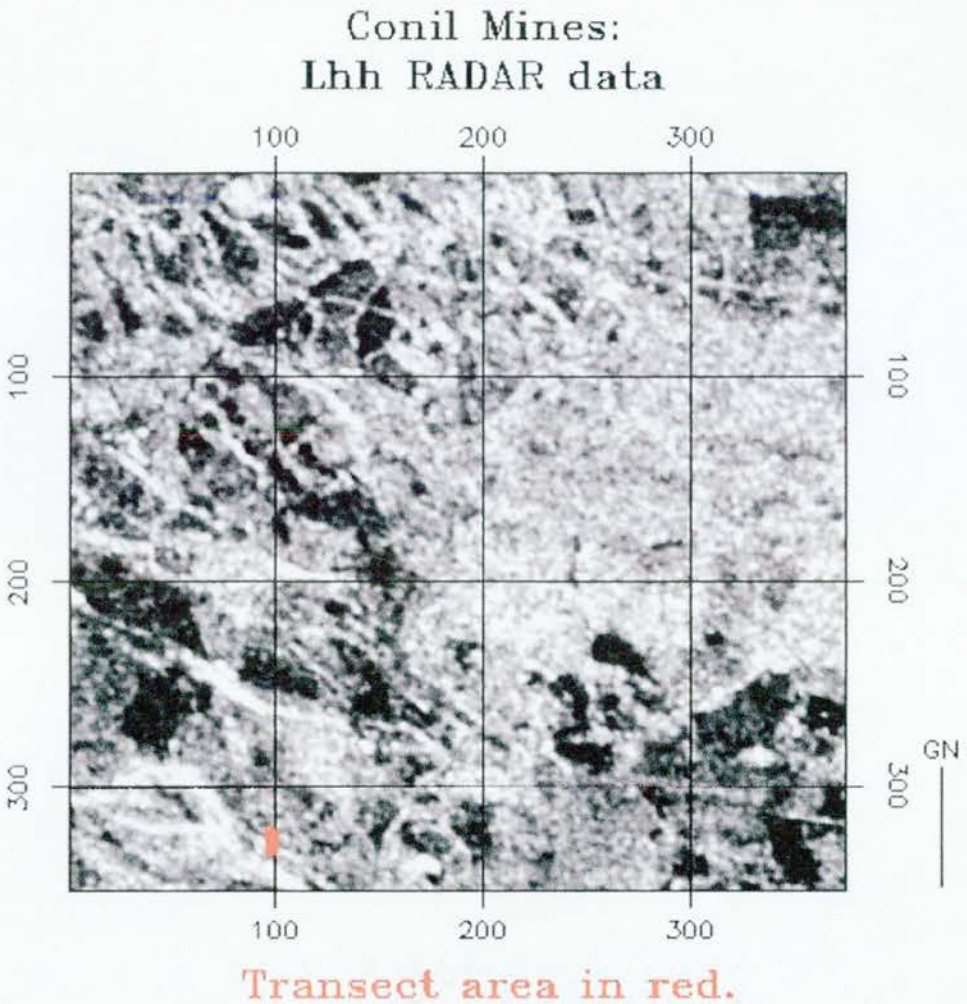

Fig. 7-24 Lhh raw RADAR data image map: Conil "C" target mine shaft. Scale is 1:22,784 approximately.

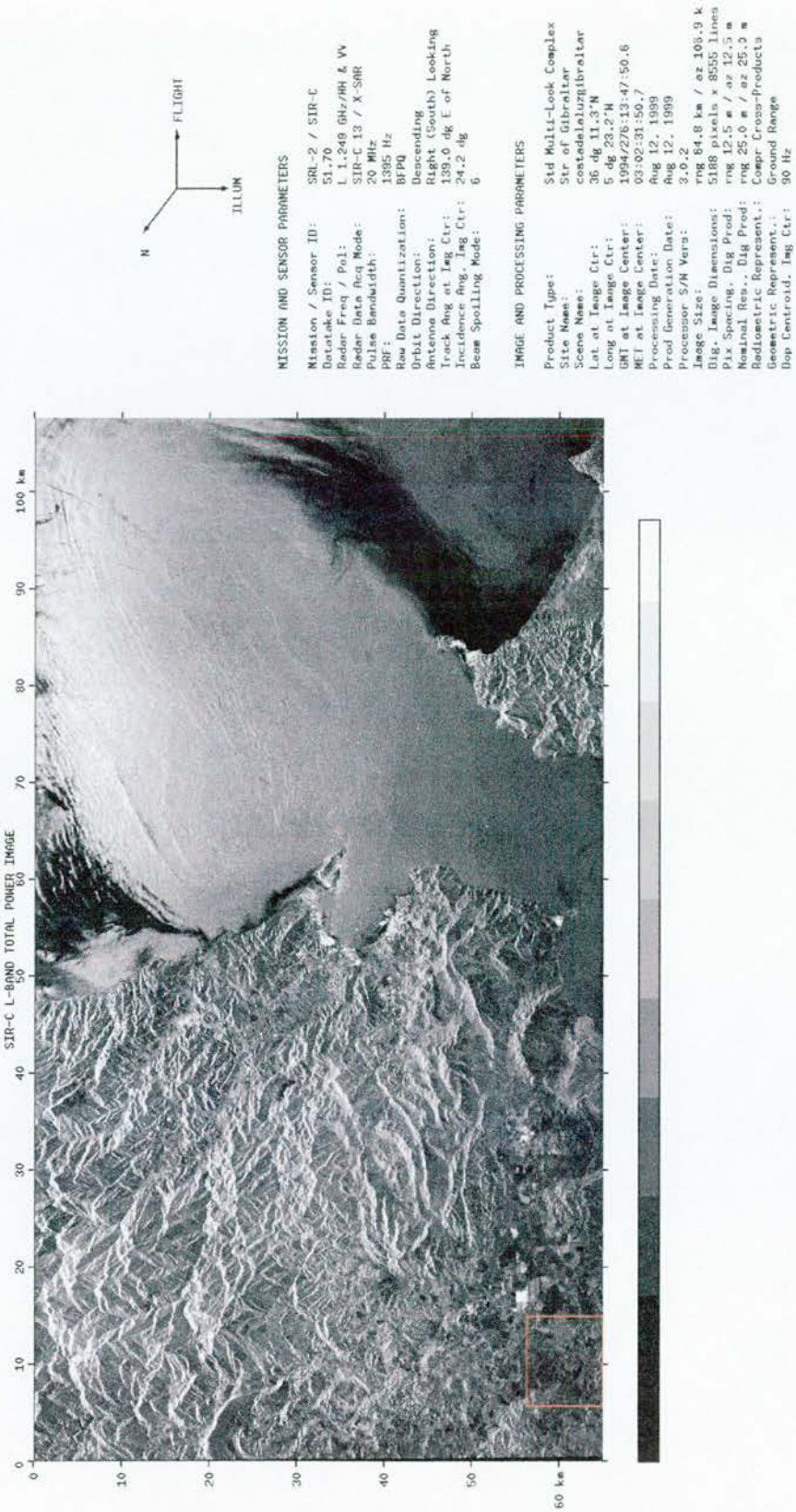

Fig. 7-25 L band, total power RADAR data image map: Conil "C" target mine area. Image and information created from CEOS software and header file, NASA/JPL. Decibel strength bar to right with data displayed at approximately 1:250,000.

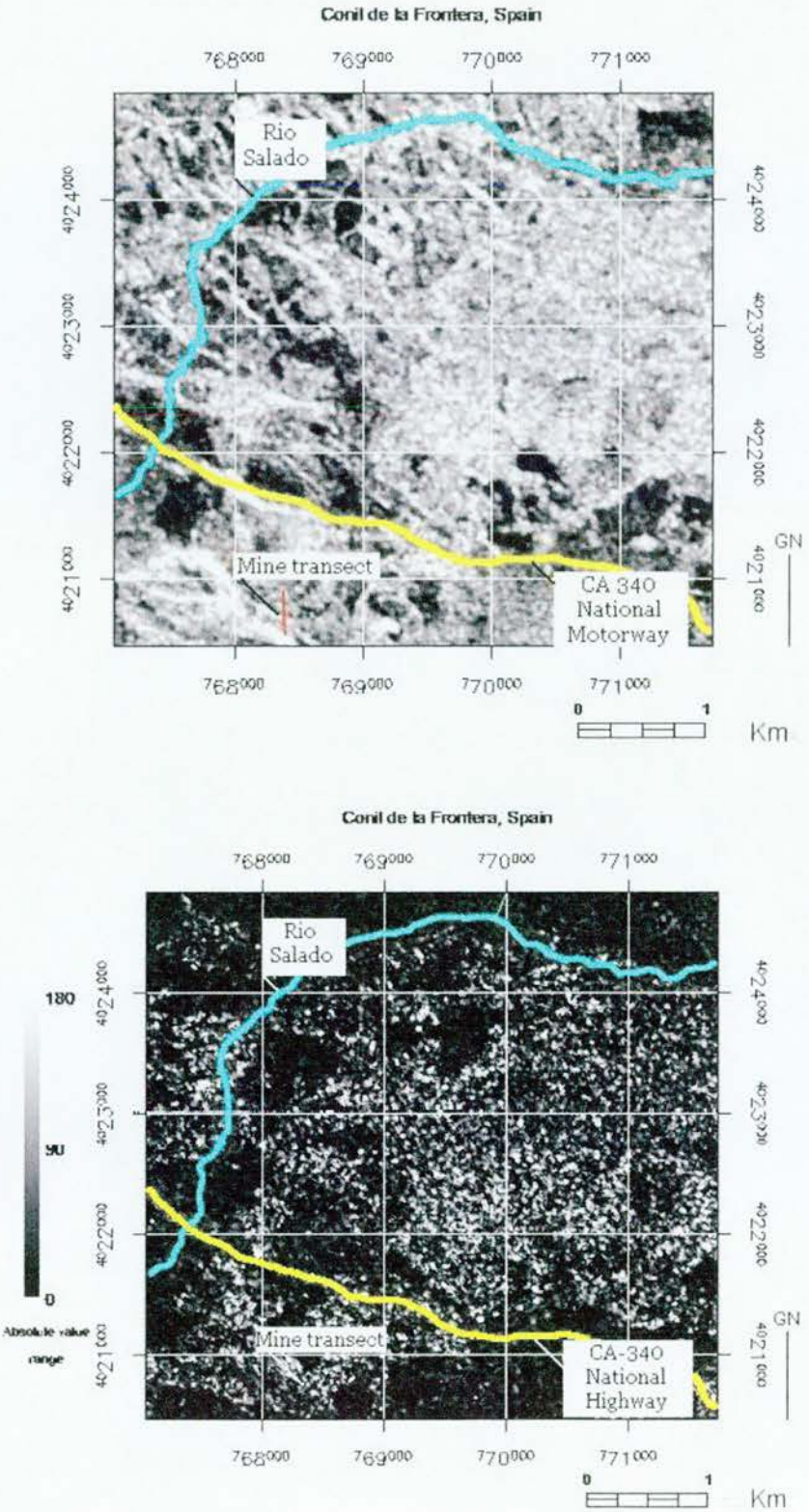

Fig. 7-26 Decibel image (above) and phase difference absolute value image (below) analysis of L band, pixels 125 by 366 to 370, Conil, Spain.

Pixel Co-ordinate	L/hh	L/vv	Phase difference
125x366	-10.88	-11.46	46.22°
125x367	-11.43	-12.28	-26.82°
125x368	-12.43	-13.21	-76.17°
125x369	-13.40	-15.02	-95.09°
125x370	-13.49	-15.11	-21.58°
125x371	-13.27	-14.27	19.37°
125x372	-14.49	-15.20	5.42°
125x373	-15.65	-16.57	-25.46°
125x374	-11.29	-14.53	-18.52°
125x375	-6.59	-8.78	-8.43°

Table 7-4 Mine site transect, Conil, Spain, L band decibel and phase difference statistics.

The L band polarimetric phase difference response of the Conil mine rake sample pixel is remarkably similar to that of the Ardachy, Islay site, displaying a difference of 5.42 (Conil) versus a 6.11 (Ardachy). The phase difference absolute value image in Fig. 7-26 (red arrow) depicts a value closer to the 180 end of the colour mapping schema employed by the software (ENVI, 2001). The terrain at Conil can be considered to be rough in microwave nomenclature (Chap. 3 and 4) with shrubs, boulders and other rocks present. It should be pointed out that in both the C and L band phase difference absolute value images, numerous points may be observed throughout the region of interest which have been mapped as having high polarimetric phase difference magnitude. As just stated when considering the terrain within the region of interest surrounding the Conil mine complex, there are numerous jagged and exposed rock outcrops, mine slag heaps and densely leafed shrubs.

The decibel responses at the Conil sample pixel for the L band phases are almost equal with the hh mode recording a -14.49 dB response versus the vv mode at -15.20. It is unknown what may be influencing the transmitted L band microwaves over the mine site. This will be further discussed in the comparative analysis section of this chapter.

7.9.3.3.1 Comparative Transect

A nearby area of the Conil mine complex was chosen to compare the capability of the multipolarimetric Imaging RADAR system. Referring back to Fig. 7-20, of the mine site, a transect was chosen which bisected the area northeast of the mine in the area in a north-south fashion. The same transect parameters are used, with each pixel encompassing 12.5 metres of earth terrain, for approximately 125 metres total. The comparative transect of decibel and phase difference analysis begins at pixel 225 by 266 and ends at 225 by 375. An overview image map of both the comparative transect and the mine site transect is provided in Fig. 7-27. The direction of analysis is from the northernmost pixel to the southernmost pixel. Again, pixel 225 by 266 is the northernmost pixel within the transect with 225 by 375 being the southernmost. Immediately following this map are the pixels analysed for their phase difference qualities and decibel response statistics with the C band data presented first, followed by the L band data.

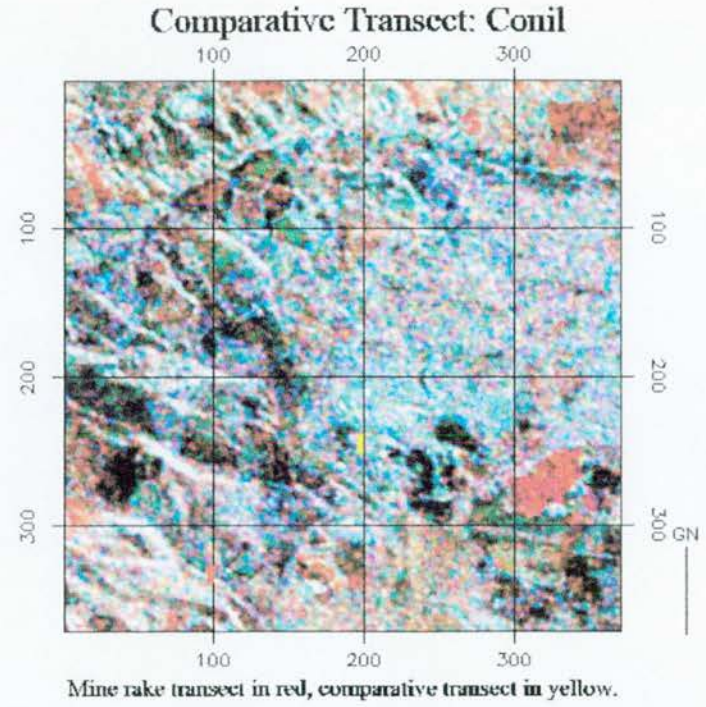

Fig. 7-27 Comparative transect, near Conil mine complex, top, image of transect area terrain, bottom. View from southwest to northeast with the hill of Cerro Cantabria in the distance.

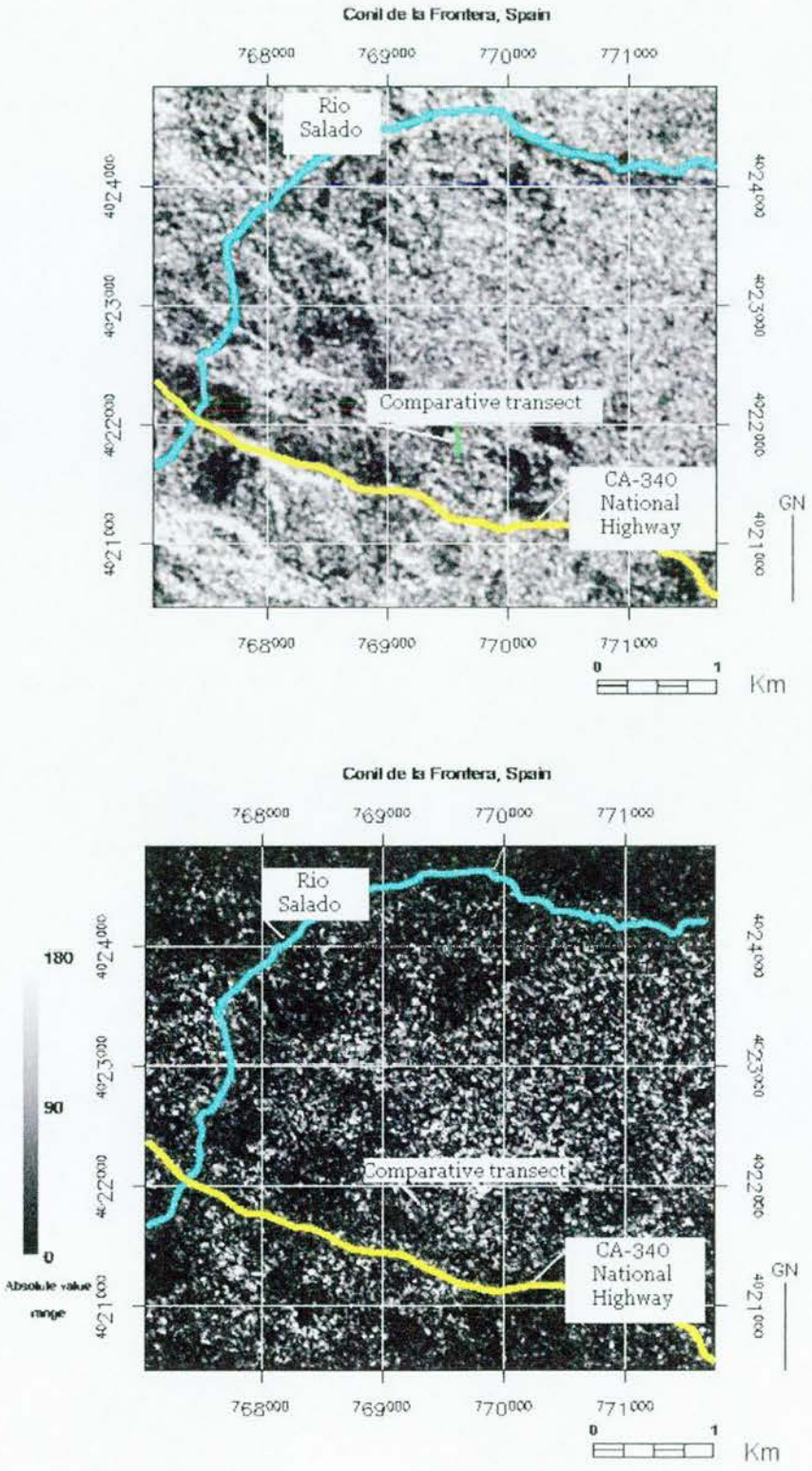

Fig. 7-28 Decibel image (above) and phase difference absolute value image (below) (C band, comparative transect), Conil, pixels 225 x 266 to 270.

Pixel Co-ordinate	Chh	Cvv	Phase difference
225x266	-6.38	-5.18	-155.58°
225x267	-6.32	-4.34	149.60°
225x268	-6.14	-3.66	55.89°
225x269	-7.38	-3.41	10.22°
225x270	-8.73	-3.02	50.92°
225x271	-9.61	-3.03	75.68°
225x272	-8.14	-4.17	66.59°
225x273	-6.50	-3.41	-65.66°
225x274	-7.06	-3.09	-84.47°
225x275	-7.03	-4.40	-11.9°

Table 7-5 Comparative transect, Conil, Spain, C band decibel and phase difference statistics.

The C-band polarimetric phase difference statistics and decibel responses for pixel 225 x 270 are not similar to those recorded over the mine rake pixel at 125 x 372, thus showing a different surface topography being illuminated by the microwaves. The C-band comparative transect in general shows lower decibel responses, though with several interesting phase difference statistics at pixels 225 x 273 through 225 x 275. By observing the phase difference absolute value image in Fig. 7-28 (red arrow) the magnitude of phase difference change may be observed along and around the transect area. As previously mentioned, the numerous and disparate high value phase difference points may be due to the occurrence of field clearance cairns composed of small stones beneath the overall vegetation canopy composed of slender, un-oriented wild flowers and exposed rock outcrops.

The L- band polarimetric phase difference statistics and decibel responses are discussed on the following page in order that they may be considered in correlation with the polarimetric phase difference absolute value image.

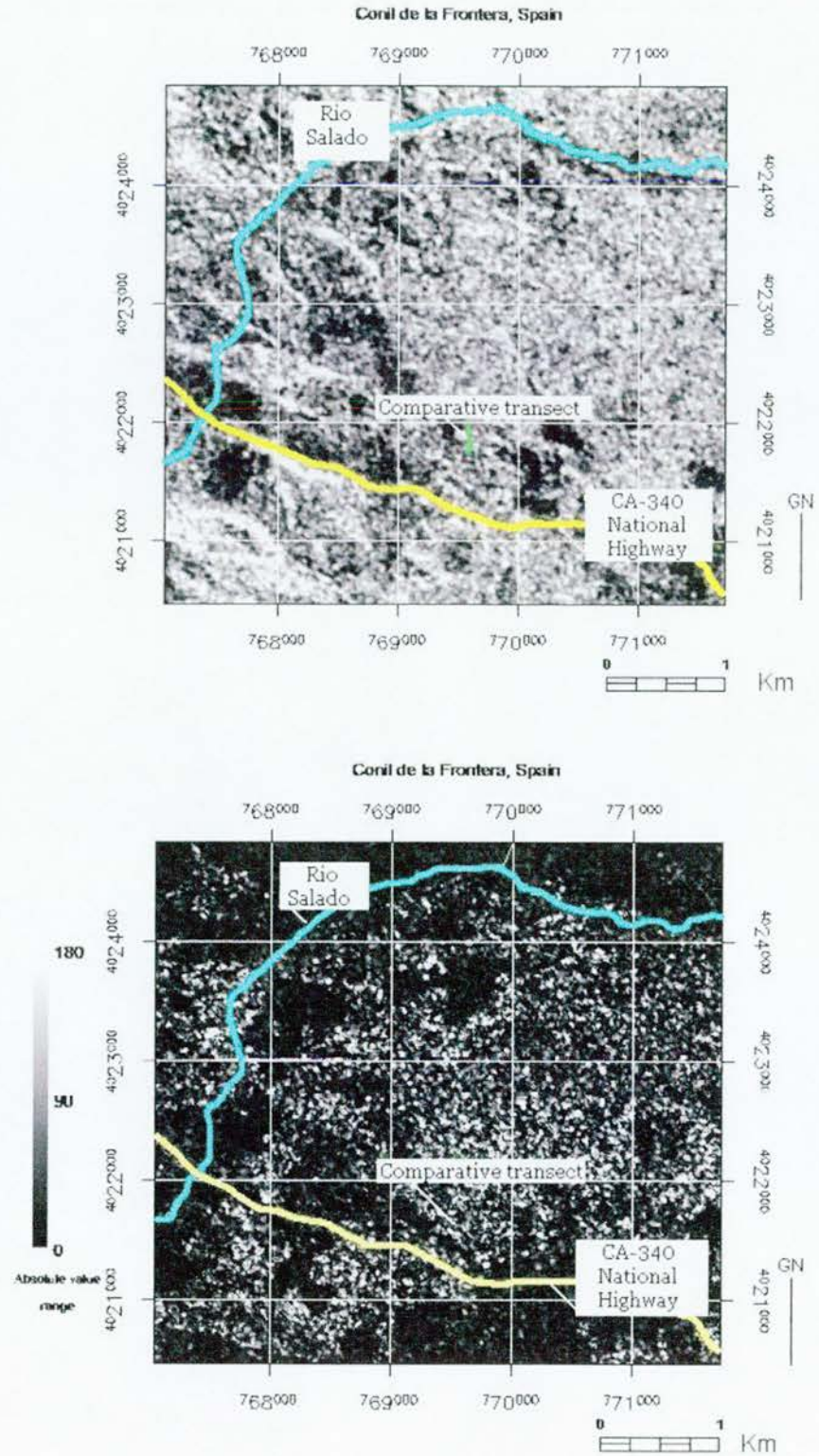

Fig. 7-29 Decibel image (above) and phase difference absolute value image analysis (below), (L band, comparative transect), Conil, pixels 225 x 266 to 270.

Pixel Co-ordinate	L/hh	L/vv	Phase difference
225x266	-6.68	-9.69	-43.19°
225x267	-4.85	-9.07	-62.41°
225x268	-3.97	-11.20	-81.62°
225x269	-4.98	-11.56	-36.15°
225x270	-7.20	-11.53	7.44°
225x271	-9.93	-13.22	-2.74°
225x272	-11.00	-13.12	-14.74°
225x273	-7.54	-9.73	8.67°
225x274	-4.37	-8.01	41.22°
225x275	-4.60	-9.91	45.77°

Table 7-6 Comparative transect, Conil, Spain, L band phase difference and decibel statistics.

L-band polarimetric phase difference statistics and decibel responses, reveal that hh mode decibel responses along the comparative transect are generally stronger than those over the mine rake transect. Conversely, the vv mode decibel responses along the comparative transect are lower in general than those recorded along the mine rake transect. It is possible that the longer wavelength Lhh band was able to peer beneath the loosely oriented wild flowers that have little or no leaf structure to impede microwaves striking the ground surface.

The L-band polarimetric phase difference recorded at the middle of the comparative transect (225 x 270) was 7.44, which, though being similar to that recorded at Ardachy, Islay and the mine rake at Conil, did not have a concordant equal decibel response in both hh and vv modes. The polarimetric phase difference absolute value image in Fig. 7-29 reflects essentially the same scenario presented by the C band, that is numerous points with high magnitudes of phase difference change caused by rock outcrops or vegetation clusters. Thus, it is unlikely that a corner reflector had been detected at pixel 225 x 270, as a dihedral would most likely produce similar decibel responses in both the hh and vv modes (Fung *et al.*, 1981). If the entire comparative transect is viewed in this light, then it can be seen that at no point is there a closely similar decibel response in both phase orientations.

7.9.3.4 Comparative analysis of the Conil mine rake site RADAR data

Pixels 125 x 366 through 373 are the pixels which coincide with the location of the primary mine rake at Site "C" in the Conil mines complex (See Fig. 7-19). It bears noting here that the Site "C" target mine is located in the portion of the Conil mine rakes located *southwest* of the N-340 coastal highway. The orientation directions within this section refer only to this portion of the rakes and should not be confused with the overall site. Finally, unlike Ardachy and Serabit El Khadim, the length and orientation of the target rake have presented several unique returns. However, only pixel 125 x 372 will be observed here in order to standardise the final comparative analysis with Ardachy and Serabit El Khadim in Chapter 8. A photo of the target mine rake may be seen in Fig. 7-30 while the C and L band phase difference with accompanying decibel responses is reported in Tables 7-7 through 7-9 for comparison.

Fig. 7-30 Mine rake of pixel 125 x 372 , Site "C", Conil mine rakes.

The dimensions of the entire Site "C" mine rake in Fig. 7-31 range from 3.5 metres in the southern terminus, to 9.8 metres in the middle, and finally, 4 metres at its northern terminus. It is approximately 2.5 metres deep at the south end, 3 metres deep in the middle section, rising to 2.5 metres at its northern end. Referring back to Fig. 7-4, it can be seen that the mine rake essentially cuts through low hills, following the surface vein of ores, thus accounting for its zigzag traverse across the terrain (See Fig. 7-31).

The dimensions of the mine rake within the coverage of pixel 125 x 372 are as follows: 4 metres in width, 2.5 metres in depth at centre, with a continuous length extending to the northeast and southeast for some 2 kilometres. The length was computed at 12.8 metres for the purposes of this study, based on deviation from the surface level.

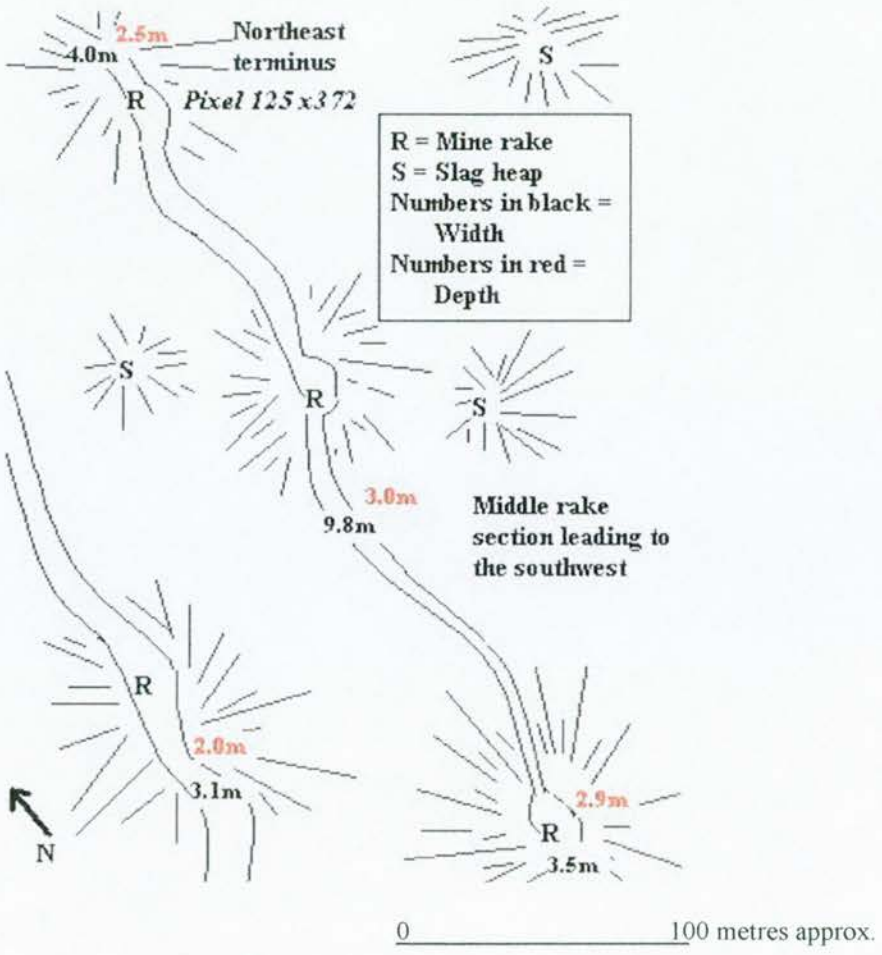

Fig. 7-31 A general map of the Site "C" target mine; pixel 125 x 372, Site "C", Conil.

Pixel Co-ordinate / Band	hh	vv	Phase difference
C band, 125x372	-9.71	-3.13	-7.84°
L band, 125x372	-14.49	-15.20	5.42°

Table 7-7 Pixel 125 x 372: Conil mine rake

A comparative pixel from the small, open pit mine, northwest of Site "C", coincides with pixel 89 x 308, seen below in Fig. 7-37. The C band and L band phase difference may be seen in Fig. 7-32, with statistics in Table 7-8. The area covered by the mine, is 15.219 hectares and covers a distance of 2.411 kilometres as measured by GPS; it is composed of sandstone. The maximum depth of the mine is 8 metres on the northwestern edge of the pit.

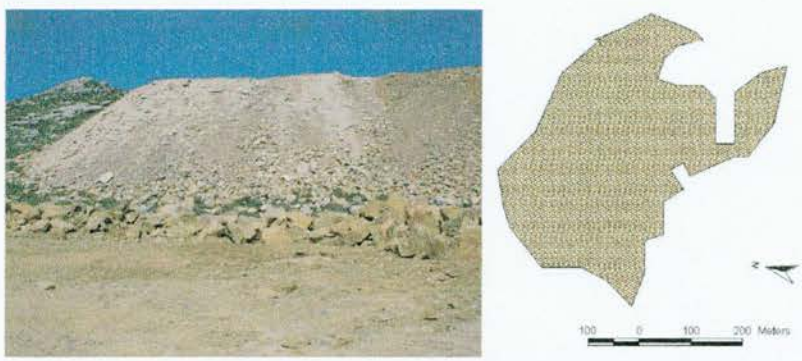

Fig. 7-32 Pixel 89 x 308; Comparative open pit mine photograph and map of mine.

Pixel Co-ordinate / Band	hh	vv	Phase difference
C band, 89x308	-2.8	-1.7	-5.38°
L band, 89x308	-1.1	-6.6	14.42°

Table 7-8 Pixel 89 x 308, C band phase difference and decibel responses on top, L band beneath; small open pit mine.

A sample pixel from the mid-section of the comparative transect as well as an image of area terrain is given below in Figures 7-33 and 7-34 with Table 7-9.

Fig. 7-33 Comparative transect area, view from southwest to northeast with hill of Cerro Cantabria in distance.

Pixel Co-ordinate / Band	hh	vv	Phase difference
C band, 225x270	-8.73	-3.02	50.92°
L band, 225x270	-7.20	-11.53	7.44°

Table 7-9 Pixel 225 x 270, Comparative transect, C and L band phase difference with decibel responses.

Dealing first with the Conil Site "C" target mine rake, located at pixel 125 x 372, it can be seen that both the C and L band phase difference statistics have similarities to those recorded at the South Ardachy Site "A" target mine (Chap. 5). The polarimetric phase difference absolute value image in Fig. 7-23 (red arrow) displayed the magnitude of change in these values and a value veering towards the upper of the grey scale mapping schema employed by the software (ENVI, 2001) Conversely, there are also differences between the two sites when decibel response is studied. At Conil, the vv polarisation of the C band decibel response is significantly stronger than that of the horizontal. It is likely that this is due to the arrayan, or myrtle bushes, and tall slender grasses covering the mine rake's peak; South Ardachy had no such vegetation cover (Chap. 5). The size of the arrayan leaves is approximately the size of the C band wavelength (5.8 cm) while the density and texture of the leaves is substantial; the orientation of the leaves is indiscriminate. The decibel responses noted in hh and vv polarisations of the C band correspond with known values for this type of surface material and vegetation cover (Ulaby and Dobson, 1989).

The L band decibel response over the Conil mine rake is remarkably similar in the vv polarisation to that of the hh mode at -14.49 dB and -15.20 dB respectively. As with the C band, a polarimetric phase difference absolute value image was produced to depict the magnitude of phase difference change along the mine transect and throughout the surrounding area. This performance of the L band was very close to that recorded at South Ardachy where hh mode in the L band saw a -15.26 dB response while the vv polarisation mode recorded a -13.99 dB response. It should be remarked that due to a particularly disturbed target area and again, the registration of image data versus actual ground range placement of the obtained RADAR data, the decibel and phase difference responses could be slightly displaced; this is an inherent problem with RADAR data analysis.

Returning to the polarimetric phase difference analysis of the mine rake, the C band at Conil shows a -7.84° phase difference versus a -6.99° at South Ardachy. The L band phase difference report at Conil notes 5.42° phase difference in comparison to a 6.11° recorded at South Ardachy. The terrain of the Conil site should be considered rough as there are intermittent shrubs, field-clearance boulders and naturally placed rocks (Chap. 3). These factors will have affected the microwave interaction with the surface, and of course the resulting recorded backscatter responses. This makes the possibility of determining whether or not the mine rake was perceived by the L band of the Imaging RADAR system as a dihedral or some other type of corner reflector difficult since it is not a perfect corner reflector.

However, the Shuttle Imaging RADAR system was shown to have the capability to topographically map the earth's surface and referring back to Chapter 3, naturally occurring corner reflectors are extremely rare and are usually man-made. In an archaeological context this is important as it means the sensor has the capacity to survey a large topographic area and potentially identify unknown man-made corner reflectors; this will be discussed further in Chapter 9.

Addressing the sample taken from a nearby modern open pit mine, the phase difference signatures and decibel responses have marked differences. Succinctly outlined the open pit mine exhibits very strong decibel responses in both RADAR bands and polarisation modes while the phase difference is lower in the L frequency. The C-band polarimetric phase difference, however, has decibel responses that are near equal in both phases, though it is impossible to categorise the pit edge as any particular type of corner reflector.

These distinct differences might be attributed to two characteristics. First, the geology of the mine is largely composed of sandstone interspersed with areas of conglomerate material, and second, vegetation is non-existent (See Fig. 32). C band decibel responses are likely a product of the numerous small pieces of rock, both natural and quarried, which litter the site. The C band polarimetric phase difference is only slightly less than that recorded at the South Ardachy and Conil mine rake, yet the decibel response is markedly different; at the open pit mine there is minimal difference between the hh and vv polarisation responses. This mimics the L band performance at both mine rakes, but it is hard to know if the C band perceives the mine pit edge as a corner reflector. L band decibel response may be the result of the hard-packed mine floor and sloping mine pit edge.

Secondly, the sample pixel extracted from the mid-section of the comparative transect reveals no similarity in decibel response or phase difference response to the Site "C" mine rake (See Fig. 7-39 and 7-40). It is interesting to note the strong vertical response in the C band, which would appear to be more consistent with vegetation containing larger scattering surfaces and oriented in an orderly fashion; this may be the result of different agriculture in 1994 as crop rotation from fallow field to soybean was evident in area farms during the year 2000 surveys. There was also evidence of intermittent clearance cairns, or rock piles, from field cleaning efforts. Some of these piles reached 1 to 2 metres in height with stones ranging from 0.5 metres in length to 1 metre with irregular widths. The current owner of the farm was unavailable for query on the point of field clearance efforts and other possible changes in field conditions.

The similarity of the C and L band phase difference responses to the Site "C" target mine rake at Conil is intriguing, though it is impossible to determine if it is functioning as some form of corner reflector due to sensor resolution (See Fig. 7-34). Again, since the target is not a perfectly formed reflector in the RADAR science sense and due to other incipient influences on the recorded backscatter, such as vegetation and surface roughness, absolute reflector identification is difficult to determine.

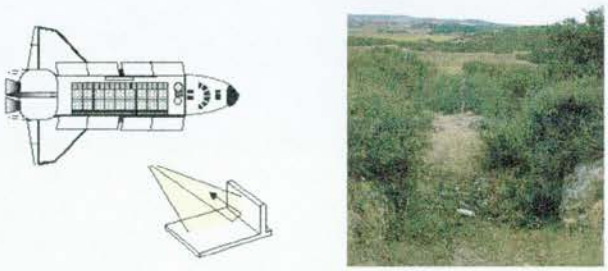

Fig. 7-34 Shuttle Imaging RADAR illumination of a theoretical dihedral reflector similar in shape to the Site "C" mine rake, Conil, Spain, seen on the right.

Finally, as an additional aid to visualising the performance of the NASA SIR-C/X-SAR sensor over all the transects discussed in this chapter, Figures 7-35a and b present comparative line charts of RADAR decibel and polarimetric phase difference performance. Pixel 1 in each chart should be understood to be the *southernmost* pixel in each transect, while Pixel 10 represents the *northernmost* pixel.

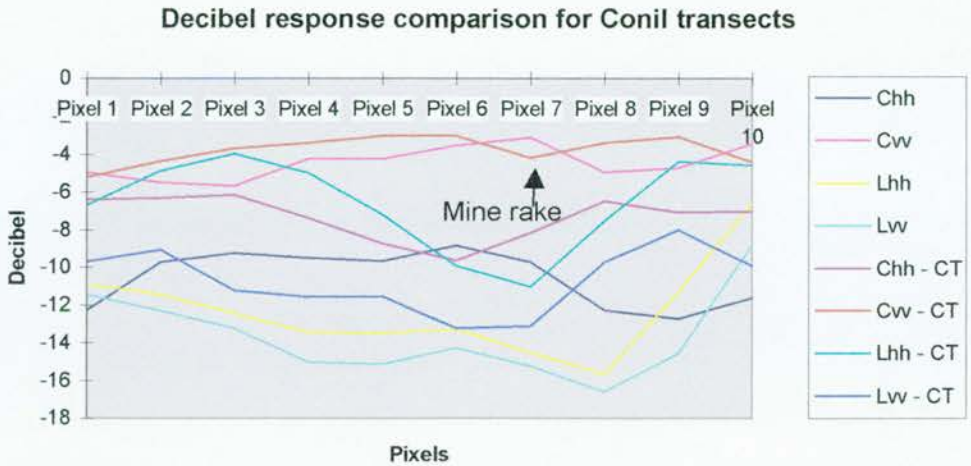

Fig. 7-35a Decibel responses for Conil de la Frontera mine and comparative transects.

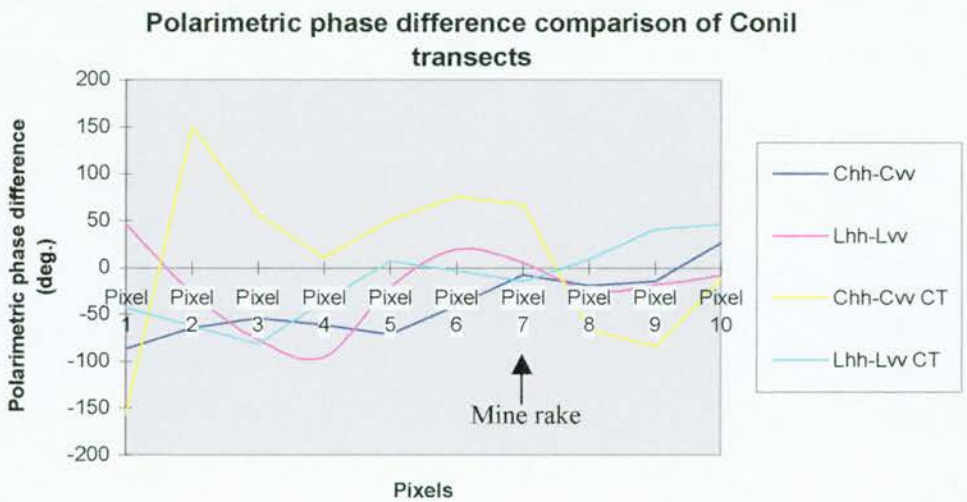

Fig. 7-35b Polarimetric phase difference statistics for Conil de la Frontera mine and comparative transects.

It was described in Chapter 4 that the wavelengths emanating from the sensor's antenna strike the earth's surface at either the horizontal or vertical axis in multipolarimetric RADAR systems. These wavelengths may or may not be received in a like manner, depending on the reception mode. Consequently, stray backscatter will occur as these broadcast wavelengths strike the earth's surface and rebound in odd manner of axis, thus creating extraneous signal noise or speckle in the final derived image. However, as was discussed in Chapter's 5 and 6, speckle may be reduced by filter processing of the Imaging RADAR data. Again, since the emphasis in using Imaging RADAR for this archaeological study was the detection of ancient mines, quite often lineal in aspect as with the Conil rakes here, it was decided to use a filtering process that would retain maximum detail while ridding extraneous noise. The results of this portion of the RADAR data analysis are described in the following section concerning visualisation.

7.9.4 Imaging RADAR topographic modelling and visualisation

7.9.4.1 Data fusion and representation

DTED (Digital Terrain Elevation Data) Level 1, a product of the Cartographic Office of the Junta de Andalucia, Spain, was used to produce a grid of the same area as the MLC data set. The RMS for the Conil data set was .027 for ground control, making it possible to verify pixel to target scene returns within the resolution of the data.

The master DTM, originally in a geographic Coordinate system and WGS-84 datum was then rectified, registered and projected into the Universal Transverse Mercator projection, using the WGS-84 spheroid, with the WGS-84 datum as its reference (NIMA, 2001).

The Cvv, Lhh and Lvv MLC polarisation images, having already been fully processed and analysed at this point, were then subjected to a filtering process before fusing the image and DTM data sets (Section 7.9.4.2).

7.9.4.2 Filter processes

An adaptive filter regimen was used against the Conil MLC data set as explained in Chapter 4.

A pseudo-colour Imaging RADAR scene was generated from polarisations of the two RADAR bands by utilising the Cvv wavelength as the Red colour band , the Lvv wavelength as the Green colour, and the Lhh wavelength as the Blue colour band to produce a false colour image (Kruse 1996). The reasoning behind these colour choices are as follows: Cvv has a wavelength of 3.8 cm ~ which since the area of Conil is relatively treeless, means that exposed rock outcroppings would give strong returns. Lvv at 23.5 cm~ is known to enjoy very subtle moisture detection capabilities, thus it was chosen as the Green colour band. Mine rakes, adits, and disused galleries and other remnants of mining activities, tend to be moisture collectors. Lhh, well known in geo-archaeological work for its lineal detection capability, was chosen as the Blue colour band (Abdelsalam *et al.*, 1995)

Finally, the composite image was created and overlaid upon the Digital Elevation Model (DEM). Three-dimensional image scenes of the fused RADAR and DTM data are presented in Figures 7-36 through 7-39 with views from the primary compass points of west, north, east and south, surrounding the Conil mine rakes. Numerous geological features may be seen in this composite image, as well as cultural features, such as the N-340 highway.

7.9.4.3 Visualisation: west

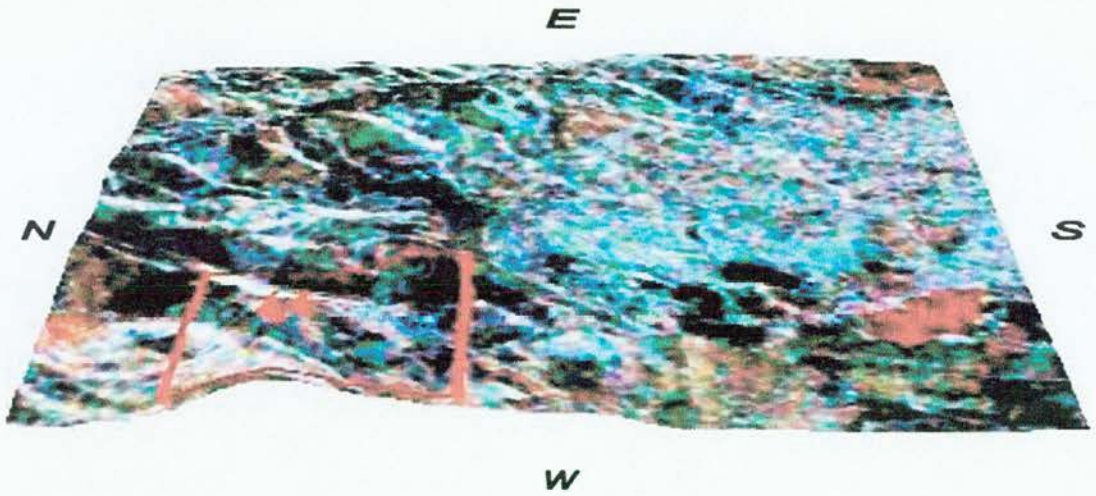

Fig. 7-36 The Conil mines viewed from the west (1:22,784).

In Figure 7-36, the main mine rake at Site "C" may be seen traversing a hill, as pointed out by the red arrow. The modern open pit mine is located just outside the left upper corner of the area of interest box. The dark areas immediately above open pit rake site and mine are the southwest oriented embankments of the N-340 coastal highway. The convolutions in the underlying geology may be seen in the low hills on the south bank of the Rio Salado, located in the upper left portion of this image. Another set of rakes is visible from this direction in a digital form and may be visible here within this analogue view, three centimetres above the left corner of the area of interest box.

Finally, all bands graphically demonstrate the interfacing of the geomorphology zones, as within the landscape to the south of the mine rakes, or right in this image, the Lvv and Lhh returns predominate, but note the purple hues. These are indicative of the Cvv band responding to the exposed rock surfaces, as this is an area devoid of trees and covered only by sparse pastoral grasses. This is an area whose geology is largely constructed of sand and loose clays with some sandstone intermixed at irregular intervals.

The distinctive area of Cvv (red) returns, located at the lower right of the image scene was found to be a *campana de girasol*, or sunflower field, under cultivation and irrigation in 1994 (Instituto de Cartografia de Andalucia, Atlas de Andalucia, 1995: CD-ROM).

7.9.4.4 Visualisation: north

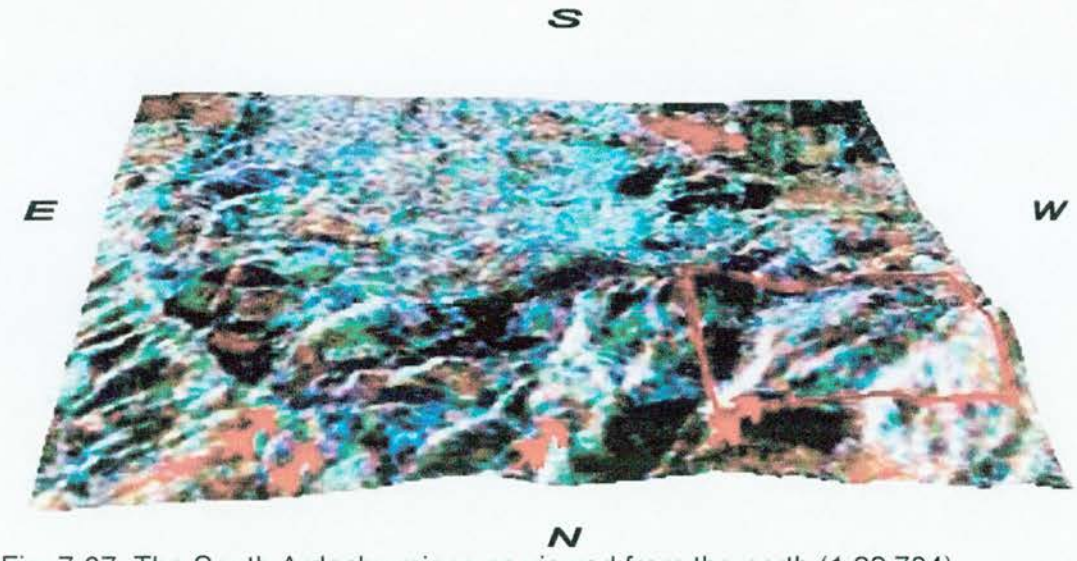

Fig. 7-37 The South Ardachy mines as viewed from the north (1:22,784).

In Fig. 7-37, the bisection of the geology by the Rio Salado is evident in the lower left corner of this image scene, which is the northeast in actual compass directions. The mine rake at Site "C" is once again evident as traverses the hillside.

The most striking feature however, is the geology that the Rio Salado crosses. Current geology maps give no evidence of a rising geology here, yet clearly there is a folding and striking process occurring which is being eroded by the passage of the stream. This process is quite likely the mechanism that has created the necessary heat and pressure for mineralisation to occur and produce mineral ore, which has extruded to surface outcrops due lifting pressures.

Finally, the mixed geomorphology of the upper portion of the image, which is the southern portion of the area of interest in reality, displays a greater tendency to report Cvv (red) returns than in the previous look angle image. This is indicative of geological and vegetational biology that is oriented more towards the RADAR sensor and which is closer in relative size to the resolution of the C band. This underlines an obvious aspect of landscape visualisation when using imaging RADAR, which is that the target are must be viewed from a multitude of angles with the location of the sensor and its incidence angle firmly in mind to clearly interpret the image data.

The area of interest will now be viewed from an easterly direction for landscape analysis.

7.9.4.5 Visualisation: east

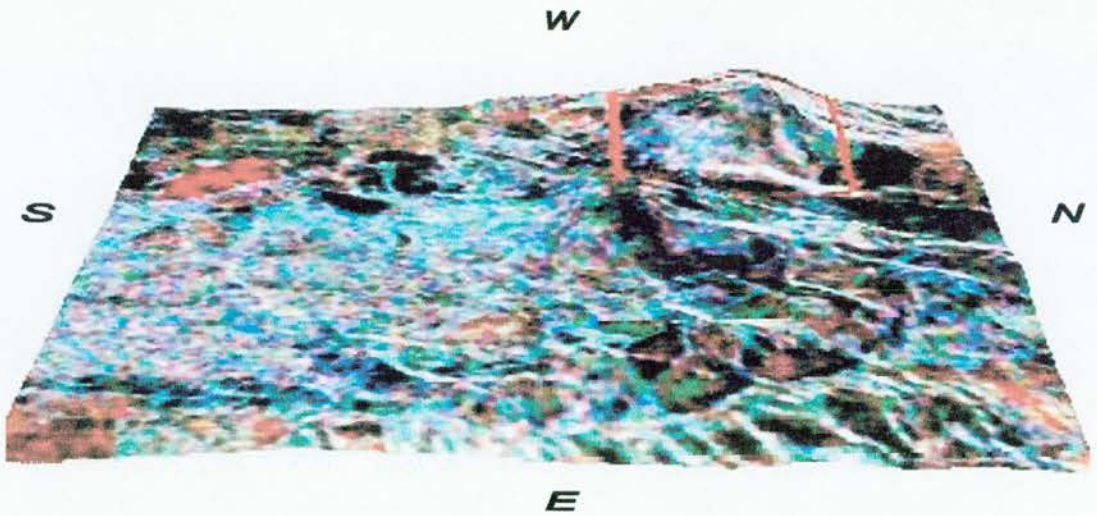

Fig. 7-38 The South Ardachy mines complex viewed from the east (1:22,784).

Fig. 7-38 gives the best perspective of the geological structure along the Rio Salado, located in the lower right portion of the image scene from this view direction. Note the areas of deep green within the banks leading down to the Rio Salado; this is a strong Lvv response over an area which functions as a catch basin for eroded materials from the northern mine rakes as well as alluvial mud deposited from inland sources.

The open pit mine, situated in this view outside the lower right corner of the Site "C" area of interest box, is seen to be intruding into the crest of the hill as well as its base. This may explain the lack of backscatter response from the interior of the mine. This is because the elevation difference from the peak of the hill to the bottom of the mine is considerable and its interior is largely filled with loose sand and crushed aggregates. If this terrain were mildly moist, which is quite likely only 1 kilometre from the ocean, then coupled with a reflecting surface which has high obscuring shoulders, a dark area might result from acting as a diffuse scattering surface (Chap. 3). However, this is speculative without further investigation.

The dark responses in the area just below the area of interest box, and corresponding to the other mine rakes, are disused dolorite extraction pits for a modern pavement factory. Another series of dark response areas may be seen to the left of the area of interest box; these are sandpits created from extraction of sand and aggregate materials to create concrete.

7.9.4.6 Visualisation: south

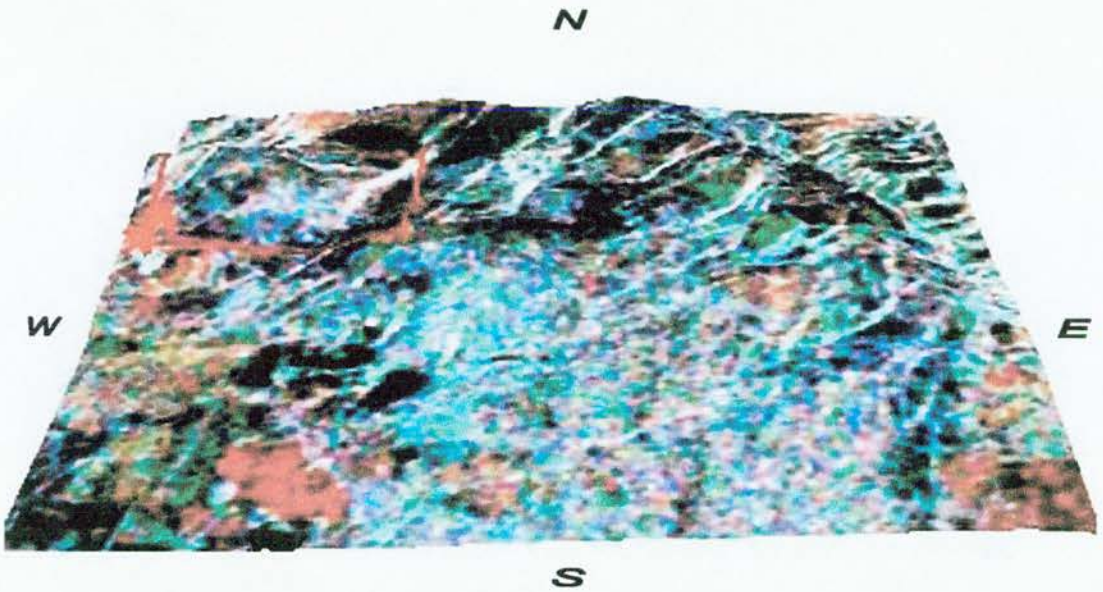

Fig. 7-39 The Conil mines as viewed from the south (1:22,784).

Fig. 7-39 gives another dramatic perspective of the folding and striking geology bisected by the Rio Salado. The stream may be seen proceeding from the lower right of the image scene, towards the top of the image, then sweeping towards the west through the folding geology of the hills.

In the lower left of the image, the field of sunflowers may be seen more clearly with the disused aggregate quarries just above. It is unknown what type of agriculture was occurring in the lower right corner of the image during the overpass of the STS imaging RADAR in 1994. In May of 2000 *harina*, or wheat populated it.

An arrow within the area of interest box draws attention to the lower mine rakes of Site "C", which can be seen roughly zigzagging across the hillsides. The open pit mine is slightly obscured in this view.

The disused dolorite mines, located to the right of the area of interest box are well defined. It is also interesting to note the strong Lvv (green) returns once again, indicative of eroded materials from the disused mines and rakes possibly containing high amounts of moisture.

This concludes the landscape analysis of the Conil mine rakes. The following section will conclude this chapter with a summary of the results obtained during the imaging RADAR survey.

7-10 Summary of results: Conil, Spain

7.10.1 Imaging RADAR and the topography

After a description of the historical and physical geographic setting behind ancient mining on the Gaditano maritime of Andalusian Spain, a detailed topographic analysis was performed on an area deemed suitable by the application of the assembled geographical model, Conil. Topographic analysis revealed a terrain surface of undulating hills, marked by a geological interface.

Imaging RADAR data analysis of the Conil mine rakes revealed phase difference responses in both the C and L band which were relatively similar to those recorded at South Ardachy (Chap. 5). The phase differences for both C and L band were mapped for their magnitude of change and presented as polarimetric phase difference absolute value images (ENVI, 2001). These analyses were derived by transecting a portion of the terrain, which began on a relatively planar terrain surface, and by then crossing the mine rake in a south to north direction. A pixel, 125 x 372, which corresponded with a target mine rake, was sampled for decibel and multipolarimetric response in both C and L bands, then compared. These were compared to response samples taken from a nearby open pit mine, located at pixel 89 x 308, and from a pixel located in the mid-section of a comparative transect. Neither of these pixel samples revealed a similar phase difference response as seen in pixel 125 x 372. While the Site "C" target mine rake exhibited interesting responses absolute identification was impossible because of sensor resolution, the shape of the mine rake, and other surface scattering influences.

Finally, a false colour composite of the Conil mines region was created from the Cvv, Lvv, and Lhh bands of the MLC data subset. This false colour composite was then draped over a DTM for three-dimensional visualisation of the archaeological landscape surrounding the mines. The false-colour composite highlighted the Imaging RADAR capability to map the geo-archaeology of the Conil region, revealing further possible areas of ancient mining activity.

The next chapter will compare the results of the investigation of the mines of Ardachy, Serabit El-Khadim, and Conil. Chapter 9, the concluding chapter, will summarise the results and discuss future research based on the data observed.

Chapter 8

Site Result Comparison

"Dentro le canta un mar de mapa". Federico Garcia Lorca, "Caracola", 1936, v: 2.

8.1 Introduction

This chapter compares the results of the Imaging RADAR (NASA SIR-C/X-SAR) archaeological survey performed on the South Ardachy, Serabit El Khadim and Conil mine sites. Section 8.2 compares the physical geography of the sites, which are followed by a comparative historical geography in Section 8.3. Comparison of site topography and analysis are outlined in Section 8.4. Section 8.5 discusses the site histories and archaeology, while Section 8.6 displays the CORONA satellite imagery. Section 8.7 compares the AVHRR data immediately preceding the overpass of the Space Shuttle and its Imaging RADAR system. Section 8.8 compares the local meteorological data immediately preceding the overpass of the Shuttle Transport System (STS). Detailed Imaging RADAR analysis data is outlined in Section 8.9. Section 8.10 concludes the chapter with a summation of the data presented.

8.2 Physical Geography and Geology

8.2.1 Comparing the Physical Geography

Characteristic	Ardachy	Serabit El Khadim	Conil de la Frontera
Distance from sea	4 km	30 km	4km
Topography	Intermediate	Complex	Intermediate
Physical Geography (Landscape)	Maritime	Maritime hinterland	Maritime

Table 8-1 Physical Geography and characterisation

The common denominator between two of the three sites, in terms of physical geography, is a maritime landscape (Table 8-1). Both Islay and Conil are heavily influenced by sea-borne weather systems, however Islay's climate is mitigated by the Gulf Stream, whilst Conil's climate is influenced by cold Atlantic currents.

All three sites have a terrain that undergoes significant change within a short distance of the sea. On Islay, the high foothills are never more than 4 kilometres from the sea, while reaching Serabit El Khadim requires surmounting low mountains only 8 kilometres from the Red Sea. At Conil, which is virtually at sea level, there are 5 major foothills within a 10-kilometre radius that have an elevation of at least 300 metres. The final observation is that the mean distance from sea for all sites is approximately 12.6 kilometres, with Serabit El Khadim being the most distant.

8.2.2 The General Geology

Characteristic	Ardachy	Serabit El Khadim	Conil de la Frontera
Geology	Limestone (Quaternary Period)	Metamorphic (Pre-Cambrian), sedimentary (Jurassic), limestone (Cenomanian-Turonian), dikes (Miocene)	Sedimentary with clays, gypsum and limestone (Cretaceos-Paleocene)
Geologic activity (major influences)	Glacial erosion	Boundary between sedimentary and metamorphic structures	Plastic sedimentary structure overlaying uplifting zone

Table 8-2 Geology and characterisation

South Ardachy and Serabit El Khadim both have metamorphic rock formations within their general geological regions, while Conil and Serabit El Khadim both have dolomite, limestone, sandstone and sediments (Table 8-2). It can then be seen that Serabit El Khadim has the most shared geological characteristics of the three mine sites, and might be regarded as the mean, if such were possible to quantify.

8.2.3 The Minerals and Mines

8.2.3.1 Minerals

Characteristic	Ardachy	Serabit El Khadim	Conil de la Frontera
Minerals	Lead, copper, silver, tin	Copper, lead, gold, iron and turquoise	Lead, copper, tin

Table 8-3 Minerals and characterisation

The minerals common to all mine site areas are copper, lead and tin (Table 8-3). All three of these minerals are representative of the great metallurgical periods in human culture, the Copper Age and the Bronze Age. The origins of copper mining on Islay are unknown and historical commentary is sparse due to the loss of Gaelic histories, both in an oral and written sense. Evidence of copper mining in southern Ireland has been demonstrated at Mt. Gabriel in the early 1st millennium BC, so it may be possible that the technology had spread around the Irish Sea to Islay (Scarre, 1995).

8.2.3.2 Mining

Characteristic	Ardachy	Serabit El Khadim	Conil de la Frontera
Area mines	Ballygrant, Kilseven, North Ardachy and Mulreesh	Umm Bugma	Unknown

Table 8-4 Mining and characterisation

Islay and the Sinai Peninsula have the most extensive record of mining (Table 8-4). The record at Conil is unclear due to a paucity of historical documents, although this may be remedied in the future by access to the library of the House of Medina Sidonia. Both Islay and Cadiz province share a unique cultural characteristic; for a great period of time both mining regions were controlled by families that had considerable economic, military and political might, they being the Lords of the Isles and the House of Medina-Sidonia. It is worth noting that these societies derived their power from a strong maritime capability, as has been discussed.

8.3 Historical Geography

8.3.1 The Historical Geography

Characteristic	Ardachy	Serabit El Khadim	Conil de la Frontera
Earliest cultural period	Mesolithic (c. 7000 - c. 3500 BC)	Mesolithic	Tartessan (preliminary)
Cultural era - mining begins	Environmental evidence, 15th century; anecdotal evidence, 11th century	Organised mining in Pre-dynastic period of Egypt (3400 BC); anecdotal evidence of earlier mining.	Celto-Iberic / Tartessan (700 BC) (preliminary)
Cultural era - mining ends	Early Industrial Age (18th century)	Industrial Age (19th century)	Roman Empire (2nd century AD - preliminary)

Table 8-5 Historical geography and characterisation

The common theme of these historical geographies is simple (Table 8-5). The extraction of minerals was a means to empire building, either in a commercial sense, such as with the Phoenicians-Carthaginians, a politico-military sense, such as the Lords of the Isles, or dynastic preservation, such as that with the Egyptian Kingdom. It must be remembered that the Lords of the Isles functioned as a confederation with a ruling council that governed its affairs, thus making it a representative political body (Williams, 1997). The Carthaginians conflicted with the Roman Empire over maritime commercial trade rights, resulting in the Punic Wars (Cotterell, 1980). Finally, Egypt needed metal to forge implements that were used to build monumental constructions, which highlighted the deification of the Pharaohs and thus preserved their place as leaders of the society (Aldred, 1998). Metals underpinned these cultures and their economies.

8.4 Location of the mine works and topographic analysis

8.4.1 Site location

Characteristic	Ardachy	Serabit El Khadim	Conil de la Frontera
Geographic co-ordinates	302097 E by 618766 N (UTM)	321176 E by 545439 N (UTM)	297685 E by 402120 N (UTM)
Climate	Temperate	Arid	Mediterranean
Ground transport (distance to sea via probable routes)	4.4 km (2 tracks)	35 km (3 tracks)	4.1 km (various routes)
Potable water (distance from mine site)	0.5 km (Loch Bharradail)	4.1 km (Wadi Bateh)	1 km (Rio Salado)

Table 8-6 Site location and characteristics

The mining regions were selected for this study on the basis of early commentaries by the classical writers, Strabo, Herodotus and Pliny, as well as representing a range of climatic types (Table 8-6). South Ardachy was selected based on its previous extensive environmental archaeological research and temperate climate, while Serabit El Khadim was selected because of the arid climate and the lack of research regarding the site, other than by Petrie in 1904-5 (Petrie, 1906). Conil was a discovery within a chosen climatic region, Mediterranean, which was found after intensive ground truthing campaign over a three-month period.

8.4.1.1 Topographic analysis

A complete topographic analysis of the region surrounding each mine complex was performed using a Digital Terrain Elevation Data subset equivalent to a level 1 parameter i.e. one verifiable elevation point every 90 meters on average (NIMA, 2001). The topographic analysis followed the methodology outlined in Chapter 3, which comprised the following examinations: slope, aspect, shaded relief, profile convexity, plan convexity, longitudinal convexity, cross sectional convexity, minimum curvature, maximum curvature and topographic feature classification (i.e. hill, peak, depression etc.). Each analysis is compared in the following sections by presenting the images side by side.

8.4.1.2 Slope

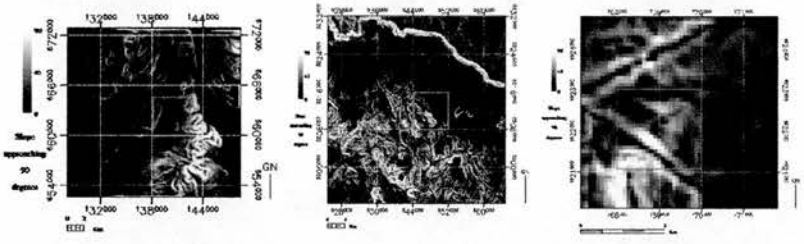

Fig. 8-1 Rate of change for slope, eastern Islay, Serabit El Khadim and Conil.

Three very distinct slope results are presented here (Fig. 8-1). At South Ardachy the need for freshwater to process minerals must have been counterbalanced by the lack of a natural drainage system. If mine workers or farmers inhabited the immediate area surrounding the works and used Loch Bharradil or other streams within the same catchment for a water supply, it is possible that their health would have been affected by heavy metal pollutants or suspended materials. Serabit El Khadim is the extreme opposite of South Ardachy. Analysis reveals a system that transports water rapidly across its surface and, coupled with an arid climate, must have made water husbanding critical. Conil, with its convoluted terrain and semi-arid climate, would have suffered the same problem but to a lesser degree. However, the nearby Rio Salado must have been utilised for freshwater in mineral production.

8.4.1.3 Aspect

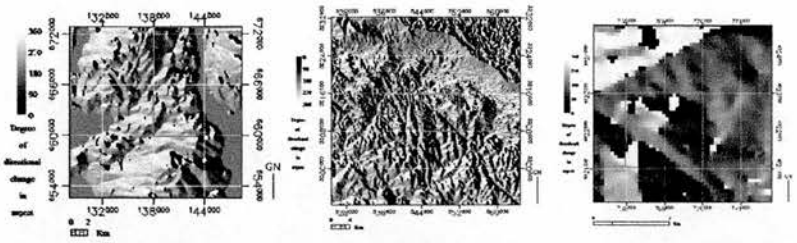

Fig. 8-2 Aspect characteristics for eastern Islay, Serabit El Khadim and Conil.

Chapter 3 described aspect, as the orientation of primary terrain faces toward a given point. Due north was used as 0° for purposes of aspect orientation.

Aspect and its relevance to these mine sites can only be theorised in the light of its importance for human populations near mine sites. At South Ardachy, Islay, would have meant that the east facing slopes of Beinn Bharradil were prime areas for habitation (Fig. 8-2). Only archaeological survey could confirm this theory. Surface faces that effectively channel water flow, solar radiation and avenues of transportation affect Serabit El Khadim. Conil shares the characteristics of South Ardachy and Serabit El Khadim in that dominant west winds over southeast facing surfaces and convoluted slopes make transport difficult.

8.4.1.4 Shaded Relief

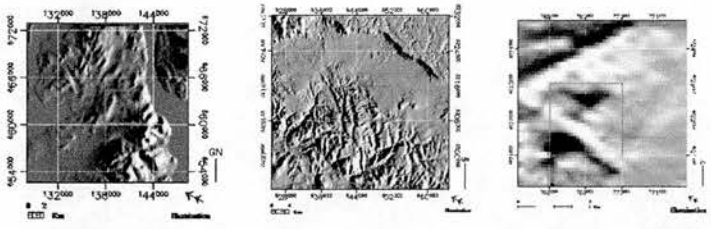

Fig. 8-3 Shaded relief of eastern Islay, Serabit El Khadim and Conil .

A shaded relief of the South Ardachy mine complex was computed using the following figures: a sun elevation angle of 18.24° in conjunction with a sun azimuth angle of 97.49°, 0730 hours. Shaded relief for the Serabit El-Khadim mine complex was computed using the following figures: a sun elevation angle of 45.25° in conjunction with a sun azimuth angle of 109.87°, 1000 hours. Finally, Conil was computed with a sun elevation angle of 40.0° with a sun azimuth angle of 135.98°, 1000 hours. Sun elevation and angle were selected based on the year 1000 AD and the date of 1 January.

The common theme between all sites is the exposed nature of their positions. None have major foothills, mountains, or tree canopies, within their topographies that can moderate the effects of solar radiation and wind. Inhabitants near South Ardachy may have utilised the sheltering western ridgeline of Beinn Bharradil and its solar illuminated eastern slopes to assist in maintaining warmth; conversely, inhabitants near Serabit El Khadim may have used the narrow wadis to escape the effects of intense solar radiation. However, it is known archaeologically that hilltop settlements in the Sinai are not uncommon (Rothenberg, 1979). Conil is an unknown quantity and requires intensive archaeological survey to define the nature of habitation around the site.

8.4.1.5 Profile convexity

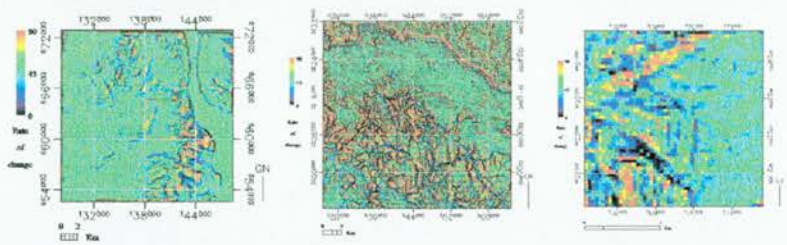

Fig. 8-4 Profile convexity for eastern Islay, Serabit El Khadim and Conil.

Profile convexity analysis was used to measure the rate of change of the slope along the profile at all site areas. Serabit El Khadim displays the most dynamic profile change of the three site areas, indicating topography difficult to traverse; the outlying great wadis display moderate profile change, possibly indicating an ancient route of access (Figure 8-4). Ardachy and Conil have area slope profiles that are indicative of the underlying ore-bearing geology. At Ardachy the north to south trend of the lead-ore bearing limestone outcrop is noticeable, while at Conil the dolorite hillocks can be detected.

8.4.1.6 Plan Convexity

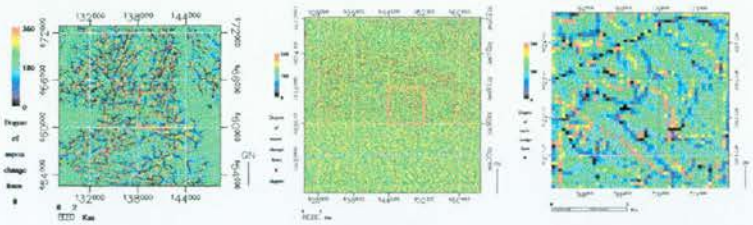

Fig. 8-5 Plan convexity of the eastern Islay area, Serabit El Khadim and Conil.

As discussed in Chapter 3, plan convexity (intersecting with the XY plane) measures the rate of change of the aspect along the plan. Serabit El Khadim exhibits the most difficult topography under plan convexity analysis (Figure 8-5). Not only are there numerous high angle slopes, but these slopes have no consistent directional orientation, making land access very difficult except from the great wadis to the east of the site. South Ardachy, to a lesser degree, suffers from the same problem, with access routes easiest from the south. Conil, located only 1 kilometre from a freshwater river, and 4 kilometres from the Atlantic Ocean, should have had the easiest transport access.

8.4.1.7 Longitudinal Convexity

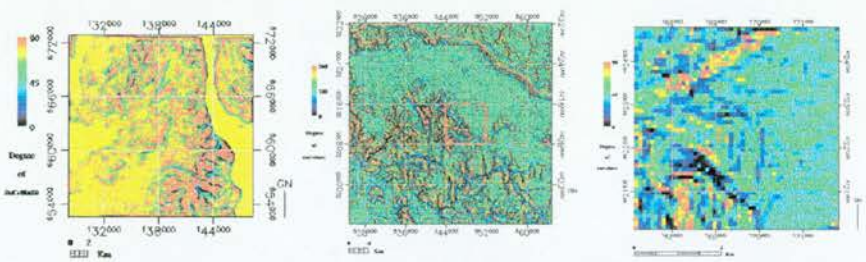

Fig. 8-6 Longitudinal curvature of the east Islay area, Serabit El Khadim and Conil.

Longitudinal curvature and cross-sectional curvature are measures of the surface curvature orthogonally in the down slope and across slope directions. Both South Ardachy and Serabit El Khadim are common in that the longitudinal convexity in the immediate area of these sites is conducive to collection of rainfall and runoff, the difference being that on Islay the thin soil overlying the rock structure and the minimal slope change create bog conditions (Fig. 8-6). Serabit El Khadim, on the other hand, will likely see water collected in the most protected of wadis, with most water being absorbed by the local geology to reappear at small springs or pools. Conil has small areas of high convexity but these are so isolated that they will suffer mostly from erosion incurred by heavy winter rainfalls and high average winds.

8.4.1.8 Cross sectional curvature

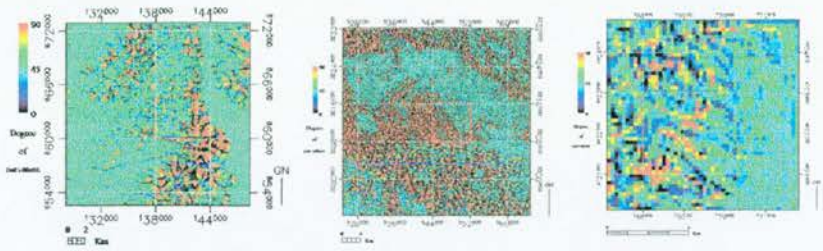

Fig. 8-7 Cross-sectional curvature of the east Islay area, Serabit El Khadim and Conil.

Cross-sectional convexity, or curvature (intersecting with the plane of the slope normal and perpendicular aspect direction) is a measure of the surface curvature orthogonally across slope directions. Analysis of Islay's eastern portion revealed cross sectional curvature resulting from the underlying geological structure, which are the contact areas that have created the necessary heat and pressure for mineralisation (Fig. 8-7). Such topography has implications for the hydrology of Islay as limited drainage networks exist to empty a large area. The possibility that the ancient mines have polluted the local environment with metals is high, largely due to the lack of mobility by heavy particulates suspended in water runoff; this is supported by the research of Cressey (1995). There are simply insufficient slope angle and outflow points to cleanse the soils.

Serabit El Khadim exhibits an extraordinary level of cross-sectional curvature. Its aridity precludes agriculture and all but the hardiest of desert vegetation. Heavy rainfall events and constant winds over such a surface topography have led to significant alluvial and arenal erosion over the centuries; limited research suggests that the climate during the early Egyptian dynasties was significantly wetter (Scarre, 1995).

At Conil the major ore bearing hillocks surrounding the rakes were detected. These hillocks, composed of dolomite, are extrusions likely exposed by the previously mentioned rising geology of the area and centuries of erosion.

Here, South Ardachy and Conil are most influenced by rising and striking geological structures. However, Serabit El Khadim and Conil are both influenced by topographies that have been created by erosion from wind and water. Serabit El Khadim has obviously seen millennia of aeolian erosion, and it is possible that this process was initially begun by past heavy rainfalls over limestone and sandstone geology.

8.4.1.9 Minimum curvature

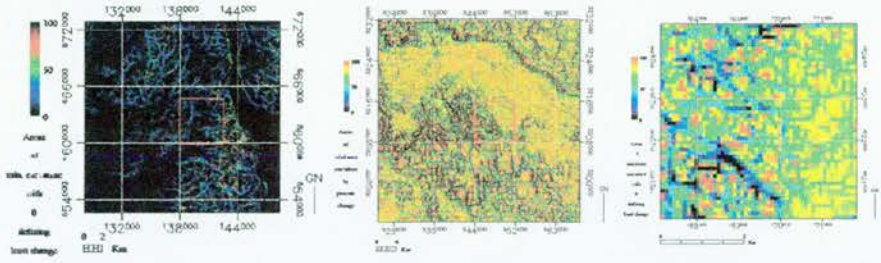

Fig. 8-8 Minimum curvature of the east Islay region, Serabit El Khadim and Conil.

Minimum curvature is the topographical analysis that determines the extent of planar surface area within a region. The essential feature between all three of the sites is the degree to which water, or the lack of it, affected the efficiency of operating a mine (Fig. 8-8). Serabit El Khadim must have had a sophisticated system to support its workings over such a long period, while Conil must also have had an engineered water supply; this is an archaeological question in need of investigation. South Ardachy, conversely, would have dealt with an overabundance of water due to the temperate climate, the marginal slope and a soil structure underpinned by rock. Water runoff with heavy metal particles was transported to Loch Bharradil via a leat as demonstrated by Cressey (1995) and seen in Chapter 5, Fig. 5-4.

8.4.1.10 Maximum curvature

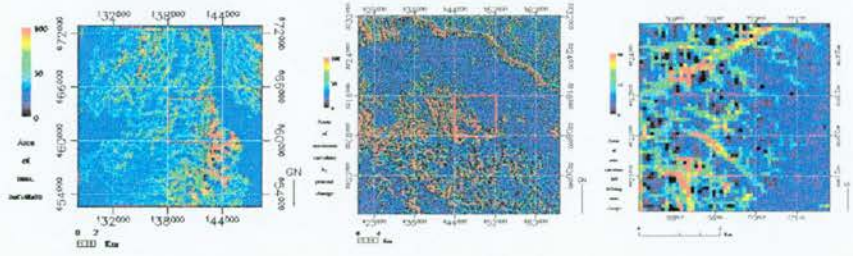

Fig. 8-9 Areas of maximum curvature in eastern Islay, Serabit, and Conil.

Maximum curvature analysis determines the extent of curved surface within a given area. Conil and South Ardachy both had minimal areas of maximum curvature (Fig. 8-9). However, due to different local soil and geological structures, they face different problems. At South Ardachy the lack of curvature, constant rainfalls, and soil underpinned by rock structures, predestine the area to drainage problems with localisation of metal pollution. Conil is the obverse with rapid water absorption due to loose, sandy soils, long hours of sun, and drying winds over a free-draining surface.

Site geology for the three mine workings will now be compared and analysed for common characteristics in Section 8.4.2.

8.4.2 Geology of the site

Characteristic	Ardachy	Serabit El Khadim	Conil de la Frontera
Site geology	Slates, phyllites, Dalriadan limestone, lead	Schists, amphiboles, migmatites, limestone, copper, turquoise	Clays, gypsum, sandstone, dolomite, copper, lead

Table 8-7 Site geology and characterisation

Copper is common to Serabit El Khadim and Conil and it should be remembered that the metal was mined on Islay as well, although not at South Ardachy, but at Kilseven (Table 8-7). Lead is common to South Ardachy and Conil, while only Serabit El Khadim reveals the presence of a precious gemstone, turquoise.

8.4.3 Geomorphology

Characteristic	Ardachy	Serabit El Khadim	Conil de la Frontera
Geomorphology	Foundland Series drift deposits of slate and phyllites; limestone outcrops covered by light loam. Peaty glays and podsols around Loch Bharradil	Entisols, typic torripsamments, and lithic torripsaments	Interface between marine and continental geomorphology classes, having both aeolian and fluvial components; mostly sand and loose clay

Table 8-8 Geomorphology and characteristics

South Ardachy has the necessary soil structure to support limited agriculture as well as pastural grazing (Table 8-8). Serabit El Khadim has virtually no capability to support agriculture, largely due to lack of water. Conil has a limited agricultural capability due to the high sand content of its soil; frequent irrigation would be necessary.

In an archaeological context, this means that the carrying capacity to support large scale industrialisation of the South Ardachy mine site would have been much easier to accomplish, while the Conil de la Frontera site would have been slightly less ideal. The Serabit El Khadim site, based on historical commentary and limited archaeological work, must have required an enormous logistical system and financial outlay to function on the scale of industrialisation that is suggested by the site.

8.4.4 Vegetation

Characteristic	Ardachy	Serabit El Khadim	Conil de la Frontera
Plant biology	*Calluna vulgaris*, *Campanula rotundifolia* and *Orchis mascula*.	*Juniperus phoenicea* , *Noaea mucronata*, *Salsola tetrandra*, *Halgeton alopecuroides*, *Artesmisia herba-alba* and *Hammada salicornica* with *A. setifera*.	*Argostis, Vulpia, Bromus Hordeum and Juneripus phoenicea.*
Plant biology thriving on mine workings: slag heaps, tailings, etc.	*Plantago lanceolata* and *Rumex obtusifolius*.	None observed.	*Myrtus communis*

Table 8-9 Vegetation and characteristics

South Ardachy and Conil mine sites are both populated with species of grasses. Serabit El Khadim is devoid of grasses (Table 8-9). South Ardachy and Conil have species of shrubs that appear to thrive atop mine slag heaps, while again Serabit El Khadem has no such species. The lack of grasses or shrubs at Serabit El Khadim's mine site may be ascribed to aridity and possibly, high soil toxicity from mine spoils, although this has not been investigated. However, Serabit El Khadem and Conil do share an intriguing species between them, that of *Juneripus phoenicea*, or Phoenician Juniper.

8.5 Site History and Archaeology

8.5.1 Historical Background

Characteristic	Ardachy	Serabit El Khadim	Conil de la Frontera
Historical background i.e. commentaries, notes or books.	Allusion in various medieval texts; books by Pennant in 18th century and Smith in 19th century with archaeological writing by Cressey in 20th century.	Limited Egyptian commentary (c. 3000 BC); archaeological writings by Petrie, Hayes, Rothenburg, in 20th century.	No historical background; area mine workings alluded to by historical documents not in public domain (Medina-Sidonia archive).

Table 8-10 Historical background and characteristics.

Serabit El Khadim has the most extensive corroborative historical and archaeological evidence to ascertain its provenance, one that extends back some 4,700 years (Table 8-10). South Ardachy has a fair quantity of historical evidence for early and middle 18th century operation of the mines. There is anecdotal evidence for late 16th century workings, although Cressey's environmental archaeological analysis points to a possible late 15th century mining effort in the area. Conil, being a new discovery, exists outside the known mining areas of ancient Iberia, such as the Rio Tinto zone, and requires a thorough investigation. However, initial ground survey of pottery fragments and mining slag point to operations from at least the 1st century BC, if not much earlier.

8.5.2 Site archaeology and survey

Characteristic	Ardachy	Serabit El Khadim	Conil de la Frontera
Type archaeological survey: reassessment, preliminary, or detailed.	Reassessment based on detailed work by Cressey 1994-95. Site includes cast workings, surface workings (trial mine shafts), spoil heaps and tailings.	Reassessment based on and survey by Petrie 1904-05. Site includes mine galleries, surface workings (quarries), spoil heaps and tailings.	Preliminary survey performed in 2000; new site. Site includes surface workings (rakes), spoil heaps and tailings.

Table 8-11 Site archaeological survey characteristics

Serabit El Khadim has the most extensive evidence of early mining and industrialisation (Table 8-11). It also has the most substantive amount of associated cultural evidence, i.e. remnants of hand tools, miners huts, monuments and commemorative inscriptions. Conil, although a new discovery, has considerable quantities of cultural evidence within a small area. South Ardachy, on the other hand, has limited cultural evidence and many of its features have been changed by farming and refuse dumping. No cultural artefacts from the site have been discovered at present.

8.5.3 Ground Features

Characteristic	Ardachy	Serabit El Khadim	Conil de la Frontera
Trial workings	X	X	X
Quarry		X	
Tailing dump	X	X	
Rakes	X		X
Adits	X		
Spoil heaps	X	X	X
Buildings	X	X	
Dimensions of target mine and type feature	9m wide *x* 11m length; 4m maximum depth / mine rake	11m wide *x* 20m length; 3m maximum depth / mine quarry	4m wide *x* 12.8 m length; 2.5 m maximum depth / mine rake

Table 8-12 Ground features and characteristics

All three sites exhibit the hallmarks of early mining archaeology, with rakes, trial works, slagheaps, and tailings (Table 8-12). Serabit El Khadim has clear evidence of miner's huts, while South Ardachy has several buildings that may have been connected with the mining works. Conil may have had structures that were associated with the mine rakes, but this awaits further archaeological investigation. The average dimensions of these sites are 8 metres in width, 3.3 metres in depth, and 14.6 metres in length.

8.5.4 Archaeological assessment

The features that most closely coincide with the historical commentary concerning South Ardachy, and which point to pre-Industrial Revolution provenance, are the open cast features. These trial shafts were noted by in the 18th century writings as pre-dating the current workings i.e. those of the 17th and 18th century when South Ardachy was in full production.

At Serabit El Khadim there are nearby tribute inscriptions to the Pharaoh Sanakht of the Third Dynasty that indicate early occupation. Intensive archaeological work would be required to establish periods of occupation and organisation around the entire site area.

The surface artefacts collected from the hill overlooking the northern end of the Site "C" Conil mine rake were analysed and compared with a diagnostic collection held by Dr. Antonio Aragon of the Casa Cultural de Barbate, Spain, a branch of the Departmento de Arqueologia, Universidad de Cadiz. These artefacts were found to match Roman pottery from the 1st century BC and 1st century AD.

Pottery shards extracted from the Conil mine rakes were found to be of mixed provenance, being of Punic and Tartessan in origin. The Punic artefacts matched samples from the 4 and 5th century BC, while those of Tartessan origin appeared to fall within the 6th century BC (Aragon, 2000: pers. comm.).

Archaeological assessment was difficult at all sites due to brevity of the ground surveys. While Serabit El Khadim has the most substantial historical and archaeological resources to work from, the remoteness of the site hinders investigation. South Ardachy has had considerable agricultural impact and archaeological investigation there may yield very little beyond what is now known. Conil has the best possibility for future discovery as its mixed archaeological provenance, and location, may provide valuable new insight into early mining in southern Iberia.

8.6 CORONA Satellite Imagery

8.6.1 CORONA Satellite Image Details

Satellite imagery from the CORONA program was obtained from the USGS GLIS Archive.

8.6.2 CORONA Satellite Imagery Subset

Characteristic	Ardachy	Serabit El Khadim	Conil de la Frontera
CORONA optical imagery	Cloud obscured target mine site, data not used. Resolution poor due to early systems problems.	Target cloud free, data used. Resolution sufficient to identify cultural features.	Target cloud free, data used. Resolution sufficient to identify vegetation clusters on mine slag heaps.

Table 8-13 CORONA satellite imagery subset characteristics

The lack of CORONA optical imagery over the Isle of Islay demonstrates the advantage which imaging RADAR has over other remote sensing systems, that being the ability to penetrate areas covered by clouds. However, the Serabit El Khadim and Conil data sets demonstrate the usefulness of high-resolution optical data when available. At Serabit El Khadim and Conil it could be used for change detection, as with Petrie's 1904-5 Sinai expedition notes, while in Spain the change in landscape use was visible when compared against the imaging RADAR data from 1994. The limitation in photographic data use in this work versus modern optical data was its ability to interrogate and analyse geology and geomorphologies, although there has been recent work in fusion of the optical and imaging RADAR data (Kruse and Dietz, 1991).

8.7 AVHRR Satellite Imagery

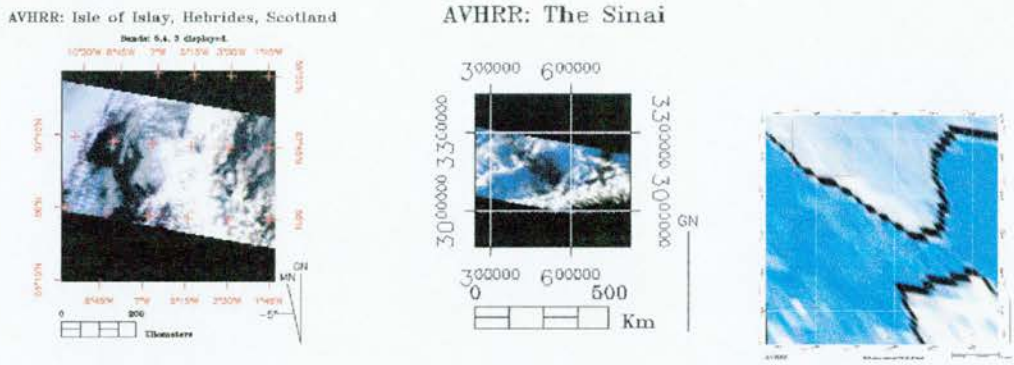

Fig. 8-10 AVHRR GAC subsets, Isle of Islay, Sinai and LAC subset for south Spain.

AVHRR Global Area Coverage (GAC) and Local Area Coverage (LAC) data for the orbital pass immediately preceding the overflight of the STS Endeavour SIR-C/X-SAR Imaging RADAR for each site was obtained from the NOAA Satellite Active Archive for analysis. Resolution was 4 km for GAC mode and 1 km for LAC mode. The LAC data is shown at a *lower* resolution due to use of another digital cartographic software (Chap. 7).

The Isle of Islay and Serabit El Khadim data sets revealed no significant visible moisture in the visible and near visible or infrared bands over Site "A" or Site "B". Conil had visible cloud and indications of moisture from the near infrared band over Site "C". As will be seen in Section 8.9.3, Imaging RADAR decibel responses for all sites were in accordance with values recorded by Ulaby and Dobson (1989) under standardised conditions. Therefore, climatic conditions had little effect on Imaging RADAR performance, though had significant amounts of moisture been present the resultant imagery would have shown the effects.

8.8 Meteorological Data

8.8.1 Isle of Islay, mid-Sinai, and outer Straits of Gibraltar Meteorological Data

Averaged weather data for the Isle of Islay region, mid-Sinai and outer Straits of Gibraltar immediately prior to the STS Endeavour overpass was provided by the Meteorological Office of the United Kingdom, the Egyptian Meteorological Service and the U.S. Navy Meteorological Command Detachment, Spain. A 24-hour averaged data comparison is presented in Table 8-14. The data for the mid-Sinai region is a monthly average as no further data was available from the Egyptian Meteorological Service.

Meteorological Details	Site "A"	Site "B"	Site "C"
Temperature (degrees, Celsius)	6.13°	21°	22°
Rainfall (mm)	.005	0	0
Wind direction (degrees, compass)	295°	No data	185°
Relative humidity (percent)	92.5	No data	83
Wind speed (km)	3.91	No data	43.2

Table 8-14 24 hour averaged regional weather data for Site "A", "B" and "C".

The weather data displays a marked difference in temperatures, but a remarkable lack of rainfall, which is unusual for both the Isle of Islay and the outer Straits of Gibraltar in October of any given year. Wind directions were out of the same quadrant, but again, considerable differences in speed, with the Isle of Islay showing marginal wind velocity, while the outer Straits of Gibraltar exhibit their normal characteristics, i.e. high average wind velocity (U.S. Navy Meteorological Command, Appendix III).

8.9 Comparative Analysis of the NASA SIR-C/X-SAR Imaging RADAR Data

8.9.1 The Imaging RADAR Data

The Imaging RADAR data for Islay were obtained on the 18th of April 1994 during NASA STS (Shuttle Transport System) Mission SRL-1; both C and L bands were in the vertical send and receive polarisation (VV) mode. The data for Serabit El Khadim were obtained on the 11th of April 1994 during NASA STS (Shuttle Transport System) Mission SRL-1 using C and L band in horizontal send and receive (hh) mode as well as horizontal send and vertical receive (hv) mode.

The data for Conil were obtained on the 3rd of October 1994, during NASA STS (Shuttle Transport System) Mission SRL-2. Both C and L bands used the horizontal send and receive polarisation (hh) mode as well as the vertical send and vertical receive mode polarisation (vv) mode. All data sets were processed as Multi-Look Complex (MLC) products, as discussed previously.

8.9.2 Data Processing

Data processing steps were presented in Chapter 3 as well as in each individual chapter for the target mine sites. Each data set was identically processed.

Ground control points (GCPs) locations for each of the sites may be seen in Figures 5-16, 6-17 and 7-18. A different process of GCP collection, registration and projection was utilised for the South Ardachy, Isle of Islay site, as discussed in Chapter 5. This was an experimental application of the principles discussed by Richards to reduce the RMS error (Richards, 1994).

8.9.3 Imaging RADAR data analysis

A reference Imaging RADAR map for each of the mine sites was presented in Chapter's 5, 6 and 7, in Figure's 5-17, 6-20 and 7-20.

8.9.3.1 Analysis form and test sites

Evaluation of the Shuttle Imaging RADAR system's ability to detect, survey and analyse ancient mine sites used a linear transect that bisected a portion of each mine site in the manner discussed in Chapter 4. At South Ardachy this was accomplished by analysing a transect covering 10 pixels, or approximately 130 metres. The UTM co-ordinate (OSGB datum) of the centre area of the mine rake was approximately 663678 N by 139730 E and corresponded to pixel 1208 by 1641 in the data sets (Chapter 5).

At Serabit El Khadim the mine site was transected and analysed in a linear fashion covering 12 pixels, or approximately 150 metres. The co-ordinate of the centre area of the mineshaft is approximately 321223 N by 544748 E, UTM, and corresponded to pixel 4274 by 1664 in the data sets (Chapter 6).

The Conil site was transected in a linear fashion crossing 10 pixels, or approximately 125 metres. The co-ordinate of the centre area of the mine rake was 402083 N by 768270 E, UTM, and corresponded to pixel 125 by 371 in the data sets (Chapter 7).

At each target site the distance was chosen to span the mine from normal signal return surface to normal signal return surface for reference purposes. Both C and L bands were analysed for decibel strength and phase difference in both HH and VV polarisation modes, although in the case of Serabit El Khadim, only HH and HV modes were available.

Each of the target mine sites also had comparative transects taken over terrain that was considered to be more planar or different in topography; these transects were analysed in the same manner described in Chapter 4.

In the following section, 8.9.3.2, the decibel returns and phase difference analysis results for the pixels concerning the targeted mine features will be compared in both C and L band, excepting Serabit El Khadim, which again did not have vv polarisation information. The associated photographs and maps will also be presented side-by-side. The comparative feature selected for each target mine site is presented in a likewise manner.

8.9.3.2 Imaging RADAR analysis

Pixel 1208 x 1640 was the pixel which coincided with the location of the mine rake at Site "A" in the South Ardachy mines complex (See Fig. 8-11 and 8-12). It was found that the Chh and Cvv decibel responses were nearly equal, while the phase difference was -6.99°; the L band displayed a drop in the difference between the hh and vv polarisations as the phase difference measured 6.11° (Table 8-15 and 8-16). These figures indicate that the Imaging RADAR system's L band perceives the mine rake, but it is unable to precisely discriminate what type of corner reflector due to its irregular shape, surface scattering influences and sensor resolution. The comparative transect showed much smaller deviation in its polarimetric phase difference results over its length, which demonstrated the planar topography of a nearby field, versus the target mine area (Chap. 5).

At Serabit El Khadim pixel 4274 x 1664 was the pixel that coincided with the Site "B" mine pit in the Serabit El Khadim mines complex (See Fig. 8-11, 8-12, Table 8-15 and 8-16). While it was not possible to perform polarimetric phase difference analysis at this site, the decibel responses from the C-hh polarisation over the mine and nearby miner's hut inferred that the Imaging RADAR system was capable of detecting a subtle change in the area's topography (Chap. 6).

Pixel 125 x 372 coincided with the location of a mine rake at Site "C" in the Conil, Spain mines complex (See Fig. 8-11, 8-12, Table 8-15 and 8-16). Here, the polarimetric phase differences were similar to South Ardachy, while decibel responses were different. Chh decibel response was -9.71 versus -3.13 for vv polarisation; phase difference was -7.84°.

Lhh and Lvv at the Conil site, on the other hand, were nearly equal in decibel response at -14.49 and -15.20 respectively while the phase difference was 5.42°. The strong response in the Cvv polarisation is thought to be from the dense myrtle shrubs atop the mine rake area, which have leaves nearly the same size as the C-band. The L-band seems to note the presence of a unique feature, although again, it cannot discriminate as to its type of reflecting surface (Chap. 3 and Chap. 7). Phase difference absolute value images were used to visualise the magnitude of phase change along all band transects and throughout the subject area, but the large number of random natural made visual detection difficult at best.

Sections 8.9.3.2.1 and 8.9.3.2.2 will discuss all of these results further.

Fig. 8-11 Left to right, South Ardachy (Site "A"), Serabit (Site "B"), and Conil, (Site "C").

Site and Pixel Coordinate	C/hh	C/vv (*C/hv for Serabit)	Phase difference
A 1208x1640	-6.26	-7.74	-6.69°
B 4274x1664	-14.69	-23.49 *	N/A
C 125x 372	-9.71	-3.13	-7.84°

Table 8-15 C band decibel returns and phase difference for Site "A", "B" and "C".

Site and Pixel Coordinate	L/hh	L/vv (*L/hv for Serabit)	Phase difference
A 1208x1640	-15.26	-13.99	6.11°
B 4274x1664	-21.74	-27.10 *	N/A
C 125x372	-14.49	-15.20	5.42°

Table 8-16 L band decibel returns and phase difference for Sites "A", "B" and "C".

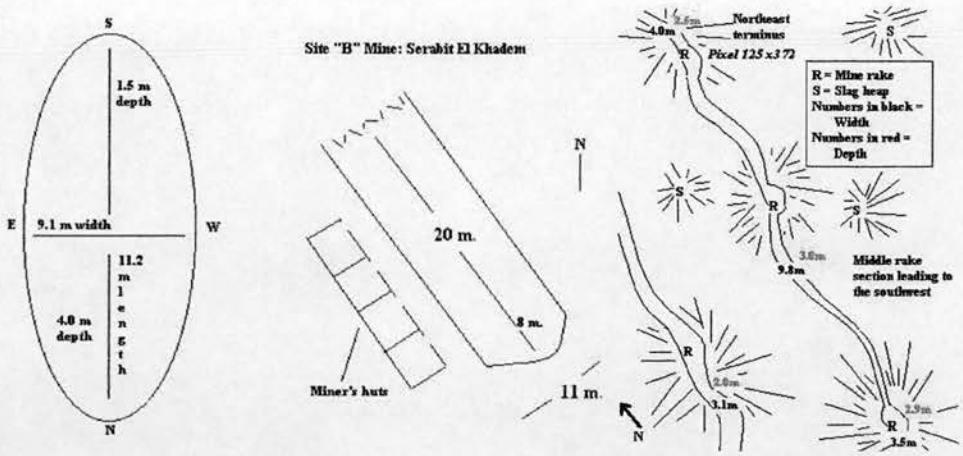

Fig. 8-12 Target mine maps for South Ardachy (Site "A", Chap. 5), Serabit El Khadim (Site "B", Chap. 6), and Conil (Site "C", Chap. 7), left to right.

8.9.3.2.1 C band polarimetric phased differences and decibel responses

With regards to polarimetric phase difference, the C band reports for South Ardachy and Conil exhibit similar values, as noted in Section 8.9.3.2. The South Ardachy (Site "A") C band phase difference report for pixel 1208 x 1640 shows a change in phase difference at -6.99, but interestingly, when viewed in the context of the overall transect via the phase difference absolute value image, it appears that the Cvv polarisation is recording strong decibel responses from the small, short-bladed grasses which grow throughout the mine area until reaching the mine rake. At the mine rake, however, vv polarisation response falls near that of the hh polarisation, thus responding to the depression in the topography. Serabit El Khadim, as discussed in Chap. 6, did not have the appropriate polarisations (hh/vv) to allow polarimetric phase difference analysis.

The Conil (Site "C") phase difference report for pixel 125 x 372 is similar in its magnitude of change to that of South Ardachy (Site "A"), although the Cvv decibel response seems to be affected by the vegetation atop the ore-bearing hillock which the mine rake bisects. The leaves of the *arrayan*, or myrtle shrubs, are dense with a leaf length between 2.5 and 3.5 centimetres and a width of some 2.0-2.5 centimetres. Since these leaves approximate the size of the C-band wavelength, they should cause higher and stronger backscatter returns to the sensor antenna, which are in the decibel return statistics in Table 8-3 and Table 8-4. This is visualised in the phase difference absolute value images for the mine site. Were the C band microwaves able to reach the mine rake unimpeded, the rake's walls might have seen a more equalised decibel return from each of the two polarisations, thus possibly giving a response similar to the South Ardachy mine rake (Site "A").

8.9.3.2.2 L band polarimetric phase difference and decibel responses

The L band phase difference reports for the two applicable mine sites, South Ardachy and Conil, have similar change in phase difference and decibel response strength. At both mine sites the pixels that correspond with the mine rakes have an almost identical hh polarisation decibel response, -15.26 for South Ardachy and -14.49 for Conil. Polarimetric phase difference is nearly equal as well at 6.11° for South Ardachy and 5.42° for Conil. Only the Lvv polarisation decibel responses of the two sites show any great difference at -13.99 for South Ardachy and -15.20 for Conil; this is likely due to the fact that at Conil the mine rake has a thin conglomerate mixture of soil which supports the previously mentioned arrayan bush and masks the underlying rock. Finally, the use of polarimetric phase difference absolute value images visualised these statistics to portray magnitude change.

Referring back to Chapter 3 and the effect of incidence angle on the quantity of backscatter which may be received by a system, it is worth noting the performance of the L band over all the sites. Site "A" had an incidence angle of 28° and a decibel of -15.26. This figure falls within the known performance range of L band in an hh polarisation over rock surfaces at that incidence angle (Ulaby and Dobson, 1989). Site "B" had a 46.9° incidence angle with a decibel response of -21.74. This statistic also meets the known performance parameters of L band in an hh polarisation over a rock surface (Ulaby and Dobson, 1989). Site "C" recorded a decibel response of –14.49 with an incidence angle of 24.1°. Unlike the previous two sites, however, this performance result corresponds with the known parameters for surfaces covered by tall grasses, or shrubs in an hh polarisation (Ulaby and Dobson, 1989). A review of the site photographs through Chapter 7 reveal that this is true, as the ore-bearing hillock which the mine rake bisects has a base covered by tall grass, while its top is covered by the *arrayan*, or myrtle, shrub.

Ideally, a model reflector, or shape, would have been constructed to the dimensions of each target mine, illuminated by polarimetric RADAR to see if similar shapes and decibel returns could be derived. Unfortunately, the practicality and remoteness of the sites made meant this was not possible; to derive the same decibel returns would require identical surface materials, construction of models, and most importantly, a polarimetric Imaging RADAR system. Computer simulation was not possible during this study, as advanced polarimetric analytical software was unavailable. Still, a method was needed to ascertain the ability of the Shuttle Imaging RADAR to discern the topography of the mine sites. Thus, as described in Chapter 4, comparative transects were obtained in the best, near-target areas to compare polarimetric phase difference change and decibel response strength, which is described in the next section.

8.9.3.3 Comparative surfaces and transects

The transect methodology was employed to graphically show the viewer that the Imaging RADAR was detecting surface shape via polarimetry. At South Ardachy (Site "A"), a comparative transect was obtained where the middle pixel, 1215 x 1660, was then compared against the mine rake (See Chapter 5, Section 5.9.3.3.1, Fig. 8-13 and Tables 8-17 and 8-18). Phase difference change was minimal over the sample pixel and decibel strength was as expected over such a surface with short grass.

Fig. 8-13 Comparative transect areas for South Ardachy (left), Serabit El Khadim (middle) and Conil (right).

Site and Pixel Coordinate	C/hh	C/vv (*C/hv for Serabit)	Phase difference
A 1215x1660	-11.53	-11.36	2.07°
B 4286x1664	-15.96	-24.54	N/A
C 225x270	-8.73	-3.02	50.92°

Table 8-17 C band decibel returns and phase difference for Site "A", "B" and "C", comparative transects

Site and Pixel Coordinate	C/hh	C/vv (*C/hv for Serabit)	Phase difference
A 1215x1660	-16.31	-14.12	-1.57°
B 4286x1664	-25.25	-184.97	N/A
C 225x270	-7.20	-11.53	7.44°

Table 8-18 L band decibel returns and phase difference for Site "A", "B" and "C", comparative transects

At Serabit El Khadim while there was sufficient planar surface to obtain a transect, the lack of proper polarimetric RADAR data made comparison impossible insofar as phase difference was concerned (See Chapter 6, Section 6.4, Fig. 8-13, Tables 8-5 and 8-6). The hh polarisation for C and L band offered the only opportunity for comparison as such (Berlin *et al.*, 1986). Referring back to Chapter 6 and the total comparative transect, little change in decibel strength was observed over its length, which was expected over a dense alluvial wadi floor.

Conil had a unique opportunity in that a modern, open pit quarry mine existed near the target mine rake; a decibel response and phase difference response were examined from an area within the mine which had similar reflecting surfaces, although much larger in size. As an aside, this may be demonstrating the limit of the sensor in determining shape and size. These results were presented in Chapter 7, Section 7.9.3.4, Figure 7-32 and Table 7-9. While the decibel response was strong, when incident angle was taken into account it did not correspond well with the known performance data for soil and rock surfaces (Ulaby and Dobson, 1989). This may be because the mine was composed of sandstone, whose response properties are somewhat different than normal rock surface (Blom and Daily, 1981).

The comparative transect at Conil had several significant changes in phase difference and decibel response over its length, although not at the centre comparative pixel; these changes are thought to be due to clearance cairns, or rock piles, beneath the slender unordered wild flowers. The phase difference absolute value images for this site show this graphically.

A thorough comparison has been made of all target mine sites. The next section will conclude the chapter with visualisations of the entire image scene for each region, the Isle of Islay, the Sinai, and southern Spain. It is impossible to compare visualisations, as each scene is unique in its own right.

8.9.4 Imaging RADAR Data fusion, modelling and visualisation

The image scene visualisations for each mining region were created in the same manner as previously discussed in Chapter's 5, 6 and 7. The difference being in that in the following visualisations it is possible to view the mines within the context of the geomorphology and geology of the entire area. Archaeologically, this is important for ascertaining access routes, lines of sight, location, and water sources, to name but a few parameters. The following visualisations illustrate the common feature for all three mine sites, their proximity to the sea. The southern Spain view is unable to depict the nearby Atlantic Ocean due to the orbital swath of the image scene terminating immediately west of the Conil mine site. The Isle of Islay may be seen in Fig. 8-14, the mid-Sinai in Fig. 8-15, and southern Spain in Fig. 8-16.

1:250,000 approx.

1:24,000 approx.

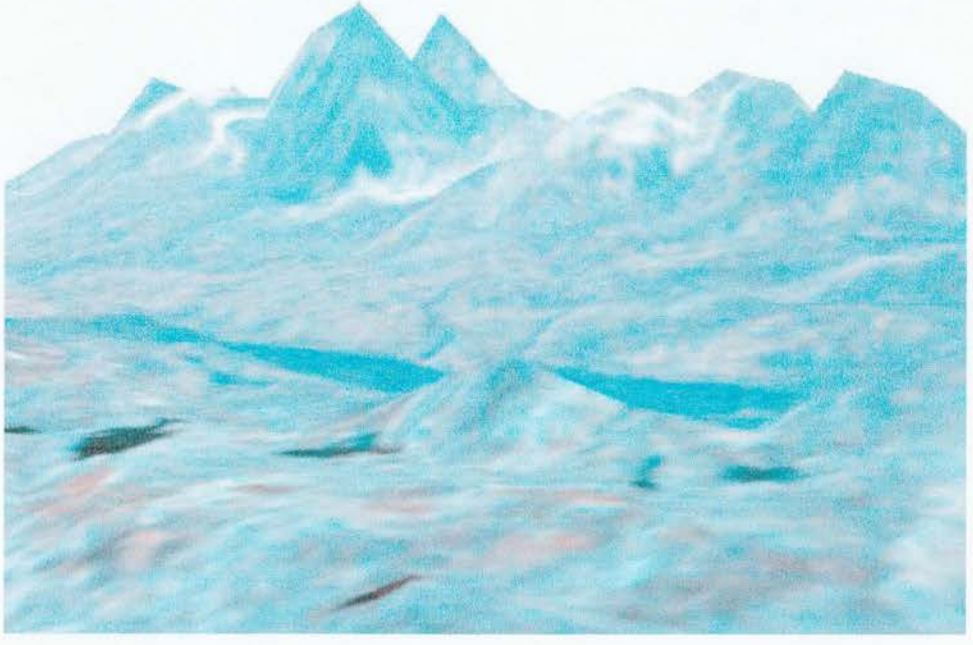

Figure 8-14 The Isle of Islay (top). Bottom, the view from South Ardachy to the Paps of Jura, on the Island of Jura. Simulated fog on the Paps was created by fusing AVHRR data onto the NASA SIR-C/X-SAR data. The terrain is *not* exaggerated as the near Pap rises to some 585 metres in height.

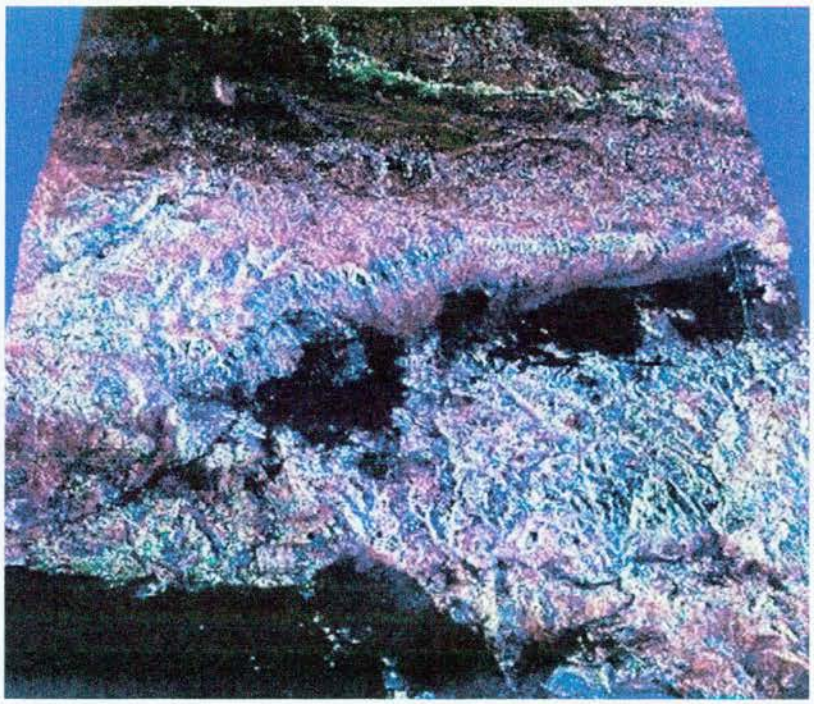

1:250,000 approx.

1:24,000 approx.

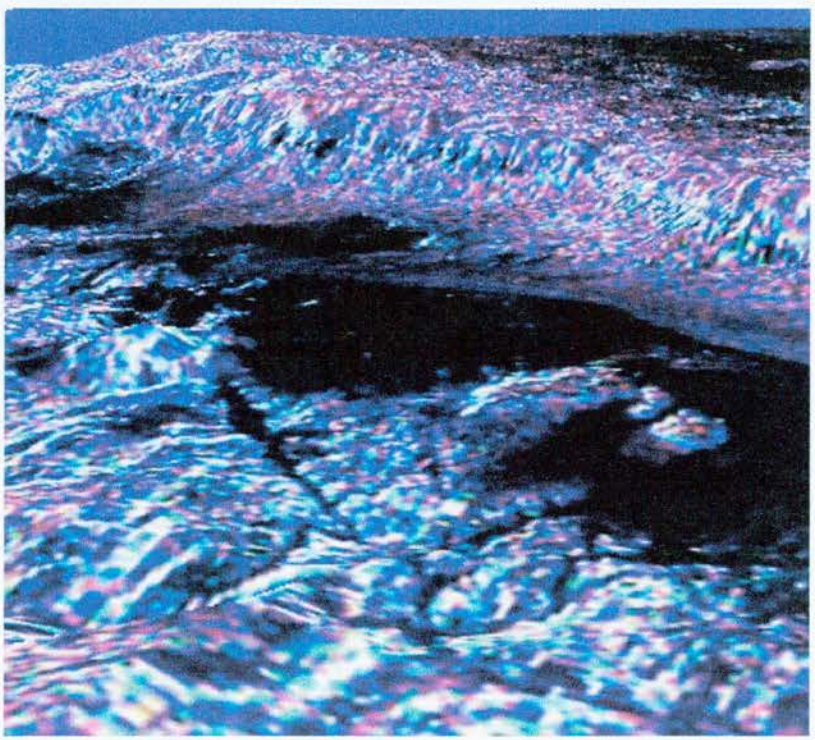

Figure 8-15. The Sinai from the Red Sea (top), foreground to the El Tigh Plateau. Bottom; view over Serabit El Khadim across the Wadi Maghara to the El Tigh Escarpment under a simulated sky.

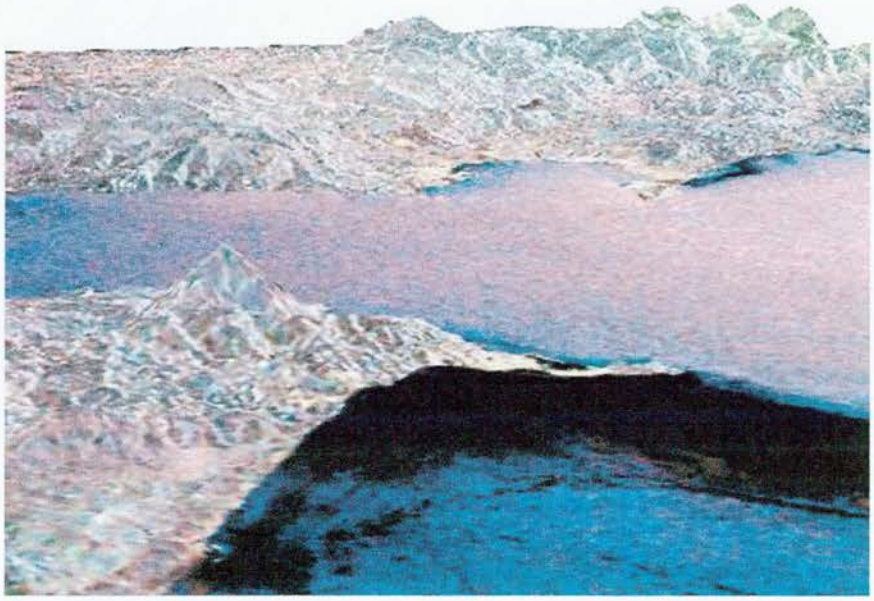

1:250,000 approx.

1:24,000 approx.

Figure 8-16 A view of the Bay of Algeciras, Gibraltar (top), and southern Spain from over Jebel Musa (Mountain of Moses) in Morocco and the Spanish colony of Ceuta. Bottom, a view from the north over Conil to Gibraltar and Morocco. Note the ocean currents detected by the L-band beneath Ceuta Peninsula in the upper image scene.

This concludes the comparison of the target mine site results for South Ardachy, Islay, Serabit El Khadim, the Sinai, and Conil, Spain. Chapter 9 will conclude this work with a concise summary and a short discussion of potential research areas related to the results seen during the course of this study.

Chapter 9
Conclusions

"Scientists have shown that the earth is spherical in shape and surrounded on all sides by water, as though it were a grape floating in water". Ibn Khaldun, c. 1379. (from Khaldun's "Prolegomena" of the "Al-Muqqadima", translated by Charles Issawi, 1987: 38).

The introduction to this study noted that the development of mineral extraction technology was poorly understood. It also noted that the reasons for this lay in the re-working of mine sites, urbanisation and changes in vegetation coverage, all of which have contributed to the loss of early mining evidence. The ability to detect, identify, survey and analyse, large geographical areas for evidence of potential ancient mining sites was deemed to be key to the problem.

This study set out to examine the usefulness of space-borne Imaging RADAR for the detection of potential ancient mineral extraction and processing sites with a view to understanding the regional impact of mineral extraction over areas too large to be amenable to conventional survey techniques; a topographic perspective drove this analytical approach.

This work then tested the capability of NASA's Space Shuttle multipolarimetric Imaging RADAR system for the detection of ancient mine sites by polarimetric means and by comparing decibel responses. Furthermore, its aim was to test Imaging RADAR detection capabilities in three distinct climatic regions of the world and to assess performance degradation via decibel response in comparison to known RADAR parameters. Next it set out to analyse, then compare, each of the ancient mine sites in the following categories, historical and physical geography, geology, geomorphology, vegetation, topography and archaeology. Finally it aimed to demonstrate visualisation of the environment by fusing digital terrain elevation data and Imaging RADAR data to create virtual landscapes. The principal conclusions of these tests are listed, item-by-item, in the following section. A discussion on further archaeological applications and remote sensing systems as well as the future of remote sensing archaeology follows in Section 9.2

9.1 Principal conclusions

- *Could references by classical writers be used to locate ancient mining regions?* In Chapter 4 and Appendix IV it was shown how references by Herodotus, Pliny the Elder and Strabo were used to locate mining regions for investigation by remote sensing.

- *Does historical geography provide sufficient historical references and geographic descriptions to select specific ancient mining sites for remote sensing analysis by Imaging RADAR?* Chapters 5, 6 and 7 presented the specific historical and geographic data which allowed specific mines within a region to be targeted for investigation; in Chapter 7 a *new* mine site, Conil, was identified by using toponymic analysis which was then analysed for its decibel response and phase difference responses; it was found to be similar in characteristics to the site at South Ardachy in Scotland (Chap. 5).
- *Can a correlation of metallurgical toponyms to the historical geography and geology of any of the mining regions be used as a means for establishing a methodology for the application of remote sensing?* Yes, in Chapter 4 and Appendix IV a toponym model was created for the targeting of potential ancient mine sites within the southern portion of Andalusian Spain. *Do toponyms concerning minerals and the corresponding geology indicate a maximum likelihood of ancient mining within an area?* The model developed during the course of the investigation was tested in only one instance, but was successful in its limited area of application. Further testing of the approach is warranted though.
- *Can the geology and geomorphology of each mine site area be analysed by Imaging RADAR?* Yes, the decibel statistics for each target mine site corresponded with the known response values for their particular geology and the RADAR bands and polarisation modes used (Ulaby and Dobson, 1989).
- *Does the local climate of each mining area affect the performance of the multipolarimetric Imaging RADAR?* No, the decibel statistics for each target mine corresponded with the known response values for the geology, RADAR bands and polarisation modes used, so no apparent degradation was found. However, local weather conditions were largely ideal with no significant atmospheric disturbances.
- *Could a comparative performance matrix showing the returns and analyses of specific polarimetry between all sites reveal a unique phase difference response for the target mine sites?* The Imaging RADAR noted topographic change at the South Ardachy mine via phase difference and decibel response in both C and L bands but was unable to discriminate a specific reflector type. At Serabit El Khadim it was not possible to undertake phase difference analysis due to the mode of the Shuttle Imaging RADAR. At the Conil mine site, as with South Ardachy, changes in topography were recorded via the C and L band information but the Imaging RADAR was again unable to discriminate a specific reflector. Phase difference absolute value imagery was able to map the magnitude of phase change for all sites.

- As observed in the Islay data set, analysis indicated that topographic differences between a mine site and its surrounding area may be detectable through an analysis of absolute phase differences. However, the presence of large phase differences co-incident to the target mine sites did not occur likely due to sensor resolution and system orientation and band selection.
- Following on with the inability to identify a unique phase difference response, this is likely due to the different spatial dimensions of the South Ardachy and Conil, obscuring vegetation at Conil and, of course, the limitations of the Imaging RADAR system in resolution and band selection. Advanced computer modelling of the mines and their interaction with microwaves would also obviously assist in matters as well.
- *Finally, could landscape visualisations for archaeological analysis of the ancient mine areas be created?* It was demonstrated that not only local area landscape visualisations could be achieved, as seen in Chapters 5, 6 and 7, but that large-scale landscape visualisations could be created which would allow efficient reconnaissance and survey of target regions.

9.2 Discussion and future prospects

When this research study began, the author hoped that the long-promised Shuttle RADAR Topographic Mission (SRTM) to map the world would take place on schedule, thereby allowing the use of its data for the topographic analysis portion of this work. Unfortunately, it did not. Still, by utilising an amalgam of cartographic data and existing digital terrain data products, a useful topographic data set was constructed for each study site and this is the most important point for archaeology and remote sensing.

Archaeology stands on the precept that it is the most interdisciplinary of all sciences, blending cultural, biological, geological, geographic, topographic and other environmental scientific analyses to construct new theorems about mankind's existence. Yet, as was pointed out in the foreword to this work, the science of topography has been abandoned due to academic lethargy, thus leading to the failure by archaeology to grasp arriving technologies such as Imaging RADAR which can perform advanced topographic analysis. What topographic science via remote sensing offers archaeology is the chance to observe and define the landscape of mankind on a scale and complexity scarcely imaginable a decade ago.

Examples of what an archaeologist could achieve from macro-topographic analysis of landscapes and micro-topographic analysis of individual sites abound. In the example of ancient mining used here, it can be determined from cross-sectional convexity and longitudinal convexity analysis what the watershed limits were surrounding each mine. This information could in turn drive the scope and scale of chemical analysis surveys in the surrounding landscapes in order to determine the spread of metals and their by-products.

As an example, Cressey's (1995) work to determine why Loch Bharradail beneath the South Ardachy mine complex showed high metal pollution and nearby Loch Fada did not, the author did not have access to digital topographic data nor topographic modelling and analysis tools and thus was unable to ascertain a satisfactory answer. Returning to Chapter 5 of this work, slope, aspect, and cross-sectional analyses show that Loch Fada is separated from Loch Bharradail by a large Dalriadan limestone outcrop that splits the landscape, thus illustrating what Cressey could not know at the time.

The definition of the watershed around a mine site such as South Ardachy may also indicate whether the earliest mining was performed in support of small-scale localised agricultural needs for implements, for example. Current work by this author at a newly discovered series of mines south of the South Ardachy mine area provide an example of this. The Airigh Guadhire mines have four hut-circles nearby, tentatively dated to the Bronze Age, several medieval fields characterised by their rather oval shape and an abandoned settlement of some 20 structures, dated to the 18th century at present (Caldwell and McKay, forthcoming). The presence of seven limestone kilns and three small rock quarries indicate considerable agricultural improvement and use over a long period of time. This landscape was noted while studying the Shuttle Imaging RADAR and topographic data for this study, then reconnoitred by high-resolution, low-altitude National Environmental Research Council (NERC) full-colour aerial photography. This imagery then was used to draw a survey plan *before* a field survey, which demonstrates the potential for topographic analysis driving further remote sensing analysis of any archaeological site.

Although not demonstrated in this work, line-of-sight (LOS) analysis via topographic analysis software offers a dramatic new opportunity for archaeologists. Forthcoming work will demonstrate how precision digital terrain models overlain with fused multi-spectral and RADAR can be used to quantify and qualify a viewshed area (Jackson, Heald and McKay, forthcoming). In a study of brochs on Scotland's north-east coast LOS analysis was used to classify the viewshed from each broch over a particular landscape i.e. maritime or land, calculate the total viewshed area and then rank them according to inter-visibility. This is a series of techniques which is immediately applicable to spatially oriented archaeology or to construct new social theorems in cultural archaeology pertaining to land use and importance.

While it is not possible to present every form of topographic analysis and its potential use to the archaeological community, this much can be said, if a complete topographic analysis has not been carried out on a given site, then the archaeologist can not be said to have a total understanding of the landscape. Any theorems created on insufficient topographic knowledge are, in this author's mind, suspect at best. Full topographic analysis offers the chance to understand the relationships of cultures within their landscapes and how these cultures viewed themselves within their landscapes by the locations of their buildings, roads, monuments and toponyms. In Scotland, where ancient Gaelic culture never constructed on the scale of cultures such as the Romans in England, only toponyms remain to give any indication as to how Gaels viewed their native landscapes. Yet, Gaelic is a language evocative of place and time requiring a topographic perspective to understand it.

Turning to the future of space-borne Imaging RADAR systems, there are several potential satellite systems that may be lofted into orbit, among them, ALOS/PALSAR, RADARSAT 2, ENVISAT and Terra-SAR. ALOS, a sensor supported by the Japanese space agency, can be considered representative of the new generation of multi-use, multi-purpose satellites that can perform optical, spectral and microwave remote sensing operations. The current specifications for the satellite are to include a 2.5m resolution panchromatic radiometer, known as PRISM, an advanced visible and near-visible sensor known as AVNIR-2, and PALSAR, a phased-array L-band synthetic aperture RADAR (NASDA, 2001). The lofting of a satellite with full-time L-band capability is, in this author's opinion, critical for future RADAR related archaeological applications. This research study was limited to target site selection, even if the Shuttle RADAR Topographic Mission data had been available, because the L-band RADAR of the SIR-C/X-SAR system was not deployed due to weight and other payload considerations (NASA, 2001). This study was thus forced to rely on the data gathered during the 1994 missions.

RADARSAT-2, sponsored by Canada and United States, will carry an improved C-band RADAR sensor giving it much higher resolution, possibly approaching 3 metres, although this has been a subject of debate due to its possible military use by unfriendly nations. Still, any C-band resolution beneath 5 metres in resolution dramatically increases its usefulness for archaeological survey and analysis, particularly pertaining to topography (NASA, 2001).

ENVISAT, another multi-purpose satellite like ALOS, is a project supported by the European Space Agency (ESA). Among the more interesting aspects of this platform is its intended use for dedicated topographic mapping. Coupled with a high-resolution spectral system ENVISAT should offer the possibility of fused spectral-RADAR image products that could dramatically enhance archaeological landscape analysis (ESA, 2001).

Other space-borne Imaging RADAR systems such as Terra-SAR and Light SAR are more ephemeral in their probability of inception. Budget cuts by NASA and other international space agencies as of the writing of this work call into question the validity of many proposed space-borne RADAR satellite programs. However, in the 2001 military and humanitarian campaign of the United States in Afghanistan, the failure to fund a full-time, fully polarimetric, multi-band space-borne Imaging RADAR, was dramatically brought home on many occasions. However unfortunate, it is hoped that this experience will be driven home before governmental funding bodies, both for military and civilian applications of Imaging RADAR systems (NASA, 2001).

These proposed RADAR satellites bring to light many of the problems faced during the course of this research study. Among them were the lack of dual polarisation RADAR data in both C and L bands at all study sites, which made polarimetric phase difference analysis and a full comparison between sites impossible, and the total lack of fully polarimetric RADAR data. Fully polarimetric data would have allowed three-dimensional images of the backscatter responses of each of the image pixels in the study transects to be generated, thus potentially more clearly identifying surface microwave interaction and helping to understand how the mines functioned as reflecting surfaces. Furthermore, problems with remote sensing software and how they induct, synthesise and display RADAR imagery and statistics, were yet another obstacle. The analysis of all the target mine sites in this work was forced to be reworked after it was discovered that the data was not correctly formatted fully polarimetric data, but merely dual polarimetric data, and then that that the remote sensing software was unable to synthesise from the dual polarimetric RADAR data a fully polarimetric data set, as was stated by the software creators. Data coverage and data type were the primary limiting factors in this study.

While not overtly stated in the text, this study was also largely an exercise in data mining of archival remote sensing data; all data sets in this work were taken some seven years before this study began. One of the worrying problems discovered while obtaining data as esoteric as the AVHRR weather sets, was the fact that some archives remove data after a period of time, reformat the data, thereby making it unusable by more modern software, or more concerning, deleting the data sets entirely. This is a problem to be considered for future remote sensing work requiring temporal data set coverage or for the archaeologist looking for imagery which covers a study area now urbanised. It is through the comparison of data sets archived through time and hence an ability to detect change that is one of remote sensing's key advantages.

Finally, the lack of financial resources for remote sensing archaeology. Archaeology has tended to treat the regimen as a technical toy understood by only a very few remote sensing specialists who treat the science as a hobby. The failure by long-established schools of archaeology throughout the world to innovate and grasp these new technologies seriously endangers their own future existence. At the closure of this work, this author sees the continued attitude that remote sensing archaeology must take place in a university-based computing centre on computer work stations. Ironically, this author, a long-time friend of Dr. Thomas Sever, Remote Sensing Archaeologist for NASA, notes that his work in the 1980s was undertaken on field deployed computers, while 95 percent of this author's study was performed aboard a computer notebook *in situ*.

The approaching retirement of Dr. Sever, Dr. El Baz at Boston's Centre for Remote Sensing and the failure of archaeological departments around the world to support remote sensing archaeology means the discipline is threatened with decline. This author's own experience where the discipline is treated as a curiosity by archaeologists and looked down upon by physical scientists does little to further any reason to support the remote sensing archaeological efforts.

The solutions to many of the technical problems may occur with the launch of the new RADAR satellites and with more advanced computer programming allow more intuitive image processing software. The new space-borne platforms will provide the necessary fully polarimetric data in the wavelengths beneficial to archaeological survey and allowing the use of double-bounce mapping routine's similar to Freeman's original MAPVEG routine; release of the SRTM interferometric data will provide the potential for a global high resolution digital terrain model of the world (NASA, 2001).

The issue of remote sensing archaeology and its decline is more problematic. The discipline can probably only be saved by schools of geography overtaking and subsuming archaeological departments whose curriculum has ceased to be innovative and timely. This would be the ultimate irony for a discipline which has its very existence predicated upon the study of the rise and fall of cultures and their failure to oft times adapt. This work, like many past civilisations, has now come to its end as well.

Bibliography

Abdelsalam, M. G., R. J. Stern, H. Schandelmeier, and M. Sultan. 1995. "Deformational history of the Neoptoterozoic Keraf Zone in NE Sudan revealed by shuttle Imaging Radar". *Journal of Geology*. Vol. 103, no. 5, USA. 475-491.

Aldred, C. 1998. *The Egyptians*. London, UK. 72-73, 75-77, 92-93, 118.

Alessandro, C. 1994. "Rome Links Ancient Cartographic Data with GIS Technology." *GeoInfo Systems*. Mar. 48.

Allan, J.A. and T.S. Richards. 1983. "Use Of Satellite Imagery In Archaeological Surveys". *Libyan Studies*, No. 14, United Kingdom. 4-8.

Angelis, F. and G. Tsetskhadze. 1994. *The Archaeology of Greek Colonization*. Insitute of Archaeology, Oxford, England. 72.

Aragon, A. *Los Fenicios en Cadiz*. 2000. Universidad de Cadiz, Spain. Unpublished.

Arribas, A. 1964. *The Iberians*. New York, USA, 1964. 32-54.

Aslam, A, M.C. Dobson, and F. Ulaby. 1978. "Effects of Vegetation Coverage on RADAR Sensitivity to Soil Moisture". *IEEE Transactions of Geoscience and Remote Sensing*, Vol. 20. WA, USA. 476 – 486.

Aubet, M. 1994. *The Phoenicians and the West.* Cambridge, UK. 218-230, 236-237.

Avery, T. E. and T.R. Lyons. 1978. *Remote Sensing: Practical Exercises on Remote Sensing In Archaeology – Practical Supplement No. 1*.Cultural Resources Management Division, National Park Service, Department of the Interior, Washington, D.C., USA. 1-6.

---------- 1981. *Remote Sensing: Aerial And Terrestrial Photography for Archaeologists – Supplement No. 7*. Cultural Resources Management Division of the U.S. Department of the Interior, Washington, D.C., USA. 1-12.

Bahn, P. 1996. "Treasure of the Atapuerca." *Archaeology*. Boston, USA. 45-48.

Baird, D. 1988. *Inside Andalusia*. Malaga, Spain. 1, 25, 12-80.

Bamford, J. 2001. "Body of Secrets". London, UK. 94.

Baramki, D. 1961. *Phoenicia and the Phoenicians*. Beirut, Lebanon, 1961. 25-47.

Barasino E. and B. Helly. 1985. "Remote Sensing and Archaeological Research in Thessaly (Greece)". *New Prospects in Archaeological Landscape* from the Proceedings EARSeL/ESA Symposium, "European Remote Sensing Opportunities", Strasbourg, France, 31 Mar-3 Apr 1985 (ESA SP-233). 203-209.

Bard, K. 2000. *"The Emergence of the Egyptian State". The Oxford History of Ancient Egypt.* I. Shaw (Ed.). Oxford, UK. 61-69.

Barnard, N. and T. Tamotsu. 1975. *Metallurgical Remains of Ancient China*. 5-8, 22-27.

Barrett, A.H. and E. Lilley. 1963. "Mariner-2 Microwave Observations of Venus", *Sky and Telescope*. New York, USA. 192-95.

Bartlett, D. 1993. *GIS and the Coastal Zone: An Annotated Bibliography.* Santa Barbara: National Center for Geographic Information and Analysis. 1-2.

Bartov, Y. 1985. "The Geological Structure of Sinai". *The Atlas of Israel*. New York, USA. 1+.

Bel Ortega, C. and A. G. Lazaro. 1990. *Guias Naturalisticas de la Privincia de Cadiz*. Vol. 1, Diputacion de Cadiz, Cadiz, Cadiz, Spain. 1-148.

Bell, F. G. 1998. *Environmental Geology: Principles and Practice.* Oxford, UK. 415-453.

Benson, V. 1989. *Great World Atlas.* New York, USA. 12-13.

Berlin, G. L., M. A. Tarabzouni, A. H. Al-Naser, K. M. Sheikho, and R. W. Larson. 1986. "SIR-B subsurface imaging of a sand-buried landscape, Al Labbah Plateau, Saudi Arabia". *IEEE Trans. Geoscience Remote Sensing*, vol. GE-24, no. 4, USA. 595-602.

Berlin, G. L., G. G. Schaber, R. C. Kozak, and P. Chavez, Jr. 1982. "Cliff- and-slope topography of part of the Grand Canyon, as characterized on a Seasat radar image". Letter Comm. in *Remote Sensing of Environment*, vol. 12. WA, USA. 81-85.

Blom, R., R. Crippen and C. Elachi. 1981. "Detection of Subsurface Features in SEASAT RADAR Images of Means Valley, Mojave Desert, CA". *Geology*, vol. 12. 346-349.

Blom, R. and M. Daily. 1982. "Radar image processing for rock type discrimination". *IEEE Trans. Geosci. Remote Sensing*, vol. GE-20, USA, 1982. 343-351.

Boardman, J. 1999. *The Greeks Overseas*. London, UK. 210-225.

Bonald, J. 2000. "Cadiz: Sierra, mar y duende". *Geo*. Madrid, Spain. May. 74-86.

Born, M. and E. Wolf. 1964. *Principles of Optics*. New York, USA. 5-37.

British Geological Survey. 1995. *The Northern Highlands of Scotland*. London, UK. 165, 177, 179.

British Geological Survey. 1997. *North Islay - Scotland Sheet 27: Soil and Drift Edition*. ISBN (folded) 0 7518 3013 5, Pub. Site unknown.

British Ordnance Survey. 1987. *Landranger Map Series: Sheet 60 – Islay*. London, UK.

Brooks, R.R. and D. Johannes. 1990. *Phyto-archaeology*. Vol. 3. ISBN 093114616X. Timber Press, USA. 1+.

Bovill, E. 1995. *The Golden Trade of the Moors*. Princeton, New Jersey, USA.

Budge, T.K. and S.A. Morain. 1978. *"Remote Sensing: Instrumentation For Nondestructive Exploration Of Cultural Resources – Supplement No. 2"*. Cultural Resources Management of the National Park Service, U.S. Department of the Interior, Washington, D.C., USA. 1+.

Burn, A.R. and A. Selincourt. 1972. *Herodotus: The Histories*. London, UK. 283-361.

Butts, A. 1954. "Copper: The Science and Technology of the Metal, Its Alloys and Compounds". *American Chemical Society Monograph Series*. New York, USA. 5-12.

Caldwell, D. and G. McKay. Forthcoming. *Airigh Guadhire*. Edinburgh, UK.

Casanova, I.R. 2000. "El Ocaso de Tartessos". *Historia 16*, No. 289. Madrid, Spain. 62-71.

Cech, B. and G. Walach. 1998. "The Importance of Integrated Prospection Techniques for Archaeological Investigations on Mining Sites in Rugged Alpine Topography". *Optical Remote Sensing for Industry and Environmental Monitoring*. Editor(s): Upendra N. Singh, NASA Langley Research Ctr., Hampton, VA, USA; Huanling Hu, Anhui Institute of Optics and Fine Mechanics, Hefei Anhui, China; Gengchen Wang, Institute of Atmospheric Physics, Beijing, China. 25.

CCRS. 2001. "A RADAR Remote Sensing Tutorial". http://www.ccrs.nrcan.gc.ca

Champion, T., C. Gamble, S. Shennan, and A. Whittle. 1984. *Prehistoric Europe*. 26.

Clark, J.G. D. 1952. *Prehistoric Europe; the economic basis*. London, UK. 34-58.

Clavero, J. 1997. *Ecoguia: Grazalema y Otras Sierras de Cadiz*. Josmar S.A. for Anaya T.C., Madrid, Spain, 1997. 140-177.

Coles, J.M. and A.F. Harding. 1979. *The Bronze Age in Europe*. London, UK. 22-87.

Collins, R. 1998. *Oxford Archaeological Guide to Spain*. Oxford, UK, 1-38, 106, 262, 270.

Collis, J. 1984. *The European Iron Age*. London, UK. 13-78.

Coronel de Militar Cartografia. 2000. *Mapa de Distrito del Vejer de la Frontera, Espana: 1:50,000*. Oficina de Militar Cartografia, Madrid, Spain.

Cotterell, A. 1980. *The Penguin Encyclopedia of Ancient Civilizations*. London, UK. 23-24, 133, 136, 304-308.

Cowan E.J. and R.A. McDonald. 2000. *Alba: Celtic Scotland in the Medieval Era*. Phantassie, UK. 167-218.

Craddock, P. 1998. *Early Metal Mining and Production*. Edinburgh, UK. 8-11.

Cressey, M. 1995. *The Identification of Early Lead Mining: Environmental, Archaeological and Historical perspectives from Islay, Inner Hebrides, Scotland*. Unpublished dissertation.

Cunliffe, B.W. 1978. *Iron Age Communities in Britain*. London, UK. 14-37.
----------. 2001. *Pytheas the Greek*. London, UK. 1+.
Curlander, J. C., F. Leberl, and F. A. Kruse. 1992. "Geometric ortho-rectification and generation of S-zero image products from multiple incidence angle synthetic aperture radar images". *Proceedings of the International Geoscience and Remote Sensing Symposium (IGARSS'92)*, 26-29 May, 1992. Houston, TX, USA. 111- 113.
Cutrona, L.J. 1970. "Synthetic Aperture RADAR". Chapter 23 of *RADAR Handbook*. New York, USA. 23-3.
Cutrona, L.J. and G.O. Hall. 1961. "A Comparison of Techniques for Achieving Fine Azimuth Resolution". *IRE Transactions*, MIL-6, USA. 119-133.
Cutrona, L.J., W.E. Vivian, E.N. Leith, and G.O. Hall. 1961. "A High Resolution RADAR Combat Surveillance System". *IRE Transactions*, MIL-5, MIT Library, Boston, USA. 128-130.
Cutting, D. and E. Jacobson, J. Meacham, and G. Tepfer. 1994. "Patterns on the Steppe: Applying GIS to the Archaeology of the Altay Mountains". *GeoInfo Systems*, March. 32-34.
Dahlin, B. and K. Pope. 1989. "Ancient Maya Wetland Agriculture: New Insights From Ecological And Remote Sensing Research". *Journal of Field Archaeology*, Vol. 16. WA, USA. 32-34.
Daily, M., T. Farr, C. Elachi, and G. Schaber. 1979. "Geologic Interpretation from Composited Radar and Landsat Imagery". *Photogram. Engr. Rem. Sens.*, 45, WA, USA. 1109-1116.
Dame and Moore's Center for International Development and Technology. 1982. *Sinai Development Study, Phase I, final Draft Report*. Vol. III. London, UK. 4-11.
Dana, P. 2001. "An Overview of the GPS System." *Gcraft*. Internet. http://www.utexas.edu/depts/grg/gcraft/notes/gps/gps.html
Danin, A. 1983. *Desert Vegetation of Israel and Sinai*. Jerusalem, Israel. 22-119.
Davis, F.W. and D.S. Simonett. 1991. *Geographic Information Systems: Principles and Applications*. Goodchild, Michael, David McGuire, and Dave Rhind. Vol. 1. New York, USA. 197.
Davy, H. 1823. *On a new phenomenon of electro-magnetism*. London, UK. 153-158.
Dawson, A.G. 1982. "Late Glacial Sea Level Changes and Ice Limits in Islay, Jura, and Scarba, Scottish Inner Hebrides". *Scottish Journal of Geology*, Vol. 18. 195-199.
Day, D., Logsdon, J.M. and B. Latell. 1998. *Eye in the Sky*. Washington, DC, USA. 48-85.
Defense Mapping Agency (DMA). 1992. "Vector Data Product Format." *Digital Chart of the World*. NIMA, Washington, DC, USA. CD-ROM.
Desroches-Noblecourt, C. 1969. *Tutenkhamen*. London, UK. 61-75.
Doren. 1991. *The Life of Benjamin Franklin*. USA. 112-145.
Druss, M. 1992. "Recovering History with GPS." *GPS World*, Apr. Boulder, USA. 32-36.
Durney, C. and C. Johnson. 1969. *Introduction to Modern Electromagnetics*. New York, USA. 39.
Ebert, J.I. 1984. "Remote Sensing Applications In Archaeology". *Advances in Archeological Method and Theory*, Vol. 7. WA, USA. 293-353.
Ebert J.I. & T.R. Lyons. 1979. "Remote Sensing In Archaeology, Cultural Resources Treatment and Anthropology: The United States Of America In 1979". *Aerial Archaeology*, No. 5, WA, USA. 1-19.
Edison, A.R., Moore, R.K. and B.D. Warner. 1960. "RADAR Return Measured at Near Vertical Incidence". *IRE Transactions*, Washington, DC, USA. 246-254.
Ehlers, M. 1989. "Integration of Remote Sensing with GIS." *PE&RS*, Nov. WA, USA. 1621+.

Ehrenreich, R. M. 1975. "*Trade, technology and the iron-working community in the Iron Age of Southern Britain*". *BAR, British Series* 144. London, UK. 66-83.

Elachi, C., C. Breed, W. E. Brown, J. B. Cimino, L. Dellwig, T. Dixon, A. England, D. Evans, J. Ford, H. MacDonald, P. Martin-Kaye, H. Masursky, J. F. McCauley, F. Sabins, R. S. Saunders, and G. Schaber. 1982. "Shuttle Imaging Radar (SIR-A) experiment: Preliminary Results". *Science*, vol. 218. Washington, DC, USA. 996-1003.

Elachi, C, W. E. Brown, J. B. Cimino, T., Dixon, D. L. Evans, J. P. Ford, R. S. Saunders, C. Breed, H. Masursky, J. F. McCauley, G. G. Schaber, L. Dellwig, A. England, H. MacDonald, P. Martin-Kaye, and F. Sabins. 1982. "Shuttle imaging radar experiment", *Science*, v. 218, no. 4576. Washington, DC, USA. 1004-1020.

Elachi, C., J. B. Cimino, and M. Settle. 1986. "Overview of the Shuttle Imaging Radar-B Preliminary scientific results". *Science*, vol. 232, Washington, DC, USA. 1511-1516.

Elachi, C., Y. Kuga, K. C. McDonald, K. Sarabandi, T. B. A. Senior, F. T. Ulaby, J. J. van Zyl, M. W. Whitt, and H. A. Zebker. *Radar polarimetry for Geoscience applications*. 1990 F.T. Ulaby and C. Elachi editors, Artech House, Inc., USA. 364.

Elachi, C., L. E. Roth, and G. G. Schaber. 1984. "Spaceborne radar subsurface imaging in Hyperarid regions". *IEEE Trans. Geosci. Remote Sensing*, GE-22, no. 4. Bellingham, WA, USA, 1984. 383-388.

El Shazly E.M. 1983. "Space Borne Imagery Interpretation of Mega Features Related To Egyptian Archaeology". *Remote Sensing - Extending Man's Horizon*, International GeoScience &Remote Sensing Symposium, No. 1. 4.1-4.6.

Encylcopedia Brittanica. 2000. "Electricity". http://www.brittanica.com

ENVI. 1997. *Users Guide: ENVI 3.4*. Better Solutions Consulting, Ltd. Liability Co., Lafayette, Colorado, USA. 343, 351, 353, 372-374.

ESA. 2001. *ENVISAT*. http://www.esa.fr

Escacena, J.L. 1985. "Gadir". *Aula Orientalis*, Vol. 3. Madrid, Spain. 39-58.

Eyal, M. 1985. "Geological History of Israel and Sinai". *Atlas of Israel*. Tel Aviv, Israel. 82.

Evans, D. L., T. G. Farr, J. P. Ford, T. W. Thompson and C. L. Werner. 1986. "Multipolarization radar images for geologic mapping and vegetation discrimination". *IEEE Trans. Geosci. Remote Sensing*, vol. 24, no. 2. Bellingham, WA, USA. 246-257.

Faraday, M. 1993. *Experimental researches in electricity*. R. & J. E. Taylor, London, UK. Original editions 1839-1855. 1+.

Farley J.A., Limp W.F. and J.Lockhart. 1990. "The Archaeologist's Workbench: Integrating GIS, Remote sensing, EDA and Database". *Interpreting space: GIS and Archaeology*. Allen K.M.S., Green S.W. & Zubrow E.B.W. (Eds.) New York, USA. 141-164.

Farr, T. G. and A. R. Gillespie. 1984. "Measurement of micro-relief on alluvial fans and its relation to age, lithology, and radar response". *Geological Society of America Abstracts with Program*, vol. 16. Washington, USA. 503-506.

Fiennes, R. 1992. *Atlantis Of The Sands*. London, UK. 1-135.

Fitzgerald, P. 1978. *Ancient China*. Oxford, UK. 112.

Forbes, R.J. 1950. *Metallurgy in Antiquity*, Leiden, Germany, 1950. 2-12, 14-17.

Fowler, M.J.F. 1996. "Declassified Intelligence Satellite Photographs". *AARGnews*, No. 13, United Kingdom. 30-35.

Fung, A., R.Moore, and F. Ulaby. 1981. *Microwave Remote Sensing, Vol. 1*. Reading, MA, USA, 1981. 1+.

---------- *Microwave Remote Sensing. Vol. II*. Reading, MA, USA. 1+.

Fung, A., R.Moore, and F. Ulaby. 1986. Microwave *Remote Sensing. Vol. III*. Reading, MA, USA. 1+.

Gaffney V., Ostir K., Podobnikar T. & Stancic Z. 1996. "Satellite Imagery And GIS Applications In Mediterranean Landscapes". *Interfacing the past: Computer applications and quantitative methods in archaeology*, CAA No. 95 Vol. II. Kamermans H. & Fennema K. (Eds.). University of Leiden, Germany. 338-342.

Galan, M.B. 2000. *"El Fabuloso Reino de Argantonio". Historia.* Madrid, Spain. 57-63.

Gallagher, M.J. "Metalliferous Veins of Islay, Scotland". Contribution to *South of Scotland Geochemical Atlas.* British Geological Survey, Interim report, 1991:1+.

Garcia, J.O. and E.U. Moron. 1991. *El Lenguaje de la Mar.* Cadiz, Spain. 1-5.

Gibbon, E. 2000. *The History of the Decline and Fall of the Roman Empire.* Penguin Books, London, UK. 11-12.

Gimbutas, M. 1965. *Bronze Age Cultures in Central and Eastern Europe.* The Hague, Netherlands. 20.

Gjerstad, E. 1973. *Early Rome.* Vol. 6 of 6. London, UK. 1+.

Goettler, G.W., N. Firth and CC. Huston. 1973. *A Preliminary Discussion of Ancient Mining in the Suktunate of Oman.* Journal of Oman Studies. Oman. 43-55.

Graham-Campbell, J. and C. E. Batey. 1998. *Vikings in Scotland.* Edinburgh, U.K. 71-95.

Greenwood. 1997. *The Sinai*, University of Texas Press, Austin, Texas, USA. 11-25.

Guo, H., L. Zhu, Y. Shao, and X. Lu. 1996. "Detection of structural and lithological features underneath a vegetation canopy using SIR-C/X-SAR data in Zhao Qing test site of southern China". *Journal of Geophysical Research*, vol. 101, no. E10, USA. 23,101-23,108.

Gutierrez Mas, J.M., M. Algara, B. Dominguez, and J.P. Moral Cardona. 1991. *Introduccion a la geologica de la Provincia de Cadiz.* Universidad de Cadiz, Spain. 1+.

Hammond, J. 1994. *Hammond: Atlas of the World-Concise Edition.* Maplewood, NJ, USA. 74-75.

Harden, D. 1962. *The Phoenicians.* New York, NY, USA. 1+.

Harger, R.O. 1970. *Synthetic Aperture RADAR Systems: Theory and Design.* New York, NY, USA. 110-127.

Harrison, R.J. 1988. *Spain at the dawn of history : Iberians, Phoenicians, and Greeks.* New York, N.Y., USA. 22-145.

Hayes, W. 1965. *Most Ancient Egypt.* Chicago, IL, USA. 35-83.

Healy, J.F. 1978. *Mining and Metallurgy in the Ancient Greek and Roman World.* London, U.K. 57-62.

Henderson, F.M. 1975. "RADAR for Small-scale Land Use Mapping". *Photogrammetric Engineering and Remote Sensing.* New York, NY., USA, 1975. 307-320.

Hendrickx, S. and P. Veermersch,. 2000. *""Prehistory: From the Paleolithic to the Badarian Culture". The Oxford History of Ancient Egypt.* Shaw (ed.). Oxford, UK. 13-43.

Herodotus. 1996. *The Histories.* London, UK. 65.

Hobbs, J. 1989. *Bedouin Life in the Egyptian Wilderness.* Austin, TX, USA. 46-78.

Hoffman, W.G. 1955. *British Industry 1700-1950.* Oxford, UK. 19-22.

Holcomb, D. W. 1992. "Shuttle Imaging RADAR and Archaeological Survey In China's Taklamakan Desert". *Journal of Field Archaeology*, Volume 19. Boston, MA, USA. 129-138.

Homer. 1967. *The Odyssey of Homer.* Translation by Richard Lattimore. New York, NY, USA. 32, v. 180.

Hopkins, A. 1995. *Spain.* New York, NY, USA. 224-239.

Hublin, J. 1996. "The First Europeans." *Archaeology.* Jan.-Feb. Boston, MA, USA, 36-44.

Hunter, James. 2000. *Last of the Free.* Edinburgh, UK. 219-221.

Hurst, H. and L.E. Stager. 1978. "A Metropolitan Landscape: the late Punic port of Carthage". *World Archaeology.* No. 9. Washington, DC, USA. 334-346.

Instituto de Cartografia de Andalucia. 2000. *Modelo digitale de los elevaciones*. Edicion: Provincia de Cadiz, LTC, Seville, Seville, Spain. CD-ROM, DTED Level 1 format.

----------. 2000. *Atlas Interactive de Andalucia*. LTC, Seville, Seville, Seville, Spain, 2000. CD-ROM.

----------. 2000. *Base de Datos de Toponimos*. Edicion: Provincia de Cadiz, escala 1:10,000, LTC, Seville, Seville, Seville, Spain. CD-ROM, DBF format.

----------. 2000. *Mapa Topografico de Andalucia*. Edicion: Cadiz, escala 1:25,000, Seville, Seville, Spain, 2000. CD-ROM, TIF format.

----------. 2000. *Mapa de los Alcornocales*. Escala, 1:75,000, LTC, Seville.

Instituto Tecnologico Geominero de Espana (ITG). 1994. *Mapa Geologico de Espana*. Edicion: *Cadiz*, 86, 3-12:1-11, 34-36, escala 1:200,000, LTC, Seville, Seville, Spain. Includes survey analysis booklet.

Instituto Tecnologico Geominero de Espana (ITG). 2000. *Mapa Geologico de Espana*. Edicion: *Tahivilla*, 1.074, 13-47: 5-6, 41, escala 1:50,000, LTC, Seville, Seville, Spain. Includes survey analysis booklet.

Jackson, A., A. Heald, G. McKay. Forthcoming. *The Tress-Barry Brochs*. Edinburgh, UK.

Jensen, John. 1986. *Introductory Digital Image Processing*. Englewood Cliffs, NJ, USA. 1+.

Jordan, R.L. 1980. "The SEASAT-A Synthetic Aperture RADAR System". *IEEE Journal of Oceanic Engineering*, OE-5, reprint, Bellingham, WA., USA. 154-164.

Jordan, R. L., B. L. Huneycutt, and M. Werner. 1995. "The SIR-C/X-SAR synthetic aperture radar system". *IEEE Trans. Geosci. Remote Sensing*, vol. 33, no. 4, 1995, USA. 829-839.

Jordan, E.C. and K.G. Balmain. 1968. *Electromagnetic Waves and Radiating Systems*, Prentice-Hall, Englewood Cliffs, NJ, USA. 18-46.

JPL. 2001. *http://southport.jpl.nasa.gov*

Junta de Andalucia. 2000. *Mapa Fisigrafico del Litoral Atlantico de Andalusia*. M.F. 05, "Cabo Roche – Ensenada de Bolonia". LTC, Seville, Spain.

Jupp, C. 1994. *The History of Islay*. The Museum of Islay Life, Port Charlotte, Isle of Islay, UK, 1994.

Kakela, P. J. 1978. "*Iron ore: energy, labor, and capital changes with technology*". *Science* 202. London, UK. 1151-1157.

Kerr, D.E. and H. Goldstein. 1951. "RADAR Targets and Echoes". *Propagation of Short Radio Waves*. Chap. 6. No. 13 in MIT Radiation Laboratory Series. New York, NY, USA. 186.

Kingsley, S. and S. Quegan. 1992. *Understanding RADAR Systems*. Berkshire, UK. 120.

Knauth, P. 1974. *The Metalsmiths*. New York, USA. 36-38.

Kober, W. 1991. "Multiple Image SAR Shape from Shading". *PE&RS*. Jan. 2+.

Kong, J.A. 1975. *The Theory of Electromagnetic Waves*. New York, NY, USA, 1975. 5-78.

Krauss, J.D. and K.R. Carver, K.R. 1973. *Electromagnetics*. New York, NY, USA, 1973. 24-105.

Kruse, F. A., and J. B. Dietz. 1991. "Integration of diverse remote sensing data sets for geologic mapping and resource exploration". SPIE Symposium on Remote Sensing for Geology and Geophysics, 1-5 April 1991, vol. 1492, Orlando, Florida, USA. 326-337.

Kruse, F. A., and J. B. Dietz. 1991. "Integration of optical and microwave images for geologic mapping and resource exploration". *Proceedings of the International Symposium on Remote Sensing of Environment*, Thematic Conference on Remote Sensing for Exploration Geology, 8th, 29 April - 2 May 1991, Denver, Colorado, Environmental Research Institute of Michigan, Ann Arbor, USA. 535- 548.

Kruse, F. A. 1996. "Geologic mapping using combined optical remote sensing and SIR-C/X-SAR data". *Proceedings, 11th Thematic Conference, Applied Geologic Remote Sensing*, 27 - 29 February 1996, Environmental Research Institute of Michigan (ERIM), Ann Arbor, MI, USA. II-142 - II-148.

Latham, C. and A. Stobbs. 1999. *Pioneers of RADAR.* Brigend, UK. 1-3.

Leakey, M.D. 1971. *Olduvai Gorge: Vol. 3. "Excavations in Beds I and II 1960-63".* Cambridge, UK. 1-8.

Lebouef, J.P. and A. Masson-DeTourbet. 1950. *La Civilisation du Tchad.* Paris, France. 3-8.

Lee, J. S. 1981. "Refined filtering of image noise using local statistics". *Computer Graphics and Image Processing*, vol. 15. Washington, DC, USA. 380-389.

Lee, J. S., I. Jurkevich, P. Dewaele, P. Wambacq, and A. Oosterlinck. 1994. "Speckle filtering of synthetic aperture radar images: A Review". *Remote Sensing Reviews*, vol. 8. Washington, DC, USA. 313-340.

Lillesand, T.M. and R.W. Kiefer. 2000. *Remote Sensing and Image Interpretation.* 4th ed., John Wiley and Sons, Inc. New York, NY, USA. 26, 616-691.

Lopes, A., E. Nezry, R. Touzi, and H. Laur. 1993. "Structure detection and statistical adaptive filtering in SAR images". *Int. J. Rem. Sens.*, vol. 14. Washington, DC, USA. 1735-1758.

Lorca, F.G. 1921. "Caracola". *Canciones.* Madrid, Spain. 6, v: 2.

Lyons, T.R. 1980. *Remote Sensing: A Handbook for Archaeologists and Cultural Resource Managers – Basic Manual Supplement: Oregon.* Archaeological Applications of Aerial Remote Sensing, Supplement 4: Cultural Resources Management, National Park Service, U.S. Department of the Interior, Washington, DC. Section 3, 7-37.

Lyons, T.R. 1981. *Remote Sensing: Multispectral Analyses Of Cultural Resources – Chaco Canyon And Bandelier National Monument, Supplement No. 5.* Cultural Resources Management of the National Park Service, U.S. Department of the Interior, Washington, DC. USA. 1-9.

McAulay, J. 1999. *Birlinn.* Isle of Harris, Scotland. 2nd ed. 74.

McCauley, J. 1982. "Subsurface Valleys and Geoarchaeology of the Eastern Sahara Revealed by Shuttle RADAR". *Science*, Vol. 318. London, UK. 1004-1020.

McCauley, J. F., C. S. Breed, and G. G. Schaber. 1986. "The megageomorphology of the RADAR rivers of the Eastern Sahara". *JPL Publication 86-26.* The Second Spaceborne Imaging Radar Symposium. JPL, Pasadena, CA, USA. 23-35.

MacDonald, H., and W. Waite. 1971. "Optimum radar depression angles for geologic analysis". *Modern Geology*, vol. 2. Washington, DC, USA. 179-193.

McDonald, R. A. 1997. *The Kingdom of the Isles.* Phantassie, UK. 17-20.

McHugh W.P., C.S. Breed, G.G. Schaber, J.F. McCauley and B.J. Szabo. 1988. "Acheulian Sites Along The "RADAR Rivers, Southern Egyptian Sahara". *Journal of Field Archaeology*, No. 15. London, UK. 361-379.

McHugh W.P., G.G. Schaber, C.S. Breed and J.F. McCauley. 1989. "Neolithic Adaptation and the Holocene Functioning Of Tertiary Palaeodrainages in Southern Egypt and Northern Sudan". *Antiquity*, No. 63. London, UK. 320-336.

McKay, G. 1996. *A Model for the Integrated Spatial Analysis of Coastal Archaeological Sites.* M.Sc. thesis, St. Cloud State University, St. Cloud, Minnesota, USA. 1-10.

---------- 2002. *The Annotated Bibliography of Remote Sensing Archaeology.* Univ. of Edinburgh, UK. http://www.arcl.ed.ac.uk/arch/remotesense/index.html.

Maddin, R. and J.D. Muhly and T.S. Wheeler. 1977. *"How The Iron Age Began".* *Scientific American*, vol. 237-77. Washington, DC, USA. 122-132.

Malek, J. 2000. *"The Old Kingdom". The Oxford History of Ancient Egypt.* Shaw (Ed.). Oxford, UK. 89-91, 93-99, 105, 111.

Meyer, C. 1997. "Bir Umm Fawakhir: Insights into Ancient Egyptian Mining". *The Journal of Metals, The Minerals, Metals & Materials Society*, New York, NY, USA. 1+.

Midant-Reyne, B. 2000. *"The Naqada Period". The Oxford History of Ancient Egypt.* Ed. Shaw. Oxford, UK. 44-60.
MIT Radiation Laboratory Series. 1952. *Technical Reports*. Vol. 5. Boston, MA, USA, 1947-1952. 1-96.
Moorey, P. R. S. 1985. *Materials and Manufacture in Ancient Mesopotamia*. BAR International Series, no. 237. London, UK. 17.
Morain, S. A., Nelson, C., White, M., Komarek, A. 1980. "Remote Detection Of Prehistoric Sites In Bandelier National Monument". *Remote Sensing: A Handbook for Archaeologists and Cultural Resource Managers*, Cultural Resources Management, National Park Service, U.S. Department of the Interior, Washington, D.C., USA. 1+.
Moscati, S. 1988. *The Phoenicians*. Milan, Italy. 226-230.
Muhly, J. D. 1985. *"Sources of tin and the beginnings of bronze metallurgy". American Journal of Archaeology*, no. 89, Boston, MA. USA. 275-291
Muir, R.J. 1994. "The Rhinns Complex: Proterozoic basement on Islay and Colonsay, Inner Hebrides, Scotland and Inishtrahull, NW Ireland". *Transactions of the Royal Society of Edinburgh*: Earth Sciences, no.85. 77-90.
NASA. 2001. http://rst.gsfc.nasa.gov/Sect8/Sect8_2.html
National Oceanographic and Atmospheric Administration. 2000. NOAA of the United States of America. "Satellite Active Archive", http://www.noaa.gov (AVHRR).
---------- Metadata for AVHRR weather image scene, Islay, UK.
---------- Metadata for AVHRR weather image scene, Serabit El-Khadim, Sinai, Egypt.
---------- Metadata for AVHRR weather image scene, Conil, Spain.
NASDA. 2001. http://alos.nasda.go.jp
NIMA. 1998. "National Imagery and Mapping Agency". Online. http://nima.mil.gov.
Nunez, M. 2001. "E-mail". Mariano_n@yahoo.com.
Ogilvie, R.M. 1980. *"Republican Rome". The Penguin Encyclopedia of Ancient Civilizations.* Cotterell (ed.). London, UK. 237, 248, 250-251.
Peake, W.H. 1959. "Interaction of Electromagnetic Waves with Some Natural Surfaces". *IRE Transactions*, AP-7. New York, NY, USA. 5342.
Pennant, T. 1998. *A Tour in Scotland and Voyage to the Hebrides: 1772.* Edinburgh UK. 1:7.
Perez, S.C. 2000. "Una Cultura Llena de Enigmas". *Historia*, Mar. Madrid, Spain. 64-70.
Pernetta, John. 1995. *Atlas of the Oceans*. London, UK. 1+.
Petrie, F. 1906. *Researches in the Sinai.* London, UK. 45-203.
Pleiner, R. 1980. "Early iron metallurgy in Europe". Wertime, T. A. and Muhly, J. D. (eds.), *The Coming of the Age of Iron*, Yale University Press, USA. 375-415.
Pliny. 1991. *Natural History: A Selection.* Trans. H. Rackham. London, UK. 43, 52-53, 296-299, 321.
Plonus, M.A. 1978. *Applied Electromagnetics.* New York, NY, USA. 25-58.
Polybius. 1922. *The Histories*. Trans. by W.R. Paton. Loeb series. New York, USA.
Prain, R. 1975. *Copper*. Mining Journal Books, London, UK. 19.
Ramo, S., J.R. Whinnery, and T. Van Duzer. 1967. *Fields and Waves in Communication Electronics*. New York, NY, USA. 5-98.
Ray, T. W., T. G. Farr, and J. J. van Zyl. 1992. "Detection of land degradation with polarimetric SAR". *Geophys. Res. Letters*. Vol. 19, no. 15, Washington, DC, USA. 1587-1590.
Renfrew, C. 1969. "The Autonomy of the Southeast European Copper Age". *Proceedings of the Prehistoric Society.* Vol. 35. London, UK. 12-46.
Rice, P.M. 1987. *Pottery Analysis.* Univ. of Chicago, Chicago, USA. 2-43.

Rice, Univ. 2001. *Degree/Radian Circle*. http://math.rice.edu/~pcmi/sphere/drg_txt.html
Richards, J.A. 1994. *Remote Sensing Digital Image Analysis*. Springer-Verlag, Berlin, Germany. 340.
Roe, M. and Davies, A. 2000. *A Survey of the Area around Jamie Mine Sun Side Allotment* Unpublished interim report for Northern Mine Research Society, UK.
Rothenburg, B. 1979. *Sinai: Pharoahs, Miners, Pilgrims and Soldiers*. Berne, Switzerland. 1+.
Rothenburg, B. and Blanco-Freijeiro, A. 1981. *Metal in History: I. Studies in Ancient Mining and Metallurgy in South-West Spain*. IAMS, London, UK. 3-21.
Rowe, A.P. 1948. *One Story of RADAR*. Cambridge University Press, New York, NY, USA, 1948. 2-21.
Sabins, Floyd. 1987. *Remote Sensing Principles and Interpretation*. New York, USA: W.H. Freeman. 190 – 238.
Sandars, N.K. 1980. "The Sea Peoples". *The Penguin Encyclopedia of Ancient Civilizations*. London, UK. 44-46.
Savory, H.N. 1968. *Spain and Portugal*. New York, New York, USA. 15-22.
Scarre, C. 1995. *The Atlas of Archaeology*. New Jersey, U.S.A. 12-18, 32-33, 106-107, 110, 118, 120.
Schaber, G. G., J. F. McCauley, C. S. Breed, and R. R. Olhoeft. 1986. "Physical controls on signal penetration and subsurface scattering in the Eastern Sahara". *IEEE Trans. Geosci. Remote Sensing*. Vol. 24. Bellingham, WA, USA. 603-623.
Schaber, G. G., J. McCauley, and C. Breed. 1997. "The use of multiwavelength and polarimetric SIR-C/X-SAR data in geologic studies of Bir Safsaf, Egypt". *Remote Sensing of Environment*, vol. 59, no. 2. Washington, DC, USA. 337- 363.
Schaber, G. G., J. F. McCauley, C. S. Breed, A. Simonin, P. M. Rebillard, N. Lancaster, and J. Teller. 1997. "SIR-C surface and subsurface responses from documented test localities in the Sahara, Namib, and Kalahari Deserts, Africa and the Jornada del Muerto, New Mexico". *Science Results from the Spaceborne Imaging Radar-C/X-Band Synthetic Aperture Radar (SIR-C/X- SAR): Progress Report*, Jet Propulsion Laboratory Publication No. 96-7, Pasadena, CA, USA. 164-169.
Schmidt, P. R. and S.T. Childs. 1995. "*Ancient African iron production*". *American Scientist* No. 83. New York, USA. 524-533.
Schmullius, C. C., and D. L. Evans. 1997. "Synthetic aperture radar (SAR) frequency and polarization requirements for applications in ecology, geology, hydrology, and oceanography: a tabular status quo after SIR-C/X-SAR". *International Journal of Remote Sensing*. Vol. 18, no. 13. London, UK, and Washington, DC, USA. 2713-2722.
Semmler, M.A. 1988. "Spain". *The Phoenicians*. Ed. Moscati. Milan, Italy. 232-236.
Sever, T. and P. Sheets. 1988. "High Tech Wizardry". *Archaeology Magazine*, Nov. Boston, USA. 28-35.
Shanmuggam, K. S., V. Narayanan, V. S. Frost, J. A. Stiles and J. C. Holtzman. 1981. "Textural features for radar image analysis". *IEEE Trans. Geosci. Remote Sensing*, vol. GE-19. Bellingham, WA, USA. 153-156.
Shackley, M. 1980. *Neanderthal Man*. London, UK. 51-65.
"Textural features for radar image analysis, IEEE Trans. Geosci. Remote Sensing, vol. GE-19. Bellingham, WA, USA. 153-156.
Shaw, I. 2000. "Introduction: Chronologies and Cultural Change in Egypt". *The Oxford History of Ancient Egypt*. I. Shaw (ed.). Oxford, UK. 1-16.
Shaw. I. 2000. "Egypt and the outside world". *The Oxford History of Ancient Egypt*. London, UK. 320, 479-480.
Shepherd, R. 1980. *Prehistoric Mining and Allied Industries*, London, UK. 3-45.
Shepherd, R. 1993. *Ancient Mining*. Essex, UK. 1-4, 11-19, 255-259.

Sherwin, C.W., J.P. Ruina and R.D. Rawcliffe. 1962. "Some Early Developments in Synthetic Aperture RADAR Systems". *IRE Transactions*, MIL-6, New York, NY, USA, 1962. 111-116.
Simmons, J. 1986. *The Railways of Britain.* London, UK. 1-4.
Singer, C.J., E.J. Holmyard and A.R. Hall. 1980. *A History of Technology, Vol. I.* Oxford, UK. 3 – 44, 56.
Sissons, J.B. 1974. "Late Glacial Marine Erosion in Scotland". *Boreas*. UK. Vol. 3. 41-8.
---------- 1977. "The Loch Lomond Readvance in Southern Skye and Some Paleoclimatic Implications". *Scottish Journal of Geology*, Vol. 3. UK. 23 – 36.
---------- 1981. "The So-called High Interglacial Rock Shoreline of Western Scotland". *Transactions Institute of British Geography*, Vol. 7. UK. 205 – 216.
---------- 1982. "The Quaternary Geomorphology of the Inner Hebrides: A Review and Reassessment. *Proceedings Geology Association*, Vol. 94, No. 2 of 2. UK. 165 – 175.
Skolnik, M. 1980. *Introduction to RADAR Systems.* Boston, MA, USA. 12-27.
Smith, A. 1895. The Book of Islay. Edinburgh, UK. 455-463.
Smith, G. 1923. *The Ancient Egyptians*. London, United Kingdom. 10-12.
Smyth , A. 1989. *Warlords and Holymen*. Edinburgh, UK. 1+.
Snodgrass, A. 1980. *Archaic Greece: The Age of Experiment.* London, UK. 75-86.
Solas, J. M. 1957. "Tartessos y las tradiciones de la colonizacion fenicia en Occidente". *Serafad*, XVII. Madrid, Spain. 23-35.
Stine R.S. and Decker T.D. 1990. "Archaeology, Data Integration And GIS". *Interpreting space: GIS and Archaeology*. London, UK. 134-140.
Strabo. 1996. *Geography*. Internet Ancient History Sourcebook, XVII.iii. 1-11. 1996.
Stuhr, F., R. Jordan, and M. Werner. 1994. "SIR-C/X-SAR: A multifaceted radar". *IEEE AES Magazine*, vol. 10, no. 10. Bellingham, WA, USA. 15-24.
Synge, F.M. and N. Stephens. 1966. "Late-postglacial shorelines, and ice-limits in Argyll and north-east Ulster". *Transactions of the Institute of British Geography.* London, UK.No. 39. 101-125.
Thomas, B.W. 1965. *The Climate of Africa.* New York, USA. 8-32.
Tylecote, R. F. 1976. *A History of Metallurgy*. London, United Kingdom, 1976. 2-12.
Ulaby, F. and M.C. Dobson. 1989. *Handbook of RADAR Scattering Statistics for Terrain.* Norwood, MA, USA. 1-4, 11-34.
United Nations. 2001. http://www.unep.com
U.S. Army. 1876. *Manual for Cavalry Troops*. West Point, NY, USA. 69-72.
U.S. Army Topographic Corp. 1958. *Tor*. Richmond, VA., USA, Map NH 36-15, 1:250,000.
U.S. Coast Guard Navigation Center (USCGNC). 2001. "GPS Bulletin Board." http://www.navcen.uscg.mil/gps/gpsff.htm
U.S. Geological Survey (USGS). 2000. "*Global Land Information System.*" http://www.usgs.gov/glis/
United States Geological Survey (USGS). 2000. "*Corona: A System Description*". http://edcwww.cr.usgs.gov/glis/hyper/guide/disp
United States Geological Survey (USGS). 2000. "*Corona: Metadata for Islay Image Scene*". http://edcwww.cr.usgs.gov/Webglis/glisbin/search.pl?DISP
United States Geological Survey (USGS). 2000. "*Corona: Metadata for Conil Image Scene*". http://edcwww.cr.usgs.gov/Webglis/glisbin/search.pl?DISP
United States Geological Survey (USGS). 2000. "*Corona: Metadata for Serabit El-Khadim Scene*". http://edcwww.cr.usgs.gov/Webglis/glisbin/search.pl?DISP

United States Navy. 1996. "Naval Electrical and Electronics Training (NEETS) Modules". United States Navy Education and Training Professional Development and Technology Center Pensacola, FL 32509, USA. Public release. 1+.
---------- 1 - *Matter, Energy, and Direct Current*
---------- 2 - *Alternating Current and Transformers*
---------- 3 - *Circuit Protection, Control, and Measurement*
---------- 4 - *Electrical Conductors, Wiring Techniques, and Schematic Reading*
---------- 5 - *Generators and Motors*
---------- 6 - *Electronic Emission, Tubes, and Power Supplies*
---------- 7 - *Solid-State Devices and Power Supplies*
---------- 8 - *Amplifiers*
---------- 9 - *Wave-Generation and Wave-Shaping Circuits*
---------- 10 - *Wave Propagation, Transmission Lines, and Antennas*. 5-35.
---------- 11 - *Microwave Principles*
---------- 12 - *Modulation Principles*
---------- 13 - *Number Systems and Logic Circuits*
---------- 14 - *Microelectronics*
---------- 15 - *Principles of Synchros, Servos, and Gyros*
---------- 16 - *Test Equipment*
---------- 17 - *Radio-Frequency Communications Principles*
---------- 18 - *Radar Principle*. 59-112.
---------- 19 - *The Technician's Handbook*
---------- 20 - *Master Glossary*
---------- 21 - *Test Methods and Practices*
---------- 22 - *Digital Computers*
---------- 23 - *Magnetic Recording*
---------- 24 - *Introduction to Fiber Optics*

Van Dijk, J. 2000. "The Amarna Period and Later New Kingdom". *The Oxford History of Ancient Egypt.* Ed. Shaw. Oxford, UK. 304-305.

van Zyl, J. J., H. A. Zebker and C. Elachi. 1990. "Imaging radar polarization signatures: Theory and observation". *Radio Science*, vol. 22, no. 4. Washington, DC, USA. 529-543.

van Zyl, J. J., 1989. "Unsupervised classification of scattering behavior using radar polarimetry data". *IEEE Trans. Geosci. Remote Sensing*, vol. 27, no. 1. Bellingham, WA, USA. 36-45.

Vidal-Madjar, D., M. Normand, O. Taconet, S. Mascle, M. Zribi, C. Emblanch, and C. Loumagne. 1996. "Test of roughness and moisture algorithms using multiparameter space borne SAR and application to surface hydrology". Science Results from the *Spaceborne Imaging Radar-C/X-Band Synthetic Aperture Radar (SIR-C/X-SAR): Progress Report*, Jet Propulsion Laboratory Publication No. 96-7, April 1996, CA, USA. 201-214.

Wainwright, G.A. 1934. "The Occurrence of Tin and Copper Near Byblos". *Journal of Egyptian Archaeology*, No. 20. London, U.K. 29-32.

Walters, C. 1988. "Ancient Egypt". *The Penguin Encyclopedia of Ancient Civilizations.* London, UK. 22-43.

Wang, L., K. H. Ding, C. C. Hsu, Y. E. Yang, and J. A. Kong. 1995. "Electromagnetic scattering model for vegetation based on L-band systems". *Proceedings of Progress in Electromagnetics Research Symposium* (PIERS) '95. Seattle, Washington, USA. 278.

Warmington, B. 1980. "Carthage". *Ancient Civilizations.* Cotterell (ed.). London, UK. 237.

Weisberger, G. and Pernicka, E. 1995. *"Ore mining in prehistoric Europe: an overview". Prehistoric Gold in Europe: Mines, Metallurgy and Manufacture.* Dordrecht, Germany. 159-182.

Wertime, T.A. and J.D. Muhly (eds.). 1980. *The Coming of the Age of Iron.* New Haven, Connecticut, USA. 3-23.

Williams, R. 1997. *The Lords of the Isles.* House of Lochar, Isle of Colonsay, Argyll, PA61 7YR, Scotland, United Kingdom. 1+.

Wilson, G.V. and Flett, J.S. 1921. "The Lead, Zinc, Copper and Nickel Ores of Scotland". Special Reports on the *Mineral Resources of Great Britain*, Vol. XVII. London, UK. 2-15.

Wittenberg, P. 2001. *RADAR Phase Measurement Accuracy.* http://home.att.net/~wittenberg/radar/chapters/ch12.dir/ch12pr.dir/c12p7.dir/c12p7.htm

Wood, J. 2001. Internet. http://www.geog.le.av.uk/jwo/research

Wood, J. 1996. *The Geomorphological Characterization of Digital Elevation Models.* Ph.D. dissertation, Univ. of Leicester, UK. 26-102.

Wysocki, J. 1991. "GPS and Selective Availability." *GPS World.* Jul. Boulder, CO, USA. 38-44.

Zebker, H. A., J. J. van Zyl and C. Elachi. 1990. "Polarimetric SAR Applications, in RADAR polarimetry for geoscience applications". Ulaby and Elachi (eds.). Norwood, MA.USA. 55-290.

Zebker, H. A., C. Elachi, and J. J. van Zyl. 1996. "Radar interferometric and penetration investigations using SIR-C data". *Science Results from the Spaceborne Imaging Radar-C/X-Band Synthetic Aperture Radar (SIR-C/X- SAR): Progress Report*, Jet Propulsion Laboratory Publication No. 96-7. Pasadena, CA, USA. 228-230.

Zebker, H. A., and J. J. van Zyl. 1991. "Imaging Radar Polarimetry: A Review". *Proceedings of the IEEE*, vol. 79. Bellingham, WA, USA. 1583-1606.

Ground Control Points

UTM, UK projection, OSGB datum.
Port Ariskaig - 142056E 673163N
Beinn Ghibheach - 136281E 627261N
Gortantoid - 133431E 672088N
Cnoc na Faire - 129581E 674763N
Loch Gorm (East) - 124006E 665763N
Loch Gorm (West) - 122181E 665639N
Traigh Mchair - 120656E 662263N
Carraigh Dubh - 130431E 662538N
Bridgend - 139181E 668188N
Loch Fada - 140556 663613N
Loch Bharradil - 138931E 663338N
Loch Ballygrant - 140569E 666463N
Loch Lossit - 140831 665163N
Finlaggan (North) - 139181 668188N
Finlaggan (South) - 137981E 666951N

CORONA

Entity Id :	DS009023026DV011
Mission Number :	9023
Frame Number :	11
Acquisition Date :	1961/08/30
Browse Availability :	YES
Camera Type :	VERTICAL
Camera/Resolution :	VERTICAL MED
Northwest Latitude :	N55 49
Northwest Longitude :	W006 27
Northeast Latitude :	N56 25
Northeast Longitude :	W001 39
Southeast Latitude :	N56 12
Southeast Longitude :	W001 35
Southwest Latitude :	N55 36
Southwest Longitude :	W006 21
Area Indicator :	Search area is within the entity coverage
Revolution :	026D
Image Type :	BLACK and WHITE
Film Type :	70mm PANORAMIC
Generation :	2
Polarity :	NEGATIVE
Browse Path :	9023/026D/V/DS009023026DV011.jpg

AVHRR

Dims: 558 x 175 x 5 [BIP]
Size: [Integer] 976,500 bytes.
Sensor Type: AVHRR
Byte Order : Host (Intel)
Projection : United Kingdom
  Datum : Ordnance Survey of Great Britain '36
  X Pixel : 4400.00 Meters
  Y Pixel : 4400.00 Meters
Wavelength : 0.6300 - 12.00

Islay C band Imaging RADAR metadata

File Descriptor Record

Record Info [1 63 192 18 18 720]
Data Format (A = ASCII) A
Format Control Doc. CEOS-SAR-CCT
Format Control Doc. Version A
Record Format rev.level A
Software ID 3.1
File Number 10
File Name pr17824_ldr_ceos

Data Set Summary

Record Info [2 10 10 50 20 2016]
SAR channel indicator 28
Scene Identifier NBC
Site name North Sea A2
GMT at Image center 1994/04/18 06:56:06.574
MET at Image center 08 19:51:06.589
Latitude at Image center 55.95
Longitude at Image center -5.80
Processed scene range (km) 53.17
Processed scene azimuth (km) 106.90
Sensor ID SIR-C -C -MD13-hvhv
Sensor Platform Heading (deg) 83.86
Incidence Angle 28.07
Radar Frequency (GHz) 5.29
Quantizer descriptor (8,4)BFPQ
Nominal PRF 1395.00
Processing Facility JPL
Processing software version 3.0.2
Product type MULTI-LOOK COMPLEX
Number of azimuth looks 18.20
Number of range looks
Line spacing (m) 12.50
Pixel spacing (m) 12.50
Orbital Direction ASCENDING

Map Projection

Record Info [3 10 20 50 20 1620]
Map projection descriptor GROUND RANGE
Geodedic alt from ellipsoid (km) 221.29
Name of reference ellipsoid GEM6
Semimajor axis ref ellipsoid (km)6378.14
Semiminor axis ref ellipsoid (km)6356.75
UTM descriptor
UTM zone signature
Map origin, false easting
Map origin, false northing
NSP descriptor
Map origin, false easting
Map origin, false northing
Projection centre longitude (deg)
Projection centre latitude (deg)
Standard parallel 1 (deg)
Standard parallel 2 (deg)
NSP central meridian 1 (deg)
NSP central meridian 2 (deg)
NSP spare 1
NSP spare 2
Near range early time latitude 56.13
Near range early time longitude -6.70
Far range early time latitude 55.65
Far range early time longitude -6.60
Far range late time latitude 55.75
Far range late time longitude -4.91
Near range late time latitude 56.23
Near range late time longitude -4.99

Platform Position

Record Info [4 10 30 50 20 800]
Number of data points 3
Year of first data 1994
Month of first data 04
Day of first data 18
Day of Year of first data pnt 108
Seconds of day of first data pnt 24958.98
Data sampling interval (sec) 8.50
Reference coordinate system GREENWICH TRUE OF DATE
Greenwich mean hour angle (deg) 0.00
Along track position error
Cross track position error
Radial position error
Along track velocity error
Cross track velocity error
Radial velocity error

Data Quality Summary
Record Info [10 10 60 50 20 464]
Calibration update date 0
Nominal azimuth ambiguity 0.00
Nominal range ambiguity 0.00
Nominal slant range resolution 0.00
Nominal azimuth range resolution 0.00
Instantaneous dynamic range 0.00
Radiometric uncertainty (dB) 0.00

Data Quality Summary
Record Info [11 10 60 50 20 464]
Calibration update date 0
Nominal azimuth ambiguity 0.00
Nominal range ambiguity 0.00
Nominal slant range resolution 0.00
Nominal azimuth range resolution 0.00
Instantaneous dynamic range 0.00
Radiometric uncertainty (dB) 0.00

Data Histograms
Record Info [12 10 70 50 20 8728]
Histogram Descriptor RAW DATA
Number of histogram bins 1 4096
Mean sample value 0000
Sample standard deviation
Minimum histogram value 0283 11.752
Maximum histogram value 0142 1.000
Histogram mean 0.00 0.00
Histogram standard deviation 0.00 0.076

Data Histograms
Record Info [13 10 70 50 20 8728]
Histogram Descriptor RAW DATA
Number of histogram bins 1 4096
Mean sample value 0000
Sample standard deviation
Minimum histogram value 3728 9.394
Maximum histogram value 3501 1.000
Histogram mean 0000 0.000
Histogram standard deviation 0000 0.091

Range Spectra
Record Info [14 10 80 50 20 4272]

Range Spectra
Record Info [15 10 80 50 20 4272]

Radar Parameter Update
Record Info [16 10 100 50 20 40]

Radar Parameter Update
Record Info [17 10 100 50 20 40]

Radar Parameter Update
Record Info [18 10 100 50 20 40]

Detailed Processing Parameters
Record Info [19 10 120 50 61 1312]
Near Slant Range (km) 237.24
Near Range Incidence Angle (deg) 21.57
Far Range Incidence Angle (deg) 32.96

Calibration Data
Record Info [20 10 130 50 20 776]

Image Records
Record Info [1 63 192 18 18 10652]
Number of Samples 2128
Number of Lines 4277
Number of bytes per pixel 5
Data Product Description COMPRESSED CROSS-PRODUCTS

Islay L band RADAR metadata

File Descriptor Record

Record Info [1 63 192 18 18 720]
Data Format (A = ASCII) A
Format Control Doc. CEOS-SAR-CCT
Format Control Doc. Version A
Record Format rev.level A
Software ID 3.1
File Number 7
File Name pr17823_ldr_ceos

Data Set Summary
Record Info [2 10 10 50 20 2016]
SAR channel indicator 18
Scene Identifier NBC
Site name North Sea A2
GMT at Image center 1994/04/18 06:56:06.574
MET at Image center 08 19:51:06.589
Latitude at Image center 55.95
Longitude at Image center -5.80
Processed scene range (km) 53.17
Processed scene azimuth (km) 106.90
Sensor ID SIR-C -L -MD13-hvhv
Sensor Platform Heading (deg) 83.86
Incidence Angle 28.076

Data Set Summary – continued

Radar Frequency (GHz)	1.249
Quantizer descriptor	(8,4)BFPQ
Nominal PRF	1395.00
Processing Facility	JPL
Processing software version	3.0.2
Product type	MULTI-LOOK COMPLEX
Number of azimuth looks	18.20
Number of range looks	
Line spacing (m)	12.50
Pixel spacing (m)	12.50
Orbital Direction	ASCENDING

Map Projection

Record Info	[3 10 20 50 20 1620]
Map projection descriptor	GROUND RANGE
Geodedic alt from ellipsoid (km)	221.2920074
Name of reference ellipsoid	GEM6
Semimajor axis ref ellipsoid (km)	6378.14
Semiminor axis ref ellipsoid (km)	6356.75
UTM descriptor	
UTM zone signature	
Map origin, false easting	
Map origin, false northing	
NSP descriptor	
Map origin, false easting	
Map origin, false northing	
Projection centre longitude (deg)	
Projection centre latitude (deg)	
Standard parallel 1 (deg)	
Standard parallel 2 (deg)	
NSP central meridian 1 (deg)	
NSP central meridian 2 (deg)	
NSP spare 1	
NSP spare 2	
Near range early time latitude	56.13
Near range early time longitude	-6.70
Far range early time latitude	55.65
Far range early time longitude	-6.60
Far range late time latitude	55.75
Far range late time longitude	-4.91
Near range late time latitude	56.23
Near range late time longitude	-4.99

Platform Position

Record Info [4 10 30 50 20 800]
Number of data points 3
Year of first data 1994
Month of first data 04
Day of first data 18
Day of Year of first data pnt 108
Seconds of day of first data pnt 24958.98
Data sampling interval (sec) 8.50
Reference coordinate system GREENWICH TRUE OF DATE
Greenwich mean hour angle (deg) 0.00
Along track position error
Cross track position error
Radial position error
Along track velocity error
Cross track velocity error
Radial velocity error

Data Quality Summary

Record Info [10 10 60 50 20 464]
Calibration update date 0
Nominal azimuth ambiguity 0.00
Nominal range ambiguity 0.00
Nominal slant range resolution 0.00
Nominal azimuth range resolution 0.00
Instantaneous dynamic range 0.00
Radiometric uncertainty (dB) 0.00

Data Quality Summary

Record Info [11 10 60 50 20 464]
Calibration update date 0
Nominal azimuth ambiguity 0.00
Nominal range ambiguity 0.00
Nominal slant range resolution 0.00
Nominal azimuth range resolution 0.00
Instantaneous dynamic range 0.00
Radiometric uncertainty (dB) 0.00

Data Histograms

Record Info [12 10 70 50 20 8728]
Histogram Descriptor RAW DATA
Number of histogram bins 1 4096
Mean sample value 0000
Sample standard deviation
Minimum histogram value 0065 13.69
Maximum histogram value 3652 1.00
Histogram mean 0000 0.000
Histogram standard deviation 0000 0.066

Data Histograms
Record Info [13 10 70 50 20 8728]
Histogram Descriptor RAW DATA
Number of histogram bins 1 4096
Mean sample value 0000
Sample standard deviation
Minimum histogram value 5679 13.930
Maximum histogram value 8796 1.000
Histogram mean 0000 0.000
Histogram standard deviation 0000 0.064

Range Spectra
Record Info [14 10 80 50 20 4272]

Range Spectra
Record Info [15 10 80 50 20 4272]

Radar Parameter Update
Record Info [16 10 100 50 20 40]

Radar Parameter Update
Record Info [17 10 100 50 20 40]

Radar Parameter Update
Record Info [18 10 100 50 20 40]

Detailed Processing Parameters
Record Info [19 10 120 50 61 1312]
Near Slant Range (km) 237.24
Near Range Incidence Angle (deg) 21.57
Far Range Incidence Angle (deg) 32.96

Calibration Data
Record Info [20 10 130 50 20 776]

Image Records
Record Info [1 63 192 18 18 10652]
Number of Samples 2128
Number of Lines 4277
Number of bytes per pixel 5
Data Product Description COMPRESSED CROSS-PRODUCTS

Appendix II - Sinai

Ground Control Points

UTM, WGS-84 datum; first number is the east coordinate, second number is north coordinate.

544658E 321231N Temple of Hathor, Serabit El Khadim.
545018 3212093 East mines, Serabit El Khadim.
544118 3211573 South mines, Serabit El Khadim.
543488 3211773 West mines, Serabit El Khadim.
544488 3212133 North mines, Serabit El Khadim.
546268 3211613 Wadi Serabit El Khadim, Wadi Garf, lower edge intersection.
555668 3223223 El Tigh escarpment, edge, due east of Serabit El Khadim.
515128 3220945 Wadi Tayibah, northwest branch.
515128 3218967 Wadi Tayibah, main section.
518078 3216989 Wadi Tayibah, north branch, terminus.
521029 3215011 Wadi Tayibah, north branch.
532830 3213034 Gebel Ragabah, northwestern extremity and terminus of wadi.
529880 3211056 Road to coastal highway and Abu Rudeis (Abu Rudays).
535781 3209078 Bir Al Deid.
538731 3207100 Wadi Ajmah.
544632 3205122 Wadi Seih, north branch, terminus.
553483 3203145 Wadi Seih.
553483 3201167 Wadi Seih, middle of main branch, atop foothill.
523979 3199189 Interior road from coastal highway and Abu Rudeis.
535618 3196053 Wadi Bir Al Adid, entrance through coastal escarpment.
541682 3197211 Bir Al Adid, middle section.
562335 3195233 Wadi Bateh, west of Serabit El Khadim.
521029 3193255 Road from Abu Zenima to Wadi Seih, to Serabit El Khadim.
529880 3191278 Track from Abu Zenima, intersection with Wadi Seih.
521029 3189300 Abu Zenima, coast road bypass.
532830 3187322 Branch wadi, intersection with main Wadi Seih.
535781 3185344 Branch wadi, leading south from Wadi Seih; name unknown.
541682 3183366 First escarpment on Wadi Seih, lower end, first mud flat.
580037 3183366 Wadi Magarah, branch.
532830 3179411 Middle mud flat at Wadi Seih.
515128 3177431 Beach, peninsula, south of Abu Rudeis.

CORONA

Meta Data Details – SERABIT EL-KHADIM	
Entity Id :	DS1048-1025DF023
Mission Number :	1048-1
Frame Number :	23
Acquisition Date :	1968/09/20
Browse Availability :	YES
Camera Type :	FORWARD
Camera/Resolution :	STEREO MED
Northwest Latitude :	N28 54
Northwest Longitude :	E031 33
Northeast Latitude :	N29 10
Northeast Longitude :	E034 16
Southeast Latitude :	N29 01
Southeast Longitude :	E034 19
Southwest Latitude :	N28 44
Southwest Longitude :	E031 32
Area Indicator :	Entity partially covers the search area
Revolution :	025D
Image Type :	BLACK and WHITE
Film Type :	70mm PANORAMIC
Generation :	2
Polarity :	NEGATIVE
Browse Path :	1048-1/025D/F/DS1048-1025DF023.jpg

AVHRR

Dims: 640 x 170 x 5 [BIP]
Size: [Integer] 1,088,000 bytes.
Sensor Type: AVHRR
Byte Order : Host (Intel)
Projection : UTM, Zone 36 North
  Datum : WGS-84
  X Pixel : 4400.00 Meters
  Y Pixel : 4400.00 Meters
Wavelength : 0.63 - 12.00

C band Sinai Imaging RADAR metadata

File Descriptor Record

Record Info [1 63 192 18 18 720]
Data Format (A = ASCII) A
Format Control Doc. CEOS-SAR-CCT
Format Control Doc. Version A
Record Format rev.level A
Software ID 3.1
File Number 4
File Name pr12498_ldr_ceos

Data Set Summary

Record Info [2 10 10 50 20 2016]
SAR channel indicator 26
Scene Identifier G20
Site name Ha Meshar, Israel (2)
GMT at Image center 1994/04/11 03:09:29.353
MET at Image center 01 16:04:29.368
Latitude at Image center 28.52
Longitude at Image center 32.84
Processed scene range (km) 70.98
Processed scene azimuth (km) 99.92
Sensor ID SIR-C -C -LO11-hh hv
Sensor Platform Heading (deg) 36.268
Incidence Angle 46.922
Radar Frequency (GHz) 5.304
Quantizer descriptor (8,4)BFPQ
Nominal PRF 1302.00
Processing Facility JPL
Processing software version 1.3.0
Product type MULTI-LOOK COMPLEX
Number of azimuth looks 2.9471152
Number of range looks
Line spacing (m) 12.50
Pixel spacing (m) 12.50
Orbital Direction ASCENDING

Map Projection

Record Info [3 10 20 50 20 1620]
Map projection descriptor GROUND RANGE
Geodedic alt from ellipsoid (km) 223.26
Name of reference ellipsoid GEM6
Semimajor axis ref ellipsoid (km)6378.14
Semiminor axis ref ellipsoid (km)6356.75
UTM descriptor
UTM zone signature
Map origin, false easting
Map origin, false northing
NSP descriptor
Map origin, false easting
Map origin, false northing

Map Projection – continued

Projection centre longitude (deg)
Projection centre latitude (deg)
Standard parallel 1 (deg)
Standard parallel 2 (deg)
NSP central meridian 1 (deg)
NSP central meridian 2 (deg)
NSP spare 1
NSP spare 2
Near range early time latitude 28.36
Near range early time longitude 32.24
Far range early time latitude 27.97
Far range early time longitude 32.82
Far range late time latitude 28.69
Far range late time longitude 33.43
Near range late time latitude 29.08
Near range late time longitude 32.85

Platform Position

Record Info [4 10 30 50 20 800]
Number of data points 3
Year of first data 1994
Month of first data 04
Day of first data 11
Day of Year of first data pnt 101
Seconds of day of first data pnt 11361.98
Data sampling interval (sec) 8.50
Reference coordinate system GREENWICH TRUE OF DATE
Greenwich mean hour angle (deg) 0.00
Along track position error
Cross track position error
Radial position error
Along track velocity error
Cross track velocity error
Radial velocity error

Data Quality Summary

Record Info [10 10 60 50 20 464]
Calibration update date 0
Nominal azimuth ambiguity 0.00
Nominal range ambiguity 0.00
Nominal slant range resolution 0.00
Nominal azimuth range resolution 0.00
Instantaneous dynamic range 0.00
Radiometric uncertainty (dB) 0.00

Data Quality Summary
Record Info [11 10 60 50 20 464]
Calibration update date 0
Nominal azimuth ambiguity 0.00
Nominal range ambiguity 0.00
Nominal slant range resolution 0.00
Nominal azimuth range resolution 0.00
Instantaneous dynamic range 0.00
Radiometric uncertainty (dB) 0.00

Data Histograms
Record Info [12 10 70 50 20 8728]
Histogram Descriptor RAW DATA
Number of histogram bins 1 4096
Mean sample value 0000
Sample standard deviation
Minimum histogram value 9384 12.66
Maximum histogram value 8184 1.00
Histogram mean 0000 0.000
Histogram standard deviation 0000 0.075

Data Histograms
Record Info [13 10 70 50 20 8728]
Histogram Descriptor RAW DATA
Number of histogram bins 1 4096
Mean sample value 0000
Sample standard deviation
Minimum histogram value 5987 5.50
Maximum histogram value 3482 1.000
Histogram mean 0000 0.000
Histogram standard deviation 0000 0.115

Range Spectra
Record Info [14 10 80 50 20 4272]

Range Spectra
Record Info [15 10 80 50 20 4272]

Radar Parameter Update
Record Info [16 10 100 50 20 40]

Radar Parameter Update
Record Info [17 10 100 50 20 40]

Radar Parameter Update
Record Info [18 10 100 50 20 40]

Detailed Processing Parameters

Record Info [19 10 120 50 61 1312]
Near Slant Range (km) 292.92
Near Range Incidence Angle (deg) 41.34
Far Range Incidence Angle (deg) 50.53

Calibration Data

Record Info [20 10 130 50 20 776]

Image Records

Record Info [1 63 192 18 18 28412]
Number of Samples 5680
Number of Lines 7995
Number of bytes per pixel 5
Data Product Description COMPRESSED CROSS-PRODUCTS

L band Sinai Imaging RADAR metadata

File Descriptor Record

Record Info [1 63 192 18 18 720]
Data Format (A = ASCII) A
Format Control Doc. CEOS-SAR-CCT
Format Control Doc. Version A
Record Format rev.level A
Software ID 3.1
File Number 1
File Name pr12497_ldr_ceos

Data Set Summary

Record Info [2 10 10 50 20 2016]
SAR channel indicator 16
Scene Identifier G20
Site name Ha Meshar, Israel (2)
GMT at Image center 1994/04/11 03:09:29.353
MET at Image center 01 16:04:29.368
Latitude at Image center 28.52
Longitude at Image center 32.84
Processed scene range (km) 70.98
Processed scene azimuth (km) 99.92
Sensor ID SIR-C -L -LO11-hh hv
Sensor Platform Heading (deg) 36.26
Incidence Angle 46.92
Radar Frequency (GHz) 1.25
Quantizer descriptor (8,4)BFPQ
Nominal PRF 1302.00
Processing Facility JPL
Processing software version 1.3.0
Product type MULTI-LOOK COMPLEX
Number of azimuth looks 2.94
Number of range looks
Line spacing (m) 12.50

Data Summary – continued

Pixel spacing (m) 12.50
Orbital Direction ASCENDING

Map Projection

Record Info [3 10 20 50 20 1620]
Map projection descriptor GROUND RANGE
Geodedic alt from ellipsoid (km) 223.26
Name of reference ellipsoid GEM6
Semimajor axis ref ellipsoid (km)6378.14
Semiminor axis ref ellipsoid (km)6356.75
UTM descriptor
UTM zone signature
Map origin, false easting
Map origin, false northing
NSP descriptor
Map origin, false easting
Map origin, false northing
Projection centre longitude (deg)
Projection centre latitude (deg)
Standard parallel 1 (deg)
Standard parallel 2 (deg)
NSP central meridian 1 (deg)
NSP central meridian 2 (deg)
NSP spare 1
NSP spare 2
Near range early time latitude 28.36
Near range early time longitude 32.24
Far range early time latitude 27.97
Far range early time longitude 32.82
Far range late time latitude 28.69
Far range late time longitude 33.43
Near range late time latitude 29.08
Near range late time longitude 32.85

Platform Position

Record Info [4 10 30 50 20 800]
Number of data points 3
Year of first data 1994
Month of first data 04
Day of first data 11
Day of Year of first data pnt 101
Seconds of day of first data pnt 11361.98
Data sampling interval (sec) 8.50
Reference coordinate system GREENWICH TRUE OF DATE
Greenwich mean hour angle (deg) 0.00
Along track position error
Cross track position error
Radial position error

Platform Position - continued

Along track velocity error
Cross track velocity error
Radial velocity error

Data Quality Summary

Record Info [10 10 60 50 20 464]
Calibration update date 0
Nominal azimuth ambiguity 0.00
Nominal range ambiguity 0.00
Nominal slant range resolution 0.00
Nominal azimuth range resolution 0.00
Instantaneous dynamic range 0.00
Radiometric uncertainty (dB) 0.00

Data Quality Summary

Record Info [11 10 60 50 20 464]
Calibration update date 0
Nominal azimuth ambiguity 0.00
Nominal range ambiguity 0.00
Nominal slant range resolution 0.00
Nominal azimuth range resolution 0.00
Instantaneous dynamic range 0.00
Radiometric uncertainty (dB) 0.00

Data Histograms

Record Info [12 10 70 50 20 8728]
Histogram Descriptor RAW DATA
Number of histogram bins 1 4096
Mean sample value 0000
Sample standard deviation
Minimum histogram value 7568 39.30
Maximum histogram value 7594 1.000
Histogram mean 0000 0.000
Histogram standard deviation 0000 0.047

Data Histograms

Record Info [13 10 70 50 20 8728]
Histogram Descriptor RAW DATA
Number of histogram bins 1 4096
Mean sample value 0000
Sample standard deviation
Minimum histogram value 9152 15.405
Maximum histogram value 6740 1.000
Histogram mean 0000 0.000
Histogram standard deviation 0000 0.088

Range Spectra

Record Info [14 10 80 50 20 4272]

Range Spectra
Record Info [15 10 80 50 20 4272]

Radar Parameter Update
Record Info [16 10 100 50 20 40]

Radar Parameter Update
Record Info [17 10 100 50 20 40]

Radar Parameter Update
Record Info [18 10 100 50 20 40]

Detailed Processing Parameters
Record Info [19 10 120 50 61 1312]
Near Slant Range (km) 292.9218445
Near Range Incidence Angle (deg) 41.34
Far Range Incidence Angle (deg) 50.53

Calibration Data
Record Info [20 10 130 50 20 776]

Image Records
Record Info [1 63 192 18 18 28412]
Number of Samples 5680
Number of Lines 7995
Number of bytes per pixel 5
Data Product Description COMPRESSED CROSS-PRODUCTS

Ground Control Points

All readings are an average of independent readings, UTM, WGS-84 datum; includes number of available satellites during GPS observation. Top coordinate is north, bottom coordinate, south.

Guadalmina

1a – 4038602N
30 319723E
5 satellites
1b - 4038601
30319722
5 satellites
Description: 5 km. North of traffic circle beneath main coastal highway, N-340.

2a - 4042677
30 317735
5 satellites
2b - 4042664
30 317736
5 satellites
Description: ascent, curve on Benahavis highway, north from N-340 traffic circle.

3a - 4043829
30 316862
5 satellites
3b - 4043838
30 316865
5 satellites
Description: Benahavis highway.

Vejer de la Frontera
4a - 4016427
30 234068
4 satellites
4b - 4016441
30 234070
4 satellites
Description: Reading taken at main traffic circle on coastal highway, N-340.

Ground Control Points – continued

Medina-Sidonia

5a - 4037156
30 238727
6 satellites
5b - 4037155
30238727
6 satellites
Description: Reading taken at Vejer-Medina-Sidonia highwat traffic circle on southwest outskirts of city.

Dona Blanca

6a - 4057272
29 754194 ZONE 29 READING**
6 satellites
6b - 4057270
29 754202 ZONE 29 READING**
6 satellites
Description: Reading taken at archaeological site.

Velez-Malaga

7a - 4078829
30 396719
5 satellites
7b - 4079933
30 396710
5 satellites
Description: Reading taken at southwest reach of Embalse de Vinuela on the A-356 highway to Riogordo and Colmenar.

Guadalmina

8a - 4042595
30 317706
5 satellites
8b - 4041513
30 318451
Description: Reading taken at closure of alluvial deposition located at north end of fan on Guadalmina River; intersects main curve of Benahavis highway as it enters river gorge.

Ground Control Points – continued

Benahavis

9a - 4043739
30 316842
5 satellites
Description: Reading taken on main thoroughfare of Benahavis at central parking zone and park.

Benalup

10a - 4043741
30 316840
3 satellites
10b - 4026262
30 247163
4 satellites
10c - 4026263
30 247171
4 satellites
Elevation check: 136 metres, 1250 Local time, Spain.
Description: Benalup traffic circle on northeast side of town.

Las Cuevas

11a - 4022875
30 254527
2 satellites - extreme obstruction from nearby rock peaks.
11b - 4022875
30254527
3 satellites - extreme obstruction from nearby rock peaks.
11c - 4022075
30 254827
3 satellites - extreme obstruction from nearby rock peaks.
Description: Bronze Age archaeological site located due southeast of Benalup, Cadiz, Andalucia, Spain.

Embalse de Charco de Redondo

12a - 4015386
30 267986
4 satellites
12b - 4015385
30 267988
4 satellites
Elevation check: 97 metres, 1356 Local time, Spain.

Rio Jara

13b - 3992103
30262870
5 satellites
13c - 3992102
30262870
6 satellites
Description: Reading taken from old Rio Jara coastal highway bridge-possible high-iron content disturbance of readings.

Betis

14a - 3994902
30 257835
5 satellites

14b - 3994910
30 257822
5 satellites

14c - 3994932
30 25778
5 satellites
Description: Taken north bank of Rio Valle as it enters behind littoral sandbar, nearby camp shelter constructed of high reflectance metal, possibly aluminum.

Monastery of Nuestra Senora, north of Tarifa, Cadiz, Andalucia, Spain

15a - 3996074
30 263514
4 satellites
15b - 3996083
30 263516
6 satellites
15c - 3996102
30 2633537
7 satellites
Elevation check: 82 metres, Local time of 1835, Spain.
Description: Active Catholic monastery located on elevated point in littoral valley, bounded on three sides by sheer, rapidly ascending arenal slopes.

Ground Control Points – continued

Rio Jara (2)

16a - 3992078N
30 262882E
4 satellites
16b - 3992087
30 262852
3 satellites
16c - 3992093
30 26847
3 satellites
16d - 3992093
30 262868
5 satellites
Description: Second attempt to verify Rio Jara, unknown if high iron content is obscuring readings due to inability to obtain 6 satellites for double triangulation.

Tarifa (2)

17a - 3990336
30 264711
6 satellites
17b - 3990336
30 264708
8 satellites
17c - 3990334
30 254708
6 satellites
Description: West traffic circle on N-340 coastal highway.

Tarifa (3)

18a - 3989632
30 265949
6 satellites
Local time check: 1245, Spain.
18b - 398963
30 265948
6 satellites
Local time check: 1245.45, Spain.

Ground Control Points - continued

Mirador el Estrecho de Gibraltar

19a - 3992983
30 269784
4 satellites
19b - 3993002
30 269837
5 satellites
19c - 3993040
30 269989
5 satellites
Description: Reading taken at N-340 overlook to Straits of Gibraltar.

Punto Carnero

20a - 3995350
30 281485
5 satellites
20b - 3995349
30 281483
5 satellites
Description: south entrance to Punto Carnero lighthouse on Bay of Gibraltar.

Punto de los Pescadores and Las Rocas

21a - 3996051
30 281209
5 satellites
21b - 3996050
30 281211
5 satellites
Description: 2km from Punto Carnero on western side of Bay of Gibraltar, significant for unusual geological structures in the water.

Rio Pelayo

21a - 3997268
30 279739
5 satellites
21b - 3997178
30 279767
6 satellites
Description: River outside Getares on Bay of Gibraltar, Spain.

Ground Control Points – continued

Punto Carabelo

22a – 39988905
30 280961
5 satellites
22b - 3998890
30 280960
6 satellites
22c - 3998831
30 280996
7 satellites
Description: Suburb of Getares and Algeciras, Spain on Bay of Gibraltar.

Algeciras

23a - 3999855
30 280090
6 satellites
23b - 3999859
30 280106
7 satellites
Description: Entrance on northwest to new Algeciras yacht basin.

Rio Palmones

24a - 4004919
30 278742
7 satellites
24b - 4004899
30 278741
7 satellites
24c - 4004897
30 278747
7 satellites
Description: River flowing south into Bay of Gibraltar, Spain.

Rio Guadalete

25a - 4006098
30 279195
4 satellites
25b - 4006206
30 279293
6 satellites

25c - 4006220
30 279327
7 satellites
Description: River flowing south into Bay of Gibraltar, Spain.

Los Barrios

26a - 4005775
30 279012
6 satellites
26b - 4005754
30 279012
6 satellites
Description: Traffic circle intersection with N-340 and A-440 north to Jerez de la Frontera.

Embalse de Almodovar (Valle de Ojen)

27a - 4004871
30 262361
3 satellites
27b - 4004871
30 262363
4 satellites
27c - 4004873
30 262370
4 satellites
27d - 4004905
30 262450
6 satellites
27e - 4004888
30 262481
7 satellites
Description: Water reservoir at the western entrance to the Valle de Oijen and west of Facinas, Cadiz, Andalucia, spain.

Tarifa (4)

28a - 3987764
30 265367
5 satellites
28b - 3987765
30 265358
5 satellites

28c - 3987778
30 265353
5 satellites
Description: Reading taken at the foot of the "Christ on the Straits of Gibraltar" statue on outer mole, or pier, of Tarifa harbor.

Puerto Sotogrande

1a - 4018725
30296032
4 satellites
1b - 4018727
30296027
4 satellites
1c - 4018729
30296026
5 satellites
Description: Position taken at intersection of beach and rock mole on eastern side at low tide.

Torre Manilva

1a - 4028388
303031672
3 satellites
1b - 4028388
30301672
3 satellites
1c - 4028404
30301653
4 satellites
Description: Position taken 25 metres behind watchtower at 6 metres above sea level.

Rio Padron

1a - 4034457
30311281
6 satellites
1b - 4034459
30311278
6 satellites
1c - 4034454
30311291
6 satellites

1d - 4034428
3011334
6 satellites
Description: Local time check, 13:51.03 Spain, elevation at 59 metres. Position taken at mouth of river some 100 metres from Kempinski Hotel on eastern shoreline. Mouth is closed at low tide and displays evidence of high nitrogen input with large algal growths.

Rio Guadalmansa

1a - 4036079
30315717
6 satellites
1b - 4036081
30315723
6 satellites
1c - 4036078
30315711
6 satellites
1d - 4036076
30315704
6 satellites
Description: Mouth of Guadalmansa on eastern shore.

Rio Guadalmina

1a - 4036850
30320361
8 satellites
1b - 4036879
30320374
8 satellites
1c - 4036873
30320361
8 satellites
1d - 4036885
30320366
8 satellites
1e - 4036888
30320372
8 satellites
1f - 4036874
30320364
8 satellites

1g - 4036872
30320364
8 satellites
Description: Local time check, 14:56.18, Spain, with elevation at 28 metres. Position taken at the mouth of the river in front of the Guadalmina Hotel golf course. Mouth is tidal with intense urbanization surrounding its shoreline. Some evidence of algal growth with deep-pooling of water behind the shallow sand barrier at its mouth.

Marbella - Ronda (Along eastern track of Rio Guadalmina north into the Sierra Bermeja)

1a - 4047233
30318657
5 satellites
1b - 4047263
30318650
5 satellites
1c - 4047311
301318642
4 satellites
Description: Position taken at Km. 160 marker.

Marbella - Ronda (Along eastern track of Rio Guadalmina north into the Sierra Bermeja)

1a - 4049348
30315383
7 satellites
1b - 4049365
30315419
7 satellites
1c - 4049369
30315425
6 satellites
Description: View of upper Rio Guadalmina valley; photograph taken.

Ronda

1a - 4070269
30307932
5 satellites
1b - 4070206
30307946
5 satellites
1c - 4070172
30307969
5 satellites
Description: Position taken at eastern traffic circle intersecting A-376 and c-341/344.

Ground Control Points – continued

Atajate

1a - 4057053
30299144
3 satellites
1b - 4057051
30299141
3 satellites
1c - 4057093
30299115
3 satellites
Description: Position taken on southeastern edge of town. Satellite view blocked on west and north by high mountain ridge.

Jimera de Libar

1a - 4058468
30296632
4 satellites
1b - 4058453
30296636
5 satellites
1c - 4058450
30296636
5 satellites
Description: Main intersection on southern edge of village.

Cortes de la Frontera

1a - 4055698
30291017
3 satellites
1b - 4055687
30290995
3 satellites
1c - 4055673
30290964
3 satellites
Description: Position taken on northern edge of village. Satellite view blocked by continuous mountain ridge running from the southwest to the northeast (Sierra de Libar).

Ubrique

1a - 4060809
30781125
4 satellites
1b - 4060815
30281133
5 satellites
1c - 4060818
30281141
5 satellites
Description: Position taken at southern edge of town 100 metres past first desvio, or turnabout.

Alcala de los Gazules

1a - 4039085
256292
5 satellites
1b - 4038737
2563005
5 satellites
1c - 4038983
30256292
5 satellites
Description: Position taken at intersection of Puerto Galiz road and Alcala by-pass (CA-511).

Conil de la Frontera

1a - 4018699
29762319
4 satellites

1b - 4018706
29762289
4 satellites

1c - 4018721
29762239
4 satellites

Description: Position taken in Gale Force 10 conditions at south traffic circle.

Playa La Barrosa Red Cross Lifesaving Station

1a - 4028607
29752790
4 satellites
1b - 4028606
29752790
4 satellites
1c - 4028606
29752790
4 satellites
Description: Position taken in Gale Force 10 conditions at station parking lot, north of main building.

Punto or Playa de Sancti Petri

1a - 4030471
29750503
5 satellites

1b - 4030491
750504
5 satellites

1c - 4030505
29750503
5 satellites

Description: Position taken at extreme reach of beach on southeastern shore across from island of Sancti Petri, an abandoned monastery. Gale Force 10 conditions.

Jerez de la Frontera

1a - 4063163
29754358
4 satellites

1b - 4063179
29754357
4 satellites

1c - 4063193
29754356
4 satellites

Description: Local time check, 14:36.02, Spain. Position taken at San Lucar de Barrameda to Jerez de la Frontera road intersection, 50 metres northwest of main traffic circle, N-IV and CA-602. Gale Force 10 conditions.

Chipiona Lighthouse

1a - 4068871
29728495
4 satellites
1b - 4068853
29728481
5 satellites
1c - 4068845
29728460
5 satellites
Description: Position taken on the eastern side of the lighthouse in Gale Force condition 10.

Chipiona Main Church (La Iglesia)

1a - 4087940
29728693
4 satellites
1b - 4087944
29728682
5 satellites
1c - 4087950
29728674
5 satellites
Description: Position taken on eastern parking lot between seawall and church wall entrance.

Bonanza

1a - 4076749
29737745
5 satellites
1b - 4076723
29737740
7 satellites
1c - 4076717
29737733
7 satellites
Description: Position taken at closest point between Rio Guadalquivir and Bonanza to La Algaida road.

Ground Control Points – continued

La Algaida Entrance to Coto De Donana

1a - 4081280
29739405
5 satellites
1b - 4081279
29739406
5 satellites
1c - 4081278
29739406
5 satellites
Description: Position taken 50 metres from end of pavement beneath clearing of coastal pine tress on sand path.

Trebujena

1a - 4084356
29752135
5 satellites
1b - 4084354
29752133
7 satellites
1c - 4084353
29752134
7 satellites
Description: Position taken near northern portion of town at Virgen de Palmares building.

Rio Guadalquivir

1a - 4086795
29746702
5 satellites
1b - 4086804
29746703
6 satellites
1c - 4086947
297466681
5 satellites
Description: Position taken at intersection with Trebujena and Guadalquivir service road.

Rio Guadalquivir Pump Station

1a - 4088738
29749488
5 satellites
1b - 40887235
29749497
5 satellites
1c - 4088741
29749483
5 satellites
Description: Position taken at intersection of main water pumping station and fresh water canal leading inland, north of access road "G". Photograph taken of landscape.

Lebrija

1a - 4091075
297538
4 satellites
1b - 4091079
29759525
4 satellites
1c - 4091092
29759509
4 satellites
Description: Train station. Local time check, 17:02.22, Spain.

Las Cabezas de Juan

1a - 4096263
30237442
7 satellites
1b - 4096264
30237438
7 satellites
1c - 4096265
30237436
7 satellites
Description: Intersection of A-4 and A-471 highways.

Espera to Bornos

1a - 4084073
250051
5 satellites
1b - 4084062
30250050
5 satellites
1c - 4084056
30250049
6 satellites
Description: Highway intersection at south end of village.

Bornos

1a - 4078169
30256682
4 satellites
1b - 4078168
30256684
4 satellites
1c - 4078168
30256688
4 satellites
Description: Position taken at northern central area of shoreline. Due to drought actual current shoreline is some 600 metres further south at present, 8 April 2000.

Arcos de la Frontera

1a - 4070860
30250542
6 satellites
1b - 4070860
30250540
6 satellites
1c - 4070860
30250540
6 satellites
Description: Position taken at Arcos de la Frontera end of Embalse de Bornos on south end of bridge.

Ground Control Points – continued

Arcos de la Frontera to El Algar

1a - 4063988
30256263
6 satellites
1b - 4064002
30256269
6 satellites
1c - 4064000
30256275
6 satellites
Description: Position taken at south end of dam bridge on CA-521 highway, Embalse de Guadalcacin.

Embalse de Guadalcacin

1a - 4061646
30260389
6 satellites
1b - 4061643
30260386
6 satellites
1c - 4061640
30260387
6 satellites
Description: Position taken on CA-521 on south end of second dam bridge heading south to El Algar. Elevation check displayed 68 metres with local time check of 17:33.16, Spain.

El Algar

1a - 4059692
30262393
5 satellites
1b - 4059689
30262384
5 satellites
1c - 4059690
30262381
5 satellites
Description: Position taken on eastern by-pass of El-Algar.

Cape Trafalgar Lighthouse

1a - 4008381
29766568
5 satellites
1b - 4008384
29766567
5 satellites
1c - 4008391
29766567
6 satellites
Description: Position taken at northern side of structure.

Torre de Palmar

1a - 4013619
29763150
5 satellites
1b - 4013620
29763161
6 satellites
1c - 4013632
29763173
7 satellites
Description: Position taken at eastern side of structure.

El Palmar North

1a - 4014816
29762700
8 satellites
1b - 4014864
2976263
8 satellites
1c - 4014918
29762638
8 satellites
Description: Position taken on southern shore of stream emptying into Atlantic Ocean. 1km south of Torre de Conil (estimate).

Rio Salado (Conil de la Frontera)

1a - 4017953
29761554
6 satellites
1b - 4017954
29761554
6 satellites
1c - 4017953
29761557
6 satellites
Description: Position taken on the northern shore of the Rio Salado at low tide, 200 metres from Atlantic Ocean.

La Muela

1a - 4018022
29769118
3 satellites
1b - 4018051
29769109
4 satellites
1c - 4018064
29769092
5 satellites
Description: Position taken at grain factory north of village centre.

El Camarinal Lighthouse

1a - 3997937
30247059
4 satellites
1b - 39977939
30247060
4 satellites
1c - 3997940
30247940
4 satellites
Description: Position taken 100 metres northeast of structure. Paasage blocked by barriers.

Ground Control Points – continued

Al Marchal

1a - 4003811
30247404
4 satellites
1b - 4003815
30247405
3 satellites
1c - 4003815
30247405
3 satellites
Description: Position taken on northern portion of village.

La Zarzeula

1a - 4005507
30246564
4 satellites
1b - 4005473
30246585
4 satellites
1c - 4005452
30246603
4 satellites
Description: Position taken in centre of village.

Tahivilla

1a - 4008128
30251919
5 satellites
1b - 4008131
30251923
5 satellites
1c - 4008132
30251924
5 satellites
Description: Position taken across from main petrol station at main turnabout.

Facinas

1a - 4003717
30256726
4 satellites

Facinas
1b - 4003717
30256734
5 satellites
1c - 4003717
30256736
5 satellites
Description: Intersection with Parque Valle de Ojen (Los Barrios road) and Facinas road, north edge of town.

Valle deOjen (El Tiradero)

1a - 4004790
3026772
4 satellites
1b - 40044797
30267707
4 satellites
1c - 40044787
30267674
Description: Position taken beneath massive acorn trees with high mountain ridges to the north and south of survey point; taken ove opening in trees on gravel road running over a small stone bridge in driving rain.

Pass of Ojen

1a - 4005680
30267878
5 satellites
1b - 4005682
30267890
5 satellites
1c - 4005684
30267886
5 satellites
5 satellites
Description: Position taken at abandoned structure overlooking high pass of Ojen.

Ojen and Old A-381 Entrance

1a - 4009918
30271489
5 satellites

1b - 4009901
30271477
5 satellites
1c - 4009928
30271490
4 satellites
Description: Old bridge of Valle de Ojen entrance to A-381 highway from Jerez de la Frontera to Las Barrios.

San Jose de Valle and Puerto de Galiz Road Intersection

1a - 4046665
30262140
4 satellites
1b - 4046667
30262167
4 satellites
1c - 40466669
30262234
4 satellites
Description: Position taken at intersection of roads over Sierra de las Cabras.

Puerto de Galis
1a - 4049239
30267218
3 satellites
1b - 4049235
302671218
4 satellites
1c - 4049235
302671218
4 satellites
Description: Position taken .5 kilometres of intersection with Ubrique highway, C-3331.

Benamahoma

1a - 4070964
30280554
5 satellites
1b - 4071021
30280503
5 satellites

Ground Control Points - continued

Benahoma

1c - 4071076
302080449
5 satellites
Description: Position taken at roadside café and bridge over stream in light rain.

El Bosque

1a - 4070901
30275915
5 satellites
1b - 4070898
30275923
5 satellites
1c - 4070897
30275924
5 satellites
Description: Position taken on the north side of the bullring.

Puerto El Boyar Mountain Pass

1a - 4070422
30286142
6 satellites
1b - 4070421
30286138
6 satellites
1c - 4070424
30286142
6 satellites
Description: Elevation check against survey point noted at 1,102 metres above sea level. GPS receiver registered 1,072 metres in elevation with a position of 4070429 N by 3028250 E. Position taken in mixture of fog, sllet, snow and rain. This should be regarded as the most accurate position in all dimensions (x, y, z and t). Local time, 15:06.16, Spain.

Grazalema

1a - 4020861
3028121
4 satellites
1b - 4020861
3028122
4 satellites

1c - 4020862
3028122
4 satellites
Description: Position taken at scenic overlook on south of town across from roadside restaurant with mountain ridge behind. Photograph taken.

Ronda Vieja or Roman Acinipo

1a - 4078766
30300564
5 satellites
1b - 4078762
30300562
5 satellites
1c - 4078754
30300562
5 satellites
Description: Position taken .5 kilometre due north of summit beneath main theater.

Montejaque

1a - 4068209
30299198
7 satellites
1b - 4068209
30299198
7 satellites
1c - 4068213
30299198
7 satellites
Description: Position taken on northern edge of village.

Benaojan

1a - 4066653
30299431
7 satellites
1b - 4066657
30299404
7 satellites
1c - 4066659
30299382
7 satellites
Description: Position taken at northern edge of town.

Ground Control Points – continued

Cueva La Pileta

1a - 4063074
30297348
6 satellites
1b - 4063071
30297347
6 satellites
1c - 4063070
30297347
6 satellites
Description: Position taken at parking lot with sheer mountain ridge to the northwest. Bronze Age archaeological site.

Benadalid

1a - 4053159
30296767
4 satellites
1b - 4053174
30296775
5 satellites
1c - 4053190
30296785
5 satellites
Description: Position taken 100 metres south of village.

Algatocin

1a - 4049835
30296072
4 satellites
1b - 4049832
30246079
4 satellites
1c - 4049826
30296081
4 satellites
Description: Position taken at south end of town.

Ground Control Points – continued

Guacin

1a - 4044371
30292560
4 satellites
1b - 4044381
30292589
4 satellites
1c - 4044381
30292614
4 satellites
Description: Position taken on north end of village.

Jimena de la Frontera

1a - 4035532
30280021
5 satellites
1b - 4035518
30280016
5 satellites
1c - 40355321
30280010
5 satellites
Description: Position taken on eastern side of town on main local access road next to power station.

CORONA

Entity Id :	DS1117-1011DA068
Mission Number :	1117-1
Frame Number :	68
Acquisition Date :	1972/05/26
Browse Availability :	YES
Camera Type :	AFT
Camera/Resolution :	STEREO HIGH
Northwest Latitude :	N36 25
Northwest Longitude :	W006 49
Northeast Latitude :	N36 07
Northeast Longitude :	W004 05
Southeast Latitude :	N35 56
Southeast Longitude :	W004 10
Southwest Latitude :	N36 14
Southwest Longitude :	W006 48
Area Indicator :	Entity partially covers the search area
Revolution :	011D
Image Type :	BLACK and WHITE
Film Type :	70mm PANORAMIC
Generation :	2
Polarity :	NEGATIVE
Browse Path :	1117-1/011D/A/DS1117-1011DA068.jpg

AVHRR

Dims: 2232 x 700 x 5 [BIP]
Size: [Integer] 3,906,000 bytes.
Sensor Type: AVHRR
Byte Order : Host (Intel)
Projection : UTM
  Datum : WGS-84
  X Pixel : 1100.00Meters
  Y Pixel : 1100.00 Meters
Wavelength : 0.63 - 12.00

C band Imaging RADAR metadata

File Descriptor Record

Record Info [1 63 192 18 18 720]
Data Format (A = ASCII) A
Format Control Doc. CEOS-SAR-CCT
Format Control Doc. Version A
Record Format rev.level A
Software ID 3.1
File Number 4
File Name pr49831_ldr_ceos

Data Set Summary

Record Info [2 10 10 50 20 2016]
SAR channel indicator 28
Scene Identifier N54
Site name Str of Gibraltar
GMT at Image center 1994/10/03 13:47:50.616
MET at Image center 03 02:31:50.641
Latitude at Image center 36.18
Longitude at Image center -5.38
Processed scene range (km) 64.83
Processed scene azimuth (km) 106.92
Sensor ID SIR-C -C -MD13-hvhv
Sensor Platform Heading (deg) 139.48
Incidence Angle 24.15
Radar Frequency (GHz) 5.29
Quantizer descriptor (8,4)BFPQ
Nominal PRF 1395.00
Processing Facility JPL
Processing software version 3.0.2
Product type MULTI-LOOK COMPLEX
Number of azimuth looks 3.97
Number of range looks
Line spacing (m) 12.50
Pixel spacing (m) 12.50
Orbital Direction DESCENDING

Map Projection

Record Info [3 10 20 50 20 1620]
Map projection descriptor GROUND RANGE
Geodedic alt from ellipsoid (km) 225.37
Name of reference ellipsoid GEM6
Semimajor axis ref ellipsoid (km)6378.14
Semiminor axis ref ellipsoid (km)6356.75
UTM descriptor

Map Projection - continued

UTM zone signature
Map origin, false easting
Map origin, false northing
NSP descriptor
Map origin, false easting
Map origin, false northing
Projection centre longitude (deg)
Projection centre latitude (deg)
Standard parallel 1 (deg)
Standard parallel 2 (deg)
NSP central meridian 1 (deg)
NSP central meridian 2 (deg)
NSP spare 1
NSP spare 2
Near range early time latitude 36.74
Near range early time longitude -5.49
Far range early time latitude 36.35
Far range early time longitude -6.04
Far range late time latitude 35.63
Far range late time longitude -5.27
Near range late time latitude 36.01
Near range late time longitude -4.72

Platform Position

Record Info [4 10 30 50 20 800]
Number of data points 3
Year of first data 1994
Month of first data 10
Day of first data 03
Day of Year of first data pnt 276
Seconds of day of first data pnt 49662.97
Data sampling interval (sec) 8.50
Reference coordinate system GREENWICH TRUE OF DATE
Greenwich mean hour angle (deg) 0.00
Along track position error
Cross track position error
Radial position error
Along track velocity error
Cross track velocity error
Radial velocity error

Data Quality Summary
Record Info [10 10 60 50 20 464]
Calibration update date 0
Nominal azimuth ambiguity 0.00
Nominal range ambiguity 0.00
Nominal slant range resolution 0.00
Nominal azimuth range resolution 0.00
Instantaneous dynamic range 0.00
Radiometric uncertainty (dB) 0.00

Data Quality Summary
Record Info [11 10 60 50 20 464]
Calibration update date 0
Nominal azimuth ambiguity 0.00
Nominal range ambiguity 0.00
Nominal slant range resolution 0.00
Nominal azimuth range resolution 0.00
Instantaneous dynamic range 0.00
Radiometric uncertainty (dB) 0.00

Data Histograms
Record Info [12 10 70 50 20 8728]
Histogram Descriptor RAW DATA
Number of histogram bins 1 4096
Mean sample value 0000
Sample standard deviation
Minimum histogram value 4626 9.921
Maximum histogram value 0854 1.00
Histogram mean 0000 0.000
Histogram standard deviation 0000 0.092

Data Histograms
Record Info [13 10 70 50 20 8728]
Histogram Descriptor RAW DATA
Number of histogram bins 1 4096
Mean sample value 0000
Sample standard deviation
Minimum histogram value 1521 7.107
Maximum histogram value 5892 1.000
Histogram mean 0000 0.000
Histogram standard deviation 0000 0.106

Range Spectra
Record Info [14 10 80 50 20 4272]

Range Spectra
Record Info [15 10 80 50 20 4272]

Radar Parameter Update
Record Info [16 10 100 50 20 40]

Radar Parameter Update
Record Info [17 10 100 50 20 40]

Radar Parameter Update
Record Info [18 10 100 50 20 40]

Detailed Processing Parameters
Record Info [19 10 120 50 61 1312]
Near Slant Range (km) 233.51
Near Range Incidence Angle (deg) 15.47
Far Range Incidence Angle (deg) 30.01

Calibration Data
Record Info [20 10 130 50 20 776]

Image Records
Record Info [1 63 192 18 18 25952]
Number of Samples 5188
Number of Lines 8555
Number of bytes per pixel 5
Data Product Description COMPRESSED CROSS-PRODUCTS

L band Andalucia Imaging RADAR metadata

File Descriptor Record
Record Info [1 63 192 18 18 720]
Data Format (A = ASCII) A
Format Control Doc. CEOS-SAR-CCT
Format Control Doc. Version A
Record Format rev.level A
Software ID 3.1
File Number 1
File Name pr49830_ldr_ceos

Data Set Summary
Record Info [2 10 10 50 20 2016]
SAR channel indicator 18
Scene Identifier N54
Site name Str of Gibraltar
GMT at Image center 1994/10/03 13:47:50.616
MET at Image center 03 02:31:50.641
Latitude at Image center 36.1887054
Longitude at Image center -5.38
Processed scene range (km) 64.83
Processed scene azimuth (km) 106.92
Sensor ID SIR-C -L -MD13-hvhv
Sensor Platform Heading (deg) 139.48
Incidence Angle 24.15

Data Set Summary - continued

Radar Frequency (GHz)	1.249
Quantizer descriptor	(8,4)BFPQ
Nominal PRF	1395.00
Processing Facility	JPL
Processing software version	3.0.2
Product type	MULTI-LOOK COMPLEX
Number of azimuth looks	3.97
Number of range looks	
Line spacing (m)	12.50
Pixel spacing (m)	12.50
Orbital Direction	DESCENDING

Map Projection

Record Info [3 10 20 50 20 1620]
Map projection descriptor GROUND RANGE
Geodedic alt from ellipsoid (km) 225.3793335
Name of reference ellipsoid GEM6
Semimajor axis ref ellipsoid (km)6378.14
Semiminor axis ref ellipsoid (km)6356.75
UTM descriptor
UTM zone signature
Map origin, false easting
Map origin, false northing
NSP descriptor
Map origin, false easting
Map origin, false northing
Projection centre longitude (deg)
Projection centre latitude (deg)
Standard parallel 1 (deg)
Standard parallel 2 (deg)
NSP central meridian 1 (deg)
NSP central meridian 2 (deg)
NSP spare 1
NSP spare 2
Near range early time latitude 36.74
Near range early time longitude -5.49
Far range early time latitude 36.35
Far range early time longitude -6.049
Far range late time latitude 35.63
Far range late time longitude -5.27
Near range late time latitude 36.01
Near range late time longitude -4.727

Platform Position

Record Info [4 10 30 50 20 800]
Number of data points 3
Year of first data 1994
Month of first data 10
Day of first data 03
Day of Year of first data pnt 276
Seconds of day of first data pnt 49662.974998474121094
Data sampling interval (sec) 8.50
Reference coordinate system GREENWICH TRUE OF DATE
Greenwich mean hour angle (deg) 0.00
Along track position error
Cross track position error
Radial position error
Along track velocity error
Cross track velocity error
Radial velocity error

Data Quality Summary

Record Info [10 10 60 50 20 464]
Calibration update date 0
Nominal azimuth ambiguity 0.00
Nominal range ambiguity 0.00
Nominal slant range resolution 0.00
Nominal azimuth range resolution 0.00
Instantaneous dynamic range 0.00
Radiometric uncertainty (dB) 0.00

Data Quality Summary

Record Info [11 10 60 50 20 464]
Calibration update date 0
Nominal azimuth ambiguity 0.00
Nominal range ambiguity 0.00
Nominal slant range resolution 0.00
Nominal azimuth range resolution 0.00
Instantaneous dynamic range 0.00
Radiometric uncertainty (dB) 0.00

Data Histograms

Record Info [12 10 70 50 20 8728]
Histogram Descriptor RAW DATA
Number of histogram bins 1 4096
Mean sample value 0000
Sample standard deviation
Minimum histogram value 8505 16.081
Maximum histogram value 2149 1.00
Histogram mean 0000 0.000
Histogram standard deviation 0000 0.055

Data Histograms
Record Info [13 10 70 50 20 8728]
Histogram Descriptor RAW DATA
Number of histogram bins 1 4096
Mean sample value 0000
Sample standard deviation
Minimum histogram value 0951 16.30
Maximum histogram value 3393 1.00
Histogram mean 0000 0.000
Histogram standard deviation 0000 0.049

Range Spectra
Record Info [14 10 80 50 20 4272]

Range Spectra
Record Info [15 10 80 50 20 4272]

Radar Parameter Update
Record Info [16 10 100 50 20 40]

Radar Parameter Update
Record Info [17 10 100 50 20 40]

Radar Parameter Update
Record Info [18 10 100 50 20 40]

Detailed Processing Parameters
Record Info [19 10 120 50 61 1312]
Near Slant Range (km) 233.55
Near Range Incidence Angle (deg) 15.47
Far Range Incidence Angle (deg) 30.01
Calibration Data
Record Info [20 10 130 50 20 776]
Image Records
Record Info [1 63 192 18 18 25952]
Number of Samples 5188
Number of Lines 8555
Number of bytes per pixel 5
Data Product Description COMPRESSED CROSS-PRODUCTS

Appendix IV

Toponym Model

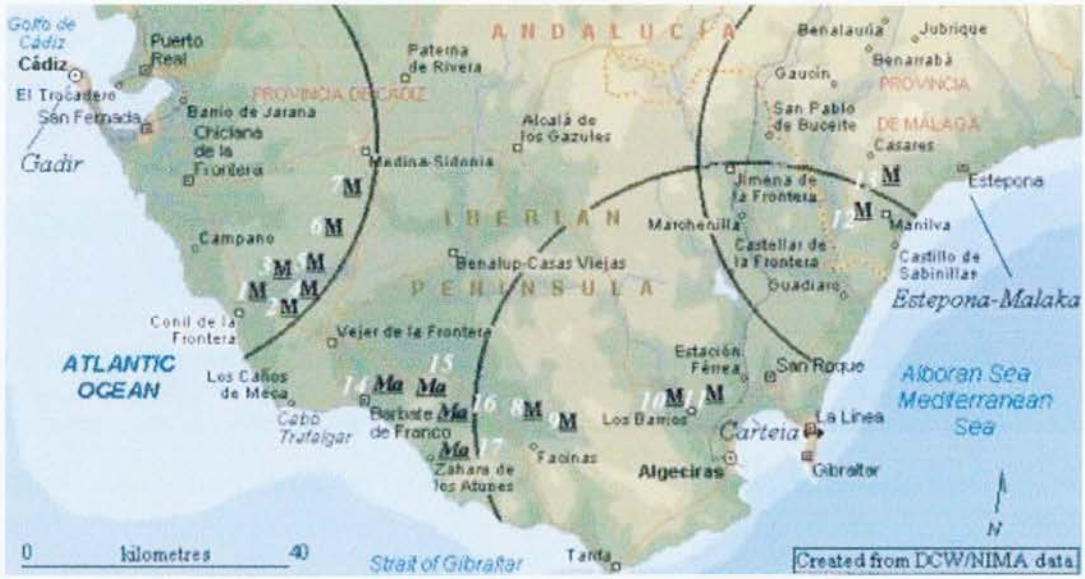

Fig. IV-I Location of metals related toponyms in Conil, Spain study region. M refers to toponyms of Celto-Iberic origin. Ma refers to later Hispano-Arabic toponyms.

IV-I The toponym model rules

The toponym model for targeting the Imaging RADAR campaign for ancient mining sites in Andalucia was constructed as follows:

a) An arbitrary maximum distance of 40 kilometres in radius was defined as a feasible trade and transport catchment area for a sea-trade entrepot, based on trafficability and least-cost path movement over the topography of the Cadiz province.

b) The three known Phoenician-Greek sea-trade entrepots of the southwestern area of the Iberian Peninsula, Gadir, Carteia and Estepona, were selected for analysis since their historical and archaeological records note a trade in metals.

c) The primary language analysed was indigenous Andalusian Spanish, with four different dialects, Bejerazano (Vejer de la Frontera), Barbateno (Barbate de Franco), Gaditano (Cadiz) and Malagueno (Malaga). Toponyms from the indigenous area dialects of Spanish were regarded as being derived from either the original Celto-Iberic languages, Latin (Roman), Greek, or Visigoth (5000 BC to 711 AD). They are signified in Figure V-1 as M. Toponyms which had a morphological structure indicating a Hispano-Arabe (Moorish) origin were regarded as more recent (711 - 1482 AD), and signified by Ma.

The Dictionary of the Royal Academy of the Spanish languages was the reference.

IV-II Toponym translations

The translations and commentaries regarding them are organised under their appropriate areas of interest, they being Gadir, Carteia and Estepona-Malaka. Another group of toponyms in the area surrounding Barbate is also included, though they are from a much later cultural period and not discussed here (711 to 1300 AD Moorish). They are *Bujar* (14), *Sierra Retin* (15), *Sierra Plata* (16) and *Punto Plata* (17). Numbers relate to map position.

Gadir –

- *Casa de la Mina (5)* – House of the mine, or "mining house". It should also be noted that in the oldest Spanish vernacular, *mina* was the word utilised for lead. *Plomo* is the world used in the modern Spanish language for this base metal. At any rate, it underscores the extent of lead mining that was carried out throughout the Iberian Peninsula. This place name is located 2-km north and east of the Conil mining complex.
- *La Mina (4)* – "The mine", or if lead was present, "the lead mine". This toponym is located 500 metres due east of *Casa de la Mina* 1.8 kilometres north and east of Conil.
- *Casa Altamina (3)* – "House of the high, or upper mine". This toponym is located some 2.2 kilometres north-northeast of the Conil mining complex. The appellation of *alta* (Eng: high, higher or upper) to the base word *mina* may describe the site's location in the midst of a chain of rolling hills which contain the ore-bearing geology of the area. The elevation at this point is 71 metres, versus a surrounding elevation of only 46 metres on average. This site was viewable from the nearby Roman era mountain fort of *Cerro Patria*, or "hill of the country or of the people".
- *Cerros de la Plata (2)* – "Hills of silver". A toponym which, according to the current topographic map of the area, is applied to the entire series of hills stretching from the Spanish national carriageway E-5 northeast to the local carriageway beneath *Los Escobones* (See map quadrant QA TF, Instituto de Cartografia de Andalucia 2000). The significance of this toponym is obvious as it points to a probable thorough survey and prospection of the geological resources within these hills over a long period of time. Further discussion over this toponym will be carried out at end of this section.
- *Casa de Poquito Aceite (1)* - "House of little oil". *Aceite* is the Spanish word for oil, but in Andalusia generally used as a colloquialism for olive oil. Olive oil was used as a processing agent in ancient mining and is mentioned by various classical writers (Pliny, tr. Rackham, 1991 and Polybius, tr. Paton, 1922). There is no evidence of present day olive grove horticulture in the immediate vicinity of this toponym, located some 3.5 km east of the main Conil mining complex.

- *Canada de la Mina (6)* – "The empty land of the mine". Pronounced "can-yah-dah deh la minah", this toponym is placed on the 1952, 1:25k topographic map (produced by the Spanish Office of Military Mapping in Madrid in an early aerial mapping campaign), in the area immediately north and west of *La Mina.* The topography of this area is flat and populated only by the occasional juniper tree and fox grasses with a light, loose soil. Whether the paucity of vegetation in the area is a by-product of mine wastes or mining is a question for archaeological survey and geo-chemical investigation. This toponym is located on a feature that extends from 2-4 km from the main Conil mine complex.
- *Algarobillos (7)* – This word is an enigma, even to the local speakers of the Bejerano (Vejer de la Frontera) dialect of Andalusian Spanish. The mountain village of *Algar*, located some 25 kilometres due east, is known to have been the site of a mining entre-pot for the Phoenicians as was *Alcala de Gazules.* While the word *Algar* has obviously passed through the lexicon of the Arabic language, due to the *al-* prefix, it is possible that *gar* is a remnant of the Phoenician language. It should remembered that the sea port of Cadiz was known to the ancients as Gadir/Gades/Gadeira, which was an adaptation of the original Phoenician spelling of *G'dr* (Bonald, 2000, Herodotus, 1996, Pliny, tr. Rackham, 1991, Polybius, tr. Paton, 1992). This is a classic example of the morphological changes of a toponym through time and language adaptation. This toponym is located 1.5 kilometres north of the Conil mine complex.

Carteia –

- *Carbones (11)* – "Coal". In the Cadiz and Malaga provinces of Andalusian Spain, the word *carbone* is used interchangeably to mean either coal or charcoal. Located in the *Valle de Ojen* region, some 20-km west of Carteia, the *Carbones* toponym is situated at the foot of small mountains, heavily populated with oak trees. Discussions with park rangers of the *Parque Nacionale de Valle de Ojen* noted that charcoal had been produced in the area up until the early 20th century.
- *Mina de Carbones (10)* – "Coal Mine". This toponym is located on the north face of a mountain (*Sierra de Carbones)* that serves as a natural boundary to the *Valle de Ojen.* It is extremely difficult to reach and required a 2 and one-half day journey by horse and foot to reach from the nearest vehicle accessible road, C-440. The site is 650 metres above sea level and has nearby springs that spill over a 30-metre cliff into the gorge that offers the only access route. There may have been opportunity mining at this site in the past, but there was no suggestion of organised extraction per the observed landscape.

- *Charcos (9)* – "Charcoal or charred wood". This toponym is located 30 km west of Carteia and due north of the *Puerto de Ojen* (Pass of Ojen, pron. "oh-hay-n"). Again, as with *Carbones*, this area suggests the creation of charcoal for localised use and not any coal extraction. However, as mentioned in Chapter 2, this is an area that was under the control of the Medina-Sidonia family for many centuries; only investigation of the family's archives might answer questions regarding mineral extraction efforts.
- *Sierra de Carbones (8)* – "Mountain of coal". See *"Mina de Carbones"*. Intensive survey over a 5-day period of this revealed no presence of coal bearing strata. However, commentary by the geological survey suggested past coal extraction (Instituto Tecnologico Geominero de Espana (ITG), Map *Tahivilla,* 2000).

Estepona-Malaka

- *Guadalmina (13)* – "River of the Mine". A toponym from the Moorish period, *Guadalmina* in the Arabic language is "*wadi al mina*". The Arabic word "*wadi*" is used throughout the Arabic world but has subtle regional differences in meaning. In Northwest Africa, today's Morocco and Western Algeria, *"wadi"* means a small rivulet, or stream, enclosed by steep slopes. This would be similar to the Scottish *glen*. In the wider Arabic-speaking world, *"wadi"* has come to be used to describe dry streambeds that may seasonally flood. This is an important distinction as the topography of the *Rio Guadalmina* is perfectly described by the Northwest Arabic regional definition; it is a permanent stream which flows through a narrow gorge, populated by various species of trees such as juniper, mytle, cedar and oak. It flows some 28 kilometres from its source in the *Sierra Bermeja* Mountains to its mouth on the Mediterranean Sea near San Pedro de Alcantara. There is an indication of modern mining (late 19th through mid-20th century) at the stream's source, southwest of the peak known as *Cascajares* (elev. 1417 m) and due west of regional highway C-339. The remains of a machinery house, transport towers for ore cars, electrical power pylons and various other related items, may be seen from highway C-339. The site is some 1000 metres beneath C-339 and is extremely dangerous to approach from this direction. The site was finally reached by all-wheel drive and foot during a three-day effort that required reaching the site from the north via Igualeja and Pujerra. No roads are marked and roads are extremely dangerous, requiring a walking guide in front on many sections; three avalanches were experienced during this reconnoitre. This site is 42 kilometres from Estepona via the modern transport network and 31 kilometres from Malaga (Malaka) by the same means.

- *Manilva (12)* – No direct translation. Manilva, the name of a small Spanish village situated some 5 kilometres due north and west of the Mediterranean Sea on regional road MA-539, is the site of modern day mining and mining during the Roman Period (Baird 1988). Modern mining in the area is strictly quarry materials, however, it is known that during the Roman period slaves were utilised for mining. *Manilva* is therefore interesting because it appears to be a corruption of two Spanish words, *manillar*, to perform by hand, and *va*, derived from the Spanish verb *ir*, which means to go. This could be a corruption of a longer, lost toponym which meant "going to a place of hand labor", which is an apt description of slave mining labor (Herodotus 1996). Heavy industrialised quarrying is performed in this area presently and no remains of ancient mining could be discerned. It should also be noted that the area has suffered significantly from the explosive development of the Spanish Mediterranean coast.

IV-III Discussion

Of the three areas of interest studied for this toponym model, it can be seen that the Gadir area grouping of mining related toponyms is the most significant and not merely for the sheer quantity. Linguistically, the Gadir toponyms display the older forms of words which are indigenous to the region and which are more likely to indicate earlier mining acitivity.

As was mentioned in the Gadir section, *mina* is a Spanish word that was used interchangeably to describe the base metal lead or an actual mine. While the word is seen in the Carteia and Estepona-Malaka groupings, what is more demonstrative in the Gadir grouping is the word *plata*, or silver. Both *plata* and *mina* are words whose morphemic and phonemic structures pre-date the introduction of Punic, Latin and Arabic linguistic influences (Bonald 2000 and Dictionary of the Royal Academy of the Spanish Languages 2001). It is well known that large quantities of high-grade lead could also yield silver. The word *plata* is not evident anywhere in the Carteia or Estepona-Malaka areas, nor is their classical reference to silver mining in this region or archaeological evidence of organised extraction (Aragorn 2000). Gadir, on the other hand, has significant evidence of not only historical, but also archaeological evidence of silver extraction in conjunction with copious amounts of lead (Aragorn 2000, Arribas 1964, Aubet 1994, Barmaki 1961, Bonald 2000, Collins 1998, Escacena 1985, Gutierrez *et al* 1991, Herodotus 1996, Junta de Andalucia *Mapa Fisografico del Litoral Atlantico de Andalusia,* Moscati 1988).

Based on the evidence indicated by this toponymic model, it was decided that the Gadir area was the best region to target using remote sensing for indications of ancient mining activity. As can be seen in Chapter 7 of this work, that evidence proved to be fruitful.

Appendix V

Mine Remote Sensing Signatures: Airigh Guadhire, Isle of Islay, Scotland

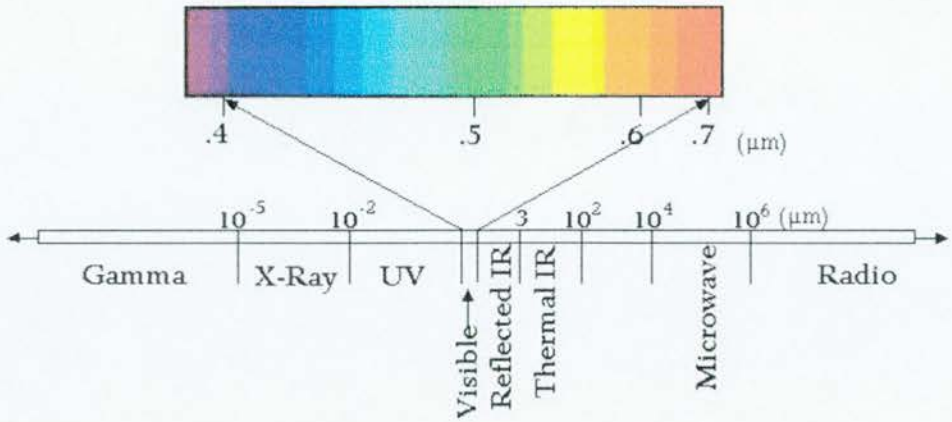

V-1 Electromagnetic spectrum (Adapted from NASA GSFC 2001)

The following image subsets of SPOT panchromatic, LANDSAT 7 (bands 3,2,1 and 7,4,1) as well as NASA Space Shuttle Imaging RADAR, are from a forthcoming work entitled *Airigh Guadhire*. They are included here to display examples of potential *visual signatures* for standard remote sensing data that might be employed for archaeological work. It may be said that these examples may also serve as a visual training cue for concepts discussed in Chapter 3 in regards to how various sensors perceive certain terrestrial features. It is beyond the scope of this work to pull individual pixels for multi-spectral data and display spectral curves, but it should be said that different remote sensing software packages will render different results based on how they induct and interpret the raw data. Therefore, images seen here are representative of how ENVI 3.4 interpreted them. Reference back to Chapter 3 and the above electromagnetic spectrum will assist in understanding these images.

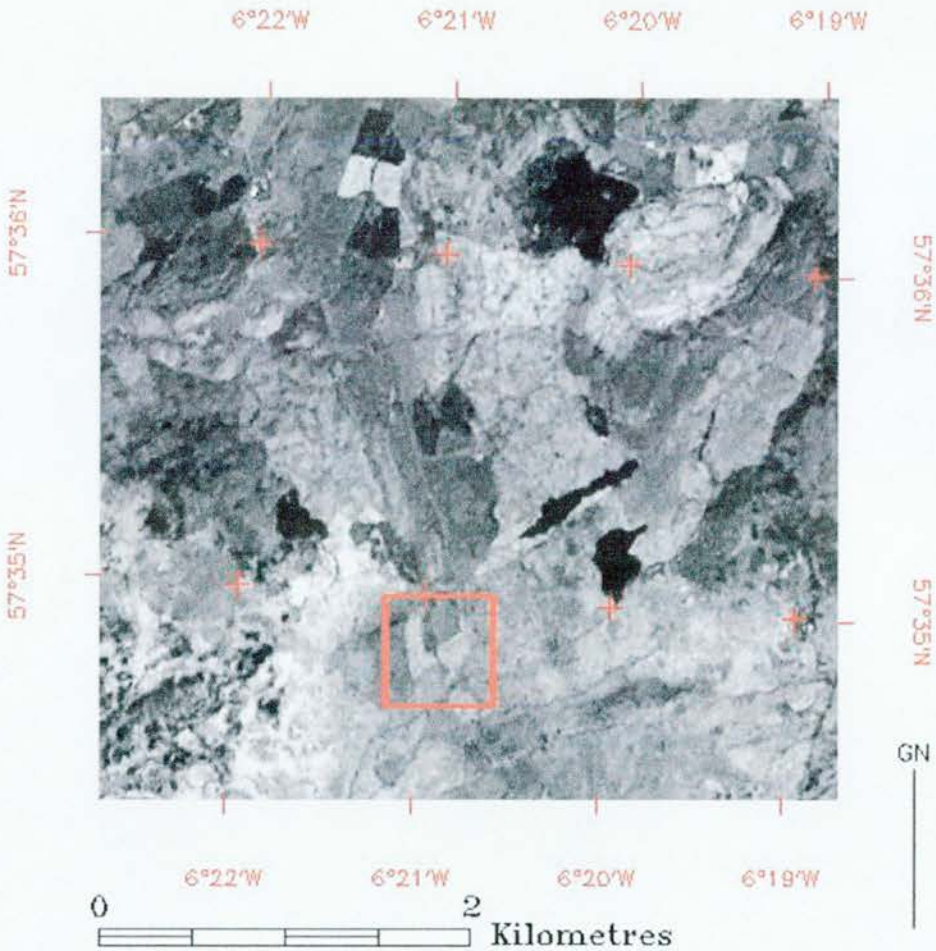

V-2 SPOT panchromatic, 10m. resolution; numerous trial mine pits in rectangle

In this image, solar radiation is optimal and the numerous trial mine pits are well illuminated without much perceptible shadow. Note the excessive brightness of the areas to the left of the red box. These are areas of former agricultural use which are now reverting to moorland.

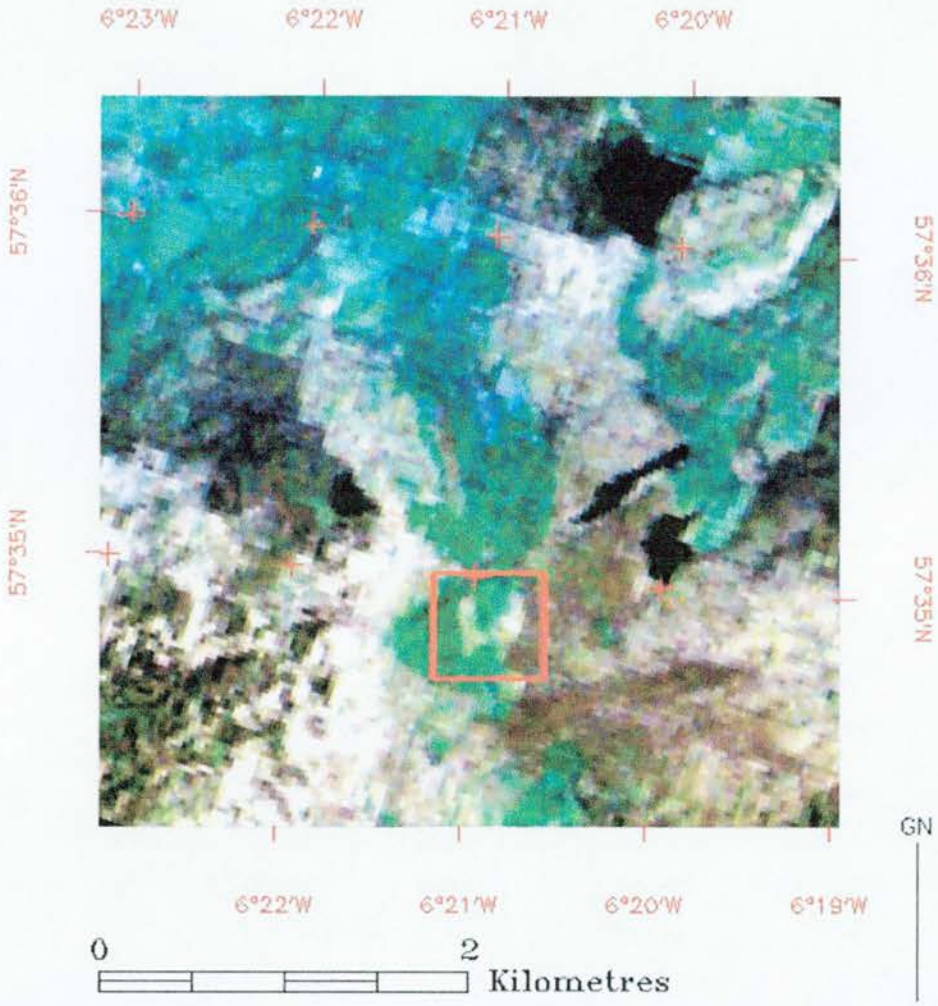

V-3 LANDSAT 7, bands 3 (red), 2 (green) and 1 (blue); re-sampled to 10m. Original resolution 30m; trial mines area denoted by rectangle.

In this image, the LANDSAT 7 image is too coarse a resolution to perceive individual trial mine pits, but it does display potential areas of vegetation stress which might be investigated by other combinations of bands. Notice that the area around the trial mine pits now presents another area to the right which appears to have had some form of disturbance in the natural vegetation growth atop a limestone outcrop with loose pelitic soils. This may be due to recent agricultural use or again, to past mining practices.

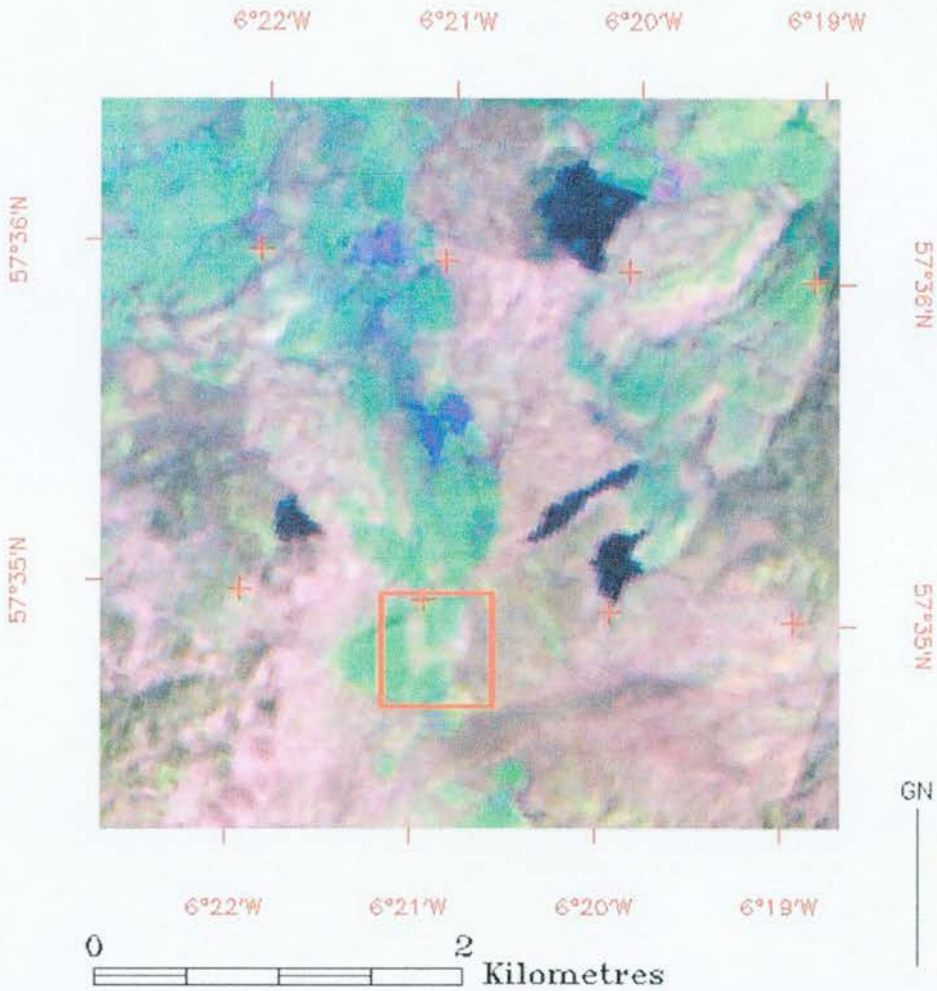

V-4 LANDSAT 7, bands 7 (red), 4 (green) and 1(blue), resolution re-sampled from 30 metres to 10 metres; trial mines area highlighted by red rectangle.

As mentioned in the last example image, different combinations of bands present different information. Here the substantial cliff created by an underlying fault and strike in the limestone outcrop of Airigh Guadhire is well highlighted in the north portion of the red box. Vegetation growth disturbance is also more well highlighted in the area around the trial mine pits with the previously mentioned area in the right of the red box showing greater delineation.

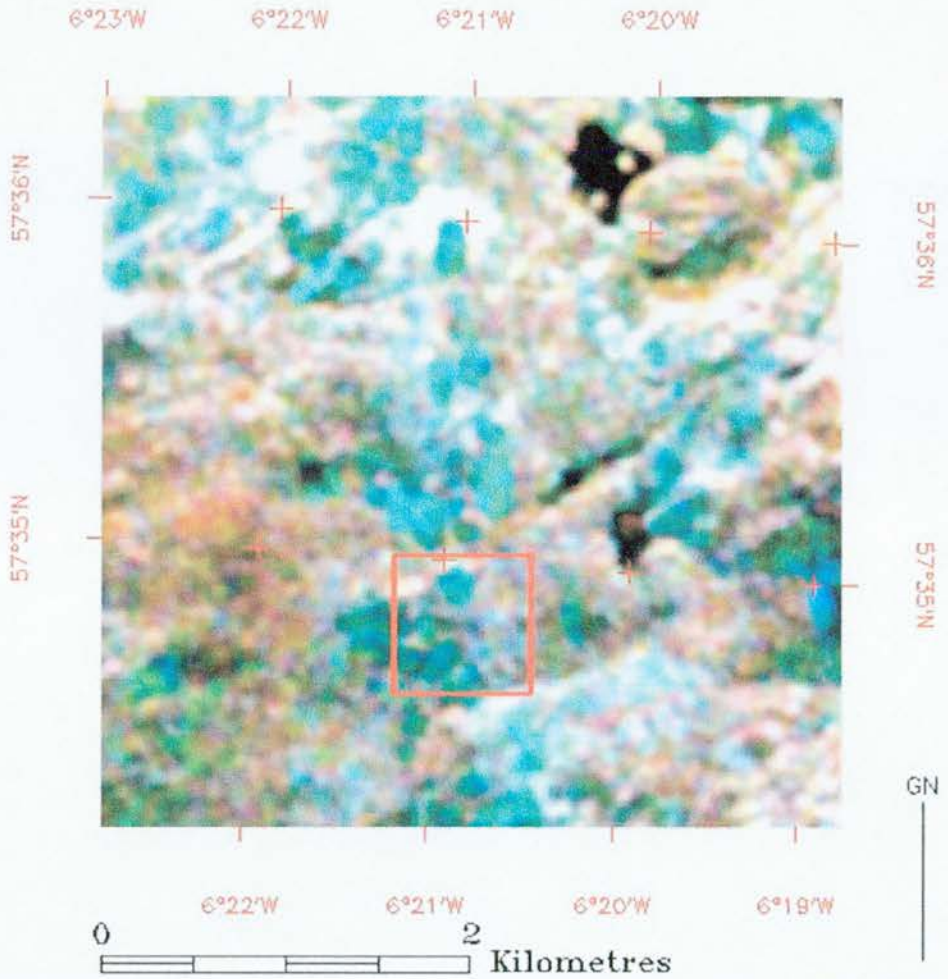

V-5 NASA Space Shuttle Imaging RADAR, MLC data, 1994. Re-sampled from 12.5 metres to 10 metres. Lvv polarisation is red, Cvv polarisation is green and Chh polarisation is blue.

In this image, the C band polarisations graphically depict the limestone outcrops and short, semi-oriented grass vegetation atop them due to their size being near the length of the wavelength, or 5.8 cm. The Lvv band, which usually detects subtle moisture areas in terrain, does so here too, with the centre area of the red box depicting a dark area linear feature which trends to the right. This is a small semi-annual burn, or stream, which is visible presently.

Band	Wavelength interval	Spectral response	Resolution	Characteristic
1	0.45-0.515	blue-green	30	Coastal water mapping, differentiation of vegetation from soils. Also useful for soil/vegetation discrimination, forest type mapping, and cultural feature identification.
2	0.525-0.605	green	30	Assessment of vegetation vigour; Also useful for cultural feature identification.
3	0.630-0.690	red	30	Chlorophyll absorption for vegetation differentiation; also useful for cultural feature identification.
4	0.75-0.900	near infra-red (ir)	30	Useful for determining vegetation types, vigour, and biomass content, for delineating water bodies, and for soil moisture discrimination.
5	1.55-1.75	mid-ir	30	Indication of vegetation moisture content and soil moisture; also useful for differentiation of snow from clouds.
6	10.40-12.50	thermal ir	60	Useful in vegetation stress analysis, soil moisture discrimination, and thermal mapping applications.
7	2.09-2.35	mid-ir	30	Hydrothermal mapping Useful for discrimination of mineral and rock types. Also sensitive to vegetation moisture content.
Pan	0.52-0.90	pan	15	Large area mapping, urban change studies.

Table V-1 LANDSAT 7 ETM+ spectral detection characteristics (Lillesand and Kiefer, 2000, USGS, 2000)

Appendix VI

The Annotated Bibliography for Remote Sensing Archaeology

The need for a comprehensive annotated bibliography of remote sensing archaeological techniques became evident early in this author's work towards a Masters of Science degree at St. Cloud State University, Minnesota in 1995. After discussing the issue with Dr. Benjamin Richason III of St. Cloud State University and Dr. McGuire Gibson of the Oriental Institute at the University of Chicago, a plan was formed for the rigorous academic assault on the subject. The research would be performed at the famous Peabody Library of Anthropology and Archaeology at Harvard University, Massachusetts. Furthermore, the work would be structured under the Chicago Manual of Writing Style to conform to the American Social Sciences standards for academic works. Lastly, the work would be thoroughly reviewed by the bibliographical research science staff at the Peabody.

The original work was completed in May 1996 and reviewed by Dr. Richard Rothaus of Ohio University, now of St. Cloud State University and the Archaeological Remote Sensing Consortium. Additional reviewers included Mr. Tony Wilkinson of the Oriental Institute of Chicago as well as the aforementioned academics, Dr. Gibson and Dr. Richardson. This 1999 edition of the work is an update to include further authors. Works who do not meet the original standards employed to create the original 1996 work are so noted.

Kind thanks are issued to Dr. Benjamin Richason III of St. Cloud State University, Dr. McGuire Gibson, Mr. Tony Wilkinson, Mr. John Sanders, Mr. Chuck Jones of the Oriental Institute of the University of Chicago, and Dr. Thomas Sever of NASA Marshall Space Center, Huntsville, Alabama. Finally, to the staff of the Jet Propulsion Laboratory, NASA, Pasadena, California, particularly Dr. Thomas Farr and Ms. Ellen O'Leary for their outstanding support in ongoing research.

Introduction

The science of remote sensing is defined as the collection of data about an object, or phenomena, without the data sensors being in direct contact with the object. Thus, the data sensors are said to be operating in a remote sensing mode that begets our terminology (Jensen 1986). While numerous sensors are commonly used to monitor geophysical processes of the earth, such as seismic events, these sensors are defined as transducers since they are in direct contact with phenomena and merely translate an analog occurrence into a digital form for scientific analysis. Remote sensing then is quite unique in its capacity to obtain data, particularly in a temporal fashion.

What then is remote sensing archaeology? Remote sensing archaeology may be defined as the methodologies and techniques pertaining to the identification, quantification, and temporal spatial analysis, of those areas of the world suspected of being impacted by humankind's cultural actions in both historic and pre-historic time periods. Furthermore, the ability of both basic and complex geophysical remote sensing systems to capture scientific data which may explain humankind's temporal position within its overall social evolution, is coupled with its capability to spatially map humankind's structural development.

The purpose of this "Annotated Bibliography of Remote Sensing Archaeology" is two-fold. First, to provide the archaeological community with a comprehensive overview of the available documentation regarding this subject and secondly, to clearly demonstrate that remote sensing archaeology is not a new, high-technology effort, as is too often trumpeted in the general and scientific media. Readers of this document will be quite likely surprised at the careful methodology of even the earliest efforts in this area of archaeology, and even more surprised at the visionary comments in what we too often consider to be the quaint past. As Prof. Thompson quoted in "Antiquity" in 1967, "...As it is, (sic) we are dealing with sensitivities beyond the human eye and, for that matter, beyond standard photographic film. Perhaps the most astounding example of this sensitivity is the possibility of distinguishing between wheat and oats as the crop in the field. The other response to Dr. St. Joseph's remarks is that the geographical and geological features he mentions are themselves of value to archaeology. To the remarks already incorporated in the paper might be added the possibility of locating, or locating more accurately, ancient trade routes. I am tempted also to underline the point in the article that satellite photography may be the impetus to lower altitude photography, and to additional types of research such as underwater remains".

Prof. Thompson's commentary would be proven true some quarter of a century later with the now renowned discovery of the "Lost City of Ubar" in the Empty Quarter of Oman by Sir Ranulph Fiennes, Prof. Juris Zarins, and Dr. Ronald Blom of NASA's Jet Propulsion Laboratory.

If a commentary from 1967 is not enough to justify in the reader's mind that remote sensing archaeology has a considerable history, then one is referred to the 1927 paper reviewed in this work by Flight Lieutenant Maitland of the Royal Air Force. Obviously, humankind has exhibited a keen interest in its past from its earliest ability to rise above its terrestrial bounds.

Looking into the future of remote sensing archaeology, many new developments and directions are evolving. With the full maturation of Geographic Information Systems technology or GIS, remote sensing archaeology has now entered into a new stage of development in relation to environmental modeling. An example of this new integration would be the PERSEUS Project that endeavors to establish the level of land change and surface degradation throughout the entire Mediterranean Sea region. On a smaller more recent scale would be the Project ZEUGMA enterprise which endeavors to map and analyse the spatial interaction of humankind within a Turkish river valley region before it is inundated by the construction of a hydrological dam.

Therein lies another one of remote sensing archaeology's great strengths, its ability to rapidly reconnoiter, survey, and analyse vast areas of the world in increasingly higher spatial resolutions, performing functions virtually impossible by humans. An increasing movement of humankind's population to the littoral zones of the world--now reported to be some 60 percent of the total global population--means that the sites to which humankind's maritime cultures first spread are being destroyed at a rate exceeding the capability of the archaeological community to examine. (Alessandro 1994) This is of course a prime opportunity for remote sensing archaeology to come to the fore.

Yet, in this rush towards the higher end of the technology bracket--the developing use of high-resolution space borne remote sensing imagery for example--basic technological developments within the easy reach of all archaeologists have been largely ignored.

Digital cameras offer a degree of terrestrial photogrammetry inconceivable some mere five years ago. Furthermore, this technology allows one to perform basic remote sensing analysis since the data captured exists in a digital form and is then eligible for image enhancement with a myriad variety of image processing software.

Global Positioning Systems are another case in point. The technology has developed to the point where unit cost is a mere fraction of its cost benefit. Current basic models are of some $100 U.S. currency and capably of some 90-meter accuracy using twelve satellites. (USGS, 2000) Clearly, there is little excuse for the failure of the widespread adoption of these technologies by either the aspiring or practicing remote sensing archaeologist.

Other avenues that are becoming increasingly important are the continuing construction of Internet databases, consisting both of imagery and archaeological reports. For the remote sensing archaeologist this is a continuing boon. While not the focus of this particular work, mention of some of the more important Internet sites relevant to remote sensing archaeology are covered in the Additional Notes portion of this paper.

The subject of obtaining imagery data and some basic image processing software is addressed within the Additional Notes section as well. The reader will note that no commercial data sources or processing software are listed. It is not the purpose of this paper to critique or to offer an opinion on commercially available products. However, it is the object of this work to point out free or minimal cost items that may enhance and further the research of archaeologists and students whom may have a limited research budget.

Finally, every effort was made to acquire and review every known article, book, or journal, regarding this subject. Readers whom may know of rare proceedings, or whom may have copies of the unavailable works listed here within are invited to forward replications to this author for ongoing review. It is impossible for this work to be complete for that is the nature of science, yet this author invites all writers on the subject to forward copies of their publications to any of the mentioned Internet databases. For until this document, remote sensing archaeology was merely a theory or doctrine within the science of archaeology. This work establishes and illustrates that there is a supporting body of scientific publications for the branch of archaeology called Remote Sensing Archaeology.

Adams, Richard E.W. *Oude Maya-Kanalen – Coordinaten En Rasters In Het Maya Oerwoud*, Oorspronklijke Engleses tekst in "Archaeology", Volume 35/ nr. 6; November 12, 1982.

This article, which is rebutted in the paper produced by Dahlin/Pope (J. of Field Archaeology, Vol. 16, 1989), expounds the hypothesis that the extensive canal structures in the Mayan areas of the Yucatan Peninsula supported the total agrarian economy of the Mayans. Adams bases his views solely on early interpretations (his own) of SAR imagery which was produced of the region by airborne means.

Critique

This reader agrees with the Dahlin/Pope arguments that Adams performed some highly improbable and suspect interpretations of the SAR imagery that was available at the time. The multi-platform assessment of area, as performed by the Dahlin/Pope (see annotation regarding this work within this paper) team appears to be the best methodology.

Adams R. M. *Heartland of Cities: Surveyal of Ancient Settlement And Land Use On The Central Floodplain Of The Euphrates*, 247 Pages, illustrations and maps; 29 cm. and map: col. on folded sheet, 72 x 42 centimetres, University of Chicago Press, Chicago, Illinois, USA; 1981.

"Heartland of Cities..." is the last volume of Prof. Adam's magnificent three-part work on settlement patterns in the Mesopotamian region. Page 33 of this volume describes a limited use of LANDSAT imagery in one particular project.

Further discussions revolve around the possible use of remote sensing technology for transport systems analysis.

Critique

It is interesting to note in this work how Prof. Adams mentions the limited application of LANDSAT imagery to his project, but how he also realises that future applications of more advanced technologies may yield more gratifying results.

Adams, Russell and Genz, Hermann. *Excavations at Wadi Fidan – A Chalcolithic Village Complex in the Copper Ore District of Feinan, Southern Jordan*, Pages 8-19, "Palestine Exploration Quarterly", No. 127, USA 1995.

A conventional archaeological expedition mounted in the present day nation of Jordan, the Wadi Fidan investigation is a classic example of Near Eastern archaeology. While no specific remote sensing efforts were made, aerial photography as well as terrestrial photogrammetry were performed (see article) to support site selection. Wadi Fidan was an extended village settlement involved in early copper mining and smelting. The authors note that these mining activities were carried out remote of the actual smelting, thus some crude transportation network existed. The authors also note that extensive Chalcolithic settlements, which were also involved in copper working, are located along the Anatolian (Turkish) border.

Critique

An interesting article in those sites such as this should be easily targeted by certain RADAR wavelengths due to their proximity to copper deposits. Furthermore, the arid desert climate would be most supportive of longer wavelength microwave remote sensing systems, which can penetrate the sub-surface structure with some degree of resolution.

Al-in, Tariq S. and Hammo, Nimmat B. *The Use of Magnetic Investigation In Iraqi Archaeological Sites – Sippar and Abu-Skhair*, Article, "Antiquities", New York, NY, USA; March 1985.

The authors discuss the application of a proton magnetometer at two long investigated sites on the central Iraqi plain, Sippar and Abu-Skhair. The Sippar site was believed to have been inhabited for only one period while Abu-Skhair experienced multiple inhabitations. Al-In and Hammat are the first archaeologists to employ this technology (at the time of the article) in Iraq and had no knowledge of previous attempts to do so. The investigators were able to define the significant objects and features of the sites to a highly accurate degree. They generated total magnetic field values, which were represented via contour maps, and computed residual magnetic values were displayed on contour and magnetic density maps. Soil, brick, and various other object samples were collected from each site area and tested for susceptibility measurements under the Kappabridge KLY I. These techniques generated very precise values in the view of the authors.

The authors noted that the Sippar site was much easier to formulate a quantitative and qualitative interpretation, largely due to its singular significant inhabitation. Conversely, Abu-Skhair was much more difficult in the view of the authors, due to increased anomalies from subsequent building over many generations.

The authors for quantitative analysis of the Sippar area site used a two-dimensional magnetic model program. This was done to generate thickness, depth, and extent of the hurled archaeological features. Various other formulae were also employed by the authors to supplement these efforts, particularly in computing depth to Center of body.

Critique

The authors give valuable information on the geology of the sites, particularly for conventional space platform imaging systems. The geology is noted as follows: "...these sites are located on the central and southern part of Iraq, which is characterised by a flat, featureless, topography. This plain represents older colian, lacustrine, delta, and flood plain deposits. The sediments are generally semi-lithified or loose consisting of all varieties of granulars, gravels, sands, silts, and clays".

A prime question here though is what effect would the increased magnetic field anomalies generated by the burnt bricks have on a spaceborne SAR system such as the SIR-C/X-SAR Shuttle Imaging RADAR or the RADARSAT satellite. This would certainly be an intriguing aside to some very useful research.

Allan J.A. & Richards T.S. *Use Of Satellite Imagery In Archaeological Surveys*, Pages 4-8, "Libyan Studies" No. 14; 1983.

A copy of this particular work was unavailable for review during the compilation of this annotated bibliography, however the work is mentioned in several remote sensing and archaeological techniques bibliographies.

Critique: Not available for review.

Anonymous. *Angkor by Satellite*, Pages 12-13, Athena Review,
No. 1; 1995.

Another ephemeral bibliographical listing pertaining to remote sensing and archaeology, yet no copy was could be retrieved for review and commentary for this annotated bibliography.

Critique: Not available for review.

Arnold H.J.P. (1989). *The Great Wall of China from space: The Exploration of A Myth*, Pages 248-252, "Spaceflight", No. 31, United Kingdom; 1989.

Arnold attempts to find the realities behind the oft-quoted quip that "the Great Wall of China is the only man-made object viewable from space". During the course of his exposition several interesting points are made in regards as to the actual usefulness of remote sensing in archaeological applications. One of his more astute observations revolves around the tendency to overlook terrestrial observations in lieu of the high technology applications.

Critique

Yet again, one of the few balanced arguments for a careful use of remote sensing technology, particularly space borne platforms. Arnold argues well for a comprehensive historical, cultural and environmental survey of any site before resorting to an often times expensive remote sensing campaign. Still, in this reader's mind a carefully planned and conservatively mounted remote sensing campaign should be a part of any archaeological exploration for the simple temporal aspect of the data collected.

Arnold, J.E., Ambos, E.L. and Larson, D.O. *Geophysical Surveys of Stratigraphically Complex Island California Sites: New Implications for Household Archaeology*, Pages 157-168, "Antiquity", No. 71, United Kingdom; 1997.

An interesting article that discusses the usefulness of both ground penetrating radar (GPR) and caesium vapour magnetometry—one of the more rarefied technologies-in a non-intrusive survey of the Californian Channel Islands (Santa Barbara, Santa Cruz, San Miguel and Anacapa.

The CVM technology is based on the theory that caesium atoms behave in a predictable fashion when their electron shells are disturbed by an imposing magnetic field. Ground penetrating RADAR, on the other hand is based on the permitivity of the various materials that its wavelengths pass through.

The authors note that CVM technology far surpasses traditional magnetometry in its precision and that in conjunction with CVM provides an extraordinary exploratory tool.
The authors also conclude that after the examination of the Prisoners Harbour Site, "researchers conducting fieldwork in other parts of the world where thick dense shell middens occur, including South Africa, Brazil, Australia, ...North America (etc.)...can benefit from these experiments. GPR and CVM are remarkably effective in detecting both major and relatively subtle features within the complex, packed shell middens, particularly when used together".

Critique

This reader agrees with the assessment of these authors that "these geophysical methods have become increasingly affordable and comprehensible to archaeological investigators during the 1990s, they have become essential tools for first-stage, non-destructive sub-surface investigations at an increasingly wide array of site types, including stratigraphically complex coastal communities".

Spinal, A. and Heathcote, C. *Some Aspects of the Use of Fluxgate Magnetometers (Gradiometers) In Geophysical Prospection in Archaeology*. Paper published by School of Archaeological Sciences, Bradford, West Yorkshire, UK; 1978.

A highly technical work that should not be undertaken by the reader without a modicum of electromagnetic wave theory, this paper pursues the analysis parameters of fluxgate potentiometers.

The authors found that when a survey was being conducted, "using a trace recording technique, the results can easily be transposed to a suitable form if the angle, between the direction of the transverse and the axis of the feature, can accurately be determined". The team also finds that the ease of operation and efficiency, in comparison to aeromagnetic surveying are inestimably easier.

Critique

This article which should not be undertaken by the technically illiterate as several complex theories involving electromagnetic theory are discussed. This author was forced to turn to electrical theory books not used in some years even with a strong technical background. Still, a refreshingly technical approach to an often times underwritten subject.

Author Unknown. *A Magnetic Survey In the Plaza Area of the Spiro Mounds Site*, Oklahoma Archaeological Reports. Oklahoma City, Oklahoma, USA; 1982.

In March 1981, a proton magnetometer test was performed on the plaza area of the Spiro Mounds Site in eastern Oklahoma. The site was an important ceremonial Center some 800 years ago and is now preserved at a State of Oklahoma park and museum. The site was divided into blocks co-ordinated with an ongoing site dig. The authors conclude that the magnetometer was highly effective in establishing hearth sites and ceremonial fire locations. A graphics software suite, the Harvard Symap system, was employed to better display the results.

Critique

It appears that magnetometric work was highly popular in the early 1980's, possibly as an alternative to the cost-prohibitive use of period satellite imagery and its low resolution. It is problematic as to whether many sites such as this would warrant a revisit with current remote sensing technologies and GIS software, but it would certainly be an intriguing issue.

Avery, Thomas E. and Lyons, Thomas R. *Remote Sensing: Practical Exercises On Remote Sensing In Archaeology – Practical Supplement No. 1*, Cultural Resources Management Division, National Park Service, Department of the Interior, Washington, DC, USA; 1978.

This supplement to the series published by the National Park Service, "Remote Sensing: A Handbook for Archaeologists and Cultural Managers", serves as a basic training manual for any hopeful future remote sensing analyst. Avery and Lyons have created an essential cookbook that strongly emphasises basic concepts with prudent exercises and short histories of various remote-sensing technologies. The manual stresses basic geometric skills, map interpretation, land surveys, and basic principles of cameras and photography.

Critique

Were this article to merely have RADAR and some few other modern remote sensing platforms mentioned, in conjunction with GPs applications, this manual would be perfectly suited for today's beginning student. As it stands on its own original merits, it is still an outstanding basic primer on basic remote sensing concepts.

Avery, Thomas E. and Lyons, Thomas R. *Remote Sensing: Aerial And Terrestrial Photography for Archaeologists – Supplement No. 7*, Cultural Resources Management Division of the U.S. Department of the Interior, Washington, DC, USA; 1981.

As the title implies, this is yet another supplement to the immensely successful handbook series known as, "Remote Sensing: A Handbook for Archaeologists and Cultural Resource Managers". This particular supplement addresses the techniques employed for obtaining high quality aerial and terrestrial photogrammetric products for the archaeologists purveyal.

Critique

Every one of the handbooks in this series should be required reading for anyone trying to grasp the subject of Remote Sensing Archaeology. This handbook addresses fundamentals of remote sensing that are too often now passed over, the basic skills of aerial interpretation and the use of optical imagery for base ground truthing for more exotic systems such as SLAR, SAR, or advanced spectral systems.

Baker, Craig and Gumerman, George J. *Remote Sensing: Archaeological Applications Of Remote Sensing In The North Central Lowlands – Supplement No. 6*, Cultural Resource Management of the National Park Service, U.S. Department of the Interior, Washington, DC, USA; 1981.

Number six in the series of supplements to the successful handbook by Avery and Lyons this particular supplement deals exclusively with the upper mid-western region of the United States surrounding the Great Lakes. An exhaustive coverage of the area is given with virtually the total knowledge needed to begin a remote sensing effort within the region. Several sample sites are presented such as the Carrier Mills site and Horseshoe investigation with analytical data extracts as well.

Critique

As with the previously reviewed documents within the series there is more information than can be imagined within a small, presented document. A further point which should be made here is that the great steppes and plains of the world are redact in the amount of attention paid to them per archaeological investigation; remote sensing offers the best opportunity for reconnaissance and survey.

Baker, James G., Garrison, Ervan G., and Hurst-Thomas, David.
Magnetic Prospection And The Discovery of Mission Santa Catalina de Guale, Georgia, "Journal of Field Archaeology", Vol. 12, USA; 1985.

From the late 16th century until the late 18th century, the predominate political and military force in the present day region of the south-eastern United States was the Spanish Empire. In the 17th century, Santa Catalina de Guale functioned a key linchpin in Spain's control of the "Ruta del Oro" along which gold shipments sailed for the Iberian Peninsula. In this paper the authors submit the reports of their investigations of present day St. Catherines Island, Georgia by proton magnetometer.

This survey was supported by computer graphics programs and test site digs. The authors propose that this methodology should be quite applicable throughout the southern eastern seaboard due to the low ferric composition of the heavily leached soils.

Critique

This reader is quite familiar with this ongoing project and proposes the view that while this method was the best available technology in the mid-1980's, the apparent ongoing failure to integrate a GIS in some form is a major failure in research vision.

Barasino E. & Helly B. *Remote Sensing And Archaeological Research In Thessaly (Greece)*, Pages 203-209, "New Prospects in "Archaeological" landscape" from the Proceedings EARSeL/ESA Symposium, "European Remote Sensing Opportunities", Strasbourg, France, 31 Mar-3 Apr 1985 (ESA SP-233); 1985.

No copy of this work was available for review after consulting the Peabody Library at Harvard University and the University of Edinburgh main library. Finally, electronic querying of the on-line European Space Agency publication database yielded no results. Quite likely this symposium report, or proceedings, is out of print or in private collections.
Critique: Not available for review.

Batey, Richard A. *Subsurface Interface RADAR At Sepphoris, Israel, 1985*, Pages 1-8, "Journal Of Field Archaeology", Vol. 14, USA; 1987.

Batey describes a season's use of an advanced subsurface RADAR system on loan from the National Geographic Society, USA, at Sepphoris, Israel, located in Biblical Galilee. This particular ground-penetrating RADAR is designed by Geophysical Survey Systems Inc. (GSSI) and consists of a RCU (RADAR Control Unit), graphic recorder, and a transceiver. Unlike the more conventional RADARs, subsurface RADAR utilises the principle of delayed return through materials with different dielectric constants. This however makes subsurface RADAR subseptible to moist soils, clays, or bodies of water such as underground aquifers. The author notes that during the course of his use of the device, medium wavelengths around the 500mhz range produced the best results. Again, as the author notes, "subsurface RADAR only displays interfaces between subsurface materials with different dielectric constants".

The techniques employed by Batey include sample dielectric testing of the Sepphoris soil by measuring two purposely-buried iron pipes. This having been established, the author proceeded with investigations of several suspected Early and Middle Roman ruins. The author states that as a result of applying this technology, "stone walls, cavities, tunnels, and hard surfaces", may be targeted for immediate investigation or future work. While the author notes the relative expense of subsurface RADAR, he believes that in the long run it is more cost efficient.

Critique

Subsurface RADAR appears to be an unique instrument which would take a high degree of familiarity to become very efficient, at least in this reader's mind, however present examples (i.e. 1990 to date) are unknown. If present technologies of this type were married to a three-dimensional graphics display for real time imaging, a tremendous breakthrough would be realised for archaeology in general.

Bewley, R.H. *Topsoil And The Archaeology Of the Solway Plain 1981-84*, Pages 19-25, "Archaeological Review of Cambridge University", 4:1, United Kingdom; 1985.

Bewley offers an outline of integrating aerial photography and various geophysical survey techniques into topsoil analysis of a suspected archaeological site in this case the Solway Plain of England. Bewley primarily dwells upon the high manpower needed to do "ground level fieldwork", when aerial photography is much more efficient for initial determination of site suitability.

Critique

An interesting observation and opinion from a British archaeologist on the effectiveness of manpower versus the technological costs of remote sensing.

Bewley, R., Brasch O. and Rog Ralmer. *An Aerial Training Week, 15-22 June 1996, Held Near Lake Balaton, Hungary*, Pages 745-750, "Antiquity", Vol. 70, United Kingdom; December 1996.

This article discusses the near 50-year drought in aerial photography within the former Iron Curtain countries. Thus, Bewley concerns himself here with re-establishing this school of archaeological survey by holding a training school near Siofok, Hungary. Mentions of the work of the Aerial Archaeological Group are covered as well as the current projects of the unit in Eastern Europe.

Aerial platforms utilised are commercially available Cessnas supplied with high-resolution hand-mounted cameras. Basic aerial survey needs are covered with no specific techniques.

Critique

A marvellous short article from a writer not heard from enough it seems. Bewley takes us back to the earliest days of remote sensing archaeology when he reminds the entire community that not everyone has a Space Shuttle or satellite down-loading data Center to do their remote sensing archaeology for them. Kudos for his efforts.

Blake, Vanessa S. *Remote Sensing in Underwater Archaeology*, Pages 3-17, Science and Archaeology, No. 33, Cambridge, United Kingdom; 1991.

A paper that details how remote sensing apparatus such as SONAR and proton magnetometers may be used to assist in underwater archaeology. A vast array of data is overviewed insofar as to what types of remote sensing technology are available for this task as well as the attendant data analysis, interpretation, and handling problems. The author concludes that very little has been done in image processing and establishing image pattern techniques to interpret the data. She also notes the inherent human factor and the types of operational environment as factors to be overcome. An extensive bibliography also accompanies this article.

Critique

An excellent overview of maritime remote sensing operations as its relates to archaeological use. The summary of past efforts in maritime archaeology is also quite welcome as it affords the less knowledgeable a foundation upon which to build an opinion.

Bouchet, J.-M and Burnez, C. *Le Camp Neolithque De Rejolles a Biron (Charente Maritime)*, Bulletin de la Societe Prehistorique Francaise, Tome 87/ 10 – 12; 1990.

A report on a Neolithic encampment first discovered in the Maritime province of Charente by aerial photography. The authors report that more remote sensing missions, in conjunction with further digs, were performed in both 1986 and 1987, again with great success.

Critique

An interesting report on a French project, especially in light of the well known remote sensing work being performed in the Rhone Valley region. It is also worth pointing out that this is one of the relative few archaeological projects reporting the use of remote sensing technology for pre-historic analysis.

Bruseth, James E., Huggins, Robert J., and Martin, William A. *Assessing Feature Extraction and Spatial Patterning Of Artefacts With Geophysical Remote Sensing Data*, Pages 701-720, "American Antiquities", 56(4), Society for American Archaeology, USA; 1991.

The authors describe the results of magnetic surveys and electromagnetic conductivity surveys at several sites located along the Richland/Chambers Reservoir in Texas. The teams used Geometrics proton magnetometers and electromagnetic conductivity sensors to conduct these operations. By first establishing a test signature by creating a fire-hardened hearth and sensing it, the team was able to benchmark an example signal image.

The group was able to not only discover new sites, but also were able to discern whether the sites had experienced long term or multiple us by their occupants. Anomalies surrounding monopolar and dipolar readings were also investigated. The authors have determined that magnetometers have significant use for assisting in archaeological work as well as a new found ability to interpret sites.

Critique

The finest article encountered to date by this reader on the application of the proton magnetometer and its relation, electrical conduction sensing. A better understanding of geology is required with such technology though, which could stymie some potential users.

Budge, Thomas K. and Morain, Stanley A. *Remote Sensing: Instrumentation For Nondestructive Exploration Of Cultural Resources – Supplement No. 2*, Cultural Resources Management of the National Park Service, U.S. Department of the Interior, Washington, DC, USA; 1978.

Another supplement in the series covering remote sensing, this particular edition covers the following subjects: the electromagnetic spectrum, theories of radiation, sensor review and applications in archaeology, image and data processing, as well as digital processing procedures. Numerous illustrations are included with a generous bibliography.

Critique

Notwithstanding the lack of a discussion of RADAR remote sensing theory, this is still an extraordinarily good and relevant series of publications. This volume should be regarded as a primer for the beginning remote sensing archaeologist.

Ciochon, Russell and James, Jamie. *The Glory That Was Angkor Wat*, Pages 39-40, "Archaeology Magazine", March/April, Boston, MA. USA; 1994.

This article, written for the general public, focuses on ongoing efforts of the international archaeological community to preserve the tremendous ruins of Angkor Wat in Kampuchea (formerly Cambodia). The article does not directly address the use of remote sensing by the various archaeological entities, however Angkor Wat has been the subject of several recent NASA Space Shuttle SIR (Shuttle Imaging RADAR) missions. The authors give a good general account of Angkor Wat's long cultural history – and more recent archaeological controversies.

Critique

The author's article should give the reader reason to ponder the fates of so-called world cultural sites, particularly when the entire world attempts to lend a hand at once.

Conant, Francis Payne. *Remote Sensing, Discovery, and Generalisations in Human Ecology*, Pages 239-250, Annual Reports of the National Geographic Society, Washington, DC, USA; 1981.

The author reports on her experiences in applying remote sensing technology in an East African region, specifically in Uganda and Kenya. The platforms utilised were LANDSAT 1 and 2 with the attendant MSS data. The author notes that her efforts are directed towards a regional human-ecology relationship and consequently does not want higher resolution imaging capability. She also notes the following organisational support: US/AID Regional Remote Sensing Center in Nairobi, Kenya, the United Nations Global Environmental Monitoring System, and the Kenya Rangeland and Environmental Monitoring System.

Critique

An unusual statement from any researcher using remote sensing technology is to hear the request for more large resolution imagery. Yet, in this particular instance, the argument remains quite relevant that in analysing the great grasslands of the world large spatial area sensing systems can derive the best basic survey results.

Conyers, Lawrence B. and Cameron, Catherine M.
Ground-penetrating Radar Techniques and Three-dimensional Computer Mapping in the American Southwest, Pages 417-430,
"Journal of Field Archaeology", No. 25, Boston, MA, USA; 1998.

New techniques of ground-penetrating radar (GPR) acquisition and computer processing were tested at archaeological sites in the American Southwest and found to be effective in producing images of buried archaeological features. These new methods, especially amplitude slice-maps, were combined with more standard data processing and interpretation techniques and tested at sites with little or no surface expression. In southern Arizona, numerous pit structures buried in terrace alluvium were discovered and mapped.

In the Four Corners region, a Chaco period great kiva and other pit structures and features were mapped by GPR and later confirmed through excavation. At some sites, GPR surveys did not successfully identify buried archaeological features. These failed surveys highlight both geological and methodological problems including soil conditions, surface disturbance, and equipment calibration that may be avoided or ameliorated in future GPR surveys.

Critique

A detailed overview of a GPR based archaeological investigation that clearly weighs and analyses the strengths and weaknesses of this ground based remote sensing system.

Couzy, Alain. *Environmental Studies Using Satellite Imagery,* Magazine du Institut Geographique National, 136 bis Rue de Grenelle, 75700, Paris, France; 1980.

Mr. Couzy's article should be regarded as the words of a too oft unheard philosopher; one who listens much and says little – unless prompted. In this instance Mr. Couzy has chosen to speak and in a tone which lends itself to be a devil's advocate on remote sensing. Without resorting to the usual technical arguments of remote sensing's benefits, the author chooses to step back and come down to earth on the true capabilities of the technology. It is that philosophy which makes this work such a thoughtful article, or as Mr. Couzy concludes, "it is neither cure-all nor gadget".

Critique

This should be required reading for all those enamoured of using remote sensing technology for archaeological applications. The pratfalls and underlying costs—both in financial and time—are well worth considering before entering into such a campaign as Mr. Couzy so aptly points out.

Comfort A. *Satellite Remote Sensing and Archaeological Survey on the Euphrates*, Pages 39-46, "AARGnews", No. 14; 1997".

This article was unavailable for review as of March 2000.

Critique

None available.

Comfort A (1997*). Satellite Remote Sensing And Archaeological Survey On The Euphrates*, Pages 1-8, "Archaeological Computing Newsletter" No. 48; 1997.

This article was unavailable for review as of March 1999.

Critique

None available.

Cox C. *Satellite Imagery, Aerial Photography And Wetland Archaeology*, "World Archaeology", No. 24; Publication site unknown; 1992.

This article was unavailable for review as of March 2000.

Critique

None available.

Custer J.F., Eveleigh T., Klemas V. & Wells I. *Application of LANDSAT Data And Synoptic Remote Sensing To Predictive Models For Prehistoric Archaeological Sites: An Example from The Delaware Coastal Plain*, Pages 572-588, "American Anthropology", No. 51, USA; 1986.

This article was unavailable for review as of March 2000.

Critique

None available.

Dahlin, Bruce H. and Pope, Kevin O. *Ancient Maya Wetland Agriculture: New Insights From Ecological And Remote Sensing Research*, "Journal of Field Archaeology", Vol. 16, USA; 1989.

The authors involved in this particular effort were attempting to ascertain the viability of the hypothesis that ancient Mayan canal systems were located throughout the Yucatan Peninsula. The authors report that, on the contrary, they are found only in northern Belize, southern Quintana Roo, Mexico, and the Candelaria River tributaries of Campeche, Mexico. Dahlin and Pope not that with the existing SAR platforms they were unable to detect small canals due to speckle noise (speckling) and spatial resolution capabilities of the technology. SAR imagery and LANDSAT TM were very useful, however, in detecting large canals which served as feeders to small lattice canal systems. Their study showed that the canals, by and large, were located near perennially moist soils and wetlands with predominately high water tables or artesian springs. The authors finally note that the karst topography of the inland regions would have precluded the possibility of effective canal systems due to the monsoonal conditions i.e. periods of deluging rainfall followed by extreme dryness. The authors believe that the Mayan culture did not depend on irrigation based agriculture.

Critique

This is a most interesting article in light of the new abilities of space borne SAR and multipolarimetric SAR systems such as the SIR-C/X-SAR, JERS-1, and RADARSAT platforms. Even more interesting is the fact that this appears to is one of the first efforts to use a multi-sensor attack on a given problem i.e. the use of the differing spatial and sensor suites of SEASAT, LANDSAT TM and AIRSAR. Certainly this can be considered to far ahead of its time in scope and thought and should be known as a milestone research event in remote sensing archaeology.

Drager, Dwight L. and Ireland, Arthur K. *Remote Sensing Of The Environmental Setting Of The Navajo Indian Irrigation Project*, U.S. Government Documents, Bureau of Land Management, Washington, DC, USA; 1980.

A report from the authors on the conclusion of a Federally mandated remote sensing project over the Navajo Indian Irrigation Project, near Farmington, New Mexico. The authors determined to use this opportunity to find if certain natural factors influenced site locations of pre-historic settlements.

The investigators found several methods by which they might analyse their findings including a rainfall contour map, a vegetation map, and a soils map, overlaying a base map. No mention is made of using a Geographic Information System (GIS), and no specific findings are suggested.

Critique

As mentioned in the author's conclusion of this work, there is considerable more work to be done in this particular area; sadly, not enough information is related within this paper for the careful reader's analysis.

Drake N.A. *Remote Sensing, Geomorphological And Archaeological Evidence For A Recent Aeolian Origin Of Surface Gypsum Crusts In Southern Tunisia*, Pages 347-354, "Proceedings of the 22nd Annual Conference of the Remote Sensing Society", RSS96 Remote Sensing Science & Industry, RSS96; 1996.

This article was unavailable for review as of March 2000.

Critique

None available.

Duller C.E. *A Case for Archaeological Reconnaissance of the Cabo Catoche-Porvenir Region of the Northeastern Yucatan Peninsula*, NASA Technical Memorandum TM-102248, USA; 1990.

This article was unavailable for review as of March 2000.

Critique

None available.

Ebert, James I. *Remote Sensing Applications in Archaeology*,
Pages 293-353, "Advances in Archaeological Method and Theory",
Vol. 7, Academic Press Inc. USA; 1984.

This is essentially a basic primer for the more advanced archaeological student, as any experienced remote sensing analyst would rapidly note, but the author does an admirable job of covering the necessary bases. From explanations of the electromagnetic spectrum – and which sensors are valid for those specific spectra – to the limitations of remote sensing techniques in archaeology, it is all explained with conciseness and clarity.

Of particular interest are Ebert's coverage of the early days of aerial photography and archaeological applications. Finally, the bibliography is excellent with numerous addresses for imagery outlets.

Critique

This is an outstanding work and should be regarded by the initiate into the uses of remote sensing for archaeology as a mandatory text.

Ebert J.I. & Lyons T.R. *Remote Sensing In Archaeology, Cultural Resources Treatment and Anthropology: The United States of America In 1979*, Pages 1-19, "Aerial Archaeology", No. 5; 1980.

This article was unavailable for review as of March 2000.

Critique

None available.

El-Baz F. *Space Age Archaeology*, Pages 40-45, "Scientific American", No. 277 (2), USA; 1997.

Prof. Baz is without a doubt one of the most renowned scientists yet in the field of remote sensing technology. His involvement with literally every aspect of the technology, from the NASA Lunar missions era, to serving on U.S. Presidential advisory committees, make him one of the true visionary and wise voices of the field.

Thus, his overview of the current status of archaeology as it has been influenced by technological developments is of significant interest. Every aspect of remote sensing archaeology, from GPS systems to Shuttle RADAR to oncoming systems, is mentioned in this concise overview of the current state of the art.

Critique

Any new articles from Prof. Baz always provide provocative reading as his views usually elucidate great commentary within the field. Once more he has illuminated the subject for the general reader while challenging the practitioners of the art of remote sensing archaeology; a significant introduction to the current status of remote sensing archaeology.

El Shazly E.M. *Space Borne Imagery Interpretation Of Mega Features Related To Egyptian Archaeology*, Pages 4.1-4.6, "Remote Sensing - Extending Man's Horizon", "International GeoScience & Remote Sensing Symposium", No. 1; 1983.

This article was unavailable for review as of March 1999.

Critique

None available.

Farley J.A., Limp W.F. & Lockhart J. *The Archaeologist's Workbench: Integrating GIS, Remote sensing, EDA and Database*, Pages 141-164, "Interpreting space: GIS and Archaeology", Allen K.M.S., Green S.W. & Zubrow E.B.W. (Eds.) Taylor and Francis; 1990.

This work was unavailable for review as of March 2000.

Critique

None available.

Fagan, Brian. *Time Detectives*, "Uluburun", Page 183, Simon and Shuster, 1230 Avenue of the Americas, New York, NY, USA; 1995.

A specially designed sonic high-accuracy ranging and positioning system (SHARPS) was used for checking the accuracy of datum points set up manually on the bottom. SHARPS is a hand held computerised acoustic distance-measuring device, invaluable for measuring the positions of such large objects as anchors.

Critique

Some very impressive technology applied to the subject, a Bronze Age galley, sailing off the present day Turkish coast when it sank. It would be interesting to see what corollary research would produce by the use of the relatively new Laser GPS systems as well as the new Laser Line-Scan Bathymetric Imaging technologies.

Fagan, Brian. *Time Detective*, "Abu Huyera on the Euphrates", Page 106, Simon and Shuster, Rockefeller Center, 1230 Avenue of the Americas, New York, NY, USA; 1995.

"Pilots on the Cairo to Baghdad airmail run photographed archaeological sites from the air, including large stone enclosures about 500 feet (150m) across, with narrow entrances. Long stone walls fanned out from theses to form narrow entrances".

Critique

This is an intriguing viewpoint of the early use of aerial platforms to gather archaeological data, in this case the Euphrates River valley of Iraq. See the annotations regarding Prof. Robert Adams within this work.

Fagan, Brian. *Time Detectives*, Page 216, "Footplows and Raised Fields", Simon and Shuster, 1230 Avenue of the Americas, New York, NY, USA; 1995.

"Timwanku's abandoned field systems covered thousands of acres, so it was a question of choosing a sample survey area. Kolata and River pored over large and small-scale aerial photographs, then settled on a 27-mile survey area in the Pampa Koani, about six miles north of Tiwanku. Here continuos tracts of ancient field systems ran from the lakeshore nearly nine miles inland. Intersecting causeways and large occupation mounds showed up clearly on the photographs. So did a large artificial canal and massive agricultural systems cut into nearby hillsides".

Critique

A real challenge for the application of aerial photography due to the extreme weather conditions of the Altiplano region of Peru. Still, the diligence and careful efforts of the researchers was rewarded, showing again the benefits of a remote sensing campaign.

Ferguson K.P., Tanis F.J. & Tyler W.A. *SPOT Bathymetric Image For Archaeological Investigations*, Pages 863-866, "Proceedings 21st International Symposium of Remote Sensing of the Environment", Ann Arbor, Michigan, USA; 1987.

This article was unavailable for review as of March 2000.

Critique

None available.

Fiennes, Ranulph. *Atlantis Of The Sands,* Chapter 1, Bloomsbury Press, Bloomsbury Ltd., 2 Soho Square, London, W1V 5DE, United Kingdom; 1992.

Fiennes' book, "Atlantis of the Sands", serves as both a personal memoir of a lifetime obsession with a near mythical "lost-city", and as a casual history of remote sensing use in Near Eastern archaeology. Fiennes notes that the celebrated adventurer T.E. Lawrence (Lawrence of Arabia),

"urged the (British) Air Ministry to route the R101 airship, Britain's answer to the German Zeppelins, over the Arabian Empty Quarter en route to India...".

Lawrence believed that much knowledge could be gained by this effort. Fiennes also describes the early efforts of Arabian explorers such as Philby, Thomas, and Thesiger, all conventional archaeologist-explorers of the period's genre.

Some three decades passed before another individual pursued the Ubar question, and when it was, it was by American oilman, Wendell Phillips. Phillips underwrote a series of aerial photographs that were taken of Wadi Ghatun and Wadi Atinah. These efforts were unsuccessful however, and for some thirty more years the Ubar question lay dormant.

Critique

This book is written for the general readership, but it should be regarded as required reading for anyone interested in the most recent applications of remote sensing and archaeology. Moreover, the discussion of early remote sensing efforts provides a unique window into the problems and ramifications of such technology in sensitive political areas.

Fiennes, Ranulph. *Atlantis Of The Sands*, Chapter 1, Bloomsbury Press, Bloomsbury Ltd., 2 Soho Square, London, W1V 5DE, United Kingdom; 1992.

In this chapter, Fiennes discusses the involvement of film documentary producer Nicholas Clapp in obtaining assistance from NASA's Jet Propulsion Laboratory for remote sensing imagery of Oman. Fiennes notes that,

"(Clapp) knew that aerial photographs had been previously used to navigate the Sands by Wendell Phillips Ubar expedition".

Clapp spoke with Dr. Ron Blom and Dr. Charles Elachi, along with Shuttle astronaut Dr. Robert Crippen, and persuaded them that the Ubar site was suitable for investigation. JPL decided to use the SIR-B (Shuttle Imaging RADAR) system aboard the Challenger Shuttle mission in mid-June 1984 to see if favourable results might be obtained. While some interesting sites were viewed, problems with the RADAR array precluded further use.

The 1986 Challenger explosion further delayed the effort. The JPL team then decided to pursue an effort with the assistance of LANDSAT and SPOT imagery. SPOT was employed due to its greater resolution, while LANDSAT was chosen for its wide image swath area. SIR-B imagery finally produced some interesting target areas, one located near a feature noticed during the Bertram Thomas Ubar expedition.

Critique

An interesting "forced" application of the multi-sensor approach to archaeology due to the loss of the Shuttle Challenger transport system and the failure of the SIR-B array system.

Fiennes, Ranulph. *Atlantis Of The Sands*, Chapter 9, Bloomsbury Press, Bloomsbury Ltd., 2 Soho Square, London, W1V 5DE, United Kingdom; 1992.

Fiennes details the exploits of archaeologist Charles Weston-Baker who hoped to view the Ubar site via a hot air balloon. Weston-Baker had discovered potsherds and shaped stones in the region of 18°, 45′ N by 52°, 45′ E. Fiennes also recounts the ongoing efforts of the JPL team with the little available imagery they had acquired. Team leader, Dr. Ronald Blom, had found several interesting ancient tracks and unexplained features in the suspected region of Oman that he contacted Fiennes and Clapp about.

Critique

The efforts of Charles Weston-Baker with a how air balloon hearken back to the early days of remote sensing. Even so, the effort proves that old technology is not necessarily bad technology.

Fiennes, Ranulph. **Atlantis Of The Sands**, Chapter 12, Bloomsbury Press, Bloomsbury Ltd., 2 Soho Square, London, W1V 5DE, United Kingdom; 1992.

The author describes the final dedicated effort to locate a probable Ubar site; an interesting observation is the problem encountered by Dr. Ronald Blom in using his GPS unit during the Gulf War – Selective Availability (SA) was instituted thus limiting use to only several hours each day. Fiennes also addresses the controversy between Clapp, who suggested in his documentary that JPL imagery led the way to Ubar, versus Juris Zarins, who believed that coincidence and pottery finds at Shisir, Oman fomented the interest.

Critique

Once again, another discussion of the classic clash between new technology and perceived old-fashioned ("hard work") archaeology. The position best taken is the middle ground, where a blend of both old and new techniques will further things along best, instead of an argument over which is more wrong!

Fiennes, Ranulph. *Atlantis Of The Sands*, Chapter 12, Bloomsbury Press, Bloomsbury Ltd., 2 Soho Square, London, W1V 5DE, United Kingdom; 1992.

A potentially overlooked detail in Fiennes' book is the use of a ground-penetrating RADAR unit, a mobile EM31 sensitivity unit. The unit utilised a scanner and was mounted on sled runners so that it may be pulled across the suspected site. Elachi and Blom noted that at a depth of 28 feet (8m approx.) beneath the sand they were able to detect the outline of a four-meter square well ahead.

Critique

A good account of meticulous remote sensing by the involvement of a ground penetrating RADAR (GPR) system. However, it is curious to note that GPS survey quality equipment was not present to accurately set up the sight. This may have been due to limited space or the relative primitive quality of the technology at the time; merely a subtle thought.

Fiennes, Ranulph. *Atlantis Of The Sands*, Postscript, Bloomsbury Press, Bloomsbury Ltd., 2 Soho Square, London, W1V 5DE, United Kingdom; 1992.

At the conclusion of Fiennes' book he addresses at some length the controversy surrounding the amount of support that remote sensing technology played in the discovery of Ubar. Fiennes concludes that,

"good vehicles, generous sponsors, the support of the Sultan and so many Omanis, a wonderful team of volunteers, including JPL, and technological aids in many forms, all contributed to our success".

Critique

A balanced view of the role which remote sensing plays in archaeology; remote sensing cannot stand alone and it is certainly not a panacea, but with proper use, it is an efficient tool for archaeologists.

Fisher, Charles L. *Archaeological Survey And Historic Preservation At The Site Of A Revolutionary War Cantonment In New Windsor, New York*, Pages 25-38, "North American Archaeologist", Vol. 6(1), Baywood Publishing Company, USA; 1984.

The author presents the results of an archaeological dig performed at the New Windsor Cantonment (near present day Newburgh, New York), a Revolutionary War encampment for the Continental Army in 1782-83. This project was undertaken by the New York State Department of Historic Sites and attempted to use a "least intrusive means" methodology in its investigations of the site. Ground penetrating RADAR units, procured from the National Heritage Grant funds, in conjunction with magnetometers and soil chemical analysis, were utilised to that end.

The author determined that ground penetrating RADAR was best suited for searching out "rubbish areas" i.e. those with a likelihood of metallic objects, while the magnetometer was best suited for locating brick or compacted earthen areas such as huts etc.

Critique

An interesting note to this project is that all sites were re-filled to preserve their contents for future evaluation by technicians with more advanced technology.

Fowler M.J.F. *Satellite Archaeology*, Pages 281-283, Spaceflight, No. 33,1991.

One of numerous articles by this author generally enumerating the avalanche of recently declassified satellite data form the U.S. Government's Central Intelligence Agency, known as the CORONA program. The author also ventures over well-trodden ground that his been written about at length in the past.

Critique

Mr. Fowler consistently brings new material to noviciate's attention in regards to remote sensing archaeology; however, it is lacking in the addition of new scientific knowledge.

Fowler M.J.F. *Satellite Image Processing For Archaeologists*, Pages 2-8, "Archaeological Computing Newsletter" No. 39, United Kingdom; 1994.

Another of the numerous articles produced by Mr. Fowler in the UK on the basics of remote sensing archaeology. Very little new techniques are covered unless the reader is completely unfamiliar with the subject. If so, they would be well off to find the "Cultural Land Use Management" series of the U.S. Department of Interior (Avery and Lyons) which covered this same ground in the 1980's and much better.

Critique

Mr. Fowler needs to focus his energies on the new development of scientific techniques in regards to remote sensing archaeology and not repeating already well done material.

Fowler M.J.F. *Ground Cover Mapping From Multispectral Satellite Imagery,* Pages 11-19, "AARGNews", No. 9, United Kingdom; 1994.

Another of the multitudinous minor works produced by Mr. Fowler. Again, no new ground is ploughed here, merely a rehash of work that has been done much more scientifically and carefully by remote sensing archaeologists in the 1980s.

Critique

The most creditable offer that this reader has for Mr. Fowler's work is that he is productive in a volumetric sense.

Fowler M.J.F. *High Resolution Russian Satellite Imagery*,
Pages 29-32. "AARGnews", No. 11, United Kingdom; 1995.

This is an overview of the Russian move towards declassification of former intelligence collection satellites for the purpose of generating much needed Western currencies by selling imagery products for environmental applications. Fowler addresses the possible benefits of this move for the archaeological remote sensing community and the ease with which new virtually real-time analytical products may be delivered.

Critique

Notwithstanding Mr. Fowler's usual proclivity towards mass production over content, this is a very good overview of a potential sea change in remote sensing technology. Furthermore, as such platforms come on-line the entire concept of how remote-sensing archaeology will be conducted in the future will be changed radically.

Fowler M.J.F. *Declassified Intelligence Satellite Photographs"*, Pages 30-35, "AARGnews", No. 13; 1996.

A short work by Mr. Fowler alerting the archaeological community to one of the many U.S. Government Central Intelligence Agency CORONA satellite image products becoming available. No remote sensing techniques or theories are discussed, merely image quality, type, and locations.

Critique

Once again, another of the productive notices by Mr. Fowler to the general archaeological community as concerning cheap available remote sensing imagery. It comes to mind to point out to the author that finances limit archaeological efforts normally and that presuming to continually point out new structures for, which there are no means to explore, may antagonise some in the science.

Fowler M.J.F. *Declassified Intelligence Satellite Photographs - An Update*, Pages 47-48, "AARGnews", No. 14, United Kingdom; 1997.

Yet another minor work by Mr. Fowler on more declassified satellite imagery from the U.S. Government's CIA CORONA program.

Critique

Once again, no discussion of remote sensing techniques is given, merely pointing out a data source.

Fowler M.J.F. *Stonehenge from Space*, Pages 130-132, "Spaceflight", No. 35, United Kingdom; 1993.

It comes so mind that Mr. Fowler feels the need to comment upon each and every new satellite image which come into his hand and to thereupon enlighten the world and archaeologists within it. However, his continuing efforts to illuminate the archaeological community with the techniques and science of remote sensing archaeology are to be commended.

Critique

See above commentary.

Fowler M.J.F. *Danebury and Its Environs From 830 Kilometres*", Pages 26-30, "HFCAS Section Newsletters", NS 21, United Kingdom; 1994.

A discussion of the Danebury, United Kingdom site and the revelations provided by a high-resolution optical space borne sensor system. New outer wall structures are noted as well as vague indications of further structural areas. Again, Fowler provides no other information other than the data source.

Critique

A further indication of Fowler's failure to provide new scientific techniques or theories as to the application of remote sensing technology in support of archaeological exploration.

Fowler M.J.F. *Detection of Archaeological Features on Satellite Imagery,* Pages 7-14, "AARGnews", No. 10, United Kingdom; 1995.

A very minor subsidiary work to one of Mr. Fowler's earlier commentaries on the usefulness of declassified U.S. Government CIA CORONA satellite imagery, recently declassified Russian satellite imagery, as well as the more well known systems, such as LANDSAT etc.

Critique

Somewhat useful to the absolute neophyte, but in of itself, little that is new or useful to the practising remote sensing archaeologist.

Fowler M.J.F. & Curtis H. *Stonehenge From 230 Kilometres"*, Pages 8-16, "AARGnews", No. 11, United Kingdom; 1995.

This is a minor notice concerning a more extended article. Please see the following annotation.

Critique

See the following annotation.

Fowler, M.J.F. *High-Resolution Satellite Imagery In Archaeological Application: A Russian Satellite Photograph Of The Stonehenge Region*, Pages 667-671, "Antiquity" No. 269, United Kingdom; 1995.

In this paper Fowler remonstrates on his previous image classification efforts over the Stonehenge site using LANDSAT TM Band 4 imagery; he notes the inability of the sensor's resolution capability to discern new features. Following on, Fowler now introduces a discussion of the KVR-1000 panchromatic sensor system, capable of producing 3-4m resolution with a spectral bandwidth range of 0.51-0.76 m, which is then "subsequently scanned for distribution as digital products". Fowler then notes introducing this data into a standard commercial digital image-processing package, "CorelDraw! 3.0" for enhancement! (Surely a new standard for the basic cheap analysis of space borne remote sensing imagery.)

Fowler also notes that KVR-1000 exceeds considerably the capabilities of LANDSAT and SPOT imagery and "for the first time—crop and soil marks".

Critique

Mr. Fowler provides some excellent insight into the capability of commercially available user-friendly image enhancement packages for providing basic image analysis functionality. However, it is interesting to note that he mentions the data costs as some 2500 pounds British or some 6000 dollars U.S.—which would make it appear that diamond quality data was mined with a low quality pick. Even so, this is still an admirable effort in all.

Gaffney V., Ostir K., Podobnikar T. & Stancic Z. *Satellite Imagery And GIS Applications In Mediterranean Landscape*s, Pages 338-342, "Interfacing the past: Computer applications and quantitative methods in archaeology", CAA No. 95 Vol. II. Kamermans H. & Fennema K. (Eds.), University of Leiden, Germany; 1996.

This article has not been found for review as of March 2000.

Critique

None available.

Garrod S.M., Clark C.D. & Parker Pearson M. *Tombs, Forests And Remote Sensing: Landscape Archaeology In The Semi-Arid Spiny Forests Of Southern Madagascar*, Pages 225-232, "Remote Sensing in Action", Proceedings of the 21st Annual Conference of the Remote Sensing Society, RSS95; 1995.

This article was unavailable for review as of March 2000.

Critique

None available.

Garrod S.M., Clark C.D., Parker Pearson M. & Wise S. *Forest And Settlement Evolution In Southern Madagascar: An Investigation Using Multi-Temporal LANDSAT TM And Archaeological Survey Data*, Pages 682-689, "Proceedings of The 22nd Annual Conference of the Remote Sensing Society", Remote Sensing Science & Industry, RSS96; 1996.

This article was unavailable for review as of March 2000.

Critique

None available.

Gibbons A. *A "New Look" For Archaeology*, Pages 918-920, "Science", No. 252, United Kingdom; Publication date unknown.

This article was not available for review as of March 2000.

Critique

None available.

Gory, Maurice. *The Environment of Petra National Park: Means of Scientific Detection in the Service of Archaeological Service,* "Archaeology", Vol. 17, ISA, USA; 1986.

Mr. Gory does an admirable job of explaining the various types of remote sensing within Jordan's famous Petra National Park. From orthochromatic photography to infrared imagery to synthetic aperture RADAR, Mr. Gory rapidly and easily explains their vices and versus' in their applications. In the end, Mr. Gory recommends the use of colour panchromatic photography in addition to oblique and vertical photography.

Critique

This article, though a bit dated today, should serve as a model for efficiency for anyone contemplating submitting a budget request for remote sensing assistance on his or her archaeological site.

Hamlin C.L. *Machine Processing Of LANDSAT data: An Introduction For Anthropologists And Archaeologists*, Pages 1-11, "MASCA Newsletter", No. 13, United Kingdom; 1977.

This article was unavailable for review as of March 2000.

Critique

None was available.

Haupt P. *1.000.000 km2 KVR-1000 Russian Satellite Imagery For 49.95DM?* Pages 31-32, "AARGnews", No. 15, United Kingdom; 1997.

This article was unavailable for review as of March 2000.

Critique

None available.

Hektor, Erich. *Photogrammetry and Archaeology*, Pages 131-142, Scollar, Publische Geddatisches Institut, Aachen, Germany; 1988.

Photogrammetry is a measuring method especially appropriate for archaeological purposes because it has a great number of advantages compared with conventional methods. The author discusses practical problems with regard to special possibilities of picture taking and picture evaluation made possible by photogrammetry. These possibilities are explained with the assistance of given examples.

Critique

A good, short overview of the basic theory behind photogrammetrics and how it is used in archaeology. It is also of worth for remote sensing archaeologists considering supplementary efforts to aerial or space borne campaigns.

Hoff, H. T., Johnson, J., Madray, S. and Sever, Thomas. *Remote Sensing and GIS Analysis in Large Scale Survey Design in North Mississippi*, Pages 124-130, "Southeastern Archaeology", Volume 7(2), Winter Edition, USA; 1988.

This work is a discussion by the authors of an ongoing attempt at the Centre for Archaeological Research at the University of Mississippi to complete a comprehensive survey of the Mississippi's six upland drainages. The authors' note that remote sensing in the eastern United States has lagged due to extensive vegetation. It is stated that, delineation of major environmental zones is highly effective, particularly,

"when combined with other types of data using a Geographic Information Systems (GIS) approach".

The authors argue that modelling offers a better analysis approach when dealing with forested areas.

Critique

An interesting article when one considers that it was published in the days well before any useful form of RADAR remote sensing was generally available.

Holcomb, Derrold W. *Shuttle Imaging RADAR And Archaeological Survey In China's Taklamakan Desert*, Pages 129-138, News and Short Contributions, "Journal of Field Archaeology", Volume 19, USA; 1992.

A spectacular report on the utilisation of Shuttle Imaging RADAR systems, more commonly known as SIR, this paper tends to support the author's view that RADAR is capable of producing much more detail than previously thought. Holcomb, a design engineer with ERDAS Inc. of Atlanta, Georgia, takes the reader through a short history of the development of the Silk Road/Tamalkan Desert region of western China and the various archaeological efforts mounted there. Holcomb then introduces previous examples of RADAR imagery and their purported lack of high-resolution, which he attributes to less skilled image analysts. In a technical tour-de-force Holcomb convincingly argues and then proves that by careful (literally) pixel by pixel manipulation, RADAR imagery can be brought to a whole new level of accuracy and detail. The author also states that,

"a comparative survey of remotely sensed data over known archaeological sites world-wide, geared toward development of a repertoire of computer regimens designed specifically for archaeological applications would be in the best interests of all".

Critique

This is, considering the date of publication, a seminal work in the development of RADAR imaging enhancement techniques. Considering the present state of space borne RADAR platforms, and the advanced capabilities of ALMAZ, RADARSAT, and SIR-C, it is of some great interest to see how Holcomb's techniques might be applied presently.

Johnson J.K., Sever T.L., Madry S.L. & Hoff H.T. *Remote Sensing And GIS analysis in Large Scale Survey Design In North Mississippi*, Pages 124-131, "Southeastern Archaeology", No. 7, USA; 1988.

This article was unavailable for review as of 2000.

Critique

None available.

Joyce C. *Archaeology takes To the Skies*, Pages 42-64, "New Scientist", No. 133, United Kingdom; 25 January 1992.

This article was unavailable for review as of March 2000.

Critique

None available.

Kennedy D. *Roman Roads and Routes in North-east Jordan*, Pages 71-93, "Levant", No. 29, United Kingdom; 1997.

This article was unavailable for review as of March 2000.

Critique

None available.

Kingsley, Simon and Quegan, Shaun. *Understanding RADAR Systems*, Chapter 11 – RADAR Remote Sensing; McGraw-Hill Book Company, Europe, Shoppenhangers Road, Berkshire, SL6 2QL, England, United Kingdom; 1992.

This chapter of Kingsley and Queghan's seminal work should be regarded as first reading by all persons interested in the future of RADAR remote sensing in archaeological work. A careful discussion of the primary types of RADAR platforms is put forth as well as their qualities. SAR, or synthetic aperture radar is noted as,

"perhaps the most sophisticated RADAR technique (certainly the most technically demanding) used in remote sensing...".

Microwave scatterometry, or high-frequency (HF) RADAR is another type of RADAR, which has applications for archaeological use, yet is little known except by specialists. Scatterometers require special calibration, note the authors, and much like SAR, is technically expensive. RADAR altimetry, the last of the technically advanced triumvirate describing the RADAR family, is being operated under the AIRSAR, TOPSAR and proposed TOPSAT platform.

Critique

A short concise primer on RADAR operating theories and principles, this book offers much needed background information to beginning users of RADAR remote sensing platforms.

Kruckman L. *The Role Of Remote Sensing In Ethnohistorical Research*, Pages 343-351, "Journal of Field Archaeology", No. 14, United Kingdom; Year unknown.

This article was unavailable for review as of March 1999.

Critique

None available.

Lange, Judith. *Passagio in Iraq*, Pages 18-33, "Archelogia Viva", Edizione Invierno, Roma, Italia; 1995.

An exquisite article, albeit in Italian, of the crisis situation which the world archaeological community finds itself in since the Gulf War of 1990-91 in Iraq. Filled with photographs, charts, maps, and text, Lange has written a succinct overview of the threat faced by the "world's patrimony", as she so correctly terms it. All aspects of every current archaeological effort in the area are covered with considerable expertise—a benefit to the reader.

Critique

It is highly recommended that the reader engage himself or herself with an Italian linguist before tackling this work. Subtle turns of word within this article can lead to wrong assumptions as occurred to this reader after several translation efforts.

Lulla K.P. *et al. Earth Observations During Space Shuttle Flight STS-41: Discovery's Mission To Planet Earth*", "Geocarto International", No. 6, United Kingdom and United States; 1991.

This article was unavailable for review as of March 1999.

Critique

None available.

Leslie, Connie with Nguyen, Lan. *The Wreck of the I-52*, Page 64, "Newsweek", New York, NY, USA; July 31, 1995.

An example of the current advanced level of undersea remote sensing was the recent discovery of the WWII Japanese submarine I-52 by Paul Tidwell, an American maritime researcher. Combining exacting research, formerly classified military technology from the U.S., and Russian commercial maritime assets, Tidwell was able to image the lost sub some 3.2 miles beneath the surface of the Equatorial Atlantic.

Tidwell plans to retrieve the 2 metric tons of gold aboard the boat, which if successful will define new boundaries in the abilities of deep-sea salvage and maritime remote sensing capabilities.

Critique

A simply stunning technological feat about which too little has been written. Tidwell has managed to assemble the finest maritime technicians available to achieve this find and should be considered on par with the descent on the "Titanic" by Dr. Robert Ballard.

Linden, Richard H. and Shurer, Pier J. *Results Of A Sub-Bottom Acoustic Survey In A Search For The Tonquin*, Pages 305-309, "The International Journal of Nautical and Underwater Exploration", Volume 13.4: 305-309, USA; 1984.

Largely passed over by most interested remote sensing aficionados is the relatively new development of underwater imaging systems. In this article the authors, both Canadian, focus on the wreck of the American trading vessel Tonquin, blown up by its crew in 1811 off the coast of present day Vancouver Island, British Columbia. The authors note that while many maritime archaeological expeditions have used magnetic detection devices, this particular search will be one of the first to use acoustic technology coupled with a computer, graphics system, and plotter – working in co-ordination with an onboard navigation system. As a result of this application of technology the authors were able to determine some 28 possible locations of the wreck, which were tested by divers using magnetic detectors. While the wreck was not located, the investigators believe that may be because the resolution of the acoustic device was not sufficient to its purpose.

Critique

Maritime remote sensing is presently supported by devices such as ROVs (Remotely Operated Vehicles), Unmanned submersibles, and some manned dive vehicles such as those used by the well-known Ballard Expedition to the "Lusitania" wreck (Irish coast). It is foreseeable that this aspect of remote sensing has applications in coastal areas for earthquake prone regions such as Greece, Italy, and Turkey, to assist conventional detection means.

Lyons, Thomas R. *Remote Sensing: A Handbook For Archaeologists And Cultural Resource Managers – Basic Manual Supplement: Oregon,* Pages 7-37, Section 3, "Archaeological Applications of Aerial Remote Sensing", Supplement 4: Cultural Resources Management, National Park Service, U.S. Department of the Interior, Washington, DC; 1980.

This supplement to the very useful NPS series, "Remote Sensing Handbook", focuses on the subject of aerial photography and in this particular instance, Oregon. Specific features are studied in depth here such as the Owyhee Canyon, Alvord and Warner Valleys, as well as several river basins.

The author is careful to address the application of aerial photography within the context of how it may be used in conjunction with satellite imagery to gain a clearer picture, so to speak. The author makes a good point as well that the analyst must consider how much a given area may have changed due to increased farming, irrigation, or as in Oregon, the creation of extensive hydro-electric dams and their associated lakes.

In a reference to these previously bodies of water, the author suggests the use of infrared films that allow subtle analysis of nearby bodies of water, such as ponds, which might be obscured by the larger bodies' massive solar reflectance.

Critique

This article has many useful hints for the imaging analyst needing to discern details near ponds, lakes, or rivers. Furthermore, with the advent of airborne hyperspectral systems and the forecast launch of a space borne hyperspectral system in the year 2000 by the United States, a whole new area of coastal archaeology will emerge.

Lyons, Thomas. *Remote Sensing: Multispectral Analyses Of Cultural Resources – Chaco Canyon And Bandelier National Monument, Supplement No. 5*, Cultural Resources Management of the National Park Service, U.S. Department of the Interior, Washington, DC, USA; 1981.

This article describes the work conducted in conjunction with the collection and analysis of multispectral data taken over Chaco Canyon, New Mexico. Five pueblos of the Anazasi were the focus of these efforts: Pueblo Alto, Kin Bineola, Pueblo Bonito, Chetro Ketl, and Wijiji. Airborne missions were conducted to provide field support by gathering soil moisture and vegetation structure data at Pueblo Alto, Kin Bineola, and Wijiji. Data was analyzed in a two-day session at EROS Data Center in Sioux Falls, South Dakota. Extensive treatment is given to the entire image-processing regimen.

Critique

A very well written analysis of a complete regional remote sensing archaeological campaign that is so often under-reported or overlooked by archaeologists.

Madry, Scott. *Remote Sensing In Archaeology*, Page 18-19, "Archaeology Magazine", American Association for the Advancement of Science, Volume 1, Issue 4, USA 1987.

This newsletter is dedicated to current issues involving the applications of remote sensing to archaeology and anthropology, as its name implies. This particular issue was concerned with close photogrammetric techniques and the special types of camera film that might be employed to enhance subtle features.

Critique

It is unknown by this reader whether or not this publication is still in existence. Due to the paucity of information available on remote sensing archaeology one would hope that the review continues its existence in some form.

Madry, Scott. *Remote Sensing In Archaeology*, Page 18-19, "Archaeology Magazine", Boston, MA. USA; May/June, 1983.

A short general publication article by the editor of the "Remote Sensing: Applications in Archaeology and Anthropology" editor. This article discusses archaeological sites around the world and how recent advances in satellite imaging systems have been used to assist in their interpretation and analysis.

Critique

While a bit dated, one statement in the article is prophetic even now in 1999. Madry notes,

"that it is possible to do research on a site from our laboratory in North Carolina – of a site in France – without ever leaving the lab".

Recent advances in technology make this even more relevant.

Madry S.L.H. & Crumley C.L. *An Application Of Remote Sensing And GIS In A Regional Archaeological Settlement Pattern Analysis: The Arroux River Valley, Burgundy, France*, Pages 364-380, "Interpreting space: GIS and Archaeology", Allen K.M.S., Green S.W. & Zubrow E.B.W. (Eds.), archaeology. Taylor, United Kingdom; 1990.

This article was unavailable for review as of March 2000.

Critique

None available.

Maitland, Flight Lieutenant. *The Works of the Old Men*, Pages 197-203, "Antiquity", Vol. 1, United Kingdom; 1927.

An extraordinary document replete with astonishingly good photography, this article may be one of the earliest known works to specifically focus on archaeological reconnaissance and survey, or what we now know as remote sensing archaeology.

Flt. Lt. Maitland describes the structures that he apparently routinely flew over on his flights carrying mail from Cairo to Baghdad and elicits from any reader a certain child-like joy at discovery. This work almost rightly belongs with the later literary genre created by Antoine Saint-Exupery.

The hand-drawn maps, which accompany his sharply detailed photographs, describe a journey across the southern portion of the Jebel Druze Mountains through what he terms "hill-fort country". Maitland studiously outlines the trade routes and paths which spots from the air, as well as providing a highly detailed map of one particular hill-fort.

A final unique detail of this foresighted work is Flt. Lt. Maitland's mention of his mission specifics,

"The air photographs were taken from a height of 2000 feet, with a lens of the focal length of 6 inches".

This is clarity and precision that would make a NASA astronaut proud even today.

Critique

The straightforward nonchalance with which Flt. Lt. Maitland writes of his subject belies the importance of this document to this particular branch of the science, remote-sensing archaeology. The detail with which this early remote sensing practitioner discusses his subject ranks this as a model even amongst today's modern technologies.

Mauelshagen, Landolf. *Architektur-Photogrammetrische Aufnahmen Und Auswertungen Von Spatantiken*, ("The Photogrammetric Survey And Plotting Of Early Byzantine Architectural Remains in Resafa, Syria"), Article, Institute Fur Photgrammetrie, Universitat Bonn, Deustschland; Berlin, Germany, 1981.

The authors make a case for the use of terrestrial photogrammetry by architectural historians and archaeologists in the analysis and study of inaccessible, or fragile, monument sites. The Resafa area is the subject of study in this instance, and the article demonstrates the use of photogrammetry as a means to record, analyse, and research archaeological architecture. Resafa is reported by the author to have been a fairly important trade Center in eastern present-day Syria and explains its geographic position in relation to great trade routes. Various techniques of applying corrected photographs to the creation of planimetric and elevation charts are also discussed, though in a very cursory manner. A further undocumented extensive work published by the German Archaeological Institute of Berlin describes the techniques in detail.

Critique

The author presents an interesting idea that is almost poignant in a fashion considering today's advances in computer technology. One is able to currently either scan in a photograph for re-assembly as a digital image, or merely use a digital camera to begin with if it is available.

It is also quite facile to utilize advanced graphics software to reconstitute a given monument and convert into a CAD frame, for example. This CAD frame can then be measured and studied for possible restoration or to estimate structural decay; obviously digital technology can be also used to simulate the edifice's original state as well.

Keywords: Terrestrial photogrammetry.

McAleer N. *Archaeology From Above*, Pages 21-25, "Space World", United Kingdom; Year unknown.

This article was unavailable for review as of March 2000.

Critique

None available.

McCauley J F. *Subsurface Valleys And Geoarcheology Of The Eastern Sahara Revealed By Shuttle RADAR*", Pages 1004-1020, "Science" No. 218, United Kingdom; 1982.

Please see annotation regarding McHugh paper that refers to the same subject.

Critique

None available.

McCauley J.F. *Palaeodrainages Of The Eastern Sahara - The RADAR Rivers Revisited (SIR-A/B Implications For A Mid-Tertiary Trans-African Drainage System)"*, Pages 624-648, "IEEE Trans Geoscience & Remote Sensing", GE-24, USA; 1986.

Please see annotation for McHugh paper that refers to the same subject.

Critique

None available.

McHugh W.P., Breed C.S., Schaber G.G., McCauley J.F. & Szabo B.J. *Acheulian Sites Along The "RADAR Rivers", Southern Egyptian Sahara*, Pages 361-379, Journal of Field Archaeology, No. 15, United Kingdom; 1988.

Please see following annotation entry for McHugh.

Critique

None available.

McHugh W.P., Schaber G.G., Breed C.S. & McCauley J.F. *Neolithic Adaptation and the Holocene Functioning of Tertiary Palaeodrainages in Southern Egypt and Northern Sudan*, Pages 320-336, "Antiquity", No. 63, United Kingdom; 1989.

"The "RADAR RIVERS" (author's italics) of the southern Eastern Sahara are systems of aggraded valleys containing inset drainage channels, now entirely obscured by wind-blown sand in the dry and hostile open desert. These features, first recognised on RADAR images, are remnants of the very different and moister landscapes of the Pleistocene and early Holocene. Proof of their attraction for early human settlement are the Acheulean artefacts that are found buried in alluvium that completely fills these old valleys and at the surface, along with Neolithic sites. The distribution of these sites follows, with good reasons, the order of the RADAR channels".

Several quite good maps and hand-held camera shots of the discussed sites are included in this discussion, as well as the SIR-B and SEASAT RADAR image data produced for this study.

Critique

An outstanding overview of one of the few space borne RADAR analysis campaigns to be carried out in support of archaeology. Of particular note are the careful descriptions of both the climatic and geological structures of the area and well worth the careful reading by any aspiring RADAR remote-sensing analyst investigating archaeological applications.

McKee B.R., Sever T.L. & Sheets P. *Prehistoric Footpaths In Costa Rica: Remote Sensing And Field Verification"*, Pages 142-157, "Archaeology, Volcanism and Remote Sensing in the Arenal Region, Costa Rica", P. Sheets & B. McKee (Eds.); 1994.

Dr. Thomas Sever, NASA Marshall Space Flight Centre, AL, holds this article.

Critique

None available.

Miller W.F., Sever T.L. & Lee D. *Applications Of Ecological Concepts And Remote Sensing Technologies In Archaeological Site Reconnaissance*, Pages 121-136, "Applications Of Space-age Technology In Archaeological Site Reconnaissance", Behrens C. & Sever T. (Eds.), Unknown publication site; 1991.

This article was unavailable for review as of March 2000.

Critique

None available.

Moore E. & Freeman A. *RADAR, Backscattering Mechanisms And The Ancient Landscape Of Angkor,* Pages 15-19, "Remote Sensing Society Archaeology Special Interest Group Newsletter", No. 1, USA; 1997.

This article was unavailable for review as of March 2000.

Critique

Not available.

Morain, S. A., Nelson, C., White, M., Komarek, A. *Remote Detection Of Prehistoric Sites In Bandelier National Monument,* "Remote Sensing: A Handbook for Archaeologists And Cultural Resource Managers, Cultural Resources Management, National Park Service, U.S. Department of the Interior, Washington, DC, USA; 1980.

The authors present the results of a test Multispectral Scanner analysis at Bandelier National Monument. The hypothesis under investigation was as follows: to subject the MSS to both supervised and unsupervised enhancement or classification techniques in a test of image analysis for cultural information. Principal component and canonical analysis were performed on an identical 512-scan line and 512-sample data mix. Each resolution cell (pixel) 3.75 feet, thus each scene covered about 1920 feet. As the authors' note,

"the basic question (is) whether the enhancement/classification techniques were capable of spectrally enhancing known prehistoric sites from the surrounding terrain".

After subjecting the test area to the hypothesis, the authors came to the following conclusions: prehistoric sites cannot be visually discerned by spectral qualities alone and pre-historic sites, even if ground data is used to direct the enhancement, cannot be visually discriminated by spectral properties. However, the authors note that a,

"supervised enhancement approach or a maximum likelihood classification technique can be used with visual interpretation to discriminate pre-historic areas".

Omokhodion, Dem. *Benin In West African Architecture,* Pages 73-80, "West African Journal of Archaeology", Volume 18, University of Benin, Nigeria; 1988.

"Recent or traditional architecture in West Africa can be and have been studied as an important dimension in the cultural development of peoples. In West Africa, form and material techniques reveal local ecological adaptation. Demarcation into social space, such as in Benin architecture, seems to offer an explanation for the relationship between the sexes, in the narrow sense, and for the social organisation in the large sense".

Critique

A rare article on activities in archaeological architecture and the use of that most basic and still quite useful remote sensing tool – the camera. Another intriguing thought is how photogrammetric or proto-magnetic sensing technology might be used to further new avenues of research on this subject.

Palmer R. *Remote Sensing and Archaeology*, Pages 18-19, "AARGnews" No. 7, United Kingdom, Year unknown.

This article was unavailable for review as of March 2000.

Critique

None available.

Parrington M. *Remote sensing*, "Annual Review of Anthropology", No. 12, United Kingdom; 1983.

This article was unavailable for review as of March 2000.

Critique

None available.

Pfieffer, John. *Remote Sensing: Archaeological Applications In Southern England*, Pages 75-82, "The Journal of New York State Archaeology", Vol. 10, State University of New York, Albany, NY, USA; 1981.

Pfieffer offers an interesting proposition to remedying rapid growth versus the necessity to conduct archaeological surveys in New England. He suggests a complete series of region-wide, low-to-medium altitude aerial photogrammetric flights for initial analysis, followed by higher resolution, larger scale flight missions over suspected sites.

This particular article describes how two such missions were carried out to success. Pfieffer also notes that in the north-eastern U.S. high-altitude black and white imagery could define sites in open areas quite well. He notes that remote sensing offers savings in time, money, and effort.

Critique

A very well written and well thought out paper on the subject of aerial photogrammetric applications in an area traditionally thought to be inaccessible.

Pope K.O. & Dahlin B.H. *Ancient Maya Wetland Agriculture: New Insights From Ecological And Remote Sensing Research"*, Pages 87-106, "Journal of Field Archaeology", No. 16; 1989.

This article was unavailable for review as of March 2000.

Critique

None available.

Pouquet J. *Remote Detection Of Terrain Features From NIMBUS I High Resolution Infrared Radiometer Night-time Measurements*, NASA Technical Notice Document (TND)-4603, United States of America; 1968.

This article was unavailable for review as of March 2000. It is quite likely that this paper may be obtained by private purchase through the U.S. Government printing office, Washington, DC, United States of America.

Critique

None available.

Richards T.S. *Evidence Of Ancient Rainwater Concentrating Structures In Northern Egypt As Seen On LANDSAT MSS Imagery*", Pages 1135-1140, "International Journal of Remote Sensing", No. 10, United Kingdom; 1989.

This journal was unavailable for review as of March 2000.

Critique

None available.

Romano D.G. & Tolba O. ***Remote Sensing And GIS In The Study Of Roman Centuriation In The Corinthia, Greece"***, Pages 457-463, "Interfacing The Past: Computer applications and quantitative methods in archaeology", CAA No. 95 Vol. II. Kamermans H. & Fennema K. (Eds.) University of Leiden, Germany; 1996.

This symposium paper was unavailable for review as of March 2000.

Critique

None available.

Sanders, John C. and Peggy. *The Nippur Expedition and Remote Sensing*, Pages 1+, "The Annual Report of the Oriental Insatiate, 1995-96", University of Chicago Press, University of Chicago, Chicago, Illinois, USA; 1996.

"During the past year a working relationship has been established between the Oriental Institute and the Center for Geographic Information Systems, in the Geography Department of St. Cloud State University (Reviewers note: Now known as the Spatial Analysis Research Center, or SARC.), St. Cloud, Minnesota. Director Benjamin Richason and his staff have been working with the Oriental Institute's McGuire Gibson, Tony J. Wilkinson, and the Computer Laboratory to co-ordinate a joint research project investigating remote sensing techniques for archaeological site identification and analysis, as well as geomorphological analysis, of a small region in south-western Iran, near the ancient site of Susa, using satellite images and ground-penetrating radar data obtained by NASA from recent Space Shuttle flights over this region of the earth."

"During this past year the Oriental Institute supplied bibliographic, map, and survey data to students at the Center for Geographic Information Systems, who then integrated this information with satellite image data of the area using the Centre's Geographic Information Systems (GIS) computer software. Preliminary results of this first test were encouraging, and discussions concerning both the data analysis procedures and the computer software techniques employed will be held during the summer of 1996, in preparation for a more focused investigation on the region around the Mesopotamian site of Nippur scheduled for the 1996/97 school year".

Critique

This reviewer participated in this project while at St. Cloud State University as part of a one year dedicated RADAR remote sensing archaeology effort to support the Oriental Institute. Specific data utilised were Space Shuttle Imaging RADAR (SIR-C/X-SAR) multipolarimetric in the Cvv, Chh, and Lhh modes. Team members were Dr. Benjamin Richason, Mr. Eric Goodman, Ms. Kathy Liljequist, Mr. Gary McKay USAR, Mr. Michael Regan, and Mr. Scott Zibell USAFR. A subsequent paper was co-authored entitled, *Image Processing Techniques for SIR-C/X-SAR Data: Karkeh River Scene*, as well as a submission to the *1996 Manual of Photogrammetric and Remote Sensing Techniques*, published by the PE&RS Society of the United States of America.

Scollar, Irwin. *Digital Image Processing And Archaeological Air Photography*, Pages 137-142, "Paper of Rhiensiches Landesmuseum, Bonn, Germany; 1988.

The author describes the history of systematic oblique aerial photography in the last sixty years as it relates to Europe's archaeological community. The author states that the Landesmuseum had obtained some 30,000 images, with ten of thousands of new archaeological sites discovered all over Northern Europe due to this effort. The author covers the efforts to obtain digitally enhance imagery of these images as well as new data.

Critique

Possibly the leading effort in Europe, this article describes in detail a highly advanced remote sensing effort that would rival, if not exceed any American effort of the time. (Note laboratory schematic within the article.)

Sever T.L. *Benchmarks In Time And Culture: An Introduction To Palestinian Archaeology*, pages 279-305, "Remote Sensing", J.F. Drinkard, G.L. Mattingly & J.M. Miller (Eds.), United Kingdom; 1988.

This article was unavailable for review as of March 2000.

Critique

None available.

Sever, T. and Sheets, P. *High Tech Wizardry*, Pages 28-35, "Archaeology Magazine", USA; November/December, 1988.

A unique article in that the authors had multiple remote sensing platforms at their disposal, Sever and Sheets detail their research on Indian trails of Costa Rica with Infrared, LIDAR (Laser Indicating Detector And Ranging), and TIMS, or Thermal Infrared Multispectral sensors. Centred on north-western Costa Rica, the investigation attempted to discover the relationship between various ancient villages, cemeteries, and other ruins, which appeared to be rather widely dispersed.

The authors first utilised LIDAR sensing technology after noting several apparent trails that appeared under infrared analysis. LIDAR is "a LASER device that makes profiles of the earth's surface. The LASER beam pulses to the ground 400 times per second, striking the surface every three and one half inches (8-9 cm. approx.), then bouncing back to its receiver.

Sever and Sheets then followed up this remote sensing analysis with a Synthetic Aperture RADAR run. Noting the application of varying wavelengths to discover subsurface features, the authors were then able to find several suspected prehistoric features. Finally, the authors used a TIMS (Thermal Infrared Multispectral Scanner) platform to investigate variegated vegetation growth. "TIMS uses six channels to measure the thermal radiation given off by the ground, with accuracy to 0.1 degree centigrade". After completing this rather extensive (by any modern standard even) remote sensing effort of the target areas, the authors then managed to have NASA's 990 Convair aerial sensing platform fly the site.

High altitude photographs, including colour infrared photography (which was used to find the original footpaths and trails) were also obtained. The authors firmly believe that remote sensing in the 1990s will be to archaeology what carbon dating was in the 1950s.

Critique

This reader believes that if there were a case for remote sensing overkill, this may be it. While the sheer array of technology is overwhelming, and the results were satisfactory, one wonders from an archaeological point of view if a little more "ground" investigation would not have been more useful.

Sever T.L. & Wagner D.W. *Analysis Of Prehistoric Roadways In Chaco Canyon Using Remotely Sensed Digital Data*, Pages 42-52, "Ancient Road Networks And Settlement Hierarchies In The New World", C. Trombold (Ed.), USA; 1991.

This article was unavailable for review as of March 2000.

Critique

None available.

Shennan I. & Donoghue D.N.M. *Remote Sensing In Archaeological Research Proceedings*, Pages 223-232, British Academy, No. 77, United Kingdom; 1992.

This article was unavailable for review as of March 2000.

Critique

None available.

Sheets, Payson D. *Geophysical Exploration For Ancient Maya Housing At Ceren, El Salvador*, Pages 645-655, "Research Reports", 1979 Annual National Geographic Reports, Washington, DC, USA; 1979.

This author details a highly unusual project in the El Salvadoran mountains in which a trio of geophysical analysis technologies will be used to detect ancient Mayan structures beneath lava fields. The project was directed at two sites, the Ilopango volcano which erupted in 300 AD, and the Laguna caldera which erupted in 600 AD

The team geophysical technicians were able to penetrate roughly five meters of tephra (lava ejections) using ground penetrating RADAR (GPR), seismic refraction, and electrical resistivity to determine the sites of several Mayan structures. These sites were verified using a ground soil-core sampling drill.

Critique

This is certainly one of the most unusual applications of remote sensing technology, that is searching beneath a geological structure which is generally perceived to be impenetrable, volcanic rock. The seismic refraction may also have applications in assisting ground truthing of RADAR target image areas, particularly in extremely dry climates.

Sheets P. & Sever T.L. *Prehistoric Footpaths In Costa Rica: Transportation And Communication In A Tropical Rainforest*, Pages 53-65, "Ancient Road Networks and Settlement Hierarchies In The New World", C. Trombold (Ed.) 53-65, Publication site unknown; 1991.

This article was unavailable for review as of March 2000.

Critique

None available.

Sherwood, Susan I., and Wynn, Jeffrey C. *The Self-Potential Method: An Inexpensive Reconnaissance and Archaeological Mapping Tool*, Pages 195-204, "Journal of Field Archaeology",
Vol. II, Boston, Massachusetts, USA; 1984.

The authors have conducted site tests of the self-potential (electrical field conductivity) method in the Harpers Ferry, Ft. Washington, and Piscataway historic sites on the Potomac River shore of Maryland. The tests were successful in identifying buried structures as well as soils disturbed in historical times.

The authors of this work also note that recent rainfall, superficial variations in soil composition (chemistry), and polarisation of electrodes can skew SP voltages. The tests are quick and are the cheapest of all geophysical exploration methods. The primary difficulty is in obtaining well-trained personnel to operate the system, as well as analysing the products.

Critique

This paper could easily have been written in a much more technically approachable manner for the neophyte archaeologist interested in using such technology. As it stands, one must consult an outside authority to fully comprehend the subtle nuances of the self-potential system.

Showalter P.S. *A Thematic Mapper Analysis Of The Prehistoric Hohokam Canal System, Phoenix, Arizona"*, Pages 77-90, "Journal of Field Archaeology", No. 20, Boston, Massachusetts, USA; 1993.

This article was unavailable for review as of March 2000.

Critique

None available.

Silverman, Helaine. *The Archaeological Identification Of An Ancient Peruvian Pilgrimage Center*, Pages 1-15, "World Archaeology", Volume 26, No. 1 – Archaeology of Pilgrimage, Routledge Inc., USA; 1994.

This article is oriented towards the more traditional archaeological site investigation and does not make any specific effort towards using remote sensing technology. However, it is useful to note the investigator's use of aerial photography to gain a better vantagepoint of the overall site, Cahuachi, on the southwest coast of Peru.

Critique

This reader finds it odd that the investigators were not opting to perform a more dedicated analysis via remote sensing. Considering the goal of this site exploration was to define Cahuachi's importance as a pilgrimage centre, remote sensing could have easily detected new transport structures such as trails, footpaths, and roads.

Stine R.S. & Decker T.D. *Archaeology, Data Integration And GIS*, Pages 134-140, "Interpreting space: GIS and Archaeology", Taylor & Francis. Allen K.M.S., Green S.W. & Zubrow E.B.W (Eds); United Kingdom; 1990.

This article was unavailable for review as of March 2000.

Critique

None available.

Streit, Richard. *Elektrische Widerstandmessungen zur Verfolgung der Hohlenverullung bei Hunas,* Publische Landesmuseum, Bonn, Germany; 1985.

An exceptionally difficult German work on the subject of electrical conductivity/resistivity of soils in conjunction with archaeological work. A contour map was generated from a highly detailed and fastidiously worked site investigation, one of the few seen by this reader. The author submits that he has obtained sensitivity in the range of 2 ohms.

Critique

A tedious effort was involved in translating this work from the German for review; howsoever it was well worth the effort as this is a very useful technique for analysis of micro-spatial patterns within a microtopography.

Thompson H.O. *A New Development in Archaeological Air Photography*, Pages 225-227, "Antiquity", No. 41. 1967.

This is a very intriguing article and well worth the search to obtain. Prof. Thompson discusses the onset of the satellite age in support of archaeological investigation in the year 1967. After an initial survey of the soon to be launched (then) Earth Resources Observation Satellite (EROS)—now known of course as LANDSAT, Thompson articulates the failure even then of U.S. Government officials to see the uses of satellite imagery to support archaeological reconnaissance and survey.

Thompson then moves on to discuss the work utilising infra-red cameras and film at the American School of Oriental Research, Jordan, as well as the then Applied Science Center for Archaeology at Pennsylvania University, USA.

The most interesting statement by Thompson in this overview of the state of remote sensing archaeology in 1967 is this rather visionary commentary,

"...As it is, however, we are dealing with sensitivities beyond the human eye and, for that matter, beyond standard photographic film. Perhaps the most astounding example of this sensitivity is the possibility of distinguishing between wheat and oats as the crop in the field. The other response to Dr. St. Joseph's remarks is that the geographical and geological features he mentions are themselves of value to archaeology. To the remarks already incorporated in the paper might be added the possibility of locating, or locating more accurately, ancient trade routes. I am tempted also to underline the point in the article that satellite photography may be the impetus to lower altitude photography, and to additional types of research such as underwater remains".

Critique

This is an outstanding article written at the dawn of space borne remote sensing archaeology. Remarkably prescient are the opinions of Prof. Thompson in regards to the ability of satellite imagery in locating more accurately, ancient trade routes.

The discovery of the lost city of Ubar in Oman (1992) was aided largely by the study of both optical, multispectral, and RADAR image data. Prof. Thompson can have scarcely dreamed of the space borne data collection systems available now, but his vision was true.

Quann J. & Bevan M. *The Pyramids From 900 Kilometres,* Pages 12-14, MASCA Newsletter No. 13, United Kingdom; 1977.

This article was unavailable for review as of March 2000.

Critique

None available.

Ursche, Joe. *Digging Up The Dead,* Page 1-2, and special supplemental section, USA TODAY, newspaper, Washington, D.C.; 28 July 1995.

A premier article for the general public on what has been dubbed the "archaeological discovery of this half of the century", the tombs of the fifty sons of Ramses II. Discovered by Kent Weeks, a veteran Egyptologist, the tombs may ultimately open some 100 tombs and reliquaries, shedding more light on Egypt's Near-Biblical times.

Critique

This story should be closely followed as the discovery of this tomb structure will draw immense financial backing, which should allow Weeks some superlative opportunities to utilize the most advanced remote sensing technologies available. As a final note, Prof. Weeks has published a book for the general readership on this subject.

Viereck, P. *A High Resolution RADAR for Detection of Shallowly Buried Objects*, Pages 295-301, "Archaeology", USA; 1985.

A prototype microwave wavelength ground penetrating RADAR system for high imaging resolution within this article by Viereck, a Danish researcher. Viereck's model relies on the principle of utilisation of the modulated microwave carrier transmission instead of the commonly used video wavelengths. Consequently, Viereck's model achieves an astounding horizontal resolution of 50 centimetres and a vertical resolution of 10 centimetres in sand. Using the 1 Ghz to 2 Ghz range, Viereck's model approaches 1-meter penetration in dry sandy soils, but water apprehends resolution and penetration if present.

Critique

A the time of this article, the technology available to Viereck's model was surely limited; one should be interested to see how a present-day working model would perform, particularly with today's digital processing capabilities.

Walker A.S. *Deserts of China*, Pages 366-375,
"American Scientist", No. 70, USA; 1982.

This article was unavailable for review as of March 2000.

Critique

None available.

Wendorf F., Close A.E. & Schild R. *A Survey Of The Egyptian RADAR Channels: An Example Of Applied Field Archaeology*, Pages 43-63, "Journal of Field Archaeology", No. 14, United Kingdom and United States; 1987.

This article was unavailable for review as of March 1999.

Critique

None available.

Wilkinson, Tony J. *Off-Site Archaeology*, Pages 196-208,
National Geographic Research and Exploration, 82): 196-207, Washington, D.C., USA; 1992.

This article addresses the question concerning the nature of interconnectivity between long-inhabited settlements of the central Iraqi plain. The author expresses the view that humankind in the area "increased pressure on the area, but avoided obvious degradation of the landscape".

The subject area is the Tell al-Hawa located north-west of the Iraqi city of Aski Mawsil. The basic argument of the author is that the areas surrounding sites may give the best indications of the cultural centre's importance.

Critique

This area has since been the subject of a remote sensing effort and is yet another example of a regional-based analytical campaign. One of the most over-looked uses of remote sensing is in the detection and extent of ancient cultural spatial structures. This effort by the Oriental Institute team is another good step towards remedying this drought.

Zayadine, Fawzi. *Caravan Routes Between Egypt And Nabatea And The Voyage of Sultan Baibars To Petra in 1276*, Pages 159-171, "Archaeology", Volume II, USA; 1981.

Zayadine offers substantial treatment of the subject of Pan-Arabian trade systems in the Ancient Near East. Several maps, as well as significant documentation, lend themselves well to the subject and provide a wealth of useful information to the novice on the subject. Of primary interest is the connection between ancient Egypt and Mesopotamia with indications of greater trade with the southern Arabian Peninsula regions than most would grant.

Critique

A thought-provoking article, especially in light of the work performed by the Fiennes' Ubar expedition and the Oriental Institute, as well as the British Museum, on trade and communication routes. While this article references no specific remote sensing issues, it is a pointer again towards the type efforts that could reveal the best results.

Additional Notes

The usefulness of the Internet and related electronic documentation make the addition of a supplementary appendix almost mandatory. However, the reader should note that due to the vagaries of the electronic data world, websites, homepages and other related Internet addresses may appear, then disappear without notification. Thus, the user should beware in utilising such resources for fundamental academic research.

This author is not responsible for the content or the verification of the existence of the documents listed in these sites which were current as of March 2000.

Internet remote sensing archaeology bibliographies:

Satellite Archaeology

http://ourworld.compuserve.com/homepages/mjff

A British homepage hosted by Martin J. Fowler primarily listing his own publications but with interesting examples of declassified CORONA imagery and recent high resolution Russian optical and multispectral data. Some publications are difficult to find due to their minimal publication numbers.

Rosetta's Remote Sensing Links

http://www.mind.net/aware/remote.htm

A homepage which lists other remote sensing archaeology interest sites such as the Archaeology Remote Sensing Consortium, Archaeometry, and the "Journal of Field Archaeology", among many others.

GIS and Remote Sensing Archaeology

http://www.geo.ryerson.ca/~michalak/html/arche.html

The *GIS and Remote Sensing Archaeology* homepage is a substantive collection of links primarily directed towards the modelling efforts of archaeologists with GIS technology. Among the more interesting links are those to the Rhone Valley Project in France and the Perseus Project, focused on the ancient Mediterranean and hosted by an U.S. consortium.

Archaeology and Remote Sensing Consortium (ARSC)

http://eleftheria.stcloud.msus.edu/arsc/

A homepage hosted by the above-mentioned organisation at St. Cloud State University, Minnesota, USA. Highlights of this homepage include a discussion group devoted solely to current remote sensing archaeology techniques and issues. Members and interested parties are free to e-mail consortium members with their questions which are sent to other members for consideration. An excellent first stop for the noviciate in remote sensing archaeology and for those searching for sources of imaging data. ARSC was begun as an outgrowth of a joint remote sensing effort between the Oriental Institute of Chicago, University of Chicago, St. Cloud State University, Minnesota, and the NASA Jet Propulsion Laboratory, Pasadena, California.

Archaeology and Geophysics

http://www.xs4all.nl/~jorbons/raap_geof.html

An excellent homepage for the more technically mined in terrestrial remote sensing or geophysical equipment. Links are given for the various manufacturers of GPS, GPR, magnetometers, and SONAR systems. This is a very good source of technical specifications for geophysical equipment.

Nautical Archaeology At Texas A&M University

http://nautarch.tamu.edu/

The University of Texas A&M in the United States, along with the University of Southampton in the United Kingdom, rank as the world's acknowledged leaders in nautical and maritime archaeology. This homepage gives an excellent start to those interested in this aspect of remote sensing archaeology. Interestingly enough, nautical archaeology is the branch of archaeology which is most dependent on remote sensing archaeological techniques, for in a purely philosophical sense, virtually all initial nautical survey work uses some form of remote sensing.

GIS and Remote Sensing For Archaeology: Burgundy, France

http://deathstar.rutgers.edu/projects/france/france.html

A very nicely done homepage detailing the nearly twenty year long research program conducted in the Burgundy region of France by Rutgers University. The focus of the project is an integrated analysis of the cultural interaction with the environment using GIS and Remote Sensing as its primary tools. The project is currently headed by Dr. Scott Madry and quite rightly should be considered as the most successful long-term remote sensing archaeological project to date. A very nicely presented group of graphical analyses are presented with general interest commentary.

Southampton Archaeology – Research

http://www.arch.soton.ac.uk/Research/

The University of Southampton homepage is an outstanding example of one of the world's premier archaeological programs. Southampton has a dedicated Center for Maritime Archaeology, as well as an Archaeological Computing program dedicated solely to the aspects of terrain and artefact reconstruction.

While most of the focus on this website is centred on nautical archaeology, as was previously discussed on the Texas A&M review, Southampton's work is directed towards a viable branch of remote sensing archaeology and is too often overlooked by terrain focused archaeologists.

ABZU – Guide to Resources for the Study of the Ancient Near East Available on the Internet
http://www-oi.uchicago.edu/OI/DEPT/RA/ABZU/ABZU.HTML

Funded, hosted, and organised by the Oriental Institute of the University of Chicago, the ABZU electronic gateway is the single largest on-line archaeological database in the world at present. Data objects within this searchable collection of on-line journals project reports and reviews number in the millions. Furthermore, while the title may describe a specific focus on Near Eastern archaeological work, numerous links to archaeological works around the world are also to be found within. The practising remote sensing archaeologist will find this to be an endless supply of data for initial topographic data about any potential survey scene.

Aerial Photographic Archive For Archaeology in the Middle East
http://www.arts.uwa.edu.au/Classics/archeology/rsame.html

Quite likely the most unheralded and little known homepage related to remote sensing archaeology, the *Aerial Photographic Archive for Archaeology in the Middle East* is an extraordinary mine of compiled data. In conjunction with topographic data which might be gleaned from the Oriental Institute's *ABZU* site, the remote sensing archaeologist working in the Middle East will come well prepared to any survey scene if also equipped with imagery from this database. This site is of very high interest for analysts using space borne RADAR systems as it offers substantial opportunity for high quality aerial optical imagery for ground truthing purposes. His Royal Highness Crown Prince Hassan Bin Talal of Jordan sponsors this project.

Project Zeugma
http://www.ist.lu/ele/html/department/zeugma/image.html

The Birecik dam, currently under construction on the river Euphrates, will be completed in the year 2000. The dam is located on the boundary between Gaziantep and Sanli Urfa provinces in Southern Turkey, about 30 km North of the border with Syria. While the dam will create a reservoir, it will also drown an area rich in history and in archaeological sites. In particular, the waters of the dam will cover much of the site of Zeugma, a Greek and Roman city located on both sides of the Euphrates.

The following Internet website addresses are those offer aerial, space borne or hydrographic sources of remotely sensed data that may support archaeological reconnaissance, survey, and analysis. The author assumes no responsibility for the existence, quality, or accuracy of the datasets nor image processing characteristics and software requirements, which are the sole responsibility of the reader or user.

Earth Science Data on the Global Land Information System

http://edcwww.cr.usgs.gov/webglis/

The gateway to the U.S. Geological Survey's "Global Land Information System". Access through this gateway to datasets of aerial photography (primarily of the United States), declassified CORONA satellite imagery, LANDSAT, NASA Space Shuttle SIR-C/X-SAR multipolarimetric SAR, and NASA Earth Observation space borne photography.

While LANDSAT data is not cost free, charges for CORONA images and negatives are minimal, while RADAR datasets are approximately $60 UD at present and take less than a week for European delivery.

EOSPSO Homepage

http://eospso.gsfc.nasa.gov/

The homepage for the NASA Earth Observation System, this site offers directions and links to multiple free datasets from the various on-going remote sensing projects. Projects of oncoming interest to the remote sensing archaeologist are the soon to be launched LANDSAT 7 and TERRA series. These platforms will offer an enhanced capability in comparison to the long operating LANDSAT MSS and TM programs and will significant gains in data quality. Links are also offered to the EOSDIS system which allow the user to link to all data sites in unison for a complete search of the entire remote sensing database including ALL sensor systems at one time. A very efficient time and labour-saving device for the hard-pressed researcher.

The X-SAR User Kit

http://isis.dlr.de/XSAR/Welcome.html

The Internet site for the German Space Remote Sensing Centre's (DLR) X-band SAR program, conducted in co-operation with NASA's Space Shuttle SIR-C/X-SAR multipolarimetry program. Datasets are offered here for the cost of the duplication and tapes (or other media) and are quite reasonable.

A very useful and well done graphical interface serves as the global search engine for data and produces highly effective coverage maps and basic metadata. The more advanced remote sensing archaeologist should be aware however that this particular wavelength of SAR is useful for precision topographic mapping primarily and best used in conjunction with high-resolution optical imagery. Still, this is clearly the most useful and easily searched remote sensing database on the Internet.

Environment Monitoring Information Systems

http://www.iki.rssi.ru/monitoring/monitor.html

Too often forgotten and overlooked by many remote sensing archaeologists are the vast resources of the Russian Space Federation. While in some contexts data is not as easily obtainable as other sources, the sheer depth and breadth of Russian geophysical and topographic analysis platforms is stunning.

It is well worth the effort and patience to retrieve a unique data set from the Russian Space Research Institute, particularly for those working in the Central Asian regions. Specific data sets mentioned on the site cover bathymetric, land-use, fire-mapping, global and regional climate change, as well as Arctic region mapping.

SMIS Home Page

http://smis.iki.rssi.ru/welcome.html

The central home page for all Russian Space Federation remote-sensing projects, "SMIS" serves as the overhead organization for direction of the myriad systems. Data acquisition sites, pricing, and even some basic image processing software are available through this gateway. Of specific interest to universities will be the pricing schemes for the image processing software, much of which are some 30 to 50 percent of its normal cost. A highly recommended site for those interested in Russian remote sensing products.

Appendix VII
RADAR Remote Sensing Addenda

VII-I Radar image distortions: slant range

Just as in other type of remote sensing system, a RADAR system's viewing geometry can produce particular geometric distortions upon the image product. Still, there are significant areas where RADAR functions much differently from conventional remote sensing systems. The primary differences of RADAR imagery lie in its side-looking viewing geometry, and that RADAR systems are essentially devices that measure distance, or *range* (CCRS, 2001). One particular effect, known as slant-range scale distortion, is created because RADAR systems measure the distance to features in slant-range instead of true horizontal distance along the ground. Consequently, an image product with a changing image scale is produced, moving from near to far range. As seen below in Fig. VII-1, even though the targets A1 and B1 are equal in size on the ground, their dimensions as perceived by the RADAR system in slant range (A2 and B2) as being quite different (CCRS, 2001). The resultant image product from such an effect shows targets in the near range to look compressed in relation to the far range. By performing a trigonometric calculation, the ground-range distance may be figured from the platform altitude and slant-range distance to change it into correct ground-range data (CCRS, 2001 and JPL, 2001).

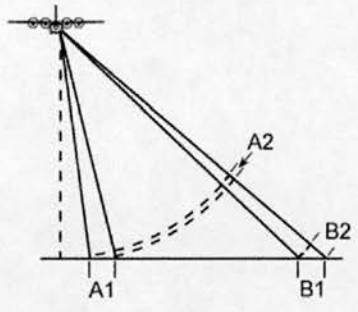

Fig. VII-1 Slant range distortion (CCRS, 2001)

As with the distorted effects seen when employing cameras and scanner systems, RADAR images have geometric distortions created from relief displacement. Just as with image products from scanners, this displacement is created perpendicular to the flight path and is one-dimensional. This displacement, in relation to RADAR systems, is reversed with the targets being displaced towards the sensor, instead of away from the sensor. The effects which are by-products of this relief displacement are known as RADAR foreshortening and layover.

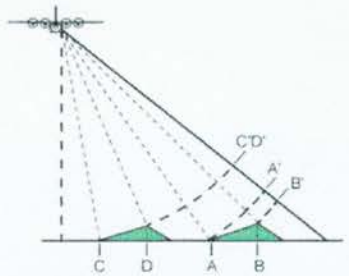

Fig. VII-2 Foreshortening (CCRS, 2001)

When a RADAR wave strikes the foot of a high feature, such as a mountain, angled in the direction of the RADAR sensor before it reaches the peak, a *foreshortening* effect is created (Fig. VII-2 and CCRS, 2001). As stated previously, since RADAR measures distance in slant-range, the slope of the mountain (A to B) will look compressed and the length of the mountain slope will not be displayed correctly (A' to B'). The angle of the mountain slope in relation to the incidence angle of the radar beam will determine the severity of the foreshortening effect upon the resultant image product. The greatest effect of foreshortening happens when the RADAR wave is perpendicular to the mountain slope, consequently producing a situation where the slope of the mountain, its base, and its peak are imaged at the same time (C to D) (CCRS, 2001). The length of the mountain slope will therefore be reduced to an effective length of zero in slant range (C'D') (CCRS, 2001). As stated in Chap. 3, pg. 36, these effects were encountered during this study and may be best seen in Chap. 7, Fig. 7-19.

VII-III Layover

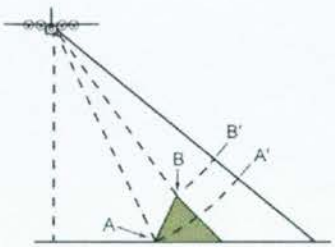

Fig. VII-3 Layover (CCRS, 2001)

Layover happens when a RADAR wave strikes the top of a high feature, such as the just discussed mountain (B), before it reaches the foot (A) of the mountain (Fig. VII-3 and CCRS, 2001). The return signal from the peak of the mountain will be received before the signal from the foot of the mountain. Therefore, the peak of the mountain is displaced in the direction of the RADAR from its actual ground position, and thus "lays over" the foot of the mountain (B' to A') (CCRS, 2001 and GSFC, 2001).

Layover effects on RADAR imagery appear much like those of foreshortening and care must be given when assessing imagery because of this. Like foreshortening, the layover effect is amplified by minimal incidence angles, at the near range of a swath, and in mountainous topography.

VII-IV Shadow

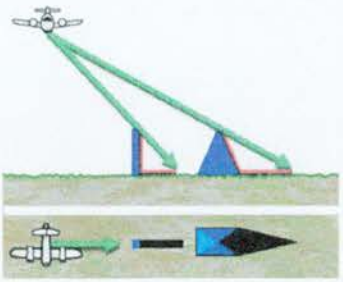

Fig. VII-4 Shadow effects; **red surfaces are completely in shadow. Black areas in image are shadowed and contain no information (CCRS, 2001).**

The foreshortening and layover effects both create another effect known as RADAR *shadow* (CCRS, 2001 and GSFC, 2001). RADAR shadow is created when the RADAR wave is unable to illuminate the target ground surface. Shadows happen in the down range dimension (i.e. towards the far range), behind vertical features or slopes that have steep sides (CCRS, 2001 and JPL 2001). Because the RADAR wave is unable to strike the surface and thereby "illuminate" it, shadowed regions will appear as dark areas on an image as no energy is available to be backscattered to the sensor's receiving antenna (CCRS, 2001 and Chap. 3). As incidence angle increases from near to far range, so will the shadow effects as the RADAR sensor's transmitted beam looks more and more obliquely at the surface (CCRS, 2001). Figure VII-4 (above) illustrates radar shadow effects upon a hypothetical vertical wall and mountain.